UNIVERSITÉ DE STRASBOURG

THÈSE présentée par :

Marine HEMMERLE

soutenue le : **08 juillet 2021**

pour obtenir le grade de : **Docteur de l'université de Strasbourg**

Discipline/ Spécialité : Sciences du vivant, Aspects moléculaires et cellulaires de la biologie

Étude de la localisation mitochondriale ou vacuolaire d'aminoacyl-ARNt synthétases cytosoliques multi-localisées chez la levure *Saccharomyces cerevisiae*

THÈSE dirigée par :

   Pr. BECKER Hubert   Professeur des Universités, IPCB (UMR 7156), Université de Strasbourg, France

RAPPORTEURS :

   Pr. SCHULDINER Maya   Professor, Weizmann Institute of Sciences, Israel
   Dr. LUQUE Ignacio   Group leader, Instituto de Bioquímica Vegetal y Fotosíntesis, Spain

EXAMINATEUR :

   Dr. FRUGIER Magali   Directrice de recherches, Université de Strasbourg, France

THESIS presented by :

Marine HEMMERLE

Defended on **July 08th, 2021**

To obtain the degree of : **Doctor of the University of Strasbourg**

Discipline/ Specialty: Life Sciences, Molecular and Cellular Biology

Study of the mitochondrial or vacuolar localization of multi-localized cytosolic aminoacyl-tRNA synthetases in the yeast *Saccharomyces cerevisiae*

THESIS supervised by:

    Pr. BECKER Hubert   Professeur, IPCB (UMR 7156), Université de Strasbourg, France

EXTERNAL JURY MEMBERS:

    Pr. SCHULDINER Maya   Professor, Weizmann Institute of Sciences, Israel

    Dr. LUQUE Ignacio   Group leader, Instituto de Bioquímica Vegetal y Fotosíntesis, Spain

EXAMINER:

    Dr. FRUGIER Magali   Directrice de recherches, Université de Strasbourg, France

Remerciements

The following acknowledgements will be written in French, but I first wanted to thank the members of my jury, Prof. Schuldiner Maya, Dr. Luque Ignacio and Dr. Frugier Magali for accepting to evaluate my thesis work and manuscript. It is an honor for me to be reviewed by a such a jury.

Déjà cinq années de passées dans la DyPS team et tant de souvenirs et de gratitude !

Je voudrais d'abord remercier le Dr. Ivan Tarassov pour son accueil au sein de l'UMR 7156. Merci également aux responsables pédagogiques de l'UE Biochimie et tout particulièrement à Joern Pütz de m'avoir permis d'enseigner durant ces 4 années. Au-delà d'une expérience professionnelle, c'est une passion que j'ai développée pour l'enseignement et l'accompagnement des étudiants. J'espère avoir réussi à leur apprendre quelque chose et à éveiller leur intérêt pour la biochimie. De mon côté j'ai tout appris à leur contact.

Hubert, par où commencer ? Peut-être par ce cours de biochimie en L1 où je me suis dit pour la première fois « Un jour je bosserai pour ce type ». Et voilà quelques années plus tard que tu acceptais de me superviser pour mon stage de Master puis enfin pour ma thèse. Merci, merci, merci pour tout ce que tu m'as appris tant sur la Science que sur moi-même. Merci d'avoir cru en moi quand je voulais tout laisser tomber, merci de m'avoir remise sur le droit chemin quand je m'égarais tout en me laissant la liberté dont j'avais besoin. Merci pour les cafés, les discussions, le soutien. Merci aussi pour cette rédaction de thèse, moi qui avais si peur de me lancer, j'ai été portée par ta bienveillance et ton enthousiasme. Merci de faire de cette équipe une petite famille. On dit de moi que je suis une mini Becker quand il s'agit de poser des questions pendant les séminaires et pour moi c'est une sacrée consécration !

Merci aux autres membres du labo, Bruno pour l'astuce de la pointe de spatule, Fred pour m'avoir aidée à appréhender les TPs de cette année. Merci Lolo pour les 1000 milliards de mini-prep à 7h du mat, les dilutions à n'en plus finir, et pour toutes les choses que tu fais pour nous au quotidien. Merci à toi Nassira pour les discussions scientifiques et autres, le girl power, ta force, tes conseils, ta bienveillance. Merci d'avoir été là pour moi, de m'avoir écoutée et soutenue.

Guillaume, aka Guigui, merci pour tout, vraiment tout. Les discussions scientifiques et ton aide, ton oreille toujours attentive (à condition que tu ne fasses pas autre chose en même temps obviously), ton enthousiasme, les fou-rires, les confidences. Merci d'avoir été mon petit rayon de soleil pendant les jours parfois gris de la thèse. Tu sais déjà tout ce que

je pense de toi, tu iras loin j'en suis sûre, tout comme je suis sûre qu'on continuera à se voir (ou au moins à s'écrire/s'appeler) lorsque je quitterai le labo (alors arrête de t'inquiéter !).

Merci également aux stagiaires que j'ai encadrés pendant ma thèse (Brenner Quentin, Beltran-Valencia Dennisse, Winterhalter Lucie), vous avez été mes petites mains et tout ce travail a été possible grâce à vous. Merci tout particulièrement à toi Juliette (aka Rouliette) d'avoir décidé de venir faire ton stage de M2 avec moi tout en sachant que j'allais rédiger mon manuscrit (quel enfer). Ton travail a été d'une aide inestimable et je suis très fière de toi (oui je l'ai dit !). Continue de poser des questions, d'être curieuse, d'avoir cette joie de vivre et de vouloir aller au fond des choses (to go further u know). De nouvelles aventures suisses t'attendent et j'espère que tu t'épanouiras dans ton travail de thèse (donne des nouvelles quand même de temps en temps !).

Merci aux anciens du labo : Gaëtan de m'avoir encadrée durant mon master et de m'avoir légué ton système Split, Sylvain pour les multiples conseils et l'entraide dans la galère, Natou pour ta folie mais aussi ton esprit scientifique aiguisé, partager ce petit bureau de 3 m^2 avec toi aura été une expérience que je n'oublierai pas ! Ludo pour les nombreux conseils scientifiques, les discussions, les soirées sur le toit de Bota et les découvertes musicales.

Merci également à Sylvie Friant et Bruno Rinaldi pour tous les petits et grands conseils, les protocoles, pour les bons moments autour d'un mojito ou d'un pot de miel.

Merci à ma famille pour leur soutien, à mes parents de toujours croire en moi et de toujours être là pour moi, à ma petite sœur de toujours trouver un mot pour me remonter le moral, à mon grand frère pour m'avoir initiée à la science dès mon plus jeune âge et de m'avoir montré que faire une thèse n'était pas (si) insurmontable. Merci également à mes amis qui ne m'ont quasiment pas vue depuis des mois, merci d'avoir compris et de toujours vous assurer que je n'ai besoin de rien.

Last but not least, merci à toi Glen, d'être toujours là, de relativiser pour deux, d'être venu à ma rescousse pendant la rédaction quand j'ai eu besoin de toi, de m'apprendre à prendre le temps. Merci de m'avoir écoutée parler des heures sur ma thèse/le labo/les manips. Merci d'être toujours une épaule sur laquelle je peux m'appuyer. Merci pour ta patience, merci pour tes encouragements, merci pour ta bienveillance. Merci d'être là.

Je ne sais pas de quoi sera fait cet après-thèse mais je sais que grâce à toutes les personnes que j'ai citées, je suis prête à l'affronter !

Table of contents

Bibliography   285

List of Figures

General introduction

Chapter I : Mitochondrial localization of proteins

Chapter II : Vacuolar localization of proteins

List of Tables

List of abbreviations

°C: degree Celsius

aa-AMP: aminoacyl-adenylate

aa-tRNA: aminoacyl-tRNA

aa: amino acid

aaRS: aminoacyl-tRNA synthetase

AdT: amidotransferase

AIMP: aaRS interacting protein

AMP: adenosine monophosphate

ATP: adenosine triphosphate

BCAA: branched-chain aa

BSA: Bovin Serum Albumin

$_c$aaRS: cytosolic aaRS

CL: cardiolipin

Da: Dalton

DNA: desoxyribonucleic acid

EMAP: endothelial monocyte-activating polypeptide

EMC: ER membrane protein complex

ER: endoplasmic reticulum

ERMES: ER-mitochondria encounter structure

Fe/S: iron-sulfur

FOA: fluoroorotic acid

FP: Fluorescent Protein

g, l, h, min, s: gram, liter, hour, minute, second

_g_: gravitational force

GAAC: General Amino Acid Control

GAP: GTPase Activating protein

GDP: guanosine diphosphate

GEF: guanine exchange factor

GFP: Green Fluorescent Protein

GST: glutathione S-transferase

GTP: guanosine triphosphate

H$^+$: proton

HOPS: homotypic fusion and vacuole protein sorting

IMM: inner mitochondrial membrane

IMP: intramembrane particle

IMS: intermembrane space

iMTS-L: internal MTS-like

kb: kilobases

LD: lipid droplet

LUCA: Last Universal Common Ancestor

M: molar

MARS: multi-aminoacyl-tRNA synthetase

MCS: membrane contact site

MCU: mitochondrial Ca^{2+} uniporter

MPP: mitochondrial processing peptidase

mRNA: messenger RNA

MSC: multisynthetasic complex

$_{mt}$aaRS: mitochondrial aaRS

mtDNA: mitochondrial DNA

mte: mitochondrial echoform

MTS: matrix targeting sequence

MVB: multivesicular bodies

NAC: nascent polypeptide-associated complex

NCR: Nitrogen Catabolic Repression

ND: non-discriminating

nER: nuclear ER

NLS: Nuclear Localization Signal

nt: nucleotide

NVJ: nucleus-vacuole junction

OD: Optical Density

OMM: outer mitochondrial membrane

OXPHOS: oxidative phosphorylation

P13, P100: pellet at 13,000 $\times$ g and 100,000 $\times$ g

PA: phosphatic acid

PAGE: PolyAcrylamide Gel Electrophoresis

PAS: phagophore assembly site

PC: phosphatidylcholine

PCR: Polymerase Chain Reaction

PE: phosphatidylethanolamine

PG: phosphatidylglycerol

pH: potential of hydrogen

PL: phospholipid

pre-tRNA: precursor tRNA

PS: phosphatidylserine

PtdIns: phosphatidylinositol

RNA: ribonucleic acid

ROS: reactive oxygen species

rpm: rotation per minute

RT: room temperature

RTD: Rapid tRNA Decay

S13, S100: soluble fraction at 13,000 $\times$ g and 100,000 $\times$ g

SAM: S-adenosylmethionine

SDS: sodium dodecyl sulfate

SPS: Ssy1-Ptr3-Ssy5

TBS: Tris Buffer Saline

TCA: trichloroacetic acid

TMD: transmembrane domain

TOM: translocase of the outer membrane

TRBD: tRNA Binding Domain

tRFS: tRNA-derived fragments

tRNA: transfer RNA

UTR: untranslated region

V: volt

vace: vacuolar echoform

vCLAMP: vacuole and mitochondria patch

VDAC: voltage-dependent anion channel

WT: wild-type

µ-, n-, m-: micro-, nano-, milli-

Amino acids			Aminoacyl-tRNA synthetases		
Name	3 letters code	1 letter code	Standard name	Short names	
Alanine	Ala	A	Alanyl-tRNA synthetase	AlaRS	ARS
Cysteine	Cys	C	Cysteinyl-tRNA synthetase	CysRS	CRS
Aspartate	Asp	D	Aspartyl-tRNA synthetase	AspRS	DRS
Glutamate	Glu	E	Glutamyl-tRNA synthetase	GluRS	ERS
Phenylalanine	Phe	F	Phenylalanyl-tRNA synthetase	PheRS	FRS
Glycine	Gly	G	Glycyl-tRNA synthetase	GlyRS	GRS
Histidine	His	H	Histidyl-tRNA synthetase	HisRS	HRS
Isoleucine	Ile	I	Isoleucyl-tRNA synthetase	IleRS	IRS
Lysine	Lys	K	Lysyl-tRNA synthetase	LysRS	KRS
Leucine	Leu	L	Leucyl-tRNA synthetase	LeuRS	LRS
Methionine	Met	M	Methionyl-tRNA synthetase	MetRS	MRS
Asparagine	Asn	N	Asparaginyl-tRNA synthetase	AsnRS	NRS
Proline	Pro	P	Prolyl-tRNA synthetase	ProRS	PRS
Glutamine	Gln	Q	Glutaminyl-tRNA synthetase	GlnRS	QRS
Arginine	Arg	R	Arginyl-tRNA synthetase	ArgRS	RRS
Serine	Ser	S	Seryl-tRNA synthetase	SerRS	SRS
Threonine	Thr	T	Threonyl-tRNA synthetase	ThrRS	TRS
Valine	Val	V	Valyl-tRNA synthetase	ValRS	VRS
Tryptophan	Trp	W	Tryptophanyl-tRNA synthetase	TrpRS	WRS
Tyrosine	Tyr	Y	Tyrosyl-tRNA synthetase	TyrRS	YRS

PREAMBLE

During my 4 years of PhD in the team Dynamic and Plasticity of Synthetases (DyPS), I have been working on the yeast *Saccharomyces cerevisiae*, a unicellular eukaryotic organism that has been extensively used as model organism. *Saccharomyces cerevisiae*'s genome was the first eukaryotic genome entirely sequenced (Goffeau *et al.*, 1996). A few years later, yeast strain libraries of deleted, overexpressed and reporter-tagged genes were created with the aim of characterizing the essentiality and localization of every single gene product (Giaever *et al.*, 2002; Huh *et al.*, 2003; Sopko *et al.*, 2006). Over the years, the yeast became a model organism to assess many biological processes ranging from mitochondrial biology, membrane trafficking, phenotype-genotype interactions, aging, human diseases or autophagy and has proven its robustness. Even now, the yeast *Saccharomyces cerevisiae* remains the favorite organism of many biologists not only because of its powerful genetics but also because of the cheapness and easiness of its handling that allows screening and phenotyping of populations of individuals at the whole genome scale (Peter and Schacherer, 2016).

Like all eukaryotic cells, yeast cells possess subcellular compartments and organelles, which are defined by specific composition and roles. This subcellular compartmentalization allows partitioning of biochemical pathways. However, such organization necessitates fine-tuned communication and coordination between the different compartments. This can be achieved by the multiple contacts between organelles formed in the cell and by vesicles that are transported from one compartment to another, both of them supporting the transfer of molecules and the transduction of signals. The mitochondria stand out as an exception compared to all the organelles, since they are considered as semi-autonomous and are not part of the endomembrane system. Nevertheless, all organelles rely on nuclear-encoded proteins for their correct functioning. These proteins, which are translated in the cytosol have thus to be targeted to their final destination. Many efforts have been made to determine the composition of the mitochondrial proteome, also called mitoproteome. Over 1000 mitochondrial proteins have been identified so far and a third of these proteins have been shown to be located in more than one subcellular compartment, a phenomenon called dual-localization (Ben-Menachem *et al.*, 2011). Yogev and Pines proposed to name "echoforms" these molecules of a single protein that can have different subcellular localizations. These echoforms are identical or nearly identical proteins but can have completely different

functions depending on their localization (Yogev and Pines, 2011).

In the DyPS research team we are particularly interested in a family of proteins called the aminoacyl-tRNA synthetases (aaRSs). These essential and ubiquitous enzymes have been extensively studied regarding their tRNA aminoacylation activity that occurs in the cytosol. However, many studies demonstrated that aaRSs can relocate to different subcellular compartments, where they either perform their "canonical" role of tRNA aminoacylation or participate to diverse processes beyond translation (Debard *et al.,* 2017; Yakobov *et al.,* 2018). These relocating aaRSs can thus be considered as echoforms, since the two identical or nearly identical proteins can have two or more different localizations. During my PhD, I took interest in the mitochondrial and vacuolar localization of cytosolic aaRSs ($_c$aaRSs), which had already been described for some $_c$aaRSs (Bonfils *et al.,* 2012; Frechin *et al.,* 2009). However, the characterization of vacuolar and mitochondrial aaRSs' echoforms ($_{vace}$aaRS and $_{mte}$aaRS respectively) is challenging. Moreover, we particularly adhere to the idea conveyed by the adage "seeing is believing", but the epifluorescence microscopy technics available at that time were not suited to discriminate the cytosolic pool of aaRSs from the discrete organellar echoform.

The aim of my PhD work was thus to create and develop microscopy tools, that would allow an unbiased and precise identification of $_{mte}$- and $_{vace}$-aaRSs in the yeast *Saccharomyces cerevisiae*. I also aimed to characterize the mode of targeting or anchoring that the proteins use to localize to these particular compartments and to investigate the possible functions of $_{vace}$aaRS and particularly of the multi-aminoacyl-tRNA synthetase complex AME from the yeast and its individual components when localized at the vacuolar surface.

To present this work, I mainly focus on eukaryotes and particularly on the yeast *Saccharomyces cerevisiae*. I decided to first introduce the actors of the eukaryotic translation process, together with their "canonical" and "non-canonical" role and/or localization in a **general introduction**. In order to make it easier to follow and to categorize the information and my results, my research work will be presented into **two chapters**; the **chapter I** about the mitochondrial localization of proteins and the **chapter II** about the vacuolar localization of proteins. Each chapter contains, an introduction that provides the necessary information regarding the organelle of interest, a section in which I introduce the context of my work and finally a section containing the articles and results of my research together with a discussion and the perspectives. After the two chapter, the **material and methods** used for

this research are described. Then I present the two scientific reviews I had the opportunity to co-author during my PhD as well as the poster I presented at the 27th International tRNA Conference. Finally, all the articles used for this manuscript are sorted by alphabetical order in the **bibliography**.

GENERAL

INTRODUCTION

A

3' OH
A 76
C
C
5' P — Discriminator N₇₃
1   72

Acceptor Stem

U 8

D-arm

17a
17b
18 G
19 G
20a 20b

15
R A 14
11
Y
R 24
A 21

TΨC-arm
61
Y A 58
C
G R
53 T Ψ C

48
Y
44
45 46

Variable loop

Anticodon arm
32 Y
33 U   R 37
34 35 36
wobble base

A Adenosine
U Uridine
G Guanosine
C Cytidine
T Thymidine
R Purine (A or G)
Y Pyrimidine (U or C)
Ψ pseudouridine

◯ additional nucleotides
● conserved nucleotides
◯ non-conserved nucleotides
◯ anticodon triplet

── Watson-Crick interaction
╌╌ non-Watson-Crick interaction

B

3'OH — A C C
5'P —

Y A
C
G R
T Ψ C

Y

G G

U

R   A
A

Y R

Y
U   R
34 35 36

C

3'   5'

Y   U
R
36 35 34

5' ········ 1 2 3 ········ 3' mRNA

anticodon	codon
position 34	position 3
C	G
A	U
G	C, U
U	A, G
I	C, A, U

Figure I-1: tRNA structures (inspired from Enkler, 2014 [1] and Debard, 2019 [2]) and codon-anticodon pairing.
A. Schematic representation of the cloverleaf secondary structure and consensus sequence of tRNAs. **B.** Representation of the same tRNA in the L-shape folding. **C.** Interaction of the codon on the mRNA with the tRNA anticodon. The interaction between the first (5') position of the anticodon (position 3) and the third position of the anticodon (position 34) involves wobble pairing (indicated in orange in the table). A: adenosine, U: uridine, G: guanosine, C: cytidine, I: inosine.

I. tRNA aminoacylation: a key step in eukaryotic protein synthesis

I.1. transfer RNA (tRNA)

In 1955, Crick proposed the "adaptor hypothesis" that suggested that the link between nucleic acid and protein sequence was performed by a dedicated class of molecules (Crick et al., 1961). In 1958 Hoagland and coworkers discovered a soluble RNA, later named transfer RNA (tRNA), that can covalently bind amino acid (aa) in the presence of ATP and an enzyme preparation able to activate the aa. They hypothesized that aa-bound soluble RNA would be the link between amino acid activation and protein translation (Hoagland et al., 1958). A few years later, the tRNA^{Ala} from yeast was sequenced and its cloverleaf-like secondary structure was determined. The subsequent sequencing data obtained for tRNA^{Tyr}, tRNA^{Phe} and tRNA^{Ser} confirmed the four-arm organization of tRNA (**Figure I-1A**). These sequencing data also led to the concept that the central base triplet of the stem-loop located in the middle of tRNA was the so-called anticodon complementary to the messenger RNA (mRNA) codon. This confirmed that tRNA was the aa carrier thus confirming the hypothesis that aa-tRNA were the adaptor molecules between mRNA and proteins (Fernández-Millán et al., 2016).

I.1.1. tRNA structure

To ensure their recognition by the ribosome and elongation factors, all tRNA should have a common scaffold. However, they should also have specific identity to allow discrimination by their cognate aaRS. The first crystal structure of yeast tRNA^{Phe} and tRNA^{Asp} obtained in the mid-seventies demonstrated that the tRNA molecules adopt a 3D L-shape (**Figure I-1B**). To form the two arms of the L-shape, the helical domains of the cloverleaf get stacked pairwise; the acceptor helix interacts with the T helix, while the D helix interacts with the anticodon helix. A network of tertiary interactions then holds the structure together (Fernández-Millán et al., 2016).

Some exceptions to this conserved shape can be found in animal mitochondria with tRNAs displaying a reduced size due to shorter loops in D or T arms, and in some cases, to complete absence of one or two arms. The most extreme case reported of a functional shortened tRNA is the 42 nucleotide (nt)-long mitochondrial tRNA^{Arg} of the worm *Romanomermis culicivorax* (Wende et al., 2013).

I.1.2. tRNA biogenesis and post-transcriptional modifications

In eukaryotes, transcription of tRNA genes is performed by the RNA Polymerase III (RNA Pol III) in the nucleus and is controlled, in response to nutrient availability and other environmental circumstances, by Maf1. In growth-limiting conditions Maf1 is dephosphorylated and imported in the nucleus to bind to RNA polymerase III and prevent tRNA transcription (Wichtowska *et al.,* 2013). Once transcribed, precursor tRNAs (pre-tRNAs) undergo several maturation steps. First the pre-tRNAs 5'-leader is cleaved by RNase P endonuclease, in the nucleus. Then the 3'-trailer is trimmed by RNase Z. The last step of tRNA maturation is the addition of CCA at the 3' end of the acceptor arm by CCA-adding enzymes (CCases). In eukaryotes all these steps are performed in the nucleus (Fernández-Millán *et al.,* 2016). The end-processed tRNAs are then exported to the cytoplasm. Throughout the tRNA processing, tRNAs are modified by enzymes that belong to two different groups. Group I enzymes either bind nucleotide in the anticodon loop or residues embedded inside the tRNA structure, while group II enzymes recognize the 3D structure of tRNA. Post-transcriptional modifications of the anticodon loop will have a major impact on the accuracy and efficacy of mRNA decoding, while modifications of the tRNA body will contribute to their folding and stability. In yeast, ten tRNA families are encoded by intron-containing genes that need to be processed. The end-processed intron-containing tRNAs are exported to the cytoplasm and introns are removed by the Sen machinery that is bound to the mitochondrial outer membrane. The cytoplasmic Trl1 ligase then ligates the tRNA half-molecules and the 2'-phosphotransferase Tpt1 catalyzes the transfer of 2'-phosphate from the splice junction to NAD^+ (Wichtowska *et al.,* 2013).

To test their maturity and integrity prior to export to the cytoplasm, tRNA can be aminoacylated inside the nucleus (Steiner-Mosonyi and Mangroo, 2004). However, other routes for tRNA export from the nucleus exist, since the aminoacylation is not absolutely necessary for the export in *S. cerevisiae* and *X. laevis*. The evidences that tRNAs undergo numerous post-transcriptional modifications arose with the initial sequencing of tRNA[Ala] that revealed the presence methylated bases, dihydrouridine, ribo-thymidine, pseudouridine... To date, more than a hundred modified nts have been identified. Among the tRNA modifications, the adenosine 34 of the tRNA, which is the first position of the anticodon, can be deaminated by Tad2 and Tad3 to form inosine. Following Crick's wobble pairing hypothesis, the presence of inosine at this position in the tRNA would extend its decoding capacity since inosine can

base pair with A, C or U (Gerber and Keller, 1999) (**Figure I-1C**). The presence of specific modifications at positions 34 and 37 that increases the repertoire of base-pairing of the anticodon loop explains why the number of tRNA species in a cell is always lower than the 61 codons. Modified nucleosides can also constitute recognition signals for cognate aaRSs and increase tRNA scaffold stability (Fernández-Millán et al., 2016).

I.1.3. tRNA turnover

In the yeast *Saccharomyces cerevisiae*, mis-processed pre-tRNAs or hypomodified (pre-) tRNAs lacking modifications are degraded by two different tRNA surveillance pathways. The newly synthesized pre-tRNAs can be polyadenylated on their 3' end by the TRAMP complex and targeted for exosome degradation. During the early steps of maturation, defective intermediates can be polyadenylated and subsequently degraded by the exosome or a CCACCA sequence can be added and the product is either degraded by the exosome or the Rapid tRNA Decay (RTD). Unstable mature tRNAs that contain mutations or that are hypomodified can be degrade by the RTD pathway (Wichtowska et al., 2013).

I.1.4. tRNA non-canonical roles

Besides their function as adaptor molecules for translation of mRNAs, tRNA have many other roles that are not always related to protein synthesis. Indeed, retroviruses can hijack host tRNAs, which serve as primers for the viral genome reverse transcription. In bacteria, the 5'-UTR-located T-box riboswitches upon binding to uncharged tRNAs adopt an anti-terminator structure that allows transcription of the downstream genes. However, charged tRNAs cannot bind T-Boxes making these riboswitches potent aa-sensors that monitor the aminoacylation state of tRNAs. They usually control the expression of genes involved in a number of functions related to aminoacylation and the metabolism of amino acids (Fernández-Millán et al., 2016).

tRNAs can be cleaved at different specific positions probably by different endonuclease activities and the tRNA cleavage products are called tRNA-derived fragments (tRFs). The tRFs are evolutionary widespread and constitute a recent and increasingly important class of small regulatory RNAs with biologically-significant functions (Fernández-Millán et al., 2016). In the yeast, tRNAs can be cleaved by the endonuclease Rny1 in their anticodon loop, producing tRNA half-molecules in certain stress conditions such as oxidative stress, stationary phase, heat, and methionine or nitrogen starvation. This cleavage seems to be a general response
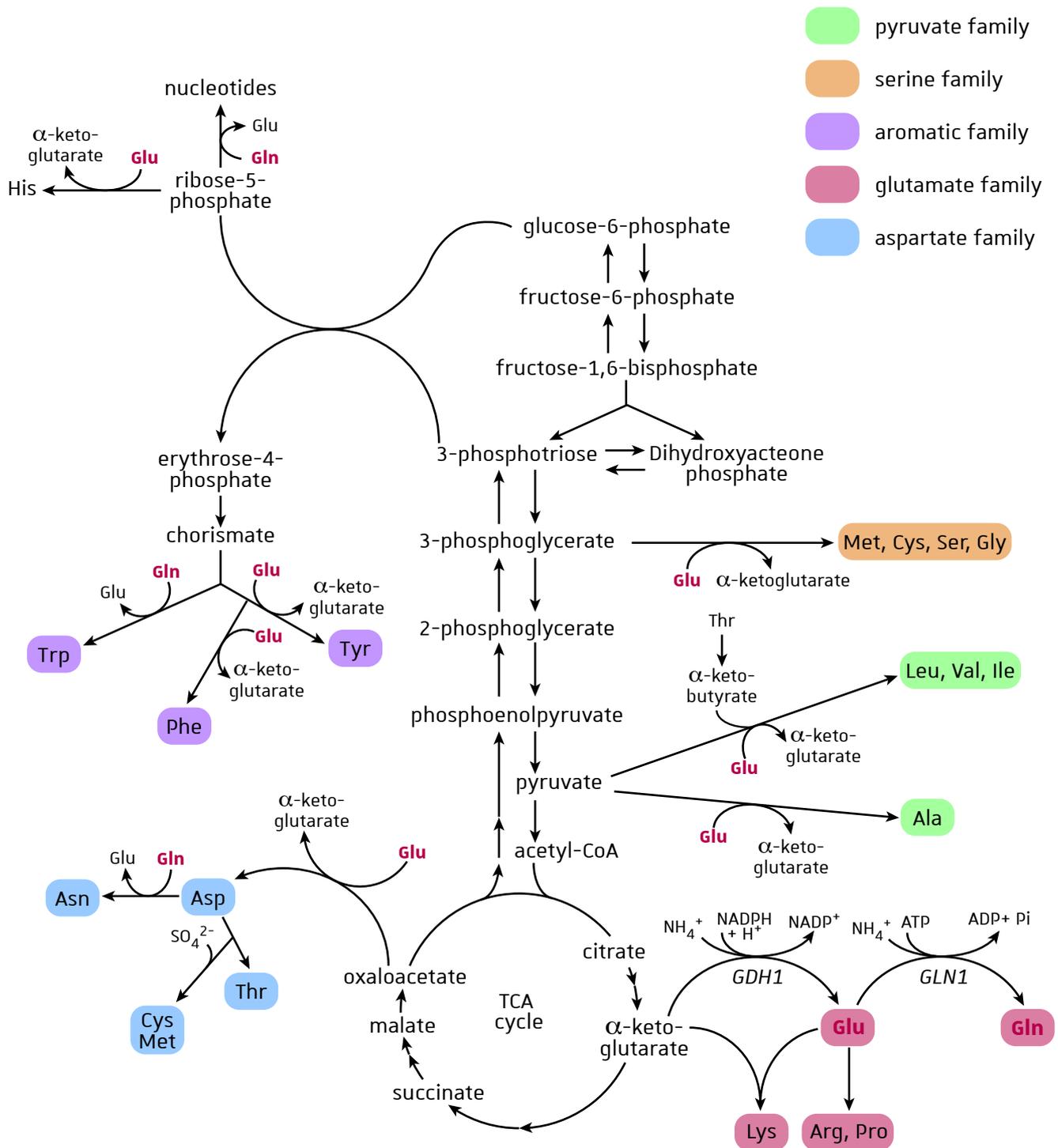
Figure I-2: Amino acids biosynthesis from glucose and ammonia (inspired from [3]). The amino acids can be grouped into families (see background colors) according to their origin or chemical properties. The ammonia is used by the NADPH-dependent glutamate dehydrogenase (*GDH1*) to produce glutamate (Glu) from α-ketoglutarate and by the glutamine synthase (*GLN1*) to produce glutamine (Gln) from Glu. Glu and Gln (in red) nitrogen is then used by the transamination reactions to produce the different amino acids.

and does not lead to a decrease of mature tRNA levels (Wichtowska *et al.*, 2013).

I.2. The proteinogenic amino acids

The proteinogenic amino acids are essential molecules that are the building blocks for protein synthesis and have a central role in general metabolism. The particularity of yeast cells compared to mammalian cells, is their ability to produce aa *de novo*, making them aa prototrophs. Yeast cells can thus grow on minimum media containing glucose and ammonium as sole source of nitrogen.

I.2.1. Biosynthesis

The aa carbon skeletons (α-keto acids) derive from the glucose catabolic pathway and the α-amino group derives from Glu and Gln that are used for the transamination reactions required in the synthesis of each aa. Glu and Gln can be produced from two anabolic reactions that assimilate ammonia; the synthesis of Glu from α-ketoglutarate by the NADPH-dependent glutamate dehydrogenase (*GDH1*) and the synthesis of Gln from Glu by the glutamine synthetase (*GLN1*). When Gln is the sole nitrogen source, Glu is synthesized from α-ketoglutarate by the catabolic reaction catalyzed by the NADH-dependent glutamate synthase (*GLT1*). On the other hand, when Glu is the sole nitrogen source, the catabolic reaction performed by NAD^+-linked glutamate dehydrogenase (*GDH2*) provides NH_4^+ that can then be used for the production of Gln. The aa that derive from a common molecule are grouped into families. The glutamate family includes Glu, Gln, Lys, Arg and Pro, the aromatic family: Phe, Trp and Tyr, the aspartate family: Asn, Asp, Thr, Cys and Met, the serine family: Met, Cys, Ser and Gly and the pyruvate family: Leu, Val, Ile and Ala. The biosynthetic pathway of His is connected to that of nucleotides (**Figure I-2**) (Ljungdahl and Daignan-Fornier, 2012).

I.2.2. Utilization

Amino acids are used for protein synthesis but can also be used as nitrogen source, with the exception of Lys, His and Cys (**Figure I-3**). The extracellular content in nitrogen sources controls the uptake of these compounds and the regulation of catabolic and anabolic processes. Even if almost all aa can be used as nitrogen source, they do not support cell growth with the same efficiency. For example, in presence of glucose as carbon source, the yeast generation time varies from approximately 2 h in presence of Asn, Gln or Arg, up to more than 4 h in presence of Met and Trp. The aa are classified as preferred and nonpreferred
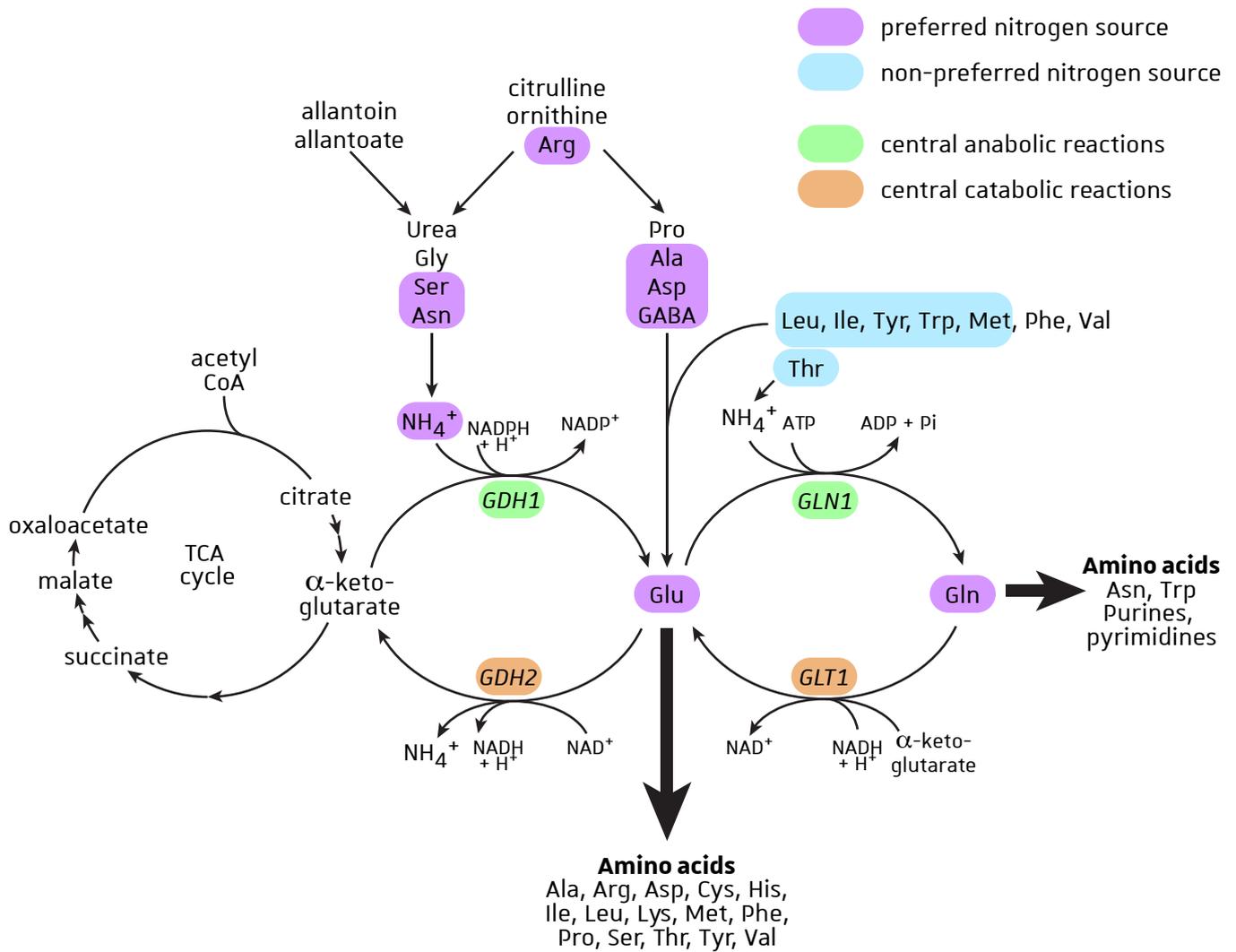
Figure I-3: Utilization of amino acids as nitrogen source (inspired from [3]). Preferred and non-preferred nitrogen sources can be used to produce glutamate.

nitrogen sources depending on *(i)* how they individually support cell growth when present as the sole nitrogen source and *(ii)* how they trigger Nitrogen Catabolic Repression (NCR) supra-pathway response to ensure preferred nitrogen sources utilization, when available. Once internalized, nitrogenous compounds can be *(i)* used directly in biosynthetic processes, *(ii)* deaminated to generate ammonium (NH_4^+) or *(iii)* used as substrates by transaminases that transfer amino groups to α-ketoglutarate to form Glu (Ljungdahl and Daignan-Fornier, 2012) (**Figure I-3**).

I.2.3. Sensing, uptake and storage

The catabolic nitrogen source utilization and anabolic aa biosynthetic pathways function in parallel and must be coordinated (**Figure I-3**). Thus, the nutrient extracellular and intracellular concentrations need to be monitored and this is performed by plasma membrane sensors, a network of intracellular sensing systems and metabolic intermediates that act as signaling molecules. The presence of external aa induces the expression of several permeases displaying broad specificities making aa inducers of their own uptake (**Figure I-4A**). The major route for aa uptake for catabolic metabolism is composed of Gap1, a high-capacity general aa permease, and Put4, a proline-specific permease (Magasanik and Kaiser, 2002). Other permeases with relatively restricted specificities can uptake aa for the translation. The general aa control (GAAC), a supra-pathway regulation mode, activates a large set of genes in response to aa starvation (Hinnebusch, 2005; Hinnebusch and Natarajan, 2002) (**Figure I-4B**). A precise response can also trigger activation or repression of specific sets of genes through the activity of specialized transcription factors. For a rapid response to adjust the catalytic properties of enzymes, modulate the degradation rates of enzymes and uptake rates of permeases and regulate the flow of metabolites in and out of intracellular organelles, post-translational modes of regulation are also used. All these modes of regulation of aa uptake and biosynthesis are reviewed in Ljungdahl and Daignan-Fornier, 2012 and Zaman *et al.*, 2008.

In yeast cells, sensing systems localized at the plasma membrane, named SPS (Ssy1-Ptr3-Ssy5) sensor, can induce the expression of genes required for aa uptake in response to micromolar amounts of extracellular aa (reviewed in Ljungdahl, 2009) (**Figure I-4A**). The SPS-sensing pathway regulates the aa permease gene expression by controlling the activity of two transcription factors, Stp1 and Stp2 (Andréasson and Ljungdahl, 2002). In presence of nutrients in the extracellular environment, genes encoding a subset of broad-specificity
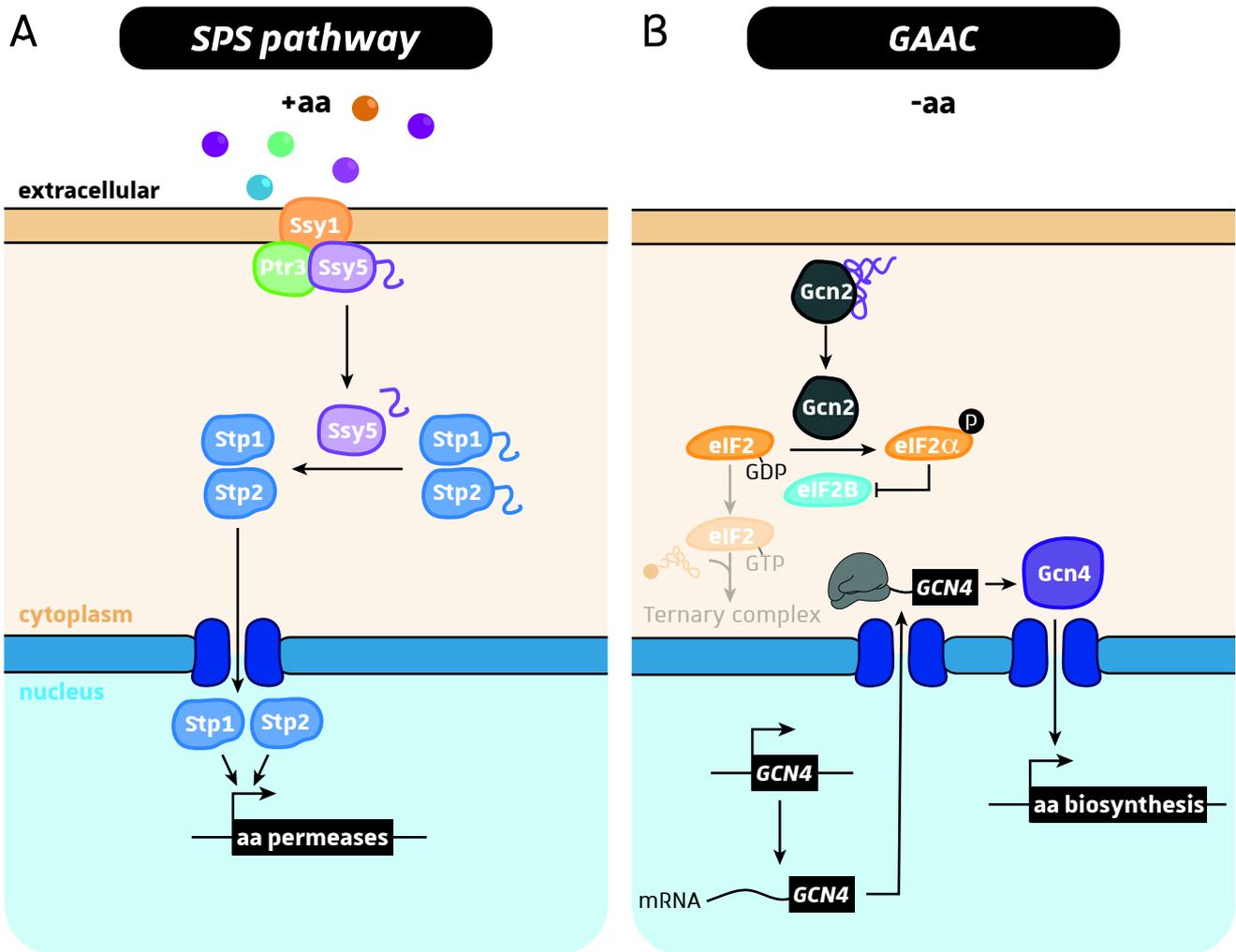
Figure I-4: Amino acid sensing. A. The SPS pathway senses the presence of micromolar amounts of extracellular amino acids (aa) and activates the transcription of amino acid permease genes to promote amino acid uptake. **B.** The general amino acid control (GAAC) monitors the intracellular concentration of amino acids through the Gcn2 kinase that binds uncharged tRNAs. In response to amino acid deprivation the general translation is inhibited while the specific translation of *GCN4* mRNA increases. Gcn4 then enters the nucleus to activate the transcription of genes involved in amino acid biosynthesis.

aa permeases are upregulated. The protein Ssy1 is an integral plasma membrane protein that interacts with extracellular aa and thus monitors the ratio of external and internal aa across the plasma membrane by undergoing conformational changes (Wu *et al.*, 2006). The signal initiated by binding of aa to Ssy1 is transduced to the peripherally-associated plasma membrane proteins Ssy5 and Ptr3, which in turn activates the Ssy5 protease activity. Ssy5 then catalyzes the endoproteolysis of the transcription factors Stp1 and Stp2 that accumulate in the nucleus to induce the expression of SPS sensor-regulated genes (Andréasson and Ljungdahl, 2002).

The intracellular aa concentration is monitored by the GAAC (**Figure I-4B**). The signal for the activation of the GAAC pathway is the presence of uncharged tRNAs that increase during aa starvation. These uncharged tRNAs are bound by and activate the Gcn2 kinase that will downregulate translation at the initiation step. In eukaryotes, the translation initiation factor eIF2 forms a ternary complex with charged $tRNA_i^{Met}$ and GTP. This ternary complex associates with the 40S ribosomal subunit to facilitate scanning of the 5' region of mRNAs to find the appropriate initiation codon. Upon phosphorylation of eIF2 by activated Gcn2 (when bound to uncharged tRNAs), the ternary complex formation is largely reduced leading to a decrease in the rate of general translation initiation. On the contrary, the reduction of ternary complex availability specifically stimulates translation of Gcn4 mRNA. Gcn4 is also controlled at the level of protein degradation. Indeed, during aa starvation, the level of Gcn4 phosphorylation is decreased, which increases its stability. Gcn4 finally enters the nucleus and activates the transcription of more than 500 genes mostly involved in aa biosynthesis (Hinnebusch, 2005; Hinnebusch and Natarajan, 2002; Natarajan *et al.*, 2001).

The transport of aa across the plasma membrane is facilitated *via* the H^+-symport energized by the plasma membrane H^+-ATPase Pma1 (Horák, 1997; Serrano *et al.*, 1986). Interestingly, individual substrates can be transported by several different systems. The redundancy of transport systems allows the extraction of nutrients from a great variety of environments (Regenberg *et al.*, 1999). The internalized aa can then be imported into the mitochondria to sustain mitochondrial translation or to the vacuole for storage (see **Chapter II section I.3**).

Table I-1: Classification and features of aaRS.

		Class I			Class II		
		aaRS	quaternary structure	editing activity	aaRS	quaternary structure	editing activity
Subclasses	A	MRS	α, α2	yes	SRS	α2	yes
		LRS	α	yes	PRS	α2	yes
		IRS	α	yes	TRS	α2	yes
		VRS	α	yes	GRS	α2	
					HRS	α2	
	B	CRS	α, α2		DRS	α2	
		QRS	α		NRS	α2	
		ERS	α		KRS	α2	yes
	C	YRS	α2		FRS	(αβ)2, α2	yes
		WRS	α2		GRS	(αβ)2	
					ARS	α2	yes
					SepRS	α4	
					PylRS	α2	
	D	**RRS**	α				
	E	**KRS**	α				
Catalytic domain organization	Structure	Rossman fold (5 parallel β-sheet connected with α-helices			7 stranded β-sheet flanked by α-helices		
	Motif sequence	HIGH and KMSKS			motif 1: +GΦXXΦXXPΦΦ motif 2: (F/Y/H)RX(E/D)...(X=4-12)...(R/H)XXXFXXX(D/E) motif 3: λXΦGΦGΦERΦΦΦΦΦ		
Mechanistic features	A76 hydroxyl group acceptor	2'OH			3'OH		
	tRNA acceptor stem binding	via minor groove of the helix (except for dimeric aaRS)			via major groove of the helix		
	aaRS-bound ATP conformation	straight conformation			bent conformation		
	tRNA 3' CCA	bent conformation			extended conformation		
	rate-limiting step	release of aa-tRNA product			formation of aa-tRNA on the enzyme		

aaRSs represented in bold require the presence of tRNA for amino acid activation. +: positively charged aa, single-letter code: invariant residues, X: any residue, λ: small aa, Φ: hydrophobic aa.

I.3. The aminoacyl-tRNA synthetase (aaRSs) family

I.3.1. The two aaRSs classes

The aminoacyl-tRNA synthetases (aaRSs) are very ancient proteins already present in the Last Universal Common Ancestor (LUCA). They are essential ubiquitous enzymes present in the three domains of life (Fournier *et al.*, 2011). The aaRSs do not show vertical inheritance from a common ancestor but are separated into two distinct evolutionary unrelated classes that exhibit functional evolutionary convergence; the class I and class II aaRSs. The two classes have different sequence motifs and thus different active site topologies (Perona and Hadd, 2012; Ribas de Pouplana and Schimmel, 2001) (**Table I-1**).

I.3.1.1. Class I

The class I aaRSs are characterized by a catalytic domain composed of a Rossmann nucleotide binding fold that binds the tRNA acceptor stem from the minor groove side and which displays the characteristic KMSKS and HIGH sequence signatures involved in binding of ATP in an extended conformation. In all class I aaRS, the Rossmann fold is split by an inserted domain, called the connective peptide 1 (CP1). In monomeric aaRS, the CP1 domain binds the 3'-end of the tRNA, while it is a dimerization interface for dimeric YRS and WRS. In IRS, VRS and LRS, this domain is greatly enlarged and is the catalytic site for the hydrolysis of misacylated tRNAs during post-transfer editing. The C-terminal region of class I aaRS, with the exception of LRS, is involved in tRNA anticodon binding and contributes to tRNA discrimination. Additional segments at the N- and C-termini and insertions within or after the Rossmann fold are also common features of class I aaRS. The class I aaRS are subdivided in five subclasses; subclass **IA** is composed of IRS, MRS, VRS, LRS, subclass **IB** of QRS, ERS, CRS, subclass **IC** of dimeric WRS and YRS, subclass ID of RRS and subclass IE of KRS-I (Perona and Hadd, 2012) (**Table I-1**).

I.3.1.2. Class II

The class II aaRSs are likely older than the class I aaRSs (Hartman and Smith, 2014). The class II is divided in three subclasses: subclass **IIA** is composed of GRS, HRS, PRS, TRS and SRS, subclass **IIB** of NRS, DRS and KRS-II, and subclass **IIC** of FRS, GRS, ARS, SepRS and PylRS. The GRS is present in distinct classes as two forms that do not directly share a common ancestor. The class II possess a catalytic domain with an anti-parallel β-fold and three motifs

A

Aminoacylation reaction

①   aaRS + aa + ATP $\xrightarrow{\text{Mg}^{2+}}$ aa~AMP•aaRS + PPi

②   aa~AMP•aaRS + tRNA^{aa} $\longrightarrow$ aa-tRNA^{aa} + aaRS
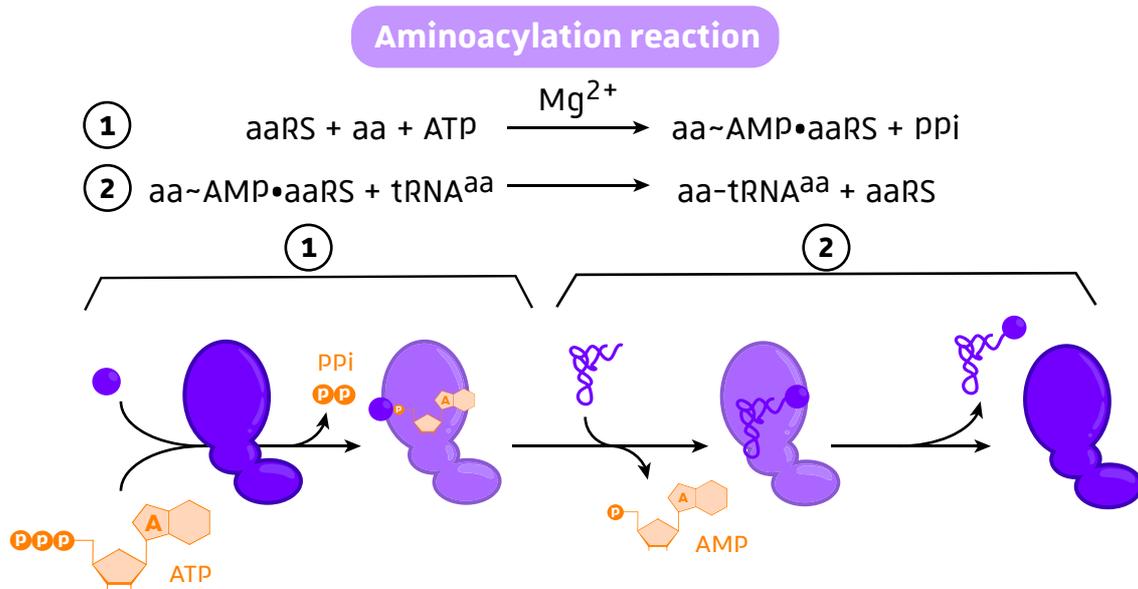
B
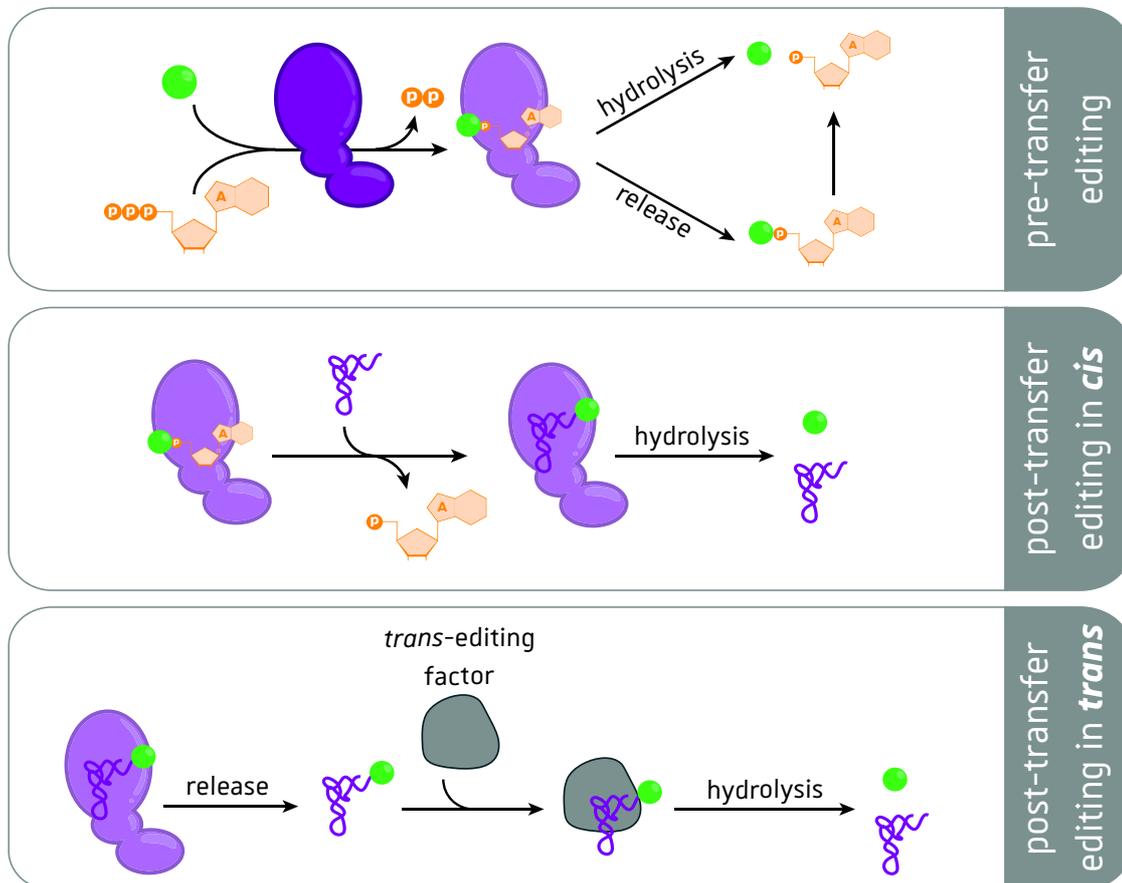
Figure I-5: tRNA aminoacylation and proofreading reactions. A. The tRNA aminoacylation is a two-steps reaction performed by aminoacyl-tRNA synthetases. 1) The amino acid is activated in the aaRS active site forming aminoacyl-AMP (aa-AMP), 2) the activated aminoacyl moiety is transferred to the 2'- or 3'-OH (class I and class II aaRS respectively) of the terminal adenine A76 of the tRNA forming an ester bond. **B.** The misaminoacylated tRNAs produced by some aaRSs can be edited by three different processes. The pre-transfer editing is performed in the aaRS active site while and post-transfer editing can be performed in *cis* by aaRS-attached editing domains or in *trans* by free-standing editing domains. ATP: adenosine triphosphate, PPi: inorganic pyrophosphate, AMP: adenosine monophosphate.

that are involved in dimerization (motif 1) and ATP and aa recognition (motifs 2 and 3). The three motifs have been characterized and they contain a strongly conserved core with an invariant residue; +GΦXXΦXXPΦΦ for motif 1, (F/Y/H)RX(E/D)...(X=4-12)...(R/H)XXXFXXX(D/E) for motif 2, and λXΦGΦGΦERΦΦΦΦ for motif 3 (+: positively charged aa, single-letter code: invariant residues, X: any residue, λ: small aa, Φ: hydrophobic aa) (Eriani *et al.*, 1990). The first and second class II motifs are separated by 40 to 80 residues, whereas the distance between motifs 2 and 3 is more variable (between 70 and 300 residues). The latter spacing region can thus be a place for insertion of additional modular domains. Most class II aaRSs form dimers, with the exception of subclass IIC that are monomers or form α_4 or $(\alpha\beta)_2$ tetramers. In the FRS $(\alpha\beta)_2$ tetramer the α-chain carries the catalytic fold and activity, while the essential catalytic residues are absent in the homologous β-chain. The tetrameric FRS thus only possess 2 active sites and binds two tRNAs that interact with all four enzyme subunits. For aa activation, class II aaRSs bind ATP in a bent conformation. Their interaction with tRNA occurs *via* the major groove side of the acceptor stem and the variable loop of tRNA faces the aaRSs (Ibba and Söll, 2000; Perona and Hadd, 2012) (**Table I-1**).

I.3.2. Canonical role of aaRSs: tRNA aminoacylation

The tRNA aminoacylation is a two-steps reaction that necessitates aa, aaRS, tRNA, ATP and Mg^{2+} (**Figure I-5A**). First, the aa activation occurs in the aaRS active site, where the α-carboxylate of aa nucleophilically attacks the α-phosphate of ATP to form aminoacyl-adenylate (aa~AMP) and an inorganic pyrophosphate. This process is tRNA-independent except for class I aaRS QRS, ERS, RRS and KRS I. During the second step of the reaction, the α-carbonyl of aa~AMP is nucleophilically attacked by the 2'- or 3'- hydroxyl of the terminal adenosine A76 of tRNAs that are substrate of class I and class II aaRSs respectively (Arnez and Moras, 1997).

The structure of QRS complexed with tRNA^Gln and ATP, which was the first structure of an aaRS-tRNA complex, gave many insights on the interaction between tRNA and aaRS. It demonstrated that binding of aaRSs to their substrates can induce sequence-dependent alternative conformations in tRNA and that tRNA binding occurs by sequence-specific interactions between aa and nucleotides. Moreover, particular protein domains were shown to be responsible for binding specific parts of the tRNA (Ibba and Söll, 2000). The specific aminoacylation of tRNA by their cognate aaRS is ensured by tRNA identity that relies on positive determinants and negative anti-determinants elements. For most tRNAs, the

identity elements are mostly located at the two distal extremities, the anti-codon loop and the aa accepting stem. These positive determinants are limited in number and can be isolated nucleotides of modified nucleotides in single-stranded regions, base pairs in helices or structural motifs. On the other hand, anti-determinants prevent tRNA recognition by non-cognate aaRS and thus tRNA misaminoacylation (Giegé *et al.*, 1998).

Despite the high selectively of aaRS for tRNAs, some aaRS can produce misacylated tRNAs. Some aaRSs are less selective than others toward aa and can generate incorrect aa-AMP during the first step of the aminoacylation reaction. These incorrect activated aa can then be transferred onto tRNA, thus generating mischarged tRNAs. To prevent the incorporation of the incorrect aa in the nascent polypeptide by the ribosome, aaRSs can either perform pre-transfer or post-transfer editing (**Figure I-5B**). Pre-transfer editing consists in the hydrolysis of the incorrect aa~AMP and is performed by the active site of the aaRS. On the other hand, post-transfer editing consists in the deacylation of the misacylated tRNA by an editing domain usually located next to the active site. Both Class I and Class II aaRSs have been shown to edit misacylated tRNAs. Class I editing domain is composed of the so called Connective Peptide 1 (CP1) editing domain, while class II aaRSs do not possess this type of domain and as such editing domains of Class I and Class II are structurally unrelated (Jakubowski, 2012). For example, the PRS contains a post-transfer editing domain inserted between motifs 2 and 3. TRS also performs post-transfer editing of misacylated Ser-tRNA^{Thr} but the editing domain is localized in N-terminus. SRS and KRS have pre-transfer editing activities that trigger the hydrolysis of misactivated aminoacyl-adenylates prior to transfer onto the tRNA (Perona and Hadd, 2012). The editing of misacylated tRNAs can also be performed in *trans*, by *trans*-editing factors that are homologous to the editing domains encoded in some aaRSs (**Figure I-5B**). The ubiquitous AlaXps *trans*-editing factors are homologous to ARS editing domain and deacylated Gly- and Ser-tRNA^{Ala}. The AlaXps are categorized in three types; AlaX-S, -M and -L, with AlaX-S being prevalent in archaea and AlaX-M and -L predominantly present in bacteria and eukaryotes. *Saccharomyces cerevisiae* contains a AlaX-L that binds aa-tRNA^{aa} but lacks editing activity. Another type of *trans*-editing factor found in archaea, eukaryotes and most bacteria are the D-aminoacyl-tRNA deacylases (DTDs). They can edit various D-aa-tRNAs in addition to selectively editing Gly-tRNA^{Ala}. In prokaryotes, Ybak prevents Cys misincorporation after tRNA^{Pro} mischarging by PRS. Other examples of trans-editing factors are listed in Kuzmishin Nagy *et al.*, 2020.

I.3.3. Indirect biosynthesis of aa-tRNAs

From the 20 standard aa encoded by the genetic code, three amino acids, Asn, Gln and Cys, can solely or additionally be charged onto their cognate tRNA by a non-canonical or indirect pathway that relies on tRNA-dependent conversion of a precursor mischarged aa-tRNA (Hemmerle *et al.*, 2020; Sheppard *et al.*, 2008). When NRS and/or QRS is/are missing an indirect route called transamidation pathway can be used to produce Asn-tRNA^{Asn} or Gln-tRNA^{Gln} through a two-step reaction. This pathway necessitates non-discriminating (ND)-DRS or ND-ERS that will aminoacylate tRNA^{Asn} and tRNA^{Gln} with Asp or Glu respectively. The misacylated tRNAs are then handled by tRNA-dependent amidotransferases (AdT). To date four types of AdT have been identified; the heterotrimeric GatCAB and GatFAB, and the heterodimeric GatDE and GatAB. In the vast majority of prokaryotes, the two-steps transamidation pathway is used to produce Gln-tRNA^{Gln}. The first step consists in the aminoacylation of tRNA^{Gln} with Glu by ND-ERS (Lapointe *et al.*, 1986). Then, the Glu moiety is transamidated into Gln by the tRNA-dependent heterotrimeric GatCAB AdT (Curnow *et al.*, 1997). In bacteria, the GatCAB AdT is usually a bi-specific Glu/Asp-AdT that can produce Gln-tRNA^{Gln} and Asn-tRNA^{Asn}, while it is a specific Asp-AdT in archaea. In order to produce Gln-tRNA^{Gln}, archaea possess an archaea-specific GatDE Glu-AdT (Tumbula *et al.*, 2000). All eukaryotes are deprived of the gene encoding the mitochondrial $_m$QRS but they possess a GatCAB-type AdT, that is a Glu-AdT producing mitochondrial Gln-tRNA^{Gln} (Gln-$_m$tRNA^{Gln}). In organelles, the mitochondrial $_m$ERS is usually the ND-ERS that participates in the organellar transamidation pathway, whereas plants have a mitochondrial and chloroplastic dual-targeted ND-ERS that participates in the transamidation pathways of both organelles. In the yeast *Saccharomyces cerevisiae*, the AdT is a GatFAB trimer that possesses the fungi-specific GatF subunit (**Figure I-6**). The real difference between the yeast mitochondrial transamidation and those of all other eukaryotes is that the $_m$ERS cannot aminoacylate $_m$tRNA^{Gln} and therefore is not the ND-ERS providing Glu-$_m$tRNA^{Gln} to the GatFAB Adt. Frechin and coworkers demonstrated that a fraction of $_c$ERS can be imported in the mitochondria and acts as the ND-ERS to produce Glu-$_m$tRNA^{Gln} (Frechin *et al.*, 2009) (**Figure I-6**).

In addition to the 20 standard genetically-encoded aa, two non-standard aa can be incorporated into proteins: selenocysteine (Sec) considered as the 21st genetically encoded aa and which is found in mammals, bacteria and archaea, and pyrrolysine (Pyl) the 22nd genetically-encoded aa found in methanogenic archaea and some bacteria. The formation of
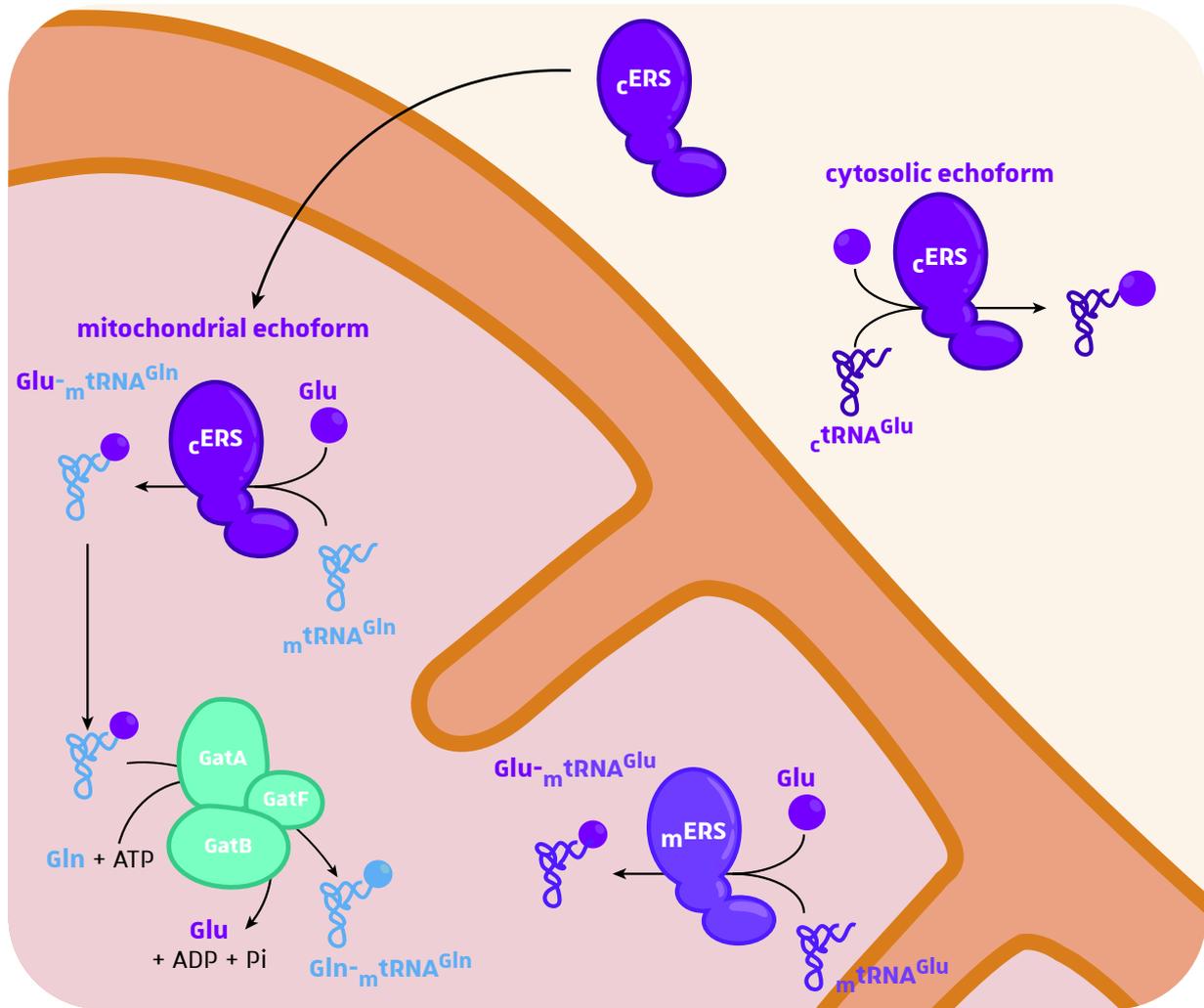
Figure I-6: Transamidation pathway used to produce Gln-tRNA^{Gln} in the yeast mitochondria. Mitochondria do not possess a $_{mt}$GlnRS. The production of mitochondrial Gln-tRNA^{Gln} thus relies on the mischarging of mitochondrial tRNA^{Gln} with Glu by the pool of cytosolic $_c$GluRS imported into michondria (mitochondrial echoform). The Glu-tRNA^{Gln} is then converted into Gln-tRNA^{Gln} by the mitochondrial GatFAB amidotransferase.

Sec-tRNA^{Sec} relies strictly on an indirect pathway. First, serine (Ser) is aminoacylated onto the opal suppressor tRNA^{Sec} by the SRS. In bacteria, the Ser moiety is directly selenylated by SelA to form Sec-tRNA^{Sec} further transported to the ribosome by a specific elongation factor SelB. While in eukaryotes and archaea, the Ser moiety is first phosphorylated by *O*-phosphoseryl-tRNA-kinase (PSTK) to form *O*-phosphoseryl-tRNA^{Sec} (Sep-tRNA^{Sec}). The Sep moiety is then selenylated in a tRNA-dependent manner by the SepSecS enzyme. Finally, the Sec-tRNA^{Sec} is transported by the eEFSec●SBP2 complex to the translating ribosomes (Hemmerle *et al.,* 2020).

I.3.4. Non-canonical roles and localizations

In addition to their canonical and essential role in tRNA aminoacylation, aaRSs can participate to many other cellular processes in prokaryotic and eukaryotic cells. In eukaryotes, these additional functions rely on additional domains and insertions that aaRSs acquired in the course of evolution. Contrary to what was believed at first, cytosolic aminoacyl-tRNA synthetases are not restricted to the cytoplasm in eukaryotic cells. Indeed, they can relocate at many different subcellular compartments where they will usually participate to other cellular processes. All these non-canonical functions and/or localizations of aaRSs are extensively described in recent reviews (Debard *et al.,* 2017; Yakobov *et al.,* 2018) and I will only present a few of them in the following paragraph.

I.3.4.1. Mitochondrial localization and missing aaRSs

Theoretically, bacteria and each translationally-active eukaryotic compartment (*e.g.*, cytoplasm, mitochondria, and chloroplasts for plants) should contain a full subset of 20 aaRSs, one for each aa of the genetic code. However, some aaRSs are missing in bacteria and there are no eukaryotic species that encode a complete and unique set of mitochondrial and/or chloroplastic aaRSs. Missing aaRSs need to be compensated either by an alternate route or by the import of a cytosolic aaRS ($_c$aaRS), that becomes a dual-localized aaRS. Surprisingly, in higher plants and *Saccharomyces cerevisiae*, $_c$aaRSs can be imported in the mitochondria even if the corresponding mitochondrial aaRS ($_m$aaRS) already exists. For their non-canonical mitochondrial import, $_c$aaRSs need a mitochondrial matrix-targeting sequence (MTS). In Humans, the KRS mRNA can undergo alternative splicing, leading to two KRS isoforms; one, that we name mitochondrial echoform aaRS ($_{mte}$aaRS), which is targeted to the mitochondria *via* a N-terminal MTS, and the other lacking this MTS which is the cytosolic echoform $_{cyte}$aaRS

that stays in the cytosol (Tolkunova *et al.*, 2000). For human GRS, the same transcript also produces the cytosolic and mitochondrial echoforms by using two different translation initiation starts (Alexandrova *et al.*, 2015).

In yeast, the mRNA of HRS and VRS contain two different AUG start codons that lead to the production of 2 isoforms (Chatton *et al.*, 1988; Natsoulis *et al.*, 1986). The long echoforms, $_{mte}$HRS and $_{mte}$VRS, contain the N-terminal MTS and localize in the mitochondria, while the short echoforms deprived of the MTS, $_{cyte}$HRS and $_{cyte}$VRS, remain in the cytosol. For yeast ARS, the translation can be initiated upstream from the AUG by an atypical ACG start codon (Tang *et al.*, 2004). Again, the long and short echoforms are mitochondrial and cytosolic, respectively. The mitochondrial localization of the yeast aaRSs echoforms was investigated by our team and the results obtained are presented in the research article I co-authored "Assigning mitochondrial localization of dual localized proteins using a yeast bi-genomic mitochondrial-split-GFP" (Bader *et al.*, 2020, **Chapter I section III.1**). In the yeast, the $_{mte}$ERS echoform of $_{c}$ERS can also be imported in the mitochondria (see **section I.3.3.**) but the $_{mte}$ERS echoform has exactly the same sequence as the cytosolic echoform. In this particular case, $_{c}$ERS is in fact a mitochondrial protein which is retained in the cytosol through its interaction with the protein Arc1 that acts as a cytosolic anchor for the aaRS (see **section II.2**). The $_{mte}$ERS corresponds, therefore, to the pool of $_{c}$ERS which is not binding to Arc1. This strategy allows to fine-tune the relocation of ERS in response to cellular compartment needs (Frechin *et al.*, 2014).

I.3.4.2. Nuclear localization; tRNA quality control and transcription regulation

Some aaRSs can also localize in the nucleus where tRNA transcription and maturation are performed. Their nuclear localization was associated with tRNA aminoacylation, which is considered as a quality control step prior to export of the tRNA towards the cytoplasm. The aminoacylation of tRNA^{Tyr} and tRNA$_i^{Met}$ was demonstrated in *X. leavis* oocytes (Lund and Dahlberg, 1998), which reinforced this idea. Moreover, nuclear localization signals (NLS) were found in many yeast aaRSs (Schimmel and Wang, 1999; Yakobov *et al.*, 2018). In the yeast, nuclear tRNA aminoacylation was demonstrated for MRS, IRS and YRS and 19 aa-tRNA species were detected in this compartment (Sarkar *et al.*, 1999; Steiner-Mosonyi and Mangroo, 2004). Interestingly, 30 % of the aa-tRNAs remain in the nucleus where they could be implicated in protein post-translational modifications (Rothbarth and Werner, 1986). In

yeast, MRS can also relocate to the nucleus to regulate transcription of Atp1 subunit of the F_1 domain of mitochondrial ATPase (Frechin *et al.,* 2014) (see **section II.2.1.**).

I.3.4.3. Implication in mammalian angiogenesis

An unexpected role for aaRSs is their implication in the process of angiogenesis in mammals. The YRS of higher eukaryotes possesses an extended C-terminus, which is 49 % identical to the sequence of Endothelial Monocyte-Activating Polypeptide (EMAP) II protein, a proinflammatory cytokine secreted by apoptotic cells to stimulate phagocytes and leukocytes migration and that represses angiogenesis (Ewalt and Schimmel, 2002; Kleeman *et al.,* 1997). Under apoptotic conditions, YRS is secreted and cleaved by extracellular proteases resulting in two fragments with cytokine properties. The C-terminal fragment, which is an EMAP II-like protein, attracts a large number of macrophages. On the other hand, the N-terminal fragment, named mini-YRS, contains a conserved Glu-Leu-Arg motif and the 3D structure typical of the interleukin-8 (IL-8) with leukocyte chemoattractant properties (Wakasugi and Schimmel, 1999). The mini-YRS also possesses a pro-angiogenic activity that relies on its Glu-Leu-Arg motif. When uncleaved, this motif is masked by the EMAP II-like domain, thus blocking the pro-angiogenic activity of mini-YRS. Like YRS, mammalian WRS contains an additional N-terminal domain. Upon alternative splicing of Trp mRNA, T1-Trp which lacks the N-terminal domain, is formed. In contrary to full-length WRS, T1-WRS blocks angiogenesis *in vivo*. A T2-WRS shorter version, produced upon T1-WRS proteolytic cleavage, displays even higher anti-angiogenic properties (Otani *et al.,* 2002; Wakasugi *et al.,* 2002)

I.3.4.4. Regulation of transcription in bacteria

In *E. coli*, the TRS binds to the operator site of its own mRNA upstream from the Shine-Dalgarno sequence (Moine *et al.,* 1990) which mimics tRNA^{Thr} anticodon stem-loop structure. By doing so, TRS prevents 30S-subunit binding to the mRNA and inhibits its translation initiation (Marzi *et al.,* 2007).

I.3.4.5. Membrane localization and *trans*-editing in cyanobacteria

In some cyanobacteria, the ERS, VRS, LRS and IRS possess a 100-200 aa-long additional domain (Luque *et al.,* 2008). This Cyanobacterial Aminoacyl-tRNA synthetases Appended Domain (CAAD) contains two putative transmembrane helices and has been shown to be essential for aaRS anchoring in thylakoid membrane (Olmedo-Verd *et al.,* 2011). In the
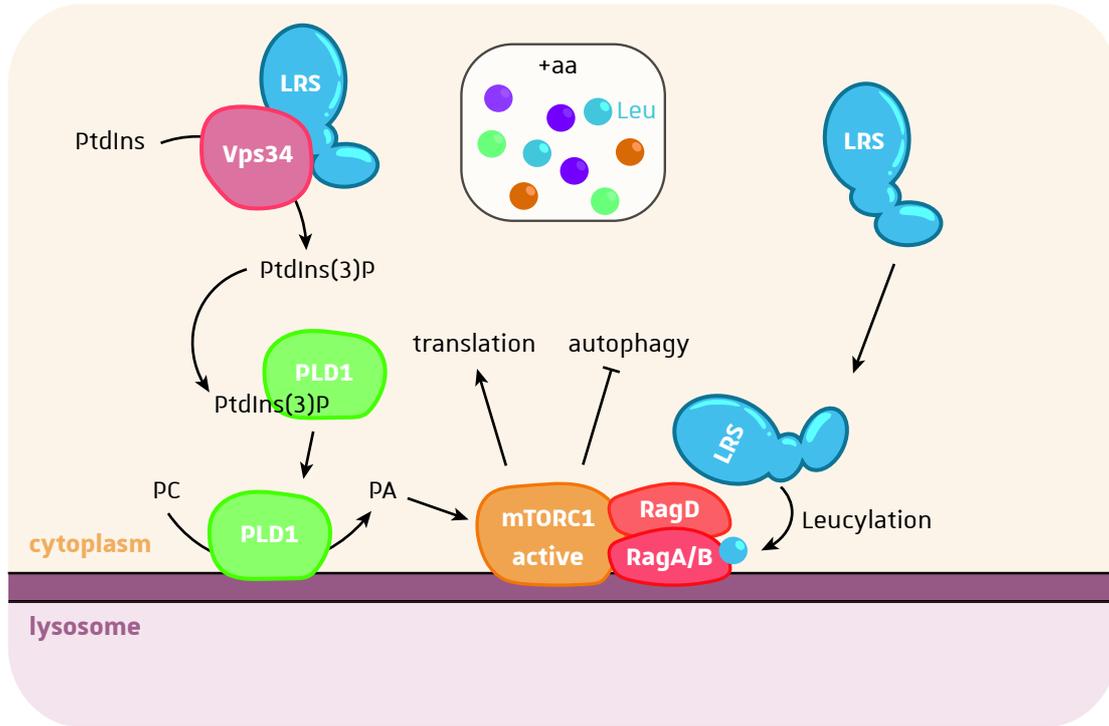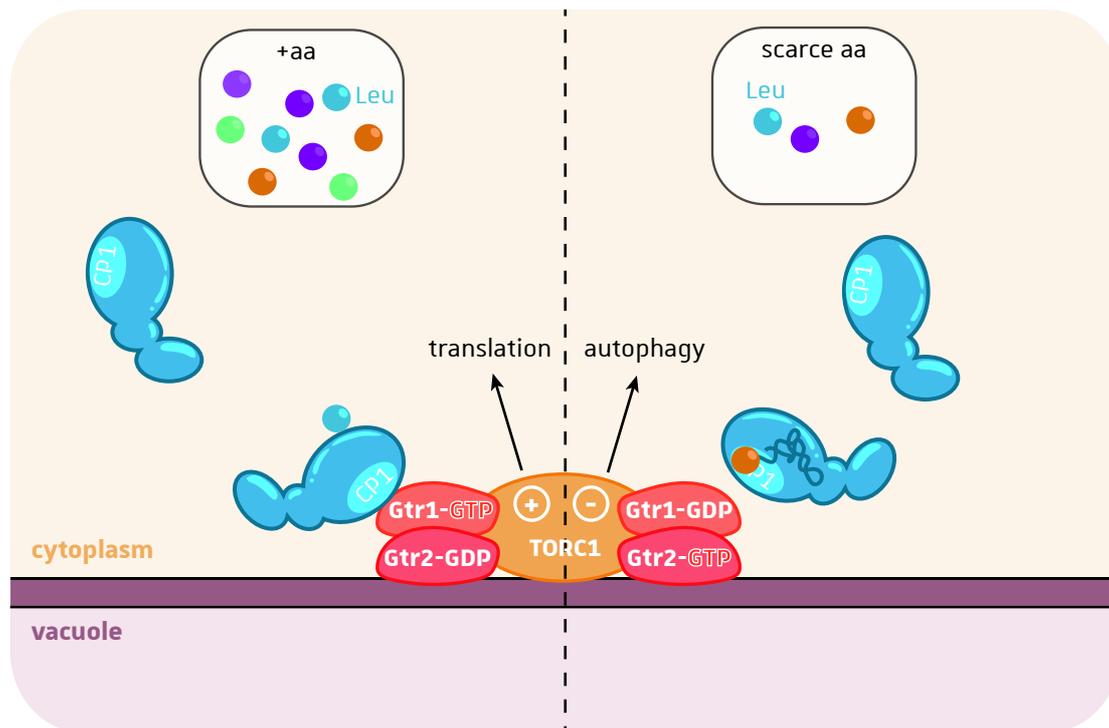
Figure I-7: Leucine sensing by the leucyl-tRNA synthetase and signaling to TORC1. A. In mammalian cells, leucine (Leu) availability is signaled to TORC1 by LeuRS in two different pathways. LeuRS can either activate mTORC1 through PLD1 or through the leucylation of the Rag GTPases RagA/B. PtdIns: phsophatidylinositol, PtdIns(3)P: phosphatidylinositol 3-phosphate, PC: phosphatidylcholine, PA: phosphatidic acid **B.** In yeast cells, LeuRS interacts with the Rag GTPase Gtr1 *via* its CP1 editing domain. In presence of leucine, LeuRS promotes TORC1 activation, while leucine deprivation leads to accumulation of mischarged tRNA^{Leu} that are edited in *cis* by the connective peptide 1 (CP1) domain of LeuRS. The conformational changes of LeuRS engaged in editing lead to disruption of the interaction and subsequent TORC1 inactivation.

cyanobacteria *Anabaena* sp. PCC 7120, the VRS CAAD triggers its accumulation in the thylakoids localized next to the junction with a neighboring cell (polar thylakoids), while thylakoids in other regions are largely devoid of VRS. This localization of VRS appears to be advantageous for faster growth under nitrogen starvation. Moreover, when localized in the thylakoids, VRS interacts with the F_1F_0 ATP synthase through its CAAD. It was thus proposed that VRS could be an aa sensor to monitor the nitrogen availability and transduce the signal to the F_1F_0 complex in order to adjust its functioning (Santamaría-Gómez *et al.,* 2016).

The cyanobacteria *Anabaena* also contains two TRS, named T1 and T2. In presence of Zn^{2+} in the medium, T1 homodimers perform the canonical aminoacylation of tRNA^{Thr}. Upon Zn^{2+} depletion, T1 dimers dissociate into monomers that have no aminoacylation activity. On the other hand, the expression of editing-defective T2 is induced leading to mischarged Ser-tRNA^{Thr}. In Zn^{2+} limitation, the editing of mischarged Ser-tRNA^{Thr} is performed in *trans* by *apo*-T1 that can form heterodimers with T2 (Rubio *et al.,* 2015).

I.3.4.6. Lipid modifications in bacteria and fungi

Another example of noncanonical localization related to noncanonical function of an aaRS in bacteria is the KRS of *Mycobacterium tuberculosis*. This organism encodes two KRS genes and one isoform contains a N-terminal MprF-like domain. This KRS localizes at the plasma membrane and acts as a lysyl-phosphatidylglycerol synthase (LysPGS) (Maloney *et al.,* 2009). The KRS domain aminoacylates tRNA^{Lys} with lysine, while the MprF-like domain transfers the lysyl moiety onto phosphatidylglycerol. Recently, a similar mechanism of lipid aminoacylation was found in *Aspergillus fumigatus* by our team (Yakobov *et al.,* 2020). This organism contains an enzyme called ErdS composed of a fusion of an DRS with a DUF2156 domain. The DRS domain aminoacylates its cognate tRNA^{Asp} with aspartate and the DUF2156 domain transfers the aspartyl moiety onto ergosterol leading to the formation of ergosteryl-3β-*O*-L-aspartate (Yakobov *et al.,* 2020). The aspartylated ergosterol could be implicated in membrane remodeling, trafficking, antimicrobial resistance, or pathogenicity.

I.3.4.7. AaRS and aa sensing

In mammalian cells, in presence of aa, LRS interacts with and activates Vps34 *via* its catalytic domain and unique C-terminal extension: UNE-L, respectively (Yoon *et al.,* 2016) (**Figure I-7A**). Vps34 in turn, produces phosphatidylinositol 3-phosphate (PtdIns(3)P) that interacts with and activates the phospholipase D (PLD) 1. Upon activation, PLD1 translocates

to the lysosomal membrane and hydrolyzes phosphatidylcholine to produce phosphatidic acid that activate mTORC1 (Yoon *et al.,* 2011). Interestingly, the activation of Vps34 by LRS does not require neither tRNA nor the production of Leu-tRNA^Leu, but only leucine. The LRS is thus considered as an amino acid sensor for the Vps34-PLD1-mTORC1 pathway (Yoon *et al.,* 2016). Independently of the previous pathway, mammalian LRS was also shown to localize at the lysosomal membrane in presence of aa, where it interacts with the Rag GTPase RagD to promote mTORC1 activity (**Figure I-7A**). Again, the tRNA charging activity of LRS is not necessary for mTORC1 activation. It was proposed that LRS preferentially binds to inactive RagD-GTP and promotes its conversion to the GDP-bound active form (Han *et al.,* 2012). However, the GTPase-activating protein (GAP) activity of LRS is under debate (Tsun *et al.,* 2013). In yeast, LRS interacts with and activates the Rag GTPase Gtr1 from the EGO complex (equivalent to the mTORC1 RAGULATOR complex in mammals) via its CP1 editing domain (**Figure I-7B**). Bonfils and coworkers demonstrated that the tRNA aminoacylation activity of LRS was not required and that leucine was sufficient for TORC1 activation. On the other hand, upon leucine deprivation, misaminoacylated tRNA^Leu are edited by the CP1 editing-domain of LRS. The conformational changes of LRS upon editing activity disrupt its interaction with Gtr1 and finally downregulate TORC1 (Bonfils *et al.,* 2012).

Recently He and coworkers reported that each aaRS is able to sense the presence of its cognate aa (He *et al.,* 2018). This process relies on the production of reactive aminoacyl adenylates by aaRSs, which are then used to modify lysine residues on target proteins. These post-translational modifications are dynamic and can be removed by sirtuins. This demonstrates that aaRSs can also be considered as aminoacyl transferases serving as aa sensors. Interestingly, upon leucine addition in the culture media or LRS overexpression the global level of leucylation and the leucylation of RagA, a component of the RAGULATOR complex, are increased. This, in turn, leads to the activation of mTORC1. LRS could thus positively regulate mTORC1 by interacting with Vps34 as previously reported (Yoon *et al.,* 2016) and by leucylating RagA. They also demonstrated that QRS can glutaminylate the pro-apoptotic protein Ask1. The post-translational modification occurs on the lysine K688 of Ask1 which is located in its ATP binding site. Upon glutaminylation, Ask1 kinase activity is inhibited and the apoptosis is suppressed (Ko *et al.,* 2001). QRS is thus an aminoacyl transferase, an aa sensor and an apoptosis repressor in human cells.

I.4. The aminoacyl-tRNAs (aa-tRNAs)

I.4.1. Canonical role; protein synthesis at the ribosomes

I.4.1.1. Initiation

The translation process can be divided in 4 phases: initiation, elongation, termination and recycling. In eukaryotes, the initiation starts with the assembly of ternary complex composed of the initiation factor eIF2, GTP and the initiator Met-tRNA$_i^{Met}$ (Levin *et al.*, 1973). The ternary complex binds to the small 40S ribosomal subunit with the help of eIF1/1A/3 (Majumdar *et al.*, 2003). The resulting complex is called the 43S complex. In eukaryotes, the mRNA 5'-end contains a 7-methylguanosine cap structure (5'-cap) where the eIF4F complex assembles (Gallie, 1998). This complex has been proposed to bind and unwind any structures found in the 5'-end to facilitate the loading of the 43S complex onto the 5'-untranslated region (UTR). In addition to the 5'-cap, eukaryotic mRNAs contain a 3'-poly(A) tail that is bound by poly(A) binding protein (PAB). PAB interacts with eIF4G, which is a component of eIF4F complex, leading to the circularization of mRNA (Tarun and Sachs, 1995). This mRNA structure facilitates binding of the 43S complex and provides a quality control mechanism preventing the synthesis of truncated proteins that could be toxic for the cell (Kapp and Lorsch, 2004). After mRNA loading, the 43S complex starts scanning down the mRNA in the 5' to 3' direction to find the AUG start codon, which is embedded in a favorable sequence context, called Kozak sequence (Kozak, 2002). Upon codon-anticodon base pairing between the initiation AUG codon and initiator tRNA$_i^{Met}$ in ternary complex (Cigan *et al.*, 1988), eIF2●GTP hydrolyses its GTP with the help of eIF5, and eIF2●GDP releases the Met-tRNA$_i^{Met}$ into the peptidyl (P) site of the 40S subunit and dissociates. The large 60S ribosomal subunit assembles with the 40S●Met-tRNA$_i^{Met}$●mRNA complex with the help of eIF5B●GTP. The hydrolysis of eIF5B's GTP leads to its dissociation from the complex, giving rise to the 80S initiation complex (Acker *et al.*, 2009; Pestova *et al.*, 2000).

I.4.1.2. Elongation

In contrast to the initiation mechanism, which is very different between prokaryotes and eukaryotes, the elongation process is conserved across the three kingdoms of life.

One cycle of elongation starts with a peptidyl-tRNA in the P-site next to a vacant A-site. The aa-tRNA, which are part of a ternary complex with GTP-bound Elongation Factor

1A (eEF1A), are carried to the ribosomal A-site. The selection of only cognate aa-tRNA is ensured by codon-anticodon base pairing between mRNA and aa-tRNA, conformational changes in the decoding center of the small ribosome subunit, and GTP hydrolysis by eEF1A (Rodnina and Wintermeyer, 2009). The aa-tRNA is then released into the A-site and the ribosomal peptidyl-transferase center catalyzes the formation of a peptide bond between the incoming aa and the P-site occupying peptidyl-tRNA. This results in a deacylated tRNA that has its acceptor end in the exit (E) site of the large ribosomal subunit and its anticodon end in the P site of small subunit. The peptidyl-tRNA is in a similar hybrid position with its acceptor end in the P-site of the large subunit and its anticodon end in the A-site of the small subunit. Complex translocation is triggered by GTP hydrolysis by ribosome bound eEF2. Upon translocation, the deacylated tRNA and the peptidyl-tRNA shift completely in the E- and P-site respectively and the mRNA moves back by 3 nucleotides to place the next codon into the A site (Ling and Ermolenko, 2016).

I.4.1.3. Termination and recycling

Termination occurs when a stop codon is placed in the A-site. This stop codon is decoded by class 1 release factor eRF1, which adopts a three dimensional structure mimicking a L-shaped tRNA (Bertram *et al.*, 2000). The class 2 release factor eRF3●GTP binds to eRF1 and promotes stop codon recognition and discrimination (Wada and Ito, 2014). Upon eRF3 dissociation after GTP hydrolysis, Rli1 factor binds to eRF1 and triggers the hydrolysis of the ester bond linking the peptide to the P-site tRNA, releasing the neo-synthesized protein from the complex (Khoshnevis *et al.*, 2010; Shoemaker and Green, 2011).

Recycling is initiated by the highly conserved protein ABCE1 that binds to the ribosomal inter-subunit space and to eRF1, inducing conformational shifts in eRF1. The conformational changes in ABCE1 are thought to destabilize inter-subunit bridges, leading to 40S and 60S ribosomal subunits separation. Deacylated tRNA and mRNA remain bound to the 40S subunit and can be released by eIF1, eIF1A, eIF3 and eIF3j subunit (Hellen, 2018). It has also been proposed that the 40S subunit may not be released and shuttle across the poly(A) tail back to the 5'-end of the mRNA thanks to the closed-loop conformation of eukaryotic mRNAs. This would facilitate the re-initiation of translation (Kapp and Lorsch, 2004).

I.4.1.4. Cotranslational assembly of protein complexes

Recently, Shiber and coworkers demonstrated that proteins belonging to a complex can assemble co-translationally (Shiber *et al.,* 2018). For this, the interactions of the nascent subunits from 12 hetero-oligomerics protein complexes in the yeast *Saccharomyces cerevisiae* were analyzed by selective ribosome profiling (seRP). Out of the 12 complexes, they identified 9 complexes that assemble co-translationally, 6 of them displaying a directional assembly mode, with one specific subunit being released from the ribosome before engaging the nascent interaction partner(s). Among the complexes which display a co-translational assembly mode, they found the AME complex, which is a multi-aminoacyl-tRNA synthetase complex (MSC) composed of the methionyl-tRNA synthetase (MRS), the glutamyl-tRNA synthetase (ERS) and the cofactor protein Arc1 (see **section II.2**). The three proteins of the complex interact with each other through their N-terminal GST-like domains. They demonstrated that both ERS and MRS engage each other and nascent Arc1 co-translationally upon emergence at the ribosome exit tunnel of the N-terminal GST-like domain. Arc1 was also shown to associate with nascent ERS but the interaction was less stable. They hypothesized that this co-translational assembly could regulate dual protein targeting and prioritize cytosolic activity (see **section II.2.**)

I.4.2. Non-canonical roles

During my PhD I participated to the redaction of a review, for which I am the first author, on aa-tRNA non-canonical utilizations (Hemmerle *et al.,* 2020). Here I will describe briefly the different roles that can be performed by aa-tRNAs (for more detailed information see publication Hemmerle *et al.,* 2020 page 228).

Besides being substrates for protein synthesis, aa-tRNA can be rerouted to participate to other cellular processes, that are equally important. In bacteria, the lysyl- and alanyl-moieties from Lys-tRNA[Lys] and Ala-tRNA[Ala] can be used by aa-phosphatidyl glycerol synthase (aaPGS) as aa donors to modify lipids. The addition of positively charged or neutral aa, changes the net negative charge of the cell envelope. These modifications of lipids by aa are decrease the susceptibility of bacteria to positively-charged antimicrobial agents, increasing the adaptation of bacteria to environmental changes, allowing the immune escape and augmenting the virulence of some strains. aa-tRNAs can also be used by FEM (Factor essential for Expression of Methicillin resistance) transferases as aa donors to form

interpeptide bridges in the peptidoglycan sacculus of bacteria.

The Glu-tRNA^{Glu} can be used as a substrate for the synthesis of δ-aminolevulinic acid which is essential in the synthesis of hemes in bacteria and green plants. This aminoacyl-tRNA is also used as a substrate by dehydratase for the modification of ribosomally-synthesized peptide-based antibiotics.

Finally, the degradation of proteins relies on the N-end rule pathway. In this process an aa-tRNA transferase uses the aa moiety of aa-tRNA to modify the N-terminal of proteins that will subsequently be degraded by the Clp protease complex in prokaryotes and the 26S proteasome in eukaryotes.

II. Multi-aminoacyl-tRNA synthetase complexes

The assembly of aaRSs into multi-aminoacyl-tRNA synthetase (MARS) complexes or multisynthetasic complexes (MSCs) together with aminoacyl-tRNA synthetase interacting proteins (AIMPs) was discovered in mammals in the early 70's (Bandyopadhyay and Deutscher, 1971; Deutscher, 1974; Mirande *et al.*, 1985). These MSCs can be found in eukaryotes and archaea and vary in size and composition (Laporte *et al.*, 2014). One study reported the existence of a MSC in bacteria, but this study is controversial (Harris, 1987). MSCs are thought to be cytosolic reservoirs for releasable and multifunctional aaRSs. Inside the MSC, aaRSs would be dedicated to their tRNA aminoacylation activity and upon release they could relocate to other compartments and/or perform noncanonical functions (Ray *et al.*, 2007). Another role proposed for MSC is that they would maintain aa-tRNAs in the ribosome vicinity and thus support the translation by a process called tRNA channeling (Han *et al.*, 2003; Kyriacou and Deutscher, 2008; Negrutskii and Deutscher, 1991).

II.1. Architecture and roles

The most documented archaeal MSC was isolated from *M. thermautotrophicus* and is composed of 3 aaRSs; L-, P- and KRS that likely assemble with a 2-2-2 stoichiometry and the elongation factor EF-1A (Hausmann *et al.*, 2007). Inside the complex, KRS and PRS bind to N-terminal and C-terminal domains of LRS respectively, while $_a$EF-1A interacts with the editing domain CP1 of LRS. This MSC is thought to enhance aa-tRNA channeling to the ribosome. *M. thermautotrophicus* contains a second MSC composed of RRS and SRS and the two ribosomal proteins L7 and L12. Upon complex formation the activity of SRS is increased, whereas RRS

activity is not impacted. This MSC could facilitate the recycling of tRNAs that have been used by the translating ribosomes (Godinic-Mikulcic *et al.*, 2014).

The smallest eukaryotic MSC is the yeast *Saccharomyces cerevisiae* AME complex, which was discovered in the mid 1990's (Simos *et al.*, 1996). It is composed of two aaRSs and one cofactor protein and will be extensively discussed below in **section II.2**.

The mammalian MSC is the biggest characterized so far and is composed of 8 aaRSs (M-, D-, K-, R-, L-, Q-, I-, and the bifunctional EPRS) and 3 AIMPs: AIMP1-3 (respectively p43, p38 and p18 in human cells). The mammalian MSC was extensively studied and particularly its composition and stoichiometry (Kaminska *et al.*, 2009). Cho and coworkers proposed a model in which MRS, EPRS, AIMP2 and AIMP3 interact together *via* their GST domains. This core complex would then serve as a nucleation platform for the assembly of the other aaRSs/AIMP. The whole MSC is suggested to be formed by the assembly of two identical symmetrically arranged subunits, each containing a single copy of the constituents, with the exception of KRS which is present as a dimer in each subunit. The two subunits would be joined by dimers of DRS and PRS domain of the EPRS and possibly KRS tetramers (Cho *et al.*, 2015). However, a recent study determined that this complex conformation was very unlikely (Khan *et al.*, 2020). Indeed, the calculated molecular weight of Cho and coworkers' model is appr. 2 MDa, whereas the mass determination by centrifugation in sucrose gradient or by gel filtration is appr. 1.0 to 1.2 MDa. According to the study of Khan and coworkers using XL-MS, the mass of the complex with monomeric constituents is appr. 930 kDa up to 1.2 MDa upon inclusion of the second monomer of the three proposed dimeric constituents (DRS, KRS and EPRS). They finally suggested, that the holo-MSC is composed of only one subunit containing mainly monomers and a few homodimers. The exact structure and stoichiometry of the MSC thus remains unclear (Khan *et al.*, 2020). The mamalian MSC has indeed been proven to be a cytosolic reservoir for cytosolic aaRSs, that can relocate to other compartments and perform noncanonical functions upon release.

II.2. Yeast *Saccharomyces cerevisiae* AME complex

In the yeast *Saccharomyces cerevisiae*, the cytosolic methionyl-tRNA synthetase ($_c$MetRS or $_c$**M**RS) and glutamyl-tRNA synthetase ($_c$GluRS or $_c$**E**RS) can associate with the aminoacylation tRNA cofactor 1, **A**rc1, to form a small multisynthetasic complex named the **AME** complex (Frechin *et al.*, 2010) (**Figure I-8A**).
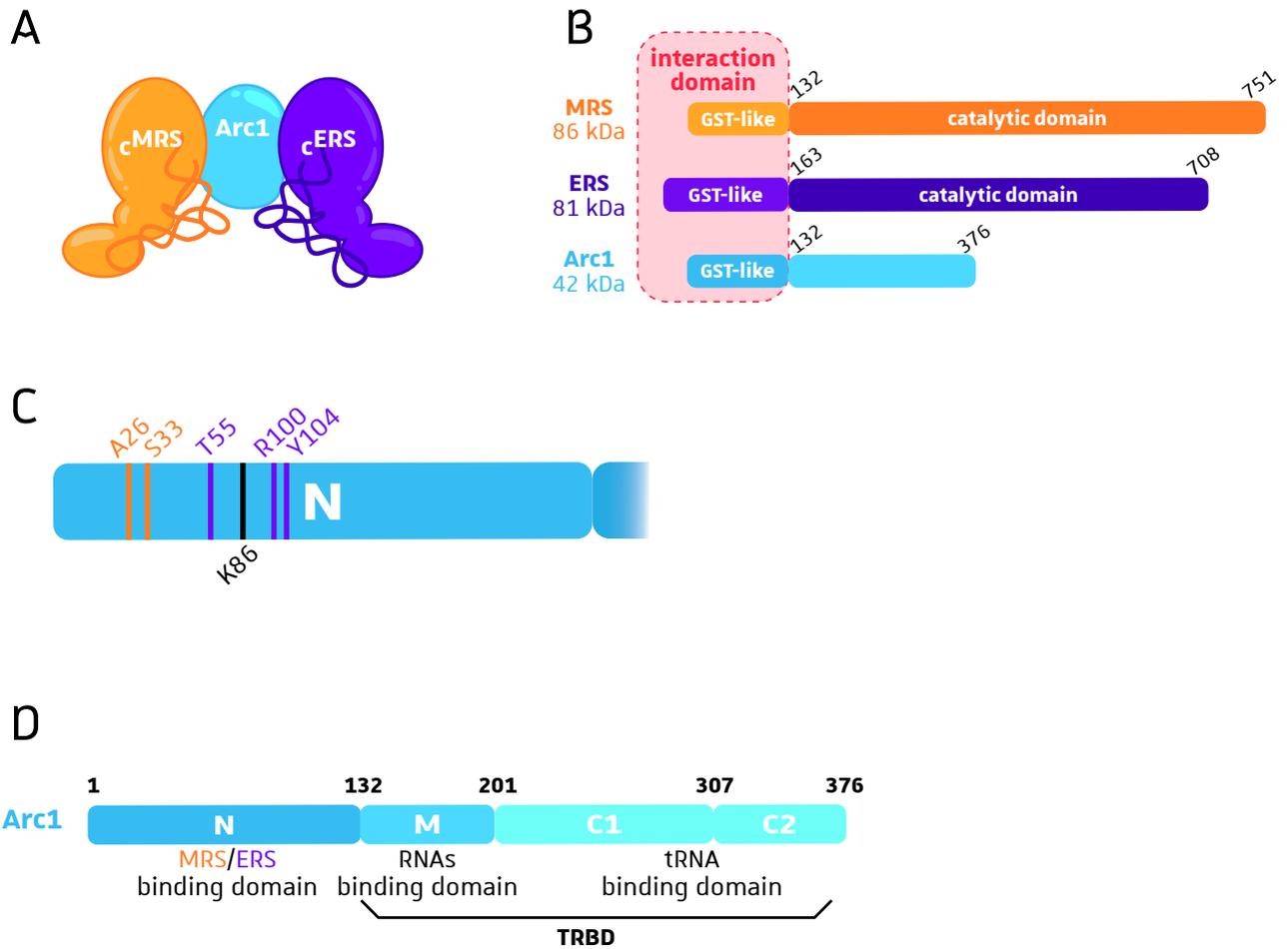
Figure I-8: *Saccharomyces cerevisiae* AME complex. A. The AME complex is composed of the cytosolic glutamyl-tRNA synthase ($_c$GluRS or $_c$**E**RS) and methionyl-tRNA synthetase ($_c$MetRS or $_c$**M**RS) and the cofactor protein **A**rc1. When bound to the two $_c$aaRSs, Arc1 binds preferentially to tRNA$_e^{Met}$ and tRNA^{Glu} [4]. **B.** The three proteins interact through their N-terminal domain that adopts a GST-like fold [5]. **C.** The residues essential for Arc1 interaction with the $_c$MRS and $_c$ERS are represented in orange and purple respectively [6]. A: alanine, S: serine, T: threonine, R: arginine, Y: tyrosine. The lysine K86 that can be biotinylated by Bpl1 is represented in black [7]. **D.** Arc1 is organized in three domains. The N-terminal (N) domain is essential for the interaction with the two $_c$aaRSs. The lysine-alanine-rich Middle (M) domain can bind different RNA molecules. The C-terminal (C) domain is subdivided into C1 and C2 subdomains. The C domain has an OB fold and can bind tRNA molecules. Together the M and C domains form the **tR**NA **B**inding **D**omain (TRBD) of Arc1 [8,9].

II.2.1. Arc1 structure, role and localization

The gene *ARC1* was discovered by Simos and coworkers in a synthetic lethal screen with *LOS1*, a gene encoding a protein involved in tRNA nuclear export (Simos *et al.*, 1996). Sequencing of the *ARC1* gene showed that it encodes an overall basic protein, composed of 376 aa distributed in three domains and with a predicted molecular mass of 42 kDa (Frechin *et al.*, 2010; Simos *et al.*, 1996). The N-terminal (N) domain (residues 1-131) adopts a GST-like fold, that promotes protein-protein interaction and thus the association of Arc1 with the two $_c$aaRSs that also contain a GST-like domain in their N-terminal domains (Simader *et al.*, 2006) (**Figure I-8B**). The residues essential for the interaction of Arc1 with $_c$MRS are Ala26 and Ser33, while Thr55, Arg100 and Tyr104 are important for the interaction with $_c$ERS (Karanasios *et al.*, 2007) (**Figure I-8C**). From residues 132 to 200, the middle (M) domain of Arc1 is lysine-/alanine-rich and has non-specific RNA binding capacities (Simos *et al.*, 1996). Finally, the C-terminal (C) domain of Arc1 shares homologies to human EMAPII. The first half of the C domain is homologous to the C-terminal of prokaryotic MRS and to a lesser extend to the N-terminal of the β subunit of FRS (Simos *et al.*, 1996). This domain has specificity for tRNA binding because of its OB fold. Together with the M domain they form the tRNA binding domain (TRBD) of Arc1 (Galani *et al.*, 2001) (**Figure I-8D**).

Since *ARC1* is synthetic lethal with *LOS1*, it very likely participates to the nuclear export of tRNA. To fulfill this role, Arc1 must thus be able to actively shuttle between the nucleus and the cytoplasm (**Figure I-9**). However, the NLS of Arc1 has not yet been identified. Moreover, Galani and coworkers showed that even upon the addition of a strong NLS, Arc1 is actively excluded from the nucleus by an Xpo1-dependent mechanism (Galani *et al.*, 2005). They could identify the 32 first aa and the C-terminal domain (aa 212-372) to be essential for nuclear exclusion but they could not find a typical Xpo1-dependent export leucine-riche Nuclear Exclusion Signal (NES) inside the Arc1 sequence. They hypothesized that Arc1 contains an atypical complex NES or that the N-terminal and/or C-terminal domains of Arc1 contain cytosolic tethering function.

Interestingly, In an attempt to identify new phospholipid-binding proteins by incubating yeast soluble extract onto membranes coated with phospholipids and subsequent mass spectrometry analysis, Fernandez-Murray and McMaster identified Arc1 as a novel lipid-binding protein (Fernandez-Murray and McMaster, 2006). Since Arc1 does not contain any known lipid-binding motif, it had never been identified or predicted as a lipid-binding
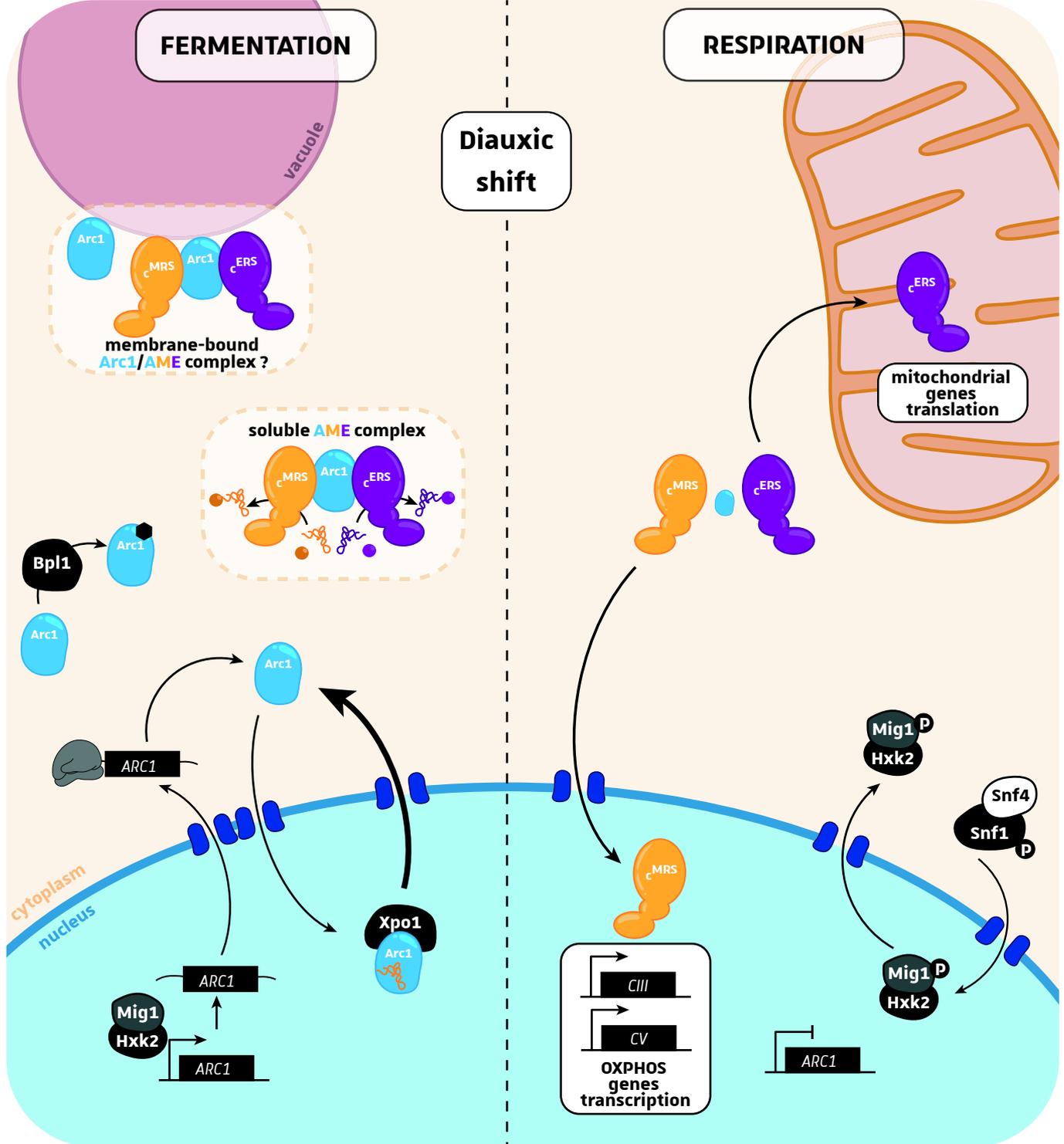
Figure I-9: Metabolism-controlled dynamic of the AME complex. When cells use a fermentable carbon source, the AME complex is soluble and sustains the translation machinery by providing aminoacyl-tRNAs. Arc1 was suggested to participate to the export of tRNAs from the nucleus and thus needs to be transiently localized in the nucleus. The Xpo1-dependent nuclear exclusion of Arc1 has been demonstrated [10]. The identification of Arc1 as a phospholipid-binding protein raises the possibility of a vacuolar relocalization of Arc1 alone or in complex with the two $_c$aaRS. Upon glucose deprivation or utilization of a non-fermentable carbon source, cells undergo a diauxic shift. The transcription of *ARC1* gene is then repressed, leading to an increase in free $_c$MRS and $_c$ERS, that relocalize into the nucleus and the mitochondria respectively. In the nucleus, $_c$MRS activates the transcription of the nuclear-encoded subunits of the complex III (CIII) and complex V (CV) of the mitochondrial respiratory chain. Upon relocalization in the mitochondria, the $_c$ERS sustains the mitochondrial translation of mtDNA-encoded respiratory complex subunits [11,12].

protein. Nonetheless, when incubated with lipids, either on membranes or with liposomes, Arc1 was shown to interact preferentially with PtdIns3P and PtdIns(3,5)P$_2$, which are enriched in the yeast endosomal and vacuolar membranes respectively. If Arc1 also interacts with these lipids *in vivo*, it could possibly bring the $_c$MRS and $_c$ERS to the vicinity of these subcellular compartments, maybe to perform non-canonical roles, like the vacuolar LRS identified by Bonfils and coworkers (Bonfils *et al.*, 2012) (**Figure I-9**).

Arc1 contains different post-translation modifications (listed in Saccharomyces Genome Database) but one of them is very surprising. Indeed, Arc1 can be biotinylated by the Bpl1 biotin-protein ligase on Lys86 and the biotinylation is abolished upon mutation of the lysine residue into arginine (Lys86Arg) (Kim *et al.*, 2004) (**Figure I-8C**). Unlike the other proteins biotinylated in the yeast, the biotin-protein BirA from *E. coli* cannot use Arc1 as a substrate. Arc1 biotinylation is not implicated in the formation of the AME complex, nor in tRNA binding. The only impact that could be observed is a decrease in Arc1 thermal stability upon biotinylation (Chang *et al.*, 2016).

II.2.2. AME complex dynamic

The association of Arc1 with the two $_c$aaRSs enhances their catalytic activities. Upon binding to Arc1, $_c$MRS catalytic efficiency (kcat/Km) increases by two orders of magnitude with a major effect on the Km (Simos *et al.*, 1996). The Arc1●$_c$MRS interaction resembles a classical GST homodimer and shows a dissociation constant (Kd) of 193 nM (Karanasios *et al.*, 2007; Simader *et al.*, 2006). On the other hand, $_c$ERS' aminoacylation efficiency is increased by a factor of 10 with a better tRNA-binding affinity when bound to Arc1 (Graindorge *et al.*, 2005). The Arc1●$_c$ERS interaction is a new type of interaction between two GST-like folds (Karanasios *et al.*, 2007). The duplex presents a Kd of 53 nM (Karanasios *et al.*, 2007) and the Arc1●$_c$ERS interaction is thus more stable than for Arc1●$_c$MRS, maybe because of the broader interaction surface (Frechin *et al.*, 2010). When not bound to $_c$MRS and $_c$ERS, Arc1 can bind to 5S RNA (weak) and a subset of tRNA species (Deinert *et al.*, 2001). However, when bound to $_c$MRS and $_c$ERS, the tRNA-binding specificity of the complex is restricted to tRNA^{Glu} and tRNA^{Met} (Frechin *et al.*, 2010). It was hypothesized that Arc1 binding to tRNAs might be involved in tRNA channeling because it directly provides tRNAs for aaRSs and prevents their release in the soluble cytosol (Simos *et al.*, 1996).

When yeast switches from fermentation to respiration, the intracellular ATP is mainly

produced by the mitochondria and thus the mitochondrial translation needs to be enhanced to produce the proteins from the respiratory chain among which the mitochondrial ATP synthase (respiratory complex V). However, in yeast the gene encoding the mitochondrial QRS is missing and the Gln-$_m$tRNA^{Gln} production relies on both the mitochondrial AdT that converts misacylated mitochondrial Glu-$_m$tRNA^{Gln} into Gln-$_m$tRNA^{Gln} (Frechin *et al.*, 2009) and on import of $_c$ERS. In other words, mitochondrial translation is directly depending on the pool of $_c$ERS which is not binding to Arc1. Previous studies achieved in the DyPS team, showed that, as expected, upon switch to respiration, the transcription of *ARC1* is inhibited by the Snf1/4 glucose-sensing pathway. This causes a drastic reduction of Arc1, leading to the release of both aaRSs (Frechin *et al.*, 2014) (**Figure I-9**). The $_c$ERS is then imported in the mitochondria to generate Glu-mtRNA^{Gln} (Frechin *et al.*, 2009) that will be converted into Gln-mtRNA^{Gln} by the GatFAB AdT. They also showed that $_c$ERS-mediated formation of Gln-mtRNA^{Gln} is particularly essential for the accumulation of the Atp9 ring of the mitochondrial ATP synthase F$_O$ domain. Meanwhile, the released $_c$MRS relocates inside the nucleus where it acts as a transcription factor that regulates expression of the *ATP1* gene, encoding a subunit of the F$_1$ catalytic sector of the mitochondrial ATP synthase (Frechin *et al.*, 2014). The protein Arc1 is thus an aminoacylation cofactor, a cytosolic retention platform for both aaRSs and most importantly it also coordinates/synchronizes the expression and assembly of the two domains (F$_O$ and F$_1$) of ATP synthase in response to the switch in nutritional carbon source (**Figure I-9**).

III.   Purpose of my thesis work

In the DyPS team, I worked on yeast aminoacyl-tRNA synthetases with the aim of identifying their non-canonical subcellular localization and, for some of them, the non-canonical role associated with this nonconventional localization. I focused on two different subcellular compartments in which aaRS relocalization has already been described in the yeast; the mitochondria and the vacuole. The challenge of such a work, is that relocalization of $_c$aaRS is not easy to visualize using conventional fluorescent protein tagging epifluorescence microscopy tools because the aaRS organellar echoforms are often less abundant than their cytosolic counterparts and the organellar fluorescence is masked by the cytosolic signal. Using biochemical approaches is even harder for the identification of organellar and cytosolic dual-localized proteins because of *(i)* the sample contaminations with cytoplasmic material and also because *(ii)* many subcellular compartments present contact sites with others.

I thus aimed to develop epifluorescence microscopy tools to unveil aaRSs' non-canonical localizations.

In a first chapter I will introduce the mitochondria and the mitochondrial localization of proteins. For the visualization of mitochondrial echoforms of dual-localized proteins we developed the BiG Mito-Split-GFP strain and this work has been recently published (Bader *et al.,* 2020). In a second chapter, I will introduce the fungal vacuole and the microscopy Vac-Split-CFP tool, I developed to visualize the vacuolar echoforms of aaRSs. The main results are presented in the form of a research article along with the supplementary work. Finally, the material and methods are presented in a distinct chapter.

CHAPTER I: MITOCHONDRIAL LOCALIZATION OF PROTEINS
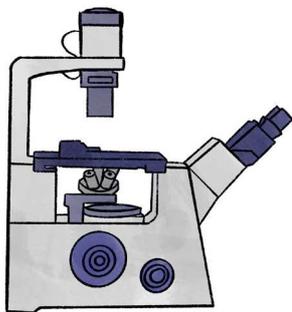
A.

- outer membrane (OM)
- intermembrane space (IMS)
- inner membrane (IM)
- matrix
- cristae
- mtDNA
- respiratory chain

mtDNA encodes:

- 7 subunits of the respiratory chain complexes: Cytb, Cox1, Cox2, Cox3, Atp6, Atp8 and Atp9
- 1 ribosomal protein: Var1
- 2 rRNAs: 15S and 21S
- complet set of tRNAs

B.

FERMENTATION — diauxic shift — RESPIRATION

glucose

| Mid-log | Mid-to-late log | late log | early stationary | late stationary |
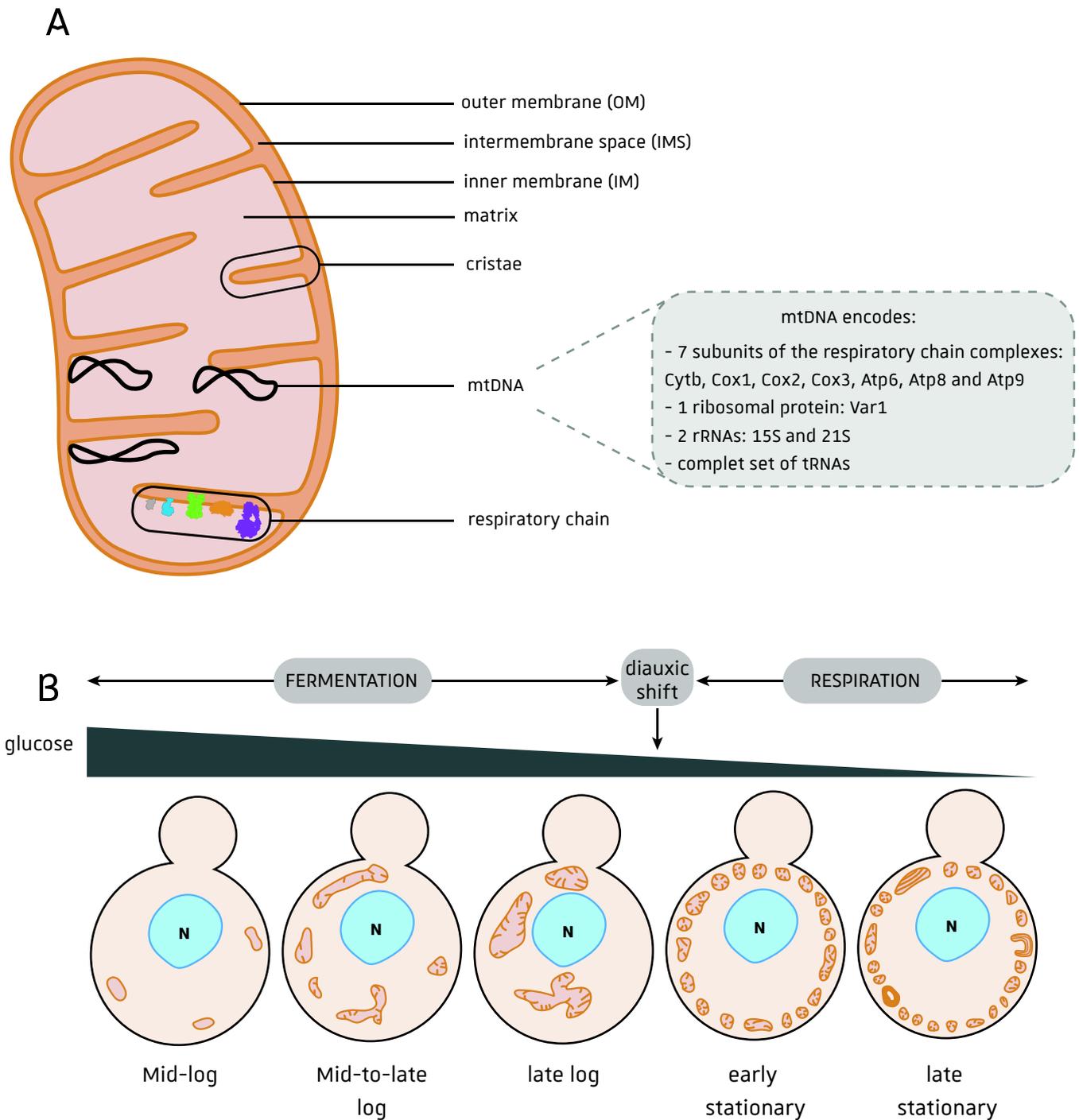
Figure ChI.I-1: Mitochondria organization and morphology. A. Mitochondria possess two membranes: inner membrane (IM) and outer membrane (OM) that delimit two soluble compartments: intermembrane space (IMS) and the matrix. The IM is invaginated in the matrix forming cristae that harbor the respiratory chain. The mitochondrial (mt)DNA consists mainly in linear molecules and encodes 8 proteins, 2 rRNAs and a full tRNA subset. **B.** The mitochondrial organization and morphology depend on the metabolic cell status. Log: logarithmic growth, N: nucleus.

I. Introduction

I.1. The mitochondria

Mitochondria are essential organelles of aerobic eukaryotic cells (**Figure ChI.I-1A**). They originate from the endosymbiosis of a prokaryotic organism, with α-proteobacteria being the closest identified relatives (Gray *et al.*, 1999). From their bacteria ancestor, mitochondria have conserved two distinct membranes, the outer and the inner membranes, which define and enclose two soluble compartments, the matrix and the intermembrane space (IMS). The two membranes of yeast mitochondria have been characterized and they are mainly composed of phospholipids, with phosphatidylcholine (PC) and phosphatidylethanolamine (PE) being the major components (40% and 27% respectively), but also phosphatidylserine (PS), phosphatidylinositol (PtdIns), phosphatidic acid (PA) and the mitochondria-specific cardiolipin (CL) (Horvath and Daum, 2013). The inner membrane has a higher content in PtdIns and CL, is highly invaginated leading to the formation of cristae and it also harbors the respiratory chain complexes. Mitochondria also possess their own DNA (mitochondrial DNA or mtDNA) remnant of their bacterial ancestor, which varies in size and content between eukaryotes. Indeed, the number of genes can be as low as five in *Plasmodium falciparum* up to 97 in *Reclinomonas americana* (Gray *et al.*, 1999). This variety in gene content is explained by the massive transfer of mitochondrial genes to the nuclear genome that occurred in the course of evolution (Thorsness and Fox, 1990). The mtDNA of *Saccharomyces cerevisiae* is composed of linear molecules of appr. 75 to 150 kb, and small amounts of circular DNA have also been observed (Maleszka *et al.*, 1991; Westermann, 2014; Williamson, 2002). The yeast mtDNA encodes 7 proteins of the oxidative phosphorylation machinery (Cytb, Cox1, Cox2, Cox3, Atp6, Atp8 and Atp9) and one protein of the mitochondrial ribosomal small subunit (Var1), two rRNAs (15S and 21S) and the complete set of tRNAs needed for mitochondrial translation (Foury *et al.*, 1998). The proteins encoded by the mitochondrial genome are almost exclusively very hydrophobic membrane proteins (also called proteolipids) which are subunits of the respiratory chain complexes. This feature explains why they cannot be synthesized in the cytosol as precursors but are co-translationally integrated into the inner membrane by mitochondrial ribosomes, which are tightly bound to the inner membrane (Fox, 2012). Most of the mitochondria-encoded proteins thus function in association with nucleus-encoded proteins that have to be imported in the mitochondria after cytosolic translation (Malina *et al.*, 2018; Pon and Schatz, 1991).

A
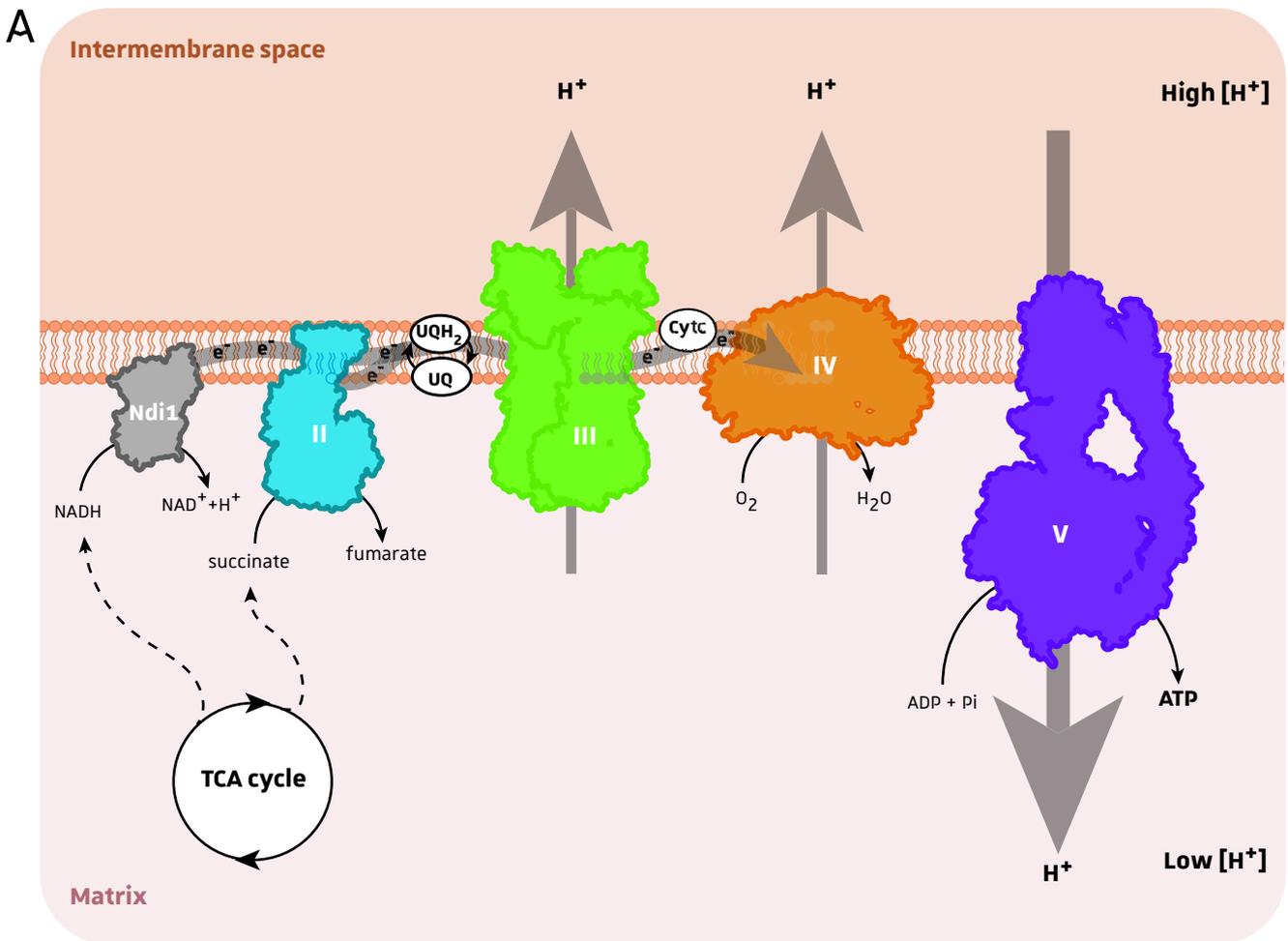
B

	NADH oxidase	Complex II Succinate dehydrogenase	Complex III Cytochrome *bc1*	Complex IV Cytochrome *c* oxidase	Complex V F$_0$F$_1$-ATP synthase	
mtDNA encoded subunit	none	none	CYTB	COX1 COX2 COX3	ATP6 ATP8 ATP9	
nulcear DNA encoded subunit	NDI1	EMI5 SDH1 SDH2 SDH3 SDH4	RIP1 COR1 QCR2 QCR6 QCR7 QCR8 QCR9 QCR10 CYT1	COX4 COX5A COX5B COX6 COX7 COX8 COX9 COX12 COX13	ATP1 ATP2 ATP3 ATP4 ATP5 ATP7 ATP14 ATP15 ATP16	ATP17 ATP18 ATP19 ATP20 ATP21

Figure ChI.I-2: Yeast respiratory chain and the genes encoding the different subunits. A. The electrons (e$^-$) flux between the different complexes is represented in gray. The [H$^+$] gradient formed by complexes III and IV is used by the complex V or F$_0$F$_1$-ATP synthase to produce ATP from ADP and inorganic phosphate (Pi). UQ: ubiquinone, UQH2: ubiquinol, Cytc: cytochrome c. **B.** With the exception of the NADH oxidase, which is only composed of the protein Ndi1, the respiratory chain complexes are composed of multiple subunits that are either encoded by the mitochondrial (mt)DNA or the nuclear DNA.

Early studies performed on the yeast *Saccharomyces cerevisiae*, demonstrated that the morphology and organization of mitochondria are greatly affected by the cell status (Pon and Schatz, 1991; Yotsuyanagi, 1962) (**Figure ChI.I-1B**). During mid- and mid-to-late logarithmic growth, cells contain only few mitochondria with poorly developed cristae. During the late logarithmic phase, the glucose starvation induces nearly full mitochondrial development; the mitochondria fuse into a mitochondrial reticulum composed of one big and several smaller tubular organelles. The switch from fermentation to respiration triggers the disruption of the mitochondrial reticulum into many small, regular mitochondria preferentially arranged at the cell periphery. During extended starvation, the mitochondria change slowly into degenerative forms composed of parallel or concentric lamellae. Later studies by Stevens showed that cells in early logarithmic phase on glucose contain only 1-2 mitochondria, while cells in stationary phase during glucose limitation contain 44 mitochondria (Stevens, 1981).

I.2. Roles

I.2.1. Production of ATP through the respiratory chain

Mitochondria are often described as the "powerhouse of the cell" because they produce the majority of cellular energy in the form of ATP through the oxidative phosphorylation (OXPHOS) (**Figure ChI.I-2A**). The OXPHOS machinery is composed of five complexes embedded in the mitochondrial inner membrane; four electron transport complexes (complex I-IV) and the F_0F_1-ATP synthase (also referred as complex V). The electrons used in the respiratory chain are generated from NADH and succinate that derive from the TCA cycle and they are passed through the respiratory chain by two transporters; the ubiquinone and the cytochrome *c*. The energy released during the transport of electrons is stored in the form of a proton (H^+) gradient across the inner membrane. This gradient is finally used by the F_0F_1-ATP synthase to generate ATP from ADP and inorganic phosphate (P_i) (Saraste, 1999). Since the mitochondria only encodes a very limited set of genes, the proteins required for the OXPHOS are from two different origins; the majority is encoded by the nuclear genome, translated in the cytosol and imported in the mitochondria, and a few proteins are directly encoded by the mtDNA and translated in this compartment (**Figure ChI.I-2B**).

In *Saccharomyces cerevisiae*, complex I is absent and replaced by Ndi1, a NADH oxidase, which faces the mitochondrial matrix (de Vries and Grivell, 1988; Marres *et al.*,

1991). The oxidation of NADH by complex I provides two electrons that are transferred to ubiquinone, which diffuses in the inner membrane to reach to complex III (cytochrome *bc1*). The complex II, or succinate dehydrogenase, transfers an electron from succinate to ubiquinone. In the yeast, the two first complex do not translocate H^+ across the membrane but only provide electrons. The complex III or cytochrome bc_1 complex delivers the electrons from ubiquinol to cytochrome *c*, a reaction that is coupled to the generation of an H^+ gradient across the membrane. The cytochrome *c*, which is a water-soluble hemoprotein, moves across the membrane to donate electrons to the complex IV, or cytochrome *c* oxidase. The electrons are transferred to the active site and used to reduce O_2 into $2H_2O$. Again, this reaction is coupled to the formation of an H^+ gradient across the membrane. The H^+ located in the intermembrane space are finally used by the F_0F_1-ATP synthase or complex V as a motive force. The ATP synthase F_0 sector contains the H^+ channel, while the F_1 sector facing the matrix side of the membrane is the catalytic component. The F_1 sector is composed of 5 subunits with a $\alpha_3\beta_3\gamma_1\delta_1\epsilon_1$ stoichiometry. The α and β subunits can bind nucleotides but only β subunits have catalytic activity, thus there are only 3 active sites within the catalytic components of complex V. Each active site passes through a cycle of different state; open, loose and tight. The open state is an empty β subunit, the loose β subunit contains ADP + P_i and the tight β subunit contains ATP that is obtained upon spontaneous conversion of ADP and P_i (Artika, 2019; Saraste, 1999). The subunit γ is located within the $(\alpha\beta)_3$ core and also interacts with subunits δ and ϵ to form a "central stalk" linking F_1 to F_0. High-resolution structures demonstrated that subunit γ only makes a few direct contacts with the F_0 *c*-ring, while subunit δ displays extensive interactions with both *c*-ring and subunit γ. The subunit ϵ on the other hand looks like a clip around γ and δ subunits (Stock *et al.*, 1999). Duvezin-Caubet and coworkers demonstrated by using δ-less mitochondria that the sole loss of subunit δ suffices to uncouple ATP synthase because of H^+ leak in the ATP synthase H^+-channel. The subunit δ thus plays a key role in connecting the F_0 *c*-ring with the F_1 subunit γ (Duvezin-Caubet *et al.*, 2003). Interestingly, the F_0 subunits *e* and *g* were shown to be important for the formation of mitochondria characteristic cristae by an oligomerization process (Paumard *et al.*, 2002).

I.2.2. Amino acid synthesis

Beside the production of ATP by the respiratory chain, mitochondria are involved in a plethora of other metabolic processes.

In the yeast mitochondria, aa can be synthesized from pyruvate and α-ketoglutarate. The aa from the pyruvate family include Ala and the branched-chain aa (BCAA) Leu, Val and Ile. Ala can be synthesized in the mitochondria by Alt1 directly from pyruvate with Glu as an ammonia donor (García-Campusano *et al.*, 2009). The entire pathway for Ile and Val biosynthesis is localized in the mitochondria, and the last step can alternatively be performed in the cytosol (Kispal *et al.*, 1996). On the other hand, Leu synthesis is localized both in the cytosol and the mitochondria (Kohlhaw, 2003). The synthesis of Arg and Lys partly occurs in the mitochondria. Indeed, ornithine, which is an intermediate in Arg biosynthesis, is synthesized in the mitochondria from Glu and acetyl-coA by 5 consecutive acetylation steps performed by Arg2, Arg5,6, Arg7 and Arg8. The synthesis of Lys from α-ketoglutarate involves by mitochondrial proteins, Lys4 and Lys12, which produce the intermediates homoisocitrate and α-ketoadipate respectively. The intermediates are then transported to the cytosol to serve as substrates for the remaining steps of Lys biosynthesis (Ljungdahl and Daignan-Fornier, 2012). In the yeast mitochondria, Asp is synthesized from the transamination reaction between Glu and oxaloacetate by the Aat1 aspartate aminotransferase. For Glu biosynthesis three different pathways can be used. Two pathways produce Glu from α-ketoglutarate and ammonia and the reaction is performed by Gdh1 or Gdh3 glutamate dehydrogenases, the latter being induced upon growth on non-fermentable carbon source and localized in the mitochondria.

In mammals, Gln can be synthesized from Glu and ammonia by the Glutamine synthase (GS). It has been demonstrated that GS has activity in the cytosol and the mitochondria and has a "weak" mitochondrial localization. In liver, the GS is imported in the mitochondria, while it remains cytosolic in astrocytes. Pro intermediate pyrroline-5-carboxylate (P5C) is synthesized in the mitochondria by the enzyme pyrroline-5-carboxylate synthase (P5CS). P5C is then reduced by pyrroline-5-carboxylate reductase (PYCR) to produce Pro. Gln can be converted by the glutaminase (GLS) to Glu and ammonia. Glu is then converted into α-ketoglutarate by transaminase or glutamate dehydrogenase (GDH), or converted by glutamate–oxaloacetate transaminase 2 (GOT2) to produce Arg. Finally, Gly is obtained by the mitochondrial conversion of tetrahydrofolate (THF) by the serine hydroxymethyltransferase (SHMT2) (Spinelli and Haigis, 2018).

I.2.3. Iron-sulfur cluster and heme biogenesis

Mitochondria are the place for mitochondrial iron-sulfur (Fe/S) clusters biogenesis and assembly and the building of cytoplasmic and nuclear Fe/S cluster proteins (Braymer and Lill, 2017). The Fe/S clusters are versatile co-factors, which can act as catalytic sites or participate to electron transfer and sensory functions. The only mitochondrial Fe/S protein that is essential for *S. cerevisiae's* growth is ferredoxin. Moreover, some cytoplasmic and nuclear Fe/S proteins are essential for viability. Thus, complete loss of mitochondrial Fe/S cluster biosynthesis is lethal. The synthesis of hemes that are involved in sensing cellular oxygen levels through the regulation of oxygen responsive genes is dually localized in the cytosol and in the mitochondrial matrix (Malina *et al.*, 2018).

I.2.4. Lipid metabolism

Mitochondria play an important role in lipid metabolism. Indeed, phosphatidic acid (PA) originating from the ER is used in mitochondria to generate cardiolipin (CL) and phosphatidylglycerol (PG) (S. C. Chang *et al.*, 1998; Osman *et al.*, 2010). Moreover, phosphatidylethanolamine (PE) is generated through the decarboxylation of phosphatidylserine (PS) by Psd1 in the mitochondria and then transported back to the ER to generate phosphatidylcholine (PC) (Clancey *et al.*, 1993). The ER-synthetized phosphatidylinositol and PC are then imported in the mitochondria. However, the mitochondria are only partly autonomous for lipid synthesis and because of their endosymbiotic origin, they are not connected to the endomembrane system. The lipids needed for mitochondrial biogenesis thus have to be provided by nonvesicular pathways (Fernández-Murray and McMaster, 2016; Horvath and Daum, 2013).

I.2.5. Calcium homeostasis and apoptosis

In mammal cells, the major organelles for calcium (Ca^{2+}) control are the endoplasmic reticulum (ER) and the mitochondria. In 1962, Vasington and Murphy provided the first evidences of Ca^{2+} uptake in isolated mitochondria and its accumulation in the matrix in an energy-dependent way (Vasington and Murphy, 1962). In order to reach the mitochondrial matrix, Ca^{2+} must cross both the outer membrane (OMM) and the ion-impermeable inner membrane (IMM) to reach the mitochondrial matrix. Uptake across the OMM is controlled by the voltage-dependent anion channel 1 (VDAC1), while the mitochondrial Ca^{2+} uniporter (MCU) controls uptake across the ion-impermeable IMM. The Ca^{2+} accumulation is counteracted

by Na⁺/ Ca²⁺ and H⁺/ Ca²⁺ exchangers (Crompton *et al.*, 1977; Gincel *et al.*, 2001; Pozzan *et al.*, 1977). Inside the mitochondria, Ca²⁺ controls the energy metabolism, by enhancing the rate of NADH production and by modulating enzymes of the tricarboxylic acid (TCA) cycle and fatty acid oxidation (Denton, 2009; Nichols and Denton, 1995). The mitochondrial Ca²⁺ homeostasis is also important for the regulation of intracellular Ca²⁺ concentration and for the activation of cell apoptotic pathways. Upon over accumulation of Ca²⁺ in mitochondria, Ca²⁺ can escape the mitochondrial matrix through the opening of large permeability transition pore (PTP). This also leads to matrix swelling, rupture of the outer membrane and release of cytochrome *c*, which will in turn activate caspases and finally the programmed cell death (Giacomello *et al.*, 2007).

Many of the signaling events leading to apoptosis in mammalian cells also take place in yeast. The key events of yeast apoptosis are the increased intracellular concentration of Ca²⁺ and reactive oxygen species (ROS). As in mammals, increased intracellular Ca²⁺ concentration will lead to increased ROS levels, cristae remodeling, mitochondria depolarization, ATP depletion, matrix swelling, OMM permeabilization and eventually release of cytochrome *c* and other pro-apoptotic proteins. Contrary to mammalian cells, yeast does not possess a MCU and cytochrome *c* release does not trigger caspase activation. However, evidences show that Ca²⁺ uptake occurs in yeast mitochondria and findings suggest that a specific Ca²⁺ transport may exist (Carraro and Bernardi, 2016). Another important difference with mammalian cells is that the major storage compartment for Ca²⁺ in yeast is the vacuole. Ca²⁺ enters the vacuole through Ca²⁺ ATPase Pmc1 and Ca²⁺/H⁺ exchanger Vcx1, a mechanism that would link Ca²⁺ homeostasis to the regulation of intracellular pH in yeast cells (Cunningham and Fink, 1994; Miseta *et al.*, 1999).

I.3. Protein import

Beside the 8 proteins encoded by the yeast mtDNA, the yeast mitoproteome has been estimated to contain approximately 1000 proteins, which are encoded by the nuclear genome, translated in the cytosol and finally imported in their respective compartment in the mitochondria (Vögtle *et al.*, 2017). For their import, precursor proteins are kept in an unfolded import-competent conformation by chaperones and other factors (Cichocki *et al.*, 2018; Jores *et al.*, 2018; Young *et al.*, 2003). The targeting and distribution of precursors to mitochondrial sub-compartments rely on targeting signals (Chacinska *et al.*, 2009) (**Figure ChI.I-3**). Most of the matrix and inner membrane proteins and some proteins of the IMS

protein destination	Type of targeting signal
Matrix	cleavable amphiphatic α-helices (MTS)
	MTS + iMTS-L
Inner membrane	Multiple internal signals
	MTS + uncleavable hydrophobic sorting signal
	iMTS-L after hydrophobic region
outer membrane	β-sheet hairpin
	C tail anchor
	signal-anchor sequence
	internal signal
intermembrane space	cysteine-containing sequence or ITS/MISS
	MTS + cleavable hydrophobic sorting signal

Figure ChI.I-3: Mitochondrial targeting signals and distribution of the mitochondrial precursors. Depending on the destination of the precursors different targeting signals can be used. Some targeting signals can be cleaved (cleavage site represented with red arrowheads) by mitochondrial peptidases . MTS: matrix-targeting sequence, iMTS-L: internal MTS-like, TMD: transmembrane domain, +: positive residues, Φ: hydrophobic residues, β-strands are represented by blue arrows and α-helices are in black.

and of the outer membrane are synthesized with a N-terminal matrix-targeting sequence (MTS). These signals are about 8 to 80 residues in length, lack negative residues, are rich in hydroxylated residues such as serine and threonine, form amphiphatic α-helices with one positively charged and one hydrophobic face (Vögtle *et al.,* 2009). Mitochondrial precursors are recognized at the mitochondrial surface by receptors that are part of the translocase of the outer membrane (TOM) complex, thus allowing their entry in the protein-conducting channel (H. Yamamoto *et al.,* 2011). The precursor proteins are then driven through the outer membrane by several binding sites and sequential interactions. The MTS facilitates binding to Tom20/Tom22 and the translocation through the TOM pore. After binding to the trans-site of the TOM complex, the presequence is handed to the translocase of the inner membrane formed by the TIM23 complex (Abe *et al.,* 2000; Melin *et al.,* 2014; Mokranjac *et al.,* 2003). Because of the accumulation of protons in the IMS, the inner membrane facing the IMS is positively charged, while the membrane side facing the matrix is negatively charged. The positively charged MTS could thus take advantage from this gradient to be translocated through the TIM23 channel. Chaperones of the matrix then bind to the incoming proteins and prevent backsliding. The MTSs are then removed by the mitochondrial processing peptidase (MPP) and rapidly degraded. Protein folding in the matrix is then supported by chaperones (Chacinska *et al.,* 2009; Hansen and Herrmann, 2019).

In addition to MTS, some proteins of the matrix and the inner membrane can contain an additional internal MTS-like structure (iMTS-L) that helps to maintain them in an import-competent state (Backes *et al.,* 2018). Some inner membrane proteins lack N-terminal targeting signals but use internal signals that are neighboring their transmembrane domain (TMD) and some other have a positively-charged stretch downstream of the TMD (Fölsch *et al.,* 1996; Wiedemann *et al.,* 2001). This region may form a hairpin-like structure that mimics a MTS. The majority of proteins of the outer membrane lack N-terminal MTSs. Some proteins are anchored to the outer membrane by C-terminal TMDs that differ from the C-terminal TMD of ER and peroxisomal proteins (Kemper *et al.,* 2008; Marty *et al.,* 2014). Another category is the signal-anchored proteins that use an N-terminal TMD to be targeted to the outer mitochondrial membrane (Ahting *et al.,* 2005). Outer membrane proteins can also belong to the group of β-barrel proteins and probably use the β-sheet hairpin structures as targeting signals (Jores *et al.,* 2016). The proteins that reside in the IMS can contain an ITS/MISS targeting signal, formed by internal amphiphatic helices in direct proximity to a cysteine residue (Milenkovic *et al.,* 2009; Sideris *et al.,* 2009). The utilization of algorithms
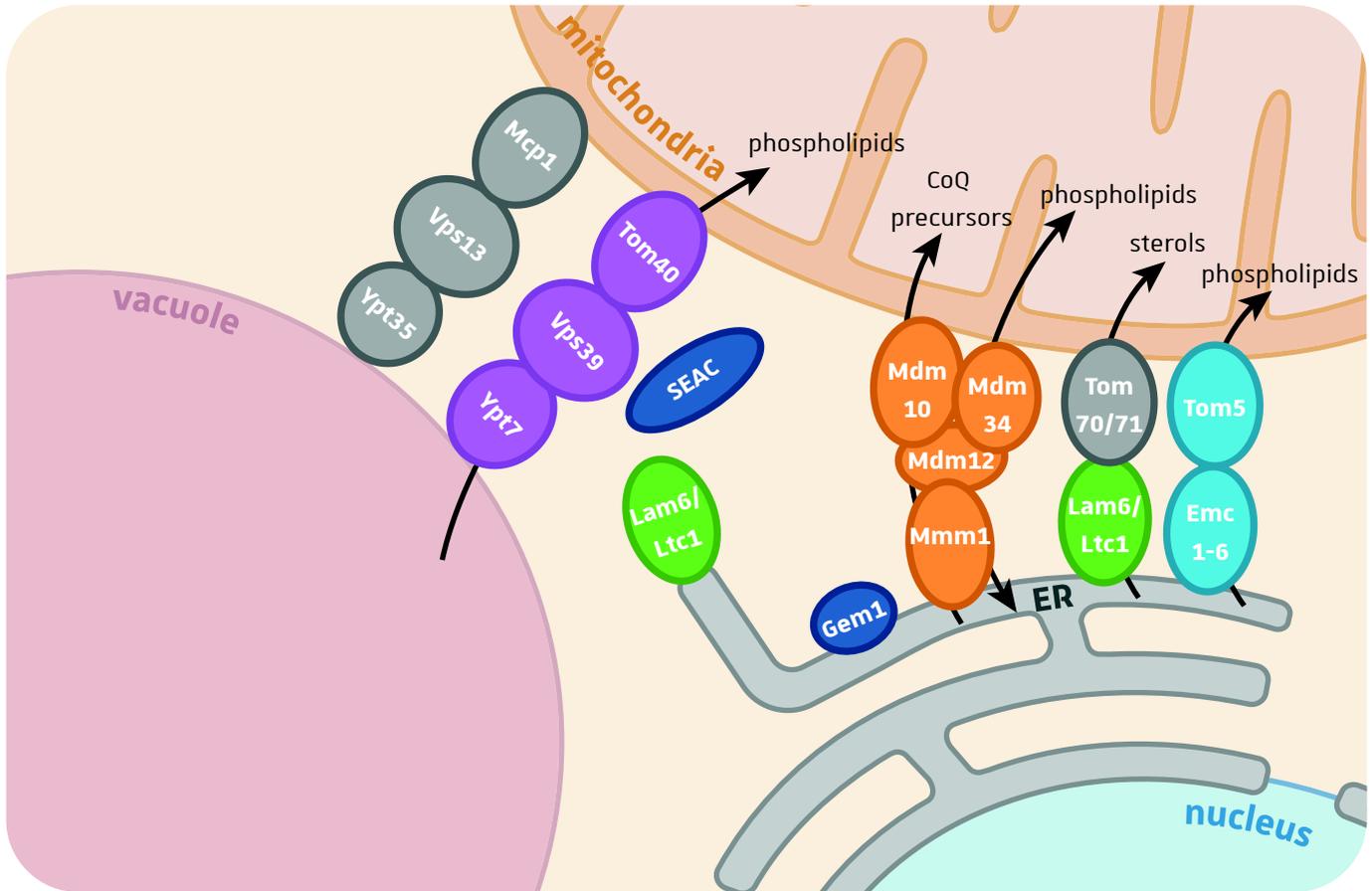
Figure ChI.I-4: Organization of vCLAMPs, ERMES and EMC contact sites. Mitochondria can contact vacuoles through vCLAMP structures and the ER by forming ERMES and EMC structures. These contact sites are involved in the transfer of lipids and other small molecules between the different subcellular compartments. The core components of ERMES, EMC and vCLAMP are represented in orange, blue and purple respectively. The other proteins participating in the contact sites are represented in gray. Upon growth on non-fermentable carbon source vCLAMPs are abolished and Vps13 relocates to the nucleus-vacuole junctions (NVJ, described in **Chapter II section I.51**). The ER protein Lam6-Ltc1 represented in green is at the interface between vCLAMP, ERMES and NVJ. SEAC and Gem1 represented in dark blue are regulatory components of vCLAMP and ERMES respectively. CoQ: Coenzyme Q.

can be useful to detect the presence of N-terminal MTSs but they are less powerful for recognizing other types of targeting signals (Claros and Vincens, 1996; Emanuelsson *et al.,* 2000; Hansen and Herrmann, 2019).

The accumulation of specific mitochondrial mRNAs binding proteins at the surface of mitochondria supports the idea that some proteins of the inner membrane can be co-translationally imported (Eliyahu *et al.,* 2010; Gadir *et al.,* 2011). The interaction of the nascent polypeptide-associated complex (NAC) with mitochondrial outer membrane protein Om14 targets cytosolic ribosomes to mitochondria (Lesnik *et al.,* 2014). The targeting of hydrophobic precursors of membrane proteins can be mediated by a recently identified targeting pathway named ER-SURF (ER surface-mediated protein targeting) (Hansen *et al.,* 2018). Indeed, mRNAs for many mitochondrial proteins are located on the ER surface, suggesting that these proteins are intentionally synthesized on the ER from which they are handed over to mitochondria.

I.4. Connection with other organelles

Membrane contact sites (MCSs) are sites of close apposition between different subcellular compartments. At MCS the organelle membranes never fuse but exchange lipids, ions (*e.g.* Ca^{2+}) or other molecules through specific complexes and thus participate to the metabolic regulation of organelles (Elbaz and Schuldiner, 2011). Studies have demonstrated that MCSs can have redundant function and that they are regulated according to the carbon sources or cell status (Elbaz-Alon *et al.,* 2014; Hönscher *et al.,* 2014). When studying MCS, it is important to consider their connections and cross-talk to completely understand their functions. For example, when yeast cells are grown on non-fermentable carbon source, the connection between vacuoles and mitochondria (vacuole and mitochondria patches, vCLAMPs) are disrupted, while contacts between mitochondria and the endoplasmic reticulum (ER) (ER-mitochondria encounter structure, ERMES) increase (Hönscher *et al.,* 2014). Moreover, the simultaneous depletion of ERMES and vCLAMP is lethal in yeast cells confirming that there is an interplay between the two structures (Elbaz-Alon *et al.,* 2014). MCS are particularly important for mitochondria that are excluded from the endomembrane system since making contacts with other organelles is a mean for them to communicate and exchange molecules.

I.4.1. ER-mitochondria encounter structure; ERMES

Mitochondria and ER are connected *via* a protein complex named ERMES (**Figure ChI.I-4**). The core components of the complex are the integral ER protein, Mmm1, the cytosolic Mdm12 protein and two mitochondrial outer membrane proteins, Mdm34 and Mdm10 (Kornmann *et al.,* 2009). The four proteins interact with each other, forming a few foci per cell at ER-mitochondria junctions (Boldogh *et al.,* 2003; Kornmann *et al.,* 2009; Youngman *et al.,* 2004). The analysis of mitochondrial phospholipid (PL) composition shows that loss of cytosolic Mdm12 and mitochondrial Mdm34 leads to a decrease in cardiolipin (CL) level, while loss of ER Mmm1 and mitochondrial Mdm10 triggers decrease of both phosphatidylethanolamine (PE) and CL (Kornmann *et al.,* 2009; Osman *et al.,* 2009). Moreover, ERMES mutants display a decrease in the rate of conversion from phosphatidylserine (PS) to PE to phosphatidylcholine (PC), indicating that ERMES complex may be directly involved in ER-mitochondria PL transport (Kornmann *et al.,* 2009). Beside its lipid transfer function, ERMES complex has other biological roles like distribution of mitochondrial nucleoids, and implications in mitophagy (Böckler and Westermann, 2014; Youngman *et al.,* 2004) Indeed, ERMES colocalizes with sites of mitophagosome formation. ERMES could be implicated in this process through its role in PLs synthesis for the expansion of the mitophagosome. The presence of ERMES is also required for the synthesis of Coenzyme Q (CoQ), which is essential for the transfer of electrons by the respiratory chain. The enzymes that synthesize CoQ form the CoQ synthome, which is located in the internal mitochondrial membrane facing the matrix but the major precursors of CoQ are synthesized in the ER. The CoQ precursors are thus transferred from the ER to the mitochondria through ERMES (Eisenberg-Bord *et al.,* 2019; Subramanian *et al.,* 2019). When ERMES is abolished, the connection of mitochondria with other compartments is mediated by other redundant MCSs (Lahiri *et al.,* 2014). For example, the ER and mitochondria can form contact sites through ER membrane protein complex (EMC) that interacts with the mitochondrial outer membrane protein Tom5. In contrast to ERMES which is absent in plants and metazoan, EMC is widely conserved among eukaryotes (Wideman *et al.,* 2013). The EMC is composed of 6 subunits (Emc1-6) and the absence of 5 of them triggers the reduction of PS to PE conversion that occurs in the mitochondria. Moreover, the quintuple mutant shows reduced contacts between ER and mitochondria and does not grow on non-fermentable carbon sources (Lahiri *et al.,* 2014). When the quintuple mutant contains a thermo-sensitive allele of *MMM1* (ERMES component), the cells are nonviable at restrictive temperature and the PS transfer to mitochondria is impaired (Lahiri *et al.,* 2014).

I.4.2. vCLAMPs

Another type of connection between mitochondria and the endomembrane system is the vacuole and mitochondria patches (vCLAMPs) (**Figure ChI.I-4**). In the yeast, formation of vCLAMPs relies on the protein Vps39, a component of the homotypic fusion and vacuole protein sorting (HOPS) complex (Elbaz-Alon *et al.*, 2014; Hönscher *et al.*, 2014). To tether the two compartments, Vps39 binds to the vacuolar protein Ypt7 and the mitochondrial protein Tom40 (González Montoro *et al.*, 2018). When ERMES components Mdm10 and Mdm12 are deleted, the overexpression of Vps39 triggers the expansion of vCLAMPs and ameliorates the growth defects of the ERMES mutants on fermentable carbon source. The lethal phenotype observed for ERMES mutants on non-fermentable carbon source was also partially rescued when Vps39 was overexpressed (Hönscher *et al.*, 2014). Moreover, mutants of Vps39 and ERMES are synthetically lethal and the depletion of ERMES complex in absence of vCLAMP leads to a severe alteration of mitochondrial PL homeostasis (Elbaz-Alon *et al.*, 2014). The endosomal protein Vps13 participates to another tethering complex between the vacuole and mitochondria *via* its interaction with vacuolar Ypt35 and mitochondrial Mcp1 (Bean *et al.*, 2018; A. Peter *et al.*, 2017). The analysis of suppressors of ERMES mutants identified two dominant mutations in Vps13 that can restore the phenotype associated with loss of ERMES (Lang *et al.*, 2015). One dominant allele of *VPS13* could restore the mitochondria morphology characteristic of ERMES mutants and also mtDNA stability, even if ERMES complex was not reassembled. When vCLAMPs are abolished on non-fermentable carbon source, Vps13 relocates to nucleus-vacuole junctions (NVJs) (Lang *et al.*, 2015). Another protein, which is at the interface of the ERMES, vCLAMP and NVJ is Lam6/Ltc1. However, loss of Lam6 does not affect the MCSs integrity, thus it is not essential for their formation but may be necessary for their cross-regulation (Elbaz-Alon *et al.*, 2015). This clearly demonstrates a direct cross-talk between nucleus, vacuoles, mitochondria and endoplasmic reticulum and some proteins could thus be at the interface and connect vCLAMPs, ERMES and NVJs.

I.5. Study of mitochondrial proteins using fluorescent proteins

With respect to the essential roles of mitochondria in eukaryotic cells, many efforts have been made to determine mitoproteomes (Malina *et al.*, 2018). However, the mitochondrial targeting signals within proteins can be cryptic and their prediction by algorithms is not always possible. Thus, in order to identify and visualize mitochondrial proteins, the approach consisting in fusing proteins to fluorescent proteins (FPs) has been extensively used and

A

B

Gly67

Tyr66

Thr65

C
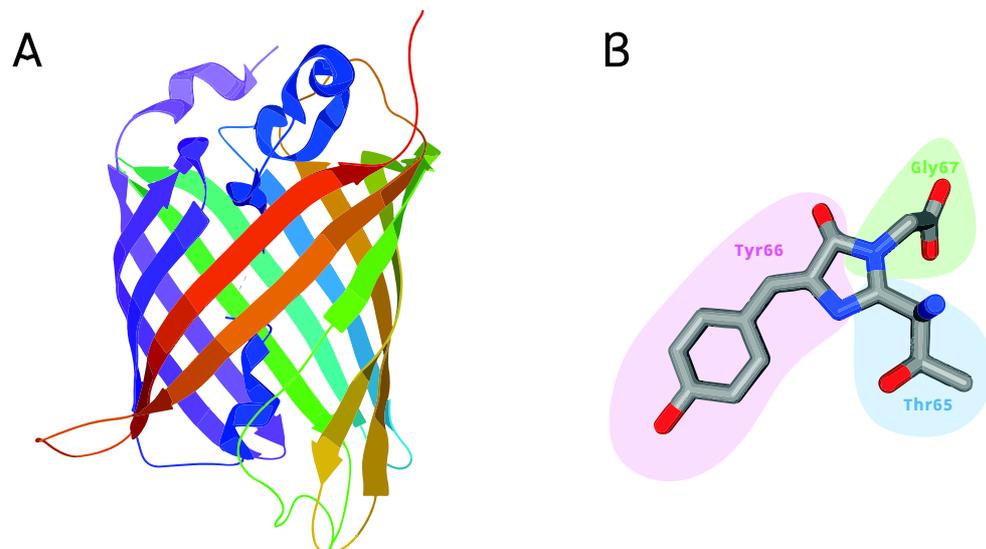
strand	β2		central helix				β4	β5		β7	β8		β10	λ (nm)		References
residue	30	39	64	65	66	80	99	105	145	153	163	171	206	Ex	Em	
avGFP	**Ser**	**Tyr**	**Phe**	**Ser**	**Tyr**	**Gln**	**Phe**	**Asn**	**Tyr**	**Met**	**Val**	**Ile**	**Ala**	**395/475**	**509**	Prasher *et al.*, 1992
frGFP			Leu	Thr		Arg	Ser			Thr	Ala			490	530	Waldo *et al.*, 1999
sfGFP	Arg	Asn	Leu	Thr		Arg	Ser	Thr	Phe	Thr	Ala	Val	Val	485	510	Pedelacq *et al.*, 2006

Figure ChI.I-5: Structure and composition of the superfolder GFP variant. A. Crystal structure of the superfolder (sf) GFP (PDB: 2B3P, [13]). The GFP is composed of 11 β-strands (each strand represented by a different color) and a central helix (dark blue) that contains the chromophore. **B.** The chromophore of the sfGFP is formed by the Thr, Tyr and Gly amino acid triade at positions 65,66 and 67 respectively. The mature chromophore is obtained upon cyclization, dehydration and oxidation of these three residues. **C.** The sequence of the initial *Aequorea victoria* GFP (avGFP) was mutated at some positions to obtain the soluble folding reporter (fr)GFP and finally the brighter sfGFP [13–15]. λ: wavelength.

among all the FPs the most famous of them remains the Green Fluorescent Protein (GFP).

The GFP from the jellyfish *Aequorea victoria* (avGFP) was first cloned in 1992 by Prasher and coworkers (Prasher *et al.,* 1992). It is composed of 238 aa organized in a 11-stranded barrel structure called "β-can" and a central helix containing the chromophore composed of three residues; Ser65, Tyr66 and Gly67. When expressed in *E. coli*, avGFP is poorly soluble. To overcome this issue, the avGFP was mutated to give rise to the folding reporter GFP (frGFP) (Waldo *et al.,* 1999), which displays better brightness and solubility when expressed alone. Nonetheless, this variant still exhibits folding defects when fused to other proteins. By expressing libraries of GFP variants N-terminally fused to poorly folded polypeptides in *E. coli*, Pedelacq and coworkers were able to isolate brighter clones corresponding to GFP variants still able to fold and they generated the superfoler GFP (sfGFP) variant (**Figure ChI.I-5**) (Pédelacq *et al.,* 2006).

Even though the GFP has been widely developed since its discovery, it still displays many limitations when it comes to its use for protein localization and even more in eukaryotic cells. Indeed, as explained in the introduction, eukaryotic cells are composed of different organelles and some proteins can simultaneously localize in different compartments. Thus, the precise identification of the subcellular localization of these multi-localized proteins by using the GFP fusions remains difficult. For proteins that localize in the cytosol and mitochondria, like the $_c$ERS in the yeast, it is nearly impossible because the cytosolic fluorescence will completely eclipse the mitochondrial signal (Frechin *et al.,* 2009).

II. Context of the study

Many efforts have been made to characterize the mitoproteome, but many mitochondrial proteins are yet not identified. The utilization of algorithms has been useful to identify proteins containing "classical" MTS but has shown limitations to unveil cryptic MTS sequences. The classical biochemical approaches, that were used for the identification of mitochondrial proteins, have many limitations. Moreover, it is almost impossible to obtain pure mitochondrial extracts because of the contact sites that occur in the cell between mitochondria and other organelles, like the vacuole or the endoplasmic reticulum. Disrupting these contacts sites could disturb the import of proteins in mitochondria and their composition. Another approach for the subcellular localization of proteins is the utilization of GFP-fused proteins. However, for dual-localized proteins, and especially for cytosolic and mitochondrial

Table ChI.I-1: Creation of the Split-GFP system and mutations present in the two fragments.

strand	β2		central helix					β4	β5				β7	β8				β10		β11			λ (nm)		
residues	30	39	64	65	66	67	80	99	105	111	128	145	153	163	166	167	171	205	206	221	223	225	Ex	Em	References
avGFP	Ser	Tyr	Phe	Ser	Tyr	Gly	Gln	Phe	Asn	Glu	Ile	Tyr	Met	Val	Lys	Ile	Ile	Ser	Ala	Leu	Phe	Thr	395/475	509	Prasher *et al.*, 1992
frGFP			Leu	Thr			Arg	Ser					Thr	Ala									490	530	Waldo *et al.*, 1999
sfGFP	Arg	Asn	Leu	Thr			Arg	Ser	Thr			Phe	Thr	Ala			Val		Val				485	510	Pedelacq *et al.*, 2006
GFP 1-10 OPT	Arg	Ile	Leu	Thr				Ser	Lys	Val	Thr	Phe	Thr		Thr	Val		Thr	Val						Cabantous *et al.*, 2005
GFP 11 M3																				His	Tyr	Asn			Cabantous *et al.*, 2005

The Split-GFP system is based on the separation of the Superfolder sfGFP [13] into two non-fluorescent fragments: GFP 1-10 and GFP 11 M3 that can self-assemble to reconstitute a fluorescent GFP [16].

echoforms, the discrimination between the cytosolic and mitochondrial fluorescence is impossible. It is even more dramatic for proteins, for which organelle pools are very limited. In this context, our team in collaboration with Pr. Roza KUCHARCZYK's team, developed a new microscopy tool called BiG Mito-Split-GFP that allows the specific fluorescent detection of mitochondrial echoforms. For this, we optimized the Split-GFP system developed by Cabantous and coworker (Cabantous *et al.*, 2005). In this system the eleven β strands of the GFP are separated into two optimized fragments, the GFP 1-10 OPT and GFP 11 M3 (named GFP$_{\beta1-10}$ and GFP$_{\beta11}$ in this work, see **Table ChI.I-1** for the mutations), that are non-fluorescent and can auto-assemble. In the strain we developed, the GFP$_{\beta1-10}$ fragment is encoded by the mitochondrial genome and thus sequestered in the mitochondrial matrix. On the other hand, the GFP$_{\beta11}$ fragment is fused to the protein of interest. If the GFP$_{\beta11}$ protein is indeed imported in the mitochondria, the GFP$_{\beta11}$ tag will be able to interact with the GFP$_{\beta1-10}$ fragment to reconstitute a fully functional and fluorescent GFP. By using this strain, it would thus be possible to detect proteins imported in the mitochondria by following the fluorescence using an ordinary epifluorescence microscope. The design of the two GFP fragments was performed by Dr. Y. Araiso, a former post-doctorate of the DyPS team. Pr. Roza KUCHARCZYK's team created the BiG Mito-Split-GFP strain in which the GFP$_{\beta1-10}$ fragment is stably expressed from the *ATP6* locus of the mitochondrial DNA. Dr. G. Bader, a former PhD student of the DyPS team, Dr. L. Enkler and myself created an expression plasmid library of aaRS, transcriptional and translational variants of aaRSs and other proteins from yeast, human and *Arabidopsis thaliana*, fused to the GFP$_{\beta11}$ tag in three consecutive copies, called in this thesis GFP$_{\beta11\textbf{chaplet}}$ or GFP$_{\beta11\textbf{ch}}$ (Bader, 2017). We then studied their mitochondrial localizations using the Big Mito-Split-GFP and further characterized their mitochondrial import signals. All the results we obtained led to the publication of a research article for which I am a second co-author (Bader *et al.*, 2020). In this thesis I will also present the study of mitochondrial import signals and especially $_c$ERS. Note that I also used the BiG Mito-Split-GFP to follow mitochondria during the process of autophagy using the epifluorescence microscope, experiments that have not yet been published but that are presented in **Chapter I section III.2**.

III.   Results & Discussion

III.1.   Research article 1: Bader *et al.,* 2020. eLife

eLife

Assigning mitochondrial localization of dual localized proteins using a yeast Bi-Genomic Mitochondrial-Split-GFP

Gaétan Bader[1‡§], Ludovic Enkler[1‡§], Yuhei Araiso[1†#], Marine Hemmerle[1†], Krystyna Binko[2], Emilia Baranowska[2], Johan-Owen De Craene[1¶], Julie Ruer-Laventie[3], Jean Pieters[3], Déborah Tribouillard-Tanvier[4**], Bruno Senger[1], Jean-Paul di Rago[4], Sylvie Friant[1], Roza Kucharczyk[2*], Hubert Dominique Becker[1*]

[1]Université de Strasbourg, CNRS UMR7156, Génétique Moléculaire, Génomique, Microbiologie, Strasbourg, France; [2]Institute of Biochemistry and Biophysics, Polish Academy of Sciences, Warsaw, Poland; [3]Biozentrum, University of Basel, Basel, Switzerland; [4]Institut de Biochimie et Génétique Cellulaires, CNRS UMR5095, Université de Bordeaux, Bordeaux, France

*For correspondence:
roza@ibb.waw.pl (RK);
h.becker@unistra.fr (HDB)

[†]These authors contributed equally to this work
[‡]These authors also contributed equally to this work
[**]Research Associate from INSERM

Present address: [§]Biozentrum, University of Basel, Basel, Switzerland; [#]Department of Clinical Laboratory Science, Division of Health Sciences, Graduate school of Medical Science, Kanazawa University, Kanazawa, Japan; [¶]EA 2106 Biomolécules et Biotechnologies Végétales, Université de Tours, Tours, France

Abstract A single nuclear gene can be translated into a dual localized protein that distributes between the cytosol and mitochondria. Accumulating evidences show that mitoproteomes contain lots of these dual localized proteins termed echoforms. Unraveling the existence of mitochondrial echoforms using current GFP (Green Fluorescent Protein) fusion microscopy approaches is extremely difficult because the GFP signal of the cytosolic echoform will almost inevitably mask that of the mitochondrial echoform. We therefore engineered a yeast strain expressing a new type of Split-GFP that we termed Bi-Genomic Mitochondrial-Split-GFP (BiG Mito-Split-GFP). Because one moiety of the GFP is translated from the mitochondrial machinery while the other is fused to the nuclear-encoded protein of interest translated in the cytosol, the self-reassembly of this Bi-Genomic-encoded Split-GFP is confined to mitochondria. We could authenticate the mitochondrial importability of any protein or echoform from yeast, but also from other organisms such as the human Argonaute 2 mitochondrial echoform.

Introduction

Mitochondria provide aerobic eukaryotes with adenosine triphosphate (ATP), which involves carbohydrates and fatty acid oxidation (*Saraste, 1999*), as well as numerous other vital functions like lipid and sterol synthesis (*Horvath and Daum, 2013*) and formation of iron-sulfur cluster (*Lill et al., 2012*). Mitochondria possess their own genome, remnant of an ancestral prokaryotic genome (*Gray, 2017*; *Margulis, 1975*) that has been considerably reduced in size due to a massive transfer of genes during eukaryotic evolution (*Thorsness and Weber, 1996*). As a result, most of the proteins required for mitochondrial structure and functions are expressed from the nuclear genome (>99%) and synthetized as precursors targeted to the mitochondria by mitochondrial targeting signals (MTS), that in some case are cleaved upon import (*Chacinska et al., 2009*). In the yeast *S. cerevisiae*, about a third of the mitochondrial proteins (mitoproteome) have been suggested to be dual localized (*Ben-Menachem et al., 2011*; *Dinur-Mills et al., 2008*; *Kisslov et al., 2014*), and have been named echoforms (or echoproteins) to accentuate the fact that two identical or nearly identical forms of a protein, can reside in the mitochondria and another compartment (*Ben-Menachem and Pines, 2017*). Due to these two coexisting forms and the difficulty to obtain pure mitochondria,

determination of a complete mitoproteome remains challenging and gave rise to conflicting results (*Kumar et al., 2002*; *Morgenstern et al., 2017*; *Reinders et al., 2006*; *Sickmann et al., 2003*).

Among all possible methods used to identify the subcellular destination of a protein, engineering green fluorescent protein (GFP) fusions has the major advantage that these fusions can be visualized in living cells using epifluorescence microscopy. This method is suitable to discriminate the cytosolic and mitochondrial pools of dual localized proteins when the cytosolic fraction has a lower concentration than the mitochondrial one (*Weill et al., 2018*). However, when the cytosolic echoform is more abundant than the mitochondrial one, this will inevitably eclipse the mitochondrial fluorescence signal. To bypass this drawback, we designed a yeast strain containing a new type of Split-GFP system termed Bi-Genomic Mitochondrial-Split-GFP (BiG Mito-Split-GFP) because one moiety of the GFP is encoded by the mitochondrial genome, while the other one is fused to the nuclear-encoded protein to be tested. By doing so, both Split-GFP fragments are translated in separate compartments and only mitochondrial proteins or echoforms of dual localized proteins trigger GFP reconstitution and can be visualized by fluorescence microscopy of living cells.

We herein first validated this system with proteins exclusively localized in the mitochondria and with the dual localized glutamyl-tRNA synthetase (cERS) that resides and functions in both the cytosol and mitochondria as we have shown previously (*Frechin et al., 2009*; *Frechin et al., 2014*). We next applied our Split-GFP strategy to the near-complete set of all known yeast cytosolic aminoacyl-tRNA synthetases. Interestingly, we discovered that two of them, cytosolic phenylalanyl-tRNA synthetase 2 (cFRS2) and cytosolic histidinyl-tRNA synthetase have a dual localization. We also confirmed the recently reported dual cellular location of cytosolic cysteinyl-tRNA synthetase (cCRS) (*Nishimura et al., 2019*). We further demonstrate that our yeast BiG Mito-Split-GFP strain can be used to better define non-conventional mitochondrial targeting sequences and to probe the mitochondrial importability of proteins from other eukaryotic species (human, mouse and plants). For instance, we show that the mammalian Argonaute 2 protein heterologously expressed in yeast localizes inside mitochondria.

Results

Construction of the BiG Mito-Split-GFP strain encoding the GFP$_{\beta1\text{-}10}$ fragment in the mitochondrial genome

We used the scaffold of the self-assembling Superfolder Split-GFP fragments designed by Cabantous and coworkers (*Cabantous et al., 2005b*; *Pédelacq et al., 2006*), where the 11 beta strands forming active Superfolder GFP are separated in a fragment encompassing the 10 first beta strands (GFP$_{\beta1\text{-}10}$) and a smaller one consisting of the remaining beta strand (GFP$_{\beta11}$). Seven amino acid (aa) residues of GFP$_{\beta1\text{-}10}$ and three of GFP$_{\beta11}$ were replaced in order to increase the stability and the self-assembly of both fragments (*Figure 1—figure supplement 1*). To increase the fluorescent signal and facilitate observation of low-abundant proteins, we concatenated and fused three β11 strands (GFP$_{\beta11\text{-chaplet;}\ \beta11ch}$) linked by GTGGGSGGGSTS spacers (see Materials and methods for DNA sequence, *Figure 1—figure supplement 1*, as in *Kamiyama et al., 2016*; *Figure 1A*).

Our objective was to integrate the gene encoding the GFP$_{\beta1\text{-}10}$ fragment into the mtDNA so that it will only be translated inside the mitochondrial matrix, while the GFP$_{\beta11ch}$ fragment is fused to the nuclear-encoded protein of interest and thus translated by cytosolic ribosomes (*Figure 1A*). To achieve this, we constructed a strain (RKY112) in which the coding sequence of the *ATP6* gene has been replaced by *ARG8m* (*atp6::ARG8m*), and where *ATP6* is integrated at the mitochondrial *COX2* locus under the control of the 5' and 3' UTRs of *COX2* gene (*Supplementary file 1*; *Table 1*; *Figure 1—figure supplement 2A–C*; see Materials and methods section for details). The RKY112 strain grew well on respiratory carbon source as wild type yeast (MR6) (*Figure 1B*), produced ATP effectively (*Figure 1C*), and expressed normally Atp6 and all the other mitochondria-encoded proteins (*Figure 1D*). We next integrated at the *atp6::ARG8m* locus of RKY112 strain mtDNA, the sequence encoding GFP$_{\beta1\text{-}10}$ (*Figure 1A*; *Figure 1—figure supplement 2*). To this end, we first introduced into the ρ^0 mitochondria (*i.e.* totally lacking mtDNA) of DFS160 strain, a plasmid carrying the *GFP$_{\beta1\text{-}10}$* sequence flanked by 5' and 3' UTR sequences of the native *ATP6* locus (pRK67, see Materials and methods for DNA sequence), yielding the RKY172 strain (bearing a non-functional synthetic ρ$^{\text{-S}}$ mtDNA, *Figure 1—figure supplement 2C*). This strain was crossed to RKY112 to enable

Figure 1. Engineering of the BiG Mito-Split-GFP system in *S. cerevisiae*. (**A**) Principle of the Split-GFP system. When present in the same subcellular compartment, two fragments of GFP namely GFP$_{\beta1-10}$ and GFP$_{\beta11ch}$ can auto-assemble to form a fluorescent BiG Mito-Split-GFP chaplet (three reconstituted GFPs). *GFP$_{\beta1-10}$* sequence encoding the first ten beta strands of GFP has been integrated into the mitochondrial genome under the control of the *ATP6* promoter. GFP$_{\beta11ch}$ consists of a tandemly fused form of the eleventh beta strand of GFP and is expressed from a plasmid under the control of a strong GPD promoter (pGPD). The molecular weight of the tag is indicated. (**B**) Growth assay on permissive SC Glu plates, respiratory plates (SC Gly), and restrictive media lacking arginine (SC Glu -Arg) of the different strains used in the study (N = 2). All generated strains are derivative from MR6. (**C**) ATP synthesis rates of the MR6 and RKY112 strains presented as the percent of the wild type control strain (N = 2). P-value was 0.7456 (not significant). 95% confidence interval was −273.4 to 229.9, R squared = 0.064 (**D**) Mitochondrial translation products in the MR6 and RKY112 strains (N = 2). Cells were grown in rich galactose medium. Pulse-chase of radiolabeled [^{35}S]methionine + [^{35}S]cysteine was performed by a 20 min incubation in the presence of cycloheximide. Total cellular extracts were separated by SDS PAGE in two different polyacrylamide gels prepared with a 30:0.8 ratio
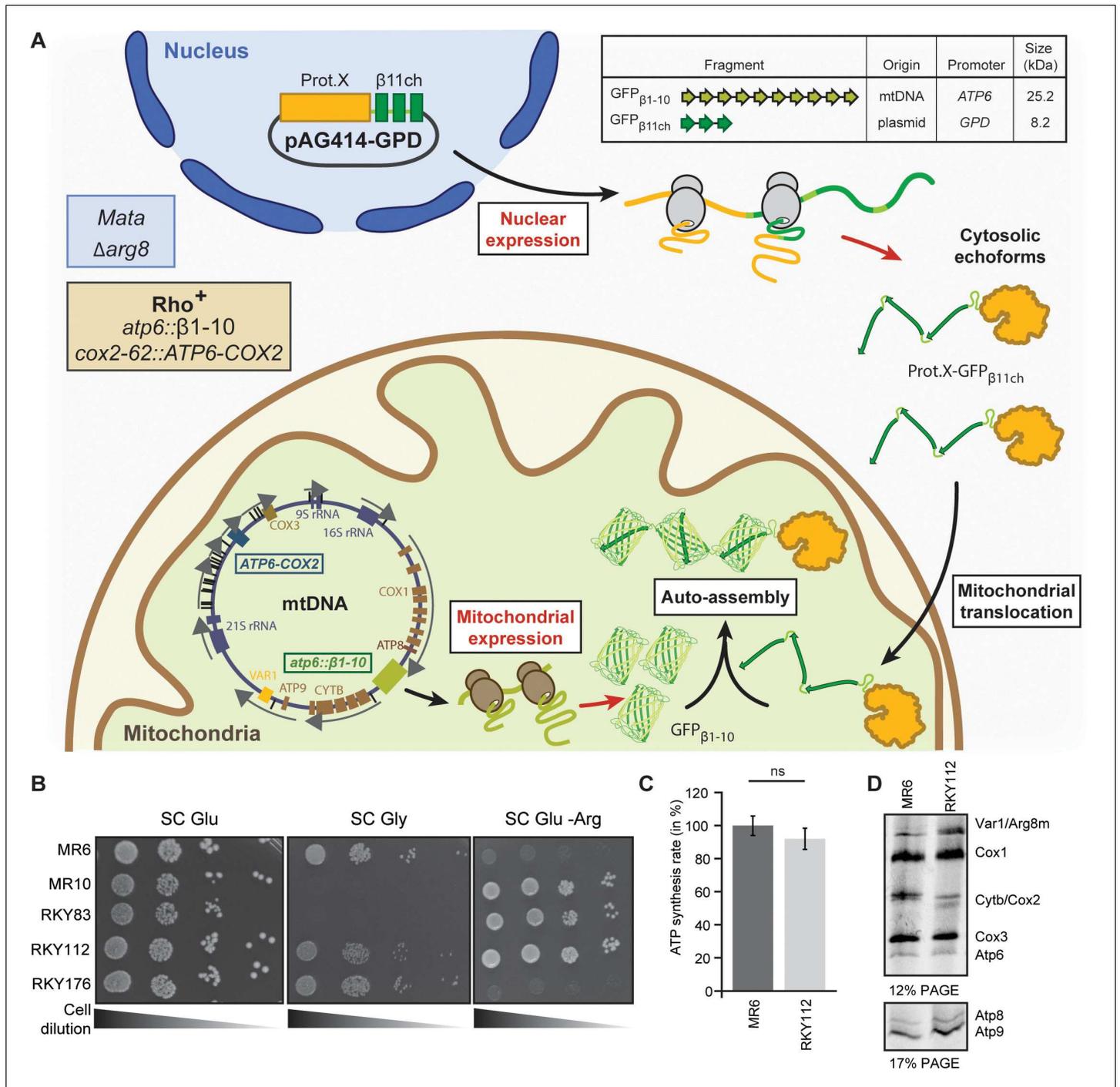*Figure 1 continued on next page*

Figure 1 continued

of acrylamide and bis-acrylamide. Upper gel: 12% polyacrylamide gel containing 4 M urea and 25% glycerol. Lower gel: 17.5% polyacrylamide gel. Gels were dried and exposed to X-ray film. The representative gels are shown.

The online version of this article includes the following source data and figure supplement(s) for figure 1:

Source data 1. Respiratory competency and translation of mtDNA-encoded respiratory subunits of the strains used in this study.

Source data 2. Statistics of the comparison of ATP synthesis rates between RKY112 and MR6 strains (related to *Figure 1C*).

Figure supplement 1. Optimized sequence and secondary structure of the GFP$_{\beta1-10}$ and GFP$_{\beta11ch}$ that were used in this study (related to *Figure 1*).

Figure supplement 2. Engineering of the strains and verification of the correct integration of *ATP6* under the control of *COX2* gene UTRs or *GFP$_{\beta1-10}$* under the control of *ATP6* gene UTRs (related to *Figure 1*).

---

replacement of *ARG8m* with *GFP$_{\beta1-10}$*. The desired recombinant clones, called RKY176, were identified by virtue of their incapacity to grow in media lacking arginine due to the loss of *ARG8m* and their capacity to grow in respiratory media (*Figure 1B*). Integration of *GFP$_{\beta1-10}$* in mtDNA was confirmed by PCR (*Figure 1—figure supplement 2E*, *Supplementary file 2*) and Western blot with anti-GFP antibodies (*Figure 2C*). Finally, the BiG Mito-Split-GFP strain (*Table 1*) was obtained by restoring the nuclear *ADE2* locus in order to eliminate interfering fluorescence emission of the vacuole due to accumulation of a pink adenine precursor (*Fisher, 1969*; *Kim et al., 2002*).

The BiG Mito-Split-GFP system restricts fluorescence emission to mitochondrially-localized proteins

The BiG Mito-Split-GFP system was first tested with Pam16 which localizes in the matrix at the periphery of the mitochondrial inner membrane and Atp4, an integral membrane protein with domains exposed to the matrix (*Kozany et al., 2004*; *Velours et al., 1988*; *Figure 2A*). The BiG Mito-Split-GFP host strain was transformed with centromeric plasmids expressing either Pam16$_{\beta11ch}$

Table 1. Genotypes of yeast strains used or generated for this study.

Strain	Nuclear genotype	mtDNA	Source
MR6	MATa ade2-1 his3-11,15 trp1-1 leu2-3,112 ura3-1 CAN1 arg8::HIS3	ρ^+	*Rak et al., 2007*
DFS160	MATα leu2Δ ura3-52 ade2-101 arg8::URA3 kar1-1	ρ^o	*Steele et al., 1996*
NB40-3C	MATa lys2 leu2-3,112 ura3-52 his3ΔHindIII arg8::hisG	ρ^+ cox2-62	*Steele et al., 1996*
MR10	MATa ade2-1 his3-11,15 trp1-1 leu2-3,112 ura3-1 CAN1 arg8::hisG	ρ^+ atp6::ARG8m	*Rak et al., 2007*
SDC30	MATα leu2Δ ura3-52 ade2-101 arg8::URA3 kar1-1	ρ^-COX2 ATP6	*Rak et al., 2007*
YTMT2	MATα leu2Δ ura3-52 ade2-101 arg8::URA3 kar1-1	ρ^+cox2-62	This study
RKY83	MATa ade2-1 his3-11,15 trp1-1 leu2-3,112 ura3-1 arg8::HIS3	ρ^+cox2-62 atp6::ARG8m	This study
RKY89	MATα leu2Δ ura3-52 ade2-101 arg8::URA3 kar1-1	ρ^-5'UTR$_{COX2}$ ATP6 3'UTR$_{COX2}$ COX2	This study
RKY112	MATa ade2-1 his3-11,15 trp1-1 leu2-3,112 ura3-1 arg8::HIS3	ρ^+ atp6::ARG8m 5'UTR$_{COX2}$ ATP6 3'UTR$_{COX2}$	This study
RKY172	MATα leu2Δ ura3-52 ade2-101 arg8::URA3 kar1-1	ρ^{-S} atp6::GFP$_{\beta1-10}$ COX2	This study
RKY176	MATa ade2-1 his3-11,15 trp1-1 leu2-3,112 ura3-1 CAN1 arg8::HIS3	ρ^+atp6::GFP$_{\beta1-10}$ 5'UTR$_{COX2}$ ATP6 3'UTR$_{COX2}$	This study
BiG Mito- Split-GFP	MATa his3-11,15 trp1-1 leu2-3,112 ura3-1 CAN1 arg8::HIS3	ρ^+atp6::GFP$_{\beta1-10}$ 5'UTR$_{COX2}$ ATP6 3'UTR$_{COX2}$	This study
BiG Mito- Split-GFP+PAM16$_{\beta11ch}$	MATa his3-11,15 trp1-1::PAM16$_{\beta11ch}$ leu2-3,112 ura3-1 CAN1 arg8::HIS3	ρ^+atp6::GFP$_{\beta1-10}$ 5'UTR$_{COX2}$ ATP6 3'UTR$_{COX2}$	This study
BiG Mito- Split-GFP+PGK1$_{\beta11ch}$	MATa his3-11,15 trp1-1::PGK1$_{\beta11ch}$ leu2-3,112 ura3-1 CAN1 arg8::HIS3	ρ^+atp6::GFP$_{\beta1-10}$ 5'UTR$_{COX2}$ ATP6 3'UTR$_{COX2}$	This study
BiG Mito- Split-GFP+GUS1$_{\beta11ch}$	MATa his3-11,15 trp1-1:: GUS1$_{\beta11ch}$ leu2-3,112 ura3-1 CAN1 arg8::HIS3	ρ^+atp6::GFP$_{\beta1-10}$ 5'UTR$_{COX2}$ ATP6 3'UTR$_{COX2}$	This study
BY 4742	MATα his3Δ1 leu2Δ0 lys2Δ0 ura3Δ0	ρ^+	*Winston et al., 1995*

• 77 •
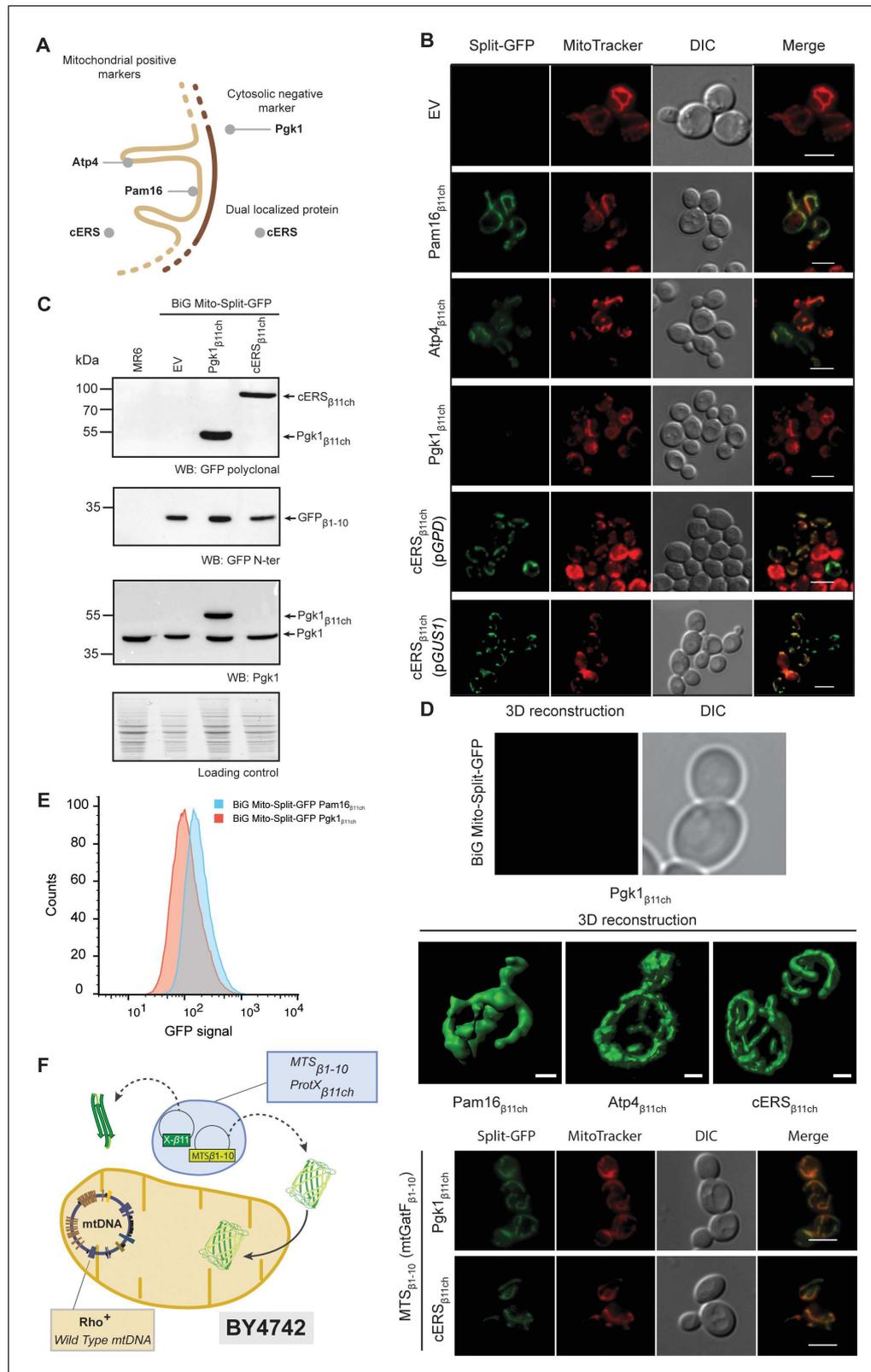
Figure 2. The reconstitution and fluorescence emission of the BiG Mito-Split-GFP is confined to mitochondria and exclusively generated by mitochondrial proteins. (A) Schematic of the spatial localization of proteins used as positive mitochondrial control proteins (Atp4, Pam16), negative cytosolic control protein (Pgk1) and as dual localized protein (cERS) in *S. cerevisiae*. (B) Empty pAG414pGPD$_{\beta11ch}$ vector (EV) or pAG414pGPD$_{\beta11ch}$ vectors expressing each of the four GFP$_{\beta11ch}$-tagged proteins used as markers in our study were transformed into the BiG Mito-Split-GFP strain. *Figure 2 continued on next page*

• 78 •

Figure 2 continued

cERS$_{β11ch}$ was either expressed under the dependence of the GPD (pGPD) or its own promoter (pGUS1) from a centromeric plasmid. GFP reconstitution upon mitochondrial import was followed by epifluorescence microscopy (N = 3). (**C**) Immunodetection of the GFP$_{β1-10}$, cERS$_{β11ch}$ and Pgk1$_{β11ch}$ fusion protein in whole cell extract from the transformed BiG Mito-Split-GFP strain using anti-GFP and -Pgk1 antibodies, confirming expression of Pgk1$_{β11ch}$. Loading control: stain-free. The representative gels are shown. (**D**) The strains described in the legend of panel (**B**) were used for three-dimensional reconstitution of yeast mitochondrial network (N = 1). Z-Stack images from Pam16$_{β11ch}$, Atp4$_{β11ch}$, cERS$_{β11ch}$ and Pgk1$_{β11ch}$ were taken using an Airyscan microscope. Scale bar: 1 μm. (**E**) Flow cytometry measurements of total GFP fluorescence of the BiG Mito-Split-GFP strain stably expressing Pgk1$_{β11ch}$ or Pam16$_{β11ch}$ (N = 3). (**F**) The mitochondrial GatF protein was fused to the GFP$_{β1-10}$ fragment (mtGatF $_{β1-10}$), thereby targeting the ten first GFP beta-strands to mitochondria after being transcribed in the nucleus and translated in the cytoplasm. This construct was co-expressed with either cERS$_{β11ch}$ or Pgk1$_{β11ch}$. The GFP reconstitution was monitored by epifluorescence microscopy. Mitochondria were stained with MitoTracker Red CMXRos. Scale bar: 5 μm. Representative fields are shown.

The online version of this article includes the following source data and figure supplement(s) for figure 2:

Source data 1. Micrographs of the BiG Mito-Split-GFP expressing Pgk1$_{β11ch}$, cERS$_{β11ch}$, Pam16$_{β11ch}$, (related to *Figure 2B*).

Source data 2. Confirmation of the expression of the GFP$_{β1-10}$, cERS$_{β11ch}$ and Pgk1$_{β11ch}$ fusion proteins in whole cell extract from the transformed BiG Mito-Split-GFP strains (Related to *Figure 2C*).

Source data 3. Flow cytometry measurements of total GFP fluorescence of the three biological replicates of the BiG Mito-Split-GFP strain stably expressing Pgk1$_{β11ch}$ or Pam16$_{β11ch}$ (related to *Figure 2F*).

Figure supplement 1. Mitochondrial relocation of mitochondrial proteins or echoforms tagged with GFP$_{β11}$ (related to *Figure 2*).

or Atp4$_{β11ch}$ bearing the GFP$_{β11ch}$ tag at their C-terminus under the constitutive GPD promoter. Expression of Pam16$_{β11ch}$ and Atp4$_{β11ch}$ resulted in strong GFP signal emissions that colocalized with MitoTracker Red CMXRos-stained mitochondria, whereas no fluorescence was detected with the corresponding empty plasmid (*Figure 2B*; *Figure 2—figure supplement 1A*). These observations confirmed that the GFP$_{β1-10}$ polypeptide is well expressed from the mtDNA, stably and correctly folded, allowing reconstitution of an active GFP upon association with the mitochondrial GFP$_{β11ch}$-tagged protein. So far, the positive controls we used for the proof of concept of the BiG Mito-Split-GFP approach are proteins more or less abundant: Atp4 (30000–40000 copies/cell) and Pam16 (3000 copies/cell) (*Morgenstern et al., 2017*; *Vögtle et al., 2017*). We will report soon, in BioRxiv, tests with other proteins with a known mitochondrial location and varying abundance to better estimate the sensitivity of the BiG Mito-Split-GFP system, including the GatF subunit of the GatFAB tRNA-dependent amidotransferase chromosomally expressed from its own promoter. This is a mitochondrial protein that has been reported to be present at only 40–80 copies (*Vögtle et al., 2017*).

We next tested the BiG Mito-Split-GFP system with a GFP$_{β11ch}$-tagged version of Pgk1, which is commonly used as negative cytosolic marker protein to probe the purity of mitochondrial preparations. Pgk1$_{β11ch}$ and endogenous Pgk1 were well detected by Western blot of total protein extracts probed with anti-Pgk1 antibodies (*Figure 2C*). No GFP fluorescence was observed with Pgk1$_{β11ch}$ (*Figure 2B*; *Figure 2—figure supplement 1A*) despite its good expression (*Figure 2C*). This is an interesting observation considering that Pgk1 localizes at the external surface of mitochondria (*Cobine et al., 2004*; *Kritsiligkou et al., 2017*; *Levchenko et al., 2016*). This provides the proof that the BiG Mito-Split-GFP system does not yield any unspecific fluorescence with cytosolic proteins even when they are externally associated to the organelle (see also Source data 4). Another negative control (His3) that further confirms the absence of false positive signal will be provided soon in Bio-Rxiv. In conclusion, these data show that any GFP$_{β11ch}$-tagged protein that localizes inside the mitochondrial matrix or at matrix side periphery of the inner membrane triggers GFP reconstitution and fluorescence emission, making this emission a robust in vivo readout for the mitochondrial importability of proteins of nuclear genetic origin.

We next tested whether the BiG Mito-Split-GFP system also allows visualization of the mitochondrial echoform of a protein located in both the cytosol and the organelle. We chose the cytosolic glutamyl-tRNA synthetase (cERS) encoded by the *GUS1* gene as a proof of concept. As we have shown, cERS is an essential and abundant protein of the cytosolic translation machinery, and a small fraction (15%) is located in mitochondria where it is required for mitochondrial protein synthesis and ATP synthase biogenesis (*Frechin et al., 2009*; *Frechin et al., 2014*). After transformation of the BiG Mito-Split-GFP strain with plasmids expressing a GFP$_{β11ch}$-tagged version of cERS under the control of either the GPD promoter (pGPD) or its own promoter (pGUS1), a GFP signal was observed only in

mitochondria (*Figure 2B*; *Figure 2—figure supplement 1A*). We also generated a stable BiG Mito-Split-GFP strain in which the gene encoding cERS$_{\beta11ch}$ was chromosomally expressed under the dependence of its own promoter at the *TRP1* locus (*Supplementary file 3*, *Figure 2—figure supplement 1B*). Again, GFP fluorescence was strictly confined to mitochondria (*Figure 2B*, *Figure 2—figure supplement 1A*). These observations demonstrate that the BiG Mito-Split-GFP system enables a specific detection in vivo of the mitochondrial pool of cERS ($_{mte}$cERS), without any interference by the cytosolic echoform, which is not possible when cERS is tagged with regular GFP (*Frechin et al., 2009*). We also expressed Pam16$_{\beta11ch}$ and Pgk1$_{\beta11ch}$ under the dependence of the GPD promoter at the *TRP1* locus. Again, as shown with the plasmid-borne strategy, Pam16$_{\beta11ch}$ expression resulted in a specific mitochondrial fluorescence, while Pgk1$_{\beta11ch}$ gave no fluorescence (*Figure 2—figure supplement 1B*).

Using high-resolution Airyscan confocal microscopy, a typical 3D mitochondrial network was reconstituted from the fluorescence induced by the expression of Pam16$_{\beta11ch}$, Atp4$_{\beta11ch}$ and cERS$_{\beta11ch}$ in the BiG Mito-Split-GFP strain whereas, as expected, no fluorescent at all was detected with Pgk1$_{\beta11ch}$ (*Figure 2D*), which further illustrates the mitochondrial detection specificity of this system. These data were corroborated by flow cytometry analyses of the BiG Mito-Split-GFP strain stably expressing Pam16$_{\beta11ch}$ and Pgk1$_{\beta11ch}$ (*Figure 2E*). These data will soon be completed (in Bio-Rxiv) with flow cytometry experiments aiming to know if the BiG Mito-Split-GFP system could be used in systematic screens for proteins with a mitochondrial localization.

We next evaluated whether the BiG Mito-Split-GFP approach represents a significant technical advance compared to the existing MTS-based Split-GFP methods that are currently used. To this end, we constructed cells (with a wild type mitochondrial genome) that co-express in the cytosol the mitochondrial protein GatF (with its own MTS) fused at its C-terminus with GFP$_{\beta1-10}$ (mtGatF$_{\beta1-10}$) and either cERS$_{\beta11ch}$ (dual localized, positive control) or Pgk1$_{\beta11ch}$ (cytosolic, negative control) (*Figure 2F*, left panel). As expected, a strong and specific mitochondrial fluorescent signal was obtained with cERS$_{\beta11ch}$ (*Figure 2F*, right panel). However, Pgk1$_{\beta11ch}$ resulted in a mitochondrial signal of similar intensity. This is presumably due to the location at the external surface of mitochondria of a small fraction of the Pgk1 pool that could interact with mtGatF$_{\beta1-10}$ prior to its import into the organelle. These results show that due to the high affinity of both self-assembling Split-GFP fragments, the MTS-based strategy can generate a mitochondrial fluorescence without mitochondrial protein internalization (*Figure 2F*, right panel). These experiments suggest that compartment-restricted expression of the GFP$_{\beta1-10}$ fragment and GFP$_{\beta11ch}$-tagged proteins increases the reliability of identifying mitochondrial echoforms of dual-localized proteins.

Screening for mitochondrial relocation of cytosolic aminoacyl-tRNA synthetases

Originally, screening cytosolic aminoacyl-tRNA synthetases (caaRSs) that can additionally relocate to mitochondria was motivated by several inconsistencies concerning this family of enzymes. The first and most documented example concerns cERS (*Frechin et al., 2009*; *Frechin et al., 2014*). We showed that the fraction of cERS which is imported ($_{mte}$cERS) into mitochondria is essential for the production of mitochondrial Gln-tRNA^{Gln} by the so-called transamidation pathway (*Frechin et al., 2009*; *Frechin et al., 2014*). In the latter, $_{mte}$cERS aminoacylates the mitochondrial tRNA^{Gln} with Glu thereby producing the Glu-tRNA^{Gln} that is then converted into Gln-tRNA^{Gln} by the GatFAB amido-transferase (AdT) (*Frechin et al., 2009*; *Frechin et al., 2014*). These results argued against the proposal that mitochondrial import of cQRS compensates for the absence of nuclear-encoded mtQRS in yeast (*Rinehart et al., 2005*). This being said, nothing excludes that cQRS can be imported into mitochondria to fulfill additional tasks beyond translation.

Another puzzling concern is the absence in *S. cerevisiae* of genes encoding six *stricto-senso* mtaaRSs: mtARS, mtCRS, mtGRS, mtHRS, mtQRS and mtVRS (*Table 2*). This suggests that the genes encoding their cytosolic equivalents ($_{cyte}$caaRS) might also encode their mitochondrial echoforms ($_{mte}$caaRSs). This has been confirmed for cARS, cGRS1, cHRS, cVRS for which alternative translation/transcription initiation allows the expression of both echoforms (*Figure 3D*; *Chang and Wang, 2004*; *Chatton et al., 1988*; *Chen et al., 2012*; *Natsoulis et al., 1986*; *Turner et al., 2000*).

We therefore applied the BiG Mito-Split-GFP strategy to the *S. cerevisiae* caaRSs (See *supplementary file 4*), aiming to discover new mitochondrial echoforms of caaRSs. We successfully expressed in the BiG Mito-Split-GFP strain the full length GFP$_{\beta11ch}$-tagged versions of 18 out of 20

Table 2. List of genes encoding *S. cerevisiae* cytosolic and mitochondrial aminoacyl-tRNA synthetases and their cytosolic or mitochondrial echoforms

	Gene coding for			
	aaRSs forms		aaRS echoforms	
aaRS	cytosolic (c)	mitochondrial (mt)	cytosolic (cyte)	mitochondrial (mte)
IRS	*ILS1*	*ISM1*	-	-
GRS	*GRS1/GRS2*	-	*GRS1*	*GRS1 −23*
SRS	*SES1*	*DIA4*	-	-
KRS	*KRS1*	*MSK1*	-	-
RRS	*RRS1*	*MSR1*	-	-
ERS	*GUS1*	*MSE1*	*GUS1*	*GUS1*
VRS	*VAS1*	-	*VAS1Δ46*	*VAS1*
YRS	*TYS1*	*MSY1*	-	-
MRS	*MES1*	*MSM1*	-	-
NRS	*DED81*	*SLM5*	-	-
PRS	*YHR020W*	*AIM10*	-	-
TRS	*THS1*	*MST1*	-	-
DRS	*DPS1*	*MSD1*	-	-
FRS	*FRS1 (β)/FRS2 (a)*	*MSF1 (a)*	-	-
CRS	*CRS1*	-	-	-
WRS	*WRS1*	*MSW1*	-	-
QRS	*GLN4*	-	-	-
ARS	*ALA1*	-	*ALA1*	*ALA1 −25*
LRS	*CDC60*	*NAM2*	-	-
HRS	*HTS1*	-	*HTS1Δ20*	*HTS1*

The *Saccharomyces* Genome Database standard gene names are used. The amino acid (aa) one-letter code is used for the aminoacyl-tRNA synthetase aa specificity and (-) means that the gene encoding the corresponding aaRS is missing. Two genes encode the cytosolic phenylalanyl-tRNA synthetase (cFRS) since the enzyme is an $\alpha_2\beta_2$ hetero-tetramer. For echoforms, the position of the alternative initiation start codon is indicated and corresponds to the nomenclature described in **Figure 3**; briefly, (- number) means that the start codon of the mteaaRS is located (number) aa upstream the one that starts translation of the corresponding cyteaaRS while (Δnumber) means that the start codon of the cyteaaRS is located (number) aa downstream the one that starts translation of the corresponding mteaaRS.

yeast caaRSs or cyteaaRSs (**Figure 3A–C**; **Figure 3—figure supplement 1**, **Supplementary files 3** and **4**). For unknown reasons, we failed to obtain the full-length GFP$_{\beta11ch}$-tagged versions of cCRS and cPRS despite repeated attempts, but successfully cloned the first hundred N-terminal aa residues of cCRS (N$_{100}$cCRS) (**Figure 3C**). An unambiguous mitochondrial fluorescent signal was observed with cFRS2$_{\beta11ch}$ (the α-subunit of the $\alpha_2\beta_2$ cFRS), cyteHRS$_{\beta11ch}$ and N$_{100}$cCRS$_{\beta11ch}$ (**Figure 3A–C**; **Figure 3—figure supplement 1**). Since the existence of a fully functional mtFRS has been demonstrated (**Koerner et al., 1987**), it is possible that supernumerary mtecFRS2 we identified is not necessary for charging mitochondrial tRNA^{Phe} but exerts some non-canonical functions, in addition to its role in cytosolic protein synthesis. The mitochondrial fluorescence triggered by expression of N$_{100}$cCRS$_{\beta11ch}$ suggests that this part of cCRS harbors a MTS, which has recently been proposed (**Nishimura et al., 2019**, see Discussion). The mitochondrial fluorescence triggered by cyteHRS$_{\beta11ch}$ is more intriguing. The most plausible hypothesis is that the MTS of the mtecHRS is longer than the one originally characterized. The other possibility is that there is indeed a second mitochondrial echoform of cHRS imported inside mitochondria through a cryptic MTS that has yet to be
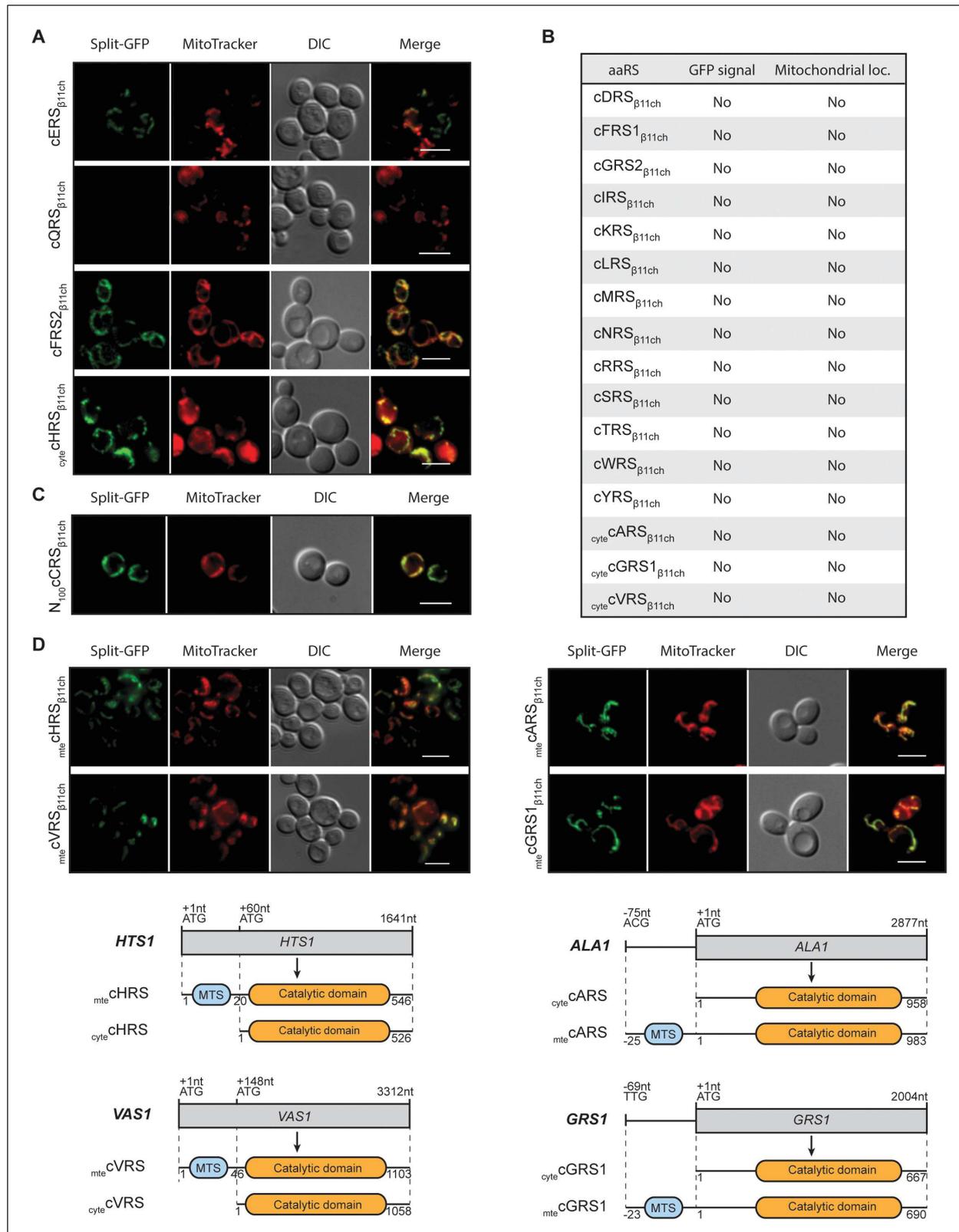
Figure 3. Identification and visualization of mitochondrial echoforms of yeast cytosolic aaRSs using the BiG Mito-Split-GFP strategy. Fluorescence microscopy analyses of BiG Mito-Split-GFP strain transformed with pAG414pGPD$_{\beta11ch}$ expressing yeast caaRSs (also see Table S3). Genes encoding 18 out of the 20 yeast caaRS, including those encoding the α- and β-subunits of the cytosolic $\alpha_2\beta_2$ FRS (cFRS2), and the cGRS2 pseudogene, as well as the four encoding the cytosolic echoforms of cGRS1 ($_{cyte}$cGRS1), cARS ($_{cyte}$cARS), cHRS ($_{cyte}$cHRS) and cVRS ($_{cyte}$cVRS) were cloned in the pAG414pGPD$_{\beta11ch}$

Figure 3 continued on next page

Cell Biology

Figure 3 continued

and expressed in the BiG Mito-Split-GFP strain (N = 2). (**A**) From the set of caaRSs tested, only cERS, cQRS, cFRS2 and $_{cyte}$cHRS micrographs are shown. (**B**) Table summarizing the GFP emission and mitochondrial localization of the caaRSs not shown in **A**). The corresponding micrographs are shown in Fig. S4A. (**C**) Fluorescence microscopy analysis of the BiG Mito-Split-GFP strain expressing the first 100 amino acids of the N-ter region of the cCRS fused to GFP$_{β11ch}$ (N = 2). (**D**) Fluorescence microscopy analyses of BiG Mito-Split-GFP strain transformed with pAG414pGPD$_{β11ch}$ expressing the mitochondrial echoforms $_{mte}$cGRS1, $_{mte}$cARS, $_{mte}$cHRS and $_{mte}$cVRS. Schematics of cARS, cGRS1, cHRS and cVRS echoforms expression in yeast. Expression can be initiated upstream of the initiator ATG$_{+1}$ ($_{mte}$cARS at ACG$_{-75}$ and $_{mte}$cGRS1 at TTG$_{-69}$) but the synthesis of this echoform can also be initiated at the ATG$_{+1}$. In this case, the expression of the cytosolic echoform is initiated downstream ($_{cyte}$cHTS at ATG$_{+60}$ and $_{cyte}$cVRS at ATG$_{+148}$). Mitochondria were stained with MitoTracker Red CMXRos. Scale bar: 5 µm. Representative fields are shown.

The online version of this article includes the following source data and figure supplement(s) for figure 3:

Source data 1. Confirmation, by WB, of the expression of the 18 full-length aaRS$_{β11ch}$ and N100cCRS$_{β11ch}$ in whole cell extracts from the transformed BiG Mito-Split-GFP strains (Related to ***Figure 3***).

Figure supplement 1. Screening of caaRSs and expression level of each GFP$_{β11ch}$-tagged proteins (related to ***Figure 3***).

identified and, like for cFRS2, this new $_{mte}$cHRS would then most probably exert a non-canonical function.

As already mentioned, cARS, cGRS1, cHRS and cVRS genes are known to produce both cytosolic and mitochondrial forms of these proteins (***Figure 3D***). When $_{mte}$cARS$_{β11ch}$, $_{mte}$cGRS1$_{β11ch}$, $_{mte}$cHRS$_{β11ch}$ and $_{mte}$cVRS$_{β11ch}$ (echoforms that start with the most upstream methionine initiator codon, ***Figure 3D***) were expressed in the BiG Mito-Split-GFP strain, a mitochondrial GFP staining was, as expected, observed with these four $_{mte}$caaRSs (***Figure 3D***). Conversely, $_{cyte}$cARS$_{β11ch}$, $_{cyte}$cGRS1$_{β11ch}$ and $_{cyte}$cVRS$_{β11ch}$, versions without their MTS) did not produce any detectable GFP signal confirming the MTS-dependency of these cytosolic echoforms for mitochondria localization (***Figure 3D***; ***Figure 3—figure supplement 1A***). The mitochondrial fluorescence produced by $_{cyte}$cHRS$_{β11ch}$ has already been discussed above.

Investigating non-conventional mitochondrial targeting signals in dual localized proteins

Unlike proteins with a MTS that is cleaved upon import into mitochondria, $_{mte}$cERS does not involve any processing (***Frechin et al., 2009***). Presumably, the mitochondrial targeting residues are located in the N-terminal (N-ter) region of cERS as in precursors of mitochondrial proteins destined to the matrix. To identify them, we tagged with GFP$_{β11ch}$ three N-ter domains of cERS of varying length that correspond to the first 30 (cERS$_{β11ch}$-N1), 70 (cERS$_{β11ch}$-N2) and 200 (cERS$_{β11ch}$-N3) residues of cERS (***Supplementary files 3*** and ***4***; ***Figure 4A***) and we tested their ability to be imported in the mitochondria of the BiG Mito-Split-GFP strain (***Figure 4B***). All three peptides produced a GFP fluorescence signal that matched the labeling of mitochondria with MitoTracker Red CMXRos (***Figure 4B***). Consistently, no GFP fluorescence was detected with cERS$_{β11ch}$ lacking the residues 1–30 or 1–200 (cERS$_{β11ch}$-ΔN1 and cERS$_{β11ch}$-ΔN2 respectively) (***Figure 4B***) despite detection by WB of these truncated proteins in cells (***Figure 4C***). For unknown reasons, cERS$_{β11ch}$-N1 and cERS$_{β11ch}$-N2 constructs were not detected by Western blot but gave a proper mitochondrial fluorescence staining (***Figure 4B*** and C). These data narrow down cERS' MTS to the 30 first aa residues of its N-ter domain; this segment is made of a short β-strand and a 13 aa long α-chain (***Simader et al., 2006***) likely harboring the import signal. This further illustrates the strength of our technique towards the identification of unconventional MTSs in dual localized proteins.

Testing mitochondrial importability of plant and mammalian proteins using the BiG Mito-Split-GFP system

The BiG Mito-Split-GFP system is based on modifications in the mitochondrial genome for expressing the GFP$_{β1-10}$ fragment inside the organelle. Modifying the mitochondrial genome is thus far only possible in *S. cerevisiae* and *Chlamydomonas reinhardtii* (***Remacle et al., 2006***). Owing to the high degree of conservation of mitochondrial protein import systems (***Lithgow and Schneider, 2010***), we used the yeast BiG Mito-Split-GFP strain to test the mitochondrial importability of proteins from various eukaryotic origins. We first tested two glutamyl-tRNA synthetases from *Arabidopsis thaliana*, *Ath*cERS and *Ath*mt/chlERS. According to independent MTS prediction tools, *Ath*cERS would be a cytosolic protein with a putative chloroplastic targeting signal (TargetP1.1), whereas *Ath*mt/chlERS is
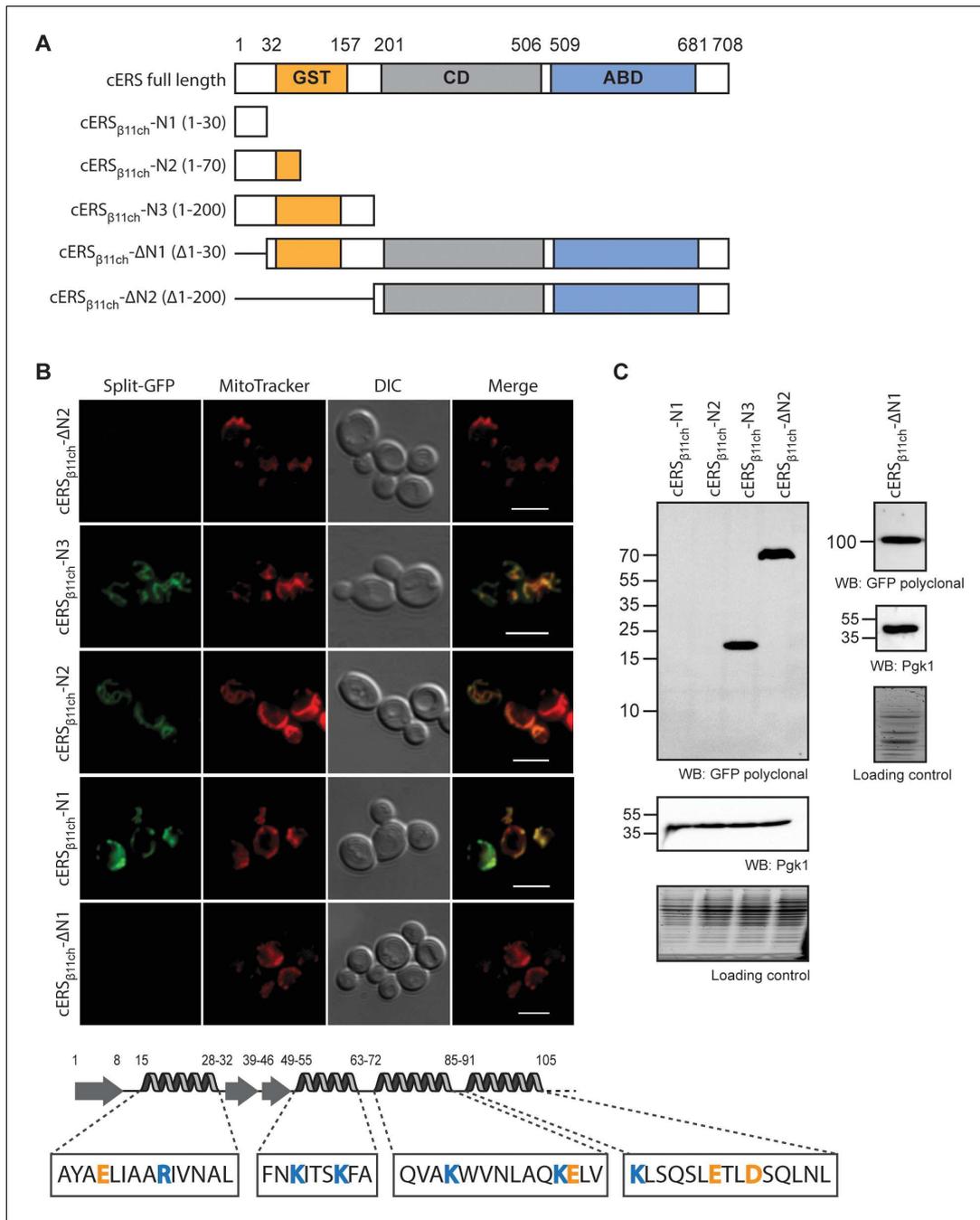
Figure 4. The BiG Mito-Split-GFP is a suitable tool to delimit regions containing non-canonical MTSs. (**A**) Schematic representation of the cERS fragments fused to GFP$_{\beta11ch}$. Orange boxes correspond to the GST-like domain necessary for Arc1 interaction (GST), the grey boxes represent the catalytic domain (CD), and the blue box, the tRNA-binding domain generally named anti-codon binding domain (ABD). Numbering above corresponds to cERS amino acids residues. (**B**) Fluorescence microscopy analyses of the BiG Mito-Split-GFP strain expressing the cERS variants shown on **A**. Mitochondria were stained with MitoTracker Red CMXRos; scale bar: 5 μm. The secondary structure (according to *Simader et al., 2006*) of the smallest peptide that still contains the non-conventional MTS of cERS is described together with the amino acid sequence of each helices. Positively and negatively charged amino acids are shown in orange and blue respectively. (**C**) Immunodetection of the cERS variants in BiG Mito-Split-GFP whole cell extracts using anti-GFP antibodies. Quantity of proteins loaded in each lane was estimated using anti-Pgk1 antibodies or by the stain-free procedure. The bands corresponding to the mutants N1 and N2 could not be detected. The representative fields or gel are shown.

The online version of this article includes the following source data and figure supplement(s) for figure 4:

Source data 1. Immunodetection of the cERS variants in BiG Mito-Split-GFP whole cell extracts using anti-GFP antibodies (related to *Figure 4C*).
Figure supplement 1. Analysis of N-terminal sequences of mitochondrial aaRSs and echoforms.

strongly predicted to be located in mitochondria and chloroplast (*Figure 5A*). cDNAs encoding the *Athc*ERS and *Ath*mt/chlERS proteins were fused to GFP$_{\beta11ch}$ (*Supplementary files 3* and *4*) and the resulting plasmids were transformed into the BiG Mito-Split-GFP strain. Expression of these proteins was confirmed by Western blot (*Figure 5C*). *Athc*ERS$_{\beta11ch}$ did not produce any GFP signal, whereas consistent with its predicted localization *Ath*mt/chlERS$_{\beta11ch}$ resulted in a specific mitochondrial fluorescence staining (*Figure 5B*). These data show that the yeast BiG Mito-Split-GFP system can be used to analyze mitochondrial localization of plant proteins.

We also used the BiG Mito-Split-GFP system to address a yet-unresolved question regarding the presence of mammalian Argonaute protein 2 (Ago2) in mitochondria. This protein mainly localizes to
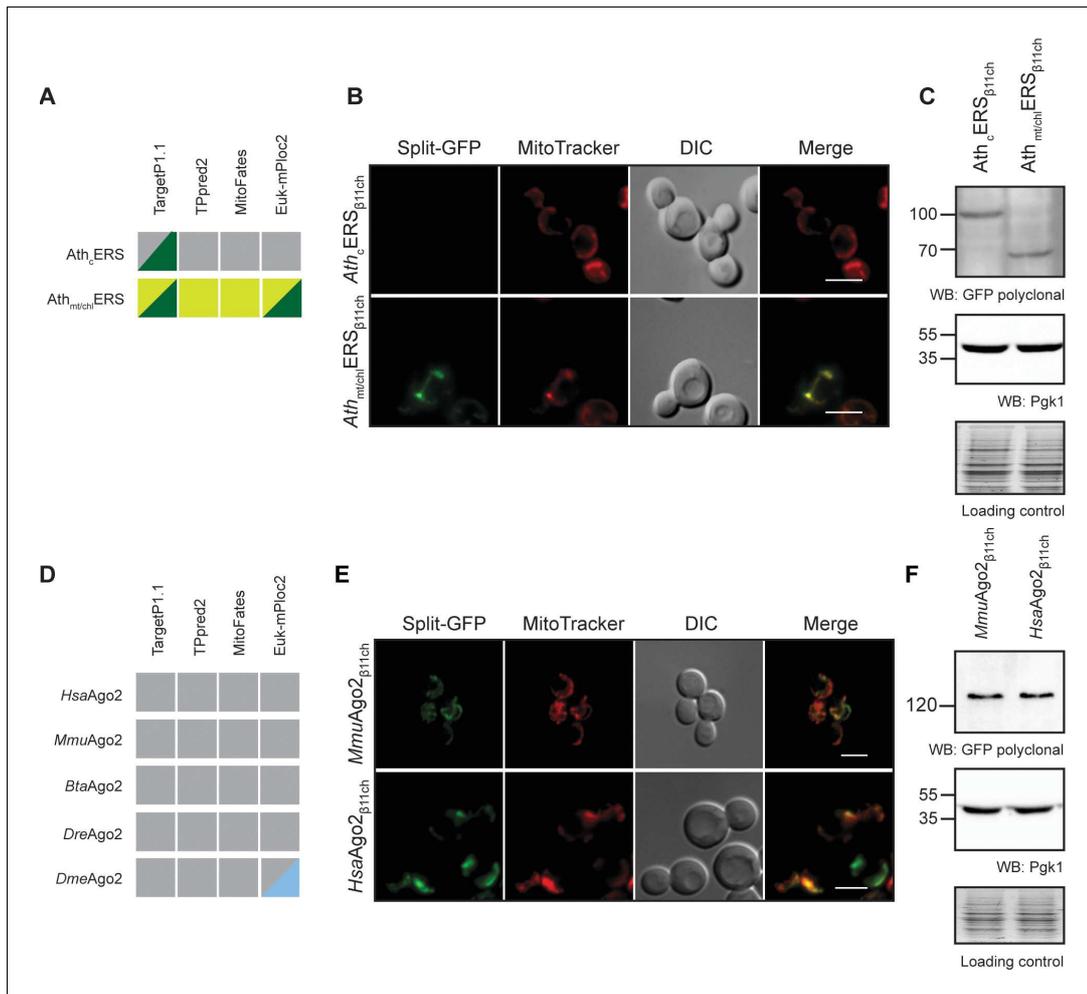
Figure 5. The BiG Mito-Split-GFP can be used to study mitochondrial importability of mammalian and plant proteins. (A, D) Prediction of MTS and mitochondrial localization of (A) two ERS from *Arabidopsis thaliana* (*Athc*ERS and *Ath*mt/chlERS) and (D) five eukaryotic Ago2 proteins [*Hsa*Ago2 (Protein argonaute-2 isoform X2 [Homo sapiens] NCBI sequence ID: XP_011515267.1), *Mmu*Ago2 (protein argonaute-2 *Mus musculus* NCBI sequence ID: NP_694818.3.), *Bta*Ago2 (*Bos Taurus*), *Dre*Ago2 (*Danio rerio*), *Dme*Ago2 (*Drosophila melanogaster*). MTS were predicted using TPpred2.0 (http://tppred2.biocomp.unibo.it/tppred2), TargetP1.1 (http://cbs.dtu.dk/services/TargetP/), MitoFates (http://mitf.cbrc.jp/MitoFates/cgibin/top.cgi) and the EukmPloc2 website (http://www.csbio.sjtu.edu.cn/bioinf/euk-multi-2/). Grey boxes indicate prediction of a cytosolic localization, light and dark green indicate prediction of mitochondrial or chloroplastic localization respectively. Blue boxes indicate prediction of nuclear localization. (B, E) Fluorescence microscopy analyses of the BiG Mito-Split-GFP strain expressing the GFP$_{\beta11ch}$-tagged $_{Ath}$cERS and $_{Ath}$mt/chlERS (N = 2) (B) and$_{Mmu}$Ago2, $_{Hsa}$Ago2 (N = 2) (E). Mitochondria were stained with MitoTracker Red CMXRos. Scale bar: 5 µm. Representative fields are shown. (C, E) Protein expression was checked by WB with anti-GFP antibodies and equal amount of loaded protein was controlled using anti-Pgk1 antibodies and by the stain-free technology (Loading control: stain-free). The representative gels are shown.
The online version of this article includes the following source data for figure 5:

Source data 1. Confirmation, by WB, of the expression of AthERS$_{\beta11ch}$ and mouse and human Ago2$_{\beta11ch}$ in whole cell extract from the transformed BiG Mito-Split-GFP strains (Related to *Figure 5C and F*).

the nucleoplasm and cell junctions where it is required for RNA-mediated gene silencing (RNAi) by the RNA-induced silencing complex (RISC) (**Hammond et al., 2000**). In some studies, Ago2 was suggested to be associated to mitochondria, but it remains unclear whether it localizes at the external surface or inside the organelle (**Barrey et al., 2011**; **Shepherd et al., 2017**). Using four different algorithms a potential MTS could not be predicted in Ago2 proteins from human, mouse, *Bos taurus*, *Danio rerio* and *Drosophila melanogaster*, casting doubts on the mitochondrial import of Ago2 (**Figure 5D**). To help resolve this question, the BiG Mito-Split-GFP yeast strain was transformed with plasmids expressing mouse and human Ago2$_{\beta11ch}$ proteins (*Mmu*Ago2$_{\beta11ch}$ and *Hsa*Ago2$_{\beta11ch}$, respectively, **Supplementary files 3** and **4**). Expression of each of these GFP$_{\beta11ch}$-tagged constructs was confirmed by WB, and both generated a solid and specific GFP fluorescence restricted to mitochondria (**Figure 5E and F**). These observations provide strong evidence that in addition to a cytosolic and nuclear location, Ago2 is also transported into mitochondria and is really a multi-localized protein with a mitochondrial echoform.

Discussion

Initially designed to study protein-protein interactions and solubility, the Split-GFP technology was almost immediately hijacked to track protein localization in various cell types and compartments (**Hyun et al., 2015**; **Kaddoum et al., 2010**; **Kamiyama et al., 2016**; **Külzer et al., 2013**; **Pinaud and Dahan, 2011**; **Van Engelenburg and Palmer, 2010**). It has also been used to study the mitochondrial localization of *PARK7* upon nutrient starvation (**Calì et al., 2015**), and to detect remodeling of MERCs (mitochondria-ER contact sites) in mammalian cells (**Yang et al., 2018**). Recently, Kakimoto and coworkers developed in yeast and mammalian cells a Split-based system to analyze inter-organelles contact sites (**Kakimoto et al., 2018**). However, in these approaches both GFP$_{\beta1-10}$ and GFP$_{\beta11}$ were anchored to proteins either translated in the cytosol or following the secretory pathway. Although the latter may avoid nonspecific interaction or reconstitution of the two GFP parts, we bring herein proofs that the simultaneous synthesis of both fragments in the cytosol, coupled to their high affinity to self-assemble, may induce potential false-positive GFP emission (**Figure 2F**).

To bypass this issue, we describe herein a new and robust Split-GFP system where the first 10 segments of beta barrel GFP (GFP$_{\beta1-10}$) is expressed from the mitochondrial genome and translated inside the organelle without interfering with mitochondrial function (**Figure 1C and D**). The remaining beta barrel is concatenated (GFP$_{\beta11ch}$), tagged to the protein of interest and expressed from cytosolic ribosomes. As a result, any detected GFP fluorescence obligatory originates from the organelle thereby demonstrating a mitochondrial localization for the tested proteins (**Figure 6A–B**).

This system was first successfully tested with two mitochondrial proteins (Atp4 and Pam16), and a cytosolic one (Pgk1) as a negative control. Moreover, the mitochondrial echoform of the cytosolic glutamyl-tRNA synthetase ($_{mte}$cERS) encoded by the *GUS1* nuclear gene was also detected with the BiG Mito-Split-GFP system (**Figures 2**, **3**, **4** and **6A**). As we already showed, synchronous release of cERS and cMRS from the cytosolic anchor Arc1 protein is required for a coordinated expression of mitochondrial and nuclear ATP synthase genes (**Frechin et al., 2009**; **Frechin et al., 2014**). Mitochondrial relocation of cERS is consistent with the functional plasticity of caaRSs with multiple locations in cells. Using GFP$_{\beta11ch}$-tagged N-ter segments of cERS, we localized its cryptic MTS within the first 30 aa residues. This region lacks amphiphilic residues (residues 15–28) and folds into a β-strand-loop-α−helix motif different than regular MTSs (**Roise et al., 1988**; **Simader et al., 2006**; **Figure 4**). These findings demonstrate that the BiG Mito-Split-GFP system allows not only to visualize in living cells the mitochondrial pool of proteins with multiple cellular locations, but also to decipher their non-conventional MTSs.

Recent efforts made to identify mitochondrial proteins and assign their submitochondrial localization revealed an exquisite precision (**Morgenstern et al., 2017**). However, resolving mitochondrial proteomes is challenging due to the difficulty of obtaining pure mitochondria and because many proteins transiently localize in mitochondria and are found elsewhere in cells. Up to 10–20% of the yeast mitoproteome was suggested to be composed of proteins with another location in cells (*i.e* the cytosol, the nucleus, ER…) (**Ben-Menachem and Pines, 2017**; **Morgenstern et al., 2017**). Our BiG Mito-Split-GFP system will be especially helpful to resolve these proteome complexities. This system was here applied to proteins involved in tRNA aminoacylation, some of which are well-known to relocate in different compartment to fulfill a wide range of cellular activities (**Han et al., 2012**;
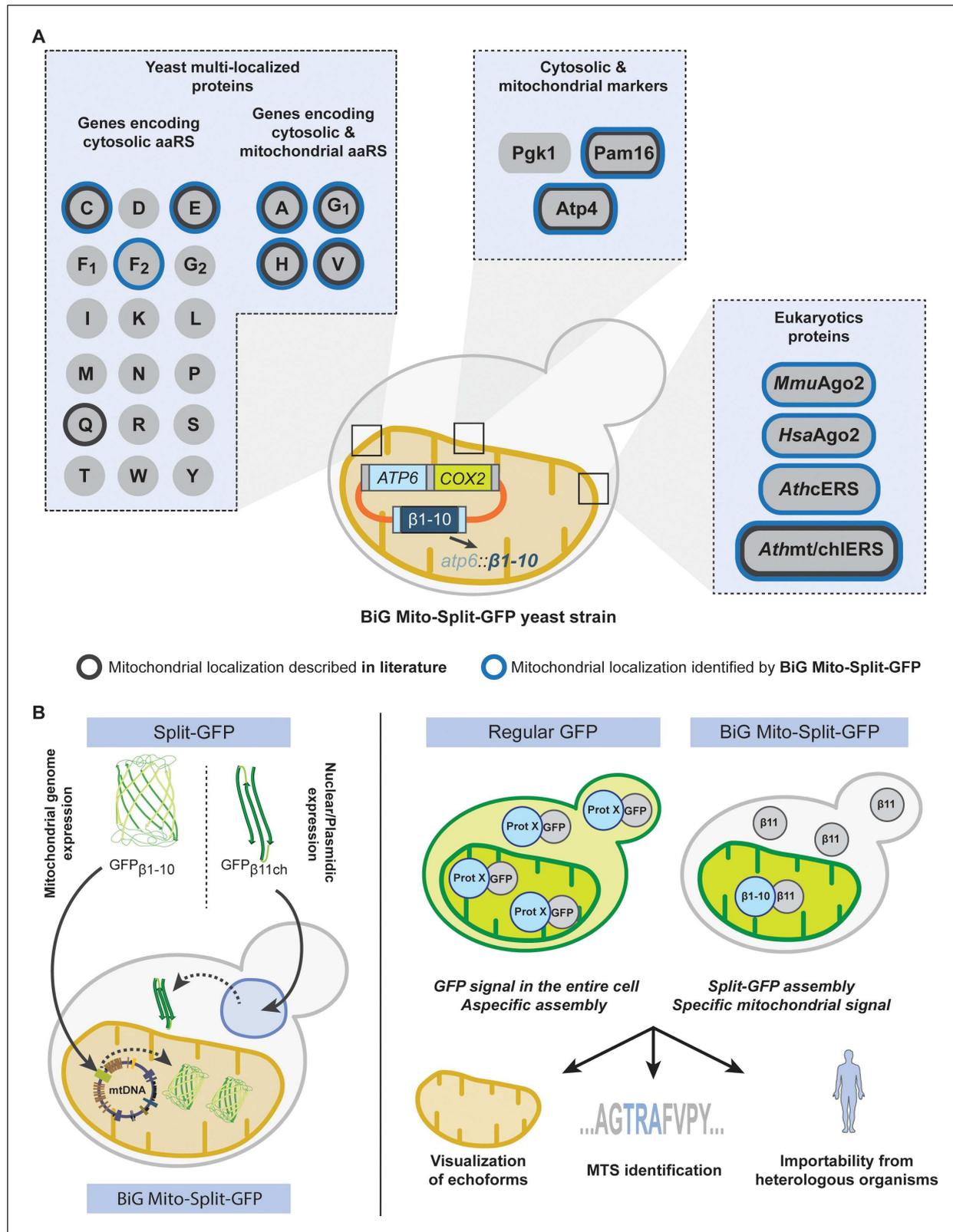
Figure 6. Schematic of the BiG Mito-Split-GFP system and its applications. (**A**) Using our engineered strain, we could show the dual localization of echoforms in the aaRS family of proteins and foster its power by studying localization of heterologous proteins originating from plants, mice and human. (**B**) The BiG Mito-Split-GFP strain was generated by integrating the sequence encoding the first 10 beta barrel segments into yeast mitochondrial DNA, and by either expressing any protein of interest fused to the 11th GFP segment from a plasmid or by integration in yeast nuclear

Figure 6 continued on next page

Figure 6 continued

DNA. As opposed to regular GFP-tagging where visualizing an echoform ultimately results in a GFP signal diffusing in the entire cell, our BiG Mito-Split-GFP system abolishes the fluorescence originating from cytosolic echoform to only display a specific mitochondrial signal. Further applications range from high-throughput experiments to identify relocating proteins involved in mitochondria homeostasis or metabolism, to identify non-conventional MTSs or seek for mitochondrial localization of heterologous proteins.

Ko et al., 2000; *Yakobov et al., 2018*). In this way, we provide strong evidence that cFRS2 and $_{cyte}$cHRS are dual localized as was observed for cERS, which suggests that these proteins may have additional roles beyond translation (*Figure 6A*). Being dually localized in the cytosol and mitochondria, and since there is no $_{mte}$cFRS1, it can be inferred that the catalytic α-subunit (cFRS2) is not inevitably in complex with the β-subunit within the $α_2β_2$ heterotetrameric form of cFRS. It will be interesting to test whether these findings in yeast extend to heterotetrameric cFRS from other eukaryotes, including humans. A *bona fide* mtFRS (encoded by the *MSF1* gene) that was shown to function as a monomer is essential to generate mitochondrial Phe-tRNA^{Phe} (F-$_{mt}$tRNA^F) in mitochondria (*Sanni et al., 1991*). This further supports the hypothesis that $_{mte}$cFRS2 is not required to produce F-$_{mt}$tRNA^F but more likely has a non-canonical yet-to-be-discovered function. Our failure to detect a mitochondrial echoform for cQRS is consistent with our previous findings (*Frechin et al., 2009*) that the only source of Q-$_{mt}$tRNA^Q in mitochondria is provided by the relocation of $_{mte}$cERS into the organelle (*Figure 3* and *Figure 3—figure supplement 1*) *de concert* with the tRNA-dependent Gat-FAB Adt (*Frechin et al., 2014*). This definitely casts in doubt the previous proposal of the existence of a cQRS mitochondrial echoform (*Rinehart et al., 2005*). In agreement with our results (*Figure 3C*), mitochondrial echoforms of cCRS were also detected in a recent study and shown to result from alternative transcription and translation starts (*Nishimura et al., 2019*), thereby unraveling how mtCRS is expressed from the *CRS1* gene and rationalizing how mitochondrial Cys-tRNA^{Cys} is produced.

Having identified new mitochondrial echoforms of caaRSs, we wondered if they carry in their N-terminal regions some common specific sequence or structural features possibly driving mitochondrial import. No specific motif was found using MAST/MEME analysis (*Bailey et al., 2009*), and there was no significant sequence similarity (as tested with Blast) (*Figure 4—figure supplement 1*). All but $_{mte}$cARS show at least one α−helix within their 50 first aa residues, and most (except cERS) are enriched in positively- vs negatively-charged aa residues, as in classical mitochondrial targeting sequences. Due to the lack of 3D structures, we cannot rule out that these N-termini adopt some specific ternary structure that are important for mitochondrial localization. As we have shown, most of the cytosolic form of cERS interacts with Arc1 in fermenting yeast, but during the diauxic shift, Arc1 expression is repressed, allowing the generation of a free pool of cERS able to relocate into mitochondria. Thus, in the case of this caaRS, interactions of its N-terminal domain seem to be important to distribute it between the cytosol and mitochondria. Future work is required to know whether such a mechanism operates also for the other dually localized caaRSs.

Our BiG Mito-Split-GFP system requires modifications of the mitochondrial genome, which can be achieved in only a limited number of organisms (*S. cerevisiae Bonnefoy and Fox, 2001* and *C. Reinhardtii Remacle et al., 2006*). However, due to the good evolutionary conservation of mitochondrial protein import, we reasoned that the system we developed in yeast could be used to test proteins of various eukaryotic origins, and we present evidence that this is indeed the case (*Figure 5*; *Figure 6C*). For instance, we showed that the mammalian Ago2 protein (*Hsa*- and *Mmu*Ago2, *Figure 5*) heterologously-expressed in yeast localize inside mitochondria. This protein was suggested to be exclusively located at the external surface of mitochondria in human cells where it would help the transport of pre- and miRNAs into the organelle, as do numerous nuclear-encoded pre- and miRNAs (*Bandiera et al., 2011*; *Barrey et al., 2011*; *Kren et al., 2009*). Several studies have suggested that mitochondrial miRNAs, also termed mitomiRs, play a role in apoptosis (*Kren et al., 2009*), mitochondrial functions (*Das et al., 2012*), and translation (*Bandiera et al., 2011*; *Jagannathan et al., 2015*; *Li et al., 2016*; *Zhang et al., 2014*), and this would require the mitochondrial import of Ago2 (*Bandiera et al., 2011*; *Das et al., 2012*; *Jagannathan et al., 2015*; *Li et al., 2016*; *Zhang et al., 2014*). However, the import of mitomiRs is still poorly understood and several possible import mechanisms have been evoked (*Barrey et al., 2011*; *Shepherd et al., 2017*). Our unambiguous detection

of Ago2 inside mitochondria of yeast cells expressing this protein sheds new light on its potential role in miRNAs import.

The yeast BiG Mito-Split-GFP system we describe here is designed to point out mitochondrial echoforms. It is robust, not expensive and can be used to test proteins from various organisms. This new approach has certainly many potential applications and opens new avenues in the study of mitochondria and their communications with other compartments of the cell.

Materials and methods

Key resources table

Reagent type (species) or resource	Designation	Source or reference	Identifiers	Additional information
Genetic reagent (*S. cerevisiae*)	BiG Mito- Split-GFP	This study		RKY176 strain with *ADE2* gene (ρ^+*atp6::GFP$_{\beta1-10}$* 5'UTR$_{COX2}$ ATP6 3 'UTR$_{COX2}$)
Genetic reagent (*S. cerevisiae*)	BiG Mito- Split-GFP+Pgk1$_{\beta11ch}$	This study		RKY176 strain (*PGK1:: β11ch::TRP1*)
Genetic reagent (*S. cerevisiae*)	BiG Mito- Split-GFP+PAM16$_{\beta11ch}$	This study		RKY176 strain (*PAM16:: β11ch::TRP1*)
Genetic reagent (*S. cerevisiae*)	BiG Mito- Split-GFP+cERS$_{\beta11ch}$	This study		RKY176 strain (*GUS1:: β11ch::TRP1*)
Antibody	Anti-GFP (Mouse polyclonal)	Sigma	Cat# G1544	WB (1:5000) Called GFP N-ter in *Figure 2C* recognizes GFPβ1–10
Antibody	Anti-GFP (Mouse monoclonal IgG$_1$κ clones 7.1 and 13.1)	Roche	Cat# 11814460001	WB (1:5000) Called GFP polyclonal in *Figure 2C* recognizes GFPβ11
Antibody	Anti-Pgk1 (Mouse monoclonal IgG1, clone 22C5D8)	Molecular Probes	Cat# 459250	WB (1:5000)
Recombinant DNA reagent	pAG414-p*GPD*-β11ch (plasmid)	This study		Template vector used for all constructs. Cloning done by Gibson assembly
Chemical compound, drug	MitoTracker Red CMXRos	ThermoFisher	Cat# M7512	Mitochondria staining
Chemical compound, drug	0.5% (v/v) 2,2,2-Trichloroethanol	Sigma	Cat# T54801	Used to detect total protein loading in SDS-PAGE, referred to Loading control

Construction of plasmids

ATP6 gene flanked by 75 bp of 5'UTR and 118 bp of 3'UTR of *COX2* was synthesized by Genescript and cloned at the EcoRI site of pPT24 plasmid bearing the sequence of *COX2* gene along with its UTRs (*Thorsness and Fox, 1993*), giving pRK49-2. The *GFP$_{\beta1-10}$* sequence (optimized for mitochondrial codon usage) encoding the first ten β-strands of GFP flanked by the regulatory sequences of *ATP6* gene and BamHI/EcoRI sites was synthesized by Genescript. The BamHI-EcoRI DNA fragment was cloned into pPT24 plasmid, giving the pRK67-2. The sequences of inserts were verified by sequencing.

The *GFP$_{\beta11ch}$* coding sequence, synthesized by Genescript, was subcloned into the pAG414 pGPD-ccdB vector to generate the pAG414pGPD-ccdB$_{\beta11ch}$. All genes encoding cytosolic or mitochondrial proteins were amplified from genomic DNA using the PrimeSTAR Max polymerase according to the manufacturer instructions (Takara), purified by PCR clean up (Macherey-Nagel) and subcloned either by Gateway (Thermofisher) (*Katzen, 2007*) or Gibson assembly (NEB)

(*Gibson et al., 2010*; *Gibson et al., 2009*) according to the manufacturer's instructions (see Table S2).

Construction of the BiG Mito-Split-GFP strain

The genotypes of strains used in this study are listed in *Table 1*. The ρ^+ indicates the wild-type complete mtDNA (when followed by deletion/insertion mutation it means the complete mtDNA with a mutation). The ρ^- synthetic genome (ρ^{-S}) was obtained by biolistic introduction into mitochondria of ρ^0 DFS160 strain (devoid of mitochondrial DNA) of the plasmids (pRK49-2 or pRK67-2) bearing indicated genes. The integration of *ATP6* gene into the mtDNA under the control of regulatory sequences of *COX2* was done using a previously described procedure (*Steele et al., 1996*). The pRK49-2 plasmid was introduced into mitochondria of DFS160 ρ^0 strain by ballistic transformation using the Particle Delivery Systems PDS-1000/He (*BIO-RAD*) as described (*Bonnefoy and Fox, 2001*), giving the ρ^{-S} strain RKY89. For the integration of the *ATP6* gene at the *COX2* locus, we first constructed a ρ^+ strain (RKY83, Fig. S2A) with a complete deletion of the coding sequence of *ATP6* (*atp6::ARG8m*) and a partial deletion in *COX2*, *cox2-62* (*Table 1*), by crossing YTMT2 (Matα derivative of strain NB40-3C carrying the *cox2-62* mutation (*Steele et al., 1996*) and MR10 (*atp6::ARG8m*) (*Rak et al., 2007*). After crossing, cells were allowed to divide during 20–40 generations to allow mtDNA recombination and mitotic segregation of the double mutation. The double *atp6::ARG8m cox2-62* mutant colonies were identified by crossing with the ρ^{-S} strain SDC30 (*Duvezin-Caubet et al., 2003*) that carries *ATP6* and *COX2* which restored the respiratory competence and by crossing with the YTMT2 strain, $\rho^+cox2-62$, which did not restored the respiratory competence of the double mutant. Next, the ρ^{-S} strain RKY89 was crossed with strain RKY83. This cross resulted in the respiratory competent progenies, named RKY112, which were growing on minimal medium without arginine (*Table 1*, *Figure 1B* and S2B). The ectopic integration of the *ATP6* gene into *COX2* locus was verified by PCR using oligonucleotides oAtp6-2, oAtp6-4, o5'UTR2 and o5'UTR1 (Table S1, Fig. S2D). To integrate $GFP_{\beta 1-10}$ into *ATP6* locus the ρ^{-S} strain RKY172 was obtained by biolistic transformation of DFS160ρ^0 with pRK67-2, as described above. RKY172 was crossed with RKY112, heterokaryons were allowed to divide during 20–40 generations to allow mtDNA recombination and mitotic segregation (Fig. S2C). The RKY176 progenies were selected by their respiratory competence and inability to grow on arginine depleted plates. The correct integration of the $GFP_{\beta 1-10}$ gene into *ATP6* locus was verified by PCR using oligonucleotides oAtp6-1, oAtp6-10, oXFP-pr and oXFP-lw (Table S1, Fig. S2E). Finally, *ADE2* WT sequence was amplified from the genomic DNA of a BY strain using oligonucleotides *ADE2* Fw and *ADE2* Rv (Table S2) and transformed into the RKY176 strain. Red/white colonies were then screened on adenine depleted plates to select *ADE2*-bearing RK176 strain.

Media and growth conditions

Yeast cell culture media and their composition: complete glucose YP medium (1% Bacto yeast extract, 1% Bacto peptone, 2% glucose, 40 mg/l adenine), complete YP Gal (1% Bacto yeast extract, 1% Bacto peptone, 2% galactose, 40 mg/l adenine), synthetic media composed of 0.67% (w/v) yeast nitrogen base without amino acids (aa), 0.5% (w/v) ammonium sulfate, either 2% (w/v) glucose (SC), galactose (SC Gal) or glycerol (SC Gly) and a mixture of aa and bases from Formedium (Norfolk, UK). Low sulfate medium LSM contained 0.67% (w/v) yeast nitrogen base without aa and ammonium sulphate, 2% galactose and 50 mg/L histidine, tryptophan, leucine, uracil, adenine, and arginine. The solid media contained 2% (w/v) of agar. Every strain was grown at 30°C with rotational shaking to mid-log ($OD_{600\ nm}$ = 0.7). SC Gal was filtered on 25 µm filters and not autoclaved before use.

Pulse-labelling of mitochondrially-synthesized proteins and ATP synthesis

Labeling of mitochondrial translation products was performed using the protocol described by *Barrientos, 2002*. Yeast cells were grown to early exponential phase (10^7 cells/mL) in 10 mL of liquid YP Gal medium. Cells were harvested by centrifugation and washed twice with LSM medium then suspended in the same medium and incubated for cysteine and methionine starvation for 2 hr at 28°C with shaking. Cells were suspended in 500 µL of LSM medium, and 1 mM cycloheximide was added. After a 5 min incubation at 28°C, 0.5 mCi of [^{35}S]methionine and [^{35}S]cysteine (Amersham

Biosciences) was added and cell suspension was further incubated for 20 min at 28°C. Total proteins were isolated by alkaline lysis and suspended in 50 µL of Laemmli buffer. Samples with the same level of incorporated radioactivity were separated by SDS-PAGE in 17.5% (w/v) acrylamide gels (to separate Atp8 and Atp9) or 12% (w/v) acrylamide containing 4 M urea and 25% (v/v) glycerol (to separate Atp6, Cox3, Cox2 and cytochrome b). After migration, the gels were dried and [^{35}S]-radio-labeled proteins were visualized by autoradiography with a PhosphorImager after a one-week exposure. To measure ATP synthase activities in the RKY112 strain, mitochondria were prepared by the enzymatic method as described in *Guérin et al., 1979*. For the rate of ATP synthesis, the mitochondria (0.15 mg/mL) were placed in a 1 mL thermostatically controlled chamber at 28°C in respiration buffer (0.65 M mannitol, 0.36 mM EGTA, 5 mM Tris-phosphate, 10 mM Tris-maleate pH 6.8) (*Rigoulet and Guerin, 1979*). The reaction was started by adding 4 mM NADH and 750 µM ADP; 100 µL aliquots were taken every 15 s and the reaction was stopped by adding 3.5% (v/v) perchloric acid and 12.5 mM EDTA. Samples were neutralized to pH 6.5 by KOH and 0.3 M MOPS. ATP was quantified using the Kinase-Glo Max Luminescence Kinase Assay (Promega) and a Beckman Coulter's Paradigm Plate Reader.

Flow cytometry analysis

5 mL of cells stably expressing Pam16$_{\beta11ch}$ and Pgk1$_{\beta11ch}$ strains (see *Table 1*) grown in YPD to confluence were diluted in 4 mL of SC Gal and grown overnight to reach mid-log phase. They were then diluted again in SC Gal and grown for 6 hr. Cells were then centrifuged and resuspended in water, passed for GFP detection on a BD FACS Canto II cytometer and Data analysis was performed using FlowJo.

Proteins extraction and western blots

10 mL of cells grown to mid-log phase were harvested and spin down 5 min at 2000 × *g* at room temperature (RT). Cells were suspended in 500 µL of deionized water, 50 µL of 1.85 M NaOH was added and the mixture was incubated 10 min on ice. After addition of 50 µL of TCA 100% and 10 min of incubation on ice, the total precipitate was pelleted by centrifugation 15 min at 13000 × *g* at 4°C. After removing the supernatant, pellets were suspended in 200 µL of Laemmli buffer (1×) supplemented with 20 µL of 1M Tris Base pH 8.

For each strain, 10 µL of total proteins were separated by SDS-PAGE on 8-, 10- or 12% (w/v) poly-acrylamide gels prior to electroblotting with a Trans-Blot Turbo system (*BIO-RAD*) onto PVDF membranes (*BIO-RAD*, #1704156). Detection was carried out using mouse monoclonal IgG anti-GFP primary antibodies (1:5000; Roche Clone 7.1 and 13.1) + mouse polyclonal for the recognition of GFP$_{\beta1-10}$ (1:5000, Sigma #G1544), and mouse monoclonal IgG1 anti-Pgk1 primary antibodies (1:5000; Molecular Probes Clone 22C5D8). Secondary antibodies were Goat anti-mouse IgG (H+L) HRP-conjugated antibodies (*BIO-RAD*; #1706516), at a concentration of 1:10000. ECL-plus reagents (*BIO-RAD*) was used according to the manufacturer's instructions and immuno-labeled proteins were revealed using a ChemiDoc Touch Imaging System (*BIO-RAD*). Total load of protein (Loading control) was assessed by UV detection using a ChemiDoc Touch Imaging System (*BIO-RAD*; Stain-free procedure) and detected by addition of 0.5% (v/v) 2,2,2-Trichloroethanol (Sigma #T54801) to the 30% acrylamide/bis-acrylamide solution.

Image acquisition and staining

Cells were incubated overnight in the appropriate media, diluted to an OD$_{600 \text{ nm}}$ of 0.3 prior to microscopy studies and stained after 6 hr of growth at 30°C. For mitochondria staining, cells were centrifuged 1 min at 1500 × *g* at room temperature, suspended in 1 mL of SC Gal supplemented with Red-Mitotracker CMXRos at a final concentration of 100 nM (Molecular Probes), and incubated 15 min at rotational shaking at 30°C. Cells were washed three times in one volume of deionized water, and suspended in 100 µL of deionized water for microscopic studies. Epifluorescence images were taken with an AXIO Observer d1 (Carl Zeiss) epifluorescence microscope using a 100 × plan apochromatic objective (Carl Zeiss) and processed with the Image J software. Images for 3D reconstruction were taken using a confocal LSM 780 high resolution module Airyscan with a 63 × 1.4 NA plan apochromatic objective (Carl Zeiss) controlled by the Zen Black 2.3 software (Carl Zeiss). Z-stack reconstruction was performed on the IMARIS 9.1.2 (Bitplane AG) software.

Additional information

Author contributions

Gaétan Bader, Conceptualization, Resources, Data curation, Formal analysis, Validation, Investigation, Methodology, Writing - original draft; Ludovic Enkler, Conceptualization, Resources, Data curation, Formal analysis, Investigation, Writing - original draft, Writing - review and editing; Yuhei Araiso, Conceptualization, Data curation, Formal analysis, Supervision, Validation, Investigation, Visualization, Methodology, Writing - original draft; Marine Hemmerle, Resources, Data curation, Formal analysis, Validation, Investigation, Visualization, Methodology, Writing - original draft; Krystyna Binko, Emilia Baranowska, Data curation, Formal analysis, Validation, Investigation, Visualization, Methodology; Johan-Owen De Craene, Conceptualization, Formal analysis, Supervision, Validation, Visualization, Writing - review and editing; Julie Ruer-Laventie, Data curation, Formal analysis, Validation, Investigation, Visualization, Methodology, Writing - original draft; Jean Pieters, Resources, Data curation, Supervision; Déborah Tribouillard-Tanvier, Formal analysis, Writing - review and editing; Bruno Senger, Conceptualization, Data curation, Formal analysis, Supervision, Validation, Investigation, Writing - review and editing; Jean-Paul di Rago, Conceptualization, Data curation, Formal analysis, Supervision, Validation, Writing - original draft, Writing - review and editing; Sylvie Friant, Data curation, Formal analysis, Validation, Investigation, Visualization, Writing - original draft, Writing - review and editing; Roza Kucharczyk, Conceptualization, Data curation, Formal analysis, Supervision, Funding acquisition, Validation, Investigation, Visualization, Writing - original draft, Project administration, Writing - review and editing; Hubert Dominique Becker, Conceptualization, Data curation, Formal analysis, Supervision, Funding acquisition, Validation, Writing - original draft, Project administration, Writing - review and editing

Author ORCIDs

Roza Kucharczyk (iD) https://orcid.org/0000-0002-8712-7535
Hubert Dominique Becker (iD) https://orcid.org/0000-0002-4102-7520

Decision letter and Author response

Additional files

Supplementary files

• Supplementary file 1. Sequence of the BamHI-EcoRI DNA fragment of GFP$_{\beta1-10}$ flanked by the regulatory sequences of *ATP6* gene Regulatory sequences of ATP6 are underlined, 5'-BamHI and 3'-EcoRI sites are in italicized bold characters. The GFP$_{\beta1-10}$ sequence is in gray background and has been codon-optimized to be expressed by *S. cerevisiae* mitochondrial translation machinery.

• Supplementary file 2. Primers used in the study to verify integration of ectopic *ATP6* or *GFP$_{\beta1-10}$* in mtDNA. The use of each oligo is described in the Materials and methods section.

• Supplementary file 3. Primers used for PCR amplifications of genes fused to GFP$_{\beta11ch}$ sequence. The primers in black and blue were used for Gateway and Gibson cloning methods respectively (see Material and methods section).

• Supplementary file 4. List of expression plasmids generated for this study.

• Transparent reporting form

Data availability

Source data for all figures showing blots and microscopy images have been provided.

References

Bailey TL, Boden M, Buske FA, Frith M, Grant CE, Clementi L, Ren J, Li WW, Noble WS. 2009. MEME SUITE: tools for motif discovery and searching. *Nucleic Acids Research* **37**:W202–W208. DOI: https://doi.org/10.1093/nar/gkp335, PMID: 19458158

Bandiera S, Rüberg S, Girard M, Cagnard N, Hanein S, Chrétien D, Munnich A, Lyonnet S, Henrion-Caude A. 2011. Nuclear outsourcing of RNA interference components to human mitochondria. *PLOS ONE* **6**:e20746. DOI: https://doi.org/10.1371/journal.pone.0020746, PMID: 21695135

Barrey E, Saint-Auret G, Bonnamy B, Damas D, Boyer O, Gidrol X. 2011. Pre-microRNA and mature microRNA in human mitochondria. *PLOS ONE* **6**:e20220. DOI: https://doi.org/10.1371/journal.pone.0020220, PMID: 21637 849

Barrientos A, Korr D, Tzagoloff A. 2002. Shy1p is necessary for full expression of mitochondrial COX1 in the yeast model of Leigh's syndrome. *The EMBO Journal* **21**:43–52. DOI: https://doi.org/10.1093/emboj/21.1.43, PMID: 11782424

Ben-Menachem R, Tal M, Shadur T, Pines O. 2011. A third of the yeast mitochondrial proteome is dual localized: a question of evolution. *Proteomics* **11**:4468–4476. DOI: https://doi.org/10.1002/pmic.201100199, PMID: 21 910249

Ben-Menachem R, Pines O. 2017. Detection of dual targeting and dual function of mitochondrial proteins in yeast. *Methods in Molecular Biology* **1567**:179–195. DOI: https://doi.org/10.1007/978-1-4939-6824-4_11, PMID: 28276019

Bonnefoy N, Fox TD. 2001. Genetic transformation *of Saccharomyces cerevisiae* mitochondria. *Methods in Cell Biology* **65**:381–396. DOI: https://doi.org/10.1016/s0091-679x(01)65022-2, PMID: 11381605

Cabantous S, Pédelacq JD, Mark BL, Naranjo C, Terwilliger TC, Waldo GS. 2005a. Recent advances in GFP folding reporter and split-GFP solubility reporter technologies application to improving the folding and solubility of recalcitrant proteins from Mycobacterium tuberculosis. *Journal of Structural and Functional Genomics* **6**:113–119. DOI: https://doi.org/10.1007/s10969-005-5247-5, PMID: 16211507

Cabantous S, Terwilliger TC, Waldo GS. 2005b. Protein tagging and detection with engineered self-assembling fragments of green fluorescent protein. *Nature Biotechnology* **23**:102–107. DOI: https://doi.org/10.1038/nbt1044, PMID: 15580262

Calì T, Ottolini D, Soriano ME, Brini M. 2015. A new split-GFP-based probe reveals DJ-1 translocation into the mitochondrial matrix to sustain ATP synthesis upon nutrient deprivation. *Human Molecular Genetics* **24**:1045–1060. DOI: https://doi.org/10.1093/hmg/ddu519, PMID: 25305074

Chacinska A, Koehler CM, Milenkovic D, Lithgow T, Pfanner N. 2009. Importing mitochondrial proteins: machineries and mechanisms. *Cell* **138**:628–644. DOI: https://doi.org/10.1016/j.cell.2009.08.005

Chang KJ, Wang CC. 2004. Translation initiation from a naturally occurring non-AUG Codon in *Saccharomyces cerevisiae*. *Journal of Biological Chemistry* **279**:13778–13785. DOI: https://doi.org/10.1074/jbc.M311269200, PMID: 14734560

Chatton B, Walter P, Ebel JP, Lacroute F, Fasiolo F. 1988. The yeast VAS1 gene encodes both mitochondrial and cytoplasmic valyl-tRNA synthetases. *The Journal of Biological Chemistry* **263**:52–57. PMID: 3275649

Chen SJ, Wu YH, Huang HY, Wang CC. 2012. *Saccharomyces cerevisiae* possesses a stress-inducible glycyl-tRNA synthetase gene. *PLOS ONE* **7**:e33363. DOI: https://doi.org/10.1371/journal.pone.0033363, PMID: 22438917

Cobine PA, Ojeda LD, Rigby KM, Winge DR. 2004. Yeast contain a non-proteinaceous pool of copper in the mitochondrial matrix. *Journal of Biological Chemistry* **279**:14447–14455. DOI: https://doi.org/10.1074/jbc.M312693200, PMID: 14729672

Das S, Ferlito M, Kent OA, Fox-Talbot K, Wang R, Liu D, Raghavachari N, Yang Y, Wheelan SJ, Murphy E, Steenbergen C. 2012. Nuclear miRNA regulates the mitochondrial genome in the heart. *Circulation Research* **110**:1596–1603. DOI: https://doi.org/10.1161/CIRCRESAHA.112.267732, PMID: 22518031

Dinur-Mills M, Tal M, Pines O. 2008. Dual targeted mitochondrial proteins are characterized by lower MTS parameters and total net charge. *PLOS ONE* **3**:e2161. DOI: https://doi.org/10.1371/journal.pone.0002161, PMID: 18478128

Duvezin-Caubet S, Caron M, Giraud MF, Velours J, di Rago JP. 2003. The two rotor components of yeast mitochondrial ATP synthase are mechanically coupled by subunit Delta. *PNAS* **100**:13235–13240. DOI: https://doi.org/10.1073/pnas.2135169100, PMID: 14581615

Fisher CR. 1969. Enzymology of the pigmented adenine-requiring mutants of Saccharomyces and Schizosaccharomyces. *Biochemical and Biophysical Research Communications* **34**:306–310. DOI: https://doi.org/10.1016/0006-291X(69)90832-8, PMID: 5767025

Frechin M, Senger B, Brayé M, Kern D, Martin RP, Becker HD. 2009. Yeast mitochondrial Gln-tRNA(Gln) is generated by a GatFAB-mediated transamidation pathway involving Arc1p-controlled subcellular sorting of cytosolic GluRS. *Genes & Development* **23**:1119–1130. DOI: https://doi.org/10.1101/gad.518109, PMID: 1 9417106

Frechin M, Enkler L, Tetaud E, Laporte D, Senger B, Blancard C, Hammann P, Bader G, Clauder-Münster S, Steinmetz LM, Martin RP, di Rago JP, Becker HD. 2014. Expression of nuclear and mitochondrial genes encoding ATP synthase is synchronized by disassembly of a multisynthetase complex. *Molecular Cell* **56**:763–776. DOI: https://doi.org/10.1016/j.molcel.2014.10.015, PMID: 25453761

Gibson DG, Young L, Chuang RY, Venter JC, Hutchison CA, Smith HO. 2009. Enzymatic assembly of DNA molecules up to several hundred kilobases. *Nature Methods* **6**:343–345. DOI: https://doi.org/10.1038/nmeth.1318, PMID: 19363495

Gibson DG, Glass JI, Lartigue C, Noskov VN, Chuang RY, Algire MA, Benders GA, Montague MG, Ma L, Moodie MM, Merryman C, Vashee S, Krishnakumar R, Assad-Garcia N, Andrews-Pfannkoch C, Denisova EA, Young L, Qi ZQ, Segall-Shapiro TH, Calvey CH, et al. 2010. Creation of a bacterial cell controlled by a chemically synthesized genome. *Science* **329**:52–56. DOI: https://doi.org/10.1126/science.1190719, PMID: 20488990

Gray MW. 2017. Lynn Margulis and the endosymbiont hypothesis: 50 years later. *Molecular Biology of the Cell* **28**:1285–1287. DOI: https://doi.org/10.1091/mbc.e16-07-0509, PMID: 28495966

Guérin B, Labbe P, Somlo M. 1979. Preparation of yeast mitochondria (*Saccharomyces cerevisiae*) with good P/O and respiratory control ratios. *Methods in Enzymology* **55**:149–159. DOI: https://doi.org/10.1016/0076-6879 (79)55021-6, PMID: 379498

Hammond SM, Bernstein E, Beach D, Hannon GJ. 2000. An RNA-directed nuclease mediates post-transcriptional gene silencing in *Drosophila* cells. *Nature* **404**:293–296. DOI: https://doi.org/10.1038/35005107, PMID: 1074 9213

Han JM, Jeong SJ, Park MC, Kim G, Kwon NH, Kim HK, Ha SH, Ryu SH, Kim S. 2012. Leucyl-tRNA synthetase is an intracellular leucine sensor for the mTORC1-signaling pathway. *Cell* **149**:410–424. DOI: https://doi.org/10. 1016/j.cell.2012.02.044, PMID: 22424946

Horvath SE, Daum G. 2013. Lipids of mitochondria. *Progress in Lipid Research* **52**:590–614. DOI: https://doi.org/ 10.1016/j.plipres.2013.07.002, PMID: 24007978

Hyun SI, Maruri-Avidal L, Moss B. 2015. Topology of endoplasmic Reticulum-Associated cellular and viral proteins determined with Split-GFP. *Traffic* **16**:787–795. DOI: https://doi.org/10.1111/tra.12281, PMID: 25761760

Jagannathan R, Thapa D, Nichols CE, Shepherd DL, Stricker JC, Croston TL, Baseler WA, Lewis SE, Martinez I, Hollander JM. 2015. Translational regulation of the mitochondrial genome following redistribution of mitochondrial MicroRNA in the diabetic heart. *Circulation. Cardiovascular Genetics* **8**:785–802. DOI: https:// doi.org/10.1161/CIRCGENETICS.115.001067, PMID: 26377859

Kaddoum L, Magdeleine E, Waldo GS, Joly E, Cabantous S. 2010. One-step split GFP staining for sensitive protein detection and localization in mammalian cells. *BioTechniques* **49**:727–736. DOI: https://doi.org/10. 2144/000113512, PMID: 20964633

Kakimoto Y, Tashiro S, Kojima R, Morozumi Y, Endo T, Tamura Y. 2018. Visualizing multiple inter-organelle contact sites using the organelle-targeted split-GFP system. *Scientific Reports* **8**:6175. DOI: https://doi.org/10. 1038/s41598-018-24466-0, PMID: 29670150

Kamiyama D, Sekine S, Barsi-Rhyne B, Hu J, Chen B, Gilbert LA, Ishikawa H, Leonetti MD, Marshall WF, Weissman JS, Huang B. 2016. Versatile protein tagging in cells with split fluorescent protein. *Nature Communications* **7**:11046. DOI: https://doi.org/10.1038/ncomms11046, PMID: 26988139

Katzen F. 2007. Gateway recombinational cloning: a biological operating system. *Expert Opinion on Drug Discovery* **2**:571–589. DOI: https://doi.org/10.1517/17460441.2.4.571, PMID: 23484762

Kim G, Sikder H, Singh KK. 2002. A colony color method identifies the vulnerability of mitochondria to oxidative damage. *Mutagenesis* **17**:375–381. DOI: https://doi.org/10.1093/mutage/17.5.375, PMID: 12202624

Kisslov I, Naamati A, Shakarchy N, Pines O. 2014. Dual-targeted proteins tend to be more evolutionarily conserved. *Molecular Biology and Evolution* **31**:2770–2779. DOI: https://doi.org/10.1093/molbev/msu221, PMID: 25063438

Ko YG, Kang YS, Kim EK, Park SG, Kim S. 2000. Nucleolar localization of human Methionyl–Trna Synthetase and Its Role in Ribosomal RNA Synthesis. *The Journal of Cell Biology* **149**:567–574. DOI: https://doi.org/10.1083/ jcb.149.3.567, PMID: 10791971

Koerner TJ, Myers AM, Lee S, Tzagoloff A. 1987. Isolation and characterization of the yeast gene coding for the alpha subunit of mitochondrial phenylalanyl-tRNA synthetase. *The Journal of Biological Chemistry* **262**:3690–3696. PMID: 3029120

Kozany C, Mokranjac D, Sichting M, Neupert W, Hell K. 2004. The J domain-related cochaperone Tim16 is a constituent of the mitochondrial TIM23 preprotein translocase. *Nature Structural & Molecular Biology* **11**:234–241. DOI: https://doi.org/10.1038/nsmb734, PMID: 14981506

Kren BT, Wong PY, Sarver A, Zhang X, Zeng Y, Steer CJ. 2009. MicroRNAs identified in highly purified liver-derived mitochondria may play a role in apoptosis. *RNA Biology* **6**:65–72. DOI: https://doi.org/10.4161/rna.6.1. 7534, PMID: 19106625

Kritsiligkou P, Chatzi A, Charalampous G, Mironov A, Grant CM, Tokatlidis K. 2017. Unconventional targeting of a thiol peroxidase to the mitochondrial intermembrane space facilitates oxidative protein folding. *Cell Reports* **18**:2729–2741. DOI: https://doi.org/10.1016/j.celrep.2017.02.053, PMID: 28297675

Külzer S, Petersen W, Baser A, Mandel K, Przyborski JM. 2013. Use of self-assembling GFP to determine protein topology and compartmentalisation in the *Plasmodium falciparum*-infected erythrocyte. *Molecular and Biochemical Parasitology* **187**:87–90. DOI: https://doi.org/10.1016/j.molbiopara.2012.11.004, PMID: 23271009

Kumar A, Agarwal S, Heyman JA, Matson S, Heidtman M, Piccirillo S, Umansky L, Drawid A, Jansen R, Liu Y, Cheung KH, Miller P, Gerstein M, Roeder GS, Snyder M. 2002. Subcellular localization of the yeast proteome. *Genes & Development* **16**:707–719. DOI: https://doi.org/10.1101/gad.970902, PMID: 11914276

Levchenko M, Lorenzi I, Dudek J. 2016. The degradation pathway of the mitophagy receptor Atg32 is Re-Routed by a posttranslational modification. *PLOS ONE* **11**:e0168518. DOI: https://doi.org/10.1371/journal. pone.0168518, PMID: 27992522

Li H, Zhang X, Wang F, Zhou L, Yin Z, Fan J, Nie X, Wang P, Fu XD, Chen C, Wang DW. 2016. MicroRNA-21 lowers blood pressure in spontaneous hypertensive rats by upregulating mitochondrial translation. *Circulation* **134**:734–751. DOI: https://doi.org/10.1161/CIRCULATIONAHA.116.023926, PMID: 27542393

Lill R, Hoffmann B, Molik S, Pierik AJ, Rietzschel N, Stehling O, Uzarska MA, Webert H, Wilbrecht C, Mühlenhoff U. 2012. The role of mitochondria in cellular iron–sulfur protein biogenesis and iron metabolism. *Biochimica Et Biophysica Acta (BBA) - Molecular Cell Research* **1823**:1491–1508. DOI: https://doi.org/10.1016/j.bbamcr.2012. 05.009

Lithgow T, Schneider A. 2010. Evolution of macromolecular import pathways in mitochondria, hydrogenosomes and mitosomes. *Philosophical Transactions of the Royal Society B: Biological Sciences* **365**:799–817. DOI: https://doi.org/10.1098/rstb.2009.0167

Margulis L. 1975. Symbiotic theory of the origin of eukaryotic organelles; criteria for proof. Symposia of the Society for Experimental Biology 21–38.

Morgenstern M, Stiller SB, Lübbert P, Peikert CD, Dannenmaier S, Drepper F, Weill U, Höß P, Feuerstein R, Gebert M, Bohnert M, van der Laan M, Schuldiner M, Schütze C, Oeljeklaus S, Pfanner N, Wiedemann N, Warscheid B. 2017. Definition of a High-Confidence mitochondrial proteome at quantitative scale. *Cell Reports* **19**:2836–2852. DOI: https://doi.org/10.1016/j.celrep.2017.06.014, PMID: 28658629

Natsoulis G, Hilger F, Fink GR. 1986. The HTS1 gene encodes both the cytoplasmic and mitochondrial histidine tRNA synthetases of *S. cerevisiae*. *Cell* **46**:235–243. DOI: https://doi.org/10.1016/0092-8674(86)90740-3, PMID: 3521891

Nishimura A, Nasuno R, Yoshikawa Y, Jung M, Ida T, Matsunaga T, Morita M, Takagi H, Motohashi H, Akaike T. 2019. Mitochondrial cysteinyl-tRNA synthetase is expressed via alternative transcriptional initiation regulated by energy metabolism in yeast cells. *Journal of Biological Chemistry* **294**:13781–13788. DOI: https://doi.org/10.1074/jbc.RA119.009203, PMID: 31350340

Pédelacq JD, Cabantous S, Tran T, Terwilliger TC, Waldo GS. 2006. Engineering and characterization of a superfolder green fluorescent protein. *Nature Biotechnology* **24**:79–88. DOI: https://doi.org/10.1038/nbt1172, PMID: 16369541

Pinaud F, Dahan M. 2011. Targeting and imaging single biomolecules in living cells by complementation-activated light microscopy with split-fluorescent proteins. *PNAS* **108**:E201–E210. DOI: https://doi.org/10.1073/pnas.1101929108, PMID: 21606345

Rak M, Tetaud E, Godard F, Sagot I, Salin B, Duvezin-Caubet S, Slonimski PP, Rytka J, di Rago JP. 2007. Yeast cells lacking the mitochondrial gene encoding the ATP synthase subunit 6 exhibit a selective loss of complex IV and unusual mitochondrial morphology. *Journal of Biological Chemistry* **282**:10853–10864. DOI: https://doi.org/10.1074/jbc.M608692200, PMID: 17261589

Reinders J, Zahedi RP, Pfanner N, Meisinger C, Sickmann A. 2006. Toward the complete yeast mitochondrial proteome: multidimensional separation techniques for mitochondrial proteomics. *Journal of Proteome Research* **5**:1543–1554. DOI: https://doi.org/10.1021/pr050477f, PMID: 16823961

Remacle C, Cardol P, Coosemans N, Gaisne M, Bonnefoy N. 2006. High-efficiency biolistic transformation of Chlamydomonas mitochondria can be used to insert mutations in complex I genes. *PNAS* **103**:4771–4776. DOI: https://doi.org/10.1073/pnas.0509501103, PMID: 16537419

Rigoulet M, Guerin B. 1979. Phosphate transport and ATP synthesis in yeast mitochondria: effect of a new inhibitor: the tribenzylphosphate. *FEBS Letters* **102**:18–22. DOI: https://doi.org/10.1016/0014-5793(79)80919-9, PMID: 378698

Rinehart J, Krett B, Rubio MA, Alfonzo JD, Söll D. 2005. *Saccharomyces cerevisiae* imports the cytosolic pathway for Gln-tRNA synthesis into the mitochondrion. *Genes & Development* **19**:583–592. DOI: https://doi.org/10.1101/gad.1269305, PMID: 15706032

Roise D, Theiler F, Horvath SJ, Tomich JM, Richards JH, Allison DS, Schatz G. 1988. Amphiphilicity is essential for mitochondrial presequence function. *The EMBO Journal* **7**:649–653. DOI: https://doi.org/10.1002/j.1460-2075.1988.tb02859.x, PMID: 3396537

Sanni A, Walter P, Boulanger Y, Ebel JP, Fasiolo F. 1991. Evolution of aminoacyl-tRNA synthetase quaternary structure and activity: *Saccharomyces cerevisiae* mitochondrial phenylalanyl-tRNA synthetase. *PNAS* **88**:8387–8391. DOI: https://doi.org/10.1073/pnas.88.19.8387, PMID: 1924298

Saraste M. 1999. Oxidative phosphorylation at the fin de siècle. *Science* **283**:1488–1493. DOI: https://doi.org/10.1126/science.283.5407.1488, PMID: 10066163

Shepherd DL, Hathaway QA, Pinti MV, Nichols CE, Durr AJ, Sreekumar S, Hughes KM, Stine SM, Martinez I, Hollander JM. 2017. Exploring the mitochondrial microRNA import pathway through polynucleotide phosphorylase (PNPase). *Journal of Molecular and Cellular Cardiology* **110**:15–25. DOI: https://doi.org/10.1016/j.yjmcc.2017.06.012, PMID: 28709769

Sickmann A, Reinders J, Wagner Y, Joppich C, Zahedi R, Meyer HE, Schönfisch B, Perschil I, Chacinska A, Guiard B, Rehling P, Pfanner N, Meisinger C. 2003. The proteome of *Saccharomyces cerevisiae* mitochondria. *PNAS* **100**:13207–13212. DOI: https://doi.org/10.1073/pnas.2135385100, PMID: 14576278

Simader H, Hothorn M, Köhler C, Basquin J, Simos G, Suck D. 2006. Structural basis of yeast aminoacyl-tRNA synthetase complex formation revealed by crystal structures of two binary sub-complexes. *Nucleic Acids Research* **34**:3968–3979. DOI: https://doi.org/10.1093/nar/gkl560, PMID: 16914447

Steele DF, Butler CA, Fox TD. 1996. Expression of a recoded nuclear gene inserted into yeast mitochondrial DNA is limited by mRNA-specific translational activation. *PNAS* **93**:5253–5257. DOI: https://doi.org/10.1073/pnas.93.11.5253, PMID: 8643562

Thorsness PE, Fox TD. 1993. Nuclear mutations in *Saccharomyces cerevisiae* that affect the escape of DNA from mitochondria to the nucleus. *Genetics* **134**:21–28. PMID: 8514129

Thorsness PE, Weber ER. 1996. Escape and migration of nucleic acids between chloroplasts, mitochondria, and the nucleus. *International Review of Cytology* **165**:207–234. DOI: https://doi.org/10.1016/s0074-7696(08)62223-8, PMID: 8900960

Turner RJ, Lovato M, Schimmel P. 2000. One of two genes encoding glycyl-tRNA synthetase in *Saccharomyces cerevisiae* provides mitochondrial and cytoplasmic functions. *The Journal of Biological Chemistry* **275**:27681–27688. DOI: https://doi.org/10.1074/jbc.M003416200, PMID: 10874035

Van Engelenburg SB, Palmer AE. 2010. Imaging type-III secretion reveals dynamics and spatial segregation of Salmonella effectors. *Nature Methods* **7**:325–330. DOI: https://doi.org/10.1038/nmeth.1437, PMID: 20228815

Velours J, Durrens P, Aigle M, Guérin B. 1988. ATP4, the structural gene for yeast F0F1 ATPase subunit 4. *European Journal of Biochemistry* **170**:637–642. DOI: https://doi.org/10.1111/j.1432-1033.1988.tb13745.x, PMID: 2892678

Vögtle FN, Burkhart JM, Gonczarowska-Jorge H, Kücükköse C, Taskin AA, Kopczynski D, Ahrends R, Mossmann D, Sickmann A, Zahedi RP, Meisinger C. 2017. Landscape of submitochondrial protein distribution. *Nature Communications* **8**:290. DOI: https://doi.org/10.1038/s41467-017-00359-0, PMID: 28819139

Weill U, Yofe I, Sass E, Stynen B, Davidi D, Natarajan J, Ben-Menachem R, Avihou Z, Goldman O, Harpaz N, Chuartzman S, Kniazev K, Knoblach B, Laborenz J, Boos F, Kowarzyk J, Ben-Dor S, Zalckvar E, Herrmann JM, Rachubinski RA, et al. 2018. Genome-wide SWAp-Tag yeast libraries for proteome exploration. *Nature Methods* **15**:617–622. DOI: https://doi.org/10.1038/s41592-018-0044-9, PMID: 29988094

Winston F, Dollard C, Ricupero-Hovasse SL. 1995. Construction of a set of *convenient Saccharomyces cerevisiae* strains that are isogenic to S288C. *Yeast* **11**:53–55. DOI: https://doi.org/10.1002/yea.320110107, PMID: 7762301

Yakobov N, Debard S, Fischer F, Senger B, Becker HD. 2018. Cytosolic aminoacyl-tRNA synthetases: unanticipated relocations for unexpected functions. *Biochimica Et Biophysica Acta (BBA) - Gene Regulatory Mechanisms* **1861**:387–400. DOI: https://doi.org/10.1016/j.bbagrm.2017.11.004

Yang Z, Zhao X, Xu J, Shang W, Tong C. 2018. A novel fluorescent reporter detects plastic remodeling of mitochondria–ER contact sites. *Journal of Cell Science* **131**:jcs208686. DOI: https://doi.org/10.1242/jcs.208686

Zhang B, Wang R, Du J, Niu J, Zhang R, Xu S, Niu X, Zhang Q, Nan Y. 2014. Upregulated microRNA-199a-5p inhibits nuclear receptor corepressor 1 translation in mice with nonalcoholic steatohepatitis. *Molecular Medicine Reports* **10**:3080–3086. DOI: https://doi.org/10.3892/mmr.2014.2592, PMID: 25269746

• 97 •
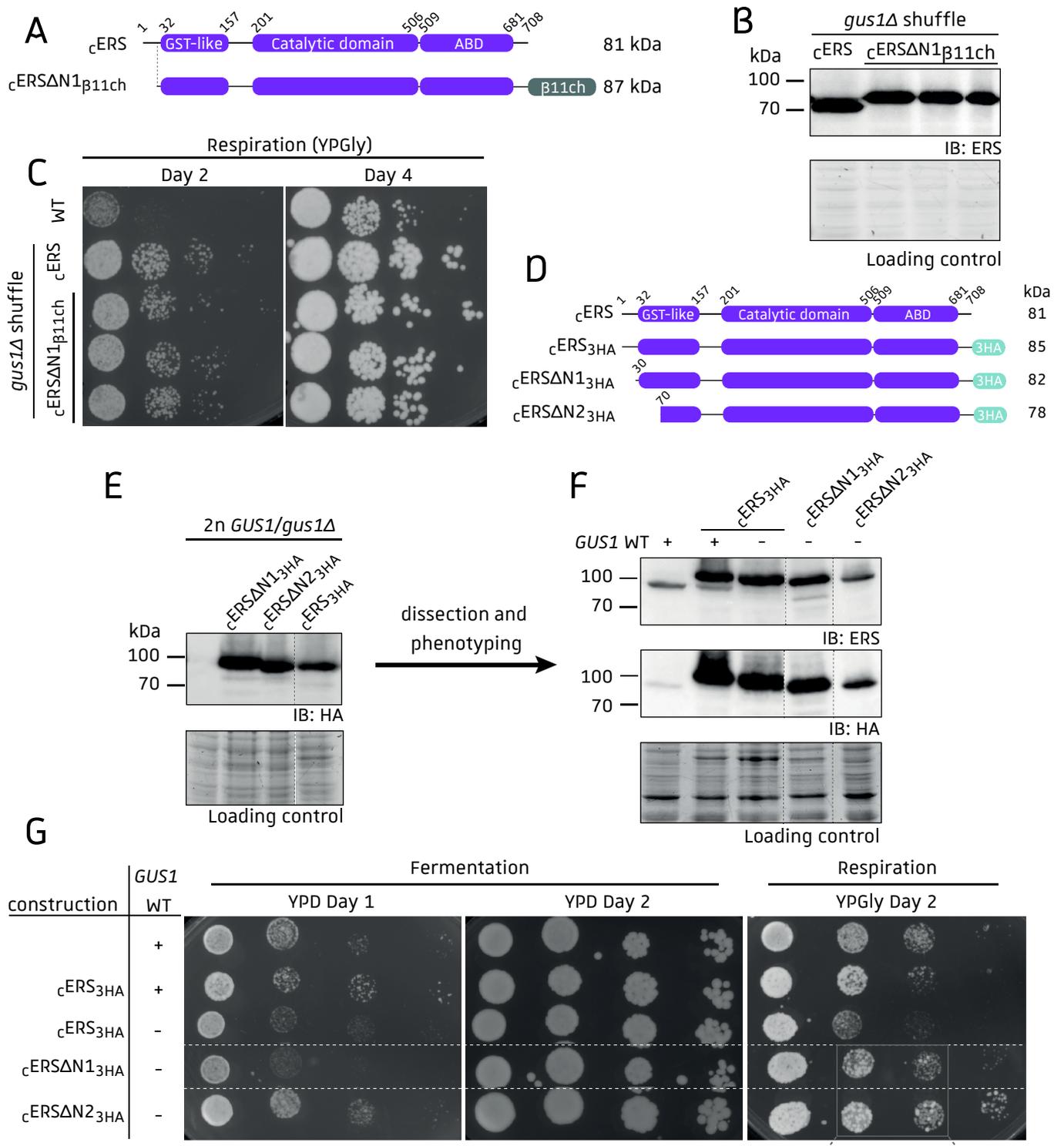
Figure ChI.R-1: Complementation of the *GUS1* deletion with ERS mutants and analysis of associated the respiratory phenotype. A. Schematic representation of the WT $_c$ERS and $_c$ERSΔN1$_{β11ch}$ mutant used in the shuffling experiment. ABD: Anticodon Binding Domain **B.** Verification of the expression of the proteins by Western blotting using anti-ERS primary antibody on the *gus1Δ* shuffle strain before transformation ($_c$ERS) and after transformation and shuffling ($_c$ERSΔN1$_{β11ch}$). **C.** Spotting assays on YPGly (respiration) medium after incubation at 30 °C. **D.** Schematic representation of the $_c$ERS mutant proteins transformed in the diploid *GUS1/gus1Δ*. **E.** Verification of the expression of the $_c$ERS deletion mutant proteins in the diploid *GUS1/gus1Δ* by Western blotting using anti-HA primary antibody before sporulation and dissection. **F.** The spores obtained after dissection were phenotyped and the expression of the constructions was verified by Western blotting with anti-ERS and anti-HA antibodies. **G.** Spotting assays on YPD (fermentation) and YPGly (respiration) for the spores containing the constructions of interest. **H.** Zoom in the spots obtained on YPGly. Suppressors colonies are highlighted by arrows.

III.2. ERS MTS identification

The mitochondrial role of $_c$ERS was first demonstrated by Frechin and coworkers, when they identified the $_c$ERS as the ND-ERS responsible for the aminoacylation of $_m$tRNA^{Gln} with Glu in the mitochondria (Frechin *et al.*, 2009). They also demonstrated that relocalization of $_c$ERS inside the mitochondria occurs during the diauxic shift, when *ARC1* expression is repressed (Frechin *et al.*, 2014). In these growth conditions, the newly synthesized $_c$ERS cannot associate with the cytosolic anchor protein Arc1. By using the BiG Mito-Split-GFP strain we developed we were able to visualize the mitochondrial pool of $_c$ERS and thus to confirm its localization. In order to identify $_c$ERS' MTS, we created GFP$_{β11ch}$-tagged $_c$ERS deletion mutants and could confirm that the signal for import was localized within the 30 first aa of $_c$ERS sequence. This $_c$ERSΔN1$_{β11ch}$ (Δ1-30) mutant protein should thus not be able to reach the mitochondria and sustain mitochondrial translation. In this regard, strains expressing $_c$ERSΔN1$_{β11ch}$ as the sole copy should not be able to grow under respiration conditions. To test this, I used a *gus1Δ shuffle* strain in which the endogenous *GUS1* essential gene has been deleted (*GUS1::HIS5*) and transferred onto a plasmid carrying the selection gene *URA3* (pRS316-*GUS1)*. I transformed this strain with the plasmid expressing cERSΔN1$_{β11ch}$ and the auxotrophy marker *TRP1* (**Figure ChI.R-1A**). In order to chase the plasmid containing the wild-type *GUS1* gene, the transformants were incubated on a solid medium containing 5-fluorooritic acid (5-FOA). Briefly, 5-FOA is a derivative of the pyrimidine precursor orotic acid, which can be converted in the toxic metabolite 5-fluorouracil by the oritidine-5'-phosphate decarboxylase encoded by *URA3*. Thus, cells that still contain the plasmid pRS316-*GUS1* (Ura$^+$ cells) will not be able to grow on medium supplemented with 5-FOA, while cells that chased the plasmid (Ura$^-$ cells) will grow, provided that the $_c$ERSΔN1$_{β11ch}$ mutant can complement the absence of *GUS1*. I was indeed able to obtain clones on medium supplemented with 5-FOA indicating that $_c$ERSΔN1$_{β11ch}$ can be the sole $_c$ERS. The absence of wild-type (WT) $_c$ERS and expression of $_c$ERSΔN1$_{β11ch}$ were verified by Western blot using an antibody directed against ERS (anti-ERS, **Figure ChI.R-1B**). I then performed drop tests on YPGly respiration medium using these strains (**Figure ChI.R-1C**). Unexpectedly, the strains expressing the truncated version as the sole $_c$ERS were still able to grow on the respiration medium. These somewhat contradictory results have to be analyzed in the light of those obtained with the BiG Mito-Split-GFP microscopy observations of the same mutant and for which there was an unambiguous absence of mitochondrial fluorescence. Note that if $_c$ERSΔN1$_{β11ch}$ still confers the capacity of growing on YPGly and thus of having a robust mitochondrial translation cannot be explained by a differential expression

of the mutant protein between the two experiments, that could have explained the absence of fluorescence, since the immunodetection signal and the loading control are similar.

In order to confirm these results, I created a diploid (2n) RS 453 strain, that I transformed with a *KanMX4* deletion cassette to replace one *GUS1* allele and obtain a 2n *GUS1/gus1Δ* strain. After verification of the presence of the two alleles (*GUS1* and *gus1Δ*) by PCR, the cells were transformed with integrative plasmids expressing $_c$ERS$_{3HA}$, $_c$ERSΔN1(Δ1-30)$_{3HA}$ or $_c$ERSΔN2(Δ1-70)$_{3HA}$ (**Figure ChI.R-1D**). After selection of the transformants, the integration of the plasmids at the *URA3* locus was verified by PCR along with the diploidy of the clones. The expression of the different constructions in the diploids was verified by Western blotting using anti-HA primary antibody (**Figure ChI.R-1E**). The diploids were then incubated on sporulation medium and dissected to obtain tetrads. The spores obtained were phenotyped (absence and presence of the *GUS1* constructions was determined on YPD + G418 and SC-Ura plates respectively). The expression of the constructs in spores presenting the phenotype of interest was again verified by Western blotting using anti-ERS and anti-HA antibodies (**Figure ChI.R-1F**). For the spore containing the WT *GUS1* gene and the $_c$ERS$_{3HA}$ construction, two bands can be observed with the anti-ERS antibody. On the contrary, for the other spores tested, only the band corresponding to the HA-tagged constructions is observed. This confirms that the constructions can complement *GUS1* deletion and that the spores are indeed *gus1Δ*. The spores containing the constructions of interest were spotted on YPD (fermentation) and YPGly (respiration) plates respectively to compare the growth rate of each spore to WT cells and to assess their capacity to sustain the mitochondrial translation in respiring cells (**Figure ChI.R-1G**). The results obtained on YPD confirm that complementation of *gus1Δ* with $_c$ERSΔN1 or $_c$ERSΔN2 is not associated with a growth delay. For the spotting assays on YPGly plates, both $_c$ERSΔN1$_{3HA}$ and $_c$ERSΔN2$_{3HA}$ display growth rates similar to the WT cells and *gus1Δ* cells complemented with $_c$ERS$_{3HA}$. These observations confirm the results obtained for the shuffling assay and indicate that even a bigger deletion of $_c$ERS N-terminus ($_c$ERSΔN2) can sustain mitochondrial translation. Moreover, when zooming in the YPGly plates, we can observe the apparition of suppressor colonies in the *gus1Δ* spores complemented with $_c$ERSΔN1$_{3HA}$ and even more with $_c$ERSΔN2$_{3HA}$ (**Figure ChI.R-1G**). This could indicate that an adaptative mechanism is used by cells to sustain mitochondrial growth in absence of an import-competent $_c$ERS.

In contrary to the *gus1Δ* shuffle strain and the *gus1Δ* spores, the BiG Mito-Split-

Figure ChI.R-2: Visualization of the GFP$_{\beta 11ch}$ fragment mitochondrial relocation. BiG Mito-Split-GFP WT (upper panel) and *por1Δ* (lower panel) were transformed with the p414-*pGPD*-GFP$_{\beta 11ch}$ plasmid. Selected transformants were grown in SCGal-Trp medium for microscopy observations.

mitochondrial porin Por1. This channel is important for the import of small molecules up to ~5 kDa in size (Lemasters and Holmuhamedov, 2006). Even if the GFP$_{\beta11ch}$ tag is bigger than the exclusion size of VDAC, I deleted the *POR1* gene in the BiG Mito-Split-GFP strain and performed microscopy analyses to assess the mitochondrial localization of the GFP$_{\beta11ch}$ tag (**Figure ChI.R-2**). The replacement of *POR1* by the *KanMX4* deletion cassette was verified by PCR. The GFP fluorescence signal obtained indicates that GFP$_{\beta11ch}$ import in the mitochondrial does not rely on VDAC and thus must translocate through the outer membrane very likely *via* the TOM complex. However, the import of GFP$_{\beta11ch}$ in the mitochondria seems to be a rare event, since among the 30 microscopy fields taken, only 3 contain cells with a fluorescent GFP signal.

III.4. Mitochondria visualization in autophagy conditions

During macroautophagy, the autophagosomes that contain organelles, proteins and other cellular constituents are delivered to the vacuole for degradation. During this process, mitochondria can be sequestered and brought to the vacuole. In order to examine the fate of mitochondria during autophagy, I decided to use the BiG Mito-Split-GFP. The advantage is that GFP reconstituted in the mitochondria is stable and cells can be further treated with different stress conditions. In a first approach, I used the BiG Mito-Split-GFP strain expressing $_c$ERS$_{\beta11ch}$ either under control of *GPD* promoter or *GUS1* promoter. In order to visualize vacuoles that are the final destination of the autophagosomes during autophagy, I used the fluorescent dye FM4-64 that stains specifically the vacuolar membrane in the experiment conditions. When grown in fermentation conditions, the mitochondria form a network that is wrapped around the vacuole, but the absence of colocalized FM4-64 and GFP signals indicate that the two organelles do not closely interact (**Figure ChI.R-3A**). On the contrary, when cells are incubated in autophagy medium (SD-N) overnight, the mitochondria network is completely abolished and mitochondria adopt a dot shape. Interestingly, the GFP signal is very close from the FM4-64 vacuolar signal. It even seems that mitochondria are not only localized at the vacuolar periphery but in the vacuole (**Figure ChI.R-3A**). Since the vacuole staining with FM4-64 is not optimal in autophagy conditions, I transformed the BiG Mito-Split-GFP strain with a plasmid expressing mCherry-Atg8 under the control of a $CuSO_4$ inducible promoter. The Atg8 protein is a component of the autophagosomes and can thus be used to follow the autophagic bodies when fused to mCherry. After induction with 1 mM $CuSO_4$, the cells were incubated during 3 h in SD-N medium before microscopy observations. The fluorescence signal observed
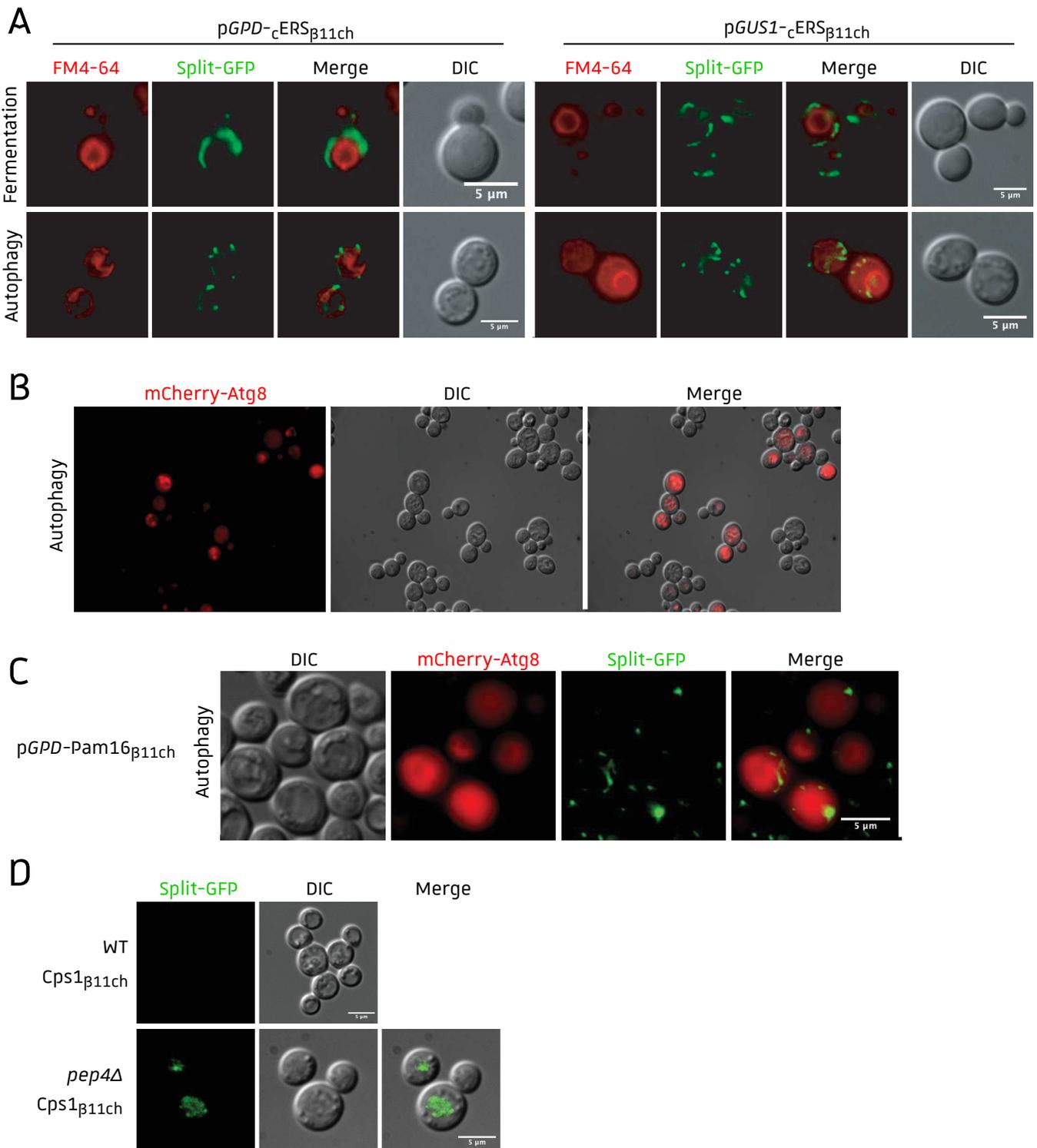
Figure ChI.R-3: Utilization of the BiG Mito-Split-GFP strain to visualize the mitochondria in autophagy conditions. A. The BiG Mito-Split-GFP strain was transformed with an integrative plasmid expressing $_c$ERS$_{\beta11ch}$ either under the control of the *GPD* or *GUS1* promoter. Cells were grown to mid-log phase in fermentation (upper panel) or incubated overnight in autophagy (SD-N) medium (lower panel) before observation. Vacuoles are stained using the FM4-64 fluorescent dye. **B.** The BiG Mito-Split-GFP strain was transformed with a plasmid expressing mCherry-Atg8. The expression of the reporter protein is induced upon addition of 1 mM CuSO$_4$. After induction, cells were incubated during 3 h in SD-N (autophagy) medium before microscopy observation. **C.** The BiG Mito-Split-GFP strain was co-transformed with plasmids expressing Pam16$_{\beta11ch}$ (*GPD* promoter, integrative plasmid) and mCherry-Atg8. For microscopy observations, cells were incubated during 3 h in SD-N medium. **D.** The WT and *pep4Δ* BiG Mito-Split-GFP strains were transformed with the plasmid expressing the vacuolar protein Cps1$_{\beta11ch}$. Cells were cultured in fermentation medium and transferred to SD-N autophagy medium overnight before microscopy observations.

confirms that mCherry-Atg8 is expressed and can be used as an autophagosome marker despite the low number of fluorescent cells (**Figure ChI.R-3B**). This strain was subsequently transformed with the integrative plasmid expressing Pam16$_{\beta11ch}$ (promoter *GPD*) to visualize the mitochondria *via* the GFP signal. Again, the mitochondria adopt a dot shape and the GFP signals of some mitochondria colocalizes with the autophagosomal mCherry-Atg8 (**Figure ChI.R-3C**). However, at this step it not possible to determine whether the mitochondria are close to the autophagosomes or in these compartments for subsequent vacuolar targeting and degradation. In order to determine if the mitochondria are degraded in the vacuoles, I fused the GFP$_{\beta11ch}$ tag to the vacuolar protease Cps1, which expression is normally induced under low-nitrogen conditions. This protein is a vacuolar resident protein and should thus not be degraded in this compartment. The idea was that if mitochondria are degraded in the vacuole during autophagy, the GFP$_{\beta1-10}$ fragment should be released in the vacuolar lumen where it could interact with Cps1$_{\beta11ch}$ and reconstitute a fluorescent GFP. When Cps1$_{\beta11ch}$ was expressed and the autophagy induced, we could not observe a GFP fluorescence localized in the vacuole (**Figure ChI.R-3D**). The absence might be due to the rapid degradation of the autophagic bodies and thus of the GFP$_{\beta1-10}$ fragment in the vacuolar lumen. In order to accumulate autophagic bodies in the vacuolar lumen, I deleted the *PEP4* gene encoding a vacuolar protease in the BiG Mito-Split-GFP strain. The replacement of *PEP4* by the *KanMX4* deletion cassette vas verified by PCR. When Cps1$_{\beta11ch}$ was expressed in this strain, we could observe a GFP fluorescence signal after an overnight induction of autophagy indicating that the GFP$_{\beta1-10}$ fragment was released in the vacuolar lumen (**Figure ChI.R-3D**). I could thus confirm that mitochondria are degraded in the vacuole during autophagy.

IV.   Conclusion & perspectives

Thanks to the BiG Mito-Split-GFP we developed, it is now possible to visualize the mitochondrial echoforms of proteins that are dual- or multi-localized in the cell. Its utilization allowed us to confirm that $_c$ARS, $_c$GRS1, $_c$HRS and $_c$VRS produced upon alternative transcription/translation initiation are indeed mitochondrial echoforms, as previously described in the literature (K. J. Chang and Wang, 2004; Chatton *et al.*, 1988; Chen *et al.*, 2012; Natsoulis *et al.*, 1986; Turner *et al.*, 2000) (**Figure ChI.CP-1**). Unexpectedly, the shorter version of $_c$HRS, which was thought to be MTS-deprived and thus logically the cytosolic echoform, was also identified as a mitochondrial echoform with our BiG Mito-Split-GFP system (**Figure ChI.CP-1**). We hypothesized that the MTS of $_c$HRS may be longer than the one initially predicted or
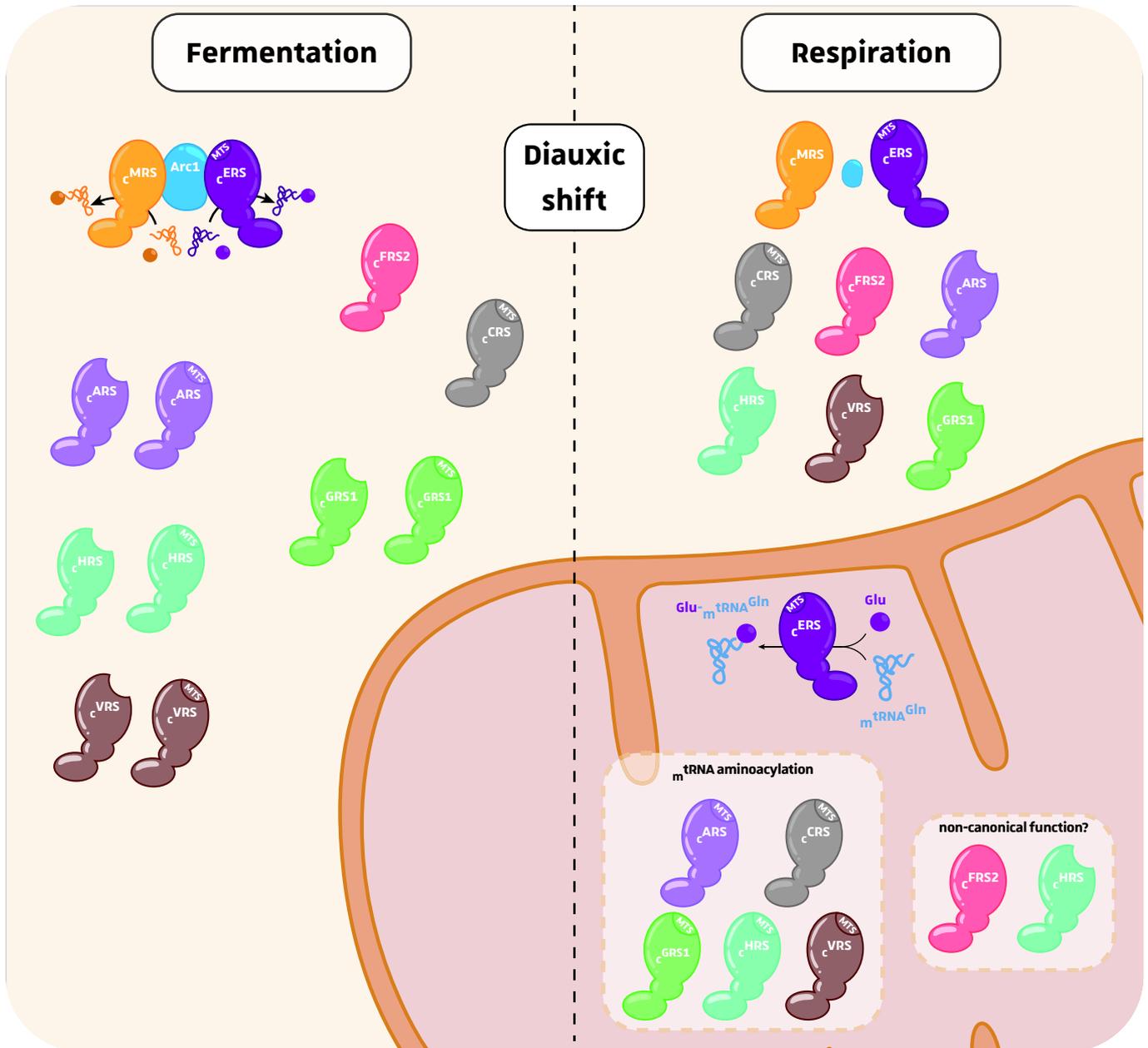
Figure ChI.CP-1: Mitochondrial localization of $_c$aaRS after diauxic shift. Summary of results obtained with the BiG Mito-Split-GFP system. The mitochondrial localization of $_c$HRS deprived of the previously identified MTS either indicate that the MTS is longer than expected or that both $_c$HRS can localize in the mitochondria. In addition, a mitochondrial echoform for $_c$FRS2 was identified despite the presence of a mitochondrial $_{mt}$FRS. The two $_c$aaRSs thus may exert non-canonical functions upon mitochondrial localization.

that both isoforms indeed localize in the mitochondria. One could be dedicated to translation while the other could be dedicated to a non-canonical function. The identification of $_c$FRS2 mitochondrial echoform was also an unexpected result since a mitochondrial $_{mt}$FRS is already present (**Figure ChI.CP-1**). We also deduced that the $_{mte}$cFRS2 could fulfill a non-canonical function when localized in the mitochondria. The BiG Mito-Split-GFP system has also proven its robustness in the identification of mitochondrial echoforms of proteins from other organisms. Indeed, we were able to confirm the mitochondrial localization of plants, mouse and human proteins. In the case of human and mouse Ago2, the prediction algorithms could not identify an MTS within the protein sequence but our system unambiguously confirmed their mitochondrial localization, making the BiG Mito-Split-GFP system a powerful tool in the identification of mitochondrial proteins with cryptic and unpredictable MTS, regardless of the organismal origin of the tested protein. Moreover, the BiG Mito-Split-GFP system can be used to identify these cryptic MTS, or at least to determine their localization in the protein sequence as was done with $_c$ERS. Indeed, we could identify the 30st residues as essential for mitochondrial localization. The apparition of suppressor colonies in the growth assays performed in respiration conditions when $_c$ERS deleted for its MTS indicates that the cells somehow develop adaptive mechanisms to bypass the absence of $_{mte}$cERS or to support $_c$ERS mutant mitochondrial import. The whole-genome sequencing analysis of these suppressors colonies could help us identify these alternative mechanisms.

Nonetheless, the BiG Mito-Split-GFP system has not been developed or explored to its maximum of possibilities and the applications are vast and diverse. I will present here the high-priority ones. Over 1200 proteins have been annotated to yeast mitochondria in the Saccharomyces Genome Database and their number is constantly increasing (Malina *et al.,* 2018). Moreover, it was estimated that a third of the mitoproteome is dual-localized (Ben-Menachem *et al.,* 2011). However, the mechanisms allowing correct distribution of the echoforms have not been identified and the MTS of numerous mitochondrial echoforms remain unidentified. By performing systematic GFP$_{\beta11ch}$-tagging of yeast proteins, we could gain insight on mitoproteome composition and on cryptic MTSs by aligning the protein sequences or by comparing crystallographic structures of mitochondrial echoforms. For example, the 30st residues of $_c$ERS that are essential for mitochondrial import and the N-terminal of Arc1 (which is also localized in the mitochondria) are made of a short β-strand followed by an α-helix. This structural signature (rather than a sequence signature) could be found in other mitochondrial proteins and thus represent a novel type of MTS. It would also be
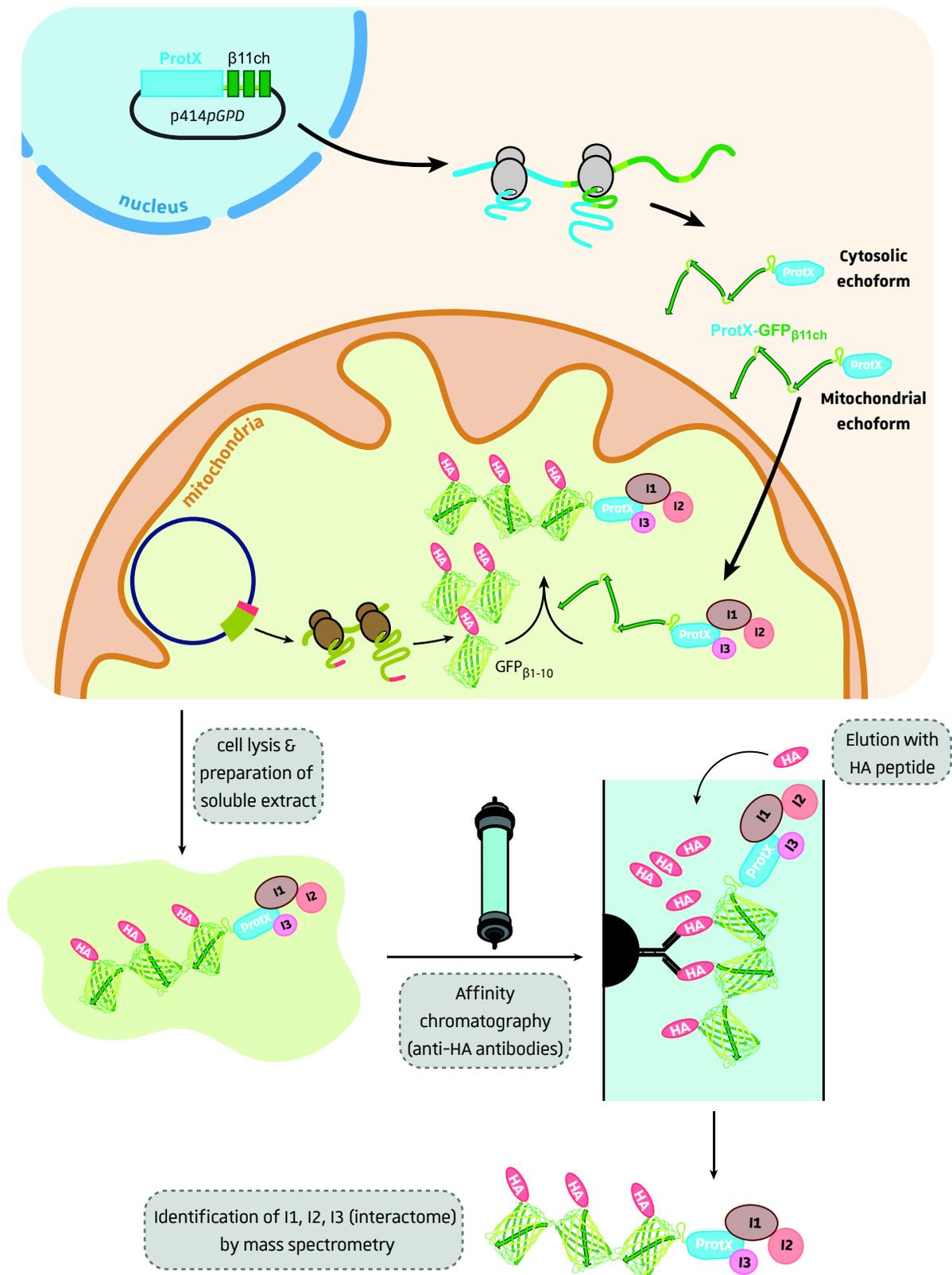
Figure ChI.CP-2: Purification of HA-GFP$_{β1-10}$ associated with GFP$_{β11ch}$-tagged protein and determination of mitochondrial protein interactome. In order to determine the interactome (I1, I2, I3...) of protein mitochondrial echoform, an HA-tag will be added in N-terminal of the mtDNA encoded GFP$_{β1-10}$ fragment. After cell lysis, the GFP$_{β1-10}$ interacting with GFP$_{β11ch}$-tagged protein will be purified by affinity chromatography (beads coupled to anti-HA antibodies). The competitive elution with HA peptides enables the purification of native protein together with its interactant. The interactome of the GFP$_{β11ch}$-tagged mitochondrial protein will then be determined by mass spectrometry.

interesting to develop the N-terminal GFP$_{\beta11ch}$-tagging of proteins to identify mitochondrial proteins carrying unprocessed N-terminal MTSs.

In order to increase the GFP fluorescence signal triggered upon mitochondrial import, three GFP$_{\beta11}$ strands were concatenated to form the GFP$_{\beta11ch}$-tag that can interact together with three mitochondrial GFP$_{\beta1-10}$. This is of particular interest for proteins that are less abundant in the mitochondria. It would be interesting to demonstrate that the concomitant reconstitution of three GFP indeed occurs and triggers a threefold increase in the GFP signal emitted. For this, the recombinant GFP$_{\beta1-10}$ fragment and GFP$_{\beta11}$ and GFP$_{\beta11ch}$ would have to be purified either alone or fused to a target protein in order to perform *in vitro* reconstitution assays. The reconstitution of GFP can be analyzed by several approaches to see how many GFPs are actually reconstituted with GFPβ_{11ch} (size-exclusion chromatography, mass spectrometry, dynamic light scattering…) and the intensity of emitted fluorescence could be measured using a spectrofluorometer. These recombinant proteins would also be essential to determine the affinity constants between the GFP$_{\beta1-10}$ and GFP$_{\beta11(ch)}$ fragments using for example Isothermal Titration Calorimetry (ITC). Indeed, the two fragments have self-assembling properties but we do not know with which strength they assemble nor in which conditions they can dissociate after reconstitution. This is particularly crucial for the utilization of the BiG Mito-Split-GFP and Vac-Split-CFP systems (see **Chapter II**) to study the dynamics of protein localization upon stress and metabolic changes.

The mitochondria are composed of two soluble compartments; the mitochondrial matrix and the intermembrane space (IMS). The BiG Mito-Split-GFP strain presented here enables the identification of proteins that localize in the mitochondrial matrix. Other submitochondrial compartments would also be interesting to explore using the BiG Mito Split-GFP strategy like the IMS which is at the center of numerous essential processes like the iron-sulfur cluster assembly and apoptosis (Herrmann and Riemer, 2010). In order to identify proteins that localize in the IMS and determine its proteome, the gene encoding the GFP$_{\beta1-10}$ fragment will have to be adequately fused to a mtDNA-encoded protein that is inserted in the inner mitochondrial membrane and which has its N- or C-terminal in the IMS.

Finally, since many mitochondrial proteins are dual-localized, the identification of their mitochondrial and submitochondrial interactome remains challenging and based on mitochondrial purification. Thus, an N-terminal HA-tag will be added to the mtDNA-encoded GFP$_{\beta1-10}$ fragment of both matrix and IMS BiG Mito-Split-GFP strains (**Figure ChI.CP-2**). By

doing so, we will be able to purify the HA-GFP$_{\beta1-10}$ fragment along with the GFP$_{\beta11ch}$-tagged protein and its interactants in native conditions. The proteins will then be eluted using HA peptides and analyzed by mass spectrometry.

CHAPTER II: VACUOLAR LOCALIZATION OF PROTEINS

medium composition (log-phase cells)	hypotonic (SC medium) carbon starvation	normal (YPD pH 5)	hypertonic (YPD pH 5 + 1 M NaCl)
cell status	Stationary phase G1 phase	log-phase	
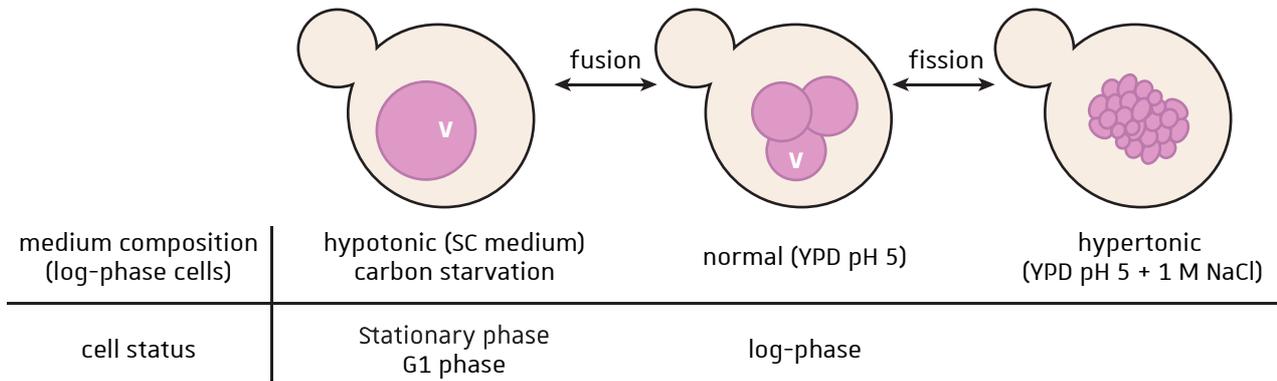
Figure ChII.I-1: Vacuole morphology. The vacuoles can undergo fusion or fission in response to the composition of the growth medium or cell status. V: vacuole.
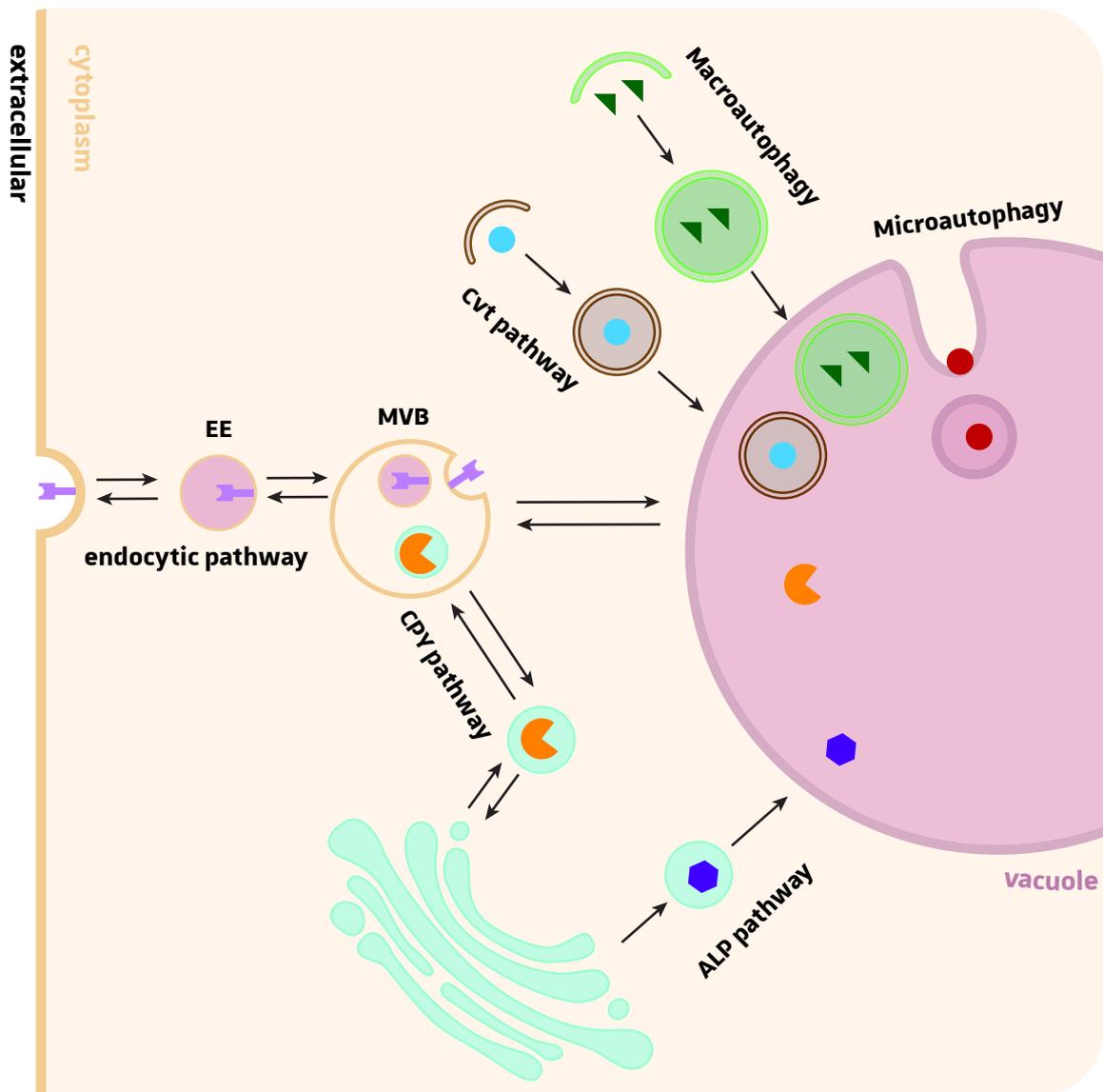
Figure ChII.I-2: Vesicular pathways for protein delivery to the vacuole. Vacuole resident proteins are sent to the vacuole by the CPY or ALP pathways that start from the late Golgi. CPY vesicles are shuttled to the vacuole through the multivesicular bodies (MVB) while the ALP vesicles are directly delivered to the vacuole. The CVT pathway has many common components with autophagy. Cargo senta to the vacuole for degradation can follow the endocytic pathway. The extracellular or plasma membrane components first traverse the early endosomes (EE) followed by the late endosome or MVB to finally reach the vacuole. In macroautophagy, the double-membrane vesicle called autophagosomes engulf cytoplasmic material and fuse with the vacuole for final degradation. During microautophagy, the vacuolar membrane invaginates to sequester cytoplasmic cargo forming vesicles that are degraded in the vacuolar lumen [17,18].

I. Introduction

I.1. The fungal vacuole

The fungal vacuole is an acidic compartment, very dynamic and sensitive to different stresses, to carbon sources and to the cell status (**Figure ChII.I-1**). The fungal vacuole represents 25 % of the cellular volume and can display different shapes. Logarithmically growing cells often have a multilobed vacuole while stationary-phase cells and cells in G1 have a single large vacuole. A carbon source starvation will also trigger vacuole fusion, a phenomenon that is rapidly reversed by the addition of a carbon source (Jones *et al.,* 1997). The fungal vacuole and the mammalian lysosome share many similarities but also differ in their function and composition. For example, the fungal vacuole can sequester high concentrations of small molecules and ions, unlike the mammalian lysosome. Indeed, the vacuoles contain a number of metabolites among which phosphate, polyphosphate, aa, *S*-adenosylmethionine (SAM), allantoin and allantoate, divalent cations (Ca^{2+}, Mg^{2+}, Mn^{2+}) and other ions (Jones *et al.,* 1997).

There are multiple pathways that deliver cargo to the vacuole (**Figure ChII.I-2**). The endocytosed receptors and their cargo contained in endocytic vesicles fuse with the early endosomes that will mature in late endosomes and finally fuse with the vacuoles (Huotari and Helenius, 2011). For proteins from the late Golgi, two different routes are possible for their delivery to the vacuole. They can either be transported through the CPY pathway to the late endosomes or multivesicular bodies (MVBs) that eventually fuse with the vacuole or they are directly delivered to the vacuole following the ALP pathway. The latter pathway requires packing of the proteins into specific vesicles coated with AP-3 complex to fuse with the vacuoles (Bowers and Stevens, 2005). Another way to deliver proteins to the vacuole are the autophagosomes, which are generated mainly during starvation and which deliver proteins and organelles to the vacuoles (Carlsson and Simonsen, 2015). The common feature of these pathways is the final fusion with the vacuole that is accomplished by membrane-embedded SNAREs after membrane contact (Kümmel and Ungermann, 2014). However, vacuoles can contact several organelles without fusing through membrane contact sites (MCSs) that will bridge organelles together (Malia and Ungermann, 2016).

I.2. The vacuolar membrane

I.2.1. Lipid composition

The vacuolar membrane contains only a low level of ergosterol and other sterols (Zinser *et al.,* 1993). It is composed of mostly of phosphatidylcholine (PC) (46.5 %) but also contains phosphatidylethanolamine (PE), phosphatidylinositol (PtdIns), and phosphatidylserine (PS) (Zinser *et al.,* 1991). Microscopy methods have also shown the presence of phosphorylated phosphatidylinositol (PPIns); phosphatidyl 3-phosphate (PtdIns(3)P), phosphatidylinositol 3,5-bisphosphate (PtdIns(3,5)P$_2$) and phosphatidylinositol 4-phosphate (PtdIns4P) (Cheng *et al.,* 2014; Obara *et al.,* 2008; Takatori *et al.,* 2016; Tomioku *et al.,* 2018). In yeast, PtdIns(3)P is generated by the phosphorylation of PtdIns by the phosphatidylinositol 3-kinase Vps34 and is asymmetrically distributed in the vacuole membrane since it is only present in the leaflet facing the cytoplasm (Cheng *et al.,* 2014; Schu *et al.,* 1993). Interestingly, Vps34 is essential for autophagy and PtdIns(3)P is a component of yeast autophagosomes, with a more prominent localization in the luminal leaflet than in the cytoplasmic leaflet (Cheng *et al.,* 2014; Kihara *et al.,* 2001). PtdIns(3,5)P$_2$ is a rare lipid, representing less than 0,1 % of total PtdIns in *Saccharomyces cerevisiae* (Mccartney *et al.,* 2014) and is synthesized by phosphorylation of PtdIns(3)P by the phosphatidylinositol 5-kinase Fab1 (Yamamoto *et al.,* 1995). Hypertonic stress induces a rapid increase in PtdIns(3,5)P$_2$ level and vacuole fragmentation within approximately 10 min (Dove *et al.,* 1997). The vacuolar fragmentation is a process that requires PtdIns(3,5)P$_2$ and Atg18 which, upon recruitment to the vacuolar membrane through binding to PtdIns(3,5)P$_2$ and PtdIns(3)P, plays a critical role through its vesicle fission activity (Gopaldass *et al.,* 2017). The vacuoles of *fab1* mutant cells have an acidification defect and are very enlarged, occupying up to 80 % of the cell volume (Yamamoto *et al.,* 1995). The enlargement of vacuoles has been shown to have an impact on correct segregation of chromosomes during cell division. PtdIns(3,5)P$_2$ also has an essential role in protein sorting at the late endosomes/MVB (Odorizzi *et al.,* 1998).

Lipid synthesis does not occur at the vacuole except for PtdIns(3,5)P$_2$. Lipids thus need to be supplied to the vacuole by vesicular and non-vesicular pathways. Most vesicles coming to the vacuole are multivesicular bodies (MVBs), the AP-3 vesicles, and autophagosomes, including the cytoplasm to vacuole-targeting (Cvt) vesicles. Non-vesicular transport of lipids is sustained by membrane contact sites, and more specifically nucleus-vacuole junction (NVJ) and vacuole-mitochondria patch (vCLAMP). At the NVJ, Lam6 and Nvj2 mediate transport

of ergosterol to the vacuole, Osh1 likely participates to the exchange of ergosterol and PtdIns4P, and Mdm1/Snx13 and Nvj3 may play some roles in lipid transfer (Gatta *et al.,* 2015; Henne *et al.,* 2015; Manik *et al.,* 2017; Murley *et al.,* 2015; Toulmay and Prinz, 2012). On the other hand, vCLAMP is thought to transport lipids from the ER to the mitochondria across the vacuolar membrane (Elbaz-Alon *et al.,* 2014; Hönscher *et al.,* 2014).

I.2.2. Vacuolar membrane domains

Interestingly, the vacuole morphology and its membrane organization drastically change according to growth conditions or upon stress. When nutrients in a medium are exhausted, yeast cells enter the stationary phase and undergo a metabolic shift from fermentation to respiration. In this condition, vacuoles fuse with each other to form a large vacuole that often takes a polyhedral shape (**Figure ChII.I-3**). In this configuration intramembrane particles (IMPs), that mainly represent transmembrane proteins, locate at the edge of polygons to form IMP-rich domains, leading to IMP-deficient polygonal faces (Moeller and Thomson, 1979). The IMP-rich domains were also demonstrated to be enriched with the V-ATPase V_o subunit Vph1 and unsaturated lipids (Toulmay and Prinz, 2013). On the other hand, the IMP-deficient areas are sterol-rich, which suggests that they are raft-like liquid-ordered (L_o) domains. The sterols are provided by the lipophagy and subsequent digestion of lipid droplets (LDs). The transport of ergosterol was shown to rely on the NPC pathway mediated by Ncr1 and Npc2 proteins (Tsuji *et al.,* 2017). Other features of IMP-deficient areas consistent with the organization in L_o domains is their capacity to merge upon collision with each other, solve and dissolve reversibly upon temperature change and their higher content in more saturated and longer acyl chains of phosphatidylcholine (Klose *et al.,* 2012; Toulmay and Prinz, 2013; Tsuji and Fujimoto, 2018). The IMP-deficient domains are also enriched with EGO complex component, Gtr2, and Ivy1 that interacts with EGO complex, suggesting that Ivy1 could regulate TORC1 (Malia and Ungermann, 2016; Toulmay and Prinz, 2013).

During hyperosmotic stress, $PtdIns(3,5)P_2$ level rapidly increases and vacuoles undergo fragmentation. In this condition, the vacuolar membrane also forms IMP-deficient and IMP-rich domains (**Figure ChII.I-3**). The IMP-deficient areas lack Vph1 and are enriched with $PtdIns(3,5)P_2$ and PtdIns(3)P, but only $PtdIns(3,5)P_2$ is required for IMP-deficient domain formation (Takatori *et al.,* 2016). These IMP-deficient domains look similar to L_o domain in stationary phase, but their ergosterol content is unknown. During hyperosmotic stress, the

Stationary phase **Hyperosmotic stress** **Nitrogen starvation** **Glucose starvation Cycloheximide**
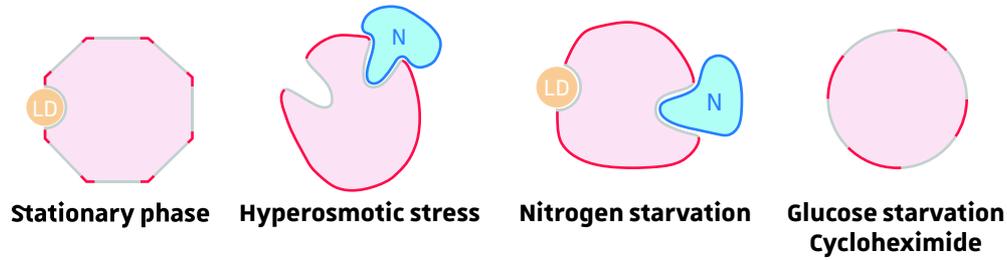
Figure ChII.I-3: Formation of Vph1-deficient vacuolar domains (adapted from [19]). During metabolic changes or upon stress the vacuolar membrane rearranges and vacuolar domains deprived of Vph1 are formed.

A

B

subcomplex	subunit	gene
V_1	A	*VMA1*
	B	*VMA2*
	C	*VMA5*
	D	*VMA8*
	E	*VMA4*
	F	*VMA7*
	G	*VMA10*
	H	*VMA13*
V_O	a	*VPH1*
	c	*VMA3*
	c'	*VMA11*
	c''	*VMA16*
	d	*VMA6*
	e	*VMA9*

C
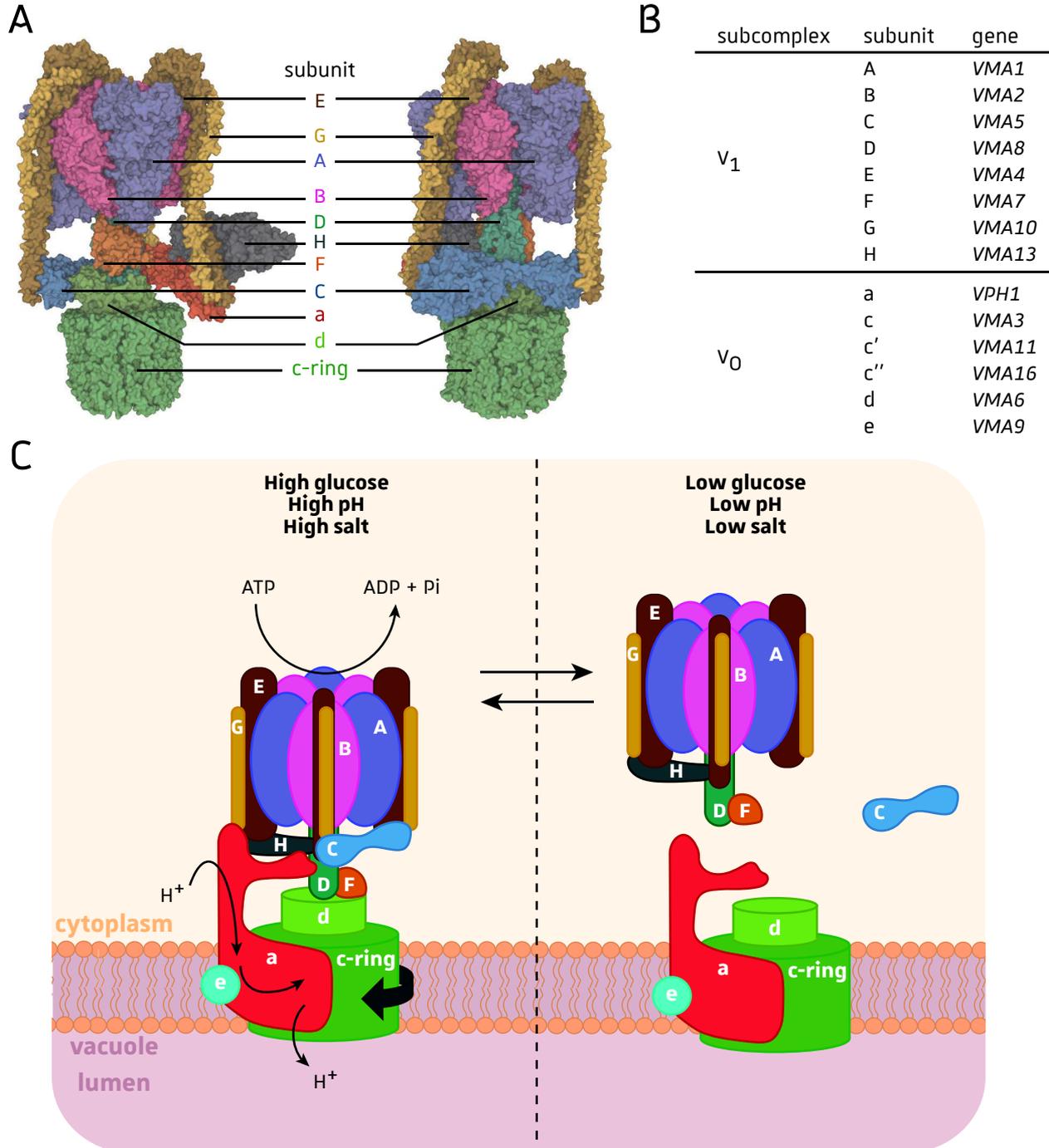
Figure ChII.I-4: Structure, composition and dynamic of the vacuolar V-ATPase. A. The 3D-structure of V-ATPase structure was obtained by electron cryomicroscopy (PDB: 3J9T, [20]). **B.** The subunits of the cytosolic V_1 and membrane V_O subcomplexes are all encoded by *VMA* genes with the exception of subunit a of V_O subcomplex encoded by *VPH1* gene. **C.** When assembled at the vacuole surface, the ATP hydrolysis by the V_1 sector is coupled to the import of protons (H^+) from the cytosol to the vacuole lumen through the V_O sector. Upon glucose, pH or salt stimuli, the V-ATPase can reversibly disassemble leading to the inhibition of H^+ import and ATPase activity [21].

vacuolar membrane constituting the nuclear-vacuole junction (NVJ) expands drastically, and ergosterol transport might occur thanks to the presence of the Vac8 protein (Takatori *et al.,* 2016; Tsuji and Fujimoto, 2018). Vph1-deficient domains also form after glucose starvation, cycloheximide treatment and weak acid stress (Toulmay and Prinz, 2013) (**Figure ChII.I-3**). During glucose starvation and cycloheximide treatment, the formation of Vph1-deficient domains depends on the ergosterol transport performed by Lct1/Lam6 at NVJ (Murley *et al.,* 2015). Finally, nitrogen starvation leads to the formation of Vph1-, IMP-deficient domain performing lipophagy in a similar manner as the IMP-deficient domain formed during the stationary phase (Tsuji *et al.,* 2017) (**Figure ChII.I-3**). The ergosterol needed for domain formation is provided by the intralumenal vesicles of MVBs and its transport depends on the NPC proteins (Müller *et al.,* 2015; Tsuji *et al.,* 2017).

I.2.3. Vacuolar V-ATPase complex

The vacuolar-type V-ATPase is a multiprotein complex that uses ATP to transport protons (H^+) from the cytosol to the vacuolar lumen (**Figure ChII.I-4**). The accumulation of H^+ into the vacuole acidifies the lumen and is also a source of energy for secondary transport systems. The V-ATPase is also necessary to maintain cytosolic pH homeostasis in a combined action with the plasma membrane ATPase Pma1 (Martínez-Muñoz and Kane, 2008). The V-ATPase is organized into two major domains; the cytosolic V_1 and membrane V_0 subcomplexes (**Figure ChII.I-4A and B**). The assembly of the two subcomplexes, that is required for V-ATPase activity, is reversible and controlled depending on different stimuli (**Figure ChII.I-4C**). The proteins required for assembly of the V-ATPase are all *VMA* (vacuolar membrane ATPase) genes, with the exception of the V_0 subunit a, also called Vph1. Cells deleted for any *VMA* gene exhibit a characteristic set of growth phenotypes. The *VMA* mutants display a loss of V-ATPase activity, an increased sensitivity to Ca^{2+}, an inability to grow in media buffered to neutral pH (pH 5.0 being the yeast optimal pH) and to use non-fermentable carbon sources (Kane, 2006). On the other hand, cells deleted of the V-ATPase V_0 subunit Vph1 do not result in complete *VMA* phenotype, but have a largely reduced V-ATPase activity and grow slowly on YPD medium buffered to pH 7.5 (Manolson *et al.,* 1994).

The V_0 subcomplex is composed of 6 subunits; a, c, c', c'', d and e. They all are integral membrane proteins, with the exception of subunit d which is peripheral and tightly associated with the V_0 subcomplex (Graham and Stevens, 1999; Parra *et al.,* 2014; Sambade and Kane, 2004). The proteolipids are inserted into the endoplasmic reticulum (ER) membrane upon

synthesis and are finally targeted to the vacuolar membrane through the secretory pathway (Graham *et al.,* 1998). The H⁺ pore of the V_o subcomplex is formed by subunits c, c′ and c′′, forming the the c-ring (Graham *et al.,* 2003). Loss of a V_o subunit affects the assembly and stability of the remaining V_o subunits and prevents the assembly of the V-ATPase (Tomashek *et al.,* 1996). The catalytic V_1 domain composed of 8 peripheral subunits (A to H) is the place where ATP hydrolysis occurs (Parra *et al.,* 2014). The subunits A and B form the catalytic ATP-hydrolyzing portion of V-ATPase in the form of an A_3B_3 hexamer (Graham *et al.,* 2000). Loss of a V_1 subunit, with the exception of subunit H, does not affect the stability of the other V_1 components but prevents their assembly into the vacuolar membrane. Upon loss of subunit H, the V-ATPase complex assembles but remains inactive (Ho *et al.,* 1993). In V_1 mutant cells, the V_o subcomplex assembles, remains stable and is successfully transported to the vacuolar membrane. The energy provided by ATP hydrolysis will allow the rotation of the rotor shaft, composed of subunits D, F and d, which is connected to the membrane c-ring. For their transfer, H⁺ bind to an acidic residue in the c-ring and, upon 360° rotation, the H⁺ exit the pore through subunit a ,encoded by the *VPH1* gene, inside the vacuolar lumen (Parra *et al.,* 2014). The subunit F of V_1 subcomplex has been proposed to be a stalk subunit bridging the two subcomplexes (Graham and Stevens, 1999).

The proteins Vma12, Vma21 and Vma22 are not subunits of the final complex but they have been demonstrated to be required for the assembly of functional V-ATPase. Loss of Vma12, Vma21 or Vma22 results in cells displaying phenotype characteristic of the *VMA* mutants. The 3 proteins have been localized in the ER membrane, where Vma12 and Vma22 form a heterodimer that interacts with Vph1 (subunit a of V_o subcomplex) (Graham *et al.,* 1998; Graham and Stevens, 1999).

When the V-ATPase disassembles, the pump becomes inactive and 3 constituents are released: the V_1 subcomplex subunit C, the V_1 subcomplex without subunit C and the V_o subcomplex (Kane, 1995) (**Figure ChII.I-4C**). In the V_1 subcomplex, there are 3 peripheral stalks made of subunits E and G (EG1-3). The subunit C has been demonstrated to interact with high affinity to EG_3, with EG_2 and with the N-terminus of V_o Vph1. The subunit C is thus a bridge between the two subcomplexes and the interactions are disrupted and reformed upon V-ATPase disassembly and reassembly (Stewart and Stock, 2012). The V-ATPase disassembly occurs in response to glucose deprivation, exposure to less-preferred carbon source (galactose, glycerol/ethanol, raffinose), changes in pH or salts, and osmotic stress

(Diakov and Kane, 2010; Kane, 1995). Upon glucose re-addition, the regulator of ATPase of vacuoles and endosomes (RAVE) complex is required for V-ATPase reassembly. The RAVE complex helps the loading of subunit C into V_1V_0 complex and its absence results in unstable and inactive V-ATPase (Smardon *et al.*, 2002; Smardon and Kane, 2007). Upon osmotic shock, the total pool of assembled V-ATPase increases. This requires the signaling lipid PtdIns(3,5)P_2 that interacts with Vph1 (Li *et al.*, 2014). Interestingly, PtdIns(3,5)P_2 has no effect on V-ATPase reassembly after glucose deprivation, indicating that the responses triggering V-ATPase reassembly after the two stimuli, are independent.

I.3. Amino acid storage and sensing

I.3.1. Amino acids transporters

The aa pool available in the cell is strictly controlled in response to the nutritional conditions. The mechanisms involved in aa concentration regulation are: the uptake activity, the aa synthesis and degradation, the protein synthesis and the proteolysis. Among all the small molecules sequestered in the vacuole, ten different aa can accumulate at high concentrations, making the vacuole a reservoir for these aa (Ishimoto *et al.*, 2012; Jones *et al.*, 1997; Kitamoto *et al.*, 1988; Messenguy *et al.*, 1980; Wiemken and Dürr, 1974). The vacuolar pool of aa is regulated by the import and export of aa across the vacuolar membrane and by the vacuolar hydrolytic enzymes, which degrade macromolecules (**Figure ChII.I-5**). Moreover, under normal growth condition, 50 % of total aa are stored in the vacuoles, comprising basic aa (Lys, His and Arg, 70-90 % of total cellular aa) , Met (66% of total cellular aa), Thr, Ser, Ile, Leu, Tyr, Phe and Trp (Ishimoto *et al.*, 2012; Tone *et al.*, 2015). However, 90 % of acidic aa (Asp and Glu) are excluded from this organelle and Val, Pro, Gly and Ala are only poorly enriched in vacuoles (Chahomchuen *et al.*, 2009; Ishimoto *et al.*, 2012). The stored aa are then redirected to the cytosol when the cells are under starvation conditions, to be used for *de novo* protein synthesis. Because of the concentration gradient between vacuole and cytosol, aa transport across the vacuolar membrane requires an active transport system, which relies on transporters from the amino acid/auxin permease (AAAP) family, the major facilitator superfamily (MSF) and the lysosomal cystine transporter (LCT) family (**Figure ChII.I-5** and **Table ChII.I-1**). These transporters are secondary active transporters that use the energy from the electrochemical H⁺-gradient generated by the V-ATPase to mediate solute:H⁺ symport (movement in the same direction) or antiport (movement in opposite directions). These active transporters have been extensively studied and characterized since
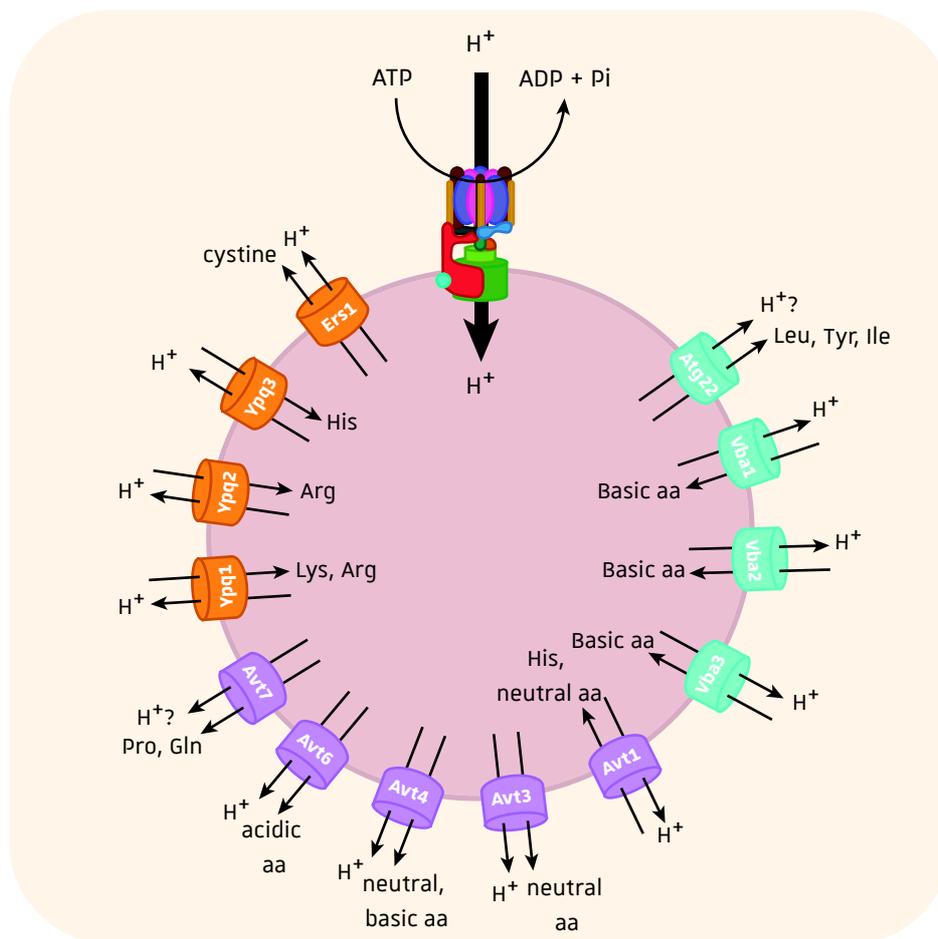
Figure ChII.I-5: Vacuolar amino acid transporters. The transport of amino acids across the vacuolar membrane relies on the energy stored in the form of an H$^+$ gradient generated by the V-ATPase. The vacuolar amino acid transporters belong to the amino acid/auxin permease (AAAP) family (represented in purple), the major facilitator superfamily (MSF, represented in blue) and the lysosomal cystine transporter (LCT) family (represented in orange) [22–26].

Table ChII.I-1: Vacuolar amino acid transporters.

Family	Protein	Substrate	direction	
			from	to
MSF	Vba1	His, Lys	cyt	vac
	Vba2	His, Lys, Arg	cyt	vac
	Vba3	His, Lys	cyt	vac
	Atg22	Ile, Leu, Tyr	vac	cyt
AAAP	Avt1	Neutral aa, His	cyt	vac
	Avt3	Neutral aa	vac	cyt
	Avt4	Neutral aa, His, Lys, Arg	vac	cyt
	Avt6	Glu, Asp	vac	cyt
	Avt7	Pro, Gln	vac	cyt
LCT	Ers1	cystine	vac	cyt
	Ypq1	Lys, Arg	cyt	vac
	Ypq2	Arg	cyt	vac
	Ypq3	His	cyt	vac

the 80's (Ohsumi and Anraku, 1981; Sato *et al.*, 1984a, 1984b) and are reviewed in Bianchi *et al.*, 2019.

I.3.2. TORC1 sensing and signaling

In the yeast, an amino acid-sensing machinery is constitutively present at the vacuole surface. It relies on the EGO complex, composed of the proteins Ego1, Ego2, Ego3, the Rag GTPases Gtr1 and Gtr2, and the Target Of Rapamycin Complex 1 (TORC1), composed mainly of Tor1 or Tor2, Lst8 and Kog1 (Dubouloz *et al.*, 2005; Powis *et al.*, 2015) (**Figure ChII.I-6**). The Ego1 subunit anchors the EGO complex in the vacuolar membrane. The Gtr1-Gtr2 heterodimer is then tethered to the membrane by its interaction with EGO complex. In the presence of aa, the Rag GTPases Gtr1 and Gtr2 are loaded with GTP and GDP respectively and associate with Kog1 component of TORC1 (Binda *et al.*, 2009). The TORC1 complex is then activated and the TOR kinases Tor1 or Tor2 phosphorylate multiple target proteins to promote anabolic processes (protein synthesis, nucleotide synthesis, lipid synthesis). On the other hand, when cells are treated with rapamycin or under nutrient starvation, GDP-bound Gtr1 inactivates the TOR kinase activity *via* the non-essential TORC1 component Tco89 leading to macroautophagy (Binda *et al.*, 2009). Interestingly, the EGO complex in conjunction with TOR has been demonstrated to be essential to counterbalance the massive macroautophagy induced upon rapamycin treatment by positively regulating microautophagy (Dubouloz *et al.*, 2005). Upon glucose starvation, TORC1 is inactivated and oligomerizes into a large hollow helix structure termed TOROID (TORC1 organized in inhibited domain). The assembly of TOROID is reversible and the disassembly relies on the Gtr GTPases (Morozumi and Shiozaki, 2021). The Gtr Rag GTPases can be regulated by different complexes (**Figure ChII.I-6**). The octameric vacuolar Seh1-associated complex (SEAC) is divided into two subcomplexes; the SEAC inhibiting TORC1 (SEACIT) and the SEAC activating TORC1 (SEACAT) (Panchaud *et al.*, 2013). The SEACIT subcomplex contains Npr2, Npr3 and Iml1 and negatively regulates TORC1. This occurs through Iml1, which stimulates Gtr1 intrinsic GTPase activity upon leucine deprivation and is thus a GTPase-activating protein (GAP) for Gtr1. The GAP activity of SEACIT is antagonized by SEACAT composed of Sea2, Sea3, Sea4, Seh1 and Sec13. By promoting the GTP-bound state of Gtr1, SEACAT promotes TORC1 activation. For Gtr1-GDP recycling, the vacuolar protein Vam6, also called Vps39, has been proposed to be a guanine exchange factor (GEF) (Binda *et al.*, 2009). During aa starvation, the heterodimeric complex Lst4-Lst7 relocates to the vacuolar membrane. Upon stimulation with aa, Lst4-Lst7 transiently binds with Gtr2 and acts as GAP
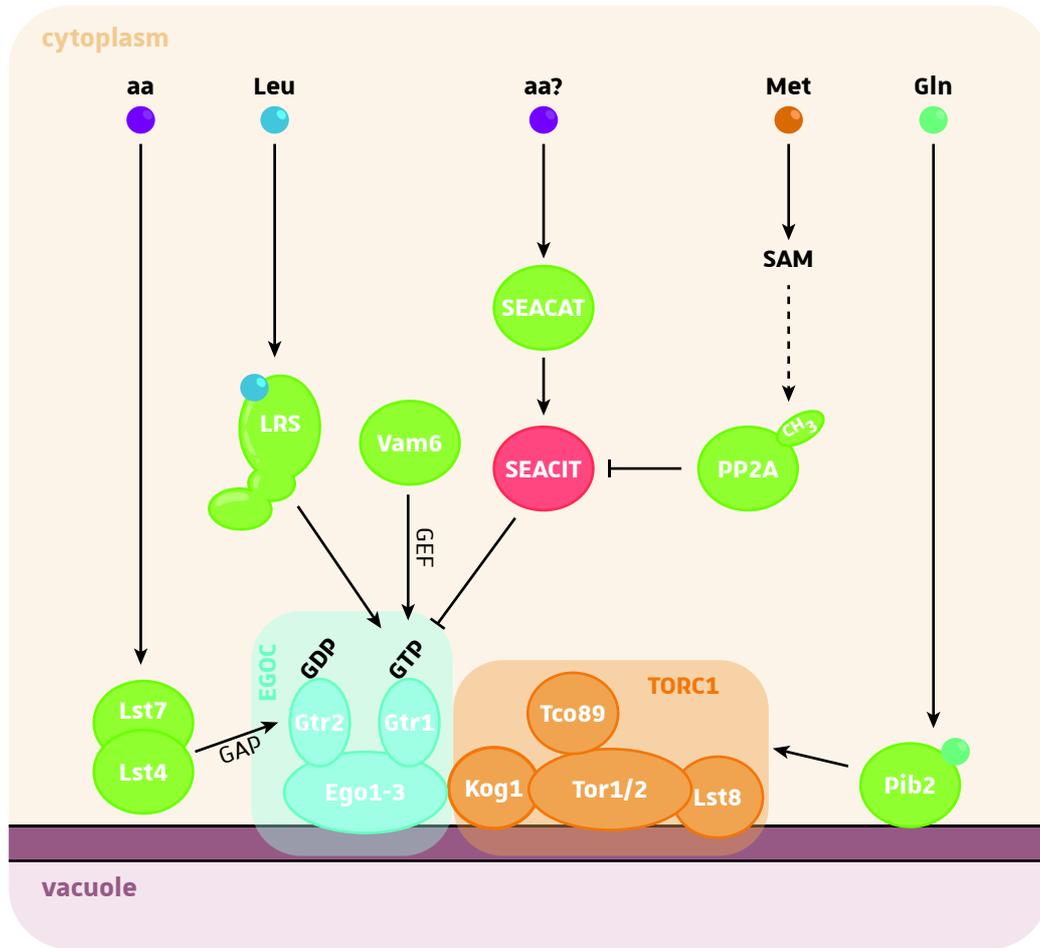
Figure ChII.I-6: Regulation of TORC1 by amino acids in yeast (adapted from [27]). The TORC1 amino acid sensing machinery is constitutively present at the vacuole surface. TORC1 complex (represented in orange) is regulated by the EGO complex (EGOC in blue) in response to amino acid stimuli. The active EGOC contains Gtr1 and Gtr2 bond to GTP and GDP respectively. The regulatory proteins represented in green promote TORC1 activation, while proteins represented in red inhibit TORC1 activation. Vam6 is a guanine exchange factor (GEF) for Gtr1 and Lst7-Lst4 complex is GTPase-activating protein (GAP) for Gtr2. Pib2 can bind glutamine (Gln) and activate TORC1 in a Gtr-independent manner. SAM: *S*-adenosylmethionine

for Gtr2 to activate TORC1 and is finally released from the vacuolar membrane (Péli-Gulli *et al.,* 2015). High (Gln or ammonium) or low-quality nitrogen sources can stimulate a rapid and transient Gtr-dependent activation of TORC1. However, only high quality or preferred nitrogen sources will sustain TORC1 activity (Stracka *et al.,* 2014). Interestingly, Gln activates TORC1 also independently of Gtr1/2, demonstrating that nutrients activate TORC1 *via* different molecular mechanisms and this explains why Gtr1/2 are not essential for TORC1 (Stracka *et al.,* 2014) (**Figure ChII.I-6**). Indeed, the protein Pib2 binds to the vacuolar membrane through its FYVE-domain and can activate TORC1 in response to aa, such as Gln and Leu. Direct binding of Pib2 to Gln was demonstrated to promote its interaction with TORC1 making Pib2 a Gln sensor for TORC1 (Morozumi and Shiozaki, 2021). Leu has also the ability to activate TORC1. For this, leucine-bound leucyl-tRNA synthetase (LRS) binds to Gtr1, this interaction being necessary and sufficient for TORC1 activation and leucine signaling to TORC1 (Bonfils *et al.,* 2012). For Met signaling, it has been proposed that when cells use lactate as a carbon source, the synthesis of *S*-adenosylmethionine (SAM) may be used to promote methylation of type 2A protein phosphatase (PP2A) leading to dephosphorylation of Npr2 preventing SEACIT assembly and thus promoting TORC1 activation (Sutter *et al.,* 2013). TORC1 activity is also regulated by the availability of glucose. In glucose-deprived cells, Snf1 is activated and phosphorylates TORC1 subunit Kog1, which dissociates from TORC1 and translocates to perivacuolar sites. The absence of Kog1 inhibits TORC1 activity and it was suggested that the inhibition is Gtr1/2-independent (Hughes Hallett *et al.,* 2015).

It has been demonstrated that a link between TORC1 and the general amino acid control (GAAC) exists in *Saccharomyces cerevisiae* (**Figure ChII.I-7A**). When active, TORC1 prevents Gcn2 Ser577 dephosphorylation, leading to a decrease in Gcn2 ability to bind uncharged tRNA. On the other hand, when TORC1 is inactivated in absence of aa, Gcn2 is activated leading to a reduction of general translation rate but an increase in *GCN4* mRNA translation, which is a transactivator of aa biosynthetic genes (Cherkasova and Hinnebusch, 2003; Kubota *et al.,* 2003). TORC1 was also shown to participate to the SPS pathway (**Figure ChII.I-7B**). In presence of aa, the SPS sensor component Ssy5 is activated and processes the transcription factors Stp1 and Stp2, that translocate to the nucleus to induce the expression of genes encoding aa permeases. Shin and coworkers demonstrated that under normal growth conditions, the processed from of Stp1 accumulates in the nucleus and is phosphorylated. On the other hand, rapamycin treatment or nitrogen starvation leads to a decrease in the nuclear accumulation of processed Stp1. They could demonstrate that the
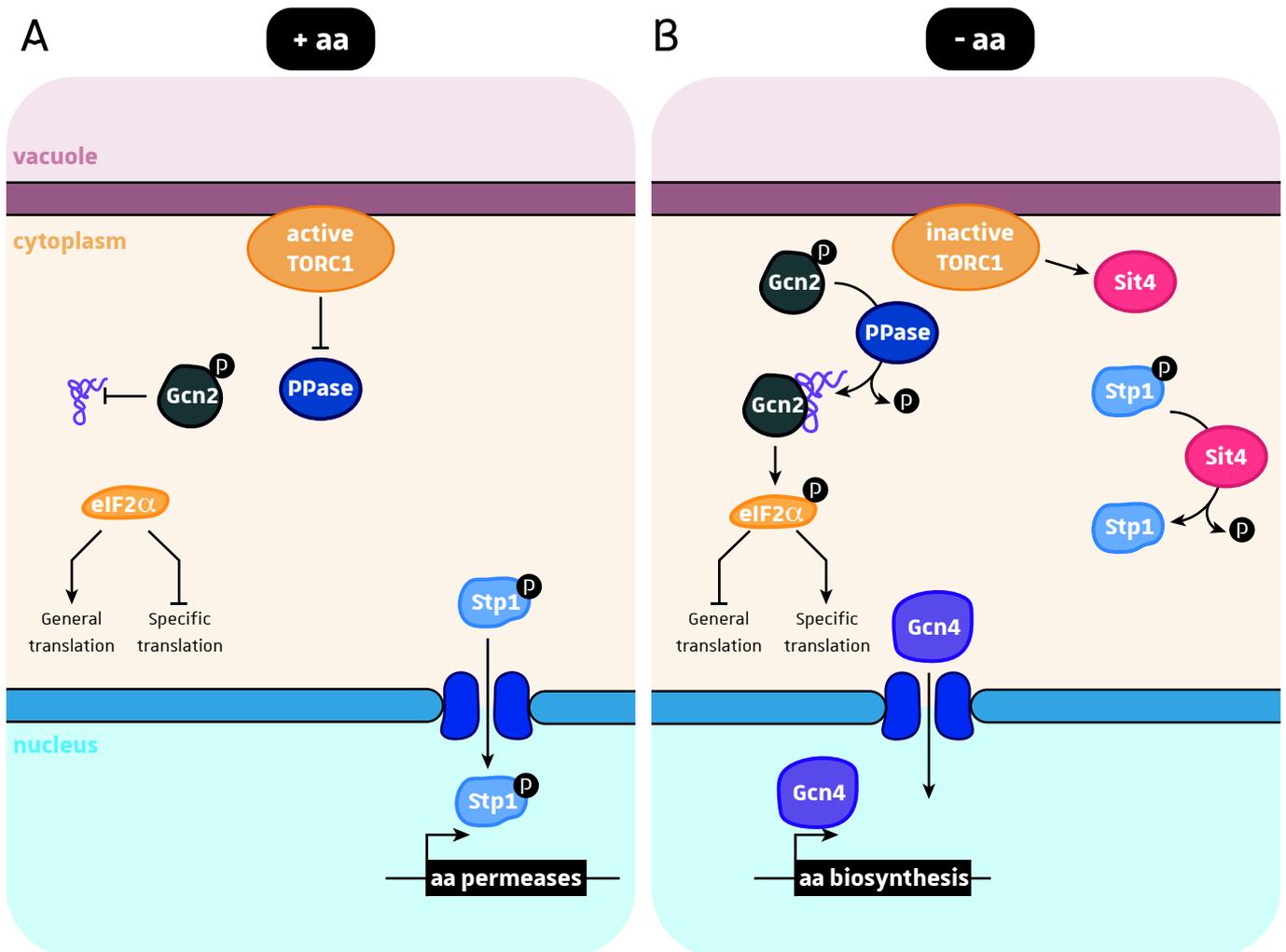
Figure ChII.I-7: Cross-talk between TORC1 and the GAAC and SPS pathways. A. In presence of amino acids, TORC1 is active and inhibits the activity of protein phosphatases (PPase) and thus the dephosphorylation of the GAAC component Gcn2. Inactivated Gcn2 cannot bind uncharged tRNAs and cannot phosphorylate eIF2α, thus promoting general translation. On the other hand, the cleaved form of Stp1 from the SPS pathway stabilized by its phosphorylation accumulates in the nucleus, where it activates the transcription of genes encoding aa permeases. **B.** In result to amino acid starvation, TORC1 is inactivated and the protein phosphatases are derepressed. Unphosphorylated Gcn2 binds to uncharged tRNAs that activate its kinase activity toward eIF2α, leading to the inhibition of general translation and activation of the specific translation of *GCN4* mRNA. Gcn4 enters the nucleus and promotes the transcription of genes implicated in amino acids biosynthesis. Inactive TORC1 promotes the activity of the PP2A-like phosphatase Sit4 that dephosphorylates Stp1 leading to the inhibition of its transcription activator activity.

PP2A-like phosphatase Sit4 mediates Stp1 dephosphorylation. Since rapamycin treatment stimulates the phosphatase activity of Sit4 in a TORC1-dependent manner, they suggested that Stp1 dephosphorylation may be a prerequisite for its degradation promoted by TORC1 inactivation (Shin *et al.*, 2009).

I.4. Autophagy

Cell survival depends on the rapid sensing of external alterations and the subsequent effective responses to maintain cell homeostasis. Under nutritional stress, one of the general responses that is triggered in eukaryotic cells is the rapid and massive induction of macroautophagy, often called autophagy (**Figure ChII.I-8**). Another type of autophagy, called microautophagy was also identified in *Saccharomyces cerevisiae* but is less studied. During microautophagy, the vacuole membrane invaginates and sequesters cytoplasmic material that is delivered to the vacuole lumen. The two mechanisms, macro- and microautophagy, are not identical since mutations in genes required for macroautophagy attenuate but do not abolish microautophagy (Sattler and Mayer, 2000). The process of autophagy in yeast was first discovered by Takeshige and coworkers and the subsequent identification of autophagy mutants helped to understand the mechanistic of this process (Takeshige *et al.*, 1992; Thumm *et al.*, 1994). In yeast, different stresses (*e.g.* removal of carbon source, auxotrophic aa or nucleic acids from the medium, rapamycin treatment) can lead to the induction of autophagy, but nitrogen starvation remains the stimulus leading to the most rapid and substantial autophagy (Noda and Ohsumi, 1998; Takeshige *et al.*, 1992; Thumm *et al.*, 1994). During the process of autophagy, cytoplasmic components are delivered to the yeast vacuole for degradation. The internal pool of molecules generated by the degradation will be sent back to the cytosol and recycled. The first step of macroautophagy is the induction that begins at a single perivacuolar site that is proximal to the vacuole, called the phagophore assembly site (PAS). During the nucleation, the PAS gradually generates a primary double-membrane-sequestering compartment called the phagophore. Next, the phagophore undergoes the expansion and the resulting double-membrane autophagosome is ultimately completed. The formation of the 300 to 900 nm-in-diameter autophagosomes during the autophagy, involves the *de novo* synthesis of cytosolic double-membrane vesicles but the origin of lipids composing the autophagosomes remains unclear. The autophagosomes then reach the vacuoles and the outer membrane fuse with the organelle membrane to release the monolayered autophagic bodies and their cargo inside the vacuole lumen. In the vacuolar
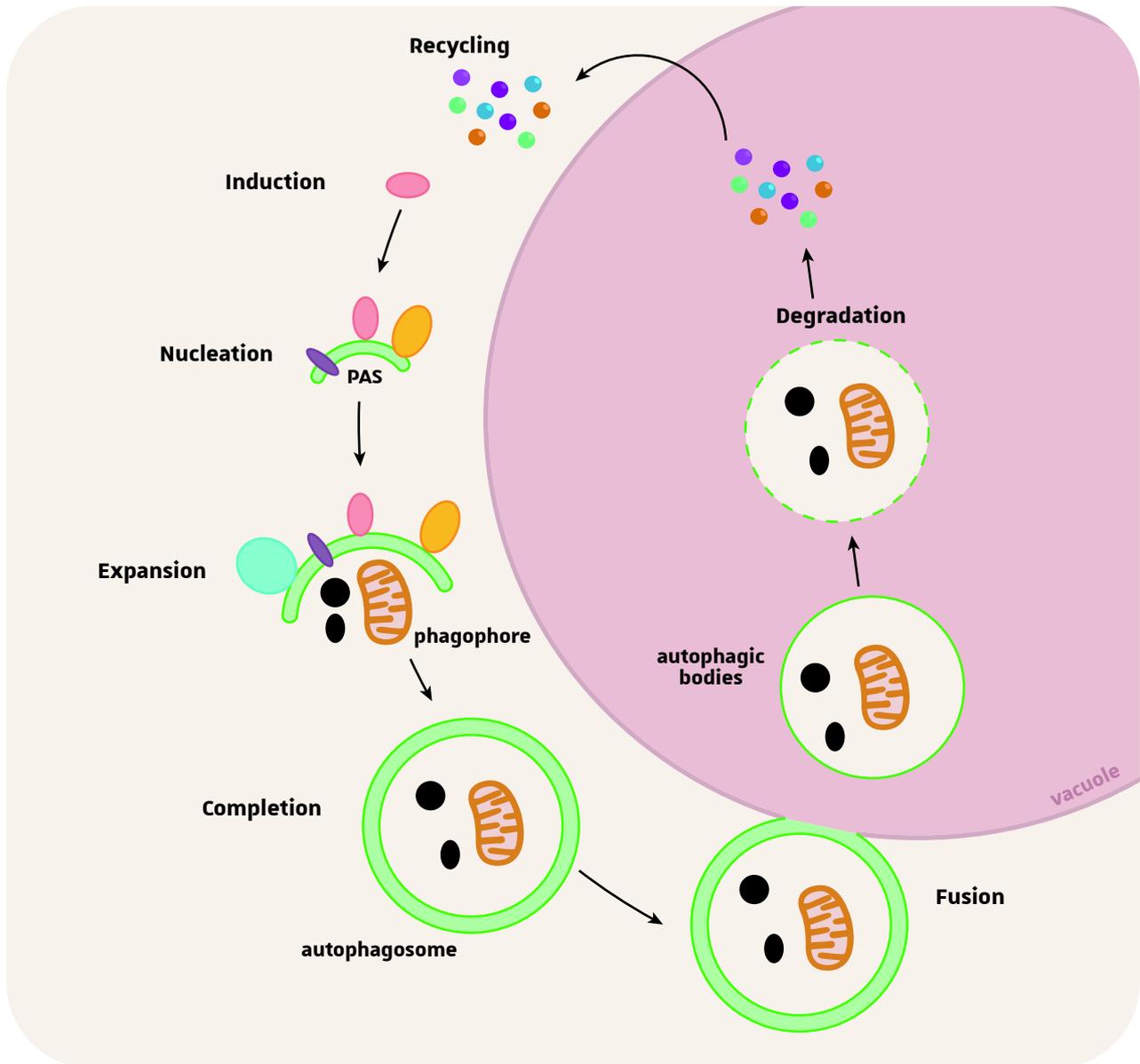
Figure ChII.I-8: The formation of autophagosomes and the process of autophagy in yeast. Autophagy is induced upon nutrient starvation and can be divided in 6 steps; induction, nucleation, expansion, completion, fusion, degradation and recycling. The main proteins participating to each stage are Atg proteins. The induction starts at a single perivacuolar site called the phagophore assemble site (PAS). From induction to nucleation, the PAS generates a double-membrane called the phagophore that non-selectively sequesters cytoplasmic material. The phagophore expands and finally closes to form the autophagosome. The autophagosome fuses with the vacuolar membrane and single-membrane autophagic bodies are delivered in the vacuole lumen and subsequently degraded by resident proteases. The resulting macromolecules are recycled back into the cytoplasm for reuse [28–31].

lumen, the resident hydrolases will degrade the autophagic bodies and the cargo. The breakdown products are finally released into the cytoplasm (Baba *et al.*, 1994; Cebollero and Reggiori, 2009; Wen and Klionsky, 2016). When the serine protease inhibitor PMSF is added to starving cells, the autophagic bodies accumulate in the vacuole and can be observed by light and electron microscopy (Thumm, 2000). Many autophagy mutants have been isolated and they almost all share typical phenotypes. When grown on rich medium, they behave like wild-type cells and their vacuolar acidification is not impaired. However, in nitrogen-free medium these mutants have a 20 to 30 % reduced vacuolar protein degradation in comparison with wild-type cells. Moreover, they cannot accumulate autophagic bodies in the vacuole, even in presence of PMSF and their survival rate is significantly reduced. Finally, they are impaired in vacuolar uptake and maturation of proaminopeptidase I which, contrary to other vacuolar proteases, does not follow the classical vacuolar protein sorting (vps-) pathway but instead uses the cytoplasm-to-vacuole targeting (Cvt) pathway (Thumm, 2000). Indeed, autophagy was shown to be implicated in the selective transport of precursor hydrolases to the vacuole through the Cvt pathway (Scott *et al.*, 1996). Moreover, the majority of genes required for Cvt pathway is also required for autophagy and both pathways rely on the formation of a double-membrane vesicle, the Cvt vesicle and autophagosome respectively. The vesicles then fuse with the vacuole membrane and release single-bilayered vesicle, the Cvt body and autophagic bodies that will be degraded (Abeliovich and Klionsky, 2001). Macroautophagy is also involved in the clearance of damaged mitochondria through a process called mitophagy (Kanki and Klionsky, 2008). Even if the process of autophagy was extensively studied, many issues remain unsolved, like the formation of the phagophore and autophagosome including the precise nature of the PAS, the origin/source(s) of the lipid/membrane used for its expansion which remain thus far unclear.

I.5. Connection with other organelles

I.5.1. NVJ

Beside the membrane contacts occurring between vacuole membrane and mitochondria (vCLAMPs, **Chapter I section I.4.2**), the vacuole is connected to the nuclear envelop of the ER (nER) through the nuclear-vacuole junctions (NVJs) (**Figure ChII.I-9**). In the yeast, the vacuolar protein Vac8 interacts with the N-terminal domain of Nvj1 that resides in the ER (Pan *et al.*, 2000). When cells are starved, Nvj1 promotes the selective turn-over of this ER region through piecemeal microautophagy of the nucleus (PMN) (Roberts *et al.*,
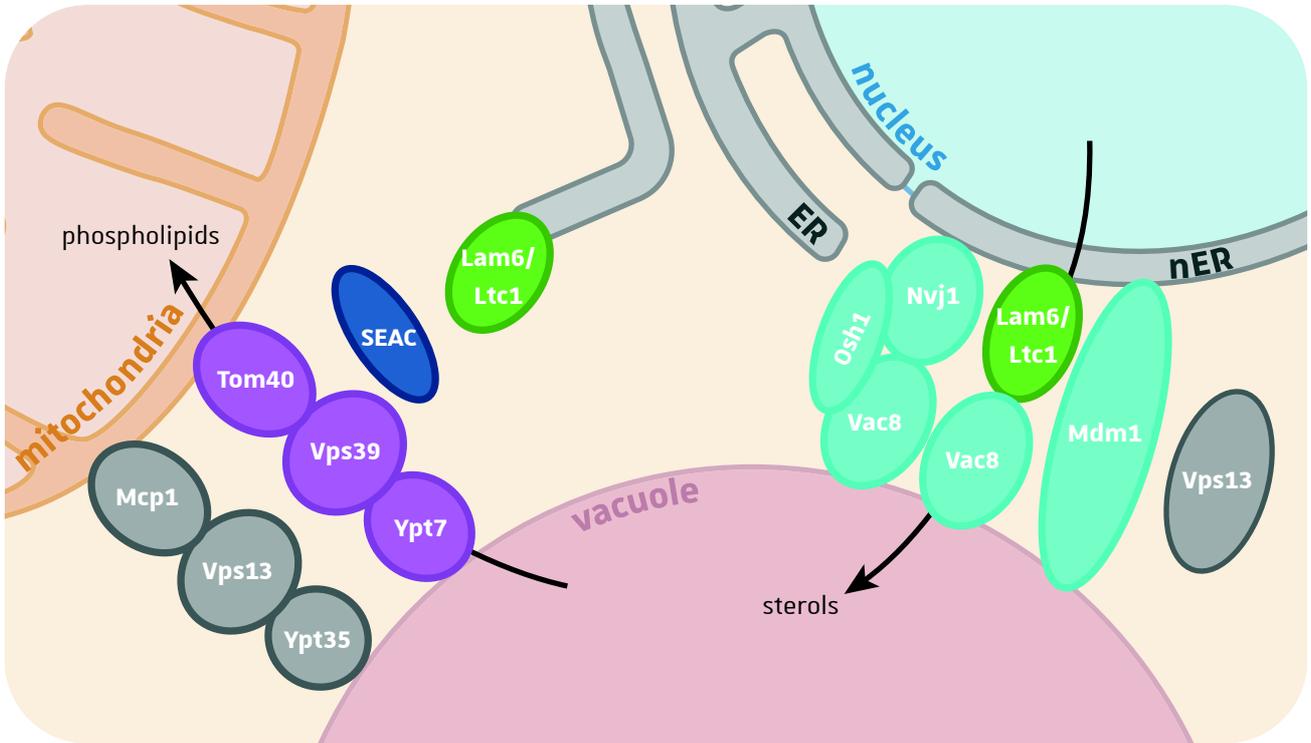
Figure ChII.I-9: Vacuole membrane contact sites. Vacuoles can form contact sites with mitochondria (vCLAMP) and nucleus (NVJ). vCLAMP are described in **Figure ChI.I-4.** The proteins implicated in NVJ formation are represented in blue. Osh1 is preferentially localized to NVJ in starvation conditions. Lam6/Ltc1 is present in NVJ as well as in vCLAMP and ERMES structures and could participate to lipid transfer from the ER to the vacuole. When non-fermentable carbon sources are used, vCLAMP are repressed and Vps13 relocalizes to NVJ. The protein Mmd1 was shown to maintain NVJ formation in the absence of other NVJ components.

2003). Osh1, a member of the oxysterol-binding protein (OSBP), localizes to the Golgi and NVJs and moves preferentially to the latter under starvation conditions (Levine and Munro, 2001). This protein binds to Nvj1 *via* its ankyrin repeats and to the Golgi *via* its PH domain (Kvam and Goldfarb, 2004; Loewen *et al.*, 2003). The integral ER membrane protein Lam6, that contains a sterol-binding motif (StART-like domain), also localizes to the NVJs through its binding to Vac8. This protein could be implicated in lipid transfer between ER and vacuoles or mitochondria (Elbaz-Alon *et al.*, 2015). Another integral ER membrane protein that is part of NVJ is Mdm1 (Henne *et al.*, 2015). It binds vacuolar PI3P *via* its PX domain and can maintain the NVJs even in the absence of other MCS proteins.

II. Context of the study

The idea of studying the vacuolar localization of Arc1 first came when I discovered that Fernandez-Murray and McMaster identified Arc1 as a new phospholipid-binding protein (Fernandez-Murray and McMaster, 2006). More precisely, Arc1 can interact *in vitro* both with PtdIns(3)P and PtdIns(3,5)P$_2$ that are specific of the endosome and vacuole membranes respectively. However, the lipid-binding domain of Arc1 has not yet been identified. The preliminary results obtained by Dr. J. De Craene, a former post-doctorate from the DyPS team, confirmed that Arc1 indeed interacts with membranes *in vivo*. Given that the main role of Arc1 is to assemble the AME complex, Arc1 could thus trigger the relocalization of the $_c$MRS and/or the $_c$ERS to membranes and in particular to the vacuolar membrane. If the two aaRSs indeed localize in the vacuole vicinity, one could ask why they would localize at the surface of this compartment, which is not considered as a translationally active location of the cell. As explained in the introduction (**section I.3.4**), the aaRSs can fulfill many roles beside aminoacylation of tRNAs and such a vacuolar/lysosomal localization of an aaRS was already demonstrated for Leucyl-tRNA synthetase (LRS) in human and yeast cells (Bonfils *et al.*, 2012; Han *et al.*, 2012). In yeast, the vacuolar localization of LRS depends on its interaction with the vacuolar Rag GTPase Gtr1. When leucine is available, LRS promotes GTP-bound Gtr1 and GDP-bound Gtr2, which interact with and activate TORC1, thus inhibiting the autophagy and promoting protein translation. However, when leucine is scarce, the CP1 editing domain of LRS undergoes a conformational change and edits mischarged Ile-tRNA^{Leu}. This conformational change of the editing domain disrupts the interaction between LRS and Gtr1 and triggers GTP hydrolysis into GDP by Gtr1 thereby leading to TORC1 downregulation and finally to autophagy. The regulation of TORC1 activity by LRS is thus leucine-dependent
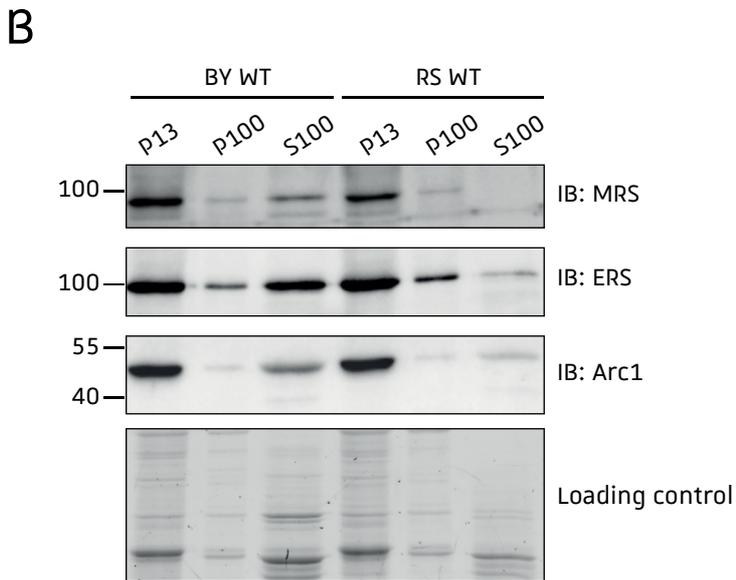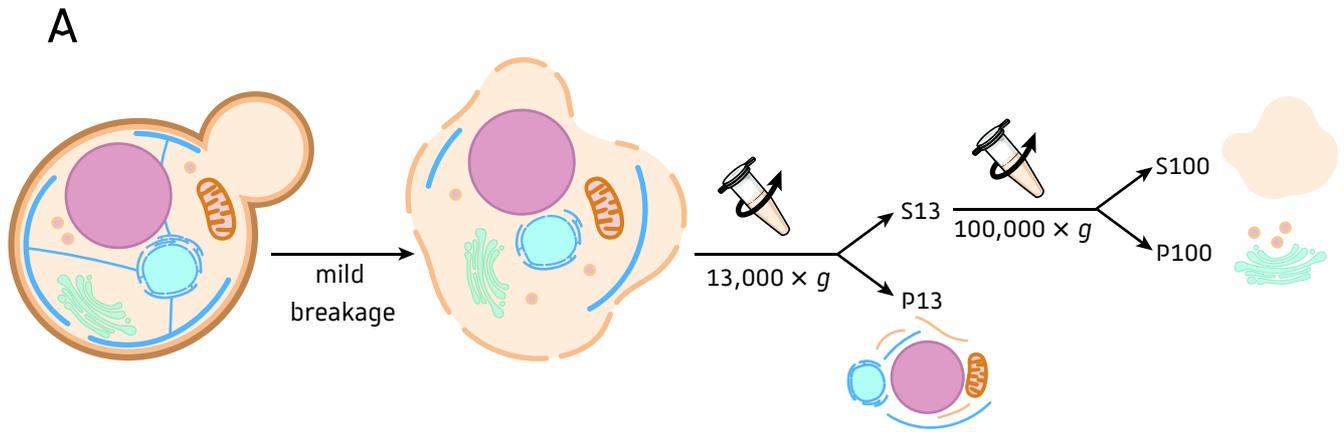
Figure ChII.R-1: Subcellular fractionation and AME complex components *in vitro* localization. A. Schematic representation of the subcellular fractionation protocol. Cells are broken using glass beads and vortex in order to maintain membrane integrity. After the first centrifugation at 13,000 × *g,* two fractions are obtained; soluble S13 and pellet P13.The S13 fraction is subsequently centrifuged at 100,000 × *g* to obtain the S100 and P100 fractions. P13: vacuole, nucleus, endoplasmic reticulum, plasma membrane, P100: Golgi and vesicles, S100: soluble fraction. **B.** Immunoblotting of the P13, P100 and S100 fractions obtained after subcellular fractionation of BY wild-type (WT) and *arc1Δ* cells. The presence of AME components was determined using anti-MRS, anti-ERS and anti-Arc1 antibodies.

but does not rely on the aminoacylation activity of LRS but on its editing domain. In regards to these observations, we hypothesized that $_c$MRS and $_c$ERS could localize at the vacuole surface (brought by the vacuolar pool of Arc1) to act as aa sensors to regulate TORC1 or another aa-sensing pathway.

To identify the vacuolar localization of proteins, biochemical approaches like subcellular fractionation or vacuole purification can be used. However, like for mitochondrial proteins identification, these methods can yield too many false positives because of impossibility to separate vacuoles from other organelles with which vacuoles make contact sites. To visualize the pool of proteins that localize at the vacuole, Dr. G. Bader and myself developed a Split-CFP system dedicated to visualize proteins binding to the vacuole compartment (Vac-Split-CFP) similar to the BiG Mito-Split-GFP. In Vac-Split-CFP system, the CFP is separated into two non-fluorescent fragments, $CFP_{\beta1-10}$ and $CFP_{\beta11ch}$, that can auto-assemble. The $CFP_{\beta1-10}$ fragment is fused to the V-ATPase protein Vph1 (Vph1-$CFP_{\beta1-10}$) and integrated in the yeast nuclear genome. On the other hand, the $GFP_{\beta11ch}$ fragment is fused to the protein of interest and expressed from plasmid DNA. Upon vacuolar localization of the $CFP_{\beta11ch}$-tagged protein, the CFP can be reconstituted and CFP fluorescence signal is emitted and observed by epifluorescence microscope. The advantage of this microscopy tool is that the fluorescence obtained is specific of a vacuolar localization. The purpose of my PhD work was to develop a microscopy tool that ensures that only vacuolar echoforms ($_{vace}$-) proteins would trigger a fluorescence signal. The main results obtained by using the Vac-Split-CFP microscopy tool along with the characterization of AME components' role at the vacuolar surface are presented in a research article for which I am the first author.

III. Results & discussion

III.1. Preliminary work: biochemical approaches to assess the AME components membrane localization

When I started working in the DyPS team, preliminary experiments had shown that Arc1 was found in membrane fractions. I thus performed subcellular fractionation of WT yeast cells from BY and RS genetic backgrounds (see **Table MM-2**) to confirm that AME components were indeed found in membrane fractions. For the subcellular fractionation cell were lysed using glass beads and the cell lysate was then separated in membrane fractions (P13 and P100) and soluble (S100) fraction by differential centrifugation (at 13,000 × g

A

B

C

D
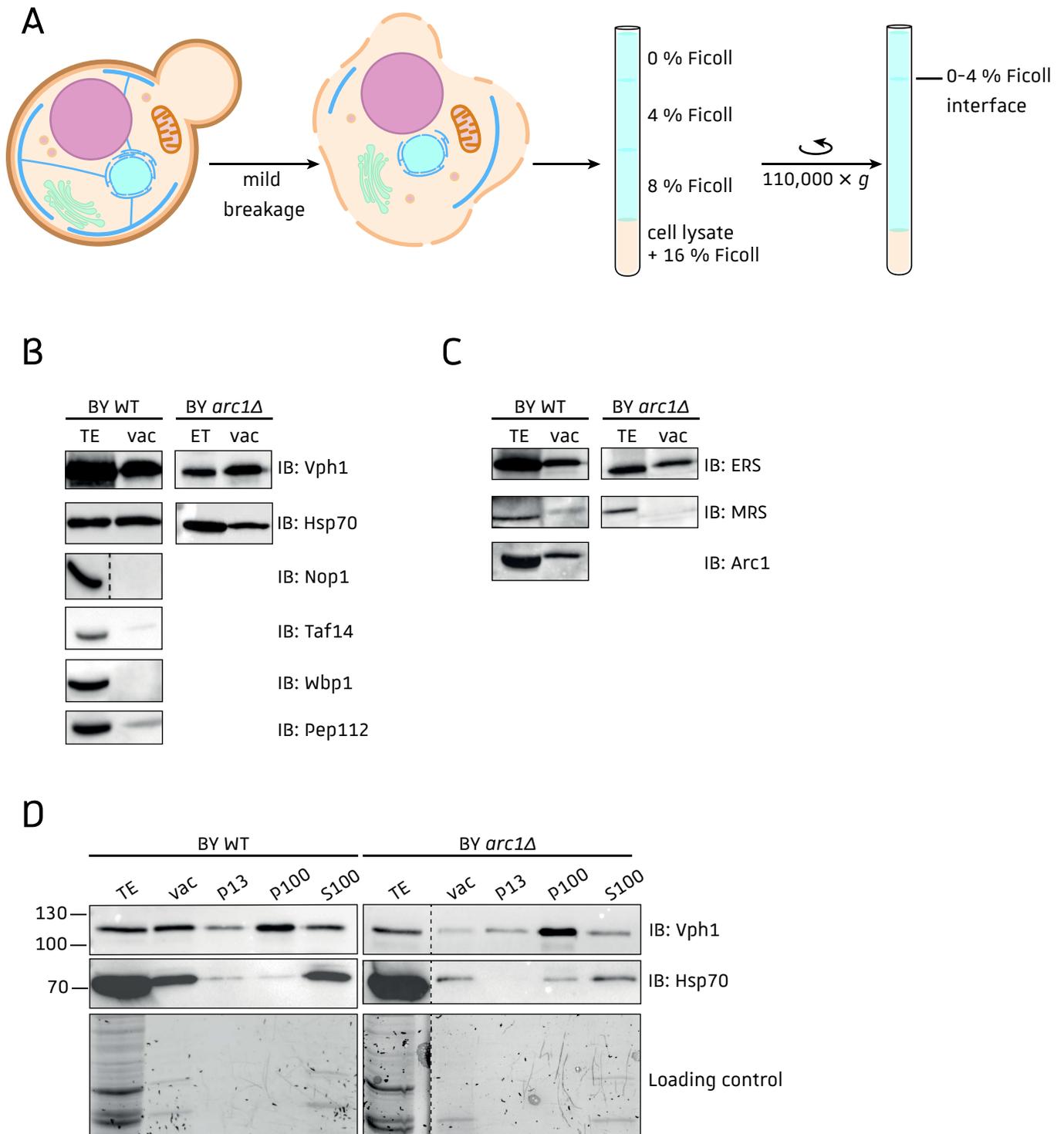
Figure ChII.R-2: Vacuole purification and AME complex components vacuolar localization. A. Schematic representation of the vacuole purification protocol. Cells are lysed using zymolyase and isoosmotic shock. Intact vacuoles are then separated from the other subcellular components using a Ficoll gradient and an ultracentriguation at 110,000 × *g* and are finally recovered at the 0-4 % Ficoll interface. **B.** Vacuole enrichment and presence of contaminating subcellular compartments were assessed by immunoblotting using antibodies directed against proteins from different subcellular compartment; Vph1: vacuole, Hsp70: mitochondria, Nop1 and Taf14: nucleus, Wbp1: endoplasmic reticulum, Pep112: endosomes. TE: total extract, vac: vacuole purification fraction. **C.** Determination of AME complex components presence in the vacuole purification fractions by immunoblotting using anti-Arc1, anti-MRS and anti-ERS. **D.** The vacuole fractions were sonicated and subsequently centrifuged at 13,000 × *g* and 100,000 × *g*. The soluble and pellet fractions were analyzed by Western blot to verify the integrity of the vacuole membrane (anti-Vph1 antibody) and the absence of mitochondrial matrix contamination (anti-Hsp70 antibody).

and 100,000 × *g* respectively) (**Figure ChII.R-1A**). The P13 pellet fraction contains nuclear, vacuolar, endoplasmic reticulum, mitochondria and plasma membranes, while the P100 fraction contains vesicles and Golgi apparatus membrane. The soluble S100 fraction contains all the cytosolic and intra-organellar proteins. The P13, P100 and S100 fractions were then analyzed by immunoblotting to assess the presence of AME complex components (**Figure ChII.R-1B**). In both backgrounds, all the AME complex components are found in mainly the P13 membrane fractions, and only slightly in the P100 fractions, indicating that they are indeed able to associate with membranes from subcellular compartments *in vivo*. The three proteins are also found in the soluble S100 fraction of BY cells. However, Arc1 and MRS are more abundant in the membrane fraction than the soluble S100 and ERS is equally distributed between both fractions. These results indicate that even if the three proteins were previously described as being exclusively cytosolic, they actually extensively associate with membranes *in vivo*. The absence of signal for the three proteins in the S100 fraction of RS cells can be explained by the lower level of proteins in this fraction (**Figure ChII.R-1B**). All together these results indicate that a substantial fraction of AME components relocate to the membranes *in vivo*. However, by using subcellular fractionation we cannot identify precisely these membranes and we cannot determine if the three components are associated with membranes in the form of a complex.

To gain insight in the vacuolar localization of AME complex components, I attempted to purify yeast vacuoles. To obtain intact vacuoles, spheroplasts were first prepared by zymolyase digestion and then lysed under isosmotic conditions using DEAE-dextran solution. The vacuoles were then isolated through flotation on a Ficoll density step gradient (**Figure ChII.R-2A**). After isolation, the enrichment and purity of the vacuole fractions were analyzed by Western blot using antibodies directed against proteins from different subcellular compartments (**Figure ChII.R-2B**). Despite a high degree of vacuole enrichment, we observed that our vacuole preparation was still contaminated with mitochondria for both BY WT and *arc1Δ* strains. This is not surprising since mitochondria and vacuoles closely interact through vCLAMP contact sites. Even if vacuoles also interact with nuclear ER, we did not identify neither nuclear nor ER contaminations within our vacuole preparation. The presence of a mitochondrial contamination makes it difficult to assess the vacuolar localization of ERS and Arc1 because they both have mitochondrial echoforms localizing in the mitochondrial matrix (Bader, 2017; Bader *et al.*, 2020). Nonetheless, the immunoblotting performed on the vacuole-mitochondria fractions could demonstrate that they indeed are present (**Figure**

ChII.R-2C). Since MRS does not localize in the mitochondria, its presence in the vacuole-mitochondria preparation is very like due to its vacuolar localization. Interestingly, when *ARC1* is deleted (BY *arc1Δ*), the presence of MRS in the vacuole fraction is abolished. These preliminary results thus indicate that MRS vacuolar localization could rely on the presence of Arc1. Since ERS and Arc1 localize in the mitochondrial matrix and are not associated with mitochondrial membranes, I attempted to get rid of mitochondrial matrix proteins in the vacuole-mitochondria fractions. For this I disrupted the organelles by sonicating the vacuole preparation and performed differential centrifugation to separate soluble proteins and membrane-associated proteins (**Figure ChII.R-2D**). The Western blot analysis indicates that the matrix protein Hsp70 indeed localizes in the soluble S100 fraction and is largely excluded from the membrane fractions P13 and P100 (**Figure ChII.R-2D**). Unfortunately, the integral vacuolar membrane protein Vph1, which is supposed to be only present in membrane fractions was also found in the soluble fraction (**Figure ChII.R-2D**). This indicates that sonicating the samples disrupts the membrane integrity and solubilizes membrane proteins. This technic thus could not be used further to unambiguously assess the association of the AME components with the vacuolar membrane.

III.2. Identification of AME components and aaRSs' vacuolar localization using the Vac-Split-CFP microscopy tool

Since biochemical approaches could not be used to identify beyond reasonable doubt, the vacuolar localization of AME complex components, we decided to create the Vac-Split-CFP epifluorescence microscopy tool based on the BiG-Mito-Split-GFP strain we previously developed (**Chapter I section III.1**). The design of the $CFP_{\beta1-10}$ fragment and its fusion to the vacuolar membrane protein Vph1 along with the integration at the *URA3* locus to create the Vac-Split-CFP strain were performed by Dr. Bader during his PhD in the DyPS team (Bader, 2017). One of the advantages of the two Split systems we developed is that only the fragment encompassing the 10 first β-strand ($GFP_{\beta1-10}$ and $CFP_{\beta1-10}$) differ but the last β-strand is the same for both systems. Thus, the $GFP_{\beta11ch}$-tagged proteins plasmid library that was developed for the study of mitochondrial proteins in **Chapter I** can also be used for the study of vacuolar localization. Nonetheless, when presenting the results obtained with the Split-Vac-CFP strain I will use the denomination $CFP_{\beta11ch}$ to avoid misunderstanding. The results I obtained after developing the system are presented here in the form of a research article.

Identifying and visualizing vacuolar echoforms of *Saccharomyces cerevisiae* cytosolic aminoacyl-tRNA synthetases

Marine Hemmerle[1], Ludovic Enkler, Guillaume Grob, Johan-Owen De Craene[1§], Gaétan Bader[1#], Bruno Senger[1], Sylvie Friant[1] and Hubert Dominique Becker[1‡]

[1.] Génétique Moléculaire, Génomique, Microbiologie, UMR 7156, CNRS, Université de Strasbourg, 4 Allée Konrad Röntgen, 67084 Strasbourg Cedex, France.

Present address: Biozentrum, University of Basel, 4056 Basel, Switzerland

§ Present address: EA 2106 Biomolécules et Biotechnologies Végétales, Université de Tours, 31, Avenue Monge, 37200 Tours, France.

‡ Correspondence to: h.becker@unistra.fr (Hubert D. Becker)

Introduction

Aminoacyl-tRNA synthetases (aaRSs) are a family of ubiquitous enzymes primarily responsible for the formation of aminoacyl-tRNA (aa-tRNA) that serve as adaptor molecules during messenger RNA translation [1]. In eukaryotes, cytosolic aaRSs ($_c$aaRSs) can assemble into multi-aminoacyl-tRNA synthetase (MARS) complexes [2,3] that are dynamical particles composed of aaRSs and accessory scaffolding proteins called AIMPs (aminoacyl-tRNA synthetase interacting multi-functional proteins) [4,5]. When inside these MSCs, aaRSs are dedicated to the production of aa-tRNAs for ribosomal protein synthesis and, in some cases their catalytic efficiency can be even be enhanced by their interacting AIMPs [6]. However, when released from the MSCs, $_c$aaRSs eventually relocate to new subcellular compartments and accomplish a variety of non-translational functions that are equally important to the cell [7,8]. The yeast *Saccharomyces cerevisiae* possesses the smallest MSC characterized thus far. This complex named AME, is composed of cytosolic methionyl- ($_c$MRS) and glutamyl-tRNA synthetase ($_c$ERS) both bound to the Arc1 AIMP [9]. Inside the AME complex, Arc1 plays the role of a cytosolic anchor preventing the release and subcellular relocation of $_c$MRS and $_c$ERS [10–12] and also enhances the aminoacylation efficiencies of the two $_c$aaRSs by binding and

delivering their cognate tRNAs [9,13–15]. So far, the AME complex has been described as exclusively cytosolic, even if the three components can have other subcellular localizations when not binding together [12,16]. Indeed, we previously demonstrated that after a metabolic switch from fermentation to respiration, the expression of the *ARC1* gene is repressed leading to the release of the $_c$MRS and $_c$ERS from the complex. Once released, $_c$MRS and $_c$ERS relocate respectively to the nucleus and to mitochondria and synchronize the nuclear transcription and mitochondrial translation of ATP synthase subunits [16]. Studies performed across species have over the past decade unraveled that a significant number of eukaryotic $_c$aaRSs are dual- if not multi-localized proteins [7,17]. It is now well accepted that eukaryotic cells use simultaneous targeting of proteins to different compartments as a way to increase protein functions with the same number of gene products. These identical or nearly identical forms that are distributed between different subcellular compartments are called echoforms [18]. Dual-localized proteins can represent up to one-third of a given species' proteome [19] and their dual-localization tend to be evolutionarily conserved across species [20]. These findings reshape our current view of what we consider as the localization and also the function of a given protein in a given organism. In the case of $_c$aaRSs, the subcellular distribution of their various echoforms is complex, dynamic and responds to a variety of stimuli [7,17]. The most frequent additional subcellular destination of $_c$aaRSs is the nucleus, and in many cases the noncanonical function of their corresponding nuclear echoforms has been identified [21]. Less frequently, $_c$aaRSs have been shown to relocate to mitochondria or at the surface of lysosome/vacuole [16,22–24].

The vacuolar/lysosomal localization of an aaRS was initially discovered for leucyl-tRNA synthetase (LRS) [23,24]. In *S. cerevisiae*, the vacuole is the main amino acid (aa) storage compartment and many transporters control the influx and efflux of aa to and from this compartment [25–29]. Moreover, the Target of Rapamycin Complex 1 (TORC1), which regulates the autophagy according to the metabolic status of the cell is constitutively present at the vacuolar surface. In the yeast, leucine-bound LRS interacts with TORC1 component Gtr1 through its CP1 editing domain. Upon leucine deprivation, the editing domain of LRS undergoes conformational changes and the interaction with Gtr1 is abolished leading to the inhibition of TORC1 activity and ultimately to autophagy. In mammalian cells, the lysosomal localization

of LRS is associated with leucylation of Rag GTPase RagA/B which promotes TORC1 activity and repress autophagy. Recently, He *et al.* demonstrated that every aaRSs, and particularly LRS and QRS, are sensing the presence of their cognate aa by reversible lysine aminoacylation of target proteins in mammalian cells [30]. Since aaRSs are highly specific for binding to their cognate aa, they could serve as aa sensors to signal aa availability to transporters and other amino acid-dependent pathways.

Interestingly, *in vitro* proteomic studies have shown that interacts with phospholipids and more specifically with phosphatidylinositol 3-phosphate (PtdIns(3)P) and phosphatidylinositol 3,5-bisphosphate (PtdIns(3,5)P_2) which are components of the yeast endosomal and vacuolar membranes respectively [31,32]. If this interaction also occurs *in vivo*, it would mean that a portion of Arc1 could also be associated with these subcellular compartments. Given that the majority of $_c$MRS and $_c$ERS is binding to Arc1, the vacuolar binding of Arc1 could trigger vacuolar localization of $_c$MRS and $_c$ERS. Unfortunately, the identification of dual-localized proteins using classical biochemical and microscopy techniques is challenging and even more for proteins which localize in the cytosol and in the vicinity of membrane organelles that face the cytoplasm. In addition, many organelles make contact with other organelles in the cell through the formation of membrane contact sites (MCSs) [33,34]. This is particularly true for vacuoles that form vCLAMP MCS with mitochondria and thus cannot be purified without mitochondrial membranes contamination. Therefore, confirming the vacuolar localization of an echoform using regular subcellular fractionation will be very difficult. Visualizing, by regular fluorescence microscopy, the vacuolar echoform of a dual localized cytosolic protein fused to a fluorescent protein (i.e. GFP, CFP, RFP…) is also extremely difficult since the fluorescence signal of the cytosolic pool of a GFP-fused echoform will eclipse that of the vacuolar one.

To circumvent this limitation, we developed a yeast strain expressing a Split-CFP system, dedicated to the visualization of vacuolar echoforms of dual-localized proteins by regular epifluorescence microscopy. This Split-CFP that we termed Vacuolar-Split-CFP (Vac-Split-CFP) allows accurate and non-ambiguous identification of echoforms localized in close proximity of the vacuolar membrane in the yeast *Saccharomyces cerevisiae*. The Vac-Split-

CFP is composed of two non-fluorescent fragments: the first fragment encompasses the ten first ß-barrel of the CFP (CFP$_{\text{ß1-10}}$) and the second fragment corresponds to the last ß-barrel of the CFP (CFP$_{\text{ß11}}$). We anchored the CFP$_{\text{ß1-10}}$ fragment at the vacuolar surface facing the cytoplasm by fusing it to the Vph1 subunit of the vacuolar V-ATPase (Vph1$_{\text{CFPß1-10}}$), while the CFP$_{\text{ß11}}$ fragment is fused to the putative dual-localized protein of interest. If there is a vacuolar echoform of the CFP$_{\text{ß11}}$-tagged protein, it will be located in the vicinity of the vacuole and thus close to the Vph1$_{\text{CFPß1-10}}$ fragment. Given that both fragments (CFP$_{\text{ß1-10}}$ and CFP$_{\text{ß11}}$) have the ability to self-assemble when in contact, the CFP is reconstituted yielding emission of a fluorescent signal detectable using conventional epifluorescence microscopy. We first verified the performances of the Vac-Split-CFP system with control proteins (i.e. using an exclusively cytosolic protein, His3, the vacuolar protein Vam13, the outer mitochondrial membrane protein Por1 and the nucleus-vacuole junction protein Nvj1) to guarantee that only a vacuolar protein triggers reconstitution of the CFP and fluorescence emission. We then tested the putative vacuolar localization of 20 $_{\text{c}}$aaRSs. As expected, we could visualize vacuolar echoforms for the two aaRSs from the AME complex. To our surprise, all the $_{\text{c}}$aaRSs we probed were also found to possess vacuolar echoforms. However, the Vac-Split-CFP does not differentiate proteins that directly bind to vacuolar lipids from those binding to vacuolar proteins. We thus performed in vitro lipid binding assays for the three components of the AME complex to determine their ability to bind directly to specific lipid species. Finally, we investigated the potential role of Arc1 and MRS vacuolar echoforms on cell growth and TORC1 activity during methionine and nitrogen starvation respectively.

Results

Construction of the Vac-Split-CFP strain

For the construction of the Vac-Split-CFP strain, the Superfolder self-assembling Split-GFP fragments designed by Cabantous and coworkers [35,36] and optimized by our team [22] were used. In this system, the 11 beta strands of the Superfolder GFP are separated into two non-fluorescent and self-assembling fragments. The Tyr66 and Asn146 residues of the fragment composed of the 10 first beta strands (GFP$_{\text{ß1-10}}$) were respectively mutated into Trp and Thr to

obtain the CFP$_{\beta1\text{-}10}$ fragment (**Supplemental Figure S1**). The second fragment composed of three concatenated beta 11 strands (GFP$_{\beta11ch}$) corresponds to the one we previously published [22] and is named CFP$_{\beta11ch}$ in this study (**Figure 1**).

To assess the vacuolar localization of proteins, the CFP$_{\beta1\text{-}10}$ fragment was fused to the vacuolar V-ATPase subunit Vph1 thereby generating Vph1$_{CFP\beta1\text{-}10}$ fusion protein (**Figure 1**). In order to stably express the Vph1$_{CFP\beta1\text{-}10}$ fusion protein, a plasmid carrying the construction under the control of GPD promoter was inserted into the *URA3* locus of BY4741 cells and the expression of the construction was verified by Western blot (**Figure 1, Supplemental Figure S2**). On the other hand, the protein of interest is fused to the CFP$_{\beta11ch}$ fragment and expressed from p414-*pGPD*-$_{\beta11ch}$ plasmid. Since the integral vacuolar protein Vph1 is delivered to the vacuole through the secretory pathway [37], its interaction with cytosolic proteins before insertion into the vacuolar membrane is very unlikely. The V-ATPase pumps protons from the cytosol into the vacuolar lumen and is thus essential to maintain cytosolic pH homeostasis. Cells with impaired Vph1 do not trigger phenotypes as drastic as cells deleted for other V-ATPase components, but have a reduced V-ATPase activity and grow slowly on medium buffered to pH 7.5 [38,39]. To ensure that the V-ATPase assembly and function were not impaired in cells expressing Vph1$_{CFP\beta1\text{-}10}$, we compared (i) the vacuole acidification (monitored by quinacrine sequestration into the vacuole, Figure 2A) between the wild-type (WT) and Vac-Split-CFP strains; (ii) the growth rate on media buffered to pH 7.5 and (iii) the vacuole morphology between both strains (**Figure 2B**). The results obtained confirm that vacuole acidification occurs in cells expressing Vph1$_{CFP\beta1\text{-}10}$ and seems even more efficient than in WT cells. In addition, Vph1$_{CFP\beta1\text{-}10}$ expressing cells have a growth rate and a vacuolar morphology similar to those of WT cells in presence of YPD medium buffered to pH 5.0 or pH 7.5. These results show that the fusion of the CFP$_{\beta1\text{-}10}$ fragment to Vph1 in the Vac-Split-CFP strain has no impact on V-ATPase activity or vacuolar morphology.

Identification of the different fluorescence patterns obtained with the Vac-Split-CFP strain

As a cytosolic control we first decided to use the His3 protein which belongs to the

histidine biosynthesis pathway (**Figure 3A**). Unexpectedly, when expressed in the Vph1$_{CFPß1-10}$ strain 14% of cells expressing His3$_{ß11ch}$ displayed CFP fluorescent dots that partially colocalize with the vacuolar FM4-64 fluorescence signal (**Figure 3B and C, Supplemental Figure S2, Supplemental Table S1**). The emission of CFP fluorescence could be triggered by a close vacuolar localization of His3 or to the nonspecific auto-assembly of the CFP$_{ß1-10}$ and CFP$_{ß11ch}$ fragments. In order to visualize the fluorescence signal emitted by a *bona fide* vacuolar protein, we generated a strain expressing Vma13$_{ß11ch}$. Vma13 is part of the V$_1$ subunit of the vacuolar V-ATPase that will dock, in fermentation conditions, to the vacuolar membrane V$_O$ subunit. When the complex is assembled, Vma13 and Vph1 are thus in close proximity [40,41]. Vma13$_{ß11ch}$ would thus localize at the surface of the vacuole and should interact with Vph1$_{CFPß1-10}$ (Figure 3A). The fluorescence signal pattern observed for Vma13$_{ß11ch}$ merges almost entirely with the FM4-64 fluorescence in contrast to the signal obtained for His3$_{ß11ch}$ and up to 80 % of FM4-64-stained vacuoles present a CFP signal (**Figure 3B and D, Supplemental Table S1**). Given that we have two different fluorescence patterns we indexed that of Vma13$_{ß11ch}$ corresponding to a vacuole-localized protein as CFP$_{all\ around}$ and that of His3$_{ß11ch}$ which is a cytosolic protein as CFP$_{dot}$ respectively (**Figure 3B and C**). These observations indicate that different fluorescence patterns can be observed with our Vac-Split-CFP strain, probably depending on the intracellular distribution of the protein.

We thus decided to analyze the fluorescence patterns of CFP$_{ß11ch}$-tagged proteins taking part to membrane contact sites (MCSs) between the vacuole and the nucleus or that are anchored in the mitochondrial outer membrane (**Figure 3A**). The fluorescence signal observed for Nvj1$_{ß11ch}$, which is anchored in the endoplasmic reticulum membrane and participate to the nucleus-vacuole junction (NVJ, **Figure 3A**), does not display the CFP$_{dot}$ or CFP$_{all\ around}$ patterns obtained for vacuolar Vma13$_{ß11ch}$ or cytosolic His3$_{ß11ch}$ (**Figure 3B and C**). Indeed, the fluorescence is not equally distributed all around the vacuole nor forms dots but appears as patches forming small arcs concentrated at a specific location that very likely corresponds to the NVJ. Since the CFP signal is more extended than the one obtained for His3, we decided to index this pattern as CFP$_{patch}$. The vacuoles and mitochondria can also be in close proximity and to test the ability of mitochondrial outer membrane protein to trigger a fluorescence signal, we

decided to use the mitochondrial porin Por1 (**Figure 3A**). Interestingly, no fluorescence signal was detected when expressing Por1$_{\text{ß11ch}}$ indicating that mitochondrial membrane proteins, which do not participate to MCS, could not trigger the reconstitution of the CFP (**Figure 3B, Supplemental Figure S2**). We then tested Atg20 which is localized at the endosomes (**Figure 3A**). The cells expressing Atg20$_{\text{ß11ch}}$ display a mix between the three different fluorescence patterns described so far (**Figure 3C, Supplemental Figure S2**). Given that endosomes will fuse to vacuoles it is not surprising that some cells display all around CFP fluorescence with Atg20$_{\text{ß11ch}}$, which is very likely the result of endosomes fusing with the vacuolar membrane even though Atg20 is not a *bona fide* vacuolar protein (**Figure 3B**). In order to assign a CFP fluorescence pattern to the described subcellular localization of the proteins we tested, we counted the distribution of each pattern we indexed and compared it to the total CFP fluorescence signal (CFP$_{\text{tot}}$) (**Supplemental Table S1**). By doing so, our data show that the cytosolic protein His3, the vacuolar protein Vam13 and the MCS Nvj1 protein, are indeed significantly represented by the CFP$_{\text{dot}}$ and CFP$_{\text{all around}}$ and CFP$_{\text{patch}}$ patterns respectively (**Figure 3C**). On the contrary, the endosomal protein Atg20 displays all three patterns equally (**Figure 3C**). The number of cells displaying the representative CFP pattern or the total CFP fluorescence were then compared to the number of cells stained with FM4-64 (**Figure D**). For all the proteins, with the exception of Atg20, there was no significant difference between the two counting methods, indicating that the vacuolar CFP fluorescence patterns distribution indeed depends on the subcellular origin of the protein. Interestingly, the ratio of CFP fluorescent cells is much higher for the vacuolar Vma13 protein, than for the other proteins (**Figure 3D**). Thus, only a *bona fide* vacuolar protein will trigger the reconstitution of the CFP in a significantly large number of cells, while proteins that are dynamically located to the vacuole vicinity will trigger CFP reconstitution in a much lower number of cells.

All together these results indicate that proteins from the mitochondrial outer membrane, that are not part of MCS between the mitochondria and the vacuole, do not trigger a detectable CFP fluorescence signal, either because their localization is not close enough from the vacuole or because the fluorescence signal triggered is below the detection limit. To the contrary, Nvj1$_{\text{ß11ch}}$, His3$_{\text{ß11ch}}$ and Atg20$_{\text{ß11ch}}$ trigger a fluorescence signal that has a specific and restricted

distribution. The CFP signal obtained for Vma13$_{\text{ß11ch}}$ confirms that a *bona fide* vacuolar protein will trigger the most efficient and extended (all around) CFP reconstitution. The interaction of the CFP$_{\text{ß1-10}}$ and CFP$_{\text{ß11ch}}$ fragments thus require a proximity that can only be achieved in the context of a membrane contact site, a direct interaction between membranes or upon interaction with a vacuolar protein. Moreover, the Vac-Split-CFP system allows the discrimination of fluorescence pattern triggered by proteins that are localized at the vacuolar surface at a well-defined and restricted area with the signal observed for a protein that is distributed all around the vacuole like Vma13.

Identification and visualization of aminoacyl-tRNA synthetase vacuolar echoforms

The vacuolar/lysosomal localization of cytosolic leucyl-tRNA synthetase (LRS) has already been demonstrated in human and yeast cells by using confocal microscopy and co-immunoprecipitation respectively [23,24]. However, these technics do not allow the specific recognition of an aaRS vacuolar echoform and the identification of the protein distribution at the vacuolar/lysosomal surface. We thus decided to use the Vac-Split-CFP strain we developed to screen the GFP$_{\text{ß11ch}}$-tagged aaRS library created in a previous work [22]. Since the mutations required for Vac-Split-CFP system are all located in the 10 first beta strands of the fluorescent protein, the last beta 11 strand is common to the previously described BiG Mito-Split-GFP and the Vac-Split-CFP systems. Surprisingly, when expressed in the Vac-Split-CFP strain, all the $_{\text{c}}$aaRS$_{\text{ß11ch}}$ tested triggered a vacuolar fluorescent CFP signal (**Figure 4, Supplemental Figure S2**). In order to characterize the vacuolar distribution of the $_{\text{c}}$aaRS, the number of cells displaying each previously-characterized fluorescent pattern was compared to the total number of cells presenting a CFP signal (**Figure 5A , Supplemental Table S1**). The results obtained unambiguously indicate that all $_{\text{c}}$aaRSs we tested localize at the vacuolar surface with a CFP$_{\text{all around}}$ pattern similar to that we obtained for the vacuolar protein Vma13. Moreover, the ratio of cells with a CFP$_{\text{all around}}$ pattern compared to the number of FM4-64 cells (**Supplemental Figure S3**) is similar to the ratio obtained when comparing the CFP$_{\text{tot}}$ signal with FM4-64 signal, indicating that this fluorescence pattern is indeed representative of the $_{\text{c}}$aaRSs. Since the $_{\text{c}}$aaRS display a fluorescence pattern similar to the one obtained for a vacuolar protein, we

compared the number of cells displaying $_c$aaRS CFP$_{\text{all around}}$ pattern to Vma13 (**Figure 5B**). By doing so, we could determine that only $_c$FRS2, $_c$NRS, $_c$LRS, $_c$ARS and $_c$GRS1 triggered a CFP$_{\text{all around}}$ fluorescence level similar to Vam13. We could thus confirm that all $_c$aaRSs tested possess a vacuolar echoform. However, differences in the frequency and probably the dynamics of the vacuolar localization event between the $_c$aaRSs are observed and will be discussed.

ERS and MRS can localize at the vacuole surface in an Arc1-independent manner

The yeast *Saccharomyces cerevisiae* contains a small Multi-Aminoacyl-tRNA Synthetase (MARS) complex, called AME complex, composed of the cytosolic glutamyl-tRNA synthetase ($_c$ERS), the methionyl-tRNA synthetase ($_c$MRS) and the aminoacylation cofactor Arc1. In fermentation conditions, the AME complex is cytosolic and participates to the production of aa-tRNA needed for protein synthesis. Upon glucose starvation, the transcription of *ARC1* gene is repressed, resulting in free $_c$MRS and $_c$ERS that relocate to the nucleus and the mitochondria respectively [16]. The AME complex is thus composed of $_c$aaRSs that have multiple subcellular localizations. Moreover, Arc1 has previously been shown to bind to phospholipids *in vitro*, and specifically to PtdIns(3)P and PtdIns(3,5)P$_2$ that are enriched in the endosomal and vacuolar membranes respectively [32]. We thus hypothesized that Arc1 could relocate at the surface of the vacuole and might escort the two $_c$aaRSs at the surface of this compartment. To confirm this, we expressed Arc1$_{\text{ß11ch}}$ in the Vac-Split-CFP *arc1Δ* strain and visualized its vacuolar localization (**Figure 6, Supplemental Figure 2**). As expected, Arc1 was localized at the vacuole surface with CFP$_{\text{all around}}$ being the representative fluorescence pattern (**Figure 6B, Supplemental Table S1**). We then assessed the vacuolar localization of $_c$ERS and $_c$MRS in the Split-Vac-CFP *arc1Δ* strain and could demonstrate that $_c$ERS$_{\text{ß11ch}}$ and $_c$MRS$_{\text{ß11ch}}$ localize at the vacuole surface in an Arc1-independent manner (**Figure 6A and B, Supplement Figure S2 and Table S**1). However, when compared to the fluorescence obtained for Vam13, none of the AME complex components reach a CFP fluorescence level comparable to the vacuolar control (**Figure 6C**). Even if the two $_c$aaRSs can localize at the vacuolar surface independently of Arc1, the distribution of the different fluorescence patterns in the arc1Δ strain differs from the WT strain (**Figure 7A**). Indeed, for both $_c$aaRSs, *ARC1* deletion triggers a significant reduction in

the number of cells displaying the $CFP_{all\ around}$ pattern and a significant increase in the number of cells with a CFP_{patch} pattern. This suggests that Arc1 somehow modulates the $_c$aaRSs' vacuolar localization. The $CFP_{all\ around}$ pattern remaining the representative pattern in Vac-Split-CFP *arc1*Δ strain, we compared it to the number of cells displaying FM4-64 fluorescence in the WT and *arc1*Δ cells (**Figure 7B**). For $_cMRS_{ß11ch}$ we observed a significant reduction in the total number of cells presenting a $CFP_{all\ around}$ pattern when *ARC1* is deleted. This demonstrates that a fraction of the vacuolar $_cMRS$ echoform is lost upon Arc1 deletion. On the contrary, *arc1*Δ cells expressing $_cERS_{ß11ch}$ display an increase in the total number of cells presenting $CFP_{all\ around}$ when compared to WT cells (**Figure 7B**). These results demonstrate that upon Arc1 loss, $_cERS$ vacuolar distribution rearranges and $_cERS$ could localize in specific vacuolar areas that appear as patches in our system. On the other hand, the increase in the total number of cells presenting a $CFP_{all\ around}$ signal observed for *arc1*Δ cells, indicate that Arc1 somehow restricts the $_cERS$ vacuolar localization event. These results demonstrate that $_cERS$ and $_cMRS$ can localize at the vacuolar surface, but the distribution and the frequency of this relocalization are impacted by Arc1. This would suggest that there might exist 2 vacuolar echoforms for both $_cERS$ and $_cMRS$, one remaining at the surface of the vacuoles by binding to Arc1(whether as a trimer or 2 distinct dimers remains to be characterized) and another either directly binding to the vacuolar membrane or interacting with a yet unknown vacuolar protein.

AME complex components in vitro interaction with phospholipids

To assess their lipid-binding ability, the three recombinant AME complex components were purified from an overexpressing *E. coli* strain and incubated on membranes coated with different phospholipid species (**Figure 8**). The results we obtained for Arc1 are similar to the ones previously reported by Fernandez and coworkers [32] (**Figure 8**). However, we could identify a strong interaction of $_{His6}$Arc1 with PtdIns(5)P and a weaker interaction with PtdIns(3,4,5)P$_3$ which is unexpected since these phosphoinositides have never been found in the yeast *Saccharomyces cerevisiae* [31]. Recombinant ERS_{His6} strongly interacts with vacuolar PtdIns(3,5)P$_2$ and more generally with all monophosphorylated and bisphosphorylated phosphoinositides (Figure 8). Again, ERS can interact with PtdIns(5)P and to a lesser extent

with PtdIns(3,4)P$_2$, and PtdIns(3,4,5)P$_3$, despite their absence it the yeast. The $_c$ERS thus does not require Arc1 to interact with lipids *in vitro*, however both proteins could bind to lipids in the form of a complex in the yeast. On the other hand, $_c$MRS does not directly interact with any tested phospholipids (**Figure 8**). Its vacuolar localization thus relies on the interaction with a vacuolar protein. To test if $_c$MRS could interact with Arc1 bound to lipids, the recombinant duplex Arc1●$_c$MRS$_{His6}$ was purified and incubated onto the lipid-coated membranes (**Figure 9**). The immunoblotting analysis using anti-$_c$MRS antibodies indicates that $_c$MRS indeed interacts with Arc1 bound to lipids *in vitro*. Arc1 could thus trigger the vacuolar localization of a portion of $_c$MRS.

Amino acid sensing and TORC1 activity are impaired in absence of Arc1-mediated vacuolar localization of $_c$MRS

In yeast, the vacuolar Target Of Rapamycin Complex 1 (TORC1) regulates the anabolic and catabolic metabolisms in response to nutrient availability [42,43]. In presence of amino acids, TORC1 is active and stimulates translation and represses autophagy by phosphorylating many target proteins and among them the ribosomal protein Rps6. In order to assess the implication of Arc1 and $_c$MRS vacuolar echoform on TORC1 activity, we monitored the phosphorylation level of Rps6 in *arc1Δ* strain and in the double mutant *arc1Δ mes1Δ* strains and in these strains complemented with $_c$MRS fused to Vph1 (MRS$_{vac}$) and thus constitutively and exclusively localized at the vacuolar membrane (**Figure 10A**). In rich medium (all amino acids are available), TORC1 activity of all mutant strains is similar to the WT. Arc1 and the possible portion of $_c$MRS vacuolar echoform brought by Arc1 thus have no impact on the activation of TORC1. On the contrary, during nitrogen depletion, TORC1, which is completely inactive in WT cells, maintains a reduced but significant activity in *arc1Δ* strain. This indicates that Arc1 and potentially the vacuolar pool of $_c$MRS interacting with Arc1 are required for the correct inhibition of TORC1 activity in absence of a nitrogen source. The overexpression of $_c$MRS$_{vac}$ restores the WT TORC1 inactivation in both *arc1Δ* and *arc1Δ mes1Δ* strains. The vacuolar localization of $_c$MRS thus has an impact on the downregulation of TORC1. However, this modulation of TORC1 activity seems to be dependent on the quantity of $_c$MRS present at

the vacuolar surface rather than on $_c$MRS interaction with Arc1. Arc1 could thus be implicated in TORC1 regulation by bringing a fraction of $_c$MRS to the vacuole vicinity. To determine if Arc1 was implicated in sensing and signaling the availability of methionine, growth assays were performed on medium depleted for methionine (**Figure 10B**). All the strains used for this experiment are prototroph for methionine and can thus produce it. While cell growth is almost totally inhibited in WT cells upon methionine depletion, *arc1*Δ cells are still able to grow even if growth is greatly reduced in comparison with rich YPD medium. The WT growth phenotype is restored upon expression of Arc1 fused to Vph1 (Arc1$_{vac}$) and thus constitutively present at the vacuolar membrane. These results indicate that Arc1 vacuolar echoform somehow participates to the signaling of methionine availability to repress translation and thus growth upon methionine depletion.

Taken together these results demonstrate that TORC1 activity and amino acid sensing and signaling pathways are modulated by Arc1 and MRS vacuolar echoform.

Discussion

In this study we present a Vacuolar-Split-CFP epifluorescence microscopy tool that allows the detection of the vacuolar echoform of cytosolic proteins. In this system, the CFP fluorescence signal emitted upon the assembly of the vacuolar CFP$_{\beta 1-10}$ fragment with the CFP$_{\beta 11ch}$-tagged protein depends on the subcellular origin of the latter. Indeed, we could demonstrate that proteins from MCS or localized in the cytosol or endosomal membranes that fuse with the vacuolar membrane will generate CFP reconstitution but i) vacuoles are never labeled entirely (dots and arcs) and ii) significantly fewer cells display a fluorescent signal (**Figure 3, Supplemental Table S1**). On the opposite, when the CFP$_{\beta 11ch}$ tag is fused to a *bona fide* vacuolar protein, the CFP signal is i) extended to the entire vacuole surface (all around) and ii) the CFP signal is observed in a large number of cells (**Figure 3**, **Supplemental Table S1**). Moreover, in order to reconstitute a fluorescent CFP, the protein has to localize extremely close to the vacuole membrane. Indeed, even if mitochondria and vacuole make close contacts in the cell, an outer mitochondrial membrane protein will not trigger CFP reconstitution (**Figure 3A, Supplemental Table S1**). We observed that a small portion of cytosolic His3 unexpectedly

generates a punctuated fluorescent signal that localizes in the vacuole vicinity (**Figure 3**). This could be explained by the fact that His3 participates to the biosynthesis of histidine and up to 90 % of this amino acid is stored in the vacuole. One could easily speculate that bringing enzymes responsible for histidine biosynthesis nearby the vacuole would potentiate histidine import in its storage compartment.

By using the Vac-Split-CFP system, we demonstrated that all $_c$aaRSs tested possess a vacuolar echoform that distributes like the vacuolar protein Vma13 all around the vacuolar surface (**Figure 4**). However, CFP reconstitution did not occur with the same efficacy for each $_c$aaRS. The $_c$aaRSs that localize at the vacuole surface in a number of cells as large as for Vma13 are $_c$FRS2, $_c$NRS, $_c$LRS, $_c$ARS and $_c$GRS1 (**Figure 5B**). These aaRSs are thus greatly enriched at the vacuole surface. Interestingly, the vacuolar localization of $_c$LRS has already been described [23]. In the model proposed by Bonfils and coworkers, the LRS interacts with vacuolar TORC1 when amino acids are available and dissociate from the vacuolar membrane upon leucine depletion. Our results confirm that $_c$LRS indeed localizes in the vacuole vicinity when amino acids are available in the growth media. For the other $_c$aaRSs, the vacuolar localization could be more dynamic or a rather rarer event regulated by different stimuli. Since aaRS can be considered as amino acid sensors [30], it would be interesting to study their vacuolar localization and the fluorescence pattern distribution upon depletion of their cognate amino acid. Concerning the AME complex, we could demonstrate that the three complex components localize at the vacuole membrane (**Figure 6**). Even if Arc1 was not absolutely necessary for $_c$MRS and $_c$ERS vacuolar localization, we showed that upon *ARC1* deletion, the distribution of $_c$MRS and $_c$ERS vacuolar echoforms displayed a more specific and restricted pattern (**Figure 7A**). Moreover, the number of cells in which vacuolar localization of both $_c$aaRSs occurred was impacted by Arc1 deletion. For $_c$MRS, the decrease in the number of cells displaying CFP fluorescence signal (**Figure 7B, Supplemental Table S1**) indicates that loss of Arc1 triggers less efficient $_c$MRS vacuolar localization, possibly because of loss of a portion of $_c$MRS vacuolar echoform. On the opposite, upon Arc1 loss, a larger number of cells displays $_c$ERS vacuolar localization indicating that Arc1somehow restricts $_c$ERS vacuolar localization. The $_c$aaRSs could thus localize at the vacuolar membrane both by binding to Arc1 and by another mechanism that has

yet to be unraveled. The *in vitro* interaction of $_c$ERS with phospholipids, and particularly with PtdIns(3,5)P$_2$, raises the possibility of a direct interaction between $_c$ERS and vacuolar lipids, *in vivo* (**Figure 8**). Interestingly, Arc1 and $_c$ERS display a broad specificity for monophosphorylated and bisphosphorylated phosphoinositides *in vitro*. We can thus hypothesize that, *in vivo*, Arc1 and $_c$ERS interaction with lipids could be extended to numerous subcellular membranes and not only to the vacuolar membrane. On the opposite, *in vitro*, $_c$MRS cannot bind directly to lipids and the interaction of $_c$MRS with phospholipids depends on the presence of Arc1 (**Figure 8 and 9**). Arc1 could thus bring a portion of $_c$MRS vacuolar echoforms to the vacuole *in vivo* and the remaining could localize at the vacuole surface by interacting with another vacuolar protein that has yet to be characterized. During amino acid starvation, TORC1 kinase activity is downregulated and translation is inhibited. However, when Arc1 is deleted, TORC1 remains partially active and cell growth is no longer impacted by methionine depletion (**Figure 10**). The amino acid availability sensing and signaling machinery to TORC1 is thus impaired upon Arc1 deletion. The overexpression of MRS or Arc1 constitutively anchored at the vacuolar membrane are sufficient to restore TORC1 downregulation and WT growth in absence of methionine respectively. We thus hypothesized that TORC1 is regulated by the amount of MRS vacuolar echoforms, and that the fraction of $_c$MRS brought to the vacuole by Arc1 can act synergistically with the Arc1-independent vacuolar $_c$MRS for efficient nitrogen starvation-induced TORC1 downregulation. $_c$MRS, and Arc1 through its possible implication in $_c$MRS vacuolar anchoring, could thus be negative regulators of TORC1 during amino acid and nitrogen starvation.

The Vac-Split-CFP system we describe here, demonstrates that all 18 caaRSs tested have a vacuolar echoform. With the exception of $_c$LRS, their localization at the vacuolar surface and implication in vacuolar functions or TORC1 signaling has never been proposed. However, they are all able to bind and activate their cognate amino acid, making them ideal candidates for amino acid sensors. Moreover, the aminoacyl-adenylate intermediate they produce during the aminoacylation reaction, has been shown to be implicated in the aminoacylation of lysine residues of target proteins in human cells [30]. If the same occurs in the yeast, one could imagine that the localization of $_c$aaRS at the surface of the storage compartment for many amino acids could be a mean to efficiently sense and transmit signals of amino acid availability to the

TORC1 machinery or to other kinases like the ones from the General Amino Acid Control for example.

Material and methods

Construction of the plasmids

The plasmid p414*pGPD*-ccdB$_{\text{ß11ch}}$ was previously created by our lab [22]. The plasmid was amplified by PCR to obtain a linearized p414*pGPD*$_{\text{ß11ch}}$ plasmid. All genes were amplified by colony PCR on BY4741 strain using the Phire Plant Direct PCR Master Mix (ThermoFisher) following the manufacturer instructions, purified by PCR clean up (Macherey-Nagel) and subcloned either by Gateway cloning or Gibson assembly in the linearized p414*pGDP*$_{\text{ß11ch}}$ plasmid.

For the creation of p306*pGPD*-Vph1$_{\text{CFPß1-10}}$ plasmid, the residues Tyr66 and Asn 146 of the previously described GFP$_{\text{ß1-10}}$ fragment [22] were mutated by site-directed mutagenesis into Trp and Thr respectively to obtain the CFP$_{\text{ß1-10}}$ fragment. The *VPH1* gene was amplified by PCR and fused to the CFP$_{\text{ß1-10}}$ fragment and subsequently cloned in the integrative plasmid p306*pGPD*-ccdB by Gateway cloning to obtain p306*pGPD*-Vph1$_{\text{CFPß1-10}}$.

Construction of the Split-vac strain

The integrative plasmid p306*pGPD*-Vph1$_{\text{CFPß1-10}}$ linearized using NsiI restriction enzyme (Fast Digest, Thermo Scientific) was transformed in BY 4742 cells and cells were selected on SC-Ura plates. For the construction of the Vac-Split-CFP *arc1Δ* strain, the Vac-Split-CFP strain was crossed with BY 4742 *arc1Δ* strain. After selection, the diploid cells were incubated on sporulation medium (potassium acetate 1 % (w/v)) and incubated at 25 °C. The tetrads were treated with zymolyase 20T (1 mg/mL) for 5 min at room temperature. Spores are then separated using a micromanipulator microscope (Singer MSM System 200). Spores having the phenotype of interest (Trp$^-$, Ura$^+$ and G418 resistant) were then selected.

Media and growth conditions

Yeast cells were cultured in complete glucose YPD medium (1% Bacto yeast extract, 1% Bacto peptone, 2% glucose) or Synthetic Complete (SC) medium (0.67% (w/v) yeast nitrogen base without amino acids (aa), 0.5% (w/v) ammonium sulfate, 2% (w/v) glucose and a mixture of aa and bases from MP biomedicals). The solid media contained 2% (w/v) of agar. Every strain was grown at 30°C with rotational shaking to mid-logarithmic growth phase (OD_{600nm} = 0.7-1.2).

Protein overexpression and purification

Bacteria were grown in LB medium (5% (w/v) Yeast extract, 10% (w/v) bacto peptone, 10% (w/v) NaCl) supplemented with ampicillin and chloramphenicol (100 mg/mL and 34 mg/mL respectively) at 37°C with rotational shaking to an OD_{600nm} = 0.5. Protein overexpression was induced with 1mM IPTG during 3 hours at 30°C.

Proteins extraction and western blots

1-1.5 OD_{600nm} units were centrifuged 5 min at 3500 rpm at room temperature (RT). Cells were suspended in 450 µL 0.185 NaOH and incubated 10 min on ice. 50 µL TCA 100% were added and after a 10 min incubation on ice the cell lysate was centrifuged 15 min at 13 000 × $\boldsymbol{g}$ at 4°C. After removing the supernatant, pellets were suspended in 50-75 µL Laemmli buffer (1 ×) buffered with Tris Base.

For each strain, 10 µL of total proteins were separated by SDS-PAGE on 8-, 10- or 12% (w/v) poly- acrylamide gels prior to electroblotting with a Trans-Blot Turbo system (BIO-RAD) onto PVDF membranes (BIO-RAD, #1704156). Detection was carried out using mouse monoclonal anti-GFP primary antibodies (1:5000; Roche Clone 7.1 and 13.1) for the recognition of $CFP_{\beta11ch}$ fragment, rabbit polyclonal anti-GFP primary antibodies for the recognition of $CFP_{\beta1-10}$ (1:5000, Sigma #G1544) and mouse monoclonal IgG1 anti-Pgk1 primary antibodies (1:5000; Molecular Probes Clone 22C5D8). Secondary antibodies were Goat anti-mouse and anti-rabbit IgG (H+L) HRP-conjugated antibodies (BIO-RAD; #1706516

and #1706515 respectively), at a concentration of 1:5000. ECL-plus reagents (BIO-RAD) was used according to the manufacturer's instructions and immuno-labeled proteins were revealed using a ChemiDoc Touch Imaging System (BIO-RAD). Total load of protein (Loading control) was assessed by UV detection using a ChemiDoc Touch Imaging System (BIO-RAD; Stain-free procedure) and detected by addition of 0.5% (v/v) 2,2,2-Trichloroethanol (Sigma #T54801) to the 30% acrylamide/bisacrylamide solution.

Image acquisition and staining

Cells were incubated overnight at 30°C in the appropriate media and diluted to an OD_{600nm} of 0.4. When the culture reached mid-logarithmic phase, 1-1.5 OD_{600nm} units were centrifuged 5 min at 3500 rpm at RT. For vacuolar staining cells were suspended in 50 μL YPD supplemented with N-(3-Triethylammoniumpropyl)-4-(6-(4-(Diethylamino) Phenyl) Hexatrienyl) Pyridinium Dibromide (FM4-64) dye at a final concentration of 7.7 μM, and incubated 15 min at 30°C. Cells were then washed with 500 μL YPD and centrifuged 2 min at 3500 rpm. FM4-64 chase was performed by a 10 min incubation at 30°C in 300 μL YPD. Cells were then centrifuged and washed with 500 μL YPD. For the microscopic studies cells were suspended in 50 μL SC medium.

Epifluorescence images were taken with an AXIO Observer d1 (Carl Zeiss) epifluorescence microscope using a 100 × plan apochromatic objective (Carl Zeiss) and processed with the Image J software.

Lipid binding assay

Recombinant proteins binding to lipids was analyzed using PIP Strip from Echelon Biosciences following the manufacturer instructions. After a 1 h incubation in blocking buffer (TBS-Tween 0.1% (v/v) fatty acid-free BSA 3% (w/v)) at RT, 10 pmol of recombinant proteins diluted in 5 mL blocking buffer were incubated for 2.5 h at RT. Detection of the protein was carried out using rabbit polyclonal anti-Arc1, -ERS and -MRS antibodies diluted 1:5000 in blocking buffer. Secondary antibodies were Goat anti-rabbit HRP-conjugated antibodies at a concentration of 1:5000. ECL-plus reagents (BIO-RAD) was used according to the

manufacturer's instructions and immuno-labeled proteins were revealed using a ChemiDoc Touch Imaging System (BIO-RAD).

[1]   M. Ibba, D. Söll, Aminoacyl-tRNA Synthesis, Annu. Rev. Biochem. 69 (2000) 617–650. https://doi.org/10.1146/annurev.biochem.69.1.617.

[2]   S. Havrylenko, M. Mirande, Aminoacyl-tRNA synthetase complexes in evolution, Int. J. Mol. Sci. 16 (2015) 6571–6594. https://doi.org/10.3390/ijms16036571.

[3]   D. Laporte, J.L. Huot, G. Bader, L. Enkler, B. Senger, H.D. Becker, Exploring the evolutionary diversity and assembly modes of multi-aminoacyl-tRNA synthetase complexes: Lessons from unicellular organisms, FEBS Lett. 588 (2014) 4268–4278. https://doi.org/10.1016/j.febslet.2014.10.007.

[4]   S.W. Lee, B.H. Cho, S.G. Park, S. Kim, Aminoacyl-tRNA synthetase complexes: Beyond translation, J. Cell Sci. 117 (2004) 3725–3734. https://doi.org/10.1242/jcs.01342.

[5]   P.S. Ray, A. Arif, P.L. Fox, Macromolecular complexes as depots for releasable regulatory proteins, Trends Biochem. Sci. 32 (2007) 158–164. https://doi.org/10.1016/j.tibs.2007.02.003.

[6]   M. Frechin, D. Kern, R.P. Martin, H.D. Becker, B. Senger, Arc1p: Anchoring, routing, coordinating, FEBS Lett. 584 (2010) 427–433.

[7]   N. Yakobov, S. Debard, F. Fischer, B. Senger, H.D. Becker, Cytosolic aminoacyl-tRNA synthetases: Unanticipated relocations for unexpected functions, Biochim. Biophys. Acta - Gene Regul. Mech. 1861 (2018) 387–400. https://doi.org/10.1016/j.bbagrm.2017.11.004.

[8]   N.H. Kwon, P.L. Fox, S. Kim, Aminoacyl-tRNA synthetases as therapeutic targets, Nat. Rev. Drug Discov. 18 (2019) 629–650. https://doi.org/10.1038/s41573-019-0026-3.

[9]   G. Simos, A. Segref, F. Fasiolo, K. Hellmuth, A. Shevchenko, M. Mann, E.C. Hurt, The yeast protein Arc1p binds to tRNA and functions as a cofactor for the methionyl- and glutamyl-tRNA synthetases, EMBO J. 15 (1996) 5437–5448. https://doi.org/10.1002/j.1460-2075.1996.tb00927.x.

[10]   K. Galani, H. Grosshans, K. Deinert, E.C. Hurt, G. Simos, The intracellular location of two aminoacyl-tRNA synthetases depends on complex formation with Arc1p, EMBO J. 20 (2001) 6889–6898. https://doi.org/10.1093/emboj/20.23.6889.

[11]   M.-P.P. Golinelli-Cohen, M. Mirande, Arc1p is required for cytoplasmic confinement of synthetases and tRNA, Mol. Cell. Biochem. 300 (2007) 47–59. https://doi.org/10.1007/s11010-006-9367-4.

[12]   M. Frechin, B. Senger, M. Brayé, D. Kern, R.P. Martin, H.D. Becker, M. Braye, D. Kern, R.P. Martin, H.D. Becker, Yeast mitochondrial Gln-tRNAGln is generated by a GatFAB-mediated transamidation pathway involving Arc1p-controlled subcellular sorting of cytosolic GluRS, Genes Dev. 23 (2009) 1119–1130. https://doi.org/10.1101/gad.518109.

[13]   J.-S. Graindorge, B. Senger, D. Tritch, G. Simos, F. Fasiolo, Role of Arc1p in the

Modulation of Yeast Glutamyl-tRNA Synthetase Activity, Biochemistry 44 (2005) 1344–1352. https://doi.org/10.1021/bi049024z.

[14]   E. Karanasios, H. Simader, G. Panayotou, D. Suck, G. Simos, Molecular Determinants of the Yeast Arc1p-Aminoacyl-tRNA Synthetase Complex Assembly, J. Mol. Biol. 374 (2007) 1077–1090. https://doi.org/10.1016/j.jmb.2007.10.010.

[15]   H. Simader, M. Hothorn, C. Kö, J. Basquin, G. Simos, D. Suck, C. Köhler, J. Basquin, G. Simos, D. Suck, Structural basis of yeast aminoacyl-tRNA synthetase complex formation revealed by crystal structures of two binary sub-complexes, Nucleic Acids Res. 34 (2006) 3968–3979. https://doi.org/10.1093/nar/gkl560.

[16]   M. Frechin, L. Enkler, E. Tetaud, D. Laporte, B. Senger, C. Blancard, P. Hammann, G. Bader, S. Clauder-Münster, L.M. Steinmetz, R.P. Martin, J.-P. di Rago, H.D. Becker, Expression of nuclear and mitochondrial genes encoding ATP synthase is synchronized by disassembly of a multisynthetase complex., Mol. Cell. 56 (2014) 763–76. https://doi.org/10.1016/j.molcel.2014.10.015.

[17]   S. Debard, G. Bader, J.O. De Craene, L. Enkler, S. Bär, D. Laporte, P. Hammann, E. Myslinski, B. Senger, S. Friant, H.D. Becker, Nonconventional localizations of cytosolic aminoacyl-tRNA synthetases in yeast and human cells, Methods. 113 (2017) 91–104. https://doi.org/10.1016/j.ymeth.2016.09.017.

[18]   R. Ben-Menachem, O. Pines, Detection of dual targeting and dual function of mitochondrial proteins in yeast, Methods Mol. Biol. 1567 (2017) 179–195. https://doi.org/10.1007/978-1-4939-6824-4_11.

[19]   R. Ben-Menachem, M. Tal, T. Shadur, O. Pines, A third of the yeast mitochondrial proteome is dual localized: A question of evolution, Proteomics. 11 (2011) 4468–4476. https://doi.org/10.1002/pmic.201100199.

[20]   S. Karniely, O. Pines, Single translation-dual destination: mechanisms of dual protein targeting in eukaryotes, EMBO Rep. 6 (2005) 420–425. https://doi.org/10.1038/sj.embor.7400394.

[21]   P. Schimmel, C.C. Wang, Getting tRNA synthetases into the nucleus, Trends Biochem. Sci. 24 (1999) 127–128. https://doi.org/10.1016/S0968-0004(99)01369-9.

[22]   G. Bader, L. Enkler, Y. Araiso, M. Hemmerle, K. Binko, E. Baranowska, J.O. De Craene, J. Ruer-Laventie, J. Pieters, D. Tribouillard-Tanvier, B. Senger, J.P. Di Rago, S. Friant, R. Kucharczyk, H.D. Becker, Assigning mitochondrial localization of dual localized proteins using a yeast bi-genomic mitochondrial-split-GFP, Elife. 9 (2020) 1–24. https://doi.org/10.7554/eLife.56649.

[23]   G. Bonfils, M. Jaquenoud, S. Bontron, C. Ostrowicz, C. Ungermann, C. De Virgilio, Leucyl-tRNA Synthetase Controls TORC1 via the EGO Complex, Mol. Cell. 46 (2012) 105–110. https://doi.org/10.1016/j.molcel.2012.02.009.

[24]   J.M. Han, S.J. Jeong, M.C. Park, G. Kim, N.H. Kwon, H.K. Kim, S.H. Ha, S.H. Ryu, S. Kim, Leucyl-tRNA synthetase is an intracellular leucine sensor for the mTORC1-signaling pathway, Cell. 149 (2012) 410–424. https://doi.org/10.1016/j.cell.2012.02.044.

[25]   M. Ishimoto, N. Sugimoto, T. Sekito, M. Kawano-Kawada, Y. Kakinuma, ATP-Dependent Export of Neutral Amino Acids by Vacuolar Membrane Vesicles of Saccharomyces cerevisiae, Biosci. Biotechnol. Biochem. 76 (2012) 1802–1804. https://doi.org/10.1271/bbb.120372.

[26]   F. Bianchi, J.S. van't Klooster, S.J. Ruiz, B. Poolman, Regulation of Amino Acid Transport in Saccharomyces cerevisiae , Microbiol. Mol. Biol. Rev. 83 (2019) 1–38. https://doi.org/10.1128/mmbr.00024-19.

[27]   M. Kawano-Kawada, Y. Kakinuma, T. Sekito, Transport of amino acids across the vacuolar membrane of yeast: Its mechanism and physiological role, Biol. Pharm. Bull. 41 (2018) 1496–1501. https://doi.org/10.1248/bpb.b18-00165.

[28]   X.D. Gao, J. Wang, S. Keppler-Ross, N. Dean, ERS1 encodes a functional homologue of the human lysosomal cystine transporter, FEBS J. 272 (2005) 2497–2511. https://doi.org/10.1111/j.1742-4658.2005.04670.x.

[29]   J.A. Simpkins, K.E. Rickel, M. Madeo, B.A. Ahlers, G.B. Carlisle, H.J. Nelson, A.L. Cardillo, E.A. Weber, P.F. Vitiello, D.A. Pearce, S.P. Vitiello, Disruption of a cystine transporter downregulates expression of genes involved in sulfur regulation and cellular respiration, Biol. Open. 5 (2016) 689–697. https://doi.org/10.1242/bio.017517.

[30]   X. Di He, W. Gong, J.N. Zhang, J. Nie, C.F. Yao, F.S. Guo, Y. Lin, X.H. Wu, F. Li, J. Li, W.C. Sun, E.D. Wang, Y.P. An, H.R. Tang, G.Q. Yan, P.Y. Yang, Y. Wei, Y.Z. Mao, P.C. Lin, J.Y. Zhao, Y. Xu, W. Xu, S.M. Zhao, Sensing and Transmitting Intracellular Amino Acid Signals through Reversible Lysine Aminoacylations, Cell Metab. 27 (2018) 151-166.e6. https://doi.org/10.1016/j.cmet.2017.10.015.

[31]   J.O. De Craene, D.L. Bertazzi, S. Bär, S. Friant, Phosphoinositides, Major Actors in Membrane Trafficking and Lipid Signaling Pathways, Int. J. Mol. Sci. 18 (2017) 634. https://doi.org/10.3390/ijms18030634.

[32]   J.P. Fernandez-Murray, C.R. McMaster, Identification of novel phospholipid binding proteins in Saccharomyces cerevisiae, FEBS Lett. 580 (2006) 82–86. https://doi.org/10.1016/j.febslet.2005.11.055.

[33]   M. Eisenberg-Bord, N. Shai, M. Schuldiner, M. Bohnert, A Tether Is a Tether Is a Tether: Tethering at Membrane Contact Sites, Dev. Cell. 39 (2016) 395–409. https://doi.org/10.1016/j.devcel.2016.10.022.

[34]   M. Bohnert, Tether Me, Tether Me Not—Dynamic Organelle Contact Sites in Metabolic Rewiring, Dev. Cell. 54 (2020) 212–225. https://doi.org/10.1016/j.devcel.2020.06.026.

[35]   S. Cabantous, T.C. Terwilliger, G.S. Waldo, Protein tagging and detection with engineered self-assembling fragments of green fluorescent protein, Nat. Biotechnol. 23 (2005) 102–107. https://doi.org/10.1038/nbt1044.

[36]   J.-D. Pédelacq, S. Cabantous, T. Tran, T.C. Terwilliger, G.S. Waldo, Engineering and characterization of a superfolder green fluorescent protein, Nat. Biotechnol. 24 (2006) 79–88. https://doi.org/10.1038/nbt1172.

[37]   K. Bowers, T.H. Stevens, Protein transport from the late Golgi to the vacuole in the yeast Saccharomyces cerevisiae, Biochim. Biophys. Acta - Mol. Cell Res. 1744 (2005) 438–

454. https://doi.org/10.1016/j.bbamcr.2005.04.004.

[38]   P.M. Kane, The Where, When, and How of Organelle Acidification by the Yeast Vacuolar H+-ATPase, Microbiol. Mol. Biol. Rev. 70 (2006) 177–191. https://doi.org/10.1128/mmbr.70.1.177-191.2006.

[39]   M.F. Manolson, B. Wu, D. Proteau, B.E. Taillon, B.T. Roberts, M.A. Hoyt, E.W. Jones, STV1 gene encodes functional homologue of 95-kDa yeast vacuolar H+- ATPase subunit Vph1p, J. Biol. Chem. 269 (1994) 14064–14074. https://doi.org/10.1016/s0021-9258(17)36755-8.

[40]   K.J. Parra, C.Y. Chan, J. Chen, Saccharomyces cerevisiae vacuolar H+-ATPase regulation by disassembly and reassembly: One structure and multiple signals, Eukaryot. Cell. 13 (2014) 706–714. https://doi.org/10.1128/EC.00050-14.

[41]   J. Zhao, S. Benlekbir, J.L. Rubinstein, Electron cryomicroscopy observation of rotational states in a eukaryotic V-ATPase, Nature. 521 (2015) 241–245. https://doi.org/10.1038/nature14365.

[42]   J. Avruch, X. Long, S. Ortiz-Vega, J. Rapley, A. Papageorgiou, N. Dai, Amino acid regulation of TOR complex 1, Am. J. Physiol. - Endocrinol. Metab. 296 (2009) 592–602 https://doi.org/10.1152/ajpendo.90645.2008.

[43]   S. Zaman, S.I. Lippman, X. Zhao, J.R. Broach, How Saccharomyces Responds to Nutrients, Annu. Rev. Genet. 42 (2008) 27–81. https://doi.org/10.1146/annurev.genet.41.110306.130206.

Table 1: Strains generated or used in this study

Strain	Genotype	Source
BY 4742	*MATa his3Δ1 leu2Δ0 lys2Δ0 trp1Δ0 ura3Δ0*	Winston *et al.,* 1995
BY 4742 trp⁻	*MATa his3Δ1 leu2Δ0 lys2Δ0 trp1Δ0 ura3Δ0*	This study
BY 4742 *arc1Δ*	*MATα arc1Δ::KanMX4 his3Δ1 leu2Δ0 ura3Δ0*	This study
Vac-Split-CFP	*MATa his3Δ1 leu2Δ0 lys2Δ0 trp1Δ0 ura3Δ0::p306-pGPD-VPH1$_{CFPβ1-10}$*	This study
Vac-Split CFP *arc1Δ*	*MAT? leu2Δ0 trp1Δ0 his3Δ1 arc1::KanMX4 ura3Δ0::p306-pGPD-VPH1$_{CFPβ1-10}$*	This study
RS 453	*MATa ade2-1 his3-11,15 leu2-3,112 trp1-1 ura3-52*	
RS 453 *arc1Δ*	*MATa ade2-1 his3-11,15 leu2-3,112 trp1-1 ura3-52 arc1Δ::KanMX4*	This study
RS 453 *arc1Δ* MRS$_{vac}$	*MAT? arc1Δ::KanMX4 ura3-52::*p306-pGPD-*MES1-VPH1*	This study
RS 453 *arc1Δ mes1Δ* MRS$_{vac}$	*MAT? mes1Δ::HIS3 arc1Δ ::KanMX4 leu2-3,112 ::*p305-pGPD-*MES1-VPH1-cMyc*	This study

fragment	size (kDa)	fused to	expressed from	promoter
CFP$_{\beta 1-10}$	25,2	Vph1	genomic DNA (*URA3* locus)	*GPD*
CFP$_{\beta 11ch}$	8,3	ProtX	plasmid	*GPD*
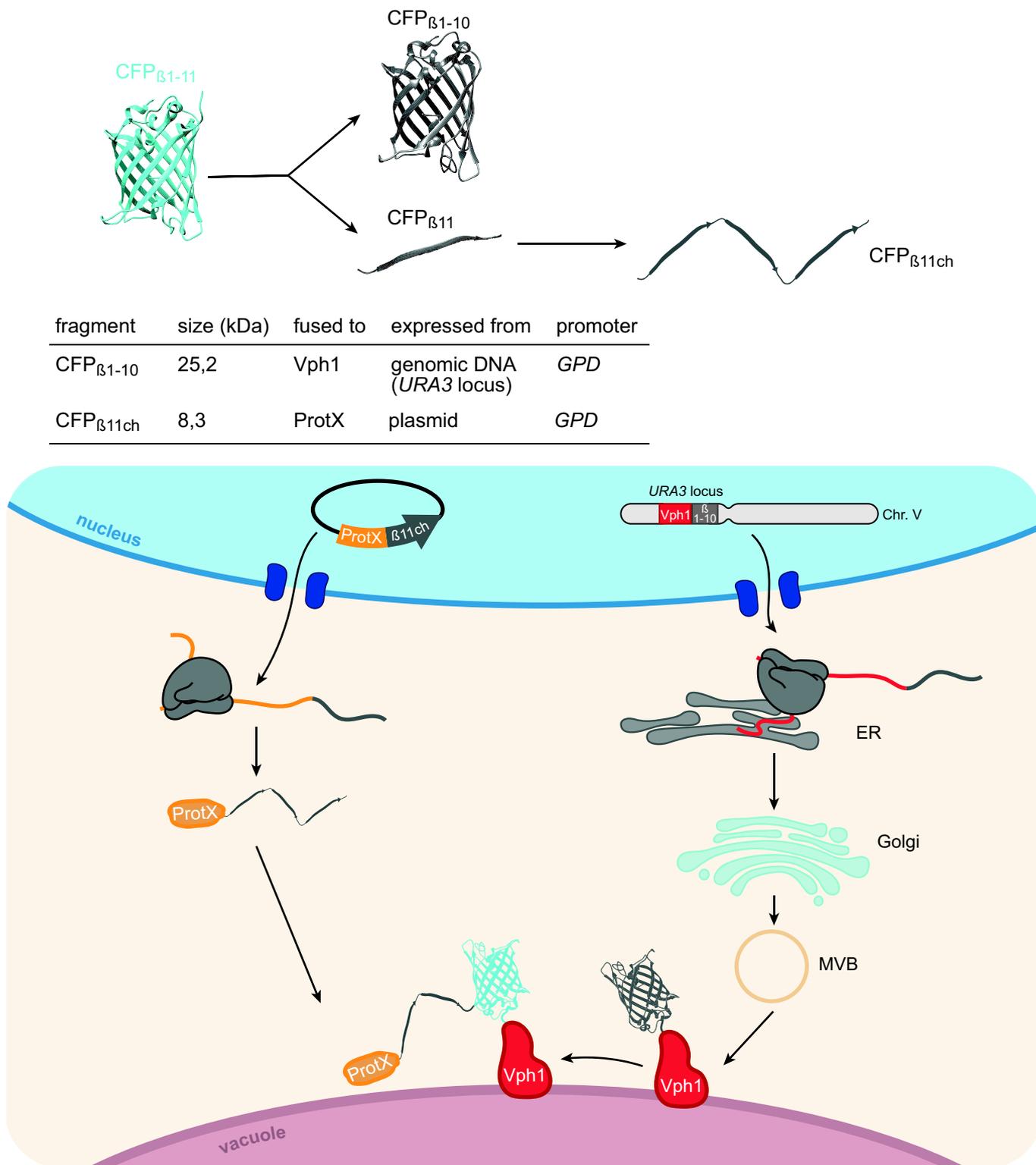
Figure 1: Engineering of Vacuolar-Split-CFP system in *Saccharomyces cerevisiae.* The CFP composed of eleven beta strands is separated into two non-fluorescent and self-assembling fragments; CFP$_{\beta 1-10}$ and CFP$_{\beta 11}$. Three CFP$_{\beta 11}$ tags are concatenated to form the CFP$_{\beta 11chapelet}$ or CFP$_{\beta 11ch}$ tag that allows the simultaneous reconstitution of three CFP. The CFP$_{\beta 1-10}$ tag fused to the gene *VPH1* is stably expressed from the genomic DNA, while the CFP$_{\beta 11ch}$ tag fused to the protein of interest is expressed from plasmidic DNA. Upon cytosolic translation, the integral membrane protein Vph1$_{CFP\beta 1-10}$ is inserted in the endoplasmic reticulum (ER) membrane and brought the vacuolar membrane through the secretory pathway. Upon vacuolar localization of the CFP$_{\beta 11ch}$-tagged protein, the two CFP fragments can self-assemble and reconstitute an active and fluorescent CFP. The emission of CFP can be monitored by epifluorescence microscopy.

A

B
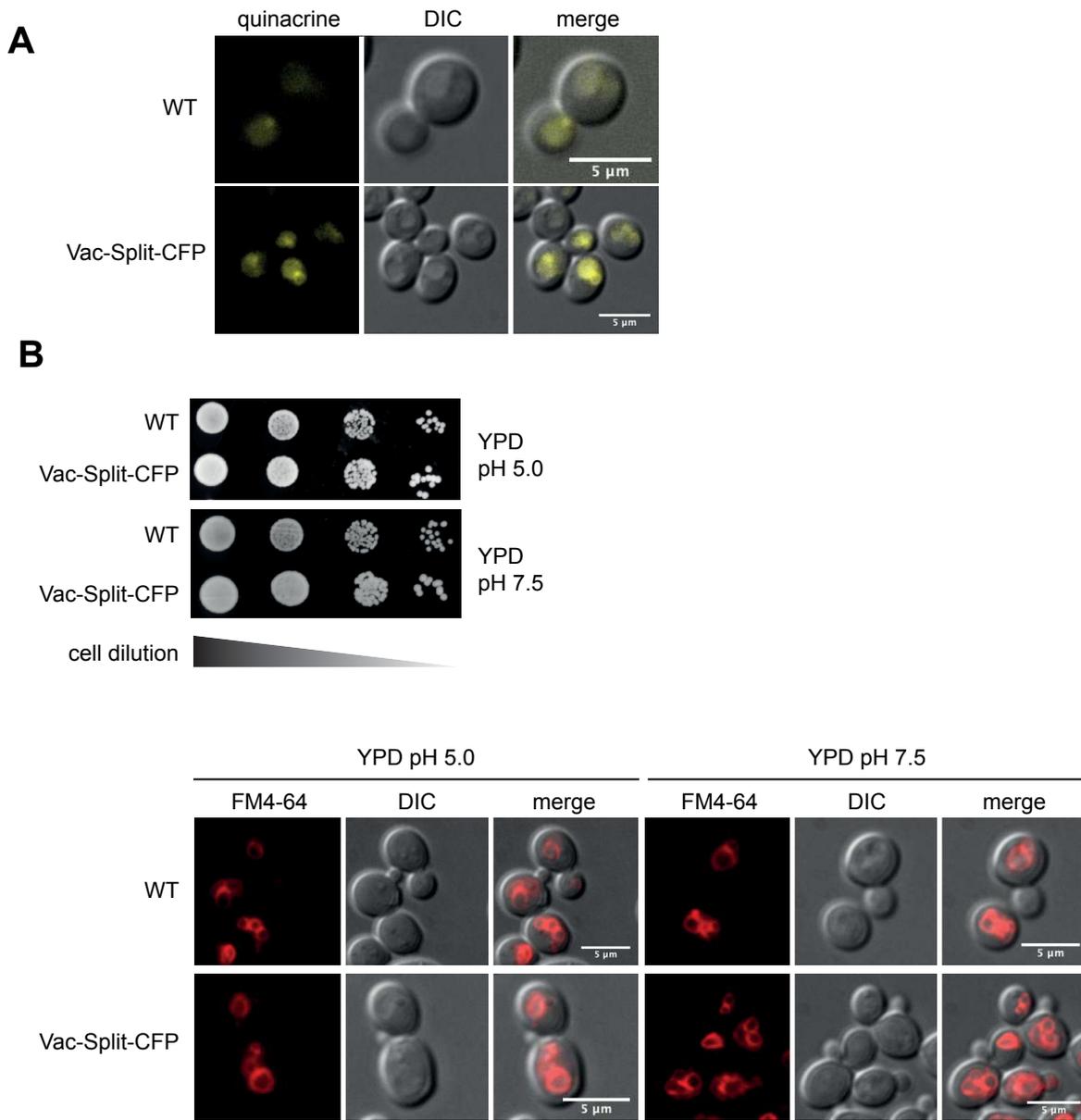
Figure 2: Impact of CFP$_{\beta1\text{-}10}$ fusion to Vph1 on vacuolar V-ATPase activity. A. Vacuolar acidification assay using quinacrine as a fluorescent probe on wild-type (WT) and Vac-Split-CFP strains. The sequestration of quinacrine in the vacuole was monitored using epifluorescence microscopy. **B.** Growth assay (N=3) and visualization of vacuole morphology using YPD medium buffered to pH 5.0 or pH 7.5 on WT and Vac-Split-CFP strains. The vacuolar membrane is stained with the fluorescent probe FM4-64. Representative fields are shown.
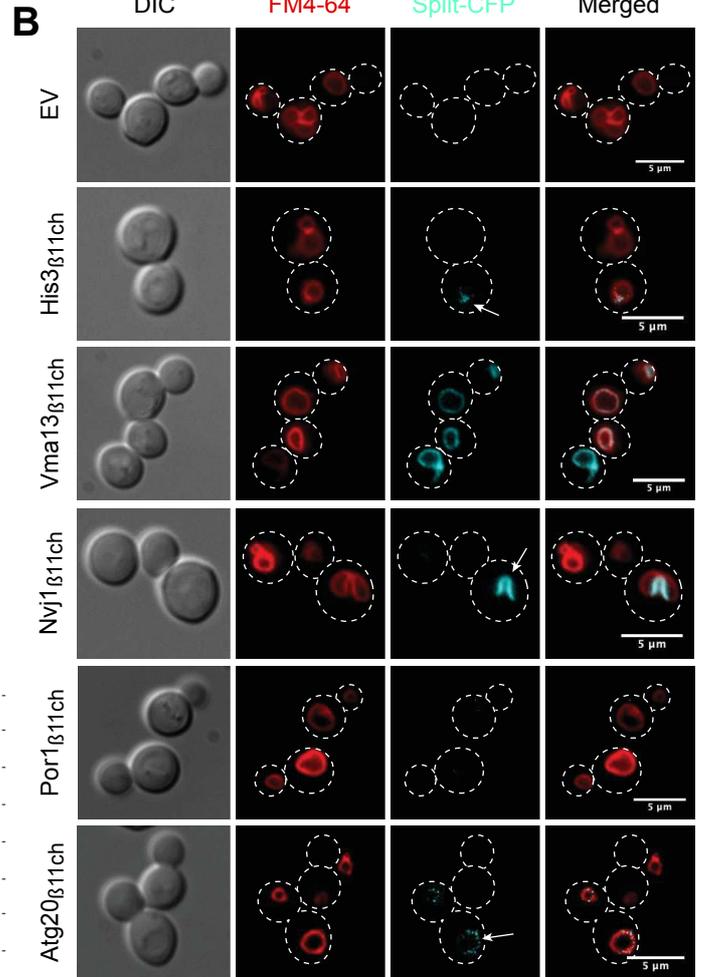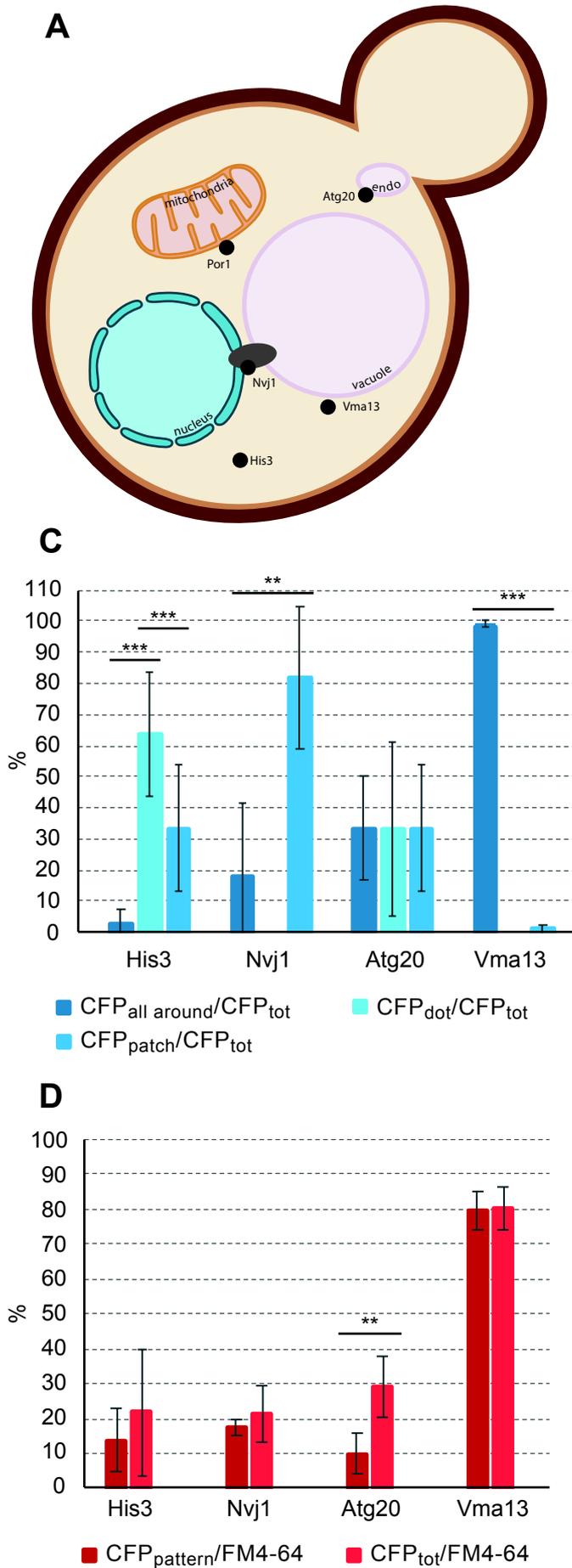
Figure 3: CFP fluorescence signal patterns triggered by proteins with different subcellular localization. A. Schematic representation of the subcellular localization of the proteins used to determine the different fluorescence patterns. His3: cytosolic protein, Por1: outer mitochondrial membrane protein, Atg20: endosomal protein, Nvj1: nuclear ER protein, part of NVJ membrane contact site, Vma13: cytosolic protein associated with the vacuolar membrane subcomplex V_O of the V-ATPase. **B.** The Vac-Split-CFP strain stably expressing Vph1$_{CFPß1-10}$ was transformed with empty p414*pGPD*-$_{ß11ch}$ vector (EV) or p414*pGPD*-$_{ß11ch}$ vectors expressing the control proteins. Vacuolar CFP reconstitution upon protein vacuolar localization was monitored using epifluorescence microscopy (N=3). The vacuole membrane was stained using FM4-64. **C.** For each control protein, the number of cells presenting a the CFP$_{all\ around}$, CFP$_{patch}$ or CFP$_{dot}$ pattern was compared to the total number of cells with a vacuolar CFP signal (CFP$_{tot}$). The difference between the most abundant pattern and the other patterns was statistically analyzed; *: p value $\leq$ 0.05, **: p value $\leq$ 0.01 and ***: p value $\leq$ 0.001. **D.** The CFP pattern representative of each protein was compared to the total number of cells with FM4-64-stained vacuoles. A significant difference was only observed for Atg20 (**: p value $\leq$ 0.01).
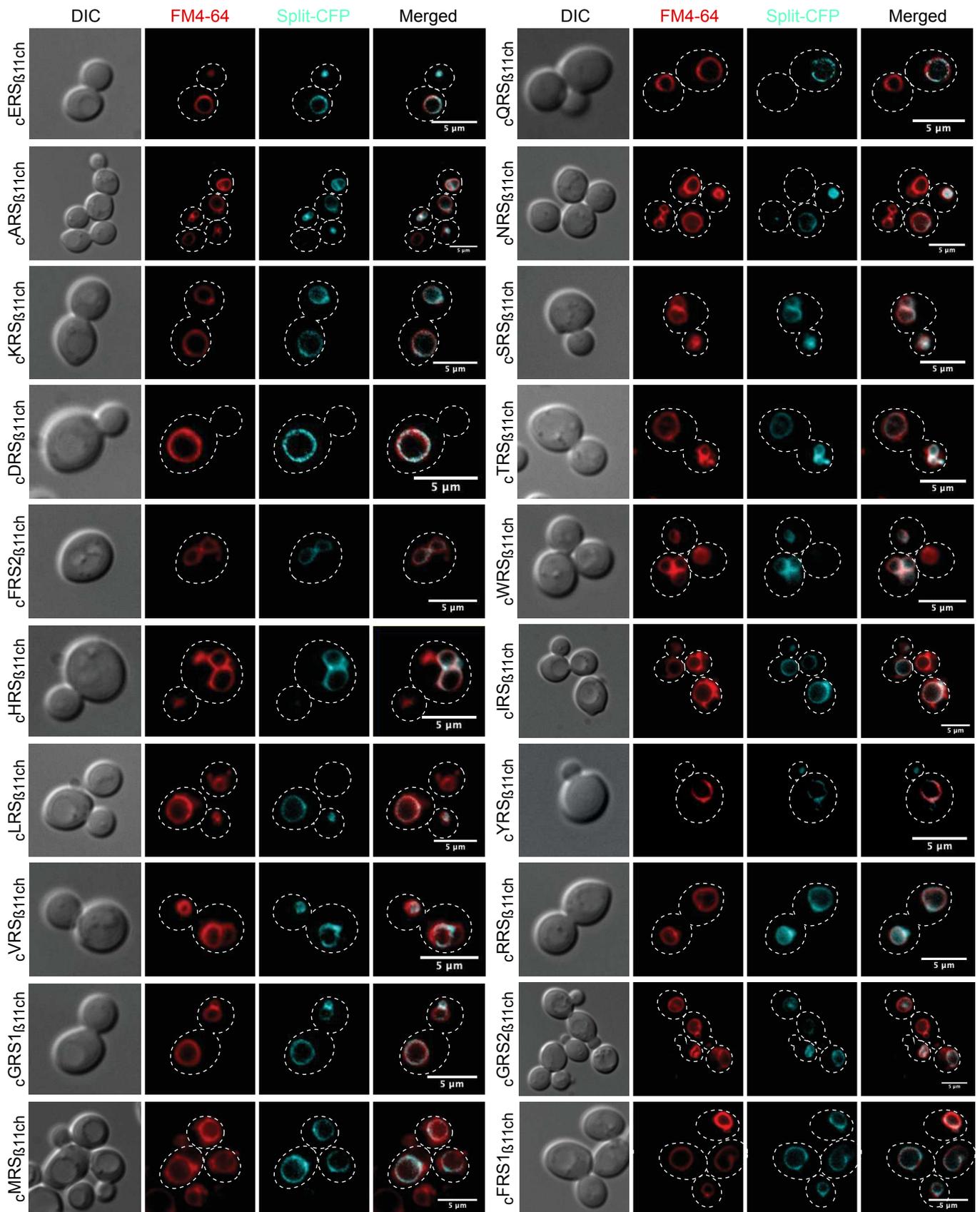
Figure 4: Identification and visualization of vacuolar echoforms of $_c$aaRSs using the Vac-Split-CFP system. The plasmids p414*pGPD*-$_{ß11ch}$ expressing 20 different aaRSs were transformed in the Vac-Split-CFP strain. The vacuolar localization triggering CFP reconstitution was followed by epifluorescence microscopy. Vacuoles were stained with FM4-64 to monitor merging of the two vacuolar signals. Representative fields are shown.

A

B
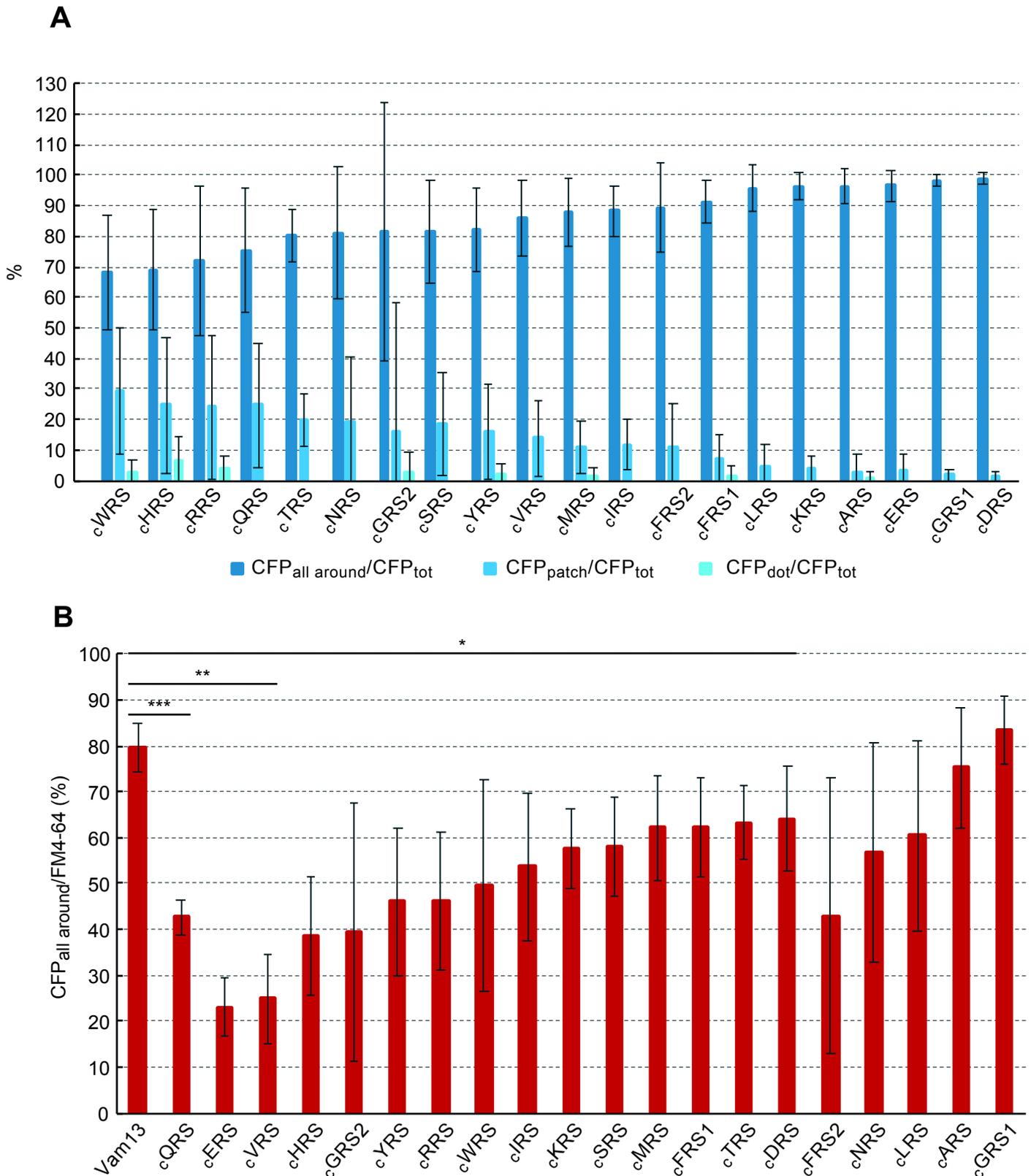
Figure 5: Analysis of vacuolar aaRS echoforms fluorescence patterns. A. The number of cells presenting the three different CFP fluorescence patterns was compared to the CFP_{tot} signal. **B.** The $CFP_{all\ around}$/FM4-64 ratio of each aaRS was compared to Vam13. The difference between each $_c$aaRS and Vma13 was statistically analyzed. Only significant differences are represented. *: p value ≤ 0.05, **: p value ≤ 0.01 and ***: p value ≤ 0.001.
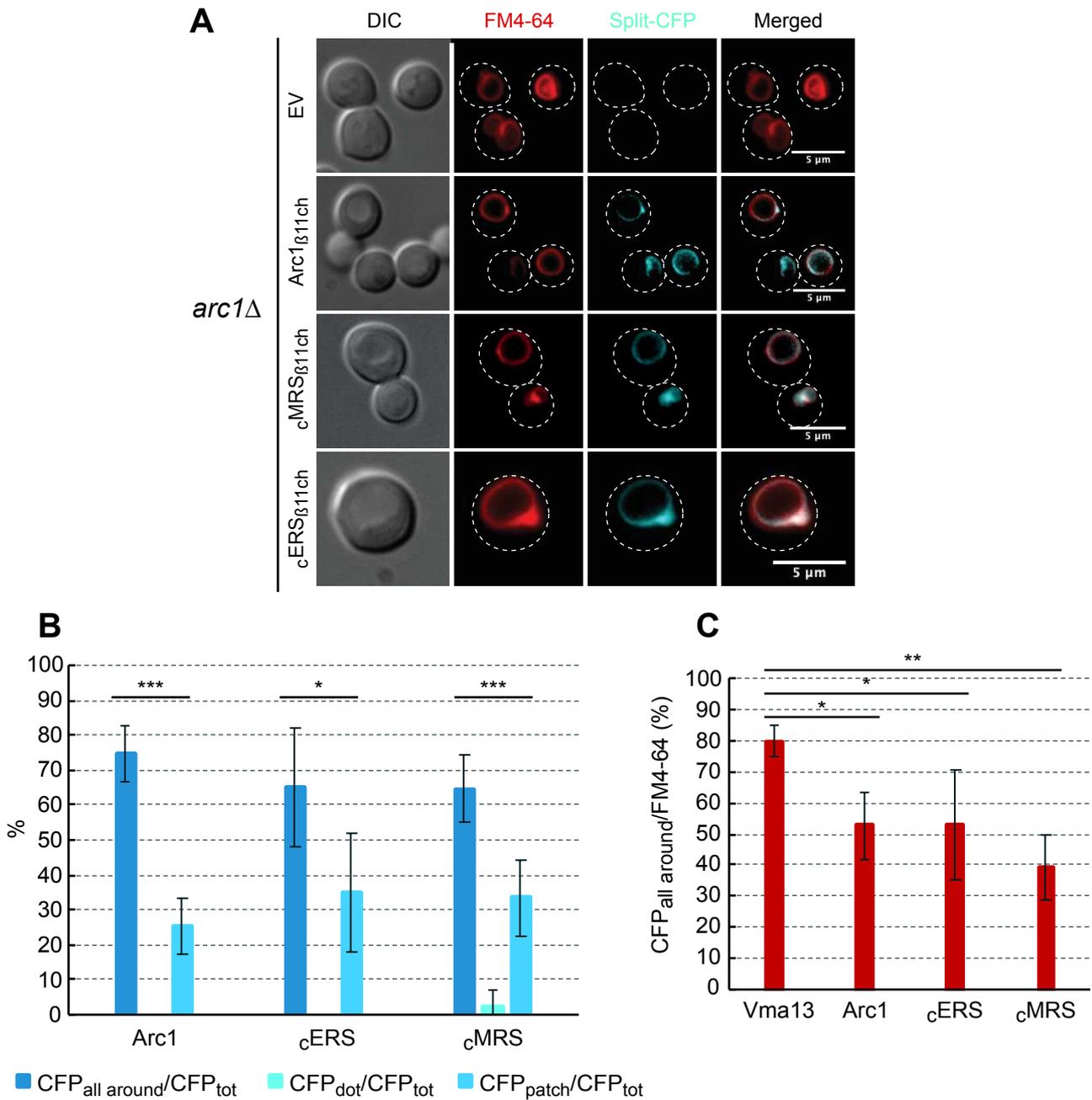
Figure 6: Vacuolar localization of the AME complex components. Cells stably expressing $Vph1_{CFP\beta1-10}$ and deleted for *ARC1* gene (*arc1Δ*) were transformed with centromeric pAG414*pGPD*-$_{\beta11ch}$ plasmid expressing either $Arc1_{\beta11ch}$, $ERS_{\beta11ch}$ or $MRS_{\beta11ch}$ (N>89 cells observed) and vacuoles were stained using FM4-64. Scale bar: 5 μm. Representative fields are shown.

A

B

■ MRS WT ■ MRS *arc1Δ* ■ ERS WT ■ ERS *arc1Δ*
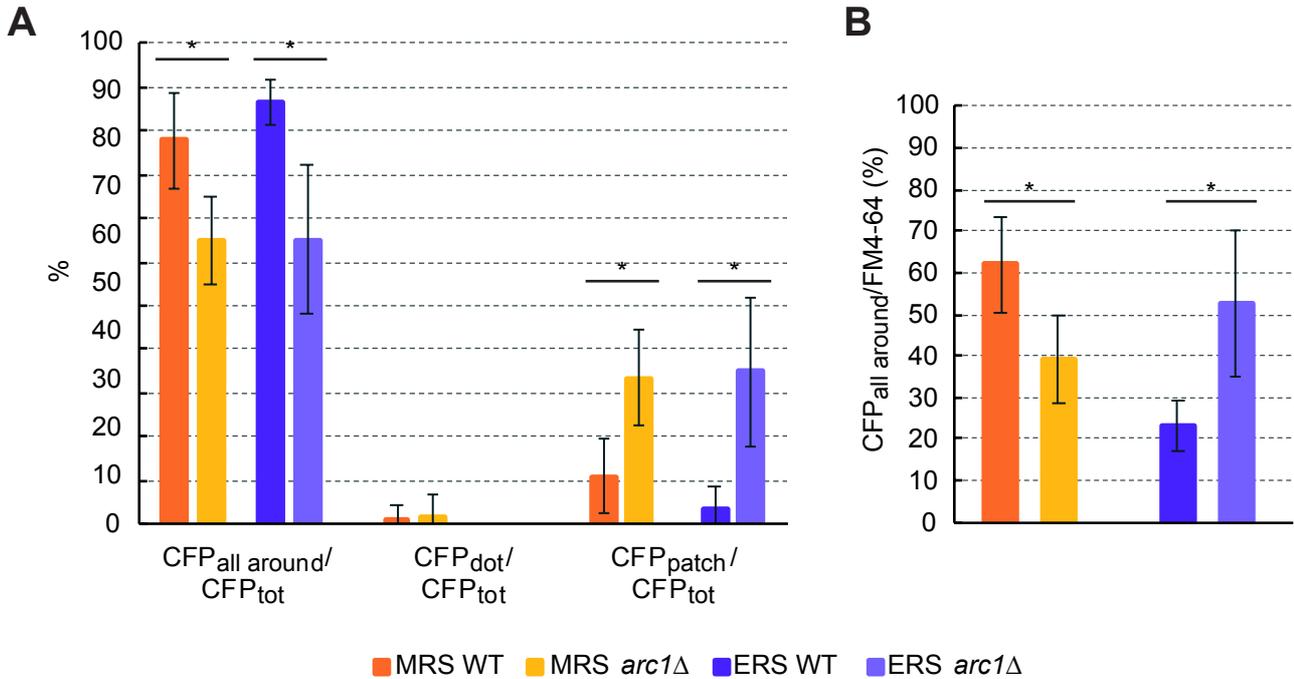
Figure 7: Arc1 modulates the vacuolar localization $_c$MRS and $_c$ERS. A. Comparison of the vacuolar CFP fluorescence pattern distribution of $_c$MRS and $_c$ERS in WT and *arc1Δ* cells. Significant difference is represented with stars. **B.** Comparison between the ratio of CFP$_{all around}$/FM4-64 cells in WT and *arc1Δ* cells expressing $_c$MRS$_{β11ch}$ or $_c$ERS$_{β11ch}$. Significant difference is represented with stars.
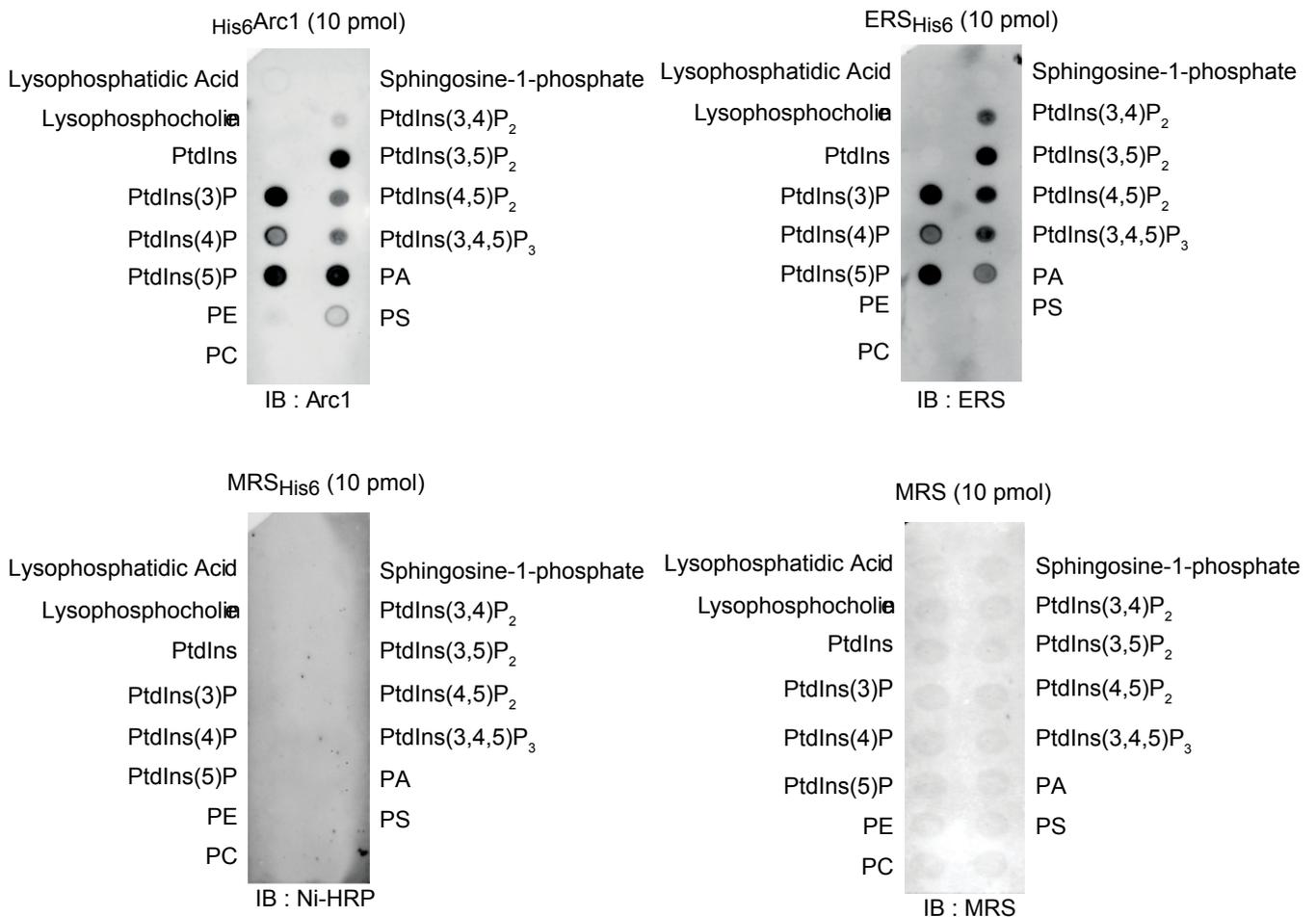
Figure 8: AME complex components *in vitro* interaction with phospholipids. Recombinant Arc1, ERS and MRS tagged with a His6-tag or native MRS (10 pmol) were incubated on membranes coated with different phospholipids. The immunoblotting was performed with anti-Arc1, anti-ERS, anti-MRS antibodies or Ni-HRP conjugate. PtdIns: phosphatidylinositiol, PA: phosphatidic acid, PE: phosphatidylethanolamine, PC: phosphatidylcholine, PS: phosphatidylserine.

Arc1•MRS$_{His6}$

IB: MRS

IB: Arc1
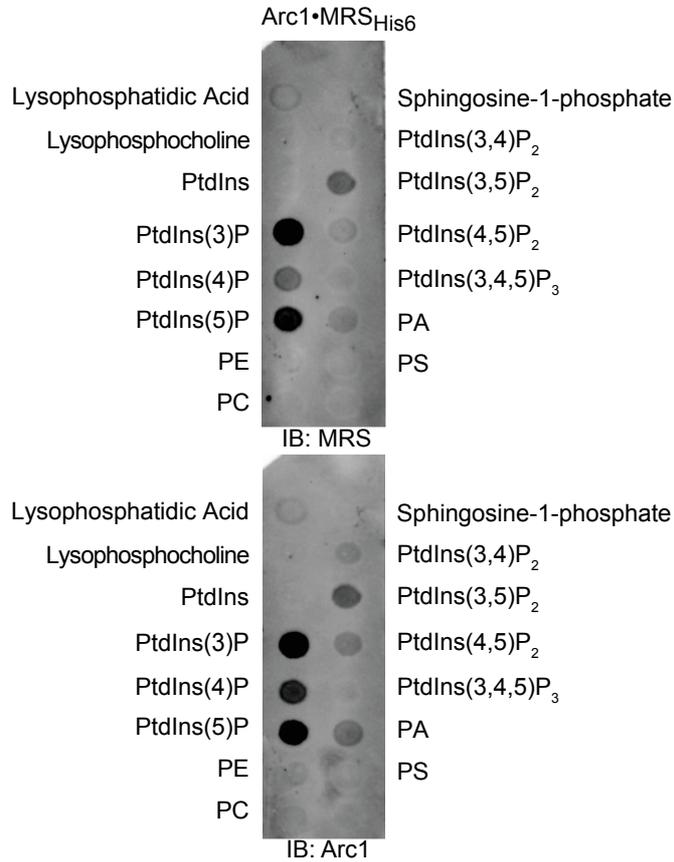
Figure 9: MRS interacts with lipid-bound Arc1 Purified recombinant Arc1•MRS$_{His6}$ duplex (10 pmol) was incubated on a membrane coated with different phospholipids. The immunoblotting was performed with anti-MRS and subsequently with anti-Arc1 antibodies.

A
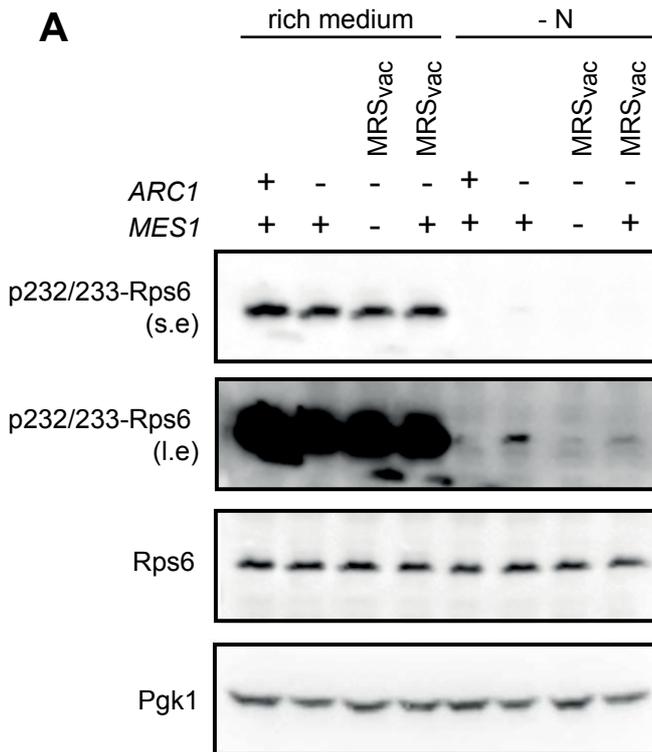
Figure 10: Sensing of amino acid availability and TORC1 activity are impaired in *arc1Δ* strain. A. The activity of TORC1 was monitored by the phosphorylation status of Rps6 in presence of rich medium or during nitrogen starvation (-N) (N=2). s.e/l.e: short and long exposition of the Western blot. MRS$_{vac}$: MRS fused to Vph1 and constitutively localized at the vacuolar surface. Pgk1: loading control. **B.** Growth assay on rich (YPD) and methionine depleted (SC-Met) medium. Arc1$_{vac}$: Arc1 fused to Vph1 and constitutively localized at the vacuole surface (N=1).

B

1 MSKGEELFTGVVPILVELDGDVNGHKFSVRGEGEGDATIGKLTLKFICTT 50

> ß1   ß2   ß3

51 GKLPVPWPTLVTTLTWGVQCFSRYPDHMKQHDFFKSAMPEGYVQERTISF 100

> ß4

101 KDDGKYKTRAVVKFEGDTLVNRIELKGTDFKEDGNILGHKLEYNFTSHNV 150

> ß5   ß6

151 YITADKQKNGIKANFTVRHNVEDGSVQLADHYQQNTPIGDGPVLLPDNHY 200

> ß7   ß8   ß9

201 FLSTQTVLSKDPNEKSGHHHHHH

> ß10
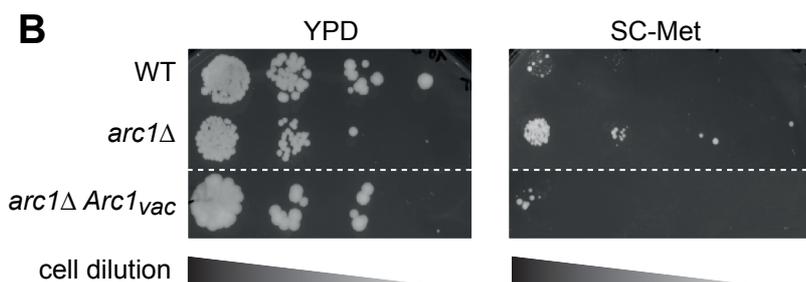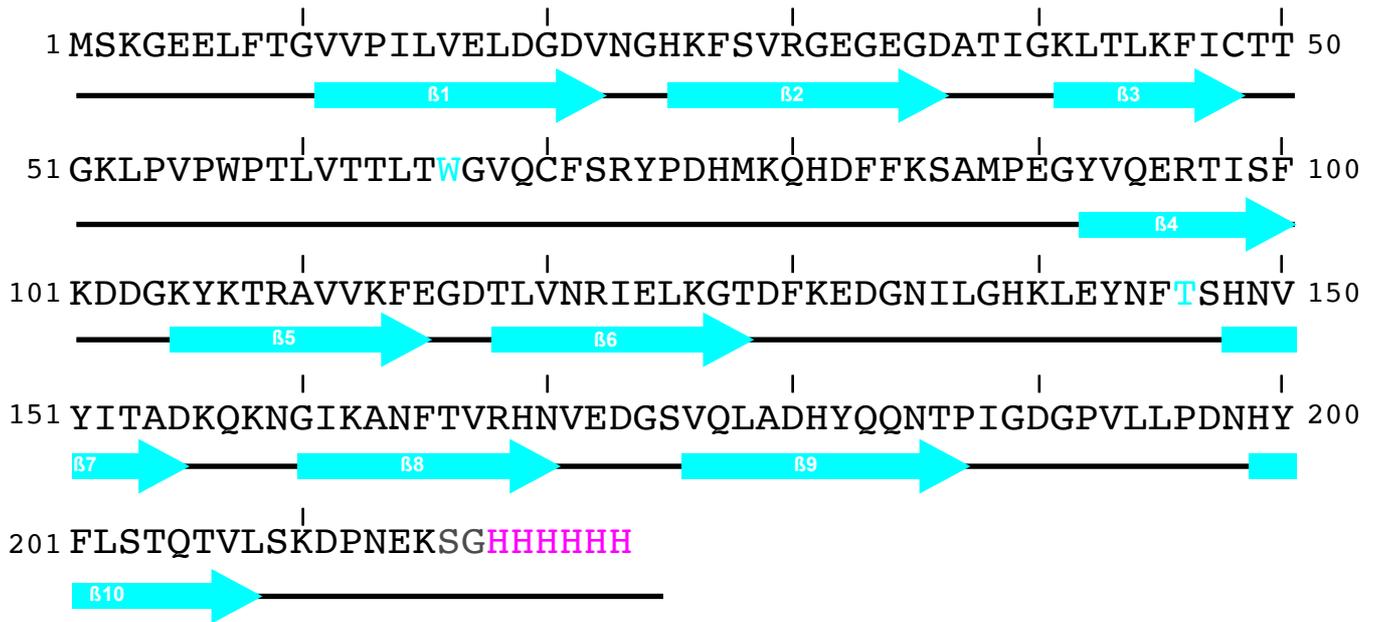
Supplemental Figure S1: CFP$_{ß1-10}$ amio acid sequence and secondary structure. The CFP$_{ß1-10}$ fragment was designed based on the BiG Mito-Split-GFP GFP$_{ß1-10}$ fragment we previously published. The amino acids represented in blue are the two mutations that were inserted in order to obtain CFP$_{ß1-10}$ from GFP$_{ß1-10}$. The ß-strands are schematized as blue arrows.
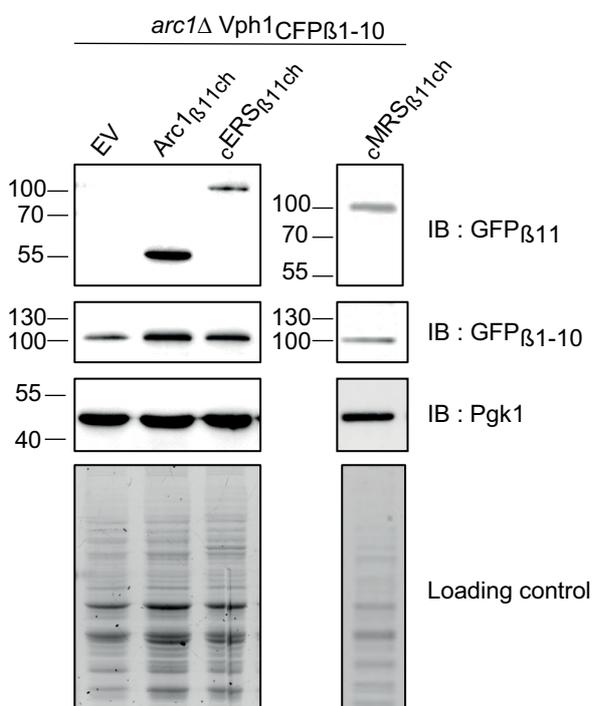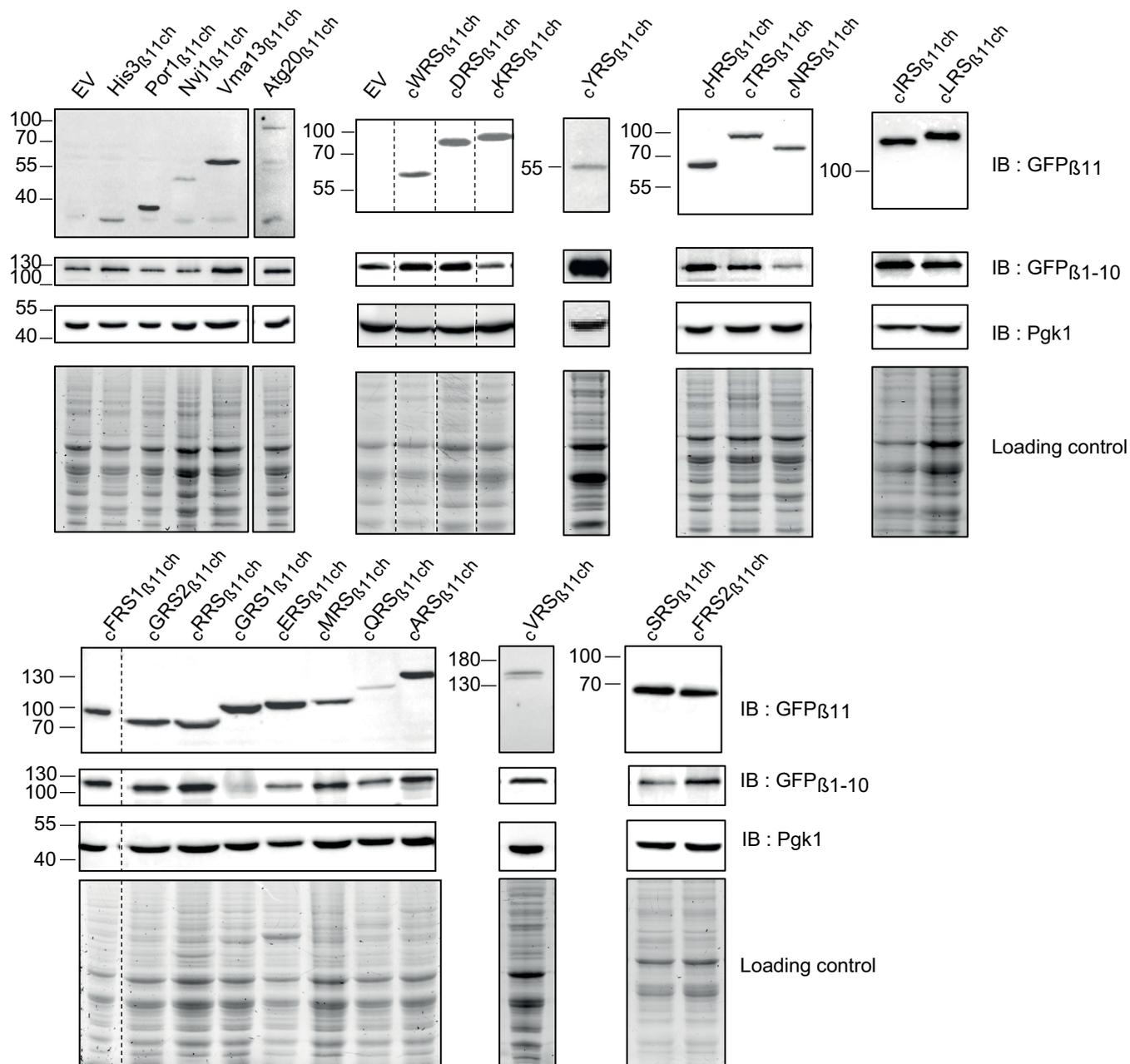
Supplemental Figure S2: Western blot analysis of the expression of the CFP$_{\beta11ch}$-tagged proteins and Vph1$_{CFP\beta1-10}$. The expression of CFP$_{\beta11ch}$-tagged proteins and Vph1$_{CFP\beta1-10}$ was verified in each strain (WT and *arc1Δ)* using anti-GFP$_{\beta11}$ and anti-GFP$_{\beta1-10}$ antibodies respectively. Pgk1: Western blot transfer control. SDS-PAGE loading control performed using the Stain free technic.
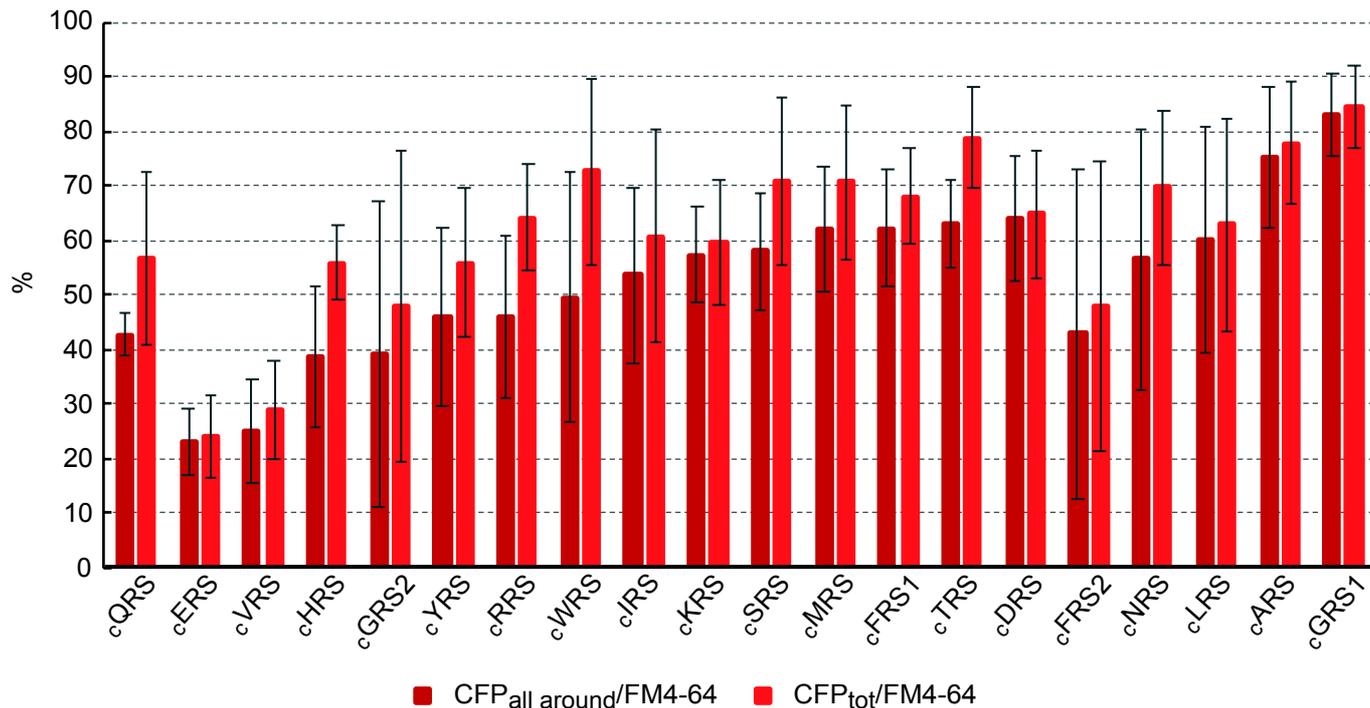
Supplemental Figure S3: Comparison of CFP$_{all\ around}$/FM4-64 and CFP$_{tot}$/FM4-64 ratio for the $_c$aaRSs. No significant difference could be detected between the two counting methods.

Supplemental Table S1: Fluorescent cells count. The total number of cells presenting the different CFP fluorescence patterns was compared to the total number of CFP fluorescent cells or to the number of cells stained with FM4-64. SD: Standard deviation.

		CFP$_{shape}$/CFP$_{tot}$ (%)						CFP/FM4-64 (%)							
		CFP$_{all around}$/CFP$_{tot}$	SD	CFP$_{dot}$/CFP$_{tot}$	SD	CFP$_{patch}$/CFP$_{tot}$	SD	CFP$_{tot}$/FM4-64	SD	CFP$_{all around}$/FM4-64	SD	CFP$_{patch}$/FM4-64	SD	CFP$_{dot}$/FM4-64	SD
	Por1	0	0	0	0	0	0	0	0	0	0	0	0	0	0
	His3	3	5	64	20	33	20	22	18	1	1	7	13	14	9
	Nvj1	18	23	0	0	82	23	21	8	4	7	17	2	0	0
	Atg20	33	17	33	28	33	20	29	9	10	6	10	10	10	8
	Vma13	99	1	0	0	1	1	80	6	80	5	1	1	0	0
	WRS	68	19	2	5	29	21	73	17	50	23				
	HRS	69	20	7	8	25	22	56	7	39	13				
	RRS	72	24	4	4	24	24	64	10	46	15				
	QRS	75	20	0	0	25	20	57	16	43	4				
	TRS	80	9	0	0	20	9	79	9	63	8				
	NRS	81	22	0	0	19	22	70	14	57	24				
Vac-Split-CFP	GRS2	82	42	3	6	16	43	48	29	39	28				
	SRS	82	17	0	0	18	17	71	16	58	11				
	YRS	82	13	2	4	16	15	56	14	46	16				
	VRS	86	12	0	0	14	12	29	9	25	10				
	MRS	88	11	1	3	11	8	71	14	62	12				
	IRS	88	8	0	0	12	8	61	19	54	16				
	FRS2	89	14	0	0	11	14	48	26	43	30				
	FRS1	91	7	2	3	7	8	68	9	62	11				
	LRS	96	8	0	0	4	8	63	20	60	21				
	KRS	96	4	0	0	4	4	60	12	57	9				
	ARS	96	6	1	2	3	6	78	11	75	13				
	ERS	96	5	0	0	4	5	24	8	23	6				
	GRS1	98	2	0	0	2	2	85	8	83	7				
	DRS	99	2	0	0	1	2	65	12	64	11				
Vac-Split-CFP *arc1Δ*	Arc1	75	8	0	0	25	8	71	12	53	11				
	ERS	65	17	0	0	35	17	81	14	53	17				
	MRS	65	10	2	5	33	11	61	8	39	10				

Figure ChII.R-3: Standalone CFP$_{\beta11ch}$ fragment cannot associate with vacuolar CFP$_{\beta1-10}$ fragment. The Vac-Split-CFP strain was transformed with p414-*pGPD*-CFP$_{\beta11ch}$ and the vacuolar localization of CFP$_{\beta11ch}$ fragment was analyzed using epifluorescence microscopy. The vacuoles are stained using FM4-64. Scale bar: 5 µm.
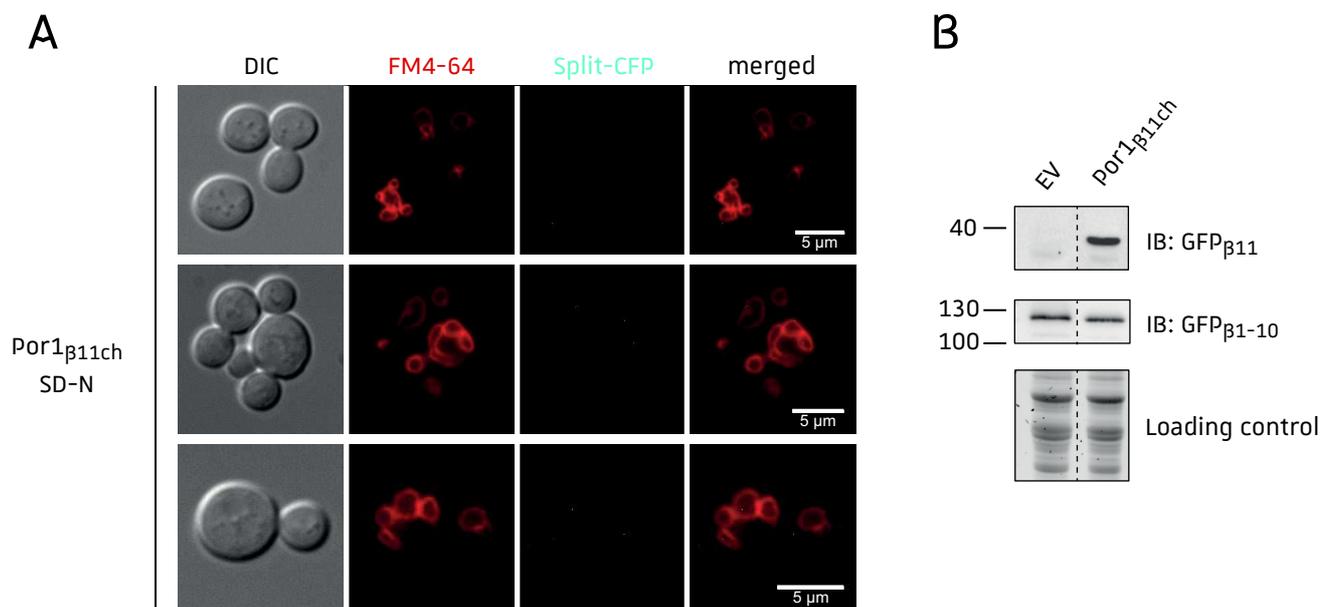
Figure ChII.R-4: Outer mitochondrial membrane protein Por1$_{\beta11ch}$ does not interact with Vph1$_{CFP\beta1-10}$ in autophagy conditions. A. The Vac-Split-CFP strain was transformed with p414-*pGPD*-Por1$_{\beta11ch}$ and incubated during 1 h in SD-N autophagy medium before microscopy observation. Vacuoles are stained using FM4-64. Scale bar : 5 µm. **B.** The expression of Por1$_{\beta11ch}$ and Vph1$_{CFP\beta1-10}$ before the induction of autophagy was verified by Western blot using anti-GFP$_{\beta11}$ and anti-GFP$_{\beta1-10}$ respectively. EV: empty vector.

III.3. Additional work performed on the Vac-Split-CFP strain

III.3.1. Study of the vacuolar localization of standalone CFP$_{\beta 11ch}$ fragment

Since the N-terminal degradation of C-terminally CFP$_{\beta 11ch}$-tagged proteins could result in the presence of standalone CFP$_{\beta 11ch}$ tag, I transformed the Vac-Split-CFP strain with p414-*pGPD*-CFP$_{\beta 11ch}$ plasmid and assessed its vacuolar localization by epifluorescence microscopy (**Figure ChII.R-3**). Because of the very small size of the CFP$_{\beta 11ch}$ fragment (~ 9 kDa) I could not verify its expression by Western blot. However, the same plasmid was used in the BiG Mito-Split-GFP strain (**Figure ChI.R-2**) and triggered the reconstitution of mitochondrial GFP, ensuring that standalone β11ch fragment is indeed expressed from this plasmid and correctly folded. The absence of CFP fluorescence signal (**Figure ChII.R-3**) thus indicates that standalone CFP$_{\beta 11ch}$ cannot localize at the vacuole surface and interact with Vph1$_{CFP\beta 1-10}$ to reconstitute an active CFP. We can thus confirm that even if proteins are N-terminally processed, the resulting CFP$_{\beta 11ch}$ fragment will not give rise to false positive vacuolar fluorescence signal.

III.3.2. Utilization of the Vac-Split-CFP strain in autophagy conditions

III.3.2.1. Outer mitochondrial membrane protein Por1 does not interact with vacuolar membrane during autophagy

By using the BiG Mito-Split-GFP strain in autophagy conditions, I could show that mitochondria seem to localize in the vacuole vicinity in this condition (**Figure ChI.R-3**). In order to determine if mitochondria were indeed close enough to the vacuolar membrane in autophagy conditions, I used the Vac-Split-CFP strain expressing the outer mitochondrial membrane protein Por1$_{\beta 11ch}$ and induced autophagy by transferring the cells to SD-N medium during 1 h (**Figure ChII.R-4**). The absence of vacuolar CFP fluorescence signal indicates that mitochondrial Por1$_{\beta 11ch}$ does not get close enough from the vacuolar membrane during autophagy to interact with Vph1$_{CFP\beta 1-10}$ and trigger CFP reconstitution (**Figure ChII.R-4A**). However, the expression of Por1$_{\beta 11ch}$ was only verified before the induction of autophagy and not after (**Figure ChII.R-4B**). The absence of CFP fluorescence could thus be explained by a reduction of Por1$_{\beta 11ch}$ expression during autophagy. The autophagy was also only induced during 1 h before observation, while the observations with BiG Mito-Split-GFP strain were performed after an overnight incubation in SD-N medium. A longer autophagy induction could thus allow the relocalization of mitochondria in the the vicinity of the vacuole and thus

A

B
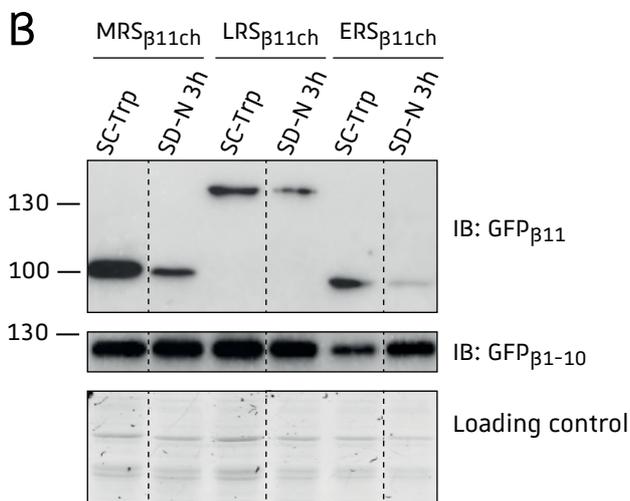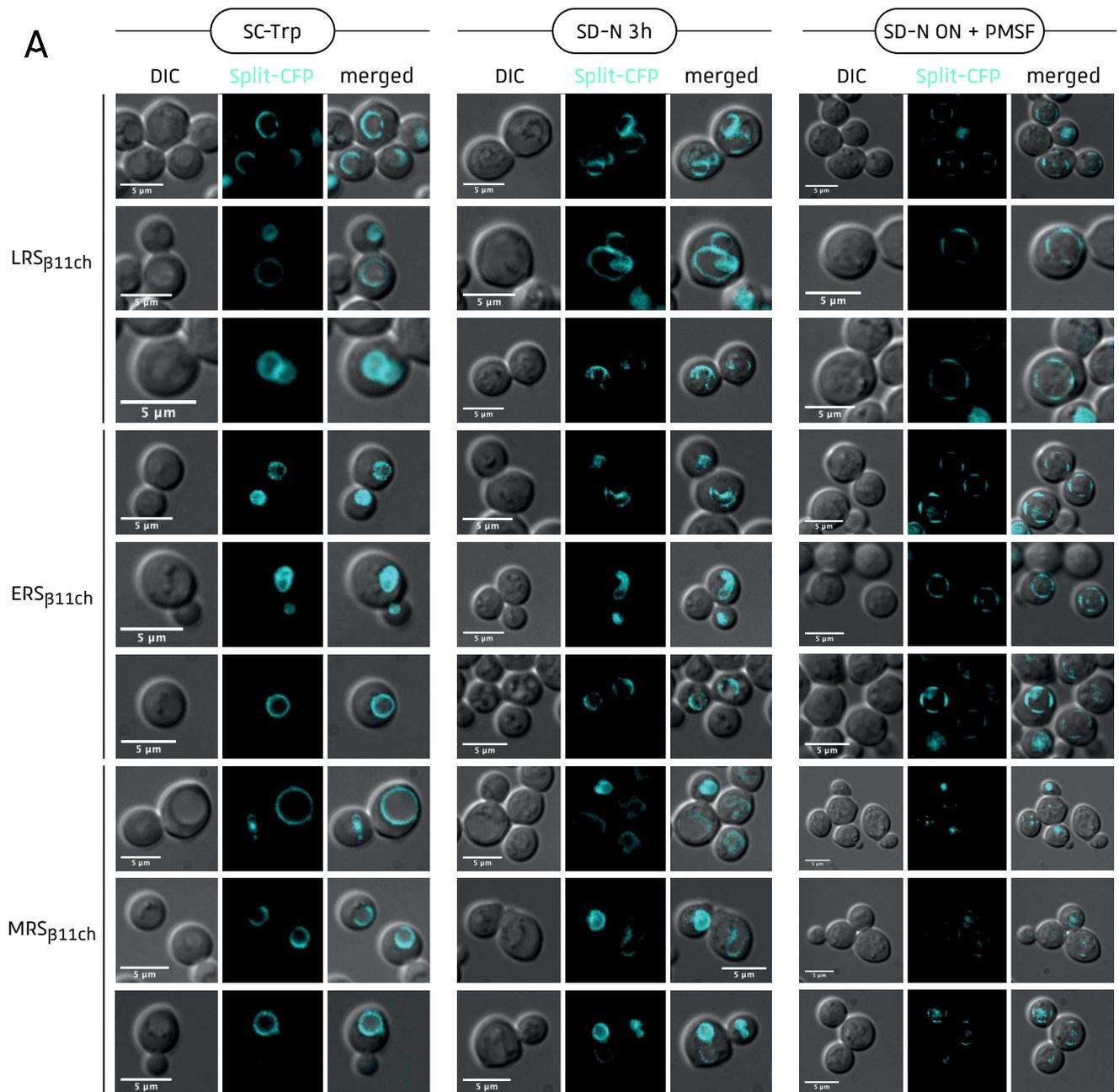
Figure ChII.R-5: LRS$_{\beta11ch}$, ERS$_{\beta11ch}$ and MRS$_{\beta11ch}$ vacuolar localization in autophagy conditions. A. The different strains were incubated in fermentation (SC-Trp) or autophagy (SD-N) conditions. For the autophagy, cells were either treated during 3 h or incubated overnight with addition of PMSF to inhibit autophagic bodies degradation. The reconstitution of vacuolar CFP was analyzed by epifluorescence microscopy. **B.** The expression of the CFP$_{\beta11ch}$-tagged proteins and Vph1$_{CFP\beta1-10}$ was determined by immunoblotting using anti-GFP$_{\beta11}$ and anti-GFP$_{\beta1-10}$ respectively.

the reconstitution of CFP.

III.3.2.2. LRS, ERS and MRS vacuolar localization during autophagy

The Vac-Split-CFP strain expressing $LRS_{\beta11ch}$, $ERS_{\beta11ch}$ or $MRS_{\beta11ch}$ was grown in fermentation condition (SC-Trp) or in autophagy medium (SD-N) either during 3 h or overnight with the addition of PMSF to inhibit autophagic bodies degradation in the vacuolar lumen. In fermentation condition, the three proteins distribute with their previously characterized $CFP_{all\ around}$ pattern at the vacuolar surface (**Figure ChII.R-5A**). In the model proposed by Bonfils and coworkers (Bonfils *et al.*, 2012), during leucine starvation the LRS starts editing misaminoacylated $tRNA^{Leu}$ leading to conformational changes and disruption of its interaction with Gtr1, a TORC1 component, and possibly to the inhibition of its vacuolar localization. However, when autophagy was induced in the Vac-Split-CFP strain expressing $LRS_{\beta11ch}$, a vacuolar CFP fluorescence signal was still observed (**Figure ChII.R-5A**) indicating that LRS still localizes at the vacuole surface, maybe through its interaction with another vacuolar protein. Another explanation is that upon self-assembly, the two CFP fragments cannot dissociate and the reconstituted CFP remains stable, thus acting as a tether that forces the vacuolar localization of LRS. A vacuolar CFP fluorescence signal is also observed for both $ERS_{\beta11ch}$ and $MRS_{\beta11ch}$ but again we first have to study the dynamic of Split-CFP dissociation before drawing conclusions about their vacuolar localization during autophagy. However, when comparing the CFP fluorescence signals obtained in these three conditions, a change in the vacuolar fluorescence pattern can be observed. Indeed, after 3 h of autophagy induction, the CFP fluorescence signal seems to be restricted to specific areas, larger than the CFP_{patch} pattern previously described. This distribution resembles that of the vacuolar domains formed during nitrogen starvation described by Tsuji and Fujimoto (Tsuji and Fujimoto, 2018, see **Chapter II section I.2.2, Figure ChII.I-3**). Indeed, the distribution of Vph1 is impacted by the metabolic status of the cell and large Vph1-deficient areas are formed during nitrogen starvation. Since the Vac-Split-CFP system is based on the fusion of $CFP_{\beta1-10}$ fragment to Vph1, the CFP fluorescence pattern observed could illustrate the vacuolar distribution of Vph1. The large vacuole areas deprived of CFP signal could thus reflect the Vph1-deficient areas. On the other hand, the reduction of CFP signal could also be explained by the reduced expression of $LRS_{\beta11ch}$, $ERS_{\beta11ch}$ and $MRS_{\beta11ch}$ during autophagy (**Figure ChII.R-5B**). When cells are incubated overnight in autophagy medium in presence of PMSF, the CFP fluorescence pattern again changes (**Figure ChII.R-5A**). For $LRS_{\beta11ch}$ and $ERS_{\beta11ch}$ we can
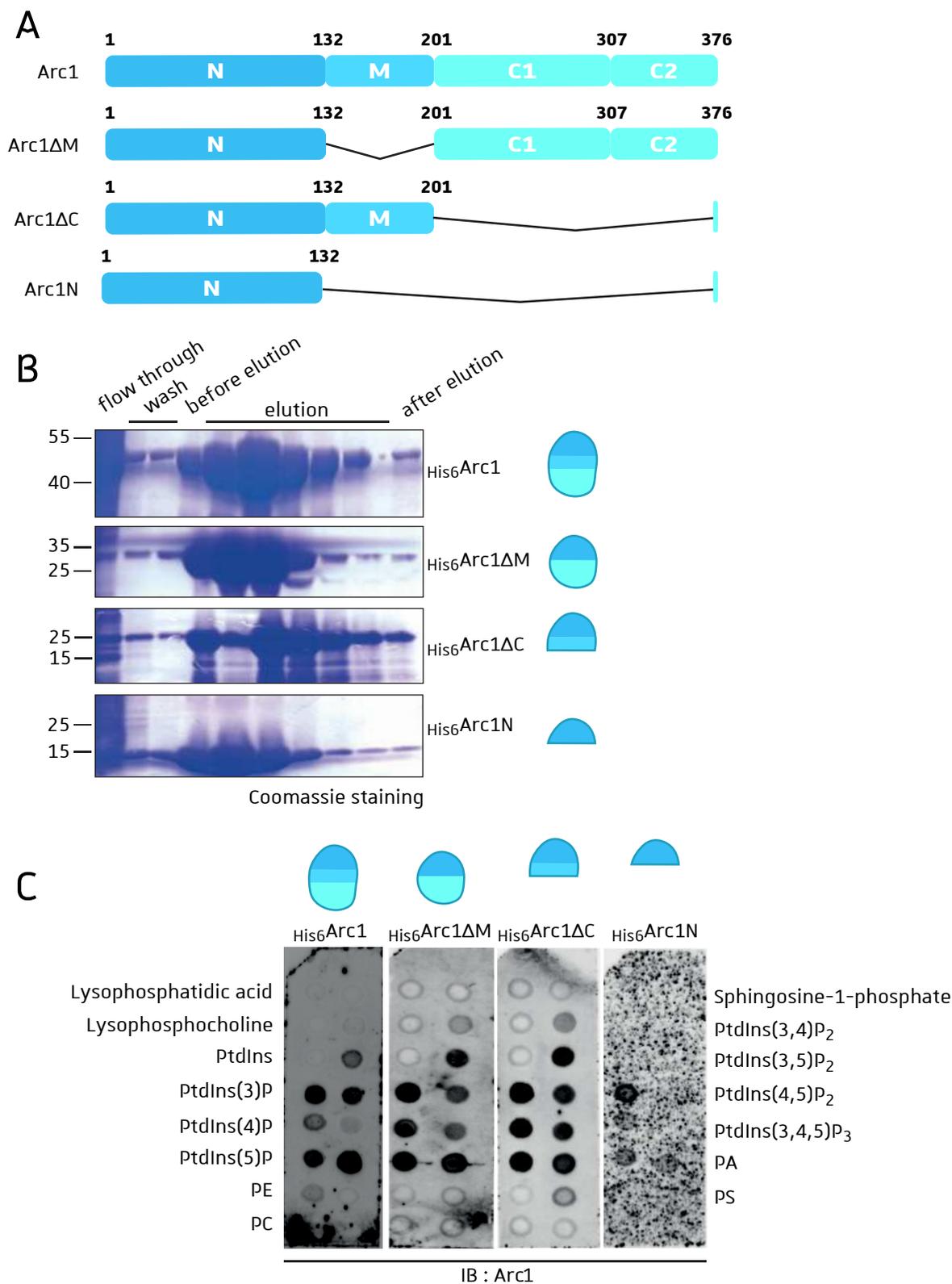
Figure ChII.R-6: Arc1 domains and interaction with lipids *in vitro*. A. Schematic representation of the Arc1 deletion mutants used for lipid binding assays. **B.** Affinity purification of the recombinant His6-tagged Arc1 deletion mutants. **C.** Lipid binding assays performed using 10 pmol of the purified deletion mutants. The immunoblotting was performed using anti-Arc1 antibody. PtdIns: phosphatidylinositol, PE: phosphatidylethanolamine, PC: phosphatidylcholine, PA: phosphatidic acid, PS: phosphatidylserine.

observe that vacuoles present regularly-arranged CFP areas separated by CFP-deprived areas. That kind of vacuolar patterns based on Vph1 distribution was also described by Tsuji and Fujimoto and is representative of cells responding to glucose starvation (**Chapter II section I.2.2, Figure ChII.I-3**). Since the cells were grown overnight in medium containing glucose as a carbon source (SD-N), the carbon source very likely became scarce over time leading to glucose starvation state. The distribution of CFP at the vacuolar surface is thus in accordance with Vph1 distribution at the surface of the vacuole during glucose starvation. Interestingly, $MRS_{\beta11ch}$ distribution after overnight incubation in autophagy medium is not similar to the one observed for $LRS_{\beta11ch}$ and $ERS_{\beta11ch}$ (**Figure ChII.R-5A**). Indeed, the CFP signal is localized in small foci or smaller patches than the ones observed for $ERS_{\beta11ch}$ or $LRS_{\beta11ch}$. This could reflect a reduced vacuolar localization of $MRS_{\beta11ch}$ during prolonged autophagy or glucose deprivation, displaying a dynamic localization of the vacualor $MRS_{\beta11ch}$ echoform depending on the cell status. In order to confirm that the diminution of CFP fluorescence is not due to $MRS_{\beta11ch}$ or $Vph1_{CFP\beta1-10}$ degradation, western blot analyses would have to be performed.

III.4. Study of AME components interaction with vacuolar membrane and lipids

III.4.1. Study of Arc1 interaction with lipids

The *in vitro* interaction of Arc1 with phospholipids had previously been described (Fernandez-Murray and McMaster, 2006) and I confirmed these results (see **Chapter II section III.2**). However, the lipid-binding domain of Arc1 has yet not been identified. Thus, we decided to create His6-tagged Arc1 deletion mutants that were expressed in *E. coli* and affinity purified (**Figure ChII.R-6A and B**). These recombinant proteins were then used to perform lipid binding assay using membranes coated with different phospholipids (**Figure ChII.R-6C**). According to the immunoblotting, the deletion of Arc1 Middle (Arc1ΔM) and C-terminal (Arc1ΔC) domains has no impact on the interaction of the mutant protein with phospholipids (**Figure ChII.R-6C**). The residues responsible for Arc1 interaction with lipids should thus be located in the N-terminal part. However, when the N-terminal domain of Arc1 is incubated in presence of phospholipids, only a slight interaction occurs and the interaction with vacuolar $PtdIns(3,5)P_2$ is completely lost. These results indicate that the N-terminal part of Arc1 alone is not sufficient to support the interaction with phospholipids. Arc1 interaction with phospholipids could thus rely on the protein conformation rather than

A

B
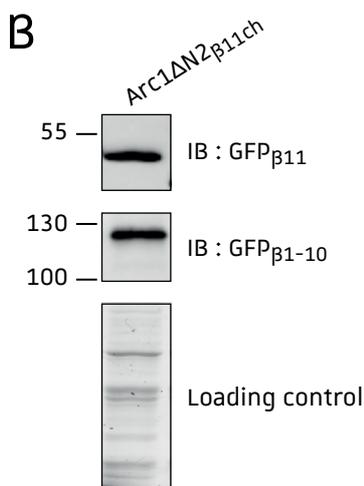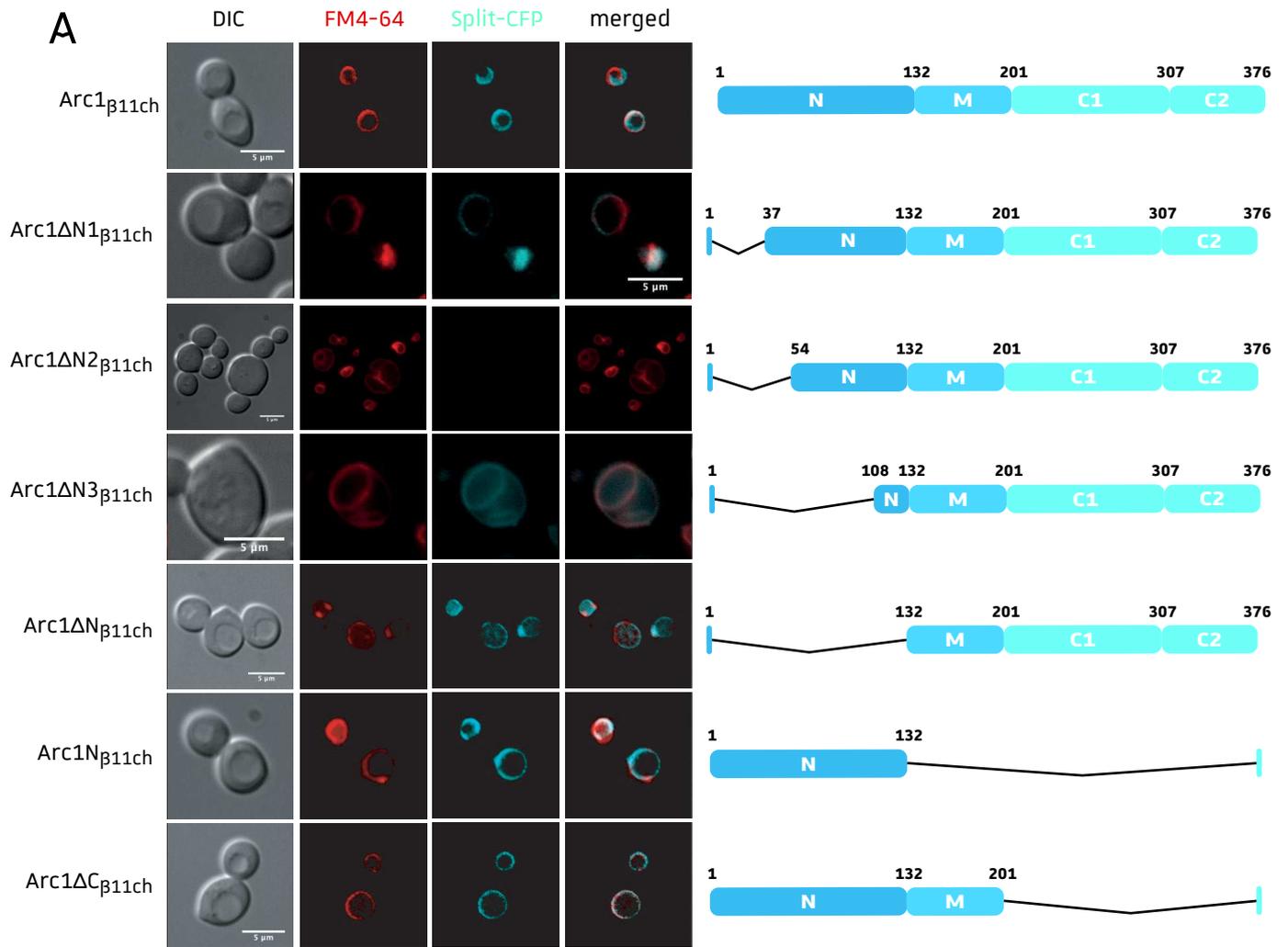
Figure ChII.R-7: Arc1 deletion mutants vacuolar localization. A. The Vac-Split-CFP strain was tranformed with different $CFP_{\beta11ch}$-tagged Arc1 deletion mutants and their vacuolar localization was determined using epifluorescence microscopy. The vacuoles are stained using FM4-64. Scale bar : 5 μm. **B.** Verification of the expression of the $Arc1\Delta N2_{\beta11ch}$ mutant and $Vph1_{CFP\beta1-10}$ by Western blot using anti-$GFP_{\beta11}$ and anti-$GFP_{\beta1-10}$ respectively.

on specific residues or domains, a hypothesis that has yet to be experimentally confirmed.

III.4.2.Utilization of the Vac-Split-CFP system to study Arc1, ERS and MRS vacuolar localization
III.4.2.1.Arc1 vacuolar anchoring domain

In order to gain insight into the Arc1 domain responsible for its interaction with the vacuolar membrane *in vivo*, several CFP$_{β11ch}$-tagged Arc1 deletion mutants were transformed in the Vac-Split-CFP strain and their vacuolar localization was assessed using epifluorescence microscopy (**Figure ChII.R-7A**). The Arc1ΔN1$_{β11ch}$ mutant deleted for the 37 first aa triggers the reconstitution of vacuolar CFP and thus localizes at the vacuole surface. These aa are therefore not essential for the interaction of Arc1 with the vacuolar membrane. For the Arc1ΔN2$_{β11ch}$ mutant deleted for the residues 1 to 54, no CFP signal could be observed even if the protein was expressed (**Figure ChII.R-7B**). These results indicate that the region located between the 37th and 54th aa residues is required for the vacuolar localization of Arc1. However, when a larger part or the entire N-terminal domain was deleted (mutants Arc1ΔN3$_{β11ch}$ and Arc1ΔN$_{β11ch}$ respectively), the vacuolar localization of Arc1 was restored (**Figure ChII.R-7B**). These results demonstrate that the N-terminal domain of Arc1 is not essential for the vacuolar localization of the protein. We thus hypothesized that the absence of fluorescence observed for mutant Arc1ΔN2$_{β11ch}$ could be explained by an important relocalization of this mutant to another subcellular compartment leading to the impossibility for this mutant to interact with the vacuolar membrane. The nuclear localization of Arc1 had been previously demonstrated by Galani and coworkers (K. Galani *et al.*, 2001) and they showed that Arc1ΔN7-32 mutant displays a cytosolic localization, while Arc1ΔN7-62 mutant localizes in the cytosol and the nucleus. These results demonstrate that the strong NES of Arc1 could be located in the region encompassing the residues 32 to 62. The Arc1ΔN1$_{β11ch}$ mutant deleted for the 37 first aa could thus still contain the NES and be restricted to the cytosol. On the other hand, the NES could be absent in the Arc1ΔN2$_{β11ch}$ mutant deleted of the 54 first residues, and this mutant could thus accumulate in the nucleus because it still bears Arc1's unidentified NLS. This would then impair Arc1's interaction with the vacuolar membrane. Since the Arc1ΔN3$_{β11ch}$ and Arc1ΔN$_{β11ch}$ localize at the vacuolar membrane, it would logically mean that they are excluded from the nucleus. The NLS of Arc1 could thus be localized between the 54th and 108th aa residues. These results also indicate that Arc1's N-terminal domain is not essential for Arc1 vacuolar localization. However, given that, when fused to

Figure ChII.R-8: ERS deletion mutants vacuolar localization. A. The Vac-Split-CFP strain was tranformed with $CFP_{\beta 11ch}$-tagged ERS and ERS1-160 deletion mutant (schematic representation on the right) and their vacuolar localization was determined using epifluorescence microscopy. The vacuoles are stained using FM4-64. Scale bar : 5 µm. **B.** Verification of the expression of the $ERS1-160_{\beta 11ch}$ mutant and $Vph1_{CFP\beta 1-10}$ by Western blot using anti-$GFP_{\beta 11}$ and anti-$GFP_{\beta 1-10}$ antibodies respectively.

Figure ChII.R-9: MRS and ERS do not require AME complex formation to localize at the vacuole surface. A. The Vac-Split-CFP *arc1Δ* strain was co-tranformed with His_{10}-tagged Arc1 mutants that cannot interact with ERS (Arc1∅ERS), MRS (Arc1∅MRS) or both aaRSs (Arc1∅MRS∅ERS) and $CFP_{\beta 11ch}$-tagged ERS or MRS. The vacuolar localization of $MRS_{\beta 11ch}$ and $ERS_{\beta 11ch}$ was determined using epifluorescence microscopy. Scale bar : 5 µm. n=5 microscopy fields were observed. **B.** Verification of the expression of the His_{10}-tagged Arc1 mutants and $CFP_{\beta 11ch}$-tagged aaRSs by Western blot using anti-Arc1 and anti-$GFP_{\beta 11}$ respectively; n=1.

CFP$_{\beta11ch}$, the N-terminal domain of Arc1 (Arc1N$_{\beta11ch}$ and Arc1ΔC$_{\beta11ch}$) triggers vacuolar CFP reconstitution (**Figure ChII.R-7A**), Arc1's N-terminal domain is able to localize at the vacuole surface. Since Arc1 interacts with ERS and MRS through its N-terminal domain and MRS and ERS localize at the vacuolar surface independently of Arc1 (see **Chapter II section III.2.**), the vacuolar localization of Arc1 N-terminal domain could thus occur through interaction with vacuolar ERS or MRS. Arc1 could thus localize at the vacuolar surface (i) through the interaction with vacuolar ERS and/or MRS *via* its N-terminal GST-like domain and (ii) through a lipid-binding domain that will encompass the Middle domain. It is also important to note that the utilization of truncated mutants also raises the possibility of protein misfolding that could ultimately trigger mislocalization of the proteins.

III.4.2.2. ERS and MRS vacuolar anchoring

For ERS, we analyzed the vacuolar localization of a deletion mutant containing the GST-like domain (aa 1-160) that allows the interaction with Arc1 (**Figure ChII.R-8A**). The absence of a vacuolar CFP signal indicates that the ERS1-160$_{\beta11ch}$ mutant cannot localize at the vacuolar surface. The expression of this mutant was confirmed by Western blot (**Figure ChII.R-8B**). The absence of vacuolar localization could result from the deletion of ERS lipid-binding domain or could be due to the localization of this mutant to another subcellular compartment. Indeed, we previously demonstrated that the MTS of ERS is localized within the 30 first aa (Bader *et al.*, 2020, **Chapter I section III.1**), the ERS1-160$_{\beta11ch}$ could thus accumulate in the mitochondria, preventing its vacuolar localization. In order to confirm that the lipid-binding domain of ERS is located after the residue 160, we could perform *in vitro* lipid binding assay with recombinant ERS1-160 and ERSΔ1-160 mutants. Moreover, since the GST-like domain of ERS is not sufficient to trigger the vacuolar localization, we can conclude that ERS' vacuolar localization does not rely on its interaction with Arc1.

In order to determine the implication of Arc1 and the AME complex formation in the vacuolar localization of ERS and MRS, the Vac-Split-CFP strain was transformed with plasmids expressing Arc1 mutants that cannot interact with MRS (Arc1⊘MRS, A26R and S33A mutants) or with ERS (Arc1⊘ERS, T55R, R100A, Y104A mutants) or with both MRS and ERS (Arc1⊘MRS⊘ERS) (**Figure ChII.R-9**). The vacuolar localization of the aaRSs was then assessed by co-transforming with plasmids expressing ERS$_{\beta11ch}$ or MRS$_{\beta11ch}$. Using Arc1 mutants that cannot interact with aaRSs is somewhat different from using an *arc1Δ* strain because of the many other subcellular localizations and roles that have been identified for Arc1. The co-

expression of MRS$_{\beta11ch}$ and Arc1$\oslash$MRS triggers a vacuolar CFP signal, confirming that MRS can bind to the vacuolar membrane in an Arc1-independent manner (**Figure ChII.R-9A**). However, the CFP signal is not equally distributed at the vacuolar surface and displays multiple foci or dots. The localization of MRS at the vacuole surface thus seems to be impacted by its interaction with Arc1 at the vacuolar surface. On the other hand, the inability of Arc1 to interact with ERS (Arc1$\oslash$ERS) does not impact MRS vacuolar localization that localizes at the vacuolar surface regardless of the presence or absence of Arc1 and therefore the formation of an AME complex (**Figure ChII.R-9A**). When Arc1$\oslash$MRS$\oslash$ERS is expressed, the MRS vacuolar localization resembles the one obtained in presence of Arc1$\oslash$MRS. Concerning ERS$_{\beta11ch}$, I was not able to co-express it with Arc1$\oslash$ERS, but the CFP signal obtained in presence of Arc1$\oslash$MRS indicates that the formation of AME complex is indeed not required for ERS$_{\beta11ch}$ vacuolar localization (**Figure ChII.R-9A**). These results confirm that the formation of AME complex is not essential for the vacuolar localization of MRS and ERS. However, even if the presence of Arc1 is not an absolute requirement for the vacuolar localization of MRS its distribution at the surface of the vacuole is impacted by its interaction with Arc1.

III.4.3. AME complex component interaction with lipid bilayer

In order to test the ability of the AME complex components to interact with lipids in a context mimicking the vacuole membrane, we used liposomes that have the same lipid composition than subcellular membranes (PolyPIPososmes from Echelon Biosciences, **Figure ChII.R-10A**). Since I am interested in the anchoring to the vacuolar membrane, the liposomes I used were enriched with vacuolar-specific phospholipid PtdIns(3,5)P$_2$. For this assay, the recombinant proteins were first purified (**Figure ChII.R-10B-G**) and then incubated with the liposomes. The advantage of these PolyPIPosomes over classical homemade liposomes, is that they contain biotinylated phosphatidylethanolamine (biotin-PE) and can thus be purified by affinity chromatography using Streptavidin beads. Since we previously demonstrated that heterologously-expressed MRS interaction with lipids relies on Arc1 (**Chapter II section III.2**), MRS$_{His6}$ was co-expressed with Arc1 in order to obtain a Arc1$\bullet$MRS$_{His6}$ duplex. Because only MRS is fused to a His$_6$-tag, the presence of Arc1 in the elution fractions of the first affinity purification (**Figure ChII.R-10E**) relies on the formation of Arc1$\bullet$MRS$_{His6}$ duplex. In order to separate Arc1$\bullet$MRS$_{His6}$ duplex from free MRS$_{His6}$ and free Arc1, a gel filtration was performed and the four main elution peaks we obtained were analyzed (**Figure ChII.R-10F and G**). The immunoblotting indicates that the two proteins are found in the four peaks. However, it is

F

Elution GF

Input | B8 | **C2** | C9 | C11

100
70

← MRS$_{His6}$

Ni-HRP

55
40

← Arc1

IB: Arc1

← MRS$_{His6}$

← Arc1

Loading control

G

H

Elution GF

Input | D3 | D4 | **D8** | D9 | D10

130
100
70
55

← MRS$_{MBP}$
← MRS

IB : MRS

← MRS$_{MBP}$

← MRS

Loading control

I

Elution GF

Input | **D7** | D8 | D9 | D10 | D11 | D12

55
40

← $_{His6}$Arc1

Ni-HRP

55
40

← $_{His6}$Arc1

IB: Arc1

← $_{His6}$Arc1

Loading control
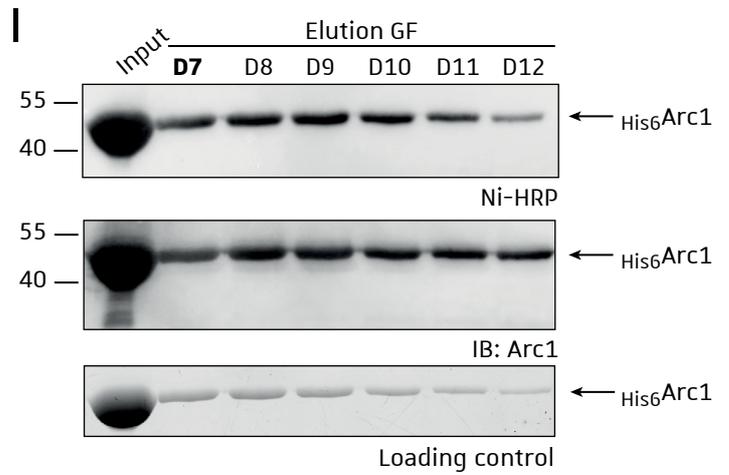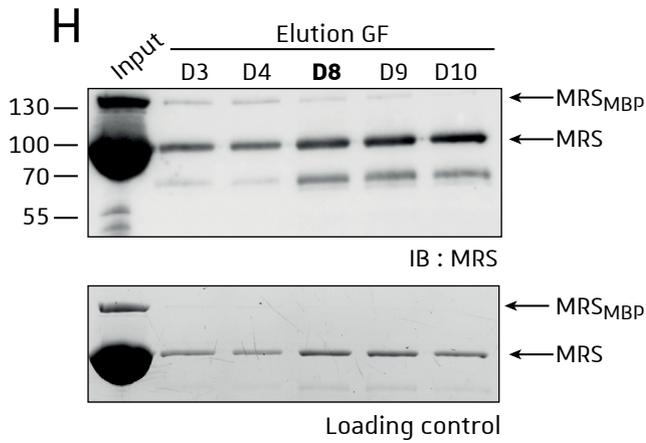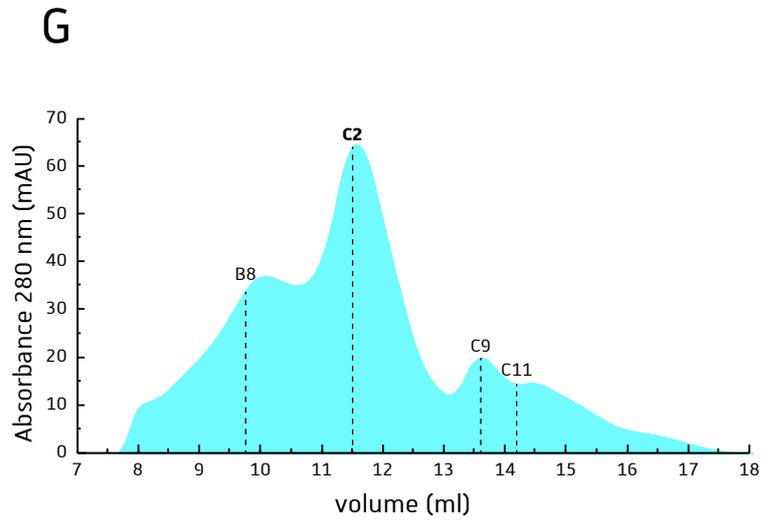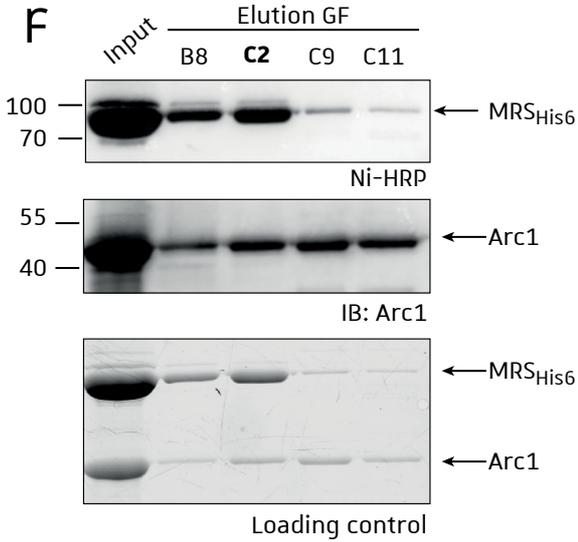
PtdIns(3,5)P$_2$
PolyPIPosome

Control
PolyPIPosome

J

100
70

← ERS$_{His6}$

IB : ERS

← ERS$_{His6}$
← BSA

Loading control

100
70

← ERS$_{His6}$

IB : ERS

← ERS$_{His6}$
← BSA

Loading control

K

100
70

IB : ERS

Loading control

100
70

← ERS$_{His6}$

IB : ERS

← ERS$_{His6}$
← BSA

Loading control
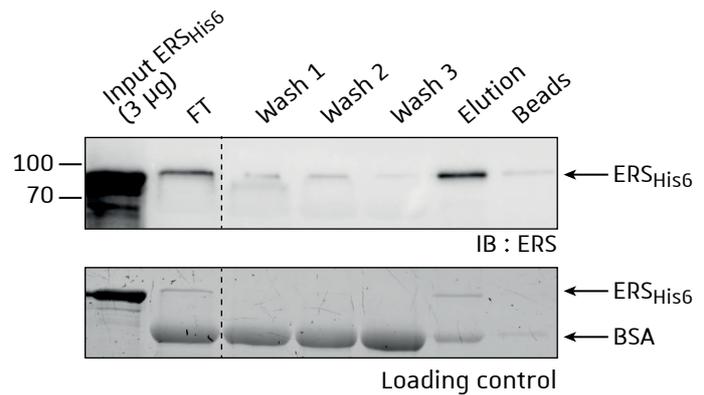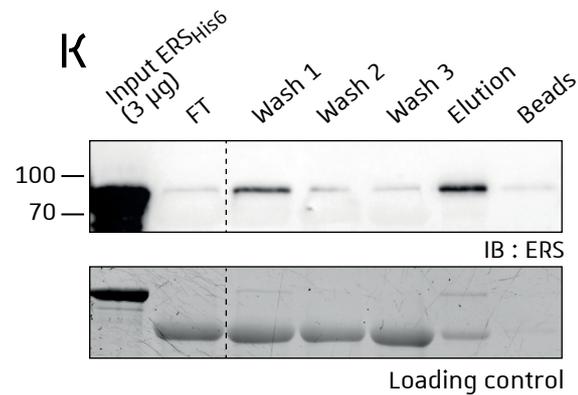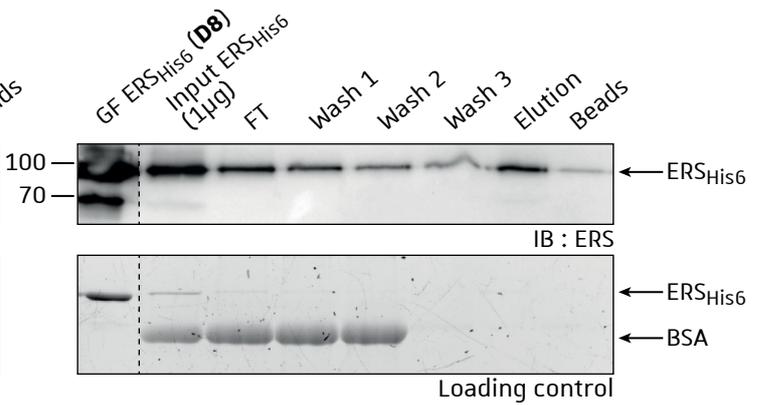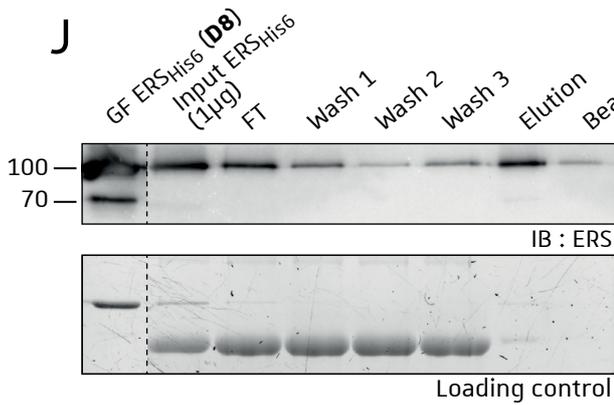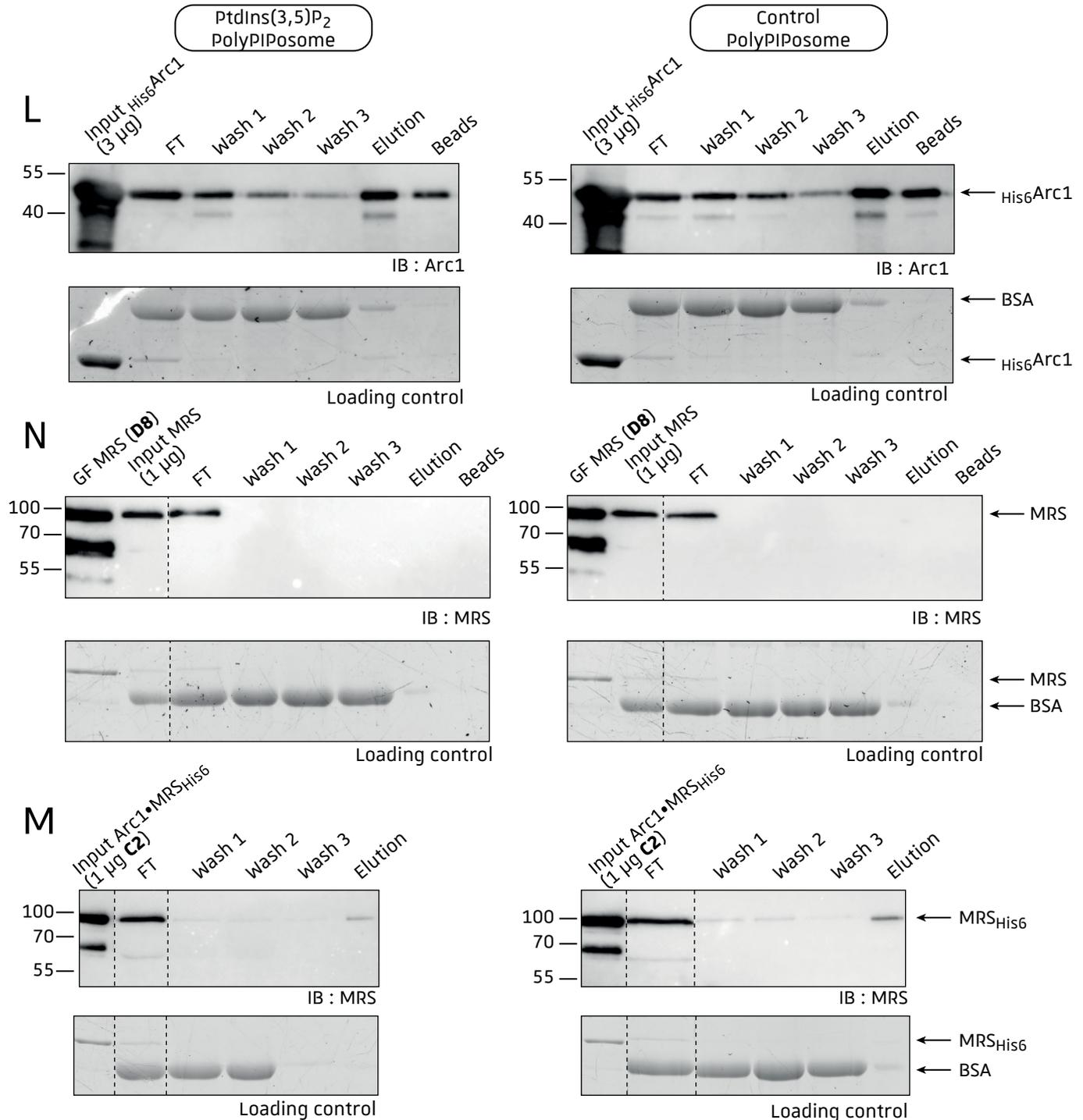
Figure ChII.R-10: Arc1, MRS, ERS and Arc1•MRS duplex interaction with liposomes. A. PtdIns(3,5)P$_2$ and control PolyPIPosomes (Echelon Biosciences) composition. The biotin-PE allows the purification of liposomes using Streptavidin affinity purification. PC: phosphatidylcholine, PE: phosphatidylethanolamine, PtdIns(3,5)P$_2$: phosphatidylinositiol 3,5-bisphosphate. **B.** Schematic representation of the liposome binding assay. The recombinant purified proteins are first incubated with liposomes and subsequently with Strepatividin beads. After washing the beads, the proteins are eluted. **C and D.** Western blot analysis of ERS$_{His6}$ affinity purification using HisTrap column (**C**) and subsequent purification of the A3 fraction using gel filtration (GF) (**D**). **E and F.** Western blot analysis of Arc1•MRS$_{His6}$ duplex affinity purification using HisTrap column (**E**) and subsequent gel filtration (**F**). The presence of MRS$_{His6}$ and Arc1 were determined using Ni-HRP conjugate and anti-Arc1 antibody respectively. **G.** Chromatogram of Arc1•MRS$_{His6}$ duplex gel filtration purification. The different fractions analyzed in **F** are represented. The fraction C2 in bold contains the duplex Arc1•MRS$_{His6}$ and was used for the liposome binding assay. **H and I.** Western blot analysis of gel filtration purification of MRS after MBP-tag cleavage using anti-MRS antibody (**H**) and of $_{His6}$Arc1 after affinity purification (**Figure ChII.R-6B**) using Ni-HRP conjugate and anti-Arc1 antibody (**I**). **J-N.** Streptavidin affinity purification of the PtdIns(3,5)P$_2$ (left panel) or Control (right panel) PolyPIPosomes incubated with ERS$_{His6}$ (**J and K**), $_{His6}$Arc1 (**L**), MRS (**M**) or Arc1•MRS$_{His6}$ duplex (**N**). For liposome binding assays **K and L**, the liposomes were first incubated with the Strepatividin beads and subsequently incubated with the recombinant proteins. FT: flowthrough, W: wash. • **183** •
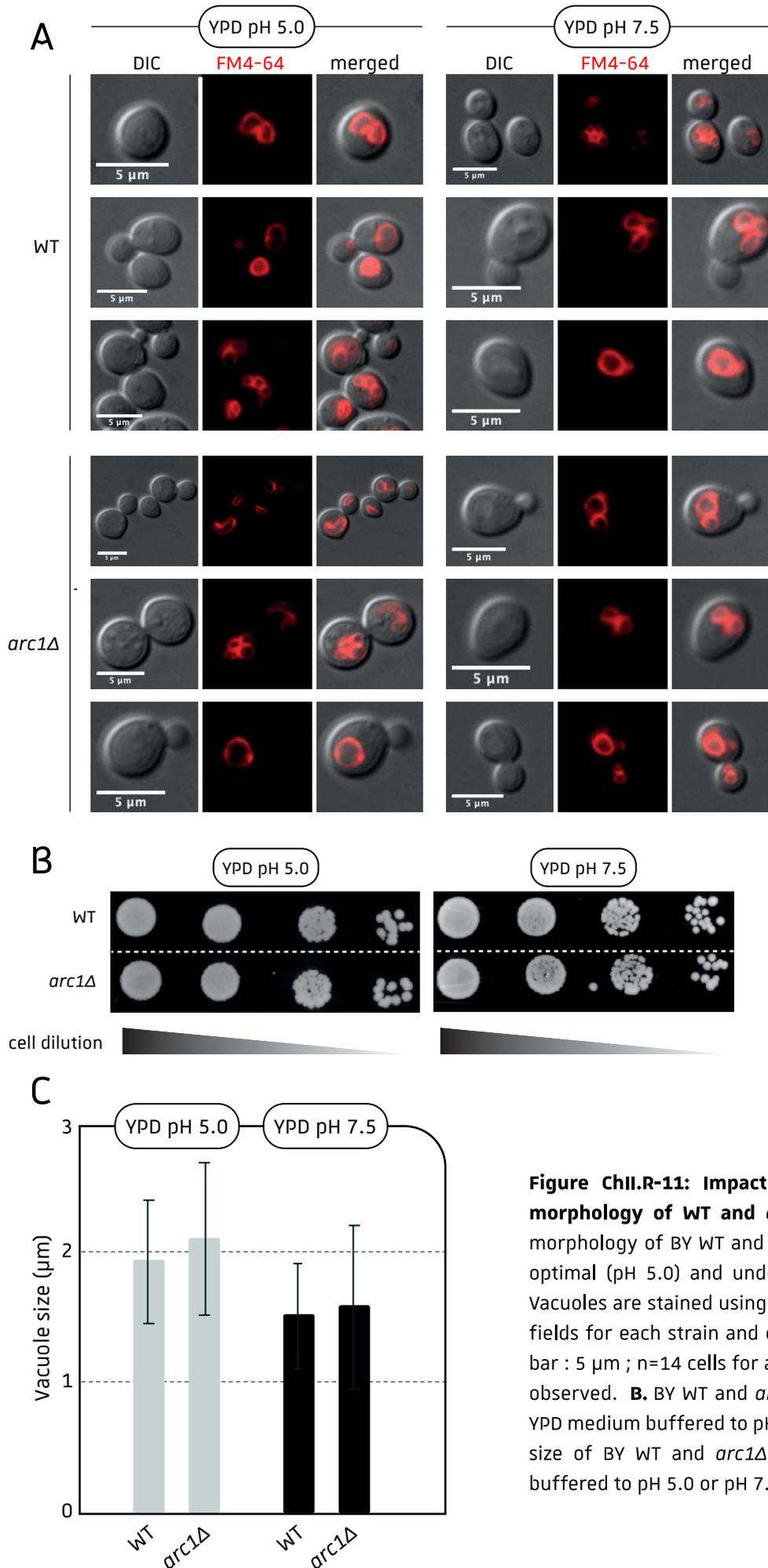
Figure ChII.R-11: Impact of pH change on vacuole morphology of WT and *arc1Δ* cells . A. The vacuole morphology of BY WT and *arc1Δ* strains was analyzed in optimal (pH 5.0) and under stress (pH 7.5) conditions. Vacuoles are stained using FM4-64. Three representative fields for each strain and condition are presented. Scale bar : 5 μm ; n=14 cells for arc1Δ and 16 cells for WT were observed. **B.** BY WT and *arc1Δ* strains growth assays on YPD medium buffered to pH 5.0 or pH 7.5. N=3. **C.** Vacuole size of BY WT and *arc1Δ* cells grown in YPD medium buffered to pH 5.0 or pH 7.5 ; n>18 cells.

impossible for the duplex to be eluted in so many fractions. Since Arc1 and MRS$_{His6}$ are 42 and 86 kDa respectively, we hypothesized that the first fraction B8 contains tetramers of Arc1 and dimers of MRS$_{His6}$ that would be 168 and 172 kDa respectively. The fraction C2, in which Arc1 and MRS are enriched (**Figure ChII.R-10F**) would contain the duplex Arc1●MRS$_{His6}$ that has a molecular weight of 128 kDa. Finally, the fractions C9 and C11, which contain smaller amount of MRS$_{His6}$ and higher amount of Arc1, would contain MRS$_{His6}$ and dimers of Arc1 that have molecular weights of 86 and 84 kDa respectively.

After purification, the liposome binding assays were performed with PtdIns(3,5)P$_2$ and control PolyPIPosomes (**Figure ChII.R-10J-N**, left and right panels respectively). For ERS$_{His6}$ (**Figure ChII.R-10J**), the presence of the protein in the flowthrough and wash fractions could indicate that ERS only weakly interacts with the liposomes. On the other hand, its presence in the elution fractions of both PtdIns(3,5)P$_2$ and control PolyPIPosomes indicates that ERS either interacts with phosphatidylcholine (PC) and/or phosphatidylethanolamine (PE) or with the biotinylated PE. However, ERS was not able to interact with the PC or PE in the previously performed lipid binding assays (**Chapter II section III.2**). In order to prevent ERS interaction with the biotin, the liposomes were first incubated with the streptavidin beads and then the protein was added (**Figure ChII.R-10K**). However, this did not diminish ERS' presence in the elution fractions of both assays. These results indicate that ERS is thus able to interact lipid bilayers in a nonspecific manner. For the assay performed with $_{His6}$Arc1, the liposomes were also previously incubated with the streptavidin beads before addition of the recombinant protein (**Figure ChII.R-10L**). The results obtained are similar to the one obtained for ERS$_{His6}$ since $_{His6}$Arc1 is found in the elution fractions of both assays. Since recombinant $_{His6}$Arc1 cannot be biotinylated by *E. coli* biotin-protein ligase BirA, the presence of Arc1 in the elution fraction is not due to its interaction with the streptavidin beads. Similar to ERS, Arc1 was not able to interact with PC and PE in the lipid biding assays, these results would thus indicate that Arc1 can interact with lipid bilayers independently of their composition in a manner similar to ERS. For MRS (**Figure ChII.R-10M**), the protein is only found in the flowthrough fraction indicating that it was not able to interact with the liposomes. These results are in accordance with the results showing that MRS cannot directly interact lipids (**Chapter II section III.2**). However, when the duplex Arc1●MRS$_{His6}$ was incubated with the liposomes (**Figure ChII.R-10N**), MRS$_{His6}$ was found in the elution fractions of both assays very likely because of the interaction of Arc1 with the lipid bilayer. These results could suggest that Arc1 anchors MRS to the subcellular membranes *in vivo*.
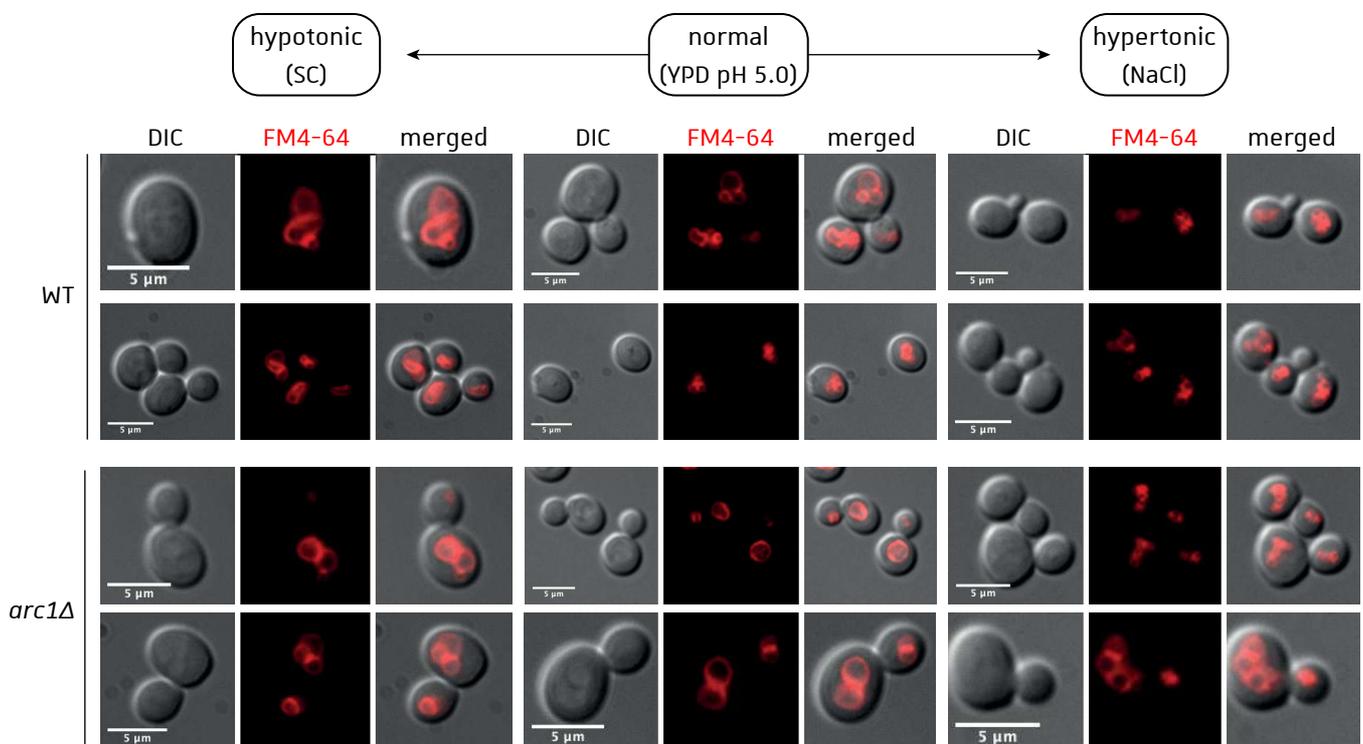
Figure CHII.R-12: Vacuole morphology of BY WT and *arc1Δ* strains in different osmotic conditions . Cells were grown in YPD pH 5.0 + 100 mM NaCl until mid-log phase. After vacuole staining with FM4-64, cells were transferred to hypotonic (SC) or hypertonic (YPD + 1 M NaCl) conditions for 10 min before epifluorescence microscopy analysis. Scale bar : 5 μm ; n>15 cells were observed.

III.5. Impact of Arc1 deletion on vacuolar morphology and cell survival upon stress

III.5.1. pH stress

Since ERS and MRS can localize at the vacuolar surface independently of Arc1, we hypothesized that the role of vacuolar Arc1 may differ from its cytosolic one meaning an aminoacylation cofactor. Moreover, the growth deficiency in presence of non-fermentable carbon source observed for *arc1Δ* cells is a phenotype that is observed for vacuolar membrane ATPase activity (*VMA*) mutants. We thus aimed to determine if Arc1 could be involved in vacuolar morphology and vacuolar functions. For this we analyzed the impact of pH stress on cells deleted for *ARC1* (**Figure ChII.R-11**). The optimal pH for yeast cell growth is 5.0 and *VMA* mutant display an inability to grow in presence of medium buffered to pH 7.5. In presence of YPD pH 5.0, WT and *arc1Δ* cells have round and multilobed vacuoles and cells display similar growth rate (**Figure ChII.R-11A and B**). There is also no difference in the size of the vacuole between the two strains (**Figure ChII.R-11C**). Upon pH change, some WT cells display more fragmented vacuoles but the overall vacuolar morphology does not change (**Figure ChII.R-11A**). Even if vacuole fragmentation could not be observed at pH 7.5 for *arc1Δ* cells, the overall vacuolar morphology of *arc1Δ* cells is not impacted by pH change. The WT and *arc1Δ* cells also display the same growth rate at pH 7.5 (**Figure ChII.R-11B**) and a diminution in the vacuole size can be observed for both strains (**Figure ChII.R-11C**). These results indicate that the Arc1 KO mutant does not display the phenotype of *VMA* mutants in presence of pH 7.5. However, *VMA* mutants display an increased sensibility to Ca^{2+} and a loss of V-ATPase activity that could also be studied in the *arc1Δ* strain. Indeed, despite being an important component of vacuolar V-ATPase, Vph1 mutants only display mild *VMA* phenotypes, which could also be the case for Arc1.

III.5.2. Osmotic stress

We also assessed the impact of *ARC1* deletion on vacuolar fusion and fragmentation during hypotonic and hypertonic stresses respectively (**Figure ChII.R-12**). For this, cells were grown to mid-log phase in "normal" condition (YPD medium supplemented with 100 mM NaCl and buffered to pH 5.0), and then transferred to hypotonic (SC medium) or hypertonic (YPD + 1 M NaCl) conditions for 10 min before epifluorescence microscopy observations. In normal condition, the WT and *arc1Δ* cells have multilobed vacuoles and the shift to hypotonic

A
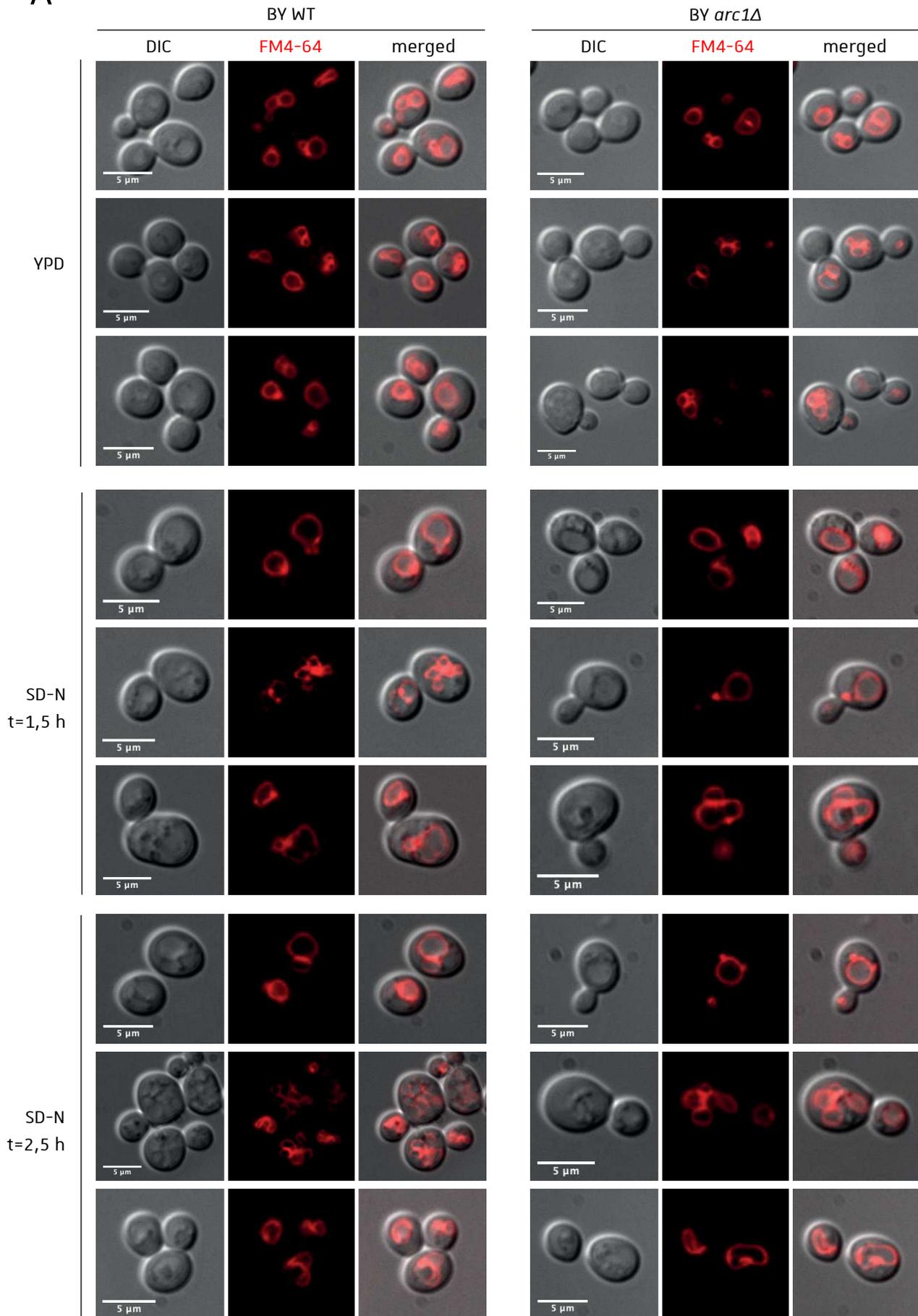
condition does not impact the vacuolar shape of both strains (**Figure ChII.R-12**, left panel). This is unexpected because vacuoles undergo fusion during hypotonic stress, there should thus be a single enlarged vacuole in both strains. Since cells were only subjected to hypotonic stress during 10 min, a prolonged incubation in hypotonic condition may be required to trigger vacuolar fusion. On the other hand, when incubated in hypertonic conditions, the vacuoles of both strains are highly fragmented (**Figure ChII.R-12**, right panel). Arc1 thus do not seem to be implicated in the process of vacuole fragmentation during hypertonic stress.

III.5.3. Prolonged starvation

The yeast vacuole is the main storage compartment for many aa, and aa uptake and export are regulated by vacuolar aa transporters. The vacuolar membrane also contains the TORC1 complex that regulates the autophagy depending on the aa and nitrogen availability. We thus studied the vacuole morphology and cell survival of WT and *arc1Δ* strains after early and prolonged amino acid and nitrogen starvations (**Figure ChII.R-13**). During early autophagy (1,5 h in SD-N), the vacuoles of WT cells start to undergo fragmentation in contrary to *arc1Δ* cells that maintain round and large vacuoles. After 2,5 h induction, the WT vacuoles are highly fragmented and display membrane invaginations. For *arc1Δ* cells, the vacuole fragmentation is less abundant and resembles the one observed for WT cells after 1,5 h starvation. Membrane invaginations can also be observed but to a lesser extent than for WT cells. The *arc1Δ* cells could thus display a delay in the apparition of the characteristic vacuolar structures associated with aa and nitrogen starvation in comparison to WT cells.

Since overnight incubation in SD-N medium was used for previous experiments, we assessed the survival of WT and *arc1Δ* cells by testing their recovery after early and prolonged starvation (**Figure ChII.R-13B**). For this, cells grown in YPD until mid-log phase were either incubated in YPD or in starvation medium for 30, 60, 120, 180 or 870 (overnight incubation) min and aliquots were plated on YPD medium. The number of colonies for each time point reflects the number of cells that survived and recovered after starvation. During the first 120 min, the recovery of WT and *arc1Δ* cells is similar in presence or in absence of aa and nitrogen. The incubation in starvation medium during 120 min thus has no impact on WT and *arc1Δ* cells survival. However, after 120 min starvation there is a slight decrease in cell survival for both WT and *arc1Δ* cells. Nonetheless, since the number of colonies does not show a decrease after prolonged starvation (870 min), we can confirm that for both strains cell division is inhibited during prolonged starvation but cell survival and recovery are not
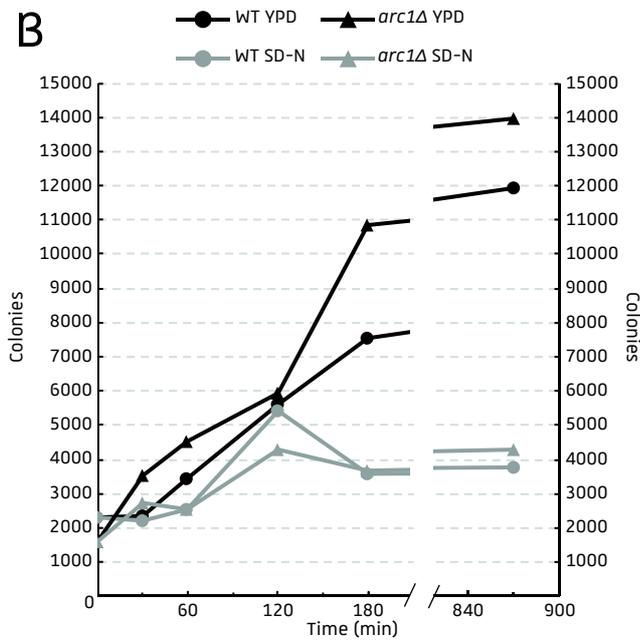
Figure ChII.R-13: Vacuole morphology and survival of BY WT and *arc1Δ* strains in autophagic conditions . A. Cells were grown in YPD and transferred in SD-N autophagy medium for 1,5 or 2,5 h. The morphology of the vacuole was assessed by epifluorescence microscopy after FM4-64 staining. Scale bar : 5 μm ; n>15 cells were observed. **B.** WT and *arc1Δ* grown in YPD medium were transferred to SD-N or YPD medium and incubated for 30, 60, 120, 180 min or overnight (870 min) before being plated on YPD medium to assess their recovery after starvation.
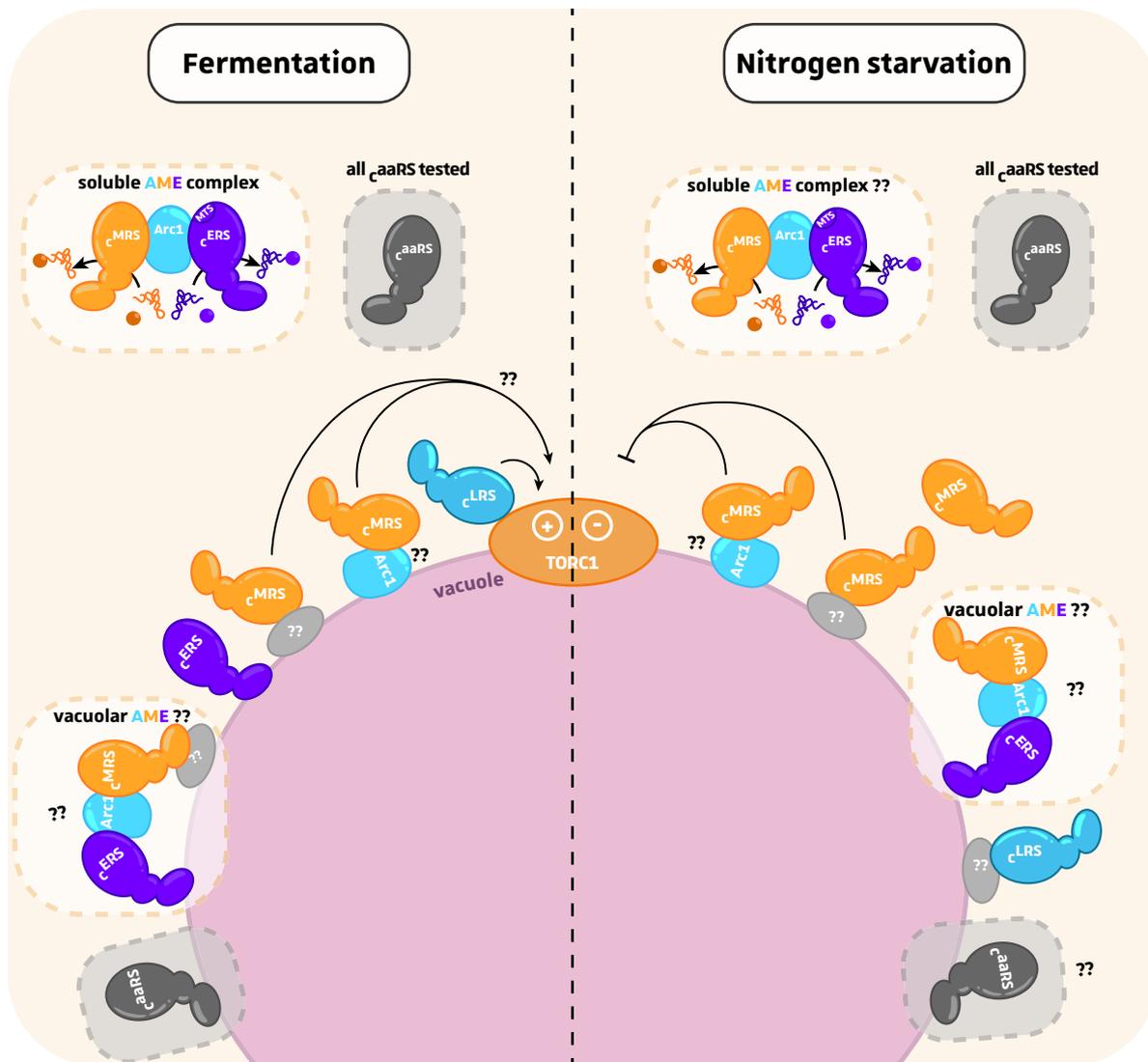
Figure ChII.CP-1: Vacuolar localization of $_c$aaRS and model for TORC1 regulation during nitrogen starvation by $_{vace}$MRS. Unexpectedly, we identified a vacuolar echoform for all the $_c$aaRSs tested by using the Vac-Split-CFP system. All the AME complex components also localize at the vacuolar surface but their precise mode of binding remains unknown. A potential role for $_{vace}$MRS in TORC1 regulation during nitrogen starvation was identified but remains to be confirmed. Moreover, the impact of $_{vace}$MRS on TORC1 activity seems to depend on the quantity of $_c$MRS present at the vacuolar surface rather than on its interaction with a specific protein.

impacted. Moreover, the number of colonies after starvation is similar for both WT and *arc1Δ* cells, the absence of Arc1 thus has no impact on cell survival after induction of autophagy.

IV. Conclusion & perspectives

The utilization of biochemical approaches confirmed that the three AME complex components are localized in subcellular membranes. However, because of the many limitations of these technics (subcellular fractionation and vacuole purification), it was not possible to clearly demonstrate the vacuolar localization of the three proteins. For these reasons, we developed the Vac-Split-CFP strain which allows the unambiguous identification of the vacuolar echoforms of cytosolic proteins. Depending on the subcellular origin of the protein tested, we were able to identify different CFP fluorescence patterns that reflect the vacuolar distribution of the proteins. We could also demonstrate that a *bona fide* vacuolar protein will trigger the most efficient and extended vacuolar CFP reconstitution. When expressed in our Vac-Split-CFP strain, all the $_c$aaRS$_{β11ch}$ tested triggered a vacuolar CFP signal, indicating that they all possess a vacuolar echoform (**Figure ChII.CP-1**). With the exception of $_c$LRS, a vacuolar localization for these $_c$aaRSs had never been described thus far. The Arc1 protein from the AME complex is also present at the vacuolar surface but is not essential for $_c$MRS and $_c$ERS vacuolar localization even though it somehow modulates the vacuolar localization/distribution of both $_c$aaRS. Indeed, Arc1 absence was linked to a remodeling in vacuolar distribution of both $_c$aaRS. Moreover, in absence Arc1, $_c$MRS vacuolar localization seems to occur more rarely, while $_c$ERS vacuolar localization occurs in a larger number of cells. Arc1 could thus promote $_c$MRS and restrict $_c$ERS vacuolar localization. Moreover, we demonstrated that the formation of AME complex is not a prerequisite for $_c$MRS and $_c$ERS vacuolar localization. Since $_c$ERS can bind to lipids and lipid bilayers *in vitro*, we hypothesized that it can bind to the vacuolar membrane *in vivo*. The lipid-binding domain of $_c$ERS could not precisely be identified but we showed that the GST-like domain of $_c$ERS is not implicated in vacuolar localization (**Figure ChII.CP-1**). On the other hand, $_c$MRS cannot bind directly to lipids or lipid bilayers and its vacuolar localization thus relies on the interaction with Arc1 and with another vacuolar protein that has yet to be identified (**Figure ChII.CP-1**). The lipid-binding domain of Arc1 could not be identified either through mutagenesis, but the results we obtained suggest that Arc1 vacuolar localization could rely on two different modes: (i) *via* a lipid-binding domain that could be located in a part of the protein that encompasses the Middle domain and (ii) *via* its interaction with $_c$ERS or $_c$MRS (**Figure ChII.CP-1**). A potential
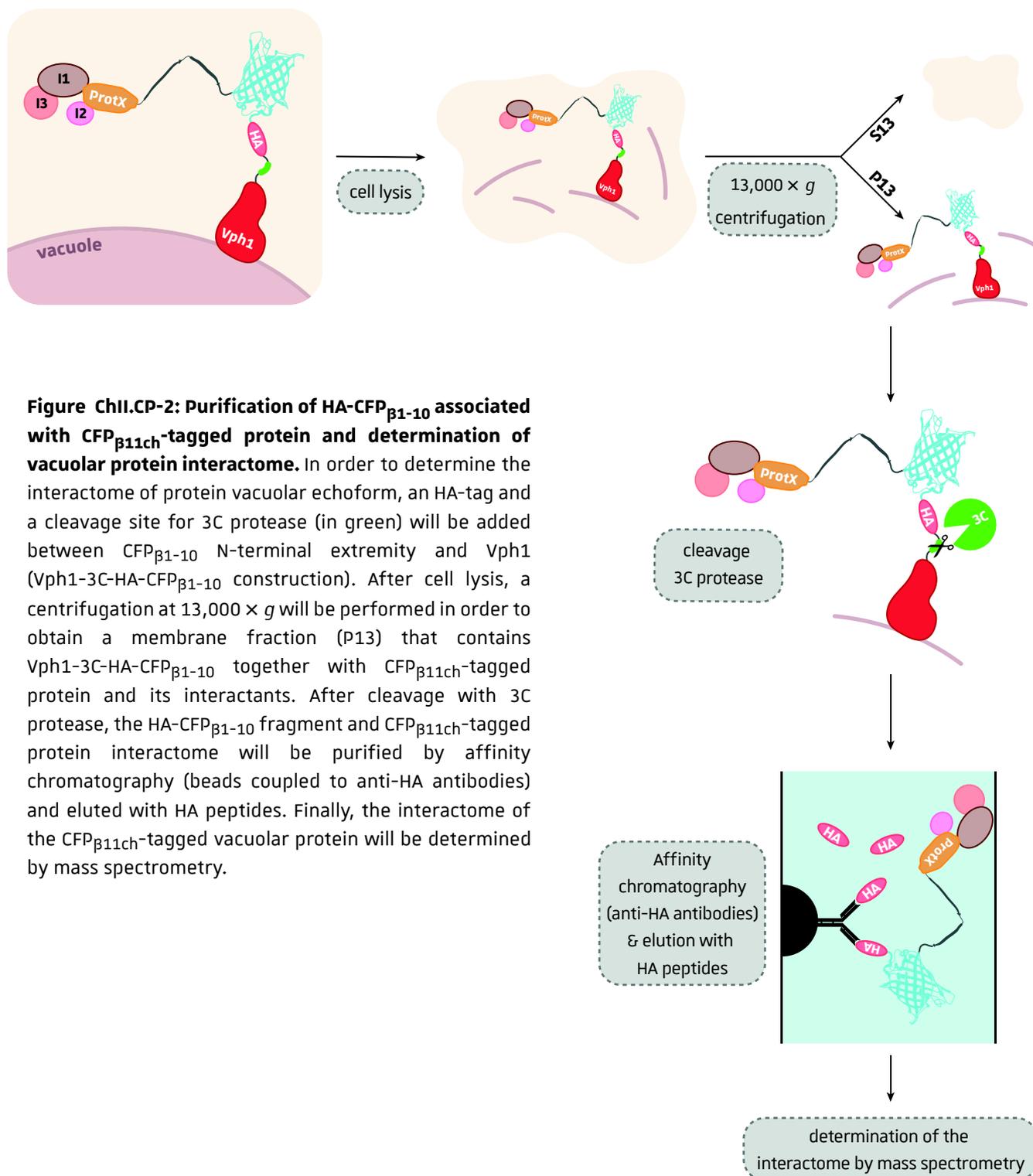
Figure ChII.CP-2: Purification of HA-CFP$_{β1-10}$ associated with CFP$_{β11ch}$-tagged protein and determination of vacuolar protein interactome. In order to determine the interactome of protein vacuolar echoform, an HA-tag and a cleavage site for 3C protease (in green) will be added between CFP$_{β1-10}$ N-terminal extremity and Vph1 (Vph1-3C-HA-CFP$_{β1-10}$ construction). After cell lysis, a centrifugation at 13,000 × *g* will be performed in order to obtain a membrane fraction (P13) that contains Vph1-3C-HA-CFP$_{β1-10}$ together with CFP$_{β11ch}$-tagged protein and its interactants. After cleavage with 3C protease, the HA-CFP$_{β1-10}$ fragment and CFP$_{β11ch}$-tagged protein interactome will be purified by affinity chromatography (beads coupled to anti-HA antibodies) and eluted with HA peptides. Finally, the interactome of the CFP$_{β11ch}$-tagged vacuolar protein will be determined by mass spectrometry.

implication in TORC1 regulation was shown for Arc1 and $_c$MRS (**Figure ChII.CP-1**). Indeed, TORC1 downregulation during nitrogen starvation and the inhibition of cell growth during methionine starvation are impaired in *arc1Δ* cells and fully restored upon overexpression and constitutive vacuolar anchoring of $_c$MRS (MRS$_{vac}$) or Arc1 (Arc1$_{vac}$) respectively. We hypothesized that the fraction of $_c$MRS brought to the vacuolar membrane by Arc1 could act synergistically with the Arc1-independent vacuolar fraction of $_c$MRS to regulate TORC1 and thus cell growth depending on the nutrient availability (**Figure ChII.CP-1**). In order to confirm these results, the phosphorylation status of TORC1 targets Rps6 and Sch9 has to be analyzed in *arc1Δ* cells overexpressing Arc1$_{vac}$. The cell growth in methionine starvation will also be assessed in *arc1Δ* and *arc1Δ mes1Δ* cells expressing MRS$_{vac}$. We could also use MRS mutants unable to activate and/or transfer the activated aminoacyl moiety onto tRNA^{Met} in these assays in order to determine if the aminoacylation function of vacuolar MRS is involved in TORC1 signaling. Medium supplemented with rapamycin could also be used for these experiments in order to determine if *arc1Δ* also blocks rapamycin-induced TORC1 downregulation. This would help us decipher the pathway(s) used by Arc1 to signal aa and/or nitrogen availability to TORC1. To understand whether TOR-signaling depends on both Arc1 and MRS or only on Arc1 or MRS, we could use variants of Arc1 and MRS that I already generated and that are unable to interact through their GST-like domains. This would allow us to generate a strain in which MRS cannot bind to vacuolar Arc1 without having to delete Arc1. If in this strain, we observe the same pattern of Rps6 phosphorylation than in an *arcΔ* strain upon shift to nitrogen starvation, this would mean that it is MRS which is responsible for modulating TOR activity and not Arc1.

Concerning the Arc1-independent MRS vacuolar echoform, it would be interesting to determine if this protein is the truncated version of MRS that has previously been identified in the yeast (Debard, 2019). Indeed, Sylvain Debard, a former PhD student of the DyPS team, demonstrated that MRS can be N-terminally processed by the vacuolar protease Pep4 and that truncation increases during autophagy. Since the GST-like domain of this MRS is absent, it cannot interact with Arc1. This could explain why a portion of vacuolar MRS relies on the interaction with Arc1, while another portion is Arc1-independent.

The epifluorescence imaging we performed upon induction of autophagy indicates that $_c$ERS, $_c$LRS and $_c$MRS still localize at the vacuole surface (**Figure ChII.CP-1**). However, for $_c$MRS we observed a fluorescence pattern different than that of $_c$LRS and $_c$ERS, with a

more restricted distribution and possibility a diminution in the vacuolar localization. The $_c$MRS could thus leave the vacuole during autophagy. However, in order to use the Vac-Split-CFP system for the study of protein dynamics, the dissociation of the $CFP_{\beta1-10}$ and $CFP_{\beta11ch}$ fragments first has to demonstrated as explained in **Chapter I section IV**. Another possibility in order to verify that the two fragments can dissociate upon metabolic change and protein relocalization, would be to incubated Vac-Split-CFP cells expressing $Vma13_{\beta11ch}$ in respiration conditions and to analyze the vacuolar CFP by epifluorescence microscopy. Indeed, Vma13, which is part of the V_1 V-ATP subcomplex, interacts with Vph1 in fermentation conditions, but the switch to respiration triggers V-ATPase dissociation and Vma13 relocalization in the cytoplasm (Parra *et al.*, 2014). A diminution in vacuolar CFP signal in respiration conditions would thus confirm the dissociation of the two CFP fragments upon $Vma13_{\beta11ch}$ cytosolic relocalization.

One of the most striking discovery we made by using the Vac-Split-CFP system is the identification of vacuolar echoforms for all the $_c$aaRSs tested (**Figure ChII.CP-1**). These observations raise two main questions that have to be answered: how do these aaRSs localize at the vacuole surface and why? To answer the first question, recombinant aaRS could be purified and incubated onto membranes coated with lipids to test their ability to directly bind to various lipid species as it was done for AME complex components. On the other hand, the Vac-Split-CFP system will be adapted to study vacuolar echoforms' interactome in a similar way as described in **Chapter section IV** (**Figure ChII.CP-2**). For this, a cleavage site for the protease 3C followed by an HA-tag will be inserted between Vph1 and the $CFP_{\beta1-10}$ fragment. After expressing the $CFP_{\beta11ch}$-tagged proteins in the Vac-Split-CFP strain, the membrane fractions will be separated by differential centrifugation (P13 and S13) and subjected to cleavage with 3C protease (P13 fraction only). The HA-$CFP_{\beta1-10}$ fragment will then be affinity purified together with the $CFP_{\beta11ch}$-tagged protein and its interactants (**Figure ChII.CP-2**). The utilization of an HA-tag allows the native elution of the proteins by using HA peptides. The eluted proteins could then be analyzed by mass spectrometry and tested enzymatically as well. The identification of the vacuolar echoforms' interactome will help us understand how the proteins localize at the vacuole surface but will also provide essential information regarding the vacuolar function of the $_c$aaRS if TORC1 components are found in the interactome, for example. For the identification of the function of membrane-associated aaRS, we are also currently developing *ex vivo* aminoacylation assays for membrane fractions to determine if aaRS aminoacylate tRNAs or proteins (lysine side chains of proteins). The

recent identification that $_c$aaRSs act as amino acid sensors for the aminoacylation of target proteins in human cells (He *et al.,* 2018) indicates that vacuolar $_c$aaRS could fulfill a similar role rather than their tRNA aminoacylation canonical role which, logically, is performed by the cytosolic echoform.

Finally, to further develop the Vac-Split-CFP system and perform large scale vacuolar localization studies, it will be necessary to automatize the counting of fluorescent cells and the recognition of the different fluorescence patterns. For this, we could try flow cytometry measurements between our different control proteins to determine if this method is accurate enough to discriminate the CFP signal emitted by a vacuolar protein with the signal emitted by a protein that reside in MCS or close to the vacuole. The other possibility would be to use a microfluidic system coupled to an epifluorescence microscope module to perform live imaging on single cells. The advantage of the microfluidic systems is that cells can be trapped into small wells and the cell environment (growth medium) can easily be changed. By using such systems, we would be able to record CFP fluorescence changes upon different stresses and gain insight into the potential dynamics of this vacuolar localization of cytosolic aaRSs, in response to environmental changes.

GENERAL CONCLUSION

My PhD work has mainly focused on the development of two imaging tools: the BiG Mito-Split-GFP and Vac-Split-CFP systems that were designed to allow the unambiguous identification of protein echoforms that localize in the mitochondrial matrix and at the vacuolar surface respectively. So far, the technics that were used for the identification of dual-localized proteins (subcellular fractionation, organelle purification, fusion to a fluorescent protein) had numerous limitations and were not really adapted to multi-localized proteins. Yet, the identification of these proteins' echoform remains crucial to gain insight into their potential role associated with relocation and to characterize organelles' proteome. This phenomenon of dual-localization is also common within cytosolic aaRSs and their unexpected relocations is often related to the non-canonical functions they can exert in the new compartment they reach which has been shown to be as important as their primary and canonical role of tRNA aminoacylation. For example, the DyPS team already identified MRS nuclear echoform and ERS mitochondrial echoform that are essential to synchronize expression of the F_0 and F_1 domains of the mitochondrial ATP synthase upon switch to the respiratory metabolism. Through the use of the BiG Mito-Split-GFP, we identified unexpected mitochondrial echoforms for $_c$aaRSs that already have a functional mitochondrial counterpart, making us logically guess that these echoforms could fulfill non-canonical roles in the mitochondria. Given the importance of aaRS and mitochondrial in numerous diseases, it would be interesting to characterize the function of these echoforms and their so far elusive import pathway. Concerning the vacuolar localization of $_c$aaRS, we were surprised to observe that all the tested $_c$aaRS do possess vacuolar echoform(s). Vacuolar/lysosomal localization had already been reported for LRS and associated with regulation of the TORC1 machinery. Even if LRS vacuolar/lysosomal localization and its mode of action differ between the two organisms, we can rationally imagine that the aaRS vacuolar echoforms identified in the yeast by using the Vac-Split-CFP tool could also localize at the lysosomal surface in human cells. Whether they will be able to sustain the function of their fungal counterparts remains to be investigated. Finally, the identification of vacuolar echoforms of Arc1, MRS and ERS and mitochondrial echoform of Arc1 adds a new degree of complexity to the dynamics and roles of the AME complex components and in a more general way to multi aminoacyl-tRNA synthetase complexes regardless of their organismal origin. Even if evidences show that AME complex formation is not required for the vacuolar localization, we cannot exclude

the possibility of the formation of a vacuolar AME complex. Nonetheless, the identification of new localizations for cytosolic proteins probably involves new organellar signaling and targeting pathways that urgently need to be explored and characterized.

MATERIAL & METHODS
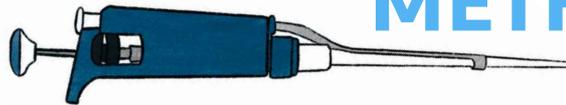
Table MM-1: *E.coli* strains used for cloning or recombinant protein overexpression.

Strain	Utilization	Genotype
DH5α	Plasmid replication	F− φ 80*lacZ* ΔM15 Δ(*lac*ZYA-*arg*F)U169 *rec*A1 *end*A1 *hsd*R17(rK−, mK+) *pho*A *sup*E44 λ− *thi-1 gyr*A96 *rel*A1
XL1 Blue		*end*A1 *gyr*A96(nal^R) *t*hi-1 *rec*A1 *rel*A1 *lac gln*V44 F'[::Tn10 *pro*AB+ lacI^q *lac*ZΔM15] *hsd*R17(r_K−m_K+) λ-
Rosetta 2	Recombinant protein production	F- *ompT hsdS*_B(r_B− m_B-) gal dcm pRARE2 (Cam^R)

Table MM-2: Yeast strains used in this study.

Strain	Genotype	Coll number
GUS1 shuffle	MATa *gus1::HIS5 ade2-1 his3-11,15 ura3-52 leu2-3,112 trp1-1 can1-100* GAL+ + pRS316-*GUS1*	49
2n RS 453	MATa/α *his3-11,15/his3-11,15 ura3-52/ura3-52 leu2-3,112/leu2-3,112 trp1-1/trp1-1 ADE2/ADE2*	
BiG Mito-Split-GFP	MATa *his3-11,15 trp1-1 leu2-3,112 ura3-1 CAN1 arg8::HIS3*, mitochondrial genome ρ⁺ *atp6::GFP*_{β1-10} _{5'UTRCOX2} *ATP6* _{3'UTRCOX2}	1820
BiG Mito-Split-GFP *por1Δ*	MATa *his3-11,15 trp1-1 leu2-3,112 ura3-1 CAN1 arg8::HIS3 por1::KanMX4*, mitochondrial genome ρ⁺ *atp6::GFP*_{β1-10} _{5'UTRCOX2} *ATP6* _{3'UTRCOX2}	2214/2215
BiG Mito-Split-GFP *pep4Δ*	MATa *his3-11,15 trp1-1 leu2-3,112 ura3-1 CAN1 arg8::HIS3 pep4::KanMX4*, mitochondrial genome ρ⁺ *atp6::GFP*_{β1-10} _{5'UTRCOX2} *ATP6* _{3'UTRCOX2}	2241/2242
BY WT	*his3Δ1 leu2Δ0 lys2Δ0 trp1Δ0 ura3Δ0*	
BY WT Trp-	MATa *his3Δ1 leu2Δ0 lys2Δ0 trp1Δ0 ura3Δ0 trp1::hphMX6*	602
BY *arc1Δ*	MATa *arc1::KanMX4 his3Δ1 leu2Δ0 ura3Δ0*	
RS WT	MATa *ade2-1 his3-11,15 leu2-3,112 trp1-1 ura3-52*	
RS *arc1Δ*	MATa *ade2-1 his3-11,15 leu2-3,112 trp1-1 ura3-52 arc1::KanMX4*	
Vac-Split-CFP	MATa *his3Δ1 leu2Δ0 lys2Δ0 trp1::hphMX6 ura3::VPH1*_{CFPβ1-10}	1642
Vac-Split-CFP *arc1Δ*	MAT? *his3Δ1 leu2Δ0 trp1::hphMX6 ura3::VPH1*_{CFPβ1-10} *arc1::KanMX4*	2019
RS *arc1Δ* MRS_vac	MAT? *arc1::KanMX4 ura3-52::MES1-VPH1*	
RS *arc1Δ mes1Δ* MRS_vac	MAT? *mes1::HIS3 arc1Δ ::KanMX4 leu2-3,112::MES1-VPH1-cMyc*	
RS *arc1Δ* Arc1_vac	MAT? *arc1::KanMX4 ura3-52::VPH1-ARC1-3HA*	

I. Biological material and growth media

I.1. Bacterial strains

Replication of plasmids is performed using bacterial strains that derive from the K-12 strain and are listed in the **Table MM-1**.

For recombinant protein production the bacterial strain Rosetta 2 that derive from BL21 strains is used (**Table MM-1**). This strain is designed to enhance the expression of eukaryotic proteins that contain codons rarely used in *E. coli*. Indeed, it carries the pRARE2 plasmid that encodes minor tRNAs specifically decoding 7 rare codons (AGA, AGG, AUA, CUA, GGA, CCC and CGG). It also carries a chromosomal copy of the T7 RNA Polymerase gene under control of the lacUV5 promoter which expression can be induced by adding isopropyl β-D-1-thiogalactopyranoside (IPTG) to the growth media. This strain is thus suitable for production of eukaryotic proteins from a plasmid carrying the gene of interest under the control of a T7 promoter.

I.2. Bacterial growth media

For bacterial growth, the rich medium LB-Miller containing 1 % (w/v) peptone, 0.5 % (w/v) yeast extract, 0.5 % (w/v) NaCl is used. The solid medium was supplemented with 1.5 % (w/v) agar-agar. Both liquid and solid media are autoclaved at 120 °C, 1.2 bars for 20 min. For plasmid selection, antibiotics are supplemented in media when the media temperature is below 50 °C, before pouring the plates for solid media or before use for liquid media. Ampicillin (Amp) is added at a final concentration of 100 mg/L and chloramphenicol (Cam) at a final concentration of 34 mg/L.

I.3. Yeast strains

The different yeast strains used in this study are listed in **Table MM-2**.

I.4. Yeast growth media

For yeast growth liquid or solid minimal (SC, synthetic Complete or SD, Synthetic Defined) or rich (YPD, Yeast extract-Peptone-Dextrose) media can be used (**Table MM-3**). SC

Table MM-3: Composition of yeast media used in this study.

		Common components	agar-agar (if solid)	Carbon source		Specific for each medium
rich media	YPD	Peptone 2% (w/v)	Yeast extract 1 % (w/v) 2% (w/v)	D-glucose 2% (w/v)	Fermentation	
	YPGly			Glycerol 2 % (w/v)	Respiration	
	YPD + G418			D-glucose 2% (w/v)	Fermentation	Geneticin (G418) 200 µg/mL
synthetic media	SC	Yeast Nitrogen Base with ammonium sulfate 6.7 g/L	2% (w/v)	D-glucose 2% (w/v)	Fermentation	CSM 0.79 g/L
	SC-aa			D-glucose 2% (w/v)	Fermentation	CSM-aa (depends on the CSM)
	SCGal			Galactose 2 % (w/v)	Fermentation + active mitochondria	CSM 0.79 g/L
	SCGal-aa			Galactose 2 % (w/v)	Fermentation + active mitochondria	CSM-aa (depends on the CSM)
Specific media	5 FOA	Yeast Nitrogen Base with ammonium sulfate 6.7 g/L	2% (w/v)	D-glucose 2% (w/v)	Fermentation	CSM 0.79 g/L + 5-fluoorotic acid (5FOA) 2.5 mM
	SD-N	Yeast Nitrogen Base without ammonium sulfate 1.7 g/L		D-glucose 2% (w/v)	Autophagy (Nitrogen starvation)	
	SPM	Potassium acetate 1 % (w/v)		None	Sporulation	

media can be supplemented with defined aa, excluding one or many of them to specifically select yeast cells according to their auxotrophic markers. The YPD media are not used for auxotrophic selection but can be supplemented with Geneticin (G418) to select clones with a *KanMX4* cassette. The carbohydrate source introduced in the media will determine the metabolism used by the yeast cells (fermentation, respiration). Liquid and solid media are autoclaved at 120 °C, 1.2 bars for 20 min, with the exception of galactose containing media that are filtered. Geneticin is added after autoclaving, once the medium temperature has dropped to 50 °C.

II. Gene amplification and cloning

II.1. Bacterial cell transformation

Competent bacteria cells are thawed slowly on ice, the plasmid DNA or 7.5 µL of Gibson assembly (see **section II.4.1.3**) are added to the cells and incubated 20 min on ice. The cells are heat-shocked in a 42 °C water bath during 40 sec. Cells are then stored on ice before being plated on LB-agar supplemented with the appropriate antibiotic. Transformed clones can be observed after an overnight incubation at 37 °C.

II.2. Plasmid extraction from bacterial cells

Isolated transformed bacterial clones are inoculated in 3 mL LB medium supplemented with the adequate antibiotic. The culture is incubated overnight at 37 °C under shaking (200 rpm, Multitron, INFORS HT). DNA extraction is performed using the EZ-10 Spin Column Plasmid DNA Miniprep Kit (BIO BASIC) following the manufacturer's instructions.

II.3. Yeast genomic DNA extraction

Cells are grown to an $OD_{600\,nm}$ = 0.8 − 1.2. 1 $OD_{600\,nm}$ unit are centrifuged and the pellet is resuspended in 200 µL lysis buffer (2 % (v/v) Triton X-100, 1 % (v/v) SDS, 100 mM NaCl, 10 mM Tris-HCl pH 8.0, 1 mM EDTA pH 8.0). Lysis is carried out by vortexing the suspension 6 times 30 sec in presence of 200 µL glass beads (Roth, $\varnothing$ 0.25 − 0.5 mm). Then, 200 µL chloroform are added and the lysate is vortexed for 2 min. After a 3 min centrifugation at 13,000 × *g* at RT, the aqueous phase is transferred in 400 µL ice-cold ethanol absolute and mixed by inversion. DNA precipitation occurs by an incubation of minimum 30 min at -80 °C. The DNA is pelleted at 13,000 × *g* for 5 min at room temperature (RT) and washed with 500 µL

Table MM-4: Primers used for the amplification of deletion cassette and for the verification of gene deletion or plasmid integration in genomic DNA.

primer MH n°	Fw/Rv	Primer use	Primer sequence (5' → 3')
169	Fw	amplification of the *KanMX4* deletion cassette for *GUS1* deletion	GAAGTATTAGTAACATTACCAGACCTCATCTGTTCC TAATAacatggaggcccagaatac
170	RV	amplification of the *KanMX4* deletion cassette for *GUS1* deletion	TGGATGATAAACTTTTACAGTCAAAGTTCTATAGGT AGACAcggcgttagtatcgaatcg
163	Fw	*GUS1* upstream primer	TTGCACTAACACCCATTGGG
173	Rv	*GUS1* downstream primer	AGCTCGTAGTCACTATTTGAACC
57	Rv	ampicillin marker	TTTTCTGTGACTGGTGAGTACTCAACC
175	Rv	verification of the plasmid integration at the *URA3* locus	AATCATTACGACCGAGATTCCC
117	Fw	amplification of the *KanMX4* deletion cassette for *POR1* deletion	CAAGCGTACCCAAAGCAAAAATCAAACCAACCTCTC AACAacatggaggcccagaatacc
118	Rv	amplification of the *KanMX4* deletion cassette for *POR1* deletion	ATGGTATATAGTGAACATATATATATTAGATATATA CGTcggcgttagtatcgaatcgac
39	Rv	verification of the insertion of the *KanMX4* deletion cassette	acaattacaaacaggaatcgaatgc
177	Fw	*POR1* upstream primer	GTGCTACGGATTCTCCCAAC
123	Fw	amplification of the *KanMX4* deletion cassette for *PEP4* deletion	ATTTAATCCAAATAAAATTCAAACAAAAACCAAAAC TAACACATGGAGCCCAGAATACC
134	Rv	amplification of the *KanMX4* deletion cassette for *PEP4* deletion	GCAGAAAAGGATAGGGCGGAGAAGTAAGAAAAGTTT AGCCGGCGTTAGTATCGAATCGAC
178	Fw	*PEP4* upstream primer	TGAGAAGCCTACCACGTAAGG

70 % (v/v) ethanol. After a centrifugation at 13,000 $\times$ *g* for 5 min at RT, the pellet is dried at RT and finally resuspended in H_2O (the volume depends on the pellet size). The concentration of DNA is determined by measuring the absorbance at 260 nm ($A_{260\,nm}$) with the Nanodrop.

II.4. PCR amplification of DNA fragments

II.4.1. Primer design

Depending on the utilization of the DNA fragment produced by PCR, the primer design will be different. However, all forward and reverse primers will anneal on the DNA region to amplify by at least 20 nucleotides and will have a guanosine or a cytidine in their 3'-ends. The melting temperature (Tm) of the primers should not be too different and is usually between 53 and 60 °C. For Gateway and Gibson cloning, when the gene will be inserted in a plasmid containing a tag, the reverse primer will be designed in order to remove the STOP codon of the gene to be cloned.

II.4.1.1. Gene deletion

Gene deletion in *Sce* genome occurs through the replacement by homologous recombination of the target gene in gDNA by a deletion cassette, obtained by PCR, usually containing the *KanMX4* gene (or an auxotrophic marker) (**Table MM-4**). To completely replace the target ORF (from ATG to STOP), the primers must be complementary to the 5'- and 3'-UTR of the target gene and allow the amplification of the *KanMX4* cassette. Usually for the homologous recombination to occur, the overlapping sequences must be approximately 40 nucleotides long.

II.4.1.2. Gateway cloning

The Gateway cloning requires the site-specific recombination between attB and attP sites located on the gene to insert and the "donor" vector respectively. Thus, the forward and reverse primers used to amplify the gene of interest must contain the attB1 and attB2 sequences in 5' and 3' respectively.

II.4.1.3. Gibson assembly

For the Gibson assembly, the primers used for the gene amplification contain the regions flanking the insertion site of the gene in the plasmid. Usually, the length of the regions used for homologous recombination is 20 nucleotides. For more detailed information

Table MM-5: PCR protocols used for DNA amplification according to the kit used.

	PrimeSTAR		Phire		
	Temperature	Time	Temperature	Time	
Initial denaturation	98 °C	1 min	98 °C	5 min	
Denaturation	98 °C	10 sec	98 °C	10 sec	
Annealing	depends on the primers	15 sec	depends on the primers	10 sec	30 ×
Extension	72 °C	5 sec/kb	72 °C	20 sec/kb	
Final extension	72 °C	1 min	72 °C	5 min	

refer to Hemmerle *et al.*, 2021, page 260.

II.4.2. DNA amplification using PrimeSTAR

To amplify a DNA fragment from a plasmid or from *Sce* genomic DNA (gDNA), the PrimeSTAR® Max DNA Polymerase (Takara) is used. The 20 µL PCR reaction is composed of 10 µL PrimeSTAR Max Premix 2 ×, 0.5 µM of each primer and 4 pg – 400 pg plasmidic DNA or 2 ng – 80 ng yeast gDNA. The PCR reaction is performed using C1000 TouchTM Thermal Cycler from Bio-Rad and protocol is described in **Table MM-5**.

II.4.3. Yeast colony PCR

Verification of the insertion of a plasmid or the deletion of a gene or amplification of a gene from *Sce* gDNA are done by colony PCR using the Phire Plant Direct PCR Master Mix (Thermo Scientific). The 10 µL reaction mixture is composed of 0,5 µM of each primer and 5 µL 2 × Phire Master Mix. Yeast cells are then swiped with a sterile pipette tip and resuspended in the PCR mix. The PCR reaction is performed using C1000 TouchTM Thermal Cycler from Bio-Rad and protocol is described in **Table MM-5**.

II.5. DNA visualization under UV light

DNA fragments are loaded onto a 1 – 2 % (w/v) agarose gel in TAE buffer (40 mM Tris, 20 mM acetate, 1 mM EDTA) and submitted to electrophoresis in the same TAE buffer for 30 min at 215 V. The gel is then incubated in a TAE solution containing 0.5 µg/mL ethidium bromide. The visualization is performed using Herolab Transilluminator.

II.6. Enzymatic restriction of plasmids

Plasmids can be digested using restriction enzymes (Fast digest enzymes from Thermo Scientific) to verify the insertion of DNA fragments in a plasmid or to linearize plasmids for further cloning steps. The 20 µL reaction contains around 0.5-1 µg plasmid, 0.5 µL restriction enzymes, 2 µL Fast digest buffer 10 ×. The reaction is incubated at 37 °C during 30 min for plasmid verification or 1 h for plasmid linearization. Digestion of DNA is verified by migration on agarose gel 1 % (w/v) and visualized as mentioned above.

II.7. Cloning strategies

During my PhD I used two different cloning strategies for DNA insertion in expression

Table MM-6: Composition of 1 × Gibson assembly mix.

	Components	Final concentration
Buffer	Tris-HCl pH 7.5	100 mM
	MgCl2	10 mM
	DTT	10 mM
	NAD+	1 mM
	each of the 4 dNTPs	2 mM
	PEG-8000	5% (w/v)
Enzymes	T5 exonuclease	7.5 U/ml
	Phusion DNA Pol	25 U/ml
	Taq DNA ligase	200 U/ml

plasmids. However, Gibson strategy was the most commonly-used technic and most of the plasmids I have constructed were assembled using this technic.

II.7.1. Gateway cloning strategy

The Gateway™ cloning strategy is a 2 steps site-specific recombination. First the gene of interest (GOI) is amplified by PCR using primers that contain the recombination sites attB1 and attB2 (see **section II.4.1.2**). The PCR product is then ligated into the linearized pJET1.2/blunt vector with the CloneJet PCR Cloning kit (Thermo Scientific) and 5 µL are transformed in chemically competent bacteria cells. After verification of the pJET1.2/GOI construction, 1 µg of plasmid is linearized with restriction enzyme (**section II.6.**) that digests outside of the GOI sequence. Restriction enzyme is inactivated following the manufacturer's instructions and 5 µL are mixed with 150 ng "donor vector" pDONR221 for BP recombination using the Gateway™ BP Clonase™ II Enzyme mix (Thermo Scientific) and incubated overnight at 25 °C. Chemically competent bacterial cells are transformed with 2 µL of recombination mix and plated on LB-agar supplemented with kanamycin. LR recombination then occurs between the pDONR221/GOI and any expression plasmid from the Gateway™ cloning collection. The LR recombination mix is composed of 150 ng of each plasmid and 10 µL of the Gateway™ LR Clonase™ II Enzyme mix (Thermo Scientific). After 2 h incubation at 25 °C, 2 µL of the LR recombination mix are transformed in competent bacteria cells subsequently plated on LB-agar supplemented with ampicillin.

II.7.2. Gibson assembly

The DNA region of interest is amplified with primers containing 20 nucleotides overhangs that will be used for the homologous recombination between the linearized plasmid and the PCR product (see **section II.4.1.3** and Hemmerle *et al.,* 2021, page 260. The DNA fragment can be amplified from *Sce* gDNA or from a plasmid. Linearization of the plasmid is performed either by enzymatic restriction or by PCR amplification. For DNA (insert and/or plasmid) obtained by PCR, a DpnI digestion is carried out for 1 h at 37 °C to remove the matrix DNA. After a PCR clean-up following the manufacturer's instructions (Macherey-Nagel) the concentration of each sample is determined by measuring the $A_{260\,nm}$ and the molar concentration is calculated using the NEBioCalculator® tool. DNA fragments are ligated in 20 µL of Gibson assembly buffer (**Table MM-6**). Finally, competent cells are transformed using 5 – 7.5 µL of the assembly.

Table MM-7: Plasmids used in this study for protein expression in the yeast (1/2).

Coll number	pMH n°	vector	promoter	Insert-tag	MW (kDa)	linearization enzyme
				Split-CFP/GFP plasmids		
1768/1769	063	p306	pGPD	Vph1-CFPβ1-10	122	NsiI
		p304	pGPD	cERS-β11ch	91	PmlI
2317	120	p304	pGUS1	cERS-β11ch	91	PmlI
2318	121	p304	pGPD	Pam16-β11ch	27	PmlI
1808	-	p414	pGPD	cERSΔN1(Δ30)-β11ch	87	-
2047-49		p414	pGPD	GFP/CFPβ11ch	9	-
2134	091	p414	pGPD	Cps1-β11ch	74	-
1505		p414	pGPD	Arc1-β11ch	52	-
1791		p414	pGPD	Arc1ΔN1(Δ37)-β11ch	47	-
1785		p414	pGPD	Arc1ΔN2(Δ54)-β11ch	45	-
1790		p414	pGPD	Arc1ΔN3(Δ108)-β11ch	39	-
1509	024	p414	pGPD	Arc1ΔN(Δ132)-β11ch	37	-
1507	006	p414	pGPD	Arc1N(1-132)-β11ch	25	-
1510	030	p414	pGPD	Arc1ΔC(1-201)-β11ch	33	-
1723		p414	pGPD	ERS1-160-β11ch	28	-
1155		p414	pGPD	His3-β11ch	34	-
2133	090	p414	pGPD	Vma13-β11ch	64	-
2315	118	p414	pGPD	Nvj1-β11ch	46	-
2332	122	p414	pGPD	Por1-β11ch	40	-
2314	117	p414	pGPD	Atg20-β11ch	82	-
1739		p414	pGPD	MRS-β11ch	96	-
1162		p414	pGPD	ERS-β11ch	91	-
1719		p414	pGPD	ARS-β11ch	118	-
1139		p414	pGPD	KRS-β11ch	78	-
1128		p414	pGPD	DRS-β11ch	74	-
1881/1882	080/081	p414	pGPD	FRS2-β11ch	67	-
1138		p414	pGPD	HRS-β11ch	70	-
1721		p414	pGPD	LRS-β11ch	134	-
1720		p414	pGPD	VRS-β11ch	136	-
1161		p414	pGPD	GRS1-β11ch	86	-

For more detailed information refer to Hemmerle et al., 2021, page 260.

II.8. Plasmid sequence verification

Plasmids obtained after cloning and DNA extraction from bacterial cells are first verified using restrictions enzymes and subsequent agarose gel electrophoresis. Clones that display the expected digestion profile are sent for Sanger DNA sequencing with specific pimers (SupremeRun Sequencing Service, Eurofins Genomics). The sequencing results are analyzed with ApE plasmid editor software.

III. Procedures used for *S. cerevisiae*

III.1. Yeast growth monitoring

Most experiments are carried out using yeast cells that are in their exponential (or mid-logarithmic, mid-log) growth phase. To determine their growth phase, the $OD_{600\ nm}$ is measured using the DU®730, Beckman Coulter spectrophotometer. For a more accurate measurement, cells are diluted 1/10 in water in a polystyrene spectrophotometer cuvette. For this spectrophotometer the exponential growth phase corresponds to an $OD_{600\ nm}$ = 0.5 – 1.5.

Usually, pre-cultures are inoculated directly from the agar plates in the appropriate medium and incubated overnight at 30 °C. In the morning, cells are diluted to an $OD_{600\ nm}$ = 0.3 – 0.4 and their growth is followed by spectrophotometer measurements.

III.2. Yeast transformation

Yeast cells are grown overnight in YPD and centrifuged at 5,000 × *g* for 5 min at RT. The pellet is washed two times with sterile H_2O and resuspended in the appropriate volume of H_2O. 10 μL of salmon sperm DNA (10 mg/mL) pre-heated at 95 °C are mixed together with 50 μL cell suspension by vortexing. 1 μg of DNA (PCR fragment or plasmid) are added to the suspension together with 350 μL transformation Mix (0.1 M lithium acetate, 34.5 % (v/v) polyethylene glycol (PEG) 4000). After a 20 - 40 min incubation at 42 °C, cells are harvested by short spin centrifugation and the pellet is washed with 1 mL H_2O. The supernatant is removed to leave approximately 100 – 150 μL in the tube to resuspend the pellet. Transformed cells are then spread on a SC-aa auxotrophic medium and incubated for 3 – 4 days at 30°C. The plasmids used in this study are listed in **Table MM-7**.

Table MM-7: Plasmids used in this study for protein expression in the yeast (2/2).

Coll number	pMH n°	vector	promoter	Insert-tag	MW (kDa)	linearization enzyme
				Split-CFP/GFP plasmids		
1163		p414	pGPD	QRS-β11ch	103	-
1215		p414	pGPD	NRS-β11ch	73	-
1160		p414	pGPD	SRS-β11ch	64	-
1137		p414	pGPD	TRS-β11ch	95	-
1216		p414	pGPD	WRS-β11ch	60	-
1738		p414	pGPD	IRS-β11ch	133	-
1166		p414	pGPD	YRS-β11ch	54	-
1154		p414	pGPD	RRS-β11ch	80	-
1874	073/074	p414	pGPD	GRS2-β11ch	80	-
		p414	pGPD	FRS1-β11ch	76	-
				Other plasmids		
1639	049	p425	pGPD	Arc1∅MRS(A26R,S33A)-3cHis10	45	-
1638	048	p425	pGPD	Arc1∅ERS(T55R, R100A, Y104A)-3cHis10	45	-
1634	044	p425	pGPD	Arc1∅MRS∅ERS-3cHis10	45	-
2135	092	p306	pGPD	cERSΔN1(Δ30)-3HA	82	PstI
2141	098	p306	pGPD	cERSΔN2(Δ70)-3HA	78	PstI
2142	099	p306	pGPD	cERS-3HA	86	PstI
2146	103	p306	pGPD	cERSΔN3(Δ160)-3HA	68	PstI
Sylvie Friant				mCherry-Atg8		-
2131	088	p306	pGPD	Vph1-Arc1-3HA	143	NsiI

III.3. Serial dilution spotting assay

Cells are grown until an $OD_{600\,nm}$ = 0.8 − 1.2 and pelleted for 3 min at 5000 rpm. After washing the cells with 1 mL sterile H_2O, the pellet is resuspended in a volume of water to obtain a $OD_{600\,nm}$ = 0.5. Serial dilutions are performed to obtain the dilutions 5.10^{-2}, 5.10^{-3}, 5.10^{-4}, 5.10^{-5}. 8 µL of each dilution are then spotted on agar plates. Cells are incubated at 30 °C for 3 − 4 days and pictures are taken every day to follow the growth of the colonies.

III.4. Yeast mating procedure

Mating of yeast cells to obtain diploid cells is performed on YPD-agar plates by mixing cells of mating type a and α. After an overnight incubation at 30 °C, cells are spread on YPD plate to obtain isolated clones. The selection of diploid is performed using the mating type tester strains PT1 (Mat a *iso1⁻ ham1⁻ cam1-*) or PT2 (Mat α *iso1⁻ ham1⁻ cam1⁻*). Indeed, when haploid cells are crossed with PT1 or PT2 strains, the diploids obtained are able to grow on SD medium. After an overnight incubation at 30 °C the plates are replica plated on SD medium and cells able to grow on this medium were not diploid in the first place. The diploid cells selected are then replica plated on various media to determine their phenotype. Finally, selected clones are tested by colony PCR to confirm their genotype.

For cells that have difficulties to mate on solid media, the mating procedure can be performed in liquid medium. Cells are first cultured until they reach an $OD_{600\,nm}$ = 0.8 − 1.2. Then equivalent volumes are mixed together and incubated at 30 °C under shaking. Every hour the tube is left on the bench for 1 min to let the cells settle. A 10 µL aliquot is taken from the bottom of the tube, diluted 1000 times and spread on YPD plate. After 3 − 5 days at 30 °C clones are cross-tested with the PT1 and PT2 strains to check for diploid cells (see the procedure above).

III.5. Diploid sporulation and tetrad dissection

To trigger sporulation, diploid cells are spread on sporulation media (1 % (w/v) acetate potassium, 2 % (w/v) agar-agar) and incubated at 25 °C or at RT. Every day cells are harvested from the plate and visualized by optical microscopy to check the presence of tetrads of four haploid spores.

Once a majority of diploid cells have undergone sporulation, tetrads are inoculated in

45 µL H$_2$O and the protective membrane surrounding spores is digested with 5 µL of zymolyase 20T (10 mg/mL) for 5 min at RT. Digested tetrads are then spread in a line on a YPD plate to form a "tetrad reservoir". After drying the plate for a few minutes tetrads are selected, picked, and the individual spores pulled apart using a micromanipulator microscope (Singer MSM System 200) that controls the movement of a fine glass needle. Plates are incubated for 3 – 4 days at 30 °C and pictures are taken up every day to monitor the growth. Genotyping of the spores is performed by replica plating on various media and mating type is determined by cross-testing with PT1 and PT2 strains.

III.6. Yeast protein extract preparation

III.6.1. Total protein extract

Cells are cultured until an OD$_{600\text{ nm}}$ = 0.8 – 1.2. The volume corresponding to 1 OD$_{600\text{ nm}}$ unit is then centrifuged at 5,000 × g for 5 min and the pellet is stored on ice. Cell lysis occurs by the addition of 450 µL NaOH 0.185 M and subsequent 10 min incubation on ice. Proteins precipitation is performed by addition of 50 µL trichloroacetic acid (TCA) 100 %. Samples are then vortexed and incubated 10 min on ice. Precipitates are centrifuged for 10 min at 13,000 × g at 4 °C. Pellets are finally resuspended in 50 µL/OD$_{600\text{ nm}}$ unit 1 × loading buffer (60 mM Tris-HCl pH 6.8, 10 % (v/v) glycerol, 2 % (v/v) β-mercaptoethanol, 2 % (w/v) SDS, 0.1 % (w/v) bromophenol blue).

III.6.2. Subcellular fractionation

Cells are cultured until they reach an OD$_{600\text{ nm}}$ = 0.8 – 1.2. The volume equivalent to 100 OD$_{600\text{ nm}}$ units is centrifuged at 5,000 × g during 10 min. From this point all steps are performed on ice and all centrifugations are carried out at 4 °C. Cells are washed with 10 mL ice-cold cytosol buffer (20 mM Hepes-Na pH 6.8, 150 mM potassium acetate, 10 mM MgCl$_2$, 250 mM sorbitol) and centrifuged at 5,000 × g during 10 min at 4°C. The pellet is resuspended in 1 mL ice-cold cytosol buffer supplemented with Protease Inhibitor Cocktail (Roche) and 1 mM phenylmethylsulfonyl fluoride (PMSF). The suspension is transferred to a 15 mL Corex tube containing 1.6 g acid-washed glass beads (Sigma, ∅ 425 – 600 µm). Cell lysis is performed by vortexing 10 times 30 s with 1 min incubation on ice between each run. The lysate is transferred in a 1.5 mL Eppendorf tube and centrifuged at 500 × g during 5 min at 4 °C. The supernatant is transferred to a new 1.5 mL Eppendorf tube and centrifuged at 13,000 × g for 10 min at 4°C to obtain the soluble S13 and the pellet P13 fractions. A 50

µL aliquot of S13 is collected for Western blot analysis and the remaining is transferred to a 1.5 mL ultracentrifugation tube. The soluble S100 and the pellet P100 fractions are obtained after a 1 h ultracentrifugation at 100,000 × g at 4°C. The P13 and P100 pellets fractions are washed using 500 µL cytosol buffer and finally resuspended with cytosol buffer in a volume equivalent to the S100 fraction. The concentration of each fraction is determined using Bradford. For Western blot analysis the same volume of each fraction is loaded onto SDS-PAGE. The quantity of proteins loaded on the gel should be at least 10 µg and at most 50 µg.

III.6.3.Yeast vacuole purification

The following protocol is adapted for a 1 L culture at an $OD_{600\ nm}$ = 0.8 – 1.2 so approximately 1000 $OD_{600\ nm}$ units. The culture is centrifuged for 2 min at 4,400 × g at RT. Cells are then resuspended by vortexing in 50 mL DTT solution (0.1 M Tris-SO_4 pH 9.4, 10 mM DTT) and incubated for 10 min in a 30 °C water-bath. Cells are pelleted at 4,400 × g at RT and resuspended in spheroplast medium A at a concentration of 20 – 30 $OD_{600\ nm}$ units/mL (1 × YNB, 2% (w/v) glucose, 1 × amino acids, 1 M sorbitol, 20 mM Tris-HCl pH 7.5). A 10 µL aliquot is diluted in 990 µL H_2O and vortexed to monitor the $OD_{600\ nm}$. Spheroplasts are prepared by the addition of zymolyase 100T at a final concentration of 3 µg/$OD_{600\ nm}$ units (stock solution at 5 mg/mL in spheroplast medium A) and incubated at 30 °C for 20 min under shaking. To monitor the cell wall digestion a 10 µL aliquot is taken and mixed with 990 µL H2O. After a 1 – 2 min incubation the mix is vortexed and the $OD_{600\ nm}$ is measured. The digestion is completed when the $OD_{600\ nm}$ reaches < 5 % of the initial $OD_{600\ nm}$ before zymolyase treatment. From this point all steps should be performed very carefully since the spheroplasts are very fragile. The spheroplasts are centrifuged 3 min at 5,380 × g at 4 °C and resuspended in 20 – 30 mL spheroplast medium B (1 × YNB, 2% (w/v) glucose, 1 × amino acids, 1 M sorbitol) by gently rotating the bottle or by using a glass rod. Spheroplast medium B is finally added to reach a concentration of 1 – 5 $OD_{600\ nm}$ units/mL and spheroplasts are centrifuged 3 min at 5,380 × g at 4°C. The washing step is repeated a second time to completely remove the zymolyase and spheroplasts are kept on ice. Spheroplasts are resuspended in 2,5 mL Ficoll 15 % (w/v) solution prepared in PS buffer (10 mM PIPES-KOH pH 6.8, 200 mM sorbitol) and 200 µL of dextran solution (0.4 mg/mL in PS buffer) are added and gently mixed. After an incubation of 5 min on ice, the spheroplasts are transferred in a 30 °C water-bath for 1.5 min with gentle mixing during the incubation and kept on ice. The cell lysate is then transferred in ultracentrifugation tubes (SW40 or SW41) and 2.5 – 3 mL of Ficoll 8 % (w/v) and then Ficoll

Table MM-8: Fluorescent probes used in this study.

Fluorescent Dye	Excitation (nm)	Emission (nm)
MitoTracker Red CMXRos	579	599
FM4-64	515	640
Quinacrine	436	525

MitoTracker : mitochondria staining, FM4-64: vacuole membrane staining after 20 min incubation, Quinacrine: accumulates in acidic compartment.

4 % (w/v) prepared in PS buffer are added onto the cell lysate. Finally, PS buffer is added to reach the top of the tube. The vacuoles are separated by a 90 min ultracentrifugation at 110,000 × g at 4°C and approximately 500 µL vacuoles can be collected at the interface between Ficoll 4 % (w/v) and PS buffer. To stabilize the vacuoles before determining the protein concentration, protease inhibitor cocktail is added to a final concentration of 0,1 ×. Vacuoles can then be frozen using liquid nitrogen and conserved at -80 °C after mixing with glycerol to 10 % (v/v) final concentration.

III.7. Fluorescence microscopic observations

III.7.1. FM™ 4-64 staining

Cells are cultured until an $OD_{600\,nm}$ = 0.8 – 1.2. The volume equivalent to 1 – 1.5 $OD_{600\,nm}$ unit is pelleted at 5,000 × g 5 min RT. The pellet is resuspended in 50 µL medium supplemented with 8 µM FM™4-64 (*N*-(3-Triethylammoniumpropyl)-4-(6-(4-(Diethylamino) Phenyl) Hexatrienyl) Pyridinium Dibromide) (**Table MM-8**). The suspension is then incubated 20 min at 30 °C to label the vacuolar membrane. Cells are then washed with 500 µL medium. After centrifugation at 5,000 × g 1 min, the pellet is resuspended in 300 µL medium and incubated 10 min at 30 °C to chase FM4-64. The suspension is centrifuged 1 min at 5,000 × g and the pellet is resuspended in 500 µL medium. After a 5,000 × g 1 min centrifugation the pellet is resuspended in 50 µL of adequate medium for microscopic observations.

III.7.2. MitoTracker™ Red CMXRos staining

Cells are cultured until mid-log phase in SC-Galactose (SCGal) medium to activate mitochondria. Approximately 1 $OD_{600\,nm}$ unit is harvested and supplemented with 1 µL 200 nM MitoTracker™ Red CMXRos (Thermo Fisher) (**Table MM-8**). After 15 min incubation at 30 °C the cells are washed three times with H_2O and resuspended in 20-50 µL SCGal.

III.7.3. Quinacrine staining

This protocol is adapted from Baggett *et al.*, 2003. Cells are cultured until mid-log phase in rich medium and 1 $OD_{600\,nm}$ unit is pelleted at 300 × g for 3 – 5 at RT. The supernatant is removed and the pellets are incubated on ice for 2 – 5 min and subsequently resuspended in 0.9 mL rich medium (SC). 100 µL Hepes 1 M pH 7.6 and quinacrine prepared in Hepes-Na 1 M pH 7.6 is added to a final concentration of 1 µM (**Table MM-8**). The suspension is incubated at growth temperature for 5 min under shaking. Cells are pelleted for 5 min at 300 × g at RT

and resuspended in 50 µL 100 mM Hepes pH 7.6, 2 % (w/v) glucose ice-cold. Cells are kept maximum 30 min on ice until microscopic observations.

IV.   Biochemisty

IV.1. Protein electrophoresis and immunoblotting

All samples for protein electrophoresis are prepared in $1 \times$ loading buffer (60 mM Tris-HCl pH 6.8, 10 % (v/v) glycerol, 2 % (v/v) β-mercaptoethanol, 2 % (w/v) SDS, 0.1 % (w/v) bromophenol blue). Before loading they are heated in a 42 °C water-bath for 5 min. For yeast total extract a volume equivalent to 0.1 $OD_{600\,nm}$ is used for SDS-PAGE analysis.

Polyacrylamide gels are prepared as followed:

-   Lower layer (resolving gel) is composed of acrylamide:bisacrylamide (30% 37.5:1) diluted in 450 mM Tris-HCl pH 8.8, 0.12 % (w/v) SDS. Acrylamide concentration was adjusted depending on the molecular weight of the proteins to analyze (usually between 8 % (v/v) and 16 % (v/v))
-   Upper layer (stacking gel) is composed of 5 % (v/v) acrylamide:bisacrylamide (30 % 37.5:1) diluted in 125 mM Tris-HCl pH 6.8, 0.1 % (w/v) SDS.

The polymerization of the polyacrylamide gels is triggered by the addition of 0.1 % (w/v) ammonium persulfate and 0.1 % (w/v) N,N,N',N Tetramethylethylenediamine (TEMED). Gels are poured between two glass plates (10×8 cm) with 0.75 mm, 1 mm or 1.5 mm integrated spacers (Mini-PROTEAN® Spacer Plates, BIO-RAD).

After sample loading, electrophoresis is performed in Tris-glycine SDS running buffer (25 mM Tris, 192 mM glycine, 0.1 % (w/v) SDS, p≈H ≈ 9) at 180 V for 10 min and then at 200 – 210 V (20 mA) for 30 – 45 min using Mini-PROTEAN® Tetra Vertical Electrophoresis Cell (BIO-RAD).

For the visualization of proteins after electrophoresis using the Stain-free technology, 0.5 % (v/v) 2,2,2-Trichloroethanol (TCE) is added to the acrylamide:bisacrylamide 30 % stock solution. Indeed, the trihalo compound is covalently bound to tryptophan residues, enhancing their fluorescence when exposed to UV light. The Stain-free procedure is performed using the ChemiDoc™ imaging system (BIO-RAD).

For Western blotting, proteins are transferred onto 0.2 μm PVDF membrane (Trans-Blot Transfer Packs, BIO-RAD) using the Trans-Blot Turbo™ transfer system (BIO-RAD) following the manufacturer's instructions. The PVDF membrane is activated by bathing it in ethanol 100 % for a few minutes. After a brief washing step with TBS-Tween buffer (50 mM Tris-HCl pH 7.6, 150 mM NaCl, 0.3 % (v/v) Tween20), the membranes are incubated in blocking buffer (TBS-Tween with 5 % (w/v) either skim milk or BSA) for 20 min at RT under shaking. Primary antibodies are incubated either overnight at 4 °C or 3 h at RT in blocking buffer at different concentrations (**Table MM-9**). After three 10 min washing steps in TBS-Tween, membranes are incubated with the HRP-couped secondary antibodies (anti-mouse or anti-rabbit goat antibodies, **Table MM-9**) diluted 1:5,000 in blocking buffer for at least 3 h at RT. Clarity Western ECL substrate (BIO-RAD) is used following the manufacturer's instructions, and the chemiluminescence detection is carried out using the ChemiDoc™ imaging system (BIO-RAD).

IV.2. Recombinant protein purification

The plasmids used for ERS_{His6}, MRS_{MBP}, $_{His6}Arc1$ (WT and truncated mutants) and $Arc1●MRS_{His6}$ overexpression are listed in **Table MM-10**. The overexpression and purification of MRS_{MBP} along with cleavage of the MBP-tag were performed by Sylvain Debard and described in Debard, 2019. After overexpression, $_{His6}Arc1$ and ERS_{His6} were first purified by nickel affinity column (HisTrap HP, Cytiva) and then submitted to gel filtration (Superdex® 200 10/300 GL, Cytiva). The His6-tagged truncated mutants of Arc1 were batch-purified using Ni-IDA agarose beads (Jena Bioscience).

IV.2.1. Protein overexpression

E. coli Rosetta 2 strains harboring the pET15b or pET20b expression plasmids (**Table MM-10**) are grown overnight in 50 mL LB medium supplemented with ampicillin (Amp) and chloramphenicol (Cam) at 37 °C under shaking. In the morning the culture is diluted to an $OD_{600\,nm} = 0.1$ in 1 L LB medium + Amp + Cam. When $OD_{600\,nm} = 0.5$, the induction is triggered by the addition of 1 mM isopropyl β-D-1-thiogalactopyranoside (IPTG) during 3 h at 30 °C. For the expression of Arc1 truncated mutants, the expression was induced upon addition of 0.2 mM IPTG and 4 h incubation at 30°C. Cells are then pelleted at 4,000 × g for 10 min at RT. At this step, cells can be stored at -20 °C.

Table MM-9: Antibodies used for immunoblotting.

Primary antibody	Type	Host	Dilution	Source
anti-MRS	polyclonal	rabbit	1:5,000	this lab
anti-Arc1	polyclonal	rabbit	1:5,000	this lab
anti-ERS	polyclonal	rabbit	1:5,000	this lab
anti-GFP N-terminal	polyclonal	rabbit	1:5,000	Sigma
anti-Vph1	monoclonal	mouse	1:1,000	gift from Dr. Friant's lab
anti-Pgk1	monoclonal	mouse	1:5,000	Abcam
anti-GFPβ11	monoclonal	mouse	1:5,000	Roche
Ni-HRP conjugate			1:10,000	Thermo Fisher

Secondary antibody	Host	Dilution	Source
anti-mouse IgG	Goat	1:5,000	BIO-RAD
anti-rabbit IgG	Goat	1:5,000	BIO-RAD

Table MM-10: Plasmids used for protein overexpression in *E. coli.*

Name	Protein-Tag	Resistance marker	induction
pET8c-Arc1	His6-Arc1	Amp	IPTG
pET8c-Arc1ΔM	His6-Arc1ΔM	Amp	IPTG
pET8c-Arc1ΔC	His6-Arc1ΔC	Amp	IPTG
pET8c-Arc1N	His6-Arc1N	Amp	IPTG
pET20b-ERS	ERS-His6	Amp	IPTG
pMALc2-MRS	MBP-MRS	Amp	IPTG
pET20b-AMRS	Arc1•MRS-His6	Amp	IPTG

IV.2.2. Soluble fraction preparation

Cells are lysed by sonicating for approximately 5 min at 40 % amplitude in lysis buffer (50 mM Hepes-Na pH 7.5, 150 mM NaCl, 1 mM $MgCl_2$, Protease Inhibitor Cocktail (tablets, Roche) and 1 mM PMSF, usually 3 mL/g of cells). The lysate is first centrifuged at 13,000 $\times$ g for 15 min at 4 °C and finally at 100,000 $\times$ g for 1 h at 4 °C to obtain a soluble fraction that can be injected on the columns. Before purification, the different fractions obtained by centrifugations are analyzed by SDS-PAGE and Stain-free procedure to confirm the solubility of the proteins.

IV.2.3. Batch purification of His6-tagged proteins

For the purification of His6-tagged proteins from 3 g of cells, 500 μl of Ni-IDA agarose beads (Jena Bioscience) are used. The resin is first washed two times with 10 volumes of Ni-IDA buffer (NaH_2PO_4 50 mM pH 8, NaCl 300 mM) supplemented with 10 mM imidazole. The soluble extract is incubated overnight with the resin at 4°C on a rotary shaker. The resin is then washed with 10 volumes of Ni-IDA buffer supplemented with 20 mM imidazole. The elution of the His6-tagged proteins is performed using Ni-IDA buffer supplemented with 250 mM imidazole. In order to remove the imidazole from the elution fractions, sample dialysis is performed. The sample is poured in a dialysis bag previously rinsed with distilled water and the dialysis bag is then soaked in ice-cold dialysis buffer under constant agitation at 4 °C for 3 h minimum (usually overnight incubation is performed). The volume of the buffer should be at least 100 times the sample volume. To concentrate the sample after dialysis, the dialysis bag is placed in a box and covered with dry polyethylene glycol (PEG6000) at 4 °C to trigger diffusion of the buffer from the dialysis bag into PEG powder.

IV.2.4. FPLC purification

ERS_{His6}, $Arc1_{His6}$ and $Arc1●MRS_{His6}$ purification was performed on ÄKTA™ pure chromatography system and analyzed with UNICORN™ software. All steps are performed in cold-room at 4 °C.

IV.2.4.1. HisTrap

The soluble extracts prepared in **section IV.2.2** are loaded onto 1 mL HisTrap™ High Performance (Cytiva) previously equilibrated with lysis buffer. The column is washed with lysis buffer and the proteins are then eluted in presence of lysis buffer and a 0-400 mM

imidazole gradient. For the elution, 500 µl fractions were collected in 96 deep-well plates using flexible fraction collector F9-C.

IV.2.4.2. Gel filtration

Depending on the protein concentration in the HisTrap elution fractions, 40-500 µL of sample are loaded onto Superdex 200 10/300 GL column (GE Healthcare) previously equilibrated with 1 × Phosphate Buffered-Saline (PBS). The elution of the proteins is performed using 1 × PBS.

IV.3. Lipid overlay assays

Interaction of proteins with lipids is determined using PIP Strip (Echelon Biosciences) membranes pre-spotted with different biologically-active lipids at 100 pmol per spot. PIP Strips are first incubated either 1 h at RT or overnight at 4 °C in 10 mL blocking buffer (Tris Buffer Saline (TBS) + 0.1 % (v/v) Tween20 + 3 % (w/v) fatty acid-free BSA). 10 pmol of recombinant protein diluted in 5 mL blocking buffer are then incubated on the membranes for 1 h à RT. After washing the membranes three times for 10 min with TBS + 0.1 % (v/v) Tween20, the primary antibody diluted 1:5,000 (**Table MM-9**) in blocking buffer is incubated on the membranes for 1 h at RT. Membranes are washed again three times with TBS + 0.1 % (v/v) Tween20 and incubated with the secondary antibody diluted 1:5,000 in blocking buffer for 1 h at RT. After three washing steps the membranes are revealed with ECL (BIO-RAD).

IV.4. Liposome binding assays

In order to perform liposome-binding assays, PolyPIPosomes from Echelon Biosciences were used. These liposomes are composed of phosphatidylcholine (PC), phosphatidylethanolamine (PE), biotin-PE and PtdIns(3,5)P$_2$ (see **Figure ChII.R-10**). For the assays, 10 µL of PolyPIPosomes are incubated with 1-3 µg of purified proteins and binding buffer (50 mM Hepes pH 7.5, 150 mM NaCl, 2 mM MgCl2, 0.1 % (w/v) fatty-acid free bovin serum albumin (BSA), 0.05 % (v/v) NP-40) for 1 h at RT on a rotary shaker (10 µL are collected for Western blot analysis).

IV.4.1. PolyPIPosome purification

The presence of biotin-PE in the PolyPIPosomes allows their purification using Dynabeads™ M-280 Streptavidin. After vortexing the beads for 30 s, 45 µL of beads are

transferred to 1 mL binding buffer and vortexed for 5 sec. The tube is then placed into a magnetic rack for 1 min and the supernatant is removed. After resuspending the beads in 45 μL binding buffer, the PolyPIPosomes are added and incubated for 1 h at RT on a rotary shaker. The tubes are then placed into the magnetic rack for 1 min and the flowthrough is collected. After three washing steps with 500 μL binding buffer, the proteins are eluted upon addition of 100 μL of SDS-PAGE loading buffer (see **section IV.1**) previously heated at 95 °C. The purification fractions are then analyzed by Western blot.

PUBLICATIONS & POSTER

Book chapter

Noncanonical inputs and outputs of tRNA aminoacylation

Marine Hemmerle, Marion Wendenbaum, Guillaume Grob, Nathaniel Yakobov, Nassira Mahmoudi, Bruno Senger, Sylvain Debard, Frédéric Fischer, Hubert Dominique Becker*

Génétique Moléculaire, Génomique, Microbiologie, UMR 7156, CNRS, Université de Strasbourg, Strasbourg, France
*Corresponding author: e-mail address: h.becker@unistra.fr

Contents

Abstract

The aminoacylation reaction is one of most extensively studied cellular processes. The so-called "*canonical*" reaction is carried out by direct charging of an amino acid (aa) onto its corresponding transfer RNA (tRNA) by the cognate aminoacyl-tRNA synthetase (aaRS), and the *canonical* usage of the aminoacylated tRNA (aa-tRNA) is to translate a messenger RNA codon in a translating ribosome. However, four out of the 22 genetically-encoded aa are made "*noncanonically*" through a two-step or indirect route that usually compensate for a missing aaRS. Additionally, from the 22 proteinogenic aa, 13 are *noncanonically* used, by serving as substrates for the tRNA- or aa-tRNA-dependent synthesis of other cellular components. These nontranslational processes range from lipid aminoacylation, and heme, aa, antibiotic and peptidoglycan synthesis

1

to protein degradation. This chapter focuses on these noncanonical usages of aa-tRNAs and the ways of generating them, and also highlights the strategies that cells have evolved to balance the use of aa-tRNAs between protein synthesis and synthesis of other cellular components.
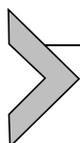
1. Introduction

Translation relies on the constant synthesis and delivery to the decoding ribosomes of a complete set of accurately aminoacylated transfer RNAs (aa-tRNAs). aa-tRNAs are the products of an enzymatic reaction termed tRNA aminoacylation, that is catalyzed by a family of ubiquitous enzymes called aminoacyl–tRNA synthetases (aaRSs) [1]. Elucidation of the aminoacylation reaction was concomitant with the characterization of tRNA and aaRSs [2–7]. In the "*canonical*" aminoacylation reaction, using a specific amino acid (aa), aaRSs catalyze the ATP-dependent formation of an aminoacyl–adenylate (aa$\sim$AMP), which enables this activated aa to be transferred directly onto the accepting 3′- or 2′OH of the terminal adenosine of the cognate tRNA (Fig. 1A). "*Canonical*" tRNA aminoacylation is often also termed "*direct*" tRNA aminoacylation and signifies that the aa and tRNA that are linked are cognate pairs and that, upon release, the aa-tRNA can be used directly in protein synthesis. Contrarily, the "*non-canonical*" tRNA aminoacylation, also termed "*alternate*" or "*indirect pathway,*" starts with an aa that is first charged onto a non–cognate tRNA by an aaRS, followed by its conversion into the cognate aa by a second enzymatic activity. The first description of a non-canonical pathway for tRNA aminoacylation occurred as early as 1968 by M. Wilcox and M. Nirenberg, who demonstrated that direct formation of glutaminyl–tRNA$^{\text{Glutamine}}$ (Gln-tRNA$^{\text{Gln}}$) by a glutaminyl–tRNA synthetase (GlnRS) was absent in three *Bacilli* species; the evidence indicated that they all required first the aminoacylation of tRNA$^{\text{Gln}}$ with glutamate (Glu), followed by the tRNA-dependent conversion of Glu into Gln, thereby demonstrating that tRNA can be a cofactor in aa biosynthesis [8]. The description of the first non-canonical aminoacylation reaction almost coincided with the first report of the non–canonical utilization of an aa–tRNA, *e.g.,* not for protein synthesis, and was that of lysyl-tRNA$^{\text{Lysine}}$ in the synthesis of *O*-lysyl phosphatidylglycerol in *Staphylococcus aureus* [9].

From the 22 genetically-encoded aa that have been identified to date, 18 are exclusively aminoacylated onto their cognate tRNAs through the
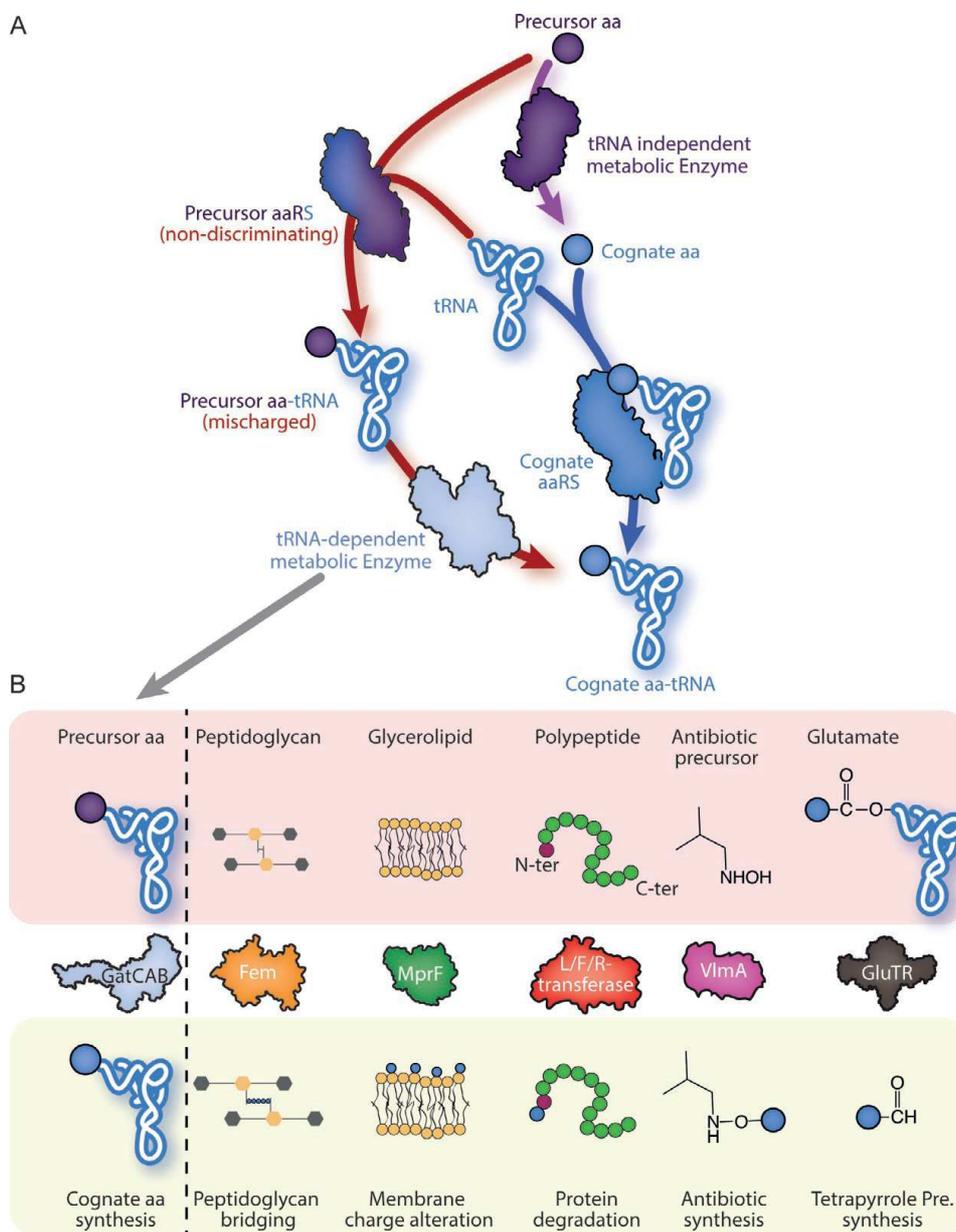
Fig. 1 Canonical and noncanonical tRNA aminoacylation reaction and nontranslational aa-tRNA usages. (A) Overview of the canonical tRNA aminoacylation (right side, blue arrows) and of the noncanonical 2-step reaction (left side, red arrows). For details see Fig. 2. (B) Schematic representations of the nontranslational usages of aa-tRNAs described in this chapter. The molecule that will be tRNA-dependently or aa-tRNA-dependently modified is indicated in the top row, the enzyme responsible for the tRNA-dependent modification in the middle and the product of the reaction or the fate of the compound tRNA-dependently modified is indicated in the bottom row.

canonical reaction (Ala, Arg, Asp, Glu, Gly, His, Ile, Leu, Lys, Met, Phe, Pro, Pyrrolysine (Pyl), Ser, Thr, Trp, Tyr and Val), one is strictly aminoacylated *via* a non-canonical aminoacylation reaction (Selenocysteine, Sec) and three are charged onto their corresponding tRNA either canonically or non-canonically (Asn, Cys and Gln). All four indirect pathways of tRNA aminoacylation have three main common features. They proceed *via* two consecutive steps (an exception is Sec-tRNA^{Sec} formation in archaea and eukaryotes that requires three reactions; see Fig. 2). The first step is the mis-charging of a tRNA with a non-cognate aa by a so-called non-discriminating aaRS (ND-aaRS) [10,11]. The second step is the conversion of the misacylated aa into the cognate one, while it is attached to the tRNA by a tRNA-dependent modifying enzyme [12]. Sometimes the ND-aaRS and the tRNA-dependent modifying enzyme form a complex that catalyzes both reactions without the release of the mischarged aa-tRNA intermediate [13]. The last common feature is that the noncognate aa of the misacylated aa-tRNA intermediate is always a metabolic precursor of the cognate final aa, in the tRNA-independent and regular metabolic pathway (*e.g.,* Asp for Asn, Glu for Gln, O-phosphoserine (Sep) for Sec; Fig. 1A). Among the 22 proteinogenic aa, 13 (Ala, Arg, Asp, Glu, Gly, Leu, Lys, Met, Phe, Thr, Trp, Val and Ser) can serve as substrates for the tRNA-dependent synthesis of other cellular components. Noteworthy, when the aa of an aa-tRNA is used for a non-canonical pathway, the tRNA carrier is generally not specific to the non-canonical usage but diverted from protein synthesis. This often requires adaptation of other components of the translation machinery that limit the negative impact that rerouting of aa-tRNAs could have on the efficiency or accuracy of protein synthesis [14]. The purpose of this chapter is to present the fascinating diversity of the non-canonical usages made by organisms of aa-tRNAs (Fig. 1B).

2. Non canonical aminoacylation of tRNAs and tRNA-dependent synthesis of amino acids

2.1 The two non-standard amino acids

In addition to the common set of 20 proteinogenic aa, two additional and non-standard aa are used for protein synthesis in some organisms: selenocysteine (Sec) and pyrrolysine (Pyl), respectively, known as the 21st and 22st genetically-encoded aa.
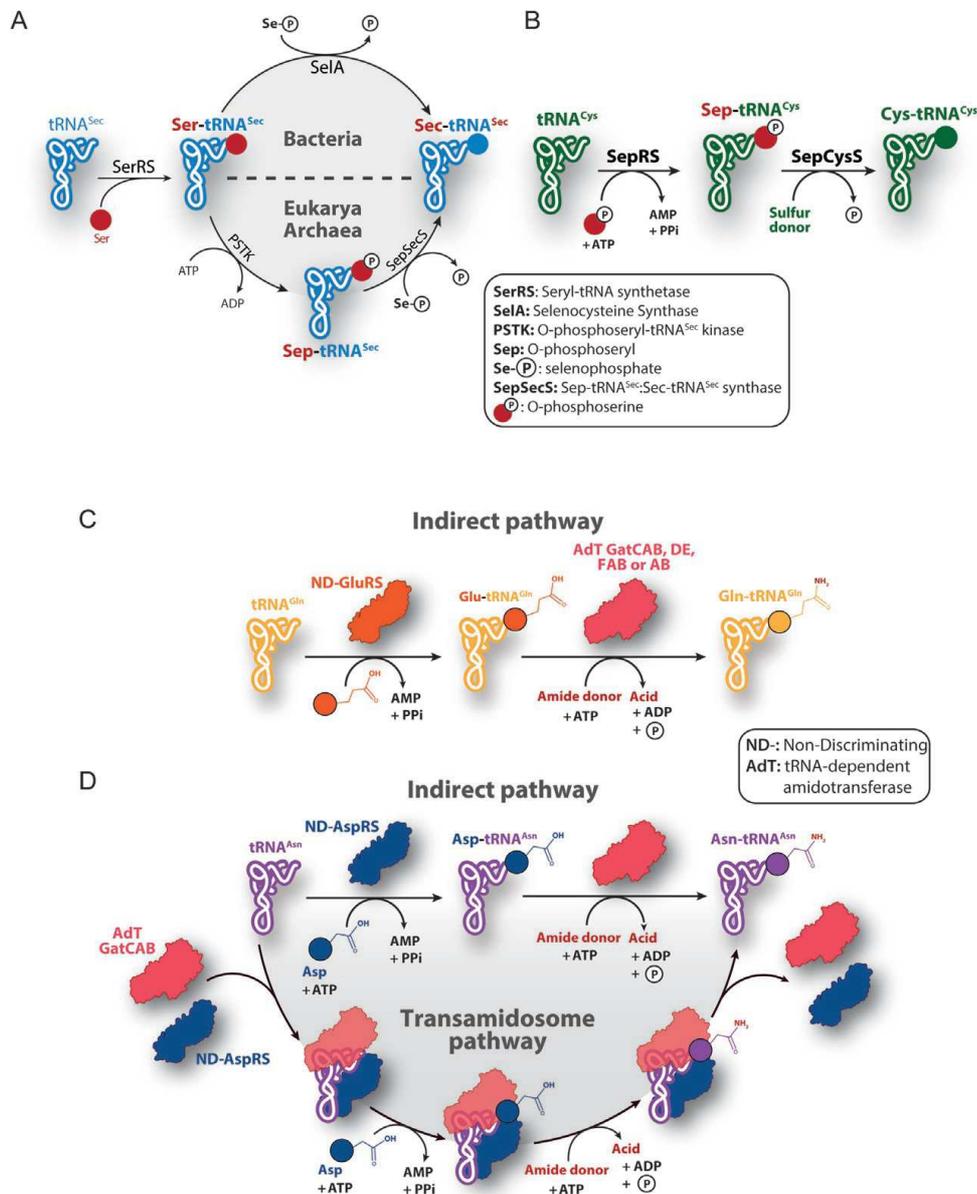
Fig. 2 Non-canonical pathways of aa-tRNA biosynthesis. (A): Biosynthesis of Sec-tRNA^{Sec} using a post-charging conversion of Sec by a two-step pathway in bacteria (upper panel) and a three-step pathway in eukaryotes and archaea (lower panel); (B) Two-step biosynthesis of Cys-tRNA^{Cys} in archaea lacking CysRS. (C) Two-step transamidation pathway of Gln-tRNA^{Gln} synthesis used by bacteria, archaea, mitochondria and chloroplasts. GatCAB AdT: Glutamyl-tRNA^{Gln} amidotransferase used by bacteria, most eukaryotic organelles; GatDE: Glutamyl-tRNA^{Gln} amidotransferase used by archaea; GatFAB AdT: Glutamyl-tRNA^{Gln} amidotransferase of yeast mitochondria; GatAB: Glutamyl-tRNA^{Gln} amidotransferase used by apicoplast. (D) Two-step transamidation pathway or transamidosome-mediated route of Asn-tRNA^{Asn} synthesis used by bacteria, archaea deprived of AsnRS or of asparagine synthetase. The amide donor is either Gln or Asn and is deaminated to form Glu or Asp (acid) during transamidation, respectively. *Panel B: adapted from J. Yuan, S. Palioura, J.C. Salazar, D. Su, P. O'Donoghue, M.J. Hohn, A.M. Cardoso, W.B. Whitman, D. Söll, RNA-dependent conversion of phosphoserine forms selenocysteine in eukaryotes and archaea, Proc. Natl. Acad. Sci. U. S. A. 103 (2006) 18923–18927.*

2.1.1 The 21st proteinogenic aa: Selenocysteine (Sec)

Selenocysteine incorporation has been discovered in 1986 both in mammals and bacteria [15,16]. Its incorporation into proteins depends on an in-frame UGA "opal" STOP codon, which is read through by ribosomes. Sec residues are found in the active sites of selenoproteins (25 genes in mammals, but none in fungi and higher plants). This non-ubiquitous proteinogenic aa has a higher nucleophilic reactivity than cysteine (Cys), thus facilitating selenoproteins in performing enhanced redox reactions and maintain redox homeostasis [17]. Sec is generated *via* two consecutive steps [18] (Fig. 2A) by tRNA-dependent modification of a Ser precursor attached to the opal suppressor tRNA^{Sec} [19]. Indeed, because tRNA^{Sec} and tRNA^{Ser} share the same tRNA identity elements, tRNA^{Sec} can be recognized by the seryl-tRNA synthetase (SerRS) and charged with Ser to form Ser-tRNA^{Sec} [20]. However, an additional base pair in the acceptor stem of tRNA^{Sec}—in comparison to all known tRNAs—prevents the recognition of the misacylated Ser-tRNA^{Sec} by the elongation factor thermo-unstable (EF-Tu), thus precluding misincorporation of Ser into proteins [21–23]. After serylation of tRNA^{Sec} by SerRS, the Ser residue is either (i) directly selenylated by SelA to form Sec-tRNA^{Sec} in bacteria [19], or (ii) phosphorylated by *O*-phosphoseryl-tRNA-kinase (PSTK) to form *O*-phosphoseryl-tRNA^{Sec} (Sep-tRNA^{Sec}), the latter activated aa being subsequently selenylated in a tRNA-dependent manner by the SepSecS enzyme in eukaryotes and archaea [24]. Both SelA and SepSecS are pyridoxal-5′-phosphate (PLP)–dependent enzymes and use selenophosphate as a selenium donor (Fig. 2A). Selenocysteinyl-tRNA^{Sec} is then transported to translating ribosomes by specific elongation factors: SelB in bacteria [25] and the eEFSec•SBP2 complex in eukaryotes [26,27]. Finally, incorporation of Sec requires pausing of the ribosomes at UGA "Sec" codons, which requires a *cis*-acting stem loop structure, called SElenoCysteine Insertion Sequence or SECIS, located downstream of the "Sec" UGA codons of selenoprotein mRNAs. Note that SECIS elements differ in length and structure between bacteria, archaea and eukaryotes [28–32].

2.1.2 The 22nd proteinogenic aa: Pyrrolysine (Pyl)

Pyrrolysine is a modified lysine with a 4-methylpyrroline-5-carboxylate group linked by an amide to the ε-amino group (ε-N). It was first discovered in 2002 in methanogenic archaea and later in several bacteria [33,34]. In methanogenic archaea, all genes encoding methylamine methyltransferases

(methane-generating enzymes) contain an in-frame UAG "amber" STOP codon that is translated into a pyrrolysyl residue. As for Sec, Pyl active site residues appear to be crucial for the activity of enzymes involved in methanogenesis [35]. Pyrrolysyl-tRNA^{Pyl} is synthesized by direct pyrrolysylation of an amber-suppressor tRNA^{Pyl} by the class IIc PylRS [36]. Pyl incorporation has become the first known example to date of direct aminoacylation of a tRNA with a non-standard proteinogenic aa. The structure of tRNA^{Pyl} differs from the classical tRNA structure because it displays for example a D- and TΨC-loop without their conserved representative residues [37]. Contrary to Sec-tRNA^{Sec} and its *trans*-specific factors, Pyl-tRNA^{Pyl} is transported to the A-site of the ribosome by the standard elongation factor EF-Tu [38]. In addition, in some cases the mRNA sequence context seems important for Pyl insertion, and a specific stem loop called PYrroLysyl Insertion Sequence or PYLIS has sometimes, but not always, been found directly next to the "amber" codon on mRNAs encoding for methylamine methyltransferases [39].

2.2 tRNA-dependent pathways of amino acid biosynthesis

Selenocysteine is not the only aa that requires multiple steps to be incorporated into proteins. In numerous organisms, analogous indirect pathways are also needed for the incorporation of standard aa into proteins. In those cases, the biosynthesis of the proteinogenic aa is tRNA-dependent and linked to the production of the corresponding cognate aa-tRNA.

For the majority of eukaryotes and very few bacteria, the 20 different types of standard aa-tRNAs are produced by a full and unique set of 20 different aaRSs. But in the majority of bacteria and all archaea, one or more aaRS genes is missing, suggesting that the aminoacylation of corresponding orphan tRNAs is performed by a non-canonical route. The organism that best illustrates missing aaRSs is the hyperthermophilic methanogenic archaea *Methanocaldococcus jannaschii*, whose genome was sequenced in 1996 and that lacks four expected aaRS genes: LysRS, CysRS, AsnRS and GlnRS [40]. It was shown in this archaeon that the lack of CysRS is compensated by a tRNA^{Cys}-dependent two-step pathway (Fig. 2B) similar to that of Sec-tRNA^{Sec} formation in bacteria. In this pathway, tRNA^{Cys} is first mischarged by a dedicated *O*-phosphoseryl-tRNA synthetase (SepRS) with Sep, before tRNA-dependent conversion of the Sep moiety into Cys by the PLP-dependent SepCysS enzyme that ressembles SepSecS [41].

AsnRS and especially GlnRS are also often missing in prokaryotes and in organelles [42]. All archaea and the majority of bacteria lack GlnRS, whereas AsnRS can be found in most bacteria and half of archaea. While all organelles do possess a dedicated AsnRS, an organellar GlnRS is never found, except in some protozoans [43]. When AsnRS and/or GlnRS is/are absent, direct tRNA charging with the two respective cognate aa—Asn and Gln—is compensated for by an indirect route called the transamidation pathway. It is a two-step pathway in which the metabolic precursors of Gln and Asn, respectively, Glu and Asp, are first attached onto the non-cognate tRNA^{Gln} and tRNA^{Asn} by ND-GluRS or ND-AspRS [10,44] (Fig. 2C). Once released from ND-aaRSs, the mischarged Glu- or Asp-tRNAs are transferred to tRNA-dependent amidotransferases (AdTs). AdTs first ATP-dependently activate the γ- or β-carboxyl group of the misacyled Glu- and Asp-tRNAs by phosphorylation, the activated side chains then being amidated, using an amido group donor, to form Gln-tRNA^{Gln} or Asn-tRNA^{Asn} [45]. All AdTs, regardless of their origins or types, usually use the γ-amide of a free Gln, with the release of Glu, to produce this amido group [46–48]. AdTs are complexes that always possess an amidase subunit to generate the amido group necessary for the amidation reaction, and a subunit that binds the misacylated aa-tRNA substrates and catalyzes the activation of the carboxyl group of the mischarged aa before amidation. The amido donor travels from one subunit to the other, enabling amidation of the misacylated tRNA, a reaction termed "transamidation." Accessory proteins also participate in the formation of the complex.

To date, four types of tRNA-dependent AdTs are known: the hetero-trimeric GatCAB and GatFAB and the heterodimeric GatDE and GatAB ("Gat" for glutamyl-tRNA^{Gln} amidotransferase). The GatCAB AdT (A: amidase, B: aa-tRNA binding, COOH activation and transamidation subunit, C: accessory chaperone) usually is a bispecific Glu/Asp-AdT that can generate Gln-tRNA^{Gln} and Asn-tRNA^{Asn}, such as in bacteria. In archaea GatCAB is a specific Asp-AdT [49]. The heterodimeric GatDE (E: amidase subunit, D: aa-tRNA binding, COOH activation and trans-amidation subunit) is an archaea-specific Glu-AdT [48] that only produces Gln-tRNA^{Gln}. In most eukaryotic organelles, such as mitochondria and chloroplasts, an organellar AdT is also required, and it is of the GatCAB-type. It functions as a Glu-AdT that synthesizes organellar Gln-tRNA^{Gln} *in vivo* [50,51]. Note that in plants, there is only a single organellar GatCAB AdT that is dually-targeted to mitochondria and chloroplasts. Of note, in mitochondria of the yeast *Saccharomyces cerevisiae*, formation of

the mitochondrial Gln-tRNA^{Gln} pool relies on a heterotrimeric GatFAB that differs from the homologous bacterial GatCAB by the presence of a fungi-specific GatF subunit that replaces structurally GatC. Recently, a heterodimeric GatAB AdT lacking a "C" subunit was found in the apicoplast of the human parasite *Plasmodium falciparum* to function as a Glu-AdT [52].

All organisms using an AdT to generate Gln-tRNA^{Gln} or Asn-tRNA^{Asn} or both also possess ND-GluRS and/or ND-AspRS that, in addition to regular Glu-tRNA^{Glu} and Asp-tRNA^{Asp}, respectively, provide the misacylated Glu-tRNA^{Gln} and Asp-tRNA^{Asn} [10,44]. Some organisms such as *Helicobacter pylori*, possess in addition to regular "discriminating" GluRS, a dedicated supernumerary tRNA^{Gln}-mischarging GluRS2 [11,53]. In organelles, the mitochondrial GluRS usually is the ND-GluRS that participates in the organellar transamidation pathway [51]. In plants, there is a dual-targeted ND-GluRS that participates in the chloroplast and mitochondrial transamidation pathways [50]. The yeast *S. cerevisiae* is however an exception, because it is the cytosolic GluRS that canonically produces the cytoplasmic Glu-tRNA^{Glu} pool which is imported into mitochondria, to specifically mischarge the mitochondrial tRNA^{Gln}. The *bona fide* mitochondrial GluRS only aminoacylates the mitochondrial tRNA^{Glu} [43,54].

Organisms that use the transamidation pathway to generate amidated aa-tRNAs have an adapted EF-Tu that has been shown to lack significant binding capacity for the misacylated Glu-tRNA^{Gln} and Asp-tRNA^{Asn} intermediates, thereby preventing misincorporation of Glu and Asp at Gln and Asn codons [13,54,55]. Another way to generate amidated aa-tRNAs without challenging the genetic code with the mischarged intermediates is the formation of so-called transamidosomes. These complexes are formed by binding of the ND-aaRS to the AdT in a tRNA-dependent manner. In the transamidosomes that have been described to date, the misacylated Asp-tRNA^{Asn} or Glu-tRNA^{Gln} generated by the complexed ND-AspRS or –GluRS are channeled to the AdT active site, without being released, and transamidated to release only the final amidated forms from the particle [56]. Bacterial (ND-AspRS•tRNA^{Asn}•GatCAB, Fig. 2D) and archaeal (ND-GluRS•tRNA^{Gln}•GatDE; [55]) transamidosomes have been characterized. The stoichiometry of their components (tRNA, ND-aaRS and AdT) varies as well as their stability and catalytic mechanism. The transamidosome of *Thermus thermophilus* is composed of 2 dimeric ND-AspRSs (four enzymes), four tRNA^{Asn} and 2 GatCAB AdTs (two enzymes); 2 tRNA^{Asn} molecules are substrates and two others are scaffolding

components that ensure the stability of the ribonucleoprotein particle throughout catalysis [14]. In *H. pylori*, only transient Glu– or Asp–transamidosomes have been identified [57,58].

While these four indirect pathways are compensatory routes for the synthesis of a given aa–tRNA when the cognate aaRS is absent, for two of them, Sec and Asn, they are (Sec) or can sometimes be (Asn) the sole metabolic pathway for the synthesis of the aa, which is therefore strictly tRNA–dependent [44].
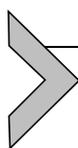
3. aa-tRNA-dependent aminoacylation of lipids and cell-wall synthesis

3.1 Multiple peptide resistance factor (MprF)

In the early 60s, Macfarlane reported the presence of *O*–L–lysyl and *O*–L–alanyl esters of phosphatidylglycerol (PG) in *Clostridium welchii* and in *Staphylococcus aureus* [59]. However, that the enzymatic synthesis of lysyl–PG in *S. aureus* involves the transfer of the lysyl moiety from Lys-tRNA^{Lys} onto PG was not demonstrated until 1966 [9]. Over the last decades, a large number of studies detected aminoacylated lipids in several bacterial species, and showed that Lys-tRNA^{Lys} and Ala-tRNA^{Ala} are usu–ally the aa donors for lipid aminoacylation and that PG, diacylglycerol or cardiolipin are the aa acceptors. Arg–PG and could also be detected but to a lesser extent [60]. In 2001, Peschel et al. demonstrated in *S. aureus* that the *mprF* gene encodes the lysyl–phosphatydyl glycerol synthase (LysPGS) responsible for LysPG synthesis [61]. They also showed that the cytoplasmic domain of LysPGS is responsible for the transfer of L–Lys from Lys-tRNA^{Lys} onto PG at the inner leaflet of the plasma membrane, whereas the N–terminal integral membrane domain flips the newly synthesized LysPG to the outer membrane leaflet [62]. The addition of positively– charged or neutral aa to PG by aminoacyl–phosphatidyl glycerol synthases (aaPGSs) reverses or neutralizes the net negative charge of the cell envelope [63], thereby decreasing the susceptibility of bacteria to positively–charged antimicrobial agents. Furthermore, aaPGS–dependent membrane remo–deling participates in the adaptation of bacteria to environmental changes (pH, osmolarity, temperature), increases immune escape [64,65] and enhances virulence of *S. aureus* and *Listeria monocytogenes* upon infection of epithelial cells and macrophages in mice [66,67].

Some aaPGSs are specific for a single aa–tRNA (*e.g.,* Lys– or Ala–tRNA), and others exhibit broader substrate specificity and can utilize up to three

different aa–tRNAs as aa donors (*e.g.,* Lys-, Ala- or Arg-tRNA) [68,69]. It has been shown that the acceptor-stem of the tRNA and in particular its fifth base pair and the $C\alpha$ of the corresponding aa are essential elements for the recognition of Ala-tRNA^{Ala} by the AlaPGS [70,71]. Structural analysis showed that the catalytic domain of AlaPGS from *Pseudomonas aeruginosa* and LysPGS from *Bacillus licheniformis* harbor a so-called dupli-GNAT (GCN5 *N*-acetyltransferase) domain, where the two GNATs are separated by a positively-charged alpha helix [72]. Such similar structures have also been described for other aminoacyl-tRNA transferases (AAT), including the Fem and L/F transferases described below. Site-directed mutagenesis based on the structures of aaPGSs, demonstrated that this positively- charged helix is essential for aa-tRNA recruitment. However, it is still not understood how bacteria regulate the balance between the usage of the aa-tRNA for protein synthesis *versus* lipid aminoacylation. Interestingly, *Mycobacterium* spp. encode a LysPGS (LysX) that is fused directly to a C-terminal lysyl-tRNA synthetase (LysRS) that is essential for the LysPG synthesis activity. This suggests that, in *Mycobacterium* spp., a dedicated pool of Lys-tRNA^{Lys} is synthesized and used by LysPGS, to produce LysPGs and that this pool escapes protein synthesis [73].

4. FemXAB

The peptidoglycan sacculus (murein) is a unique and essential structural element of bacterial cell walls found outside of the plasma membrane. It contributes to the maintenance of cell shape to preserve the cell integrity, and serves as a scaffold for the anchoring of other cell envelope components such as proteins and teichoic acids in Gram-positive bacteria.

Peptidoglycan synthesis is achieved by a succession of enzymatic events, that start with the formation of the well-known lipid II. This lipid harbors a so-called stem-peptide composed of the L-Ala$_1$-D-Glu$_2$-X$_3$-D-Ala$_4$-D-Ala$_5$ pentapeptide where X$_3$ is variable among species (L-Lys, δ-L-ornithine or ω-L, L-diaminopimelic acid) (Fig. 3A). At this stage, Fem transferases, which are non-ribosomal peptidyl transferases, use aa-tRNA as aa donors to form an "interpeptide bridge" that, in a later step, serves to cross-link the X$_3$ of the newly-synthesized peptidoglycan subunit (Lipid II released from its undecaprenyl-diphosphate) to the D-Ala$_4$ of an adjacent peptidoglycan stem-peptide [74,75]. The formation of the stem-peptide is tRNA-independent, whereas Fem ligase-mediated formation of the interpeptide bridge was shown to be tRNA-dependent.
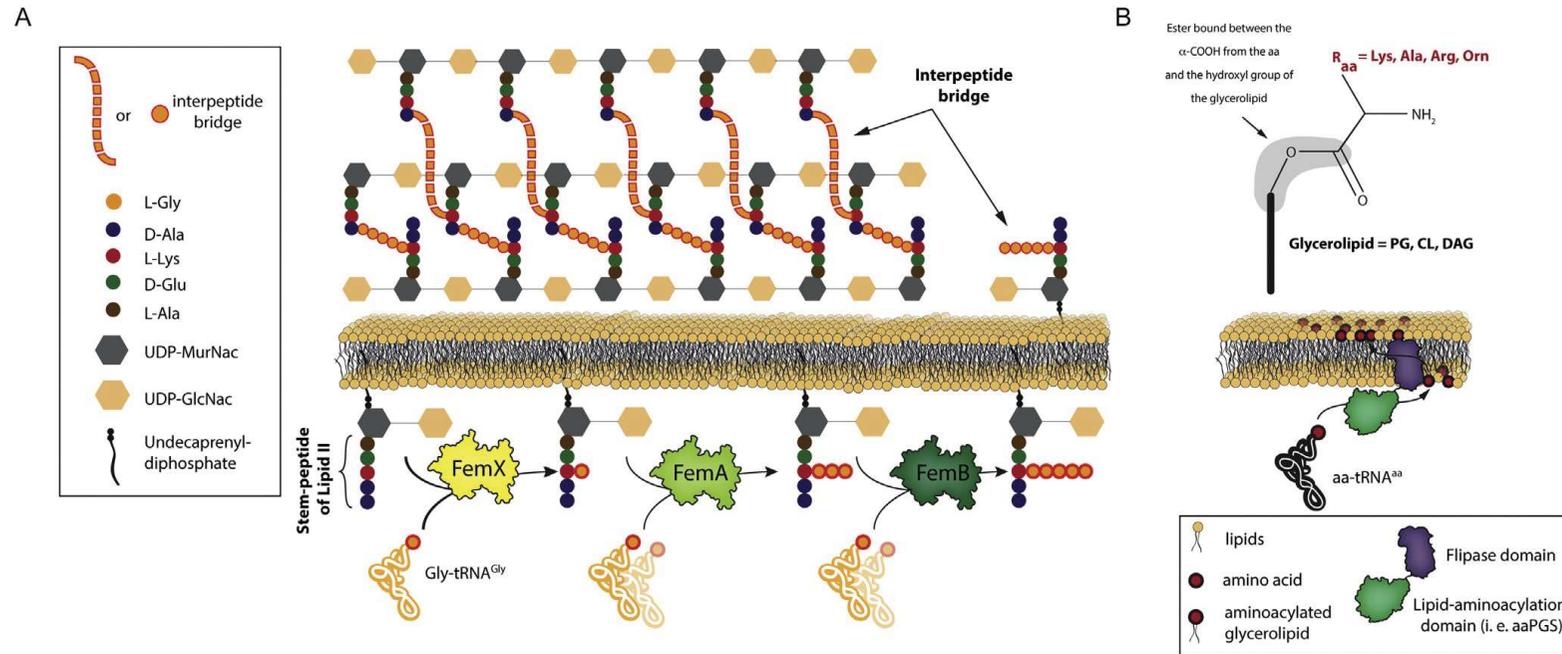
Fig. 3 Aminoacyl-tRNA-dependent cell wall remodeling in prokaryotes. (A) In *S. aureus*, the stem peptide composed of L-Ala$_1$-D-Glu$_2$-Lys$_3$-D-Ala$_4$-D-Ala$_5$ is added onto Lipid I to form the well-characterized Lipid II. Aminoacyl-tRNA transferases (ATT) belonging to the Fem ligases family then successively add a variable number of aa to form the interpeptide bridge. For example, in *S. aureus* FemX adds a single glycine, FemA adds Gly2 and Gly3 and finally, FemB adds Gly4 and Gly5 onto the L-Lys of the stem-peptide. The resulting peptidoglycan subunit is then flipped out to the outer cytoplasmic-membrane leaflet, and the link to the growing peptidoglycan saccule is made by PBP tran-speptidases. MurNac: N-Acetylmuramic acid, GlcNac: N-Acetylglucosamine. (B) MprF and MprF-like proteins contain a C-terminal ATT domain (green) that reroutes aa-tRNA^{aa} from the translational machinery and transfers the aa moiety onto glycerolipids, and a N-terminal flipase domain (purple) that exposes the aminoacylated glycerolipid to the outer membrane leaflet. As schematized in the upper panel, different aa/ lipid combinations were documented in prokaryotes as reviewed by Slavetinsky et al. [60]. PG: phosphatidylglycerol, DAG: diacylglycerol, CL: cardiolipin, R$_{aa}$: lateral chain of the indicated aa.

In *S. aureus*, 3 Fem ligases are required. FemX adds the first glycine residue (Gly_1) onto the stem-peptide at the ε-NH_2 group of L-Lys_3 [76,77], while FemA and FemB are essential for the addition of $Gly_{2,3}$ and $Gly_{4,5}$, respectively. These proteins are highly specific with respect to the position of the Gly residues that they attach [78]. Among the five tRNA^{Gly} isoacceptors encoded by *S. aureus*, three of them have a weak binding capacity to EF-Tu, due to the replacement of G_{49}-U_{65} and G_{51}-C_{63} by A_{49}-U_{65} and A_{51}-U_{63} base pairs in the T-loop [79,80]. Furthermore, Rohrer et al. showed that the three tRNA^{Gly} capable of escaping the translational machinery have G_{18} and G_{19} replaced by UU or CU [81]. The Fem factors are known to be essential for methicillin resistance, and are found in both resistant and susceptible *S. aureus* strains. The phenotypes of the FemAB null mutants of *S. aureus* showed a reduction of cell wall Gly content and strong morphological aberrations during cell division and separation [76]. The inactivation of the *femAB* operon reduces the interpeptide to a monoglycine, inducing a poorly crosslinked peptidoglycan. Decreased growth rate and hypersusceptibility to antibiotics such as methicillin were observed in *femAB* deleted strains, making FemAB a potential target to restore β-lactam susceptibility in methicillin-resistant *S. aureus* (MRSA) [82].

Staphylococcus simulans, *S. epidermidis* and *S. capitis* incorporate a variable ratio of L-Ser/Gly residues (but also L-Ala for *S. epidermidis*) into the interpeptide bridges to escape pentaglycine endopeptidase-mediated degradation. To our knowledge, tRNA^{Ser} modifications are not involved in the distribution of Ser-tRNA^{Ser} between peptidoglycan cross-linking and translation. Thus, bacteria may adapt the ratio of Ser-tRNA^{Ser} used for each mechanism according to environmental conditions. *S. epidermis* encodes at least two tRNA^{Gly} isoacceptors employed exclusively for interpeptide-chain formation [83]. Both contain CC or UU instead of the universal G_{18} and G_{19} di-nucleotide. Furthermore, the supplementary C_{32}-G_{38} base pair in the anticodon loop and, to a lesser extent, the impaired U_{10}-U_{25} base pairs as well as the weak post-transcriptional modification ratio in the D-loop are also considered as crucial to determine the fate of Gly-tRNA^{Gly} isoacceptors.

In *S. pneumoniae*, MurM (homologue of the *S. aureus* FemA) adds L-Ser or L-Ala as the first residue to the L-Lys of the stem peptide [78,84], and MurN then adds L-Ala to form an interpeptide chain composed only of two residues [84].

Finally, *Weissella viridescens* harbors either a L-Ala-L-Ser or a L-Ala-L-Ser-L-Ala interpeptide chain [85]. Villet et al. showed that the C_{71} and C_{72}

from the tRNA^{Ala} are critical nucleotides for recognition by FemX, whereas the G_3–U_{70}, base pair considered as a strong identity determinant for recognition by AlaRS is dispensable [86]. Because MurM and FemX of *W. viridescens* recognize only two aa-tRNAs [87,88], it has been suggested that these two proteins may be involved in the complex discrimination between protein and peptidoglycan synthesis [89].

In summary, Gly-tRNA^{Gly}, Ala-tRNA^{Ala}, Ser-tRNA^{Ser} but also Thr-tRNA^{Thr} participate in peptidoglycan interpeptide chain formation. For a more detailed review of the interpeptide composition across bacterial species, refer to reports of Dare & Ibba or Schleifer & Kandler [83,90].

5. aa-tRNA-dependent synthesis of hemes

Only a small subset of the aa produced by the cell are used in protein synthesis, and we have seen that from this small pool some can be deviated to build molecules other than proteins. There are also several other pathways that require non-proteogenic aa and among them, the synthesis of heme necessitates δ-aminolevulinic acid (ALA), a pathway that is tRNA-dependent. ALA can be synthesized either from free glycine and succinyl-CoA (eukaryotes) or glutamate (bacteria and green plants), when the latter is bound to its cognate tRNA^{Glu} (reviewed in [91], Fig. 4).

ALA is the first molecule in the tetrapyrrole synthesis pathway that leads to heme biosynthesis in mammals and chlorophyll in plants. ALA biogenesis in plants and bacteria has been studied for more than four decades, and employs a simple three-step pathway. First, Glu is charged onto tRNA^{Glu} by GluRS [92–94]. Second, tRNA^{Glu}-bound Glu is reduced to glutamate
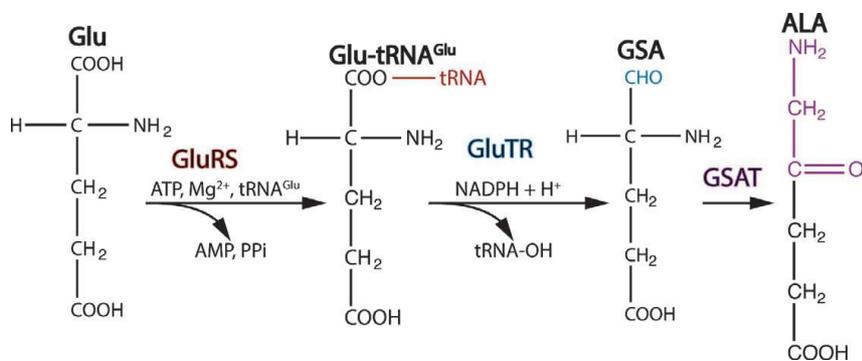

Fig. 4 C5 pathway of ALA formation. Glutamate (Glu) is attached directly onto tRNA^{Glu} by GluRS. Glu is then reduced to glutamate-1 semi-aldehyde (GSA) by glutamyl-tRNA reductase (GluTR) and further converted by glutamate aminomutase (GSAT) to δ-aminolevulinic acid (ALA).

semi–aldehyde (GSA) and detached from tRNA^{Glu} by glutamyl–tRNA reductase (GluTR) [95,96]. Finally, GSA is converted to the final product ALA by GSA aminomutase (GSAT) [97].

The finding that Glu is used to produce ALA in green plants [98,99] preceded the discovery that tRNA^{Glu} is required for ALA production [92–94]. Thus, Glu-tRNA^{Glu} formation is an absolute intermediate in the GSA formation by GluTR, an enzyme that has been shown to form a complex with GluRS [100] and together, both proteins have strict requirements for tRNA^{Glu} [101,102].

In bacteria, GluTR is encoded by the *hemA* gene that is part of the *hemAXCDBL* operon in which *hemX* codes for an integral membrane protein capable of negatively affecting the cellular concentration of *hemA* [103]. GluTR activity is rate-limiting in ALA formation [104] and in plants, it represents an ideal target for designing herbicides [105]. Its activity has been shown to be regulated by acting on the protein stability that is increased in heme limiting conditions in *S. typhimurium* [106]. Later, FLU, another negative regulator of GluTR was identified. Flu is a membrane-bound protein involved in chlorophyll biosynthesis that interacts directly with GluTR but not with GSAT [107,108]. It must be noted that although the levels of GluTR and GSAT control ALA production, they do not control directly chlorophyll synthesis in *Chlamydomonas reinhardtii*. A complex between GSAT and GluTR has been identified and proposed to protect the highly- reactive GSA intermediate [109].

ALA is the universal precursor of tetrapyrroles like hemes, and the latter have been shown to downregulate not only the activity of GluTR but also of GluRS, which is more surprising [110]. In addition, hemes are also capable of inhibiting aminoacylation activity of a Zn^{2+}–deprived form of human tryptophanyl-tRNA synthetase [111]. Moreover, holocytochrome *c* (*e.g.,* heme bound) can interact with tRNA, and this interaction was shown to mediate caspase-mediated apoptosis [112].

An essential GluTR–interacting protein named GluTRB that is localized in the thylakoid membrane, participates in the sub–compartmentalization of GluTR, to separate ALA pools in order to balance production of heme and chlorophyll [113]. The interaction of GluTRBP with GluTR stimulates its activity, but the latter is still inhibited in a heme–dependent concentration [114]. Binding of GluTRBP to GluTR also prevents FLU from inhibiting GluTR, but a ternary complex consisting of GluTR, GluTRBP and FLU can be formed, suggesting a biological role for the ternary complex in the regulation of the plant GluTR [115]. The complexity of this regulation

of GluTR expression/activity is reinforced by the finding that GluTR can be degraded from its N-terminus by the Clp protease, but not when protected by GluTRBP [116].

ALA utilization by bacteria leads to heme, an essential cofactor for *S. aureus* growth and colonization that becomes toxic at high concentrations, thereby underlining the necessity for these organisms to control tightly heme homeostasis [117]. In plants, subplastidial allocation of GluTR in the stroma and in membrane fractions reveals that when membrane-bound, GluTR is less active, and this is the result of the concerted actions of GluTR interacting proteins (FLU, GluTRBP, Clp protease and cpSRP43) [118,119]. Finally, in higher plants there are two isoforms for GluTR: GluTR1 that is expressed predominantly in green tissue, and GluTR2 that is expressed constitutively in all organs. It was recently shown that heme binding to GluTRBP inhibits its interaction with GluTR, thereby making it accessible to Clp protease, which participates in GluTR regulation [120].

Overall, the utilization of Glu-tRNA^{Glu} outside translation represents an intriguing example of how various metabolic pathways are interconnected. Glu-tRNA^{Glu} utilization for ALA production controls heme and chlorophyll biosynthesis, two molecules that are crucial for other cellular events that contribute to the life cycle of various organisms, and whose production seems to be subjected to tight and complex control.
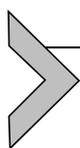
6. aa-tRNA-dependent formation of antibiotics

Peptide-based antibiotics can, at least in part, be synthesized tRNA-dependently, and are an important class of molecules because they provide organisms with defenses to fight against invading microbes, or to help them survive in a given ecological niche [89,121]. There is a group of antibiotics whose composition is based on peptides. There are two ways of synthesizing peptide-based antibiotics that both require tRNA: ribosomally- or non-ribosomally-synthesized peptidic antibiotics [122]. Those that are ribosomally-synthesized include defensins (30–40 aa in length; disrupt membrane integrity) that are a large class of Cys–rich peptide antibiotics whose Cys residues are regionally-specifically oxidized to stabilize the molecule and provide protease resistance. Similarly, lantibiotics are low molecular weight lanthionine-containing cyclic peptides that, like defensins, perturb membrane integrity. This class of molecules belongs to the superfamily of RiPP (ribosomally synthesized peptides that undergo extensive post-translational modifications). They are synthesized as precursors that

consist of an N–terminal leader peptide fused to a C–terminal core peptide containing modifications. Interestingly for some of them, a Glu-tRNA^{Glu} is used by a dehydratase to modify aa residues of the ribosomally-made peptide parts (reviewed in [123]). Aromatic heterocyclic peptide scaffolds derived from Cys, Ser and Thr residues [124] are another large family of ribosomally-derived antibiotics like microcin B17, patellamides and streptolysin S. It is noteworthy that microcins have a broad diversity of chemical structures and modifications, and are widely used as antitumoral and/or antimicrobial drugs [125]. The synthesis of these antibiotic compounds is rather complex and there are tens of genes that are required, and tRNAs are either involved as regulators of this process [122] or as carrier molecules for additional modifications with aa. tRNA-based regulation of antibiotic production is, for example, used by *Streptomyces coelicolor*. In this filamentous bacterium there is a single gene (*bldA*) that encodes the only tRNA^{Leu} capable of decoding the UUA rare Leu codon. The expression of this specific tRNA^{Leu} is very low in fresh cultures, but increases to reach its maximum as cultures get older. The tRNA^{Leu} expression pattern correlates with morphological differentiation and changes in antibiotic production [126]. This suggests a means of limiting ribosomal-mediated antibiotic synthesis in the host to physiologically appropriate circumstances by modulating tRNA availability. A similar mode of regulation has also been proposed for biofilm production, in which Hha proteins decrease biofilm production by repressing transcription of tRNAs decoding rare codons (argU and proL) normally involved in fimbriae production [127].

The second tRNA-dependent mode of synthesizing peptide-based antibiotics are the non-ribosomal antibiotic pathways. These rely on a series of enzymatic reactions that involve at one step an aa-tRNA. For example, valanimycin production involves a gene cluster containing 14 genes in *Streptomyces viridifaciens*, in which the VlmA protein catalyzes the transfer of a seryl residue from Ser-tRNA^{Ser} to the hydroxyl group of isobutylhydroxylamine to produce the O-seryl-isobutylhydroxylamine ester [128]. An intriguing fact concerning valanimycin production is that the Ser-tRNA^{Ser} used in the reaction is produced by a dedicated SerRS, named VlmL, encoded by the *vlmL* gene [129]. Similarly, production of a streptothricin-related antibiotic requires an intermediate, in which an amino sugar is aminoacylated with Gly by a Fem-like enzyme in a tRNA-dependent manner [130]. Overall, the enzymes involved in these types of modifications belong to the class of the aa-tRNA-dependent transferases that were identified over 50 years ago [131–133].

Although aa-tRNAs can be used to remodel several compounds, they can also be substrates for the synthesis of cyclic dipeptide-based antibiotics. They were long thought to be products released prematurely from the ribosome until the discovery of cyclodipeptides synthases [134]. Cyclodipeptides are further subjected to various modifications until the final product is obtained [135]. A strategy employing various enzymes to modify a core scaffold to produce differential tailoring is often used in nature to generate structural diversity. Such small molecule diversity enables easy evolution of new biological functions, and allows fine-tuning of existing ones [135,136]. Cyclodipeptide synthases genes, are often clustered with tailoring enzyme genes, most likely to facilitate the overall regulation of the cyclodipeptide-based compound production (for a review see [123]). Cyclic dipeptides are an interesting class of molecules because they constitute a rather convincing alternative over conventional antibiotics, as exemplified in their role in preventing quorum sensing pathogenesis of uropathogens [137].

7. aa-tRNA-dependent degradation of proteins

In 1963, the participation of aa-tRNAs in protein degradation was first reported in prokaryotes, in which it was shown that ribosome-deprived extracts were still able to catalyze tRNA-dependent aminoacylation of proteins [138]. In eukaryotes, it was noted 23 years later that specific aa residues found in the N-terminus (N-t) of proteins could decrease dramatically the half-life of the corresponding protein in *S. cerevisiae* [139]. An enzymatic activity able to transfer the aa moiety of an aa-tRNA to the N-t of proteins leading to protein degradation was also identified in eukaryotes [140], and is presently termed the N-end rule pathway [141].

In bacteria, the N-end rule pathway includes three components: an aa-tRNA transferase responsible for the transfer of the aa moiety onto the protein that will be degraded, a N-recognin that binds the aminoacylated protein signaling it to the degradation machinery, the Clp protease complex. In eukaryotes, an additional preliminary step involving deamination of amide aa residues in N-t of the protein is catalyzed by a deamination enzyme. This enables the subsequent recognition by the aa-tRNA transferase, followed by signaling of the protein for degradation by the proteasome [142].

7.1 N-end rule pathway in prokaryotes

In 1963, Kaji et al. identified a protein fraction in *E. coli* that was able to transfer radioactively-labeled Leu onto proteins in the absence of ribosomes [138], thereby describing for the first time the activity of a leucyl-tRNA protein transferase. In 1973, Soffer demonstrated that Leu, Phe, and to a lower extent Met and Trp, can also be transferred onto the N-t residue of α–casein [143]. Later, it was discovered that the nature of the N-t residue of the targeted protein modulates the aa conjugation efficiency [139]. The residues onto which aa are efficiently transferred efficiently include the basic residues Arg, Gln, Lys and Pro, which were thereafter termed destabilizing residues. However, the mechanism linking addition of aa to the N-t of a protein to its degradation was not identified until Tobias et al. showed in 1991that a bacterial strain lacking the Clp ATP-dependent protease degraded much less efficiently a protein carrying destabilizing residues [144]. This proved that Leu (or Phe) conjugation mediates degradation by recruiting the Clp protease [144]. The gene coding the leucyl−/phenylalanyl-tRNA transferase (L/F transferase) was identified 2 years later [145]. Notably, this gene is located near the gene encoding ClpA, a component of the Clp protease complex, which participates in the N-end rule pathway. In 1995, the gene encoding the protein was cloned, overexpressed and purified, allowing the development of an *in vitro* assay that lead to the characterization of its catalytic mechanism [146]. Since then, the structure of the aa-tRNA transferase was determined in complex with an aa-tRNA analog [147], and the mechanism of the peptide bond formation between the N-t residue and the aa transferred by the aa-tRNA transferase has been elucidated [148].

In sum, protein aminoacylation in prokaryotes is mediated by L/F transferases that modify a residue in N-t (preferentially recognizing a basic residue), which enables the recognition of the protein by ClpS, which in turn signals delivery of the proteins to the Clp protease complex for degradation. Note that ClpS belongs to the family of N-recognins, which are proteins that bind to aminoacylated proteins and enable their delivery to the degradation machinery (Fig. 5C).

7.2 N-end rule pathway in eukaryotes

In *S. cerevisiae* and higher eukaryotes, proteins are not aminoacylated directly to induce their degradation (Fig. 5B). Instead, a first step of deamidation converts the amide aa Asn and Gln to Asp and Glu. These deamination
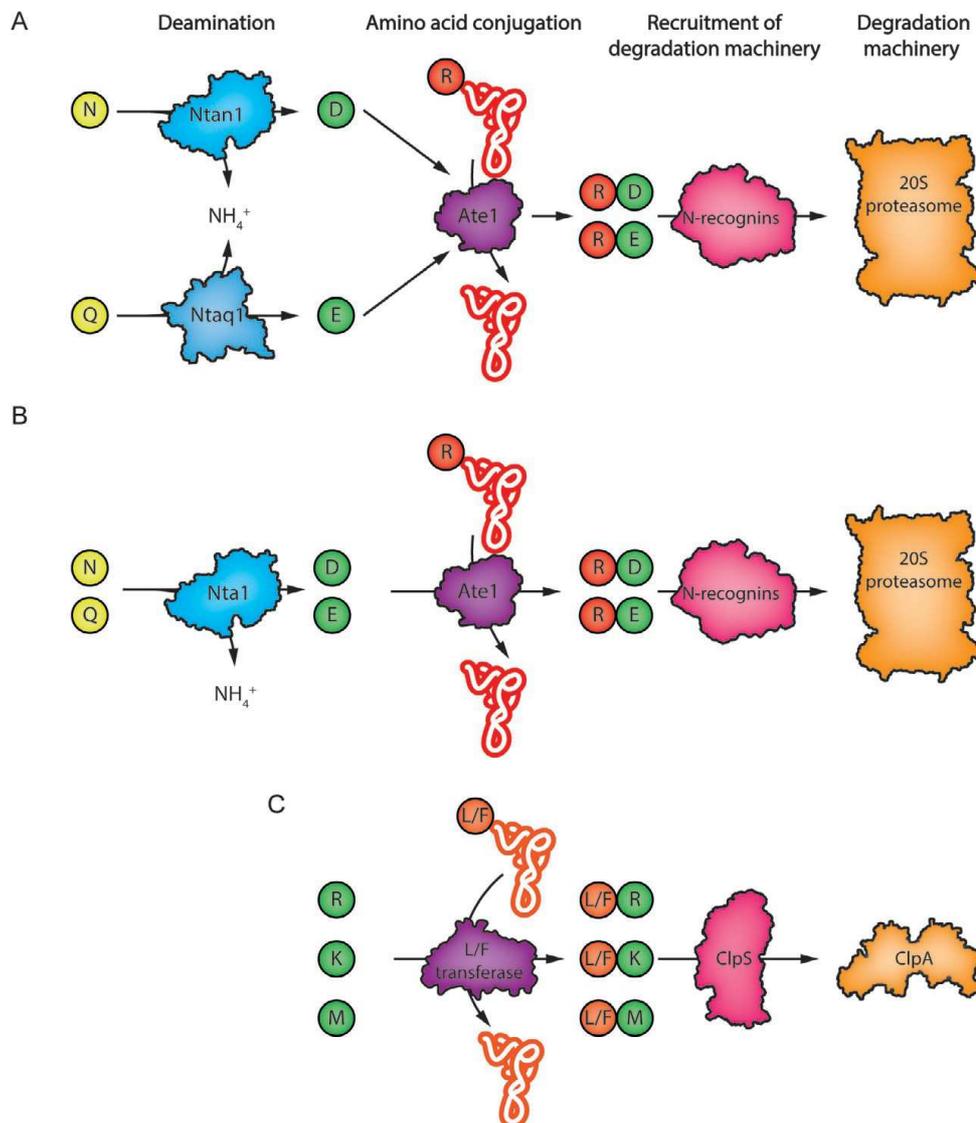
Fig. 5 Overview of the N-end rule pathway leading to protein degradation. (A) In mammals, protein degradation starts by the deamination of Gln (Q) or Asn (N) in first position at the N-ter of the protein. This leads to the arginylation of the N-ter of by Ate1, and subsequently to the binding of the protein by a N-recognin, which delivers it to the proteasome. (B) In fungi, the pathway is very similar, the sole difference being that the deamination step is performed by one enzyme both for Gln and Asn. (C) In prokaryotes there is no deamination step: Arg (R), Lys (K) and Met (M) are recognized by a leucyl-phenylalanine-tRNA transferase (L/F transferase) which transfers either Leu (L) or Phe (P) on the first amino acid in the N-ter of the protein. This so-called destabilizing residue is recognized by ClpS, which delivers the protein to the ClpA protease for degradation. *Panel C: adapted from T. Tasaki, S.M. Sriram, K.S. Park, Y.T. Kwon, The N-end rule pathway, Annu. Rev. Biochem. 81 (2012) 261–289.*

reactions are performed by Nta1 in fungi [149]. In mammals, deamination of Gln and Asn is performed by Ntaq1 and Ntan1, respectively [141,150] (Fig. 5A). After deamination, these residues can be aminoacylated by a unique arginyl-tRNA transferase, Ate1, both in *S. cerevisiae* and mammals [151,152]. Upon arginylation, the protein can be ubiquitinylated, a step mediated by a N-recognin. This leads finally to the degradation of the protein by the 26S proteasome.

This N-end rule mechanism is the only noncanonical pathway in which proteinogenic aa-tRNAs are used for protein degradation rather than for their synthesis. In this case, aa-tRNAs are diverted not only from their anabolic use, but become essential components of the protein catabolic pathway.
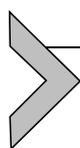
8. Concluding remarks

This chapter has been dedicated. Mainly to the fascinating diversity of the nontranslational mechanisms and processes that employ the aa moiety of an aa-tRNA. The first descriptions of these noncanonical usages of aa-tRNAs (Leu-tRNA^{Leu} to modify proteins and of Lys-tRNA^{Lys} in *O*-lysyl-phosphatidylglycerol synthesis) coincided with the characterization of the conventional aminoacylation reaction for protein synthesis [5–7,9]. Yet, these nontranslational usages are generally less well known than the primary historical role of aa-tRNA in protein synthesis, despite being equally essential for the cell. There is no doubt that new processes and functions will be unraveled in the future, and will enrich the existing functional repertoire of aa-tRNAs. As an example, the arginyltransferase Ate1, which transfers the arginyl moiety from Arg-tRNA^{Arg} to the N-terminus of proteins targeted for degradation by the N-end rule pathway, has recently also been shown in mammalian cells and in *Dictyostelium discoideum* to be implicated in the aminoacylation of internal residues of β-actin [153,154]. Interestingly the steady-state level of arginylated β-actin is relatively low but tends to increase in migratory cells, demonstrating that this post-translational aminoacylation is actively regulated in cells [153]. Arginylation of protein is not restricted to β-actin, because an increasing number of eukaryotic proteins appear to undergo Ate1-mediated arginylation of internal Asp and Glu residues; these arginylated proteins participate in myriad cellular processes ranging from embryogenesis, to cell migration and protein homeostasis [155].

There are however many unanswered issues when considering the non-translational processes that rely on the use of aa-tRNAs. One of the most important is how aa-tRNAs escape the translational machinery, and how cells achieve a balance between the use of the same aa-tRNA species for protein synthesis and/or for other cellular processes? In fact, though the various non-canonical usages of aa-tRNAs we describe in this chapter have been studied actively, it remains largely unknown how aa-tRNAs are diverted from their primary and canonical usage. In some cases, organisms have found a strategy that eliminates the competition between translation and nontranslational usages of an aa-tRNA by producing a dedicated pool of aa-tRNAs for a given non-canonical process. For example, *S. epidermis* encodes two tRNA^{Gly} isoacceptors dedicated exclusively to interpeptide-chain formation. Moreover, sometimes organisms have even acquired or evolved a supernumerary aaRS dedicated to the synthesis of specific aa-tRNAs (*e.g.,* LysRS fused to LysPGS in *Mycobacterium* for LysPG synthesis). Dedicating a given pool of tRNAs to nontranslational processes could also be accomplished by post-transcriptionally modifying tRNA nucleotides. Indeed, tRNAs undergo a series of post-transcriptional modifications, and some of them could potentially also serve to assign a given tRNA pool to a given nontranslational function. Finally, it was recently shown that, in eukaryotes, a single aaRSs can be localized in two or more subcellular compartments, and that these spatially-distinguished isoforms (called echoforms) can serve different roles, including the noncanonical roles that rely on the synthesis of a compartment–specific aa-tRNA [156].

Acknowledgments

References

[1] M. Ibba, D. Söll, Aminoacyl-tRNA synthesis, Annu. Rev. Biochem. 69 (2000) 617–650.

[2] N. Kresge, R.D. Simoni, R.L. Hill, The discovery of tRNA by Paul C .Zamecnik a soluble ribonucleic acid intermediate in protein synthesis, J. Biol. Chem. 280 (2005) 37–40.

[3]   M.B. Hoagland, E.B. Keller, P.C. Zamecnik, Enzymatic carboxyl activation of amino acids, J. Biol. Chem. 218 (1956) 345–358.

[4]   J.A. DeMoss, S.M. Genuth, G.D. Novelli, The enzymatic activation of amino acids via their acyl–adenylate derivatives, Proc. Natl. Acad. Sci. 42 (1956) 325–332.

[5]   P. Berg, Acyl adenylates; an enzymatic mechanism of acetate activation, J. Biol. Chem. 222 (1956) 991–1013.

[6]   P. Berg, Acyl adenylates; the interaction of adenosine triphosphate and L–methionine, J. Biol. Chem. 222 (1956) 1025–1034.

[7]   M.B. Hoagland, M.L. Stephenson, J.F. Scott, L.I. Hecht, P.C. Zamecnik, A soluble ribonucleic acid intermediate in protein synthesis, J. Biol. Chem. 231 (1958) 241–257.

[8]   M. Wilcox, M. Nirenberg, Transfer RNA as a cofactor coupling amino acid synthesis with that of protein, Proc. Natl. Acad. Sci. U. S. A. 61 (1968) 229–236.

[9]   W.J. Lennarz, J.A. Nesbitt, J. Reiss, The participation of sRNA in the enzymatic synthesis of O-L-lysyl phosphatidylgylcerol in *Staphylococcus aureus*, Proc. Natl. Acad. Sci. U. S. A. 55 (1966) 934–941.

[10] J. Lapointe, L. Duplain, M. Proulx, A single glutamyl–tRNA synthetase aminoacylates tRNA(Glu) and tRNA(Gln) in Bacillus subtilis and efficiently misacylates *Escherichia coli* tRNA1(Gln) in vitro, J. Bacteriol. 165 (1986) 88–93.

[11] H.D. Becker, H. Roy, L. Moulinier, M.H. Mazauric, G. Keith, D. Kern, Thermus thermophilus contains an eubacterial and an archaebacterial aspartyl–tRNA synthetase, Biochemistry 39 (2000) 3216–3230.

[12] J. Yuan, K. Sheppard, D. Söll, Amino acid modifications on tRNA, Acta Biochim. Biophys. Sin. Shanghai 40 (2008) 539–553.

[13] H. Roy, H.D. Becker, M.H. Mazauric, D. Kern, Structural elements defining elongation factor Tu mediated suppression of codon ambiguity, Nucleic Acids Res. 35 (2007) 3420–3430.

[14] M. Blaise, M. Bailly, M. Frechin, M.A. Behrens, F. Fischer, C.L.P. Oliveira, H.D. Becker, J.S. Pedersen, S. Thirup, D. Kern, Crystal structure of a transfer-ribonucleoprotein particle that promotes asparagine formation, EMBO J. 29 (2010) 3118–3129.

[15] I. Chambers, J. Frampton, P. Goldfarb, N. Affara, W. McBain, P.R. Harrison, The structure of the mouse glutathione peroxidase gene: the selenocysteine in the active site is encoded by the 'termination' codon, TGA, EMBO J. 5 (1986) 1221–1227.

[16] F. Zinoni, A. Birkmann, T.C. Stadtman, A. Bock, Nucleotide sequence and expression of the selenocysteine-containing polypeptide of formate dehydrogenase (formate-hydrogen-lyase-linked) from *Escherichia coli*, Proc. Natl. Acad. Sci. U. S. A. 83 (1986) 4650–4654.

[17] E.S.J. Arnér, Selenoproteins-what unique properties can arise with selenocysteine in place of cysteine? Exp. Cell Res. 316 (2010) 1296–1303.

[18] B.J. Lee, P.J. Worland, J.N. Davis, T.C. Stadtman, D.L. Hatfield, Identification of a selenocysteyl-tRNA(Ser) in mammalian cells that recognizes the nonsense codon, UGA, J. Biol. Chem. 264 (1989) 9724–9727.

[19] W. Leinfelder, E. Zehelein, M.A. Mandrand-Berthelot, A. Böck, Gene for a novel tRNA species that accepts L-serine and cotranslationally inserts selenocysteine, Nature 331 (1988) 723–725.

[20] K.M. Holman, A.K. Puppala, J.W. Lee, L.E.E. Hyun, M. Simonović, Insights into substrate promiscuity of human seryl–tRNA synthetase, RNA 23 (2017) 1685–1699.

[21] Y. Itoh, S. Chiba, S.I. Sekine, S. Yokoyama, Crystal structure of human selenocysteine tRNA, Nucleic Acids Res. 37 (2009) 6259–6268.

[22] C. Baron, E. Westhof, A. Böck, R. Giegé, Solution structure of selenocysteine-inserting tRNA(Sec) from *Escherichia coli*. Comparison with canonical tRNA(Ser), J. Mol. Biol. 231 (1993) 274–292.

[23] C. Sturchler, E. Westhof, P. Carbon, A. Krol, Unique secondary and tertiary structural features of the eucaryotic selenocysteine tRNA(Sec), Nucleic Acids Res. 21 (1993) 1073–1079.

[24] J. Yuan, S. Palioura, J.C. Salazar, D. Su, P. O'Donoghue, M.J. Hohn, A.M. Cardoso, W.B. Whitman, D. Söll, RNA-dependent conversion of phosphoserine forms selenocysteine in eukaryotes and archaea, Proc. Natl. Acad. Sci. U. S. A. 103 (2006) 18923–18927.

[25] K. Forchhammer, W. Leinfelder, A. Böck, Identification of a novel translation factor necessary for the incorporation of selenocysteine into protein, Nature 342 (1989) 453–456.

[26] P.R. Copeland, J.E. Fletcher, B.A. Carlson, D.L. Hatfield, D.M. Driscoll, A novel RNA binding protein, SBP2, is required for the translation of mammalian selenoprotein mRNAs, EMBO J. 19 (2000) 306–314.

[27] D. Fagegaltier, N. Hubert, K. Yamada, T. Mizutani, P. Carbon, A. Krol, Characterization of mSelB, a novel mammalian elongation factor for selenoprotein translation, EMBO J. 19 (2000) 4796–4805.

[28] F. Zinoni, J. Heider, A. Böck, Features of the formate dehydrogenase mRNA necessary for decoding of the UGA codon as selenocysteine, Proc. Natl. Acad. Sci. U. S. A. 87 (1990) 4660–4664.

[29] S. Halboth, A. Klein, Methanococcus voltae harbors four gene clusters potentially encoding two [NiFe] and two [NiFeSe] hydrogenases, each of the cofactor F420-reducing or F420-non-reducing types, Mol. Gen. Genet. 233 (1992) 217–224.

[30] M.J. Berry, L. Banu, Y. Chen, S.J. Mandel, J.D. Kieffer, J.W. Harney, P.R. Larsen, Recognition of UGA as a selenocysteine codon in type I deiodinase requires sequences in the 3′ untranslated region, Nature 353 (1991) 273–276.

[31] S.C. Low, M.J. Berry, Knowing when not to stop: selenocysteine incorporation in eukaryotes, Trends Biochem. Sci. 21 (1996) 203–208.

[32] P. Cravedi, G. Mori, F. Fischer, R. Percudani, Evolution of the selenoproteome in helicobacter pylori and epsilonproteobacteria, Genome Biol. Evol. 7 (2015) 2692–2704.

[33] B. Hao, W. Gong, T.K. Ferguson, C.M. James, J.A. Krzycki, M.K. Chan, A new UAG-encoded residue in the structure of a methanogen methyltransferase, Science 296 (2002) 1462–1466 (80-..

[34] Y. Zhang, V.N. Gladyshev, High content of proteins containing 21st and 22nd amino acids, selenocysteine and pyrrolysine, in a symbiotic deltaproteobacterium of gutless worm Olavius algarvensis, Nucleic Acids Res. 35 (2007) 4952–4963.

[35] J.A. Krzycki, Function of genetically encoded pyrrolysine in corrinoid-dependent methylamine methyltransferases, Curr. Opin. Chem. Biol. 8 (2004) 484–491.

[36] S.K. Blight, R.C. Larue, A. Mahapatra, D.G. Longstaff, E. Chang, G. Zhao, P.T. Kang, K.B. Green-Church, M.K. Chan, J.A. Krzycki, Direct charging of tRNACUA with pyrrolysine in vitro and in vivo, Chem 17 (2004) 503–507.

[37] G. Srinivasan, C.M. James, J.A. Krzycki, Pyrrolysine encoded by UAG in archaea: charging of a UAG-decoding specialized tRNA, Science 296 (2002) 1459–1462. 80.

[38] A. Théobald-Dietrich, M. Frugier, R. Giegé, J. Rudinger-Thirion, Atypical archaeal tRNA pyrrolysine transcript behaves towards EF-Tu as a typical elongator tRNA, Nucleic Acids Res. 32 (2004) 1091–1096.

[39] A. Théobald-Dietrich, R. Giegé, J. Rudinger-Thirion, Evidence for the existence in mRNAs of a hairpin element responsible for ribosome dependent pyrrolysine insertion into proteins, Biochimie 87 (2005) 813–817.

[40] C.J. Bult, O. White, G.J. Olsen, L. Zhou, R.D. Fleischmann, G.G. Sutton, J.A. Blake, L.M. Fitzgerald, R.A. Clayton, D. Jeannine, A.R. Kerlavage, J.C. Venter, et al., Complete genome sequence of the methanogenic archaeon, Methanococcus jannaschii, Science 273 (1996) 1058–1073. 80.

[41] A. Sauerwald, W. Zhu, T.A. Major, H. Roy, S. Palioura, D. Jahn, W.B. Whitman, J.R. Yates, M. Ibba, D. Söll, RNA-dependent cysteine biosynthesis in archaea, Science 307 (2005) 1969–1972. 80.

[42] A. Chaliotis, P. Vlastaridis, D. Mossialos, M. Ibba, H.D. Becker, C. Stathopoulos, G.D. Amoutzias, The complex evolutionary history of aminoacyl-tRNA synthetases, Nucleic Acids Res. 45 (2017) 1059–1068.

[43] M. Frechin, B. Senger, M. Braye, D. Kern, R.P. Martin, H.D. Becker, Yeast mitochondrial Gln-tRNAGln is generated by a GatFAB-mediated transamidation pathway involving Arc1p-controlled subcellular sorting of cytosolic GluRS, Genes Dev. 23 (2009) 1119–1130.

[44] H.D. Becker, D. Kern, Thermus thermophilus: a link in evolution of the tRNA-dependent amino acid amidation pathways, Proc. Natl. Acad. Sci. U. S. A. 95 (1998) 12832–12837.

[45] A.W. Curnow, K.W. Hong, R. Yuan, S. Il Kim, O. Martins, W. Winkler, T.M. Henkin, D. Söll, Glu-tRNAGln amidotransferase: a novel heterotrimeric enzyme required for correct decoding of glutamine codons during translation, Proc. Natl. Acad. Sci. U. S. A. 94 (1997) 11819–11826.

[46] D. Jahn, Y.C. Kim, Y. Ishino, M.W. Chen, D. Söll, Purification and functional characterization of the Glu-tRNA(Gln) amidotransferase from *Chlamydomonas reinhardtii*, J. Biol. Chem. 265 (1990) 8059–8064.

[47] A.W. Curnow, M. Ibba, D. Soll, tRNA-dependent asparagine formation, Nature 382 (1996) 589–590.

[48] D.L. Tumbula, H.D. Becker, W. Chang, D. Söll, Domain-specific recruitment of amide amino acids for protein synthesis, Nature 407 (2000) 106–110.

[49] K. Sheppard, J. Yuan, M.J. Hohn, B. Jester, K.M. Devine, D. Söll, From one amino acid to another: tRNA-dependent amino acid biosynthesis, Nucleic Acids Res. 36 (2008) 1813–1825.

[50] C. Pujol, M. Bailly, D. Kern, L. Maréchal-Drouard, H. Becker, A.-M. Duchêne, Dual-targeted tRNA-dependent amidotransferase ensures both mitochondrial and chloroplastic Gln-tRNAGln synthesis in plants, Proc. Natl. Acad. Sci. U. S. A. 105 (2008) 6481–6485.

[51] A. Nagao, T. Suzuki, T. Katoh, Y. Sakaguchi, T. Suzuki, Biogenesis of glutaminyl-mt tRNAGln in human mitochondria, Proc. Natl. Acad. Sci. U. S. A. 106 (2009) 16209–16214.

[52] B.M. Mailu, L. Li, J. Arthur, T.M. Nelson, G. Ramasamy, K. Fritz-Wolf, K. Becker, M.J. Gardner, Plasmodium apicoplast Gln-tRNAGln biosynthesis utilizes a unique GatAB amidotransferase essential for erythrocytic stage parasites, J. Biol. Chem. 290 (2015) 29629–29641.

[53] S. Skouloubris, L.R. De Pouplana, H. De Reuse, T.L. Hendrickson, A noncognate aminoacyl-tRNA synthetase that may resolve a missing link in protein evolution, Proc. Natl. Acad. Sci. U. S. A. 100 (2003) 11297–11302.

[54] J. Rinehart, B. Krett, M.A.T. Rubio, J.D. Alfonzo, D. Söll, *Saccharomyces cerevisiae* imports the cytosolic pathway for Gln-tRNA synthesis into the mitochondrion, Genes Dev. 19 (2005) 583–592.

[55] T. Rampias, K. Sheppard, D. Söll, The archaeal transamidosome for RNA-dependent glutamine biosynthesis, Nucleic Acids Res. 38 (2010) 5774–5783.

[56] M. Bailly, M. Blaise, B. Lorber, H.D. Becker, D. Kern, The transamidosome: a dynamic ribonucleoprotein particle dedicated to prokaryotic tRNA-dependent asparagine biosynthesis, Mol. Cell 28 (2007) 228–239.

[57] J.L. Huot, F. Fischer, J. Corbeil, É. Madore, B. Lorber, G. Diss, T.L. Hendrickson, D. Kern, J. Lapointe, Gln-tRNAGln synthesis in a dynamic transamidosome from Helicobacter pylori, where GluRS2 hydrolyzes excess Glu-tRNAGln, Nucleic Acids Res. 39 (2011) 9306–9315.

[58] F. Fischer, J.L. Huot, B. Lorber, G. Diss, T.L. Hendrickson, H.D. Becker, J. Lapointe, D. Kern, The asparagine-transamidosome from Helicobacter pylori: a dual-kinetic mode in non-discriminating aspartyl-tRNA synthetase safeguards the genetic code, Nucleic Acids Res. 40 (2012) 4965–4976.

[59] M.G. Macfarlane, Characterization of lipoamino-acids as O-amino-acid esters of phosphatidyl-glycerol, Nature 196 (1962) 136–138.

[60] C. Slavetinsky, S. Kuhn, A. Peschel, Bacterial aminoacyl phospholipids—biosynthesis and role in basic cellular processes and pathogenicity, Biochim. Biophys. Acta Mol. Cell Biol. Lipids 1862 (2017) 1310–1318.

[61] A. Peschel, R.W. Jack, M. Otto, L.V. Collins, P. Staubitz, G. Nicholson, H. Kalbacher, W.F. Nieuwenhuizen, G. Jung, A. Tarkowski, K.P.M. Van Kessel, J.A.G. Van Strijp, *Staphylococcus aureus* resistance to human defensins and evasion of neutrophil killing via the novel virulence factor MprF is based on modification of membrane lipids with L-lysine, J. Exp. Med. 193 (2001) 1067–1076.

[62] C.M. Ernst, P. Staubitz, N.N. Mishra, S.J. Yang, G. Hornig, H. Kalbacher, A.S. Bayer, D. Kraus, A. Peschel, The bacterial defensin resistance protein MprF consists of sep-arable domains for lipid lysinylation and antimicrobial peptide repulsion, PLoS Pathog. 5 (2009) 1–9.

[63] H. Roy, M. Ibba, Broad range amino acid specificity of RNA-dependent lipid remodeling by multiple peptide resistance factors, J. Biol. Chem. 284 (2009) 29677–29683.

[64] C. Weidenmaier, A. Peschel, V.A.J. Kempf, N. Lucindo, M.R. Yeaman, A.S. Bayer, DltABCD- and MprF-mediated cell envelope modifications of *Staphylococcus aureus* confer resistance to platelet microbicidal proteins and contribute to virulence in a rabbit endocarditis model, Infect. Immun. 73 (2005) 8033–8038.

[65] L. Friedman, J.D. Alder, J.A. Silverman, Genetic changes that correlate with reduced susceptibility to daptomycin in *Staphylococcus aureus*, Antimicrob. Agents Chemother. 50 (2006) 2137–2145.

[66] K. Thedieck, T. Hain, W. Mohamed, B.J. Tindall, M. Nimtz, T. Chakraborty, J. Wehland, L. Jänsch, The MprF protein is required for lysinylation of phospholipids in listerial membranes and confers resistance to cationic antimicrobial peptides (CAMPs) on *Listeria monocytogenes*, Mol. Microbiol. 62 (2006) 1325–1339.

[67] J. Zemansky, B.C. Kline, J.J. Woodward, J.H. Leber, H. Marquis, D.A. Portnoy, Development of a mariner-based transposon and identification of *Listeria monocytogenes* determinants, including the peptidyl-prolyl isomerase PrsA2, that contribute to its hemolytic phenotype, J. Bacteriol. 191 (2009) 3950–3964.

[68] R.N. Fields, H. Roy, Deciphering the tRNA-dependent lipid aminoacylation systems in bacteria: novel components and structural advances, RNA Biol. 15 (2018) 480–491.

[69] W. Arendt, S. Hebecker, S. Jäger, M. Nimtz, J. Moser, Resistance phenotypes mediated by aminoacyl-phosphatidylglycerol synthases, J. Bacteriol. 194 (2012) 1401–1416.

[70] H. Roy, M. Ibba, RNA-dependent lipid remodeling by bacterial multiple peptide resistance factors, Proc. Natl. Acad. Sci. U. S. A. 105 (2008) 4667–4672.

[71] S. Hebecker, W. Arendt, I.U. Heinemann, J.H.J. Tiefenau, M. Nimtz, M. Rohde, D. Söll, J. Moser, Alanyl-phosphatidylglycerol synthase: mechanism of substrate recognition during tRNA-dependent lipid modification in *Pseudomonas aeruginosa*, Mol. Microbiol. 80 (2011) 935–950.

[72] S. Hebecker, J. Krausze, T. Hasenkampf, J. Schneider, M. Groenewold, J. Reichelt, D. Jahn, D.W. Heinz, J. Moser, Structures of two bacterial resistance factors mediating tRNA-dependent aminoacylation of phosphatidylglycerol with lysine or alanine, Proc. Natl. Acad. Sci. U. S. A. 112 (2015) 10691–10696.

[73] E. Maloney, D. Stankowska, J. Zhang, M. Fol, Q.J. Cheng, S. Lun, W.R. Bishai, M. Rajagopalan, D. Chatterjee, M.V. Madiraju, The two-domain LysX protein of *Mycobacterium tuberculosis* is required for production of lysinylated phosphatidylglycerol and resistance to cationic antimicrobial peptides, PLoS Pathog. 5 (2009) 1–14.

[74] A. Bouhss, A.E. Trunkfield, T.D.H. Bugg, D. Mengin-Lecreulx, The biosynthesis of peptidoglycan lipid-linked intermediates, FEMS Microbiol. Rev. 32 (2008) 208–233.

[75] M. Jarick, U. Bertsche, M. Stahl, D. Schultz, K. Methling, M. Lalk, C. Stigloher, M. Steger, A. Schlosser, K. Ohlsen, The serine/threonine kinase Stk and the phosphatase Stp regulate cell wall synthesis in *Staphylococcus aureus*, Sci. Rep. 8 (2018) 1–13.

[76] U. Kopp, M. Roos, J. Wecke, H. Labischinski, Staphylococcal peptidoglycan interpeptide bridge biosynthesis: a novel antistaphylococcal target? Microb. Drug Resist. 2 (1996) 29–41.

[77] H. Labischinski, Consequences of the interaction of β-lactam antibiotics with penicillin binding proteins from sensitive and resistant *Staphylococcus aureus* strains, Med. Microbiol. Immunol. 181 (1992) 241–265.

[78] T. Schneider, M.M. Senn, B. Berger-Bächi, A. Tossi, H.G. Sahl, I. Wiedemann, In vitro assembly of a complete, pentaglycine interpeptide bridge containing cell wall precursor (lipid II-Gly5) of *Staphylococcus aureus*, Mol. Microbiol. 53 (2004) 675–685.

[79] S. Giannouli, A. Kyritsis, N. Malissovas, H.D. Becker, C. Stathopoulos, On the role of an unusual tRNAGly isoacceptor in *Staphylococcus aureus*, Biochimie 91 (2009) 344–351.

[80] L.E. Sanderson, O.C. Uhlenbeck, The 51-63 base pair of tRNA confers specificity for binding by EF-Tu, RNA 13 (2007) 835–840.

[81] S. Rohrer, K. Ehlert, M. Tschierske, H. Labischinski, B. Berger-Bachi, The essential *Staphylococcus aureus* gene fmhB is involved in the first step of peptidoglycan pentaglycine interpeptide formation, Proc. Natl. Acad. Sci. U. S. A. 96 (1999) 9351–9356.

[82] J. Hübscher, A. Jansen, O. Kotte, J. Schäfer, P.A. Majcherczyk, L.G. Harris, G. Bierbaum, M. Heinemann, B. Berger-Bächi, Living with an imperfect cell wall: compensation of femAB inactivation in *Staphylococcus aureus*, BMC Genomics 8 (2007) 1–14.

[83] K. Dare, M. Ibba, Roles of tRNA in cell wall biosynthesis, Wiley Interdiscip. Rev. RNA 3 (2012) 247–264.

[84] S.R. Filipe, A. Tomasz, Inhibition of the expression of penicillin resistance in *Streptococcus pneumoniae* by inactivation of cell wall muropeptide branching genes, Proc. Natl. Acad. Sci. U. S. A. 97 (2000) 4891–4896.

[85] S. Biarrotte-Sorin, A.P. Maillard, J. Delettré, W. Sougakoff, M. Arthur, C. Mayer, Crystal structures of Weissella viridescens FemX and its complex with UDP-MurNAc-pentapeptide: insights into FemABX family substrates recognition, Structure 12 (2004) 257–267.

[86] R. Villet, M. Fonvielle, P. Busca, M. Chemama, A.P. Maillard, J.E. Hugonnet, L. Dubost, A. Marie, N. Josseaume, S. Mesnage, C. Mayer, J.M. Valéry, M. Ethève-Quelquejeu, M. Arthur, Idiosyncratic features in tRNAs participating in bacterial cell wall synthesis, Nucleic Acids Res. 35 (2007) 6870–6883.

[87] M. Fonvielle, M. Chemama, M. Lecerf, R. Villet, P. Busca, A. Bouhss, M. Ethève-Quelquejeu, M. Arthur, Decoding the logic of the tRNA regiospecificity of nonribosomal FemX(Wv) aminoacyl transferase, Angew. Chem. Int. Ed. Engl. 49 (2010) 5115–5119.

[88] J. Shepherd, Characterisation of Pneumococcal Peptidoglycan Cross-linking Enzymology, 2011, pp. 1–330. https://www.semanticscholar.org/paper/Characterisation-of-pneumococcal-peptidoglycan-Shepherd/c432b7bb6343829e651d635c9f4b1251378cb54b.

[89] J. Shepherd, M. Ibba, Direction of aminoacylated transfer RNAs into antibiotic synthesis and peptidoglycan–mediated antibiotic resistance, FEBS Lett. 587 (2013) 2895–2904.

[90] K.H. Schleifer, O. Kandler, Peptidoglycan types of bacterial cell walls and their taxonomic implications, Bacteriol. Rev. 36 (1972) 407–477.

[91] P.A. Castelfranco, S.I. Beale, Chlorophyll biosynthesis: recent advances and areas of current interest, Annu. Rev. Plant Physiol. 34 (1983) 241–276.

[92] D.D. Huang, W.Y. Wang, S.P. Gough, C.G. Kannangara, δ–aminolevulinic acid–synthesizing enzymes need an RNA moiety for activity, Science 225 (1984) 1482–1484. 80.

[93] D.D. Huang, W.Y. Wang, Chlorophyll biosynthesis in Chlamydomonas starts with the formation of glutamyl–tRNA, J. Biol. Chem. 261 (1986) 13451–13455.

[94] A. Schön, G. Krupp, S. Gough, S. Berry-Lowe, C.G. Kannangara, D. Söll, The RNA required in the first step of chlorophyll biosynthesis is a chloroplast glutamate tRNA, Nature 322 (1986) 281–284.

[95] C. Gamini Kannangara, S.P. Gough, P. Bruyant, J. Kenneth Hoober, A. Kahn, D. von Wettstein, tRNAGlu as a cofactor in δ–aminolevulinate biosynthesis: steps that regulate chlorophyll synthesis, Trends Biochem. Sci. 13 (1988) 139–143.

[96] D. Peterson, A. Schön, D. Söll, The nucleotide sequences of barley cytoplasmic glutamate transfer RNAs and structural features essential for formation of δ–aminolevulinic acid, Plant Mol. Biol. 11 (1988) 293–299.

[97] B. Grimm, A. Bull, K.G. Welinder, S.P. Gough, C.G. Kannangara, Purification and partial amino acid sequence of the glutamate 1-semialdehyde aminotransferase of barley and Synechococcus, Carlsberg Res. Commun. 54 (1989) 67–79.

[98] S.I. Beale, P.A. Castelfranco, 14C incorporation from exogenous compounds into δ–aminolevulinic acid by greening cucumber cotyledons, Biochem. Biophys. Res. Commun. 52 (1973) 143–149.

[99] S.I. Beale, S.P. Gough, S. Granick, Biosynthesis of δ aminolevulinic acid from the intact carbon skeleton of glutamic acid in greening barley, Proc. Natl. Acad. Sci. U. S. A. 72 (1975) 2719–2723.

[100] D. Jahn, Complex formation between glutamyl–tRNA synthetase and glutamyl–tRNA reductase during the tRNA-dependent synthesis of 5-aminolevulinic acid in *Chlamydomonas reinhardtii*, FEBS Lett. 314 (1992) 77–80.

[101] R.D. Willows, C.G. Kannangara, B. Pontoppidan, Nucleotides of tRNA (Glu) involved in recognition by barley chloroplast glutamyl–tRNA synthetase and glutamyl–tRNA reductase, Biochim. Biophys. Acta Gene Struct. Expr. 1263 (1995) 228–234.

[102] L. Randau, S. Schauer, A. Ambrogelly, J.C. Salazar, J. Moser, S.I. Sekine, S. Yokoyama, D. Söll, D. Jahn, tRNA recognition by glutamyl–tRNA reductase, J. Biol. Chem. 279 (2004) 34931–34937.

[103] I. Schroder, P. Johansson, L. Rutberg, L. Hederstedt, The hemX gene of the Bacillus subtilis hemAXCDBL operon encodes a membrane protein, negatively affecting the steady-state cellular concentration of HemA (glutamyl–tRNA reductase), Microbiology 140 (1994) 731–740.

[104] L.Y. Wang, L. Brown, M. Elliott, T. Elliott, Regulation of heme biosynthesis in Salmonella typhimurium: activity of glutamyl–tRNA reductase (HemA) is greatly elevated during heme limitation by a mechanism which increases abundance of the protein, J. Bacteriol. 179 (1997) 2907–2914.

[105] P.J. Loida, R.L. Thompson, D.M. Walker, C.A. Cajacob, Novel inhibitors of glutamyl–tRNA(Glu) reductase identified through cell-based screening of the heme/chlorophyll biosynthetic pathway, Arch. Biochem. Biophys. 372 (1999) 230–237.

[106] L. Wang, M. Elliott, T. Elliott, Conditional stability of the HemA protein (Glutamyl-tRNA reductase) regulates heme biosynthesis in Salmonella typhimurium, J. Bacteriol. 181 (1999) 1211–1219.

[107] R. Meskauskiene, K. Apel, Interaction of FLU, a negative regulator of tetrapyrrole biosynthesis, with the glutamyl-tRNA reductase requires the tetratricopeptide repeat domain of FLU, FEBS Lett. 532 (2002) 27–30.

[108] D. Goslings, R. Meskauskiene, C. Kim, K.P. Lee, M. Nater, K. Apel, Concurrent interactions of heme and FLU with Glu tRNA reductase (HEMA1), the target of metabolic feedback inhibition of tetrapyrrole biosynthesis, in dark- and light-grown Arabidopsis plants, Plant J. 40 (2004) 957–967.

[109] C. Lüer, S. Schauer, K. Möbius, J. Schulze, W.D. Schubert, D.W. Heinz, D. Jahn, J. Moser, Complex formation between glutamyl-tRNA reductase and glutamate-1-semialdehyde 2,1-aminomutase in *Escherichia coli* during the initial reactions of porphyrin biosynthesis, J. Biol. Chem. 280 (2005) 18568–18572.

[110] G. Levicán, A. Katz, M. De Armas, H. Núñez, O. Orellana, Regulation of a glutamyl-tRNA synthetase by the heme status, Proc. Natl. Acad. Sci. U. S. A. 104 (2007) 3135–3140.

[111] K. Wakasugi, Human tryptophanyl-tRNA synthetase binds with heme to enhance its aminoacylation activity, Biochemistry 46 (2007) 11291–11298.

[112] M. Gorla, N.B.V. Sepuri, Perturbation of apoptosis upon binding of tRNA to the heme domain of cytochrome c, Apoptosis 19 (2014) 259–268.

[113] O. Czarnecki, B. Hedtke, M. Melzer, M. Rothbart, A. Richter, Y. Schröter, T. Pfannschmidt, B. Grimm, An Arabidopsis GluTR binding protein mediates spatial separation of 5-Aminolevulinic acid synthesis in chloroplasts, Plant Cell 23 (2011) 4476–4491.

[114] A. Zhao, Y. Fang, X. Chen, S. Zhao, W. Dong, Y. Lin, W. Gong, L. Liu, Crystal structure of Arabidopsis glutamyl-tRNA reductase in complex with its stimulator protein, Proc. Natl. Acad. Sci. U. S. A. 111 (2014) 6630–6635.

[115] Y. Fang, S. Zhao, F. Zhang, A. Zhao, W. Zhang, M. Zhang, L. Liu, The Arabidopsis glutamyl-tRNA reductase (GluTR) forms a ternary complex with FLU and GluTR-binding protein, Sci. Rep. 6 (2016) 4–10.

[116] J. Apitz, K. Nishimura, J. Schmied, A. Wolf, B. Hedtke, K.J. van Wijk, B. Grimm, Posttranslational control of ALA synthesis includes GluTR degradation by clp protease and stabilization by GluTR-binding protein, Plant Physiol. 170 (2016) 2040–2051.

[117] J.E. Choby, C.M. Grunenwald, A.I. Celis, S.Y. Gerdes, J.L. Dubois, P. Skaar, *Staphylococcus aureus* HemX modulates glutamyl-tRNA reductase abundance to regulate heme biosynthesis, MBio 9 (2018) 1–19.

[118] J. Schmied, Z. Hou, B. Hedtke, B. Grimm, Controlled partitioning of Glutamyl-tRNA reductase in stroma- and membrane-associated fractions affects the synthesis of 5-Aminolevulinic acid, Plant Cell Physiol. 59 (2018) 2204–2213.

[119] P. Wang, F.C. Liang, D. Wittmann, A. Siegel, S.O. Shan, B. Grimm, Chloroplast SRP43 acts as a chaperone for glutamyl-tRNA reductase, the rate-limiting enzyme in tetrapyrrole biosynthesis, Proc. Natl. Acad. Sci. U. S. A. 115 (2018) E3588–E3596.

[120] A.S. Richter, C. Banse, B. Grimm, The GluTR-binding protein is the heme-binding factor for feedback control of glutamyl-tRNA reductase, Elife 8 (2019) 1–18.

[121] E.C. Ulrich, W.A. van der Donk, Cameo appearances of aminoacyl-tRNA in natural product biosynthesis, Curr. Opin. Chem. Biol. 35 (2016) 29–36.

[122] E.M. Nolan, C.T. Walsh, How nature morphs peptide scaffolds into antibiotics, Chembiochem 10 (2009) 34–53.

[123] M. Moutiez, P. Belin, M. Gondry, Aminoacyl-tRNA-utilizing enzymes in natural product biosynthesis, Chem. Rev. 117 (2017) 5578–5618.

[124] R.S. Roy, A.M. Gehring, J.C. Milne, P.J. Belshaw, C.T. Walsh, Thiazole and oxazole peptides: biosynthesis and molecular machinery, Nat. Prod. Rep. 16 (1999) 249–263.

[125] S. Rebuffat, Microcins, Elsevier Inc., second ed., 2013.

[126] B.K. Leskiw, R. Mah, E.J. Lawlor, K.F. Chater, Accumulation of bldA-specified tRNA is temporally regulated in Streptomyces coelicolor A3(2), J. Bacteriol. 175 (1993) 1995–2005.

[127] R. García-Contreras, X.S. Zhang, Y. Kim, T.K. Wood, Protein translation and cell death: the role of rare tRNAs in biofilm formation and in activating dormant phage killer genes, PLoS One 3 (2008) 1–15.

[128] R.P. Garg, X.L. Qian, L.B. Alemany, S. Moran, R.J. Parry, Investigations of valanimycin biosynthesis: elucidation of the role of seryl-tRNA, Proc. Natl. Acad. Sci. U. S. A. 105 (2008) 6543–6547.

[129] R.P. Garg, J.M. Gonzalez, R.J. Parry, Biochemical characterization of VlmL, a seryl-tRNA synthetase encoded by the valanimycin biosynthetic gene cluster, J. Biol. Chem. 281 (2006) 26785–26791.

[130] C. Maruyama, H. Niikura, M. Izumikawa, J. Hashimoto, K. Shin-ya, M. Komatsu, H. Ikeda, M. Kuroda, T. Sekizuka, J. Ishikawa, Y. Hamano, tRNA-dependent aminoacylation of an amino sugar intermediate in the biosynthesis of a streptothricin-related antibiotic, Appl. Environ. Microbiol. 82 (2016) 3640–3648.

[131] A. Kaji, H. Kaji, G.D. Novelli, Soluble amino acid-incorporating system. I. Preparation of the system and nature of the reaction, J. Biol. Chem. 240 (1965) 1185–1191.

[132] A. Kaji, H. Kaji, G.D. Novelli, Soluble amino acid-incorporating system. II. Soluble nature of the system and the characterization of the radioactive product, J. Biol. Chem. 240 (1965) 1192–1197.

[133] M. Matsuhashi, C.P. Dietrich, J.L. Strominger, Biosynthesis of the peptidoglycan of bacterial cell walls iii. the role of soluble ribonucleic acid and of lipid intermediates in glycine incorporation in *staphylococcus aureus*, J. Biol. Chem. 242 (1967) 3191–3206.

[134] M. Gondry, L. Sauguet, P. Belin, R. Thai, R. Amouroux, C. Tellier, K. Tuphile, M. Jacquet, S. Braud, M. Courçon, C. Masson, S. Dubois, S. Lautru, A. Lecoq, S.I. Hashimoto, R. Genet, J.L. Pernodet, Cyclodipeptide synthases are a family of tRNA-dependent peptide bond-forming enzymes, Nat. Chem. Biol. 5 (2009) 414–420.

[135] T.W. Giessen, M.A. Marahiel, Ribosome-independent biosynthesis of biologically active peptides: application of synthetic biology to generate structural diversity, FEBS Lett. 586 (2012) 2065–2075.

[136] M.A. Fischbach, C.T. Walsh, J. Clardy, The evolution of gene collectives: how natural selection drives chemical innovation, Proc. Natl. Acad. Sci. U. S. A. 105 (2008) 4601–4608.

[137] S. Gowrishankar, S.K. Pandian, B. Balasubramaniam, K. Balamurugan, Quorum quelling efficacy of marine cyclic dipeptide –cyclo(L-leucyl-L-prolyl) against the uropathogen Serratia marcescens, Food Chem. Toxicol. 123 (2019) 326–336.

[138] H. Kaji, G.D. Novelli, A. Kaji, A soluble amino acid-incorporating system from rat liver, Biochim. Biophys. Acta 76 (1963) 474–477.

[139] A. Bachmair, D. Finley, A. Varshavsky, In vivo half-life of a protein is a function of its amino-terminal residue, Science 234 (1986) 179–186. 80.

[140] B. Bartel, I. Wünning, A. Varshavsky, The recognition component of the N-end rule pathway, EMBO J. 9 (1990) 3179–3189.

[141] S. Grigoryeve, A.E. Stewart, Y.T. Kwon, S.M. Arfin, R.A. Bradshaw, N.A. Jenkins, N.G. Copeland, A. Varshavsky, A mouse amidase specific for N-terminal asparagine: the gene, the enzyme, and their function in the N-end rule pathway, J. Biol. Chem. 271 (1996) 28521–28532.

[142] T. Tasaki, S.M. Sriram, K.S. Park, Y.T. Kwon, The N-end rule pathway, Annu. Rev. Biochem. 81 (2012) 261–289.

[143] R.L. Soffer, Peptide acceptors in the arginine transfer reaction, J. Biol. Chem. 248 (1973) 2918–2921.

[144] J.W. Tobias, T.E. Shrader, G. Rocap, A. Varshavsky, The N-end rule in bacteria, Science 254 (1991) 1374–1377. 80.

[145] T.E. Shrader, J.W. Tobias, A. Varshavsky, The N-end rule in *Escherichia coli*: cloning and analysis of the leucyl, phenylalanyl-tRNA-protein transferase gene aat, J. Bacteriol. 175 (1993) 4364–4374.

[146] G. Abramochkin, T.E. Shrader, The leucyl/phenylalanyl-tRNA-protein transferase. Overexpression and characterization of substrate recognition, domain structure, and secondary structure, J. Biol. Chem. 270 (1995) 20621–20628.

[147] K. Suto, Y. Shimizu, K. Watanabe, T. Ueda, S. Fukai, O. Nureki, K. Tomita, Crystal structures of leucyl/phenylalanyl-tRNA-protein transferase and its complex with an aminoacyl-tRNA analog, EMBO J. 25 (2006) 5942–5950.

[148] K. Watanabe, Y. Toh, K. Suto, Y. Shimizu, N. Oka, T. Wada, K. Tomita, Protein-based peptide-bond formation by aminoacyl-tRNA protein transferase, Nature 449 (2007) 867–871.

[149] R.T. Baker, A. Varshavsky, Yeast N-terminal Amidase, J. Biol. Chem. 270 (1995) 12065–12074.

[150] H. Wang, K.I. Piatkov, C.S. Brower, A. Varshavsky, Glutamine-specific N-terminal amidase, a component of the N-end rule pathway, Mol. Cell 34 (2009) 686–695.

[151] E. Balzi, M. Choder, W. Chen, A. Varshavsky, A. Goffeau, Cloning and functional analysis of the arginyl-tRNA-protein transferase gene ATE1 of *Saccharomyces cerevisiae*, J. Biol. Chem. 265 (1990) 7464–7471.

[152] A. Ciechanovers, S. Ferber, D. Ganoth, S. Elias, A. Hershko, S. Arfin, Purification and characterization of Arginyl-tRNA-protein transferase from rabbit reticulocytes, J. Biol. Chem. 263 (1988) 11155–11167.

[153] L. Chen, A. Kashina, Quantification of intracellular N-terminal β-actin arginylation, Sci. Rep. 9 (2019) 1–9.

[154] P. Batsios, H.C. Ishikawa-Ankerhold, H. Roth, M. Schleicher, C.C.L. Wong, A. Müller-Taubenberger, Ate1-mediated posttranslational arginylation affects substrate adhesion and cell migration in Dictyostelium discoideum, Mol. Biol. Cell 30 (2019) 453–466.

[155] J. Wang, I. Pavlyk, P. Vedula, S. Sterling, N.A. Leu, D.W. Dong, A. Kashina, Arginyltransferase ATE1 is targeted to the neuronal growth cones and regulates neurite outgrowth during brain development, Dev. Biol. 430 (2017) 41–51.

[156] N. Yakobov, S. Debard, F. Fischer, B. Senger, H.D. Becker, Cytosolic aminoacyl-tRNA synthetases: unanticipated relocations for unexpected functions, Biochim. Biophys. Acta, Gene Regul. Mech. 1861 (2018) 387–400.

Method article

Hemmerle *et al.*, 2021

Visualizing mitochondrial importability of a protein using the yeast Bi-genomic Mitochondrial-Split-GFP strain and an ordinary fluorescence microscope

Visualizing mitochondrial importability of a protein using the yeast Bi-genomic Mitochondrial-Split-GFP strain and an ordinary fluorescence microscope

Marine Hemmerle[1], Bruno Senger[1], Roza Kucharczyk[2] and Hubert D. Becker[1‡]

[1]Université de Strasbourg, CNRS, Génétique Moléculaire, Génomique, Microbiologie, UMR 7156, 4 Allée Konrad Röntgen, 67084 Strasbourg Cedex, France. [2]Institute of Biochemistry and Biophysics, Polish Academy of Sciences, Warsaw, Poland.

‡ Correspondence to: h.becker@unistra.fr

Running Title: Visualizing mitochondrial proteins using BiG Mito-Split-GFP

Key words

Mitochondria, localization, dual localized, BiG Mito-Split-GFP, living cells, *Saccharomyces cerevisiae*, epifluorescence microscopy

Abstract

Proving with certainty that a GFP-tagged protein is imported inside mitochondria by visualizing its fluorescence emission with an epifluorescence microscope is currently impossible using regular GFP-tagging. This is particularly true for proteins dual localized in the cytosol and mitochondria, which have been estimated to represent up to one third of the established mitoproteomes. These proteins are usually composed of a surpassingly abundant pool of the cytosolic isoform compared to the mitochondrial isoform. As a consequence, when tagged with a regular GFP, the fluorescence emission of the cytosolic isoform will inevitably eclipse that of the mitochondrial one and prevent the detection of the mitochondrial echoform. To overcome this technical limit, we engineered a yeast strain expressing a new type of GFP called Bi-Genomic Mitochondrial-Split-GFP (BiG Mito-Split-GFP). In this strain one moiety of the GFP is encoded by the mitochondrial DNA while the second moiety of the GFP can be tagged to any nuclear-encoded protein (suspected to be dual localized or bona fide mitochondrial). By doing so, only mitochondrial proteins or echoforms of dual localized proteins, regardless of their organismal origin, trigger GFP reconstitution that can be visualized by regular fluorescence microscopy. The strength of the BiG Mito-Split-GFP system is that proof of the mitochondrial localization of a given protein rests on a simple and effortless microscopy observation.

1.   **Introduction**

Fusing green fluorescent protein (GFP) or any other fluorescent protein still remains the fastest approach to visualize, using epifluorescence or confocal microscopy, the localization of a given protein in a given subcellular compartment and notably in mitochondria. However, a growing number of proteins studied in yeast and Human, display a dual cytosolic and mitochondrial localization [1, 2]. It is therefore very difficult, if not impossible, to distinguish the fluorescence of the mitochondrial pool (also called mitochondrial echoform) of such kind of GFP-tagged dual-localized protein from the cytosolic pool (cytosolic echoform) by epi- or confocal microscopy [3]. The fact that, in most cases, the proportion of the cytosolic pool largely exceeds that of the mitochondrial one, dramatically accentuates this difficulty. Confirming the mitochondrial relocation of a small pool of a cytosolic protein usually necessitates obtaining highly pure mitochondria by subcellular fractionation and verifying the purity of the mitochondria using antibodies directed against sub-compartment-specific markers. However, getting ultra-pure mitochondria devoid of cytosolic contaminants is technically almost impossible to achieve since disrupting and isolating compartments tightly bound together in the cell *via* contact sites like the ER-mitochondria ERMES complex [4] or the vacuole-mitochondria vCLAMP [5], is currently very challenging and laborious.

Owing to the constantly increasing number of mitochondrial echoforms in established mitoproteomes, there is a crucial need for a reliable unbiased, cost effective and rapid new tool that could validate the presence of a protein inside mitochondria and that also enables the specific visualization of only the mitochondrial echoform of a dual-localized protein. To this end, we re-engineered the two-fragments self-assembling Split-GFP originally designed by Cabantous and co-workers [6] and engineered a yeast strain harboring a so-called Bi-Genomic Mitochondrial-Split-GFP (BiG Mito-Split-GFP). In this strain, the gene encoding the ß1-10

fragment of the Split-GFP (GFP$_{\beta1-10}$) was biolistically integrated [7, 8] into the mitochondrial genome and is thus only translated inside the mitochondrial matrix by mitoribosomes. On the other hand, the second Split-GFP fragment (GFP$_{\beta11}$) sequence can be fused to any nuclear-encoded protein that will be translated by the cytosolic translation machinery **Fig. 1**. By doing so, the cytosolic echoform of GFP$_{\beta11}$-tagged dual-localized protein will not generate a GFP signal because it will never be in contact with the GFP$_{\beta1-10}$ complementing fragment which is synthesized and entrapped inside the mitochondria. On the opposite, upon mitochondrial import, the GFP$_{\beta11}$ fragment fused to the mitochondrial echoform will be able to interact with the mitochondrially-produced GFP$_{\beta1-10}$ and trigger assembly of a fully functional GFP emitting a fluorescent signal that can be visualized by conventional fluorescence microscopy. To guarantee that any mitochondrial protein will generate a fluorescent signal regardless of its expression level, we did not use a single ß11 to tag the nuclear-encoded gene of interest but concatenated three $\beta11$ strands ($\beta11$-chaplets or GFP$_{\beta11ch}$, [7]) and mutagenized both original Split-GFP fragments in order to increase their stability and self-assembly [7, 9]. The BiG Mito-Split-GFP system not only allows specific and unbiased visualization of discrete pools of mitochondrial echoforms of yeast dual-localized proteins but also constitutes a suitable and reliable tool to test mitochondrial importability of proteins from other organisms like plants and Human [7]. We describe herein (i) how to generate the plasmid expressing the GFP$_{\beta11ch}$-tagged gene of interest, (ii) how to transform and grow the BiG Mito-Split-GFP strain, (iii) how to visualize the mitochondrial GFP signal with an ordinary epi-fluorescence microscope and (iv) how to verify expression of the GFP$_{\beta11ch}$ and GFP$_{\beta1-10}$ fragments using commercially-available antibodies.

2. Materials

2.1. PCR and Isothermal assembly

Description of the buffers and isothermal assembly enzymes used to fuse the GFP$_{\beta 11ch}$ sequence at the 3'-end of the gene of interest (GOI). The design of the oligonucleotide primers used for the PCR and isothermal assembly of the plasmid are described in **Fig. 2**.

1. Thermal Cycler (C1000 Touch™ Thermal Cycler (BIO-RAD)).

2. 5× isoT master mixture (mix): 3 mL Tris-HCl pH 7.5 1 M, 150 µL MgCl$_2$ 2 M, 600 µL of dNTP mix (10 mM each), 300 µL DTT 1 M, 300 µL NAD$^+$ 100 mM, 1.5 g of PEG-8000 and sterile ultrapure water up to 6 mL final volume. Store 320 µL aliquots in a -80 °C freezer.

3. 2× reaction master mix: 320 µL 5× isoT master mix, 1.2 µL of T5 exonuclease (New England Biolabs, 10 U/µL), 20 µL Phusion DNA polymerase (ThermoFisher Scientific, 2 U/µL), 8 µL Taq DNA ligase (New England Biolabs, 40 U/µL) and water up to 800 µL. Freeze 11 µL aliquots and keep at -80 °C.

4. Dry Heating block for 1.5 mL microtubes.

2.2. BiG Mito-Split-GFP transformation

1. BiG Mito-Split-GFP Strain (see **Table 1**).

2. Liquid Yeast extract Peptone Dextrose (YPD): Peptone 2 % (w/v), Yeast extract 1 % (w/v), Dextrose 2 % (w/v). Autoclaved at 120 °C, 1.2 bars for 20 min.

3. Bench Top Centrifuge.

4. Dry Heating Block for 1.5 mL microtubes.

5. Salmon sperm DNA (10 mg/mL).

6. Lithium acetate 1 M (no need to adjust pH).

7. Polyethylene glycol (PEG)-4000 50 % (w/v).

8. Water bath.

9. Solid Synthetic Complete Dextrose without tryptophane (SCD-Trp): 0.675 % Yeast Nitrogen Base (without amino acids), 2 % Dextrose, amino acid (-Trp) dropout mix, 2 % agar. Autoclaved at 120 °C, 1.2 bars for 20 min.

10. Glass beads (2.5 – 4.5 mm in diameter).

11. Incubator.

2.3. BiG Mito-Split-GFP growth

1. Liquid Synthetic Complete Dextrose without tryptophane (SCD-Trp): 0.675 % Yeast Nitrogen Base (without amino acids), 2 % Dextrose, amino acid (-Trp) dropout mix. Autoclaved at 120 °C, 1.2 bars for 20 min.

2. Incubator Shaker

3. Liquid Synthetic Complete Galactose without tryptophane (SCGal-Trp): 0.675 % Yeast Nitrogen Base (without amino acids), 2 % Galactose, amino acid (-Trp) dropout mix. Do not autoclave, but rather use vacuum filtration system with 0.2 μm pores.

2.4. Epi-fluorescence Microscopy

1. AXIO Observer d1 (Carl Zeiss) epifluorescence microscope using a 100 × plan apochromatic objective (Carl Zeiss).

2. 76 × 26 mm microscope slide and 22 × 22 mm cover slip.

3. MitoTracker™ Red CMXRos (Thermo Fisher).

4. Liquid SC-Gal: 0.675 % Yeast Nitrogen Base (without amino acids), 2 % Galactose, aminoacid (-Trp) dropout mix. Do not autoclave, but rather use vacuum filtration system with 0.2 μm pores.

2.5. SDS-PAGE electrophoresis, Western Blotting and Immunodetection

1. NaOH 0.185 M.

2. Trichloroacetic acid 100 % (w/v).

3. Laemmli buffer 1 × (see **Note 1**).

4. Mini-PROTEAN® 3 System Glass Plates (BIO-RAD)

5. SDS polyacrylamide gels. The resolving gel is composed of acrylamide:bisacrylamide (30% 37.5:1) supplemented with 0.5 % (v/v) 2,2,2-Trichloroethanol (TCE) (optional, see **Note 2**) diluted in 450 mM Tris-HCl pH 8.8, 0.12 % (w/v) SDS and the acrylamide concentration is adjusted depending on the molecular weight of the proteins to analyze (usually 8- , 10- or 12 % (v/v)). After addition of 0.1 % (w/v) ammonium persulfate (APS) and 0.1 % (v/v) N,N,N',N Tetramethylethylenediamine (TEMED), immediately pour the solution between two 10×8 cm Mini-PROTEAN® Spacer Plates from BIO-RAD with integrated spacers of 0.75, 1 or 1.5 mm. Cover the surface with ethanol 100 % and discard the ethanol after polymerization. The stacking gel, which is poured on top of the resolving gel, is composed of 5 % (v/v) acrylamide:bisacrylamide (30 % 37.5:1) supplemented with TCE diluted in 125 mM Tris-HCl pH 6.8, 0.1 % (w/v) SDS. The polymerization is triggered upon addition of 0.1 % APS and 0.1 % TEMED and the comb is added right after pouring the gel.

6. Mini-PROTEAN® Tetra Vertical Electrophoresis Cell from BIO-RAD.

7. 0.2 μm PVDF membranes.

8. Trans-Blot Transfer Packs (BIO-RAD).

9. Trans-Blot Turbo™ transfer system from BIO-RAD.

10. Ethanol 100 %.

11. TBS-Tween20: 50 mM Tris-HCl pH 7.6, 150 mM NaCl and 0.3 % (v/v) Tween20.

12. Skim milk powder.

13. Heidolph Duomax shaker.

14. Primary antibody (see **Table 2**).

15. Secondary antibody (see **Table 3**).

16. Clarity Western ECL substrate from BIO-RAD.

17. Chemidoc™ imaging system from BIO-RAD.

18. Red Ponceau.

3. Methods

3.1. Engineering the plasmid expressing the GFP$_{\text{ß11ch}}$-tagged gene of interest using the Gibson assembly procedure

1. PCR-amplify the gene of interest using the G1-for and G2-rev primer (see **Fig. 2** for details)

2. The isothermal assembly is performed as follows :11 µL 2× reaction master mix is added to 9 µL DNA solution that is classically obtained by mixing PCR fragments (1-5 fragments, approximately 1 µL each) and sterile ultapure water. The reaction mixture is immediately incubated at 50 °C for 30-60 min. Parental plasmid DNA present within PCR products can be eliminated *via* DpnI digestion (see **Note 3**). 5 µL of the whole mixture is used to transform chemically-competent *Escherichia coli* cells [10] and yields classically 10-800 colonies.

3.2. Transforming the BiG Mito-Split-GFP strain

1. Inoculate BiG Mito-Split-GFP Strain from a YPD rich medium plate in 3 mL liquid YPD medium and grow overnight (ON) at 30 °C under 200 rpm rotational shaking.

2. Pellet cells by centrifugation at 5,000 × g for 5 minutes (min) at room temperature (RT).

3. Heat the salmon sperm DNA (10 mg/mL) at 95 °C for 5 min to solubilize it.

4. Wash cells with 1 mL sterile ultrapure water and centrifuge at 5,000 × g for 5 min at RT.

5. Repeat step 4.

6. Resuspend the pellet in the appropriate volume of sterile ultrapure water (see **Note 4**).

7. In a 1.5 mL microtube add 10 µL of cooled salmon sperm DNA before adding 50 µL of cell suspension (see **Note 5**). Mix by vortexing for 5 seconds (s).

8. Add 1 μg of the p414-pGPD-GOI-GFP$_{ß11ch}$ (see **Fig. 2**) to the cells and then 72 μL sterile ultrapure water, 36 μL lithium acetate 1 M and 240 μL polyethylene glycol (PEG)-4000 50 % (w/v). Mix by vortexing for 5 s.

9. Incubate cells in a 42 °C water bath for 20 to 40 min.

10. Harvest cells by short spin centrifugation (approximately 10 s). Add 1 mL sterile ultrapure water (see **Note 6**), mix by inversion without resuspending the pellet and immediately remove the supernatant to leave $100 - 150$ μL liquid in the tube.

11. Resuspend the pellet using the remaining supernatant.

12. Spread cells on a Petri dish containing solid SCD-Trp medium using sterile glass beads.

13. Incubate the plate at 30 °C for $3 - 4$ days until colonies appear.

14. Streak colonies on a new SCD-Trp plate and incubate at 30 °C for $2 - 3$ days.

15. Select the clones that can grow on SCD-Trp and store the SCD-Trp plate at 4 °C.

3.3. Culture of the transformed BiG Mito-Split-GFP strain

1. Grow $3 - 4$ selected clones overnight (ON) in 3 mL liquid SCD-Trp medium at 30 °C under 200 rpm rotational shaking.

2. In the morning, dilute the cells to an $OD_{600\ nm} = 0.4$ in 3 mL SC Galactose (SCGal)-Trp medium and incubate them at 30 °C under 200 rpm rotational shaking to an $OD_{600\ nm} = 0.8 - 1.2$.

3. Separate equally the whole culture into two 1.5 ml sterile microtubes, one for the preparation of total protein extract and Western blot (to verify expression of the GFP$_{ß11ch}$-tagged protein; see **section 3.5.**) and the other one for mitochondria staining and microscopy imaging.

4. Centrifuge the cells for total protein extract at 5,000 × *g* for 5 min at RT and discard the supernatant.

5. Keep the cell pellet for total protein extract on ice and proceed with mitochondria staining and microscope imaging.

3.4. Visualizing mitochondrial importability of the GFP$_{ß11ch}$-tagged protein

1. Add MitoTracker™ Red CMXRos (Thermo Fisher) to a final concentration of 100 µM to the cells prepared at **section 3.3. step 3.** for mitochondria staining.

2. Incubate the cells at 30 °C for 15 min.

3. Centrifuge the cells at 5,000 × *g* for 5 min at RT.

4. Wash cells with 1 mL sterile deionized water.

5. Repeat **step 4.** twice.

6. Resuspend cells in 50 µL SCGal medium.

7. Drop 2.3 µL of stained cells between 76 × 26 mm microscope slide and 22 × 22 mm cover slip (see **Note 7**).

8. Perform epifluorescence imaging (see **Fig. 3**) using an AXIO Observer d1 (Carl Zeiss) epifluorescence microscope using a 100 × plan apochromatic objective (Carl Zeiss). The images are acquired using the GFP, TRITC and Nomarski filters and using the camera CoolSnap HQ2 photometrix (Roper Scientific). For image processing and montage, the software ImageJ is used.

3.5. Verifying expression of the GFP$_{ß11ch}$-tagged protein and/or of the mitochondrial GFP$_{ß1-10}$ fragment

1. Resuspend the pellet in 450 µL NaOH 0.185 M.

2. Incubate the suspension 10 min on ice.

3. Add 50 µL trichloroacetic acid 100 %.

4. Incubate the suspension 10 min on ice.

5. Pellet the precipitated proteins at 13,000 × *g* for 15 min at 4 °C.

6. Remove the supernatant (see **Note 8**) and resuspend the pellet in 75 µL Laemmli buffer 1 × (see **Note 9**).

7. Prepare polyacrylamide gels and load 7.5 µL of total protein extract in Laemmli buffer onto the polyacrylamide gel and perform the electrophoresis at 180 V for 10 min and then at 200 V using Mini-PROTEAN® Tetra Vertical Electrophoresis Cell from BIO-RAD.

8. If TCE was added to the polyacrylamide gel, proteins having migrated can be detected using Stain-free procedure on Chemidoc™ imaging system from BIO-RAD (see **Note 2**).

9. Transfer proteins onto 0.2 µm PVDF membranes using Trans-Blot Transfer Packs and Trans-Blot Turbo™ transfer system from BIO-RAD (see **Note 10**).

10. Shortly incubate the membrane in ethanol 100 % and wash with 10 ml TBS-Tween20 solution.

11. Block the membrane with 10 ml TBS-Tween20 solution supplemented with 5 % (w/v) skim milk for 30 min at RT under shaking on Heidolph Duomax 1030 at 10 rpm. Discard the blocking solution.

12. Incubate the membrane overnight at 4 °C under shaking with 10 mL blocking solution containing the primary antibody (see **Table 2**) diluted 1:5,000 (see **Note 11**).

13. The next day, remove the primary antibody solution.

14. Wash the membrane with 10 ml TBS-Tween20 solution for 10 min at RT under shaking. Discard the washing solution.

15. Repeat step 14 two times

16. Add 10 mL of the secondary antibody (see **Table 2**) diluted 1:5,000 in blocking solution and incubate for 3 hours at RT under shaking.

17. Remove the secondary antibody solution.

18. Wash the membrane with 10 mL TBS-Tween20 solution for 10 min at RT under shaking.

19. Repeat step 18 twice.

20. Wash the membrane with 10 mL TBS 1 × solution.

21. Add the Clarity Western ECL substrate from BIO-RAD (750 µL of each reagent for one membrane).

22. Perform immunodetection using the Chemidoc™ imaging system from BIO-RAD and the Chemiluminescence program (manual acquisition and optimal time exposure).

23. Rinse the membrane with TBS-Tween20 solution shortly and add undiluted Red Ponceau staining to the membrane (see **Note 12**). Incubate 20 min at RT under shaking.

24. Remove the Red Ponceau staining solution and wash the membrane with 10 mL TBS-Tween20 solution until the red staining of the membrane disappear.

25. Start from step 11 using a second set of primary and secondary antibodies.

4. **Notes**

1. 4X Laemmli buffer: 0.5 M Tris-HCl pH 6.8, 8 % (w/v)SDS, 40 % (v/v) glycerol, 0.05 % (w/v) Bromophenol blue

2. 2,2,2-Trichloroethanol is added to the acrylamide:bisacrylamide 30 % (v/v) stock solution to visualize proteins that have migrated inside the gel by UV detection using the Stain-free procedure using a ChemiDoc Touch Imaging System. This procedure can serve as loading control to assess that all lanes were initially loaded with comparable amounts of proteins. Alternatively, Red Ponceau staining of the membrane can be performed after transfer to verify the migration and transfer.

3. In order to remove the parental plasmid DNA used as a matrix for PCR amplification, DpnI digestion can be performed. For this, the isothermal assembly reaction is supplemented with 2 μL of 10 × FastDigest buffer and 10 U (1 μL) DpnI (Thermo Fisher) and incubated at 37 °C for 1 h. Subsequently, DpnI is heat-inactivated (5 min at 95 °C). Removing the template DNA from the isoT reaction decreases the possibility to transform *E. coli* cells with an empty plasmid and thus the number of false positives.

4. The cell suspension should be milky without being too dense. Usually for a volume of 1 mL of an overnight culture, 100 μL deionized water are used to resuspend the pellet.

5. Make sure the salmon sperm DNA is not too hot when adding the cells to avoid heat shock, that would cause cell death and thus reduce transformation efficiency.

6. The pellet should not be resuspended when deionized water is added after heat shock. Addition of water will dilute the transformation mix.

7. To avoid bubbles, even in the middle of the coverslip, press on the corners. Pressing in the middle of the coverslip would cause cell burst.

8. Ensure to remove all the droplets when discarding the protein precipitation solution. Residual trichloroacetic acid droplets will change the blue color of Laemmli solution to a yellow/orange color. This indicates that pH of the sample is too acid which can cause troubles during SDS-PAGE electrophoresis.

9. If the solution has a yellow or orange color after adding the $1 \times$ Laemmli solution to the cells, Tris-Base 1 M should be added until the color turns to deep blue (start using 1 µL Tris-Base and increase the volume if the color does not change). Laemmli buffer $1 \times$ can also be supplemented with 1 M Tris-Base.

10. We used the Trans-Blot Turbo transfer system from BIO-RAD for our experiments, but any transfer system can be used.

11. The primary antibody can also be incubated at RT for 3 h under shaking. However, better results were obtained with an ON incubation at 4 °C.

12. Red Ponceau staining solution is used to denaturate the HRP coupled to the secondary antibody. By doing so, it is possible to incubate the membrane with another set of primary and secondary antibodies, without being disturbed by the HRP signal emitted by the first secondary HRP-coupled antibody. However, this method does not remove HRP-coupled secondary antibody from membrane. In order to reuse the membrane with a second set of antibodies, other stripping methods (heat and detergent, low pH or kits provided by different manufacturers) can be used.

5. References

1. Ben-Menachem R, Pines O (2017) Detection of Dual Targeting and Dual Function of Mitochondrial Proteins in Yeast. Methods Mol Biol 1567: 179-195

2. Ben-Menachem R, Tal M, Shadur T, Pines O (2011) A third of the yeast mitochondrial proteome is dual localized: a question of evolution. Proteomics 11: 4468-4476

3. Kisslov I, Naamati A, Shakarchy N, Pines O (2014) Dual-targeted proteins tend to be more evolutionarily conserved. Mol Biol Evol 31: 2770-2779

4. Lang A, John Peter AT, Kornmann B (2015) ER-mitochondria contact sites in yeast: beyond the myths of ERMES. Curr Opin Cell Biol 35: 7-12

5. Elbaz-Alon Y, Rosenfeld-Gur E, Shinder V, Futerman AH, Geiger T, Schuldiner M (2014) A dynamic interface between vacuoles and mitochondria in yeast. Dev Cell 30: 95-102

6. Cabantous S, Terwilliger TC, Waldo GS (2005) Protein tagging and detection with engineered self-assembling fragments of green fluorescent protein. Nat Biotechnol 23: 102-107

7. Bader G, Enkler L, Araiso Y, Hemmerle M, Binko K, Baranowska E, De Craene O J, Ruer-Laventie J, Pieters J, Tribouillard-Tanvier D, Senger B, di Rago J-P, Friant S, Kucharczyk R, Becker, HD (2020) Assigning mitochondrial localization of dual localized proteins using a yeast Bi-Genomic Mitochondrial-Split-GFP. eLife 9: e56649

8. Bonnefoy N, Fox TD (2001) Genetic transformation of Saccharomyces cerevisiae mitochondria. Methods Cell Biol 65: 381-396

9. Pedelacq JD, Cabantous S, Tran T, Terwilliger TC, Waldo GS (2006) Engineering and characterization of a superfolder green fluorescent protein. Nat Biotechnol 24: 79-88

10.   Inoue H, Nojima H, Okayama H (1990) High efficiency transformation of *E. coli* with plasmids. Gene 96: 23-28.

11.   Frechin M, Senger B, Braye M, Kern D, Martin RP, Becker HD (2009) Yeast mitochondrial Gln-tRNA(Gln) is generated by a GatFAB-mediated transamidation pathway involving Arc1p-controlled subcellular sorting of cytosolic GluRS. Genes Dev 23: 1119-1130

Bi-Genomic Mitochondrial-Split-GFP
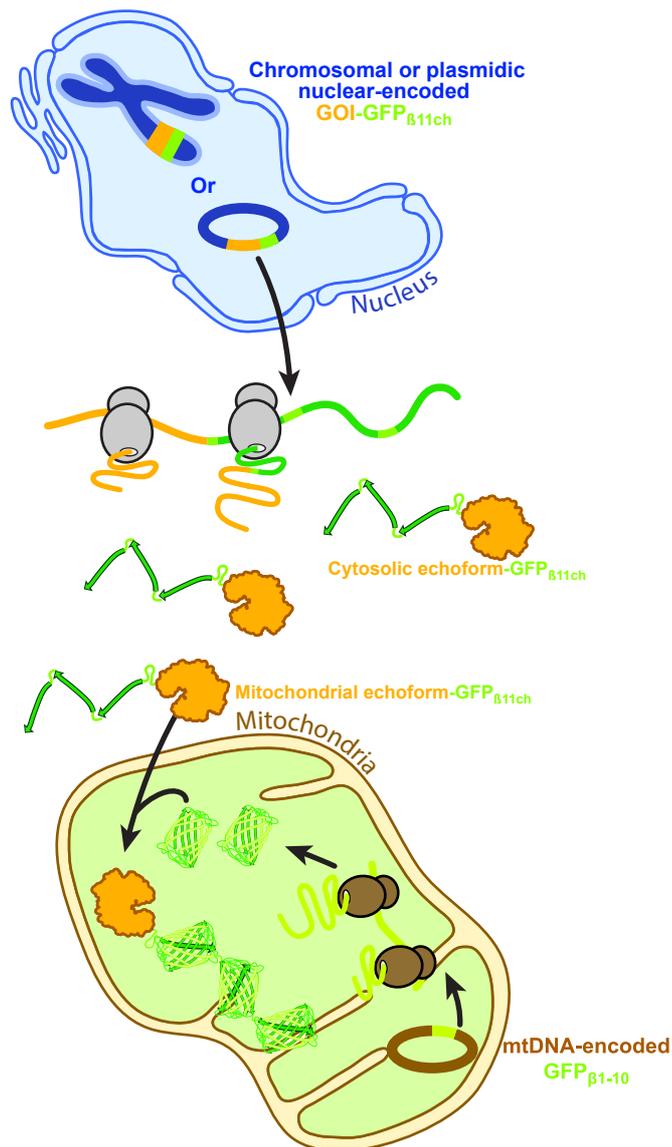
Figure 1. Principle of the BiG Mito-Split-GFP system. The gene of interest (GOI) encoding a dual-localized protein has been tagged at its 3'-end with the sequence of three interspaced ß11 fragments of the Split-GFP (ß11chaplet; $GFP_{ß11ch}$). The mRNA of this $GOI_{ß11ch}$ gene will be translated by cytosolic ribosomes into the corresponding protein fused at its C-terminus with the ß11ch tag. The pool corresponding to the cytosolic ß11ch-tagged echoform stays in the cytoplasm and is thus not generating any fluorescent signal, while the mitochondrial ß11ch-tagged echoform will translocate inside the mitochondrial matrix. Upon mitochondrial import the ß11ch appended to the mitochondrial echoform will bind to $GFP_{ß1-10}$ fragment of the Split-GFP translated by mitoribosomes from transcripts transcribed from a mtDNA-integrated ß1-10 gene. Upon interaction both mitochondria-restricted Split-GFP fragments will reconstitute a functional GFP yielding fluorescent restricted to mitochondria that can be visualized by epifluorescence microcopy.

a. GFP$_{ß11ch}$ sequence

ggc	tgc	agg	aat	tcg	ata	tca	agc	tta	CGT	GCA	CAA	GCT	AGC	GGC	GGA	TCA	ACA	AGT	AGA
G	C	R	N	S	I	S	S	L	R	A	Q	A	S	G	G	S	T	S	R

GAT	CAT	ATG	GTT	TTG	CAC	GAA	TAT	GTC	AAT	GCT	GCT	GGT	ATT	ACT	GGT	ACC	GGT	GGT	GGT
D	H	M	V	L	H	E	Y	V	N	A	A	G	I	T	G	T	G	G	G

TCT	GGT	GGT	GGT	TCT	ACC	AGT	AGA	GAT	CAT	ATG	GTT	TTG	CAC	GAA	TAT	GTC	AAT	GCT	GCT
S	G	G	G	S	T	S	R	D	H	M	V	L	H	E	Y	V	N	A	A

GGT	ATT	ACT	GGT	ACA	GGT	GGT	GGT	TCT	GGT	GGT	GGT	TCT	ACC	AGT	AGA	GAT	CAT	ATG	GTT
G	I	T	G	T	G	G	G	S	G	G	G	S	T	S	R	D	H	M	V

TTG	CAC	GAA	TAT	GTC	AAT	GCT	GCT	GGT	ATT	ACT	GGT	ACC	TGA	ctc	gag
L	H	E	Y	V	N	A	A	G	I	T	G	T	*		

b. Final construct

p414-pGPD
GOI-GFP$_{ß11ch}$

(plasmid map labels: pGPD, GOI, GFP$_{ß11ch}$, ColE1, bla, A-C, TRP1)

c. PCR step

p414-pGPD
xxx-GFP$_{ß11ch}$

(labels: P2-for, xxx, P1-rev, A-rev, A-for)
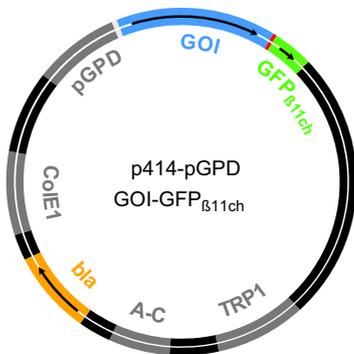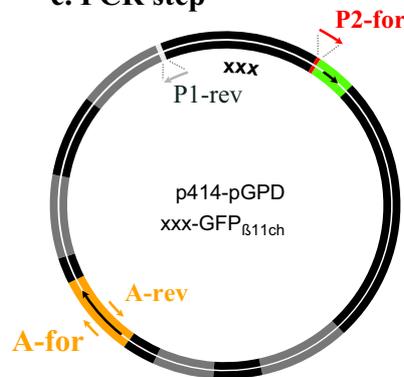
Primers :

P1-rev : TAGTTCTAGAATCCGTCGAAAC

G1-for : GTTTCGACGGATTCTAGAACTA *-ATG of GOI + 20-25 nt*

P2-for: GGCTGCAGGAATTCGATATCAAGC

G2-rev: GCTTGATATCGAATTCCTGCAGCC *-20-25 nt of GOI without stop codon*

A-for: TTGAGTACTCACCAGTCACAGAAAAGC

A-rev: TTTTCTGTGACTGGTGAGTACTCAACC

G1-for → GOI → G2-rev

3 PCR produts :
1× GOI
2× plasmid

d. Isothermal assembly

GOI
plasmid #2
(P1-rev+A-for)

plasmid #1
(P2-for+A-rev)
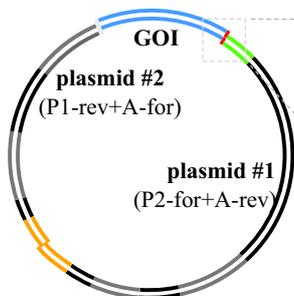
Step1: cohesive end production
5'
3'
T5 exonuclease

Step 2 : Hybridization + polymerization
5'
3'
Phusion DNA polymerase
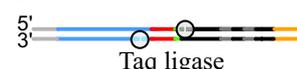
Step 3 : Ligation
5'
3'
Taq ligase
↓
Final product

Figure 2. Adding the GFPß11ch tag (a) at the 5'-end of gene of interest using the isothermal assembly strategy. (a) Sequence (Nucleotides and amino acids) of the GFP$_{ß11ch}$ tag. The ß-strands (arrows) of the GFP$_{ß11ch}$ tag are in green and the spacers between the ß11 fragments are in black. Nucleotides in red correspond to the downstream isoT tag (used for P2-for and G2-rev). Note that underlined nucleotides show EcoRI (red) and XhoI (black) restriction sites at both ends of the GFP$_{ß11ch}$. (b) *In silico* assembly of the desired construct (p414-pGPD-GOI- GFP$_{ß11ch}$) showing showing the selection marker (bla (ampicillin resistance), yellow), the gene of interest (GOI, blue), the GFP$_{ß11ch}$ tag (green) with a small linker region (red), the GPD promoter (pGPD), the yeast auxotrophy marker *TRP1*, the *E. coli* origin of replication (ColE1) and the yeast centromeric origin of replication (A-C : ARS/CEN). **(b)** To obtain the final construct, PCR amplification is used for the GOI and the two plasmidic fragments. The template used to amplify the destination vector is a similar plasmid containing an irrelevant GOI (named xxx here). The position and the sequence of the primers is indicated. Please note that for primer G2-rev the reverse-complement sequence of your GOI has to be considered (without stop codon) since the primer has the same sequence than the minus strand of the GOI. **(c)** Gibson assembly of the 3 PCR products (the GOI and the two plasmid halves). This assembly is performed at 50°C and has three steps : i) T5 exonuclease (5'→ 3') creates short 3' overhangs since it gets rapidly inactivated at 50°C, ii) the single stranded overhangs can hybridize and become substrates for Phusion DNA polymerase and iii) the fragments are ligated together by Taq DNA ligase to yield the final product.
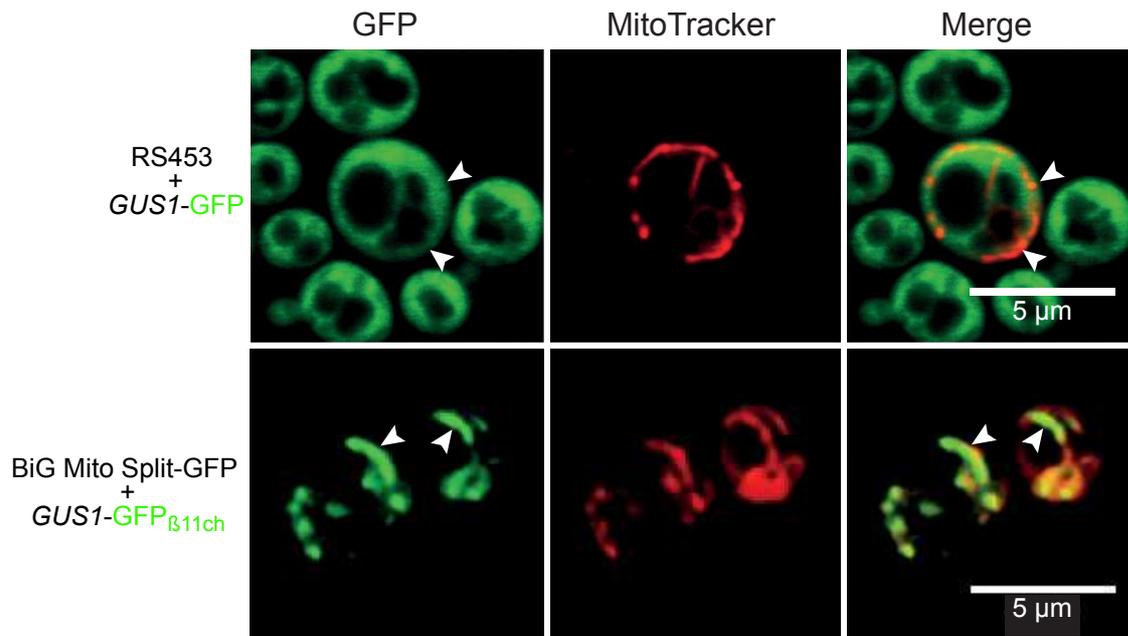
Figure 3. Fluorescence emission patterns of a dual-localized protein ß11ch tagged and expressed in the BiG Mito-Split-GFP to that of the same protein tagged with regular GFP. Micrographs of the RS453 strain expressing *GUS1* tagged with regular GFP (top) and of the BiG Mito-Split-GFP strain expressing *GUS1* tagged with ß11ch (bottom). *GUS1* encodes glutamyl-tRNA synthetase which has been shown to be dual-localized both in the cytosol and the mitochondria [11]. Cells were treated as described in section 3.4. steps 1-7 and images were taken as described in section 3.4., step 8 and processed with the ImageJ software. Mitochondrial echoforms of glutamyl-tRNA synthetase are indicated with white arrowheads.

Poster

Aminoacyl-tRNA synthetases and signaling pathways

27th tRNA conference, September 23-27 2018, Strasbourg, France

Aminoacyl-tRNA synthetases and signaling pathways

Marine Hemmerle, Hubert D. Becker

GMGM UMR7156, Université de Strasbourg, 28 rue Goethe, F-67081 Strasbourg

Background

In the yeast *Saccharomyces cerevisiae* the cytosolic methionyl- (MRS) and glutamyl-tRNA synthetase (ERS) associate with Arc1 to form the AME multisynthetasic complex. In this complex, Arc1 is a cytosolic anchor and an aminoacylation cofactor for the two aaRSs [1].

The AME complex has been described as exclusively cytosolic until a proteomic study showed that Arc1 can bind to PI(3)P and PI(3,5)P$_2$ which are specific of the endosomes and vacuolar membranes respectively [2]. Localization at the surface of vacuoles is not restricted to AME as was shown for Leucyl-tRNA synthetase (LRS) that regulates autophagy by sensing the amino acids availabilty in the cell and aminoacylating proteins of the TORC1 pathway [3,4] .

Our aim was to decipher the subcellular distribution of the AME complex components. Our hypothesis was that if Arc1 can bind to lipids *in vitro* it could bind to organellar membranes *in vivo* and redirect ERS and MRS to form a membrane-associated AME complex.
The localization of the AME components, the interaction domain of Arc1 with lipids and the aminoacylation activity of the membrane-bound aaRSs were analyzed using biochemical approaches and a Split-GFP-based microscopy stratregy we designed.
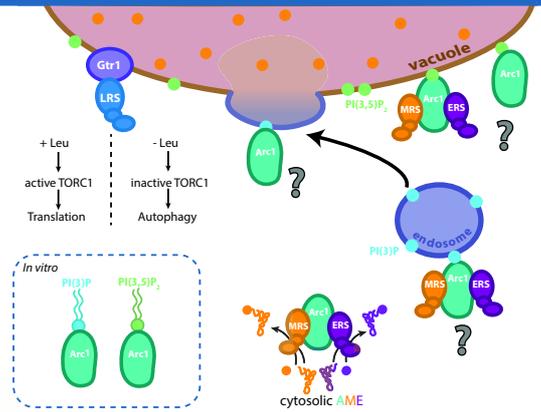

1 AME components localize in membrane fractions and at the vacuole surface

Subcellular fractionation consists in the separation of the «heavy» membranes (P13; mitochondria, vacuoles, endoplasmic reticulum, nucleus, plasmic membrane) from the «light» membranes (P100; endosomes and golgi) and the soluble fraction (S100; cytosol and vesicles) by differential centrifugations (13 000 x *g* and 100 000 x *g*) (Fig.2A).

The split-GFP system is composed of two non-fluorescent fragments (ß11 and ß1-10) and allows the specific detection of multi-localized proteins through compartment-specific reconstitution of the GFP protein (Fig. 2A). This technic was used to visualize the vacuolar localization of the AME components (Fig. 2B). To determine whether Arc1 mediates the anchoring of the 2 aaRS at the vacuolar membrane, vacuoles from a WT and an arc1Δ strain were purified on Ficoll gradient (Fig. 2C).
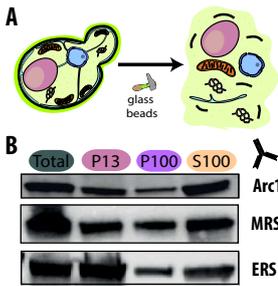
AME components localize in membrane fractions (Fig. 2B) and at the vacuolar surface (Fig. 2D). MRS anchoring is mediated by the protein Arc1 whereas ERS binding is Arc1-independent (Fig. 2E).
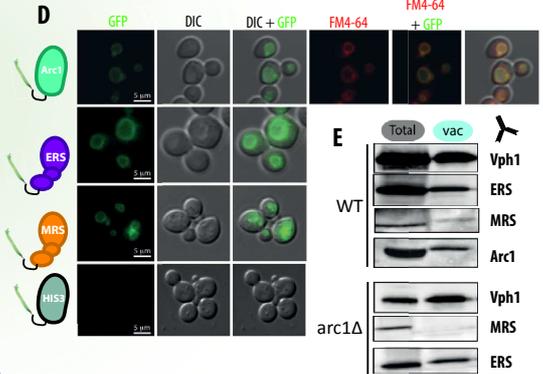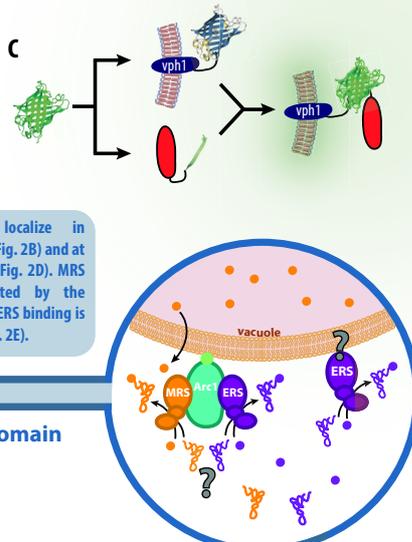
2 Identification of Arc1 lipid-interacting domain
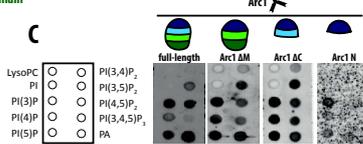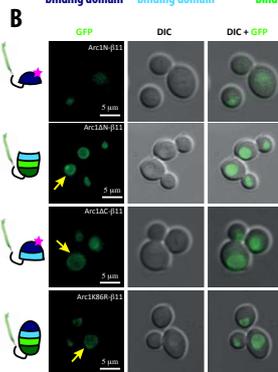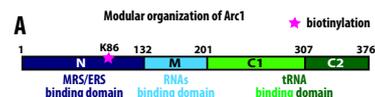
Arc1 is organized in 3 modules and can be biotinylated in the aaRS-binding domain (K86) (Fig. 3A) [5]. Arc1 does not contain any conventional PIP-binding site and the role of biotinylated Arc1 is still unknown. Arc1 mutants were tested on lipid- and PIP-coated membranes (Fig. 3B) and with the Split-GFP system (Fig. 3C) to identify the lipid-binding domain.

Arc1 lipid-binding domain could not be identified using these mutants. However, the mutant Arc1N seems to have a reduced affinity for lipids and its vacuolar localization is not as clear as for the full-length protein.
Arc1 anchoring may be mediated by its tridimentional structure or another post-translational modification since Arc1 can be succinylated, phosphorylated, ubiquitinylated...

3 Aminoacylation activity of membrane-bound aaRS
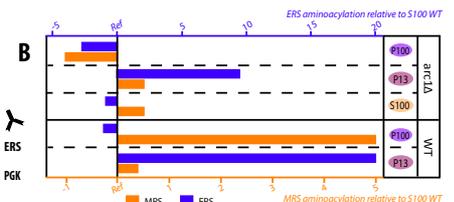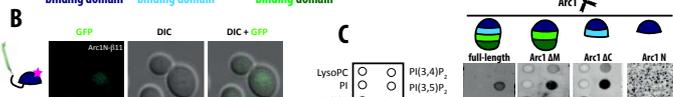
The primary role of the cytosolic AME complex is to produce Glu- and Met-tRNAs. The aminoacylation activity of the membrane-bound AME components was tested on the P13, P100 and S100 fractions (Fig. 4A). In the WT strain (lower pannel) the MRS and ERS are both active in the P13 and P100 fractions (membrane) respectively. However, in the arc1Δ strain only the ERS remains active in the membrane fraction. Indeed, ERS remains anchored to membrane fractions even in the absence of Arc1 (Fig. 4B).

MRS and ERS are both active in the membrane fractions.
Only ERS remains active when Arc1 is absent.
The possibility that aaRSs also aminoacylate proteins instead of tRNAs when localized at the vacuole to regulate signaling pathways will be checked.

Perspectives

1. Confirm that MRS vacuolar binding is Arc1-dependent and that ERS anchoring is Arc1-indepedent using the Split-GFP system in an arc1Δ strain.
2. Determine if Arc1, MRS and ERS use the endosomes pathway to localize at the vacuolar surface.
3. Understand the binding strategy of the AME components (use hemi-complexes AE, AM)
4. Compare Arc1/MRS/ERS interactome in absence or presence of Glu/Met.
5. Analyze methionylation/glutamylation of TORC1 pathway proteins (Gtr1).

References

1. Frechin, M. (2014), *Mol Cell*, **56**(6): 763-776
2. Fernandez-Murray, J. (2006), *FEBS letter*, **580**(1): 82-86
3. He, X. (2018), *Cell Metab*, **27**(1): 1-16
4. Bonfils, G. (2012), *Mol Cell*, **46**(1): 105-110
5. Kim, H. (2004), *J. Biol. Chem*, **279**(41): 42445-42452

Université de Strasbourg

BIBLIOGRAPHY

I. References in text

Ā

Abe, Y., Shodai, T., Muto, T., Mihara, K., Torii, H., Nishikawa, S. ichi, Endo, T., and Kohda, D. (2000). Structural basis of presequence recognition by the mitochondrial protein import receptor Tom20. *Cell*, *100*(5), 551–560.

Abeliovich, H., and Klionsky, D. J. (2001). Autophagy in Yeast: Mechanistic Insights and Physiological Function. *Microbiology and Molecular Biology Reviews*, *65*(3), 463–479.

Acker, M. G., Shin, B. S., Nanda, J. S., Saini, A. K., Dever, T. E., and Lorsch, J. R. (2009). Kinetic Analysis of Late Steps of Eukaryotic Translation Initiation. *Journal of Molecular Biology*, *385*(2), 491–506.

Ahting, U., Waizenegger, T., Neupert, W., and Rapaport, D. (2005). Signal-anchored proteins follow a unique insertion pathway into the outer membrane of mitochondria. *Journal of Biological Chemistry*, *280*(1), 48–53.

Alexandrova, J., Paulus, C., Rudinger-Thirion, J., Jossinet, F., and Frugier, M. (2015). Elaborate uORF/IRES features control expression and localization of human glycyl-tRNA synthetase. *RNA Biology*, *12*(12), 1301–1313.

Andréasson, C., and Ljungdahl, P. O. (2002). Receptor-mediated endoproteolytic activation of two transcription factors in yeast. *Genes and Development*, *16*(24), 3158–3172.

Artika, I. M. (2019). Current understanding of structure, function and biogenesis of yeast mitochondrial ATP synthase. *Journal of Bioenergetics and Biomembranes, 51*(5), 315–328.

B

Baba, M., Takeshige, K., Baba, N., and Ohsumi, Y. (1994). Ultrastructural analysis of the autophagic process in yeast: Detection of autophagosomes and their characterization. *Journal of Cell Biology*, *124*(6), 903–913.

Backes, S., Hess, S., Boos, F., Woellhaf, M. W., Gödel, S., Jung, M., Mühlhaus, T., and Herrmann, J. M. (2018). Tom70 enhances mitochondrial preprotein import efficiency by binding to internal targeting sequences. *Journal of Cell Biology*, *217*(4), 1369–1382.

Bader, G. (2017). *Ingénierie d'un outil basé sur une GFP fragmentée pour l'étude des protéines multi-localisées chez les eucaryotes*. University of Strasbourg.

Bader, G., Enkler, L., Araiso, Y., Hemmerle, M., Binko, K., Baranowska, E., De Craene, J. O., Ruer-Laventie, J., Pieters, J., Tribouillard-Tanvier, D., Senger, B., Rago, J. P. Di, Friant, S., Kucharczyk, R., and Becker, H. D. (2020). Assigning mitochondrial localization of dual localized proteins using a yeast bi-genomic mitochondrial-split-GFP. *ELife*, *9*, 1–24.

Baggett, J. J., Shaw, J. D., Sciambi, C. J., Watson, H. A., and Wendland, B. (2003). Fluorescent

Labeling of Yeast. In *Current Protocols in Cell Biology* (Vol. 20, Issue 1, pp. 4.13.1-4.13.28). Wiley.

Bandyopadhyay, A. K., and Deutscher, M. P. (1971). Complex of aminoacyl-transfer RNA synthetases. *Journal of Molecular Biology*, *60*(1), 113–122.

Bean, B. D. M., Dziurdzik, S. K., Kolehmainen, K. L., Fowler, C. M. S., Kwong, W. K., Grad, L. I., Davey, M., Schluter, C., and Conibear, E. (2018). Competitive organelle-specific adaptors recruit Vps13 to membrane contact sites. *The Journal of Cell Biology*, *217*(10), 3593–3607.

Ben-Menachem, R., Tal, M., Shadur, T., and Pines, O. (2011). A third of the yeast mitochondrial proteome is dual localized: A question of evolution. *Proteomics*, *11*(23), 4468–4476.

Bertram, G., Bell, H. A., Ritchie, D. W., Fullerton, G., and Stansfield, I. (2000). Terminating eukaryote translation: Domain 1 of release factor eRF1 functions in stop codon recognition. *RNA*, *6*(9), 1236–1247.

Bianchi, F., van't Klooster, J. S., Ruiz, S. J., and Poolman, B. (2019). Regulation of Amino Acid Transport in Saccharomyces cerevisiae . *Microbiology and Molecular Biology Reviews*, *83*(4), 1–38.

Binda, M., Péli-Gulli, M. P., Bonfils, G., Panchaud, N., Urban, J., Sturgill, T. W., Loewith, R., and De Virgilio, C. (2009). The Vam6 GEF Controls TORC1 by Activating the EGO Complex. *Molecular Cell*, *35*(5), 563–573.

Böckler, S., and Westermann, B. (2014). Mitochondrial ER contacts are crucial for mitophagy in yeast. *Developmental Cell*, *28*(4), 450–458.

Boldogh, I. R., Nowakowski, D. W., Yang, H.-C., Chung, H., Karmon, S., Royes, P., and Pon, L. A. (2003). A Protein Complex Containing Mdm10p, Mdm12p, and Mmm1p Links Mitochondrial Membranes and DNA to the Cytoskeleton-based Segregation Machinery. *Molecular Biology of the Cell*, *14*(11), 4618–4627.

Bonfils, G., Jaquenoud, M., Bontron, S., Ostrowicz, C., Ungermann, C., and De Virgilio, C. (2012). Leucyl-tRNA Synthetase Controls TORC1 via the EGO Complex. *Molecular Cell*, *46*(1), 105–110.

Bowers, K., and Stevens, T. H. (2005). Protein transport from the late Golgi to the vacuole in the yeast Saccharomyces cerevisiae. *Biochimica et Biophysica Acta - Molecular Cell Research*, *1744*(3 SPEC. ISS.), 438–454.

Braymer, J. J., and Lill, R. (2017). Iron–sulfur cluster biogenesis and trafficking in mitochondria. *Journal of Biological Chemistry*, *292*(31), 12754–12763.

C

Cabantous, S., Terwilliger, T. C., and Waldo, G. S. (2005). Protein tagging and detection with engineered self-assembling fragments of green fluorescent protein. *Nature Biotechnology*, *23*(1), 102–107.

Carlsson, S. R., and Simonsen, A. (2015). Membrane dynamics in autophagosome biogenesis. *Journal of Cell Science*, *128*(2), 193–205.

Carraro, M., and Bernardi, P. (2016). Calcium and reactive oxygen species in regulation of the mitochondrial permeability transition and of programmed cell death in yeast. *Cell Calcium*, *60*(2), 102–107.

Cebollero, E., and Reggiori, F. (2009). Regulation of autophagy in yeast Saccharomyces cerevisiae. *Biochimica et Biophysica Acta*, *1793*(9), 1413–1421.

Chacinska, A., Koehler, C. M., Milenkovic, D., Lithgow, T., and Pfanner, N. (2009). Importing Mitochondrial Proteins: Machineries and Mechanisms. *Cell*, *138*(4), 628–644.

Chahomchuen, T., Hondo, K., Ohsaki, M., Sekito, T., and Kakinuma, Y. (2009). Evidence for Avt6 as a vacuolar exporter of acidic amino acids in Saccharomyces cerevisiae cells. *The Journal of General and Applied Microbiology*, *55*(6), 409–417.

Chang, C. Y., Chang, C. P., Chakraborty, S., Wang, S. W., Tseng, Y. K., and Wang, C. C. (2016). Modulating the structure and function of an aminoacyl-trna synthetase cofactor by biotinylation. *Journal of Biological Chemistry*, *291*(33), 17102–17111.

Chang, K. J., and Wang, C. C. (2004). Translation Initiation from A Naturally Occurring Non-AUG Codon in Saccharomyces cerevisiae. *Journal of Biological Chemistry*, *279*(14), 13778–13785.

Chang, S. C., Heacock, P. N., Mileykovskaya, E., Voelker, D. R., and Dowhan, W. (1998). Isolation and characterization of the gene (CLS1) encoding cardiolipin synthase in Saccharomyces cerevisiae. *Journal of Biological Chemistry*, *273*(24), 14933–14941.

Chatton, B., Walter, P., Ebel, J. P., Lacroute, F., and Fasiolo, F. (1988). The yeast VAS1 gene encodes both mitochondrial and cytoplasmic valyl-tRNA synthetases. *Journal of Biological Chemistry*, *263*(1), 52–57.

Chen, S.-J., Wu, Y.-H., Huang, H.-Y., and Wang, C.-C. (2012). Saccharomyces cerevisiae possesses a stress-inducible glycyl-tRNA synthetase gene. *PloS One*, *7*(3), e33363.

Cheng, J., Fujita, A., Yamamoto, H., Tatematsu, T., Kakuta, S., Obara, K., Ohsumi, Y., and Fujimoto, T. (2014). Yeast and mammalian autophagosomes exhibit distinct phosphatidylinositol 3-phosphate asymmetries. *Nature Communications*, *5*(1), 1–12.

Cherkasova, V. A., and Hinnebusch, A. G. (2003). Translational control by TOR and TAP42 through dephosphorylation of eIF2α kinase GCN2. *Genes and Development*, *17*(7), 859–872.

Cho, H. Y., Maeng, S. J., Cho, H. J., Choi, Y. S., Chung, J. M., Lee, S., Kim, H. K., Kim, J. H., Eom, C. Y., Kim, Y. G., Guo, M., Jung, H. S., Kang, B. S., & Kim, S. (2015). Assembly of Multi-tRNA Synthetase Complex via Heterotetrameric Glutathione Transferase-homology Domains. *The Journal of biological chemistry, 290*(49), 29313–29328.

Cichocki, B. A., Krumpe, K., Vitali, D. G., and Rapaport, D. (2018). Pex19 is involved in importing dually targeted tail-anchored proteins to both mitochondria and peroxisomes. *Traffic*, *19*(10), 770–785.

Cigan, A. M., Feng, L., and Donahue, T. F. (1988). tRNAimet functions in directing the scanning

ribosome to the start site of translation. *Science*, *242*(4875), 93–97.

Clancey, C. J., Chang, S.-C., and Dowhans, W. (1993). Cloning of a Gene (PSDl) Encoding Phosphatidylserine Decarboxylase from Saccharomyces cerevisiae by Complementation of an Escherichia coli Mutant*. *Journal of Biological Chemistry*, *268*(33), 24580–24590.

Claros, M. G., and Vincens, P. (1996). Computational method to predict mitochondrially imported proteins and their targeting sequences. *European Journal of Biochemistry*, *241*(3), 779–786.

Crick, F. H. C., Leslie Barnett, F. R. S., Brenner, S., and Watts-Tobin, R. J. (1961). General Nature of the Genetic Code for Proteins. *Nature*, *192*, 1227–1232.

Crompton, M., Künzi, M., and Carafoli, E. (1977). The Calcium-Induced and Sodium-Induced Effluxes of Calcium from Heart Mitochondria: Evidence for a Sodium-Calcium Carrier. *European Journal of Biochemistry*, *79*(2), 549–558.

Cunningham, K. W., and Fink, G. R. (1994). Ca2+ transport in Saccharomyces cerevisiae. *Journal of Experimental Biology*, *196*, 157–166.

Curnow, A. W., Hong, K. W., Yuan, R., Kim, S. Il, Martins, O., Winkler, W., Henkin, T. M., and Söll, D. (1997). Glu-tRNAGln amidotransferase: A novel heterotrimeric enzyme required for correct decoding of glutamine codons during translation. *Proceedings of the National Academy of Sciences of the United States of America*, *94*(22), 11819–11826.

D

de Vries, S., and Grivell, L. A. (1988). Purification and characterization of a rotenone-insensitive NADH: Q6 oxidoreductase from mitochondria of Saccharomyces cerevisiae. *European Journal of Biochemistry*, *176*(2), 377–384.

Debard, S. (2019). *Molecular dynamic of the methionyl-tRNA synthetase and its novel non-canonical functions in the yeast S. cerevisiae*. University of Strasbourg.

Debard, S., Bader, G., De Craene, J. O., Enkler, L., Bär, S., Laporte, D., Hammann, P., Myslinski, E., Senger, B., Friant, S., and Becker, H. D. (2017). Nonconventional localizations of cytosolic aminoacyl-tRNA synthetases in yeast and human cells. *Methods*, *113*, 91–104.

Deinert, K., Fasiolo, F., Hurt, E. C., and Simos, G. (2001). Arc1p Organizes the Yeast Aminoacyl-tRNA Synthetase Complex and Stabilizes Its Interaction with the Cognate tRNAs. *Journal of Biological Chemistry*, *276*(8), 6000–6008.

Denton, R. M. (2009). Regulation of mitochondrial dehydrogenases by calcium ions. *Biochimica et Biophysica Acta - Bioenergetics*, *1787*(11), 1309–1316.

Deutscher, M. P. (1974). Aminoacyl-tRNA Synthetase Complex from Rat Liver. *Methods in Enzymology*, *29*(C), 577–583.

Diakov, T. T., and Kane, P. M. (2010). Regulation of vacuolar proton-translocating ATPase activity and assembly by extracellular pH. *Journal of Biological Chemistry*, *285*(31), 23771–

23778.

Dove, S. K., Cooke, F. T., Douglas, M. R., Sayers, L. G., Parker, P. J., and Michell, R. H. (1997). Osmotic stress activates phosphatidylinositol-3,5-bisphosphate synthesis. *Nature*, *390*(6656), 187–192.

Dubouloz, F., Deloche, O., Wanke, V., Cameroni, E., and De Virgilio, C. (2005). The TOR and EGO protein complexes orchestrate microautophagy in yeast. *Molecular Cell*, *19*(1), 15–26.

Duvezin-Caubet, S., Caron, M., Giraud, M. F., Velours, J., and Di Rago, J. P. (2003). The two rotor components of yeast mitochondrial ATP synthase are mechanically coupled by subunit δ. *Proceedings of the National Academy of Sciences of the United States of America*, *100*(23), 13235–13240.

E-F

Eisenberg-Bord, M., Tsui, H. S., Antunes, D., Fernández-del-Río, L., Bradley, M. C., Dunn, C. D., Nguyen, T. P. T., Rapaport, D., Clarke, C. F., and Schuldiner, M. (2019). The Endoplasmic Reticulum-Mitochondria Encounter Structure Complex Coordinates Coenzyme Q Biosynthesis. *Contact*, *2*, 1–14.

Elbaz-Alon, Y., Eisenberg-Bord, M., Shinder, V., Stiller, S. B., Shimoni, E., Wiedemann, N., Geiger, T., and Schuldiner, M. (2015). Lam6 Regulates the Extent of Contacts between Organelles. *Cell Reports*, *12*(1), 7–14.

Elbaz-Alon, Y., Rosenfeld-Gur, E., Shinder, V., Futerman, A. H., Geiger, T., and Schuldiner, M. (2014). A dynamic interface between vacuoles and mitochondria in yeast. *Developmental Cell*, *30*(1), 95–102.

Elbaz, Y., and Schuldiner, M. (2011). Staying in touch: The molecular era of organelle contact sites. *Trends in Biochemical Sciences*, *36*(11), 616–623.

Eliyahu, E., Pnueli, L., Melamed, D., Scherrer, T., Gerber, A. P., Pines, O., Rapaport, D., and Arava, Y. (2010). Tom20 Mediates Localization of mRNAs to Mitochondria in a Translation-Dependent Manner. *Molecular and Cellular Biology*, *30*(1), 284–294.

Emanuelsson, O., Nielsen, H., Brunak, S., and Von Heijne, G. (2000). Predicting subcellular localization of proteins based on their N-terminal amino acid sequence. *Journal of Molecular Biology*, *300*(4), 1005–1016.

Eriani, G., Delarue, M., Poch, O., Gangloff, J., and Moras, D. (1990). Partition of tRNA synthetases into two classes based on mutually exclusive sets of sequence motifs. *Nature*, *347*(6289), 203–206.

Ewalt, K. L., and Schimmel, P. (2002). Activation of angiogenic signaling pathways by two human tRNA synthetases. *Biochemistry*, *41*(45), 13344–13349.

Fernández-Millán, P., Schelcher, C., Chihade, J., Masquida, B., Giegé, P., and Sauter, C. (2016). Transfer RNA: From pioneering crystallographic studies to contemporary tRNA biology. *Archives of Biochemistry and Biophysics*, *602*, 95–105.

Fernandez-Murray, J. P., and McMaster, C. R. (2006). Identification of novel phospholipid binding proteins in Saccharomyces cerevisiae. *FEBS Letters*, *580*(1), 82–86.

Fernández-Murray, J. P., and McMaster, C. R. (2016). Lipid synthesis and membrane contact sites: A crossroads for cellular physiology. *Journal of Lipid Research*, *57*(10), 1789–1805.

Fölsch, H., Guiard, B., Neupert, W., and Stuart, R. A. (1996). Internal targeting signal of the BCS1 protein: A novel mechanism of import into mitochondria. *EMBO Journal*, *15*(3), 479–487.

Fournier, G. P., Andam, C. P., Alm, E. J., and Gogarten, J. P. (2011). Molecular Evolution of Aminoacyl tRNA Synthetase Proteins in the Early History of Life. *Orig Life Evol Biosph*, *41*, 621–632.

Foury, F., Roganti, T., Lecrenier, N., and Purnelle, B. (1998). The complete sequence of the mitochondrial genome of *Saccharomyces cerevisiae*. *FEBS Letters*, *440*(3), 325–331.

Fox, T. D. (2012). Mitochondrial protein synthesis, import, and assembly. *Genetics*, *192*(4), 1203–1234.

Frechin, M., Enkler, L., Tetaud, E., Laporte, D., Senger, B., Blancard, C., Hammann, P., Bader, G., Clauder-Münster, S., Steinmetz, L. M., Martin, R. P., di Rago, J.-P., and Becker, H. D. (2014). Expression of nuclear and mitochondrial genes encoding ATP synthase is synchronized by disassembly of a multisynthetase complex. *Molecular Cell*, *56*(6), 763–776.

Frechin, M., Kern, D., Martin, R. P., Becker, H. D., and Senger, B. (2010). Arc1p: Anchoring, routing, coordinating. *FEBS Letters*, *584*(2), 427–433.

Frechin, M., Senger, B., Brayé, M., Kern, D., Martin, R. P., Becker, H. D., Braye, M., Kern, D., Martin, R. P., and Becker, H. D. (2009). Yeast mitochondrial Gln-tRNAGln is generated by a GatFAB-mediated transamidation pathway involving Arc1p-controlled subcellular sorting of cytosolic GluRS. *Genes and Development*, *23*(9), 1119–1130.

G

Gadir, N., Haim-Vilmovsky, L., Kraut-Cohen, J., and Gerst, J. E. (2011). Localization of mRNAs coding for mitochondrial proteins in the yeast Saccharomyces cerevisiae. *RNA*, *17*(8), 1551–1565.

Galani, K., Grosshans, H., Deinert, K., Hurt, E. C., and Simos, G. (2001). The intracellular location of two aminoacyl-tRNA synthetases depends on complex formation with Arc1p. *The EMBO Journal*, *20*(23), 6889–6898.

Galani, Kyriaki, Hurt, E., and Simos, G. (2005). The tRNA aminoacylation co-factor Arc1p is excluded from the nucleus by an Xpo1p-dependent mechanism. *FEBS Letters*, *579*(5), 969–975.

Gallie, D. R. (1998). A tale of two termini: A functional interaction between the termini of an mRNA is a prerequisite for efficient translation initiation. *Gene*, *216*(1), 1–11.

García-Campusano, F., Anaya, V. H., Robledo-Arratia, L., Quezada, H., Hernández, H., Riego, L., and González, A. (2009). ALT1 -encoded alanine aminotransferase plays a central role in the metabolism of alanine in Saccharomyces cerevisiae. *Canadian Journal of Microbiology*, *55*(4), 368–374.

Gatta, A. T., Wong, L. H., Sere, Y. Y., Calderón-Noreña, D. M., Cockcroft, S., Menon, A. K., and Levine, T. P. (2015). A new family of StART domain proteins at membrane contact sites has a role in ER-PM sterol transport. *ELife*, *4*, 1–46.

Gerber, A. P., and Keller, W. (1999). An adenosine deaminase that generates inosine at the wobble position of tRNAs. *Science*, *286*(5442), 1146–1149.

Giacomello, M., Drago, I., Pizzo, P., and Pozzan, T. (2007). Mitochondrial Ca2+ as a key regulator of cell life and death. *Cell Death and Differentiation*, *14*(7), 1267–1274.

Giaever, G., Chu, A. M., Ni, L., Connelly, C., Riles, L., Véronneau, S., Dow, S., Lucau-Danila, A., Anderson, K., André, B., Arkin, A. P., Astromoff, A., El Bakkoury, M., Bangham, R., Benito, R., Brachat, S., Campanaro, S., Curtiss, M., Davis, K., … Johnston, M. (2002). Functional profiling of the Saccharomyces cerevisiae genome. *Nature*, *418*(6896), 387–391.

Giegé, R., Sissler, M., and Florentz, C. (1998). Universal rules and idiosyncratic features in tRNA identity. *Nucleic Acids Research*, *26*(22), 5017–5035.

Gincel, D., Zaid, H., and Shoshan-Barmatz, V. (2001). Calcium binding and translocation by the voltage-dependent anion channel: A possible regulatory mechanism in mitochondrial function. *Biochemical Journal*, *358*(1), 147–155.

Godinic-Mikulcic, V., Jaric, J., Greber, B. J., Franke, V., Hodnik, V., Anderluh, G., Ban, N., and Weygand-Durasevic, I. (2014). Archaeal aminoacyl-tRNA synthetases interact with the ribosome to recycle tRNAs. *Nucleic Acids Research*, *42*(8), 5191–5201.

Goffeau, A., Barrell, G., Bussey, H., Davis, R. W., Dujon, B., Feldmann, H., Galibert, F., Hoheisel, J. D., Jacq, C., Johnston, M., Louis, E. J., Mewes, H. W., Murakami, Y., Philippsen, P., Tettelin, H., and Oliver, S. G. (1996). Life with 6000 genes. *Science*, *274*(5287), 546–567.

González Montoro, A., Auffarth, K., Hönscher, C., Bohnert, M., Becker, T., Warscheid, B., Reggiori, F., van der Laan, M., Fröhlich, F., and Ungermann, C. (2018). Vps39 Interacts with Tom40 to Establish One of Two Functionally Distinct Vacuole-Mitochondria Contact Sites. *Developmental Cell*, *45*(5), 621-636.e7.

Gopaldass, N., Fauvet, B., Lashuel, H., Roux, A., and Mayer, A. (2017). Membrane scission driven by the PROPPIN Atg18. *The EMBO Journal*, *36*(22), 3274–3291.

Graham, L. A., Flannery, A. R., and Stevens, T. H. (2003). Structure and Assembly of the Yeast V-ATPase. *Journal of Bioenergetics and Biomembranes*, *35*(4), 301–312.

Graham, L. A., Hill, K. J., and Stevens, T. H. (1998). Assembly of the yeast vacuolar H+-ATPase occurs in the endoplasmic reticulum and requires a Vma12p/Vma22p assembly complex. *Journal of Cell Biology*, *142*(1), 39–49.

Graham, L. A., Powell, B., and Stevens, T. H. (2000). Composition and assembly of the yeast vacuolar H+-ATPase complex. *Journal of Experimental Biology*, *203*(1), 61–70.

Graham, L. A., and Stevens, T. H. (1999). Assembly of the yeast vacuolar proton-translocating atpase. *Journal of Bioenergetics and Biomembranes*, *31*(1), 39–47.

Graindorge, J.-S., Senger, B., Tritch, D., Simos, G., and Fasiolo, F. (2005). Role of Arc1p in the Modulation of Yeast Glutamyl-tRNA Synthetase Activity †. *Biochemistry*, *44*(4), 1344–1352.

Gray, M. W., Burger, G., and Lang, B. F. (1999). Mitochondrial evolution. *Science*, *283*(5407), 1476–1481.

H

Han, J. M., Jeong, S. J., Park, M. C., Kim, G., Kwon, N. H., Kim, H. K., Ha, S. H., Ryu, S. H., and Kim, S. (2012). Leucyl-tRNA synthetase is an intracellular leucine sensor for the mTORC1-signaling pathway. *Cell*, *149*(2), 410–424.

Han, J. M., Kim, J. Y., and Kim, S. (2003). Molecular network and functional implications of macromolecular tRNA synthetase complex. *Biochemical and Biophysical Research Communications*, *303*(4), 985–993.

Hansen, K. G., Aviram, N., Laborenz, J., Bibi, C., Meyer, M., Spang, A., Schuldiner, M., and Herrmann, J. M. (2018). An ER surface retrieval pathway safeguards the import of mitochondrial membrane proteins in yeast. *Science*, *361*(6407), 1118–1122.

Hansen, K. G., and Herrmann, J. M. (2019). Transport of Proteins into Mitochondria. *The Protein Journal*, *38*(3), 330–342.

Harris, C. (1987). An aminoacyl-tRNA synthetase complex in Escherichia coli. *Journal of Bacteriology*, *169*(6), 2718–2723.

Hartman, H., and Smith, T. F. (2014). The evolution of the ribosome and the genetic code. *Life*, *4*(2), 227–249.

Hausmann, C. D., Prætorius-Ibba, M., and Ibba, M. (2007). An aminoacyl-tRNA synthetase: Elongation factor complex for substrate channeling in archaeal translation. *Nucleic Acids Research*, *35*(18), 6094–6102.

He, X. Di, Gong, W., Zhang, J. N., Nie, J., Yao, C. F., Guo, F. S., Lin, Y., Wu, X. H., Li, F., Li, J., Sun, W. C., Wang, E. D., An, Y. P., Tang, H. R., Yan, G. Q., Yang, P. Y., Wei, Y., Mao, Y. Z., Lin, P. C., ... Zhao, S. M. (2018). Sensing and Transmitting Intracellular Amino Acid Signals through Reversible Lysine Aminoacylations. *Cell Metabolism*, *27*(1), 151-166.e6.

Hellen, C. U. T. (2018). Translation termination and ribosome recycling in eukaryotes. *Cold Spring Harbor Perspectives in Biology*, *10*(10).

Hemmerle, M., Senger, B., Kucharczyk, R., and Becker, H. D. (2021). Visualizing mitochondrial importability of a protein using the yeast Bi-genomic Mitochondrial-Split-GFP strain and an ordinary fluorescence microscope. *Methods in Molecular Biology*, in press.

Hemmerle, M., Wendenbaum, M., Grob, G., Yakobov, N., Mahmoudi, N., Senger, B., Debard, S., Fischer, F., and Becker, H. D. (2020). Noncanonical inputs and outputs of tRNA aminoacylation.

In *Enzymes* (Vol. 48, pp. 117–147). Academic Press.

Henne, W. M., Zhu, L., Balogi, Z., Stefan, C., Pleiss, J. A., and Emr, S. D. (2015). Mdm1/Snx13 is a novel ER-endolysosomal interorganelle tethering protein. *Journal of Cell Biology*, *210*(4), 541–551.

Herrmann, J. M., and Riemer, J. (2010). The intermembrane space of mitochondria. *Antioxidants and Redox Signaling*, *13*(9), 1341–1358.

Hinnebusch, A. G. (2005). Translational regulation of GCN4 and the general amino acid control of yeast. *Annual Review of Microbiology*, *59*, 407–450.

Hinnebusch, A. G., and Natarajan, K. (2002). Gcn4p, a master regulator of gene expression, is controlled at multiple levels by diverse signals of starvation and stress. *Eukaryotic Cell*, *1*(1), 22–32.

Ho, M. N., Hirata, R., Umemoto, N., Ohya, Y., Takatsuki, A., Stevens, T. H., and Anraku, Y. (1993). VMA13 encodes a 54-kDa vacuolar H+-ATPase subunit required for activity but not assembly of the enzyme complex in Saccharomyces cerevisiae. *Journal of Biological Chemistry*, *268*(24), 18286–18292.

Hoagland, M. B., Stephenson, M. L., Scott, J. F., Hecht, L. I., and Zamecnik, P. C. (1958). A soluble ribonucleic acid intermediate in protein synthesis. *The Journal of Biological Chemistry*, *231*(1), 241–257.

Hönscher, C., Mari, M., Auffarth, K., Bohnert, M., Griffith, J., Geerts, W., van der Laan, M., Cabrera, M., Reggiori, F., and Ungermann, C. (2014). Cellular metabolism regulates contact sites between vacuoles and mitochondria. *Developmental Cell*, *30*(1), 86–94.

Horák, J. (1997). Yeast nutrient transporters. *Biochimica et Biophysica Acta - Reviews on Biomembranes*, *1331*(1), 41–79.

Horvath, S. E., and Daum, G. (2013). Lipids of mitochondria. *Progress in Lipid Research*, *52*(4), 590–614.

Hughes Hallett, J. E., Luo, X., and Capaldi, A. P. (2015). Snf1/AMPK promotes the formation of Kog1/raptor-bodies to increase the activation threshold of TORC1 in budding yeast. *eLife, 4, e09181*

Huh, W. K., Falvo, J. V., Gerke, L. C., Carroll, A. S., Howson, R. W., Weissman, J. S., and O'Shea, E. K. (2003). Global analysis of protein localization in budding yeast. *Nature*, *425*(6959), 686–691.

Huotari, J., and Helenius, A. (2011). Endosome maturation. *EMBO Journal*, *30*(17), 3481–3500.

I-J

Ibba, M., and Söll, D. (2000). Aminoacyl-tRNA Synthesis. *Annual Review of Biochemistry*, *69*(1), 617–650.

Ishimoto, M., Sugimoto, N., Sekito, T., Kawano-Kawada, M., and Kakinuma, Y. (2012). ATP-Dependent Export of Neutral Amino Acids by Vacuolar Membrane Vesicles of Saccharomyces cerevisiae. *Bioscience, Biotechnology, and Biochemistry*, *76*(9), 1802–1804.

Jakubowski, H. (2012). Quality control in tRNA charging. *Wiley Interdisciplinary Reviews: RNA*, *3*(3), 295–310.

Jones, E. W., Webb, G. C., and Hiller, M. A. (1997). Biogenesis and Function of the Yeast Vacuole. In *Cold Spring Harbor Monograph Archive* (Vol. 21, Issue 0, pp. 363–470).

Jores, T., Klinger, A., Groβ, L. E., Kawano, S., Flinner, N., Duchardt-Ferner, E., Wöhnert, J., Kalbacher, H., Endo, T., Schleiff, E., and Rapaport, D. (2016). Characterization of the targeting signal in mitochondrial β-barrel proteins. *Nature Communications*, *7*(1), 1–16.

Jores, T., Lawatscheck, J., Beke, V., Franz-Wachtel, M., Yunoki, K., Fitzgerald, J. C., Macek, B., Endo, T., Kalbacher, H., Buchner, J., and Rapaport, D. (2018). Cytosolic Hsp70 and Hsp40 chaperones enable the biogenesis of mitochondrial β-barrel proteins. *Journal of Cell Biology*, *217*(9), 3091–3108.

K

Kaminska, M., Havrylenko, S., Decottignies, P., Le Maréchal, P., Negrutskii, B., and Mirande, M. (2009). Dynamic organization of aminoacyl-tRNA synthetase complexes in the cytoplasm of human cells. *Journal of Biological Chemistry*, *284*(20), 13746–13754.

Kane, P. M. (1995). Disassembly and reassembly of the yeast vacuolar H+-ATPase in vivo. *Journal of Biological Chemistry*, *270*(28), 17025–17032.

Kane, P. M. (2006). The Where, When, and How of Organelle Acidification by the Yeast Vacuolar H+-ATPase. *Microbiology and Molecular Biology Reviews*, *70*(1), 177–191.

Kanki, T., and Klionsky, D. J. (2008). Mitophagy in yeast occurs through a selective mechanism. *Journal of Biological Chemistry*, *283*(47), 32386–32393.

Kapp, L. D., and Lorsch, J. R. (2004). The molecular mechanics of eukaryotic translation. *Annual Review of Biochemistry*, *73*, 657–704.

Karanasios, E., Simader, H., Panayotou, G., Suck, D., and Simos, G. (2007). Molecular Determinants of the Yeast Arc1p-Aminoacyl-tRNA Synthetase Complex Assembly. *Journal of Molecular Biology*, *374*(4), 1077–1090.

Kemper, C., Habib, S. J., Engl, G., Heckmeyer, P., Dimmer, K. S., and Rapaport, D. (2008). Integration of tail-anchored proteins into the mitochondrial outer membrane does not require any known import components. *Journal of Cell Science*, *121*(12), 1990–1998.

Khan, K., Baleanu-Gogonea, C., Willard, B., Gogonea, V., and Fox, P. L. (2020). 3-Dimensional architecture of the human multi-tRNA synthetase complex. *Nucleic Acids Research*, *48*(15), 8740–8754.

Khoshnevis, S., Gross, T., Rotte, C., Baierlein, C., Ficner, R., and Krebber, H. (2010). The iron-

sulphur protein RNase L inhibitor functions in translation termination. *EMBO Reports*, *11*(3), 214–219.

Kihara, A., Noda, T., Ishihara, N., and Ohsumi, Y. (2001). Two distinct Vps34 phosphatidylinositol 3-kinase complexes function in autophagy and carboxypeptidase y sorting in Saccharomyces cerevisiae. *Journal of Cell Biology*, *153*(3), 519–530.

Kim, H. S., Hoja, U., Stolz, J., Sauer, G., and Schweizer, E. (2004). Identification of the tRNA-binding protein Arc1p as a novel target of in vivo biotinylation in Saccharomyces cerevisiae. *Journal of Biological Chemistry*, *279*(41), 42445–42452.

Kispal, G., Steiner, H., Court, D. A., Rolinski, B., and Lill, R. (1996). Mitochondrial and cytosolic branched-chain amino acid transaminases from yeast, homologs of the myc oncogene-regulated Eca39 protein. *Journal of Biological Chemistry*, *271*(40), 24458–24464.

Kitamoto, K., Yoshizawa, K., Ohsumi, Y., and Anraku2, Y. (1988). Dynamic Aspects of Vacuolar and Cytosolic Amino Acid Pools of Saccharomyces cerevisiae. *Journal of Bacteriology*, 170(6), 2683–2686.

Kleeman, T. A., Wei, D., Simpson, K. L., and First, E. A. (1997). Human tyrosyl-tRNA synthetase shares amino acid sequence homology with a putative cytokine. *Journal of Biological Chemistry*, *272*(22), 14420–14425.

Klose, C., Surma, M. A., Gerl, M. J., Meyenhofer, F., Shevchenko, A., and Simons, K. (2012). Flexibility of a Eukaryotic Lipidome – Insights from Yeast Lipidomics. *PLoS ONE*, *7*(4), e35063.

Ko, Y. G., Kim, E. K., Kim, T., Park, H., Park, H. S., Choi, E. J., and Kim, S. (2001). Glutamine-dependent Antiapoptotic Interaction of Human Glutaminyl-tRNA Synthetase with Apoptosis Signal-regulating Kinase 1. *Journal of Biological Chemistry*, *276*(8), 6030–6036.

Kohlhaw, G. B. (2003). Leucine Biosynthesis in Fungi: Entering Metabolism through the Back Door. *Microbiology and Molecular Biology Reviews*, *67*(1), 1–15.

Kornmann, B., Currie, E., Collins, S. R., Schuldiner, M., Nunnari, J., Weissman, J. S., and Walter, P. (2009). An ER-mitochondria tethering complex revealed by a synthetic biology screen. *Science*, *325*(5939), 477–481.

Kozak, M. (2002). Pushing the limits of the scanning mechanism for initiation of translation. *Gene*, 299(1–2), 1–34.

Kubota, H., Obata, T., Ota, K., Sasaki, T., and Ito, T. (2003). Rapamycin-induced translational derepression of GCN4 mRNA involves a novel mechanism for activation of the eIF2α kinase GCN2. *Journal of Biological Chemistry*, *278*(23), 20457–20460.

Kümmel, D., and Ungermann, C. (2014). Principles of membrane tethering and fusion in endosome and lysosome biogenesis. *Current Opinion in Cell Biology*, 29(1), 61–66.

Kuzmishin Nagy, A. B., Bakhtina, M., and Musier-Forsyth, K. (2020). Trans-editing by aminoacyl-tRNA synthetase-like editing domains. In *Enzymes* (1st ed., Vol. 48). Elsevier Inc.

Kvam, E., and Goldfarb, D. S. (2004). Nvj1p is the outer-nuclear-membrane receptor for oxysterol-binding protein homolog Osh1p in Saccharomyces cerevisiae. *Journal of Cell*

Science, *117*(21), 4959–4968.

Kyriacou, S. V., and Deutscher, M. P. (2008). An Important Role for the Multienzyme Aminoacyl-tRNA Synthetase Complex in Mammalian Translation and Cell Growth. *Molecular Cell*, *29*(4), 419–427.

L

Lahiri, S., Chao, J. T., Tavassoli, S., Wong, A. K. O., Choudhary, V., Young, B. P., Loewen, C. J. R., and Prinz, W. A. (2014). A Conserved Endoplasmic Reticulum Membrane Protein Complex (EMC) Facilitates Phospholipid Transfer from the ER to Mitochondria. *PLoS Biology*, *12*(10), e1001969.

Lang, A. B., John Peter, A. T. A. T., Walter, P., and Kornmann, B. (2015). ER-mitochondrial junctions can be bypassed by dominant mutations in the endosomal protein Vps13. *Journal of Cell Biology*, *210*(6), 883–890.

Lapointe, J., Duplain, L., and Proulx, M. (1986). A single glutamyl-tRNA synthetase aminoacylates tRNA(Glu) and tRNA(Gln) in Bacillus subtilis and efficiently misacylates Escherichia coli tRNA1(Gln) in vitro. *Journal of Bacteriology*, *165*(1), 88–93.

Laporte, D., Huot, J. L., Bader, G., Enkler, L., Senger, B., and Becker, H. D. (2014). Exploring the evolutionary diversity and assembly modes of multi-aminoacyl-tRNA synthetase complexes: Lessons from unicellular organisms. *FEBS Letters*, *588*(23), 4268–4278.

Lemasters, J. J., and Holmuhamedov, E. (2006). Voltage-dependent anion channel (VDAC) as mitochondrial governator - Thinking outside the box. *Biochimica et Biophysica Acta - Molecular Basis of Disease*, 1762(2), 181–190.

Lesnik, C., Cohen, Y., Atir-Lande, A., Schuldiner, M., and Arava, Y. (2014). OM14 is a mitochondrial receptor for cytosolic ribosomes that supports co-translational import into mitochondria. *Nature Communications*, *5*(1), 1–11.

Levin, D. H., Kyner, D., and Acs, G. (1973). Protein initiation in eukaryotes: formation and function of a ternary complex composed of a partially purified ribosomal factor, methionyl transfer RNA, and guanosine triphosphate. *Proceedings of the National Academy of Sciences of the United States of America*, *70*(1), 41–45.

Levine, T. P., and Munro, S. (2001). Dual targeting of Osh1p, a yeast homologue of oxysterol-binding protein, to both the Golgi and the nucleus-vacuole junction. *Molecular Biology of the Cell*, *12*(6), 1633–1644.

Li, S. C., Diakov, T. T., Xu, T., Tarsio, M., Zhu, W., Couoh-Cardel, S., Weisman, L. S., and Kane, P. M. (2014). The signaling lipid PI(3,5)P2 stabilizes V1-Vo sector interactions and activates the V-ATPase. *Molecular Biology of the Cell*, *25*(8), 1251–1262.

Ling, C., and Ermolenko, D. N. (2016). Structural insights into ribosome translocation. *Wiley Interdisciplinary Reviews: RNA*, *7*(5), 620–636.

Ljungdahl, P. O. (2009). Amino-acid-induced signalling via the SPS-sensing pathway in yeast.

Biochemical Society Transactions, *37*(1), 242–247.

Ljungdahl, P. O., and Daignan-Fornier, B. (2012). Regulation of amino acid, nucleotide, and phosphate metabolism in Saccharomyces cerevisiae. *Genetics*, *190*(3), 885–929.

Loewen, C. J. R., Roy, A., and Levine, T. P. (2003). A conserved ER targeting motif in three families of lipid binding proteins and in Opi1p binds VAP. *EMBO Journal*, *22*(9), 2025–2035.

Lund, E., and Dahlberg, J. E. (1998). Proofreading and aminoacylation of tRNAs before export from the nucleus. *Science*, *282*(5396), 2082–2085.

Luque, I., Riera-Alberola, M. L., Andújar, A., and Ochoa De Alda, J. A. G. (2008). Intraphylum diversity and complex evolution of cyanobacterial aminoacyl-tRNA synthetases. *Molecular Biology and Evolution*, *25*(11), 2369–2389.

M

Magasanik, B., and Kaiser, C. A. (2002). Nitrogen regulation in Saccharomyces cerevisiae. *Gene*, *290*(1–2), 1–18.

Majumdar, R., Bandyopadhyay, A., and Maitra, U. (2003). Mammalian translation initiation factor eIF1 functions with eIF1A and eIF3 in the formation of a stable 40 S preinitiation complex. *Journal of Biological Chemistry*, *278*(8), 6580–6587.

Maleszka, R., Skelly, P. J., and Clark-Walker, G. D. (1991). Rolling circle replication of DNA in yeast mitochondria. *EMBO Journal*, *10*(12), 3923–3929.

Malia, P. C., and Ungermann, C. (2016). Vacuole membrane contact sites and domains: emerging hubs to coordinate organelle function with cellular metabolism. *Biochemical Society Transactions*, *44*(2), 528–533.

Malina, C., Larsson, C., and Nielsen, J. (2018). Yeast mitochondria: An overview of mitochondrial biology and the potential of mitochondrial systems biology. *FEMS Yeast Research*, 18(5).

Maloney, E., Stankowska, D., Zhang, J., Fol, M., Cheng, Q. J., Lun, S., Bishai, W. R., Rajagopalan, M., Chatterjee, D., and Madiraju, M. V. (2009). The two-domain LysX protein of Mycobacterium tuberculosis is required for production of lysinylated phosphatidylglycerol and resistance to cationic antimicrobial peptides. *PLoS Pathogens*, *5*(7).

Manik, M. K., Yang, H., Tong, J., and Im, Y. J. (2017). Structure of Yeast OSBP-Related Protein Osh1 Reveals Key Determinants for Lipid Transport and Protein Targeting at the Nucleus-Vacuole Junction. *Structure*, *25*(4), 617-629.e3.

Manolson, M. F., Wu, B., Proteau, D., Taillon, B. E., Roberts, B. T., Hoyt, M. A., and Jones, E. W. (1994). STV1 gene encodes functional homologue of 95-kDa yeast vacuolar H+- ATPase subunit Vph1p. *Journal of Biological Chemistry*, *269*(19), 14064–14074.

Marres, C. A. M., de Vries, S., and Grivell, L. A. (1991). Isolation and inactivation of the nuclear gene encoding the rotenone-insensitive internal NADH: ubiquinone oxidoreductase of mitochondria from Saccharomyces cerevisiae. *European Journal of Biochemistry*, *195*(3),

857–862.

Martínez-Muñoz, G. A., and Kane, P. (2008). Vacuolar and plasma membrane proton pumps collaborate to achieve cytosolic pH homeostasis in yeast. *Journal of Biological Chemistry*, *283*(29), 20309–20319.

Marty, N. J., Teresinski, H. J., Hwang, Y. T., Clendening, E. A., Gidda, S. K., Sliwinska, E., Zhang, D., Miernyk, J. A., Brito, G. C., Andrews, D. W., Dyer, J. M., and Mullen, R. T. (2014). New insights into the targeting of a subset of tail-anchored proteins to the outer mitochondrial membrane. *Frontiers in Plant Science*, *5*(SEP).

Marzi, S., Myasnikov, A. G., Serganov, A., Ehresmann, C., Romby, P., Yusupov, M., and Klaholz, B. P. (2007). Structured mRNAs Regulate Translation Initiation by Binding to the Platform of the Ribosome. *Cell*, *130*(6), 1019–1031.

Mccartney, A. J., Zhang, Y., and Weisman, L. S. (2014). Phosphatidylinositol 3,5-bisphosphate: Low abundance, high significance. *BioEssays*, *36*(1), 52–64.

Melin, J., Schulz, C., Wrobel, L., Bernhard, O., Chacinska, A., Jahn, O., Schmidt, B., and Rehling, P. (2014). Presequence Recognition by the Tom40 Channel Contributes to Precursor Translocation into the Mitochondrial Matrix. *Molecular and Cellular Biology*, *34*(18), 3473–3485.

Messenguy, F., Colin, D., and Have, J. TEN. (1980). Regulation of Compartmentation of Amino Acid Pools in Saccharomyces cerevisiae and Its Effects on Metabolic Control. *European Journal of Biochemistry*, *108*(2), 439–447.

Milenkovic, D., Ramming, T., Müller, J. M., Wenz, L. S., Gebert, N., Schulze-Specking, A., Stojanovski, D., Rospert, S., and Chacinska, A. (2009). Identification of the signal directing Tim9 and Tim10 into the intermembrane space of mitochondria. *Molecular Biology of the Cell*, *20*(10), 2530–2539.

Mirande, M., Corre, D., and Waller, J.-P. (1985). A complex from cultured Chinese hamster ovary cells containing nine aminoacyl-tRNA synthetases. Thermolabile leucyl-tRNA synthetase from the tsH1 mutant cell line is an integral component of this complex. *European Journal of Biochemistry*, *147*(2), 281–289.

Miseta, A., Kellermayer, R., Aiello, D. P., Fu, L., and Bedwell, D. M. (1999). The vacuolar Ca2+/H+ exchanger Vcx1p/Hum1p tightly controls cytosolic Ca2+ levels in S. cerevisiae. *FEBS Letters*, *451*(2), 132–136.

Moeller, C. H., and Thomson, W. W. (1979). An ultrastructural study of the yeast tonoplast during the shift from exponential to stationary phase. *Journal of Ultrasructure Research*, *68*(1), 28–37.

Moine, H., Romby, P., Springer, M., Grunberg-Manago, M., Ebel, J. P., Ehresmann, B., and Ehresmann, C. (1990). Escherichia coli threonyl-tRNA synthetase and tRNAThr modulate the binding of the ribosome to the translational initiation site of the ThrS mRNA. *Journal of Molecular Biology*, *216*(2), 299–310.

Mokranjac, D., Paschen, S. A., Kozany, C., Prokisch, H., Hoppins, S. C., Nargang, F. E., Neupert, W., and Hell, K. (2003). Tim50, a novel component of the TIM23 preprotein translocase of

mitochondria. *EMBO Journal*, *22*(4), 816–825.

Morozumi, Y., and Shiozaki, K. (2021). Conserved and divergent mechanisms that control torc1 in yeasts and mammals. *Genes*, *12*(1), 1–14.

Müller, M., Schmidt, O., Angelova, M., Faserl, K., Weys, S., Kremser, L., Pfaffenwimmer, T., Dalik, T., Kraft, C., Trajanoski, Z., Lindner, H., and Teis, D. (2015). The coordinated action of the MVB pathway and autophagy ensures cell survival during starvation. *ELife*, *4*, e07736.

Murley, A., Sarsam, R. D., Toulmay, A., Yamada, J., Prinz, W. A., and Nunnari, J. (2015). Ltc1 is an ER-localized sterol transporter and a component of ER-mitochondria and ER-vacuole contacts. *Journal of Cell Biology*, *209*(4), 539–548.

N-O

Natarajan, K., Meyer, M. R., Jackson, B. M., Slade, D., Roberts, C., Hinnebusch, A. G., and Marton, M. J. (2001). Transcriptional Profiling Shows that Gcn4p Is a Master Regulator of Gene Expression during Amino Acid Starvation in Yeast. *Molecular and Cellular Biology*, *21*(13), 4347–4368.

Natsoulis, G., Hilger, F., and Fink, G. R. (1986). The HTS1 gene encodes both the cytoplasmic and mitochondrial histidine tRNA synthetases of S. cerevisiae. *Cell*, *46*(2), 235–243.

Negrutskii, B. S., and Deutscher, M. P. (1991). Channeling of aminoacyl-tRNA for protein synthesis in vivo. *Proceedings of the National Academy of Sciences of the United States of America*, *88*(11), 4991–4995.

Nichols, B. J., and Denton, R. M. (1995). Towards the molecular basis for the regulation of mitochondrial dehydrogenases by calcium ions. *Molecular and Cellular Biochemistry*, *149–150*(1), 203–212.

Noda, T., and Ohsumi, Y. (1998). Tor, a phosphatidylinositol kinase homologue, controls autophagy in yeast. *Journal of Biological Chemistry*, *273*(7), 3963–3966.

Obara, K., Noda, T., Niimi, K., and Ohsumi, Y. (2008). Transport of phosphatidylinositol 3-phosphate into the vacuole via autophagic membranes in Saccharomyces cerevisiae. *Genes to Cells*, *13*(6), 537–547.

Odorizzi, G., Babst, M., and Emr, S. D. (1998). Fab1p PtdIns(3)P 5-kinase function essential for protein sorting in the multivesicular body. *Cell*, *95*(6), 847–858.

Ohsumi, Y., and Anraku, Y. (1981). Active transport of basic amino acids driven by a proton motive force in vacuolar membrane vesicles of Saccharomyces cerevisiae. *Journal of Biological Chemistry*, *256*(5), 2079–2082.

Olmedo-Verd, E., Santamaría-Gómez, J., Ochoa De Alda, J. A. G., De Pouplana, L. R., and Luque, I. (2011). Membrane anchoring of aminoacyl-tRNA synthetases by convergent acquisition of a novel protein domain. *Journal of Biological Chemistry*, *286*(47), 41057–41068.

Osman, C., Haag, M., Potting, C., Rodenfels, J., Dip, P. V., Wieland, F. T., Brügger, B., Westermann,

B., and Langer, T. (2009). The genetic interactome of prohibitins: Coordinated control of cardiolipin and phosphatidylethanolamine by conserved regulators in mitochondria. *Journal of Cell Biology*, *184*(4), 583–596.

Osman, C., Haag, M., Wieland, F. T., Brügger, B., and Langer, T. (2010). A mitochondrial phosphatase required for cardiolipin biosynthesis: The PGP phosphatase Gep4. *EMBO Journal*, *29*(12), 1976–1987.

Otani, A., Slike, B. M., Dorrell, M. I., Hood, J., Kinder, K., Ewalt, K. L., Cheresh, D., Schimmel, P., and Friedlander, M. (2002). A fragment of human TrpRS as a potent antagonist of ocular angiogenesis. *Proceedings of the National Academy of Sciences of the United States of America*, *99*(1), 178–183.

Ᵽ-Ꝛ

Pan, X., Roberts, P., Chen, Y., Kvam, E., Shulga, N., Huang, K., Lemmon, S., and Goldfarb, D. S. (2000). Nucleus-vacuole junctions in Saccharomyces cerevisiae are formed through the direct interaction of Vac8p with Nvj1p. *Molecular Biology of the Cell*, *11*(7), 2445–2457.

Panchaud, N., Péli-Gulli, M. P., and De Virgilio, C. (2013). SEACing the GAP that nEGOCiates TORC1 activation: Evolutionary conservation of Rag GTPase regulation. *Cell Cycle*, *12*(18), 2948–2952.

Parra, K. J., Chan, C. Y., and Chen, J. (2014). Saccharomyces cerevisiae vacuolar H+-ATPase regulation by disassembly and reassembly: One structure and multiple signals. *Eukaryotic Cell*, *13*(6), 706–714.

Paumard, P., Vallier, J., Coulary, B., Schaeffer, J., Soubannier, V., Mueller, D. M., Brèthes, D., di Rago, J.-P., and Velours, J. (2002). The ATP synthase is involved in generating mitochondrial cristae morphology. *EMBO Journal*, *21*(3), 221–230.

Pédelacq, J. D., Cabantous, S., Tran, T., Terwilliger, T. C., and Waldo, G. S. (2006). Engineering and characterization of a superfolder green fluorescent protein. *Nature Biotechnology*, *24*(1), 79–88.

Péli-Gulli, M. P., Sardu, A., Panchaud, N., Raucci, S., and De Virgilio, C. (2015). Amino Acids Stimulate TORC1 through Lst4-Lst7, a GTPase-Activating Protein Complex for the Rag Family GTPase Gtr2. *Cell Reports*, *13*(1), 1–7.

Perona, J. J., and Hadd, A. (2012). Structural diversity and protein engineering of the aminoacyl-tRNA Synthetases. *Biochemistry*, *51*(44), 8705–8729.

Pestova, T. V., Lomakin, I. B., Lee, J. H., Choi, S. K., Dever, T. E., and Hellen, C. U. T. (2000). The joining of ribosomal subunits in eukaryotes requires eIF5B. *Nature*, *403*(6767), 332–335.

Peter, A., Herrmann, B., Antunes, D., Rapaport, D., Dimmer, K. S., and Kornmann, B. (2017). Vps13-Mcp1 interact at vacuole-mitochondria interfaces and bypass ER-mitochondria contact sites. *Journal of Cell Biology*, *216*(10), 3219–3229.

Peter, J., and Schacherer, J. (2016). Population genomics of yeasts: towards a comprehensive

view across a broad evolutionary scale. *Yeast*, *33*(3), 73–81.

Pon, L., and Schatz, G. (1991). *The Molecular and Cellular Biology of the Yeast Saccharomyces, Volume 1: Genome Dynamics, Protein Synthesis, and Energetics* (J. R. Broach, J. R. Pringles, & E. W. Jones (eds.)). Cold Spring Harbor Laboratory Press.

Powis, K., Zhang, T., Panchaud, N., Wang, R., De Virgilio, C., and Ding, J. (2015). Crystal structure of the Ego1-Ego2-Ego3 complex and its role in promoting Rag GTPase-dependent TORC1 signaling. *Cell Research*, *25*(9), 1043–1059.

Pozzan, T., Bragadin, M., and Azzone, G. F. (1977). Disequilibrium between Steady-State ca2+ Accumulation Ratio and Membrane Potential in Mitochondria. Pathway and Role of ca2+ Efflux. *Biochemistry*, *16*(25), 5618–5625.

Prasher, D. C., Eckenrode, V. K., Ward, W. W., Prendergast, F. G., and Cormier, M. J. (1992). Primary structure of the Aequorea victoria green-fluorescent protein. *Gene*, *111*(2), 229–233.

Ray, P. S., Arif, A., and Fox, P. L. (2007). Macromolecular complexes as depots for releasable regulatory proteins. *Trends in Biochemical Sciences*, *32*(4), 158–164.

Regenberg, B., Düring-Olsen, L., Kielland-Brandt, M. C., and Holmberg, S. (1999). Substrate specificity and gene expression of the amino acid permeases in Saccharomyces cerevisiae. *Current Genetics*, *36*(6), 317–328.

Ribas de Pouplana, L., and Schimmel, P. (2001). Two classes of tRNA synthetases suggested by sterically compatible dockings on tRNA acceptor stem. *Cell*, *104*(2), 191–193.

Roberts, P., Moshitch-Moshkovitz, S., Kvam, E., O'Toole, E., Winey, M., and Goldfarb, D. S. (2003). Piecemeal microautophagy of nucleus in Saccharomyces cerevisiae. *Molecular Biology of the Cell*, *14*(1), 129–141.

Rodnina, M. V., and Wintermeyer, W. (2009). Recent mechanistic insights into eukaryotic ribosomes. *Current Opinion in Cell Biology*, *21*(3), 435–443.

Rothbarth, K., and Werner, D. (1986). Amino-acid-transfer reactions in isolated nuclei of Ehrlich ascites tumor cells. *European Journal of Biochemistry*, *155*(1), 149–156.

Rubio, M. Á., Napolitano, M., Ochoa De Alda, J. A. G., Santamaría-Gómez, J., Patterson, C. J., Foster, A. W., Bru-Martínez, R., Robinson, N. J., and Luque, I. (2015). Trans-oligomerization of duplicated aminoacyl-tRNA synthetases maintains genetic code fidelity under stress. *Nucleic Acids Research*, *43*(20), 9905–9917.

S

Sambade, M., and Kane, P. M. (2004). The Yeast Vacuolar Proton-translocating ATPase Contains a Subunit Homologous to the Manduca sexta and Bovine e Subunits That Is Essential for Function. *Journal of Biological Chemistry*, *279*(17), 17361–17365.

Santamaría-Gómez, J., Ochoa de Alda, J. A. G., Olmedo-Verd, E., Bru-Martínez, R., and Luque,

I. (2016). Sub-cellular localization and complex formation by aminoacyl-tRNA synthetases in cyanobacteria: Evidence for interaction of membrane-anchored ValRS with ATP synthase. *Frontiers in Microbiology*, *7*(JUN).

Saraste, M. (1999). Oxidative phosphorylation at the fin de siecle. *Science*, 283(5407), 1488–1493.

Sarkar, S., Azad, A. K., and Hopper, A. K. (1999). Nuclear tRNA aminoacylation and its role in nuclear export of endogenous tRNAs in Saccharomyces cerevisiae. *Proceedings of the National Academy of Sciences of the United States of America*, *96*(25), 14366–14371.

Sato, T., Ohsumi, Y., and Anraku, Y. (1984a). An arginine/histidine exchange transport system in vacuolar-membrane vesicles of Saccharomyces cerevisiae. *Journal of Biological Chemistry*, *259*(18), 11509–11511.

Sato, T., Ohsumi, Y., and Anraku, Y. (1984b). Substrate specificities of active transport systems for amino acids in vacuolar-membrane vesicles of Saccharomyces cerevisiae. Evidence of seven independent proton/amino acid antiport systems. *Journal of Biological Chemistry*, *259*(18), 11505–11508.

Sattler, T., and Mayer, A. (2000). Cell-free Reconstitution of Microautophagic Vacuole Invagination and Vesicle Formation. *The Journal of Cell Biology*, *151*(3), 529–538.

Schimmel, P., and Wang, C. C. (1999). Getting tRNA synthetases into the nucleus. *Trends in Biochemical Sciences*, *24*(4), 127–128.

Schu, P. V., Takegawa, K., Fry, M. J., Stack, J. H., Waterfield, M. D., and Emr, S. D. (1993). Phosphatidylinositol 3-kinase encoded by yeast VPS34 gene essential for protein sorting. *Science*, *260*(5104), 88–91.

Scott, S. V., Hefner-Gravink, A., Morano, K. A., Noda, T., Ohsumi, Y., and Klionsky, D. J. (1996). Cytoplasm-to-vacuole targeting and autophagy employ the same machinery to deliver proteins to the yeast vacuole. *Proceedings of the National Academy of Sciences of the United States of America*, *93*(22), 12304–12308.

Serrano, R., Kielland-Brandt, M. C., and Fink, G. R. (1986). Yeast plasma membrane ATPase is essential for growth and has homology with (Na+ + K+), K+- and Ca2+-ATPases. *Nature*, *319*(6055), 689–693.

Sheppard, K., Yuan, J., Hohn, M. J., Jester, B., Devine, K. M., and Söll, D. (2008). From one amino acid to another: tRNA-dependent amino acid biosynthesis. *Nucleic Acids Research*, *36*(6), 1813–1825.

Shiber, A., Döring, K., Friedrich, U., Klann, K., Merker, D., Zedan, M., Tippmann, F., Kramer, G., and Bukau, B. (2018). Cotranslational assembly of protein complexes in eukaryotes revealed by ribosome profiling. *Nature*, *561*(7722), 268–272.

Shin, C. S., Kim, S. Y., and Huh, W. K. (2009). TORC1 controls degradation of the transcription factor Stp1, a key effector of the SPS amino-acidsensing pathway in Saccharomyces cerevisiae. *Journal of Cell Science*, *122*(12), 2089–2099.

Shoemaker, C. J., and Green, R. (2011). Kinetic analysis reveals the ordered coupling of

translation termination and ribosome recycling in yeast. *Proceedings of the National Academy of Sciences of the United States of America*, *108*(51), E1392–E1398.

Sideris, D. P., Petrakis, N., Katrakili, N., Mikropoulou, D., Gallo, A., Ciofi-Baffoni, S., Banci, L., Bertini, I., and Tokatlidis, K. (2009). A novel intermembrane space-targeting signal docks cysteines onto Mia40 during mitochondrial oxidative folding. *Journal of Cell Biology*, *187*(7), 1007–1022.

Simader, H., Hothorn, M., Kö, C., Basquin, J., Simos, G., Suck, D., Köhler, C., Basquin, J., Simos, G., and Suck, D. (2006). Structural basis of yeast aminoacyl-tRNA synthetase complex formation revealed by crystal structures of two binary sub-complexes. *Nucleic Acids Research*, *34*(14), 3968–3979.

Simos, G., Segref, A., Fasiolo, F., Hellmuth, K., Shevchenko, A., Mann, M., and Hurt, E. C. (1996). The yeast protein Arc1p binds to tRNA and functions as a cofactor for the methionyl- and glutamyl-tRNA synthetases. *EMBO Journal*, *15*(19), 5437–5448.

Smardon, A. M., and Kane, P. M. (2007). RAVE is essential for the efficient assembly of the C subunit with the vacuolar H+-ATPase. *Journal of Biological Chemistry*, *282*(36), 26185–26194.

Smardon, A. M., Tarsio, M., and Kane, P. M. (2002). The RAVE complex is essential for stable assembly of the yeast V-ATpase. *Journal of Biological Chemistry*, *277*(16), 13831–13839.

Smirnova, E. V., Lakunina, V. A., Tarassov, I., Krasheninnikov, I. A., and Kamenski, P. A. (2012). Noncanonical functions of aminoacyl-tRNA synthetases. *Biochemistry (Moscow)*, *77*(1), 15–25.

Sopko, R., Huang, D., Preston, N., Chua, G., Papp, B., Kafadar, K., Snyder, M., Oliver, S. G., Cyert, M., Hughes, T. R., Boone, C., and Andrews, B. (2006). Mapping pathways and phenotypes by systematic gene overexpression. *Molecular Cell*, *21*(3), 319–330.

Spinelli, J. B., and Haigis, M. C. (2018). The multifaceted contributions of mitochondria to cellular metabolism. Nature cell biology, 20(7), 745–754.

Steiner-Mosonyi, M., and Mangroo, D. (2004). The nuclear tRNA aminoacylation-dependent pathway may be the principal route used to export tRNA from the nucleus in Saccharomyses cerevisiae. *Biochemical Journal*, *378*(3), 809–816.

Stevens, B. (1981). Mitochondrial Structure. *Cold Spring Harbor Monograph Archive*, *11*(0), 471–504.

Stewart, A. G., and Stock, D. (2012). Priming a molecular motor for disassembly. *Structure*, 20(11), 1799–1800.

Stock, D., Leslie, A. G. W., and Walker, J. E. (1999). Molecular architecture of the rotary motor in ATP synthase. *Science*, *286*(5445), 1700–1705.

Stracka, D., Jozefczuk, S., Rudroff, F., Sauer, U., and Hall, M. N. (2014). Nitrogen source activates TOR (Target of Rapamycin) complex 1 via glutamine and independently of Gtr/Rag proteins. *Journal of Biological Chemistry*, *289*(36), 25010–25020.

Subramanian, K., Jochem, A., Le Vasseur, M., Lewis, S., Paulson, B. R., Reddy, T. R., Russell, J. D., Coon, J. J., Pagliarini, D. J., and Nunnari, J. (2019). Coenzyme Q biosynthetic proteins assemble in a substrate-dependent manner into domains at ER–mitochondria contacts. *Journal of Cell Biology*, *218*(4), 1353–1369.

Sutter, B. M., Wu, X., Laxman, S., and Tu, B. P. (2013). XMethionine inhibits autophagy and promotes growth by inducing the SAM-responsive methylation of PP2A. *Cell*, *154*(2), 403.

T

Takatori, S., Tatematsu, T., Cheng, J., Matsumoto, J., Akano, T., and Fujimoto, T. (2016). Phosphatidylinositol 3,5-Bisphosphate-Rich Membrane Domains in Endosomes and Lysosomes. *Traffic*, *17*(2), 154–167.

Takeshige, K., Baba, M., Tsuboi, S., Noda, T., and Ohsumi, Y. (1992). Autophagy in yeast demonstrated with proteinase-deficient mutants and conditions for its induction. *Journal of Cell Biology*, *119*(2), 301–312.

Tang, H. L., Yeh, L. S., Ghen, N. K., Ripmaster, T., Schimmel, P., and Wang, C. C. (2004). Translation of a yeast mitochondrial tRNA synthetase initiated at redundant non-AUG codons. *Journal of Biological Chemistry*, *279*(48), 49656–49663.

Tarun, S. Z., and Sachs, A. B. (1995). A common function for mRNA 5′ and 3′ ends in translation initiation in yeast. *Genes and Development*, *9*(23), 2997–3007.

Thorsness, P. E., and Fox, T. D. (1990). Escape of DNA from mitochondria to the nucleus in Saccharomyces cerevisiae. *Nature*, *346*, 376–379.

Thumm, M. (2000). Structure and function of the yeast vacuole and its role in autophagy. *Microscopy Research and Technique*, *51*(6), 563–572.

Thumm, M., Egner, R., Koch, B., Schlumpberger, M., Straub, M., Veenhuis, M., and Wolf, D. H. (1994). Isolation of autophagocytosis mutants of Saccharomyces cerevisiae. *FEBS Letters*, *349*(2), 275–280.

Tolkunova, E., Park, H., Xia, J., King, M. P., and Davidson, E. (2000). The human lysyl-tRNA synthetase gene encodes both the cytoplasmic and mitochondrial enzymes by means of an unusual: Alternative splicing of the primary transcript. *Journal of Biological Chemistry*, *275*(45), 35063–35069.

Tomashek, J. J., Sonnenburg, J. L., Artimovich, J. M., and Klionsky, D. J. (1996). Resolution of subunit interactions and cytoplasmic subcomplexes of the yeast vacuolar proton-translocating ATPase. *Journal of Biological Chemistry*, *271*(17), 10397–10404.

Tomioku, K. na, Shigekuni, M., Hayashi, H., Yoshida, A., Futagami, T., Tamaki, H., Tanabe, K., and Fujita, A. (2018). Nanoscale domain formation of phosphatidylinositol 4-phosphate in the plasma and vacuolar membranes of living yeast cells. *European Journal of Cell Biology*, *97*(4), 269–278.

Tone, J., Yoshimura, A., Manabe, K., Murao, N., Sekito, T., Kawano-Kawada, M., and

Kakinuma, Y. (2015). Characterization of Avt1p as a vacuolar proton/amino acid antiporter in *Saccharomyces cerevisiae*. *Bioscience, Biotechnology, and Biochemistry*, *79*(5), 782–789.

Toulmay, A., and Prinz, W. A. (2012). A conserved membrane-binding domain targets proteins to organelle contact sites. *Journal of Cell Science*, *125*(1), 49–58.

Toulmay, A., and Prinz, W. A. (2013). Direct imaging reveals stable, micrometer-scale lipid domains that segregate proteins in live cells. *Journal of Cell Biology*, *202*(1), 35–44.

Tsuji, T., Fujimoto, M., Tatematsu, T., Cheng, J., Orii, M., Takatori, S., and Fujimoto, T. (2017). Niemann-Pick type C proteins promote microautophagy by expanding raft-like membrane domains in the yeast vacuole. *ELife*, *6*.

Tsuji, T., and Fujimoto, T. (2018). Lipids and lipid domains of the yeast vacuole. *Biochemical Society Transactions*, *46*(5), 1047–1054.

Tsun, Z. Y., Bar-Peled, L., Chantranupong, L., Zoncu, R., Wang, T., Kim, C., Spooner, E., and Sabatini, D. M. (2013). The folliculin tumor suppressor is a GAP for the RagC/D GTPases that signal amino acid levels to mTORC1. *Molecular Cell*, *52*(4), 495–505.

Tumbula, D. L., Becker, H. D., Chang, W. Z., and Söll, D. (2000). Domain-specific recruitment of amide amino acids for protein synthesis. *Nature*, *407*(6800), 106–110.

Turner, R. J., Lovato, M., and Schimmel, P. (2000). One of two genes encoding glycyl-tRNA synthetase in Saccharomyces cerevisiae provides mitochondrial and cytoplasmic functions. *Journal of Biological Chemistry*, *275*(36), 27681–27688.

V-W

Vasington, F. D., and Murphy, J. V. (1962). Ca++ Uptake by Rat Kidnev Mitochondria and Its Dependence J on Respiration and Phosphorylation. In *Journal of Biological Chemistry* (Vol. 237, Issue 8).

Vögtle, F. N., Burkhart, J. M., Gonczarowska-Jorge, H., Kücükköse, C., Taskin, A. A., Kopczynski, D., Ahrends, R., Mossmann, D., Sickmann, A., Zahedi, R. P., and Meisinger, C. (2017). Landscape of submitochondrial protein distribution. *Nature Communications*, *8*(1).

Vögtle, F. N., Wortelkamp, S., Zahedi, R. P., Becker, D., Leidhold, C., Gevaert, K., Kellermann, J., Voos, W., Sickmann, A., Pfanner, N., and Meisinger, C. (2009). Global Analysis of the Mitochondrial N-Proteome Identifies a Processing Peptidase Critical for Protein Stability. *Cell*, *139*(2), 428–439.

Wada, M., and Ito, K. (2014). A genetic approach for analyzing the co-operative function of the tRNA mimicry complex, eRF1/eRF3, in translation termination on the ribosome. *Nucleic Acids Research*, *42*(12), 7851–7866.

Wakasugi, K., and Schimmel, P. (1999). Highly differentiated motifs responsible for two cytokine activities of a split human tRNA synthetase. *Journal of Biological Chemistry*, *274*(33), 23155–23159.

Wakasugi, K., Slike, B. M., Hood, J., Otani, A., Ewalt, K. L., Friedlander, M., Cheresh, D. A., and Schimmel, P. (2002). A human aminoacyl-tRNA synthetase as a regulator of angiogenesis. *Proceedings of the National Academy of Sciences of the United States of America*, *99*(1), 173–177.

Waldo, G. S., Standish, B. M., Berendzen, J., and Terwilliger, T. C. (1999). Rapid protein-folding assay using green fluorescent protein. *Nature Biotechnology*, *17*(7), 691–695.

Wen, X., and Klionsky, D. J. (2016). An overview of macroautophagy in yeast. *Journal of Molecular Biology*, *428*(9), 1681–1699.

Wende, S., Platzer, E. G., Jühling, F., Pütz, J., Florentz, C., Stadler, P. F., & Mörl, M. (2014). Biological evidence for the world's smallest tRNAs. *Biochimie, 100,* 151–158.

Westermann, B. (2014). Mitochondrial inheritance in yeast. *Biochimica et Biophysica Acta - Bioenergetics*, *1837*(7), 1039–1046.

Wichtowska, D., Turowski, T. W., and Boguta, M. (2013). An interplay between transcription, processing, and degradation determines tRNA levels in yeast. *Wiley Interdisciplinary Reviews: RNA*, *4*(6), 709–722.

Wideman, J. G., Gawryluk, R. M. R., Gray, M. W., and Dacks, J. B. (2013). The ancient and widespread nature of the ER-mitochondria encounter structure. *Molecular Biology and Evolution*, *30*(9), 2044–2049.

Wiedemann, N., Pfanner, N., and Ryan, M. T. (2001). The three modules of ADP/ATP carrier cooperate in receptor recruitment and translocation into mitochondria. *EMBO Journal*, *20*(5), 951–960.

Wiemken, A., and Dürr, M. (1974). Characterization of amino acid pools in the vacuolar compartment of Saccharomyces cerevisiae. *Archives of Microbiology*, *101*(1), 45–57.

Williamson, D. (2002). The curious history of yeast mitochondrial DNA. *Nature Reviews Genetics*, *3*(6), 475–481.

Wu, B., Ottow, K., Poulsen, P., Gaber, R. F., Albers, E., and Kielland-Brandt, M. C. (2006). Competitive intra- and extracellular nutrient sensing by the transporter homologue Ssy1p. *Journal of Cell Biology*, *173*(3), 327–331.

Y-Z

Yakobov, N., Debard, S., Fischer, F., Senger, B., and Becker, H. D. (2018). Cytosolic aminoacyl-tRNA synthetases: Unanticipated relocations for unexpected functions. *Biochimica et Biophysica Acta - Gene Regulatory Mechanisms*, *1861*(4), 387–400.

Yakobov, N., Fischer, F., Mahmoudi, N., Saga, Y., Grube, C. D., Roy, H., Senger, B., Grob, G., Tatematsu, S., Yokokawa, D., Mouyna, I., Latgé, J. P., Nakajima, H., Kushiro, T., and Becker, H. D. (2020). RNA-dependent sterol aspartylation in fungi. *Proceedings of the National Academy of Sciences of the United States of America*, *117*(26), 14948–14957.

Yamamoto, A., DeWald, D. B., Boronenkov, I. V., Anderson, R. A., Emr, S. D., and Koshland, D. (1995). Novel PI(4)P 5-kinase homologue, Fab1p, essential for normal vacuole function and morphology in yeast. *Molecular Biology of the Cell*, *6*(5), 525–539.

Yamamoto, H., Itoh, N., Kawano, S., Yatsukawa, Y. I., Momose, T., Makio, T., Matsunaga, M., Yokota, M., Esaki, M., Shodai, T., Kohda, D., Aiken Hobbs, A. E., Jensen, R. E., and Endo, T. (2011). Dual role of the receptor Tom20 in specificity and efficiency of protein import into mitochondria. *Proceedings of the National Academy of Sciences of the United States of America*, *108*(1), 91–96.

Yogev, O., and Pines, O. (2011). Dual targeting of mitochondrial proteins: Mechanism, regulation and function. *Biochimica et Biophysica Acta - Biomembranes*, *1808*(3), 1012–1020.

Yoon, M. S., Du, G., Backer, J. M., Frohman, M. A., and Chen, J. (2011). Class III PI-3-kinase activates phospholipase D in an amino acid-sensing mTORC1 pathway. *Journal of Cell Biology*, *195*(3), 435–447.

Yoon, M. S., Son, K., Arauz, E., Han, J. M., Kim, S., and Chen, J. (2016). Leucyl-tRNA Synthetase Activates Vps34 in Amino Acid-Sensing mTORC1 Signaling. *Cell Reports*, *16*(6), 1510–1517.

Yotsuyanagi, Y. (1962). Études sur le chondriome de la levure. I. Variation de l'ultrastructure du chondriome au cours du cycle de la croissance aérobie. *Journal of Ultrasructure Research*, *7*(1–2), 121–140.

Young, J. C., Hoogenraad, N. J., and Hartl, F. U. (2003). Molecular chaperones Hsp90 and Hsp70 deliver preproteins to the mitochondrial import receptor Tom70. *Cell*, *112*(1), 41–50.

Youngman, M. J., Hobbs, A. E. A., Burgess, S. M., Srinivasan, M., and Jensen, R. E. (2004). Mmm2p, a mitochondrial outer membrane protein required for yeast mitochondrial shape and maintenance of mtDNA nucleoids. *Journal of Cell Biology*, *164*(5), 677–688.

Zaman, S., Lippman, S. I., Zhao, X., and Broach, J. R. (2008). How Saccharomyces Responds to Nutrients. *Annual Review of Genetics*, *42*(1), 27–81.

Zinser, E., Paltauf, F., and Daum, G. (1993). Sterol composition of yeast organelle membranes and subcellular distribution of enzymes involved in sterol metabolism. *Journal of Bacteriology*, *175*(10), 2853–2858.

Zinser, E., Sperka-Gottlieb, C. D. M., Fasch, E. V., Kohlwein, S. D., Paltauf, F., and Daum, G. (1991). Phospholipid synthesis and lipid composition of subcellular membranes in the unicellular eukaryote Saccharomyces cerevisiae. *Journal of Bacteriology*, *173*(6), 2026–2034.

II. References in figures

[1]   L. Enkler, Le complexe multisynthétasique AME de levure : Dynamique de l'édifice et rôles non canoniques de ces composants, University of Strasbourg, 2014.

[2]   S. Debard, Molecular dynamic of the methionyl-tRNA synthetase and its novel non-canonical functions in the yeast S. cerevisiae, University of Strasbourg, 2019.

[3]   P.O. Ljungdahl, B. Daignan-Fornier, Regulation of amino acid, nucleotide, and phosphate metabolism in Saccharomyces cerevisiae, Genetics. 190 (2012) 885–929.

[4]   K. Deinert, F. Fasiolo, E.C. Hurt, G. Simos, Arc1p Organizes the Yeast Aminoacyl-tRNA Synthetase Complex and Stabilizes Its Interaction with the Cognate tRNAs, J. Biol. Chem. 276 (2001) 6000–6008.

[5]   H. Simader, M. Hothorn, C. Kö, J. Basquin, G. Simos, D. Suck, C. Köhler, J. Basquin, G. Simos, D. Suck, Structural basis of yeast aminoacyl-tRNA synthetase complex formation revealed by crystal structures of two binary sub-complexes, Nucleic Acids Res. 34 (2006) 3968–3979.

[6]   E. Karanasios, H. Simader, G. Panayotou, D. Suck, G. Simos, Molecular Determinants of the Yeast Arc1p-Aminoacyl-tRNA Synthetase Complex Assembly, J. Mol. Biol. 374 (2007) 1077–1090.

[7]   H.S. Kim, U. Hoja, J. Stolz, G. Sauer, E. Schweizer, Identification of the tRNA-binding protein Arc1p as a novel target of in vivo biotinylation in Saccharomyces cerevisiae, J. Biol. Chem. 279 (2004) 42445–42452.

[8]   G. Simos, A. Segref, F. Fasiolo, K. Hellmuth, A. Shevchenko, M. Mann, E.C. Hurt, The yeast protein Arc1p binds to tRNA and functions as a cofactor for the methionyl- and glutamyl-tRNA synthetases, EMBO J. 15 (1996) 5437–5448.

[9]   K. Galani, H. Grosshans, K. Deinert, E.C. Hurt, G. Simos, The intracellular location of two aminoacyl-tRNA synthetases depends on complex formation with Arc1p, EMBO J. 20 (2001) 6889–6898.

[10]   K. Galani, E. Hurt, G. Simos, The tRNA aminoacylation co-factor Arc1p is excluded from the nucleus by an Xpo1p-dependent mechanism, FEBS Lett. 579 (2005) 969–975.

[11]   M. Frechin, L. Enkler, E. Tetaud, D. Laporte, B. Senger, C. Blancard, P. Hammann, G. Bader, S. Clauder-Münster, L.M. Steinmetz, R.P. Martin, J.-P. di Rago, H.D. Becker, Expression of nuclear and mitochondrial genes encoding ATP synthase is synchronized by disassembly of a multisynthetase complex., Mol. Cell. 56 (2014) 763–76.

[12]   M. Frechin, D. Kern, R.P. Martin, H.D. Becker, B. Senger, Arc1p: Anchoring, routing, coordinating, FEBS Lett. 584 (2010) 427–433.

[13]   J.D. Pédelacq, S. Cabantous, T. Tran, T.C. Terwilliger, G.S. Waldo, Engineering and characterization of a superfolder green fluorescent protein, Nat. Biotechnol. 24 (2006) 79–88.

[14]   D.C. Prasher, V.K. Eckenrode, W.W. Ward, F.G. Prendergast, M.J. Cormier, Primary structure of the Aequorea victoria green-fluorescent protein (Bioluminescence; Cnidaria; aequorin; energy transfer; chromophore; cloning), Biochem. Mol. Biol. Mayo Found. 111 (1992) 284–2065.

[15]   G.S. Waldo, B.M. Standish, J. Berendzen, T.C. Terwilliger, Rapid protein-folding assay using green fluorescent protein, Nat. Biotechnol. 17 (1999) 691–695.

[16]   S. Cabantous, T.C. Terwilliger, G.S. Waldo, Protein tagging and detection with engineered self-assembling fragments of green fluorescent protein, Nat. Biotechnol. 23 (2005) 102–107.

[17]   S.C. Li, P.M. Kane, The yeast lysosome-like vacuole: Endpoint and crossroads, Biochim. Biophys. Acta - Mol. Cell Res. 1793 (2009) 650–663.

[18]   K. Bowers, T.H. Stevens, Protein transport from the late Golgi to the vacuole in the yeast Saccharomyces cerevisiae, Biochim. Biophys. Acta - Mol. Cell Res. 1744 (2005) 438–454.

[19]   T. Tsuji, T. Fujimoto, Lipids and lipid domains of the yeast vacuole, Biochem. Soc. Trans. 46 (2018) 1047–1054.

[20]   A. Zhao, Y. Fang, X. Chen, S. Zhao, W. Dong, Y. Lin, W. Gong, L. Liu, Crystal structure of Arabidopsis glutamyl-tRNA reductase in complex with its stimulator protein, Proc. Natl. Acad. Sci. U. S. A. 111 (2014) 6630–6635.

[21]   K.J. Parra, C.Y. Chan, J. Chen, Saccharomyces cerevisiae vacuolar H+-ATPase regulation by disassembly and reassembly: One structure and multiple signals, Eukaryot. Cell. 13 (2014) 706–714.

[22]   F. Bianchi, J.S. van't Klooster, S.J. Ruiz, B. Poolman, Regulation of Amino Acid Transport in Saccharomyces cerevisiae , Microbiol. Mol. Biol. Rev. 83 (2019) 1–38.

[23]   M. Kawano-Kawada, Y. Kakinuma, T. Sekito, Transport of amino acids across the vacuolar membrane of yeast: Its mechanism and physiological role, Biol. Pharm. Bull. 41 (2018) 1496–1501.

[24]   M. Kawano-Kawada, K. Manabe, H. Ichimura, T. Kimura, Y. Harada, K. Ikeda, S. Tanaka, Y. Kakinuma, T. Sekito, A PQ-loop protein Ypq2 is involved in the exchange of arginine and histidine across the vacuolar membrane of Saccharomyces cerevisiae, Sci. Rep. 9 (2019) 3–5.

[25]   X.D. Gao, J. Wang, S. Keppler-Ross, N. Dean, ERS1 encodes a functional homologue of the human lysosomal cystine transporter, FEBS J. 272 (2005) 2497–2511.

[26]   J.A. Simpkins, K.E. Rickel, M. Madeo, B.A. Ahlers, G.B. Carlisle, H.J. Nelson, A.L. Cardillo, E.A. Weber, P.F. Vitiello, D.A. Pearce, S.P. Vitiello, Disruption of a cystine transporter downregulates expression of genes involved in sulfur regulation and cellular respiration, Biol. Open. 5 (2016) 689–697.

[27]   A. González, M.N. Hall, Nutrient sensing and TOR signaling in yeast and mammals , EMBO J. 36 (2017) 397–408.

[28]   H. Nakatogawa, K. Suzuki, Y. Kamada, Y. Ohsumi, Dynamics and diversity in autophagy mechanisms: lessons from yeast, Nat. Rev. Mol. Cell Biol. 10 (2009) 458–467.

[29]   E. Cebollero, F. Reggiori, Regulation of autophagy in yeast Saccharomyces cerevisiae, Biochim. Biophys. Acta. 1793 (2009) 1413–1421.

[30]   A.S. Gross, M. Graef, Mechanisms of Autophagy in Metabolic Stress Response, J. Mol. Biol. 432 (2020) 28–52.

[31]   X. Wen, D.J. Klionsky, An overview of macroautophagy in yeast, J. Mol. Biol. 428 (2016) 1681–1699.

Marine HEMMERLE

Étude de la localisation mitochondriale ou vacuolaire d'aminoacyl-ARNt synthétases cytosoliques multi-localisées chez la levure *Saccharomyces cerevisiae*

Les aminoacyl-ARNt synthétases (aaRSs) catalysent la formation des aminoacyl-ARNt utilisés par la machinerie traductionnelle. La relocalisation subcellulaire de ces enzymes est souvent associée à des fonctions non-canoniques. La levure *S. cerevisiae* contient un complexe multisynthétasique, appelé complexe AME, composé de la méthionyl- et de la glutamyl-ARNt synthétases (MRS et ERS) et du cofacteur Arc1. Bien que le complexe ait été décrit comme exclusivement cytosolique, les deux aaRSs peuvent se relocaliser dans différents compartiments subcellulaires. On parle alors d'échoformes cytosoliques et organellaires. De plus, Arc1 interagit avec des lipides vacuolaires *in vitro*, suggérant une localisation vacuolaire *in vivo.* Pour identifier les échoformes mitochondriales et vacuolaires (vace) de protéines cytosoliques, nous avons élaboré deux outils de microscopie à épifluorescence. Nous avons pu identifier une nouvelle échoforme mitochondriale pour deux aaRSs, ainsi que des échoformes vacuolaires pour toutes les aaRSs testées et pour les composants du complexe AME. Une potentielle implication de vaceMRS dans l'inhibition du complexe TORC1 vacuolaire a également été mise en évidence.

Mots clés : aminoacyl-ARNt synthétase, *S. cerevisiae*, échoformes, mitochondrie, vacuole, TORC1

The aminoacyl-tRNA synthetases (aaRSs) are responsible for the formation of aminoacyl-tRNAs used by the translational machinery. The subcellular relocalization of these proteins is often associated with non-canonical functions. The yeast *S. cerevisiae* contains a multisynthetasic complex, called AME complex, composed of the methionyl- and glutamyl-tRNA synthetases (MRS and ERS) and the cofactor Arc1. Even if the complex has been described as exclusively cytosolic, the two aaRSs can relocate in different subcellular compartments. These proteins are thus referred as cytosolic or organellar echoforms. Moreover, Arc1 interacts with vacuolar lipids *in vitro*, suggesting a vacuolar localization *in vivo*. To visualize mitochondrial and vacuolar (vace) echoforms of cytosolic proteins, we engineered two epifluorescence microscopy tools. We identified a new mitochondrial echoform for two aaRSs, as well as vacuolar echoforms for all the cytosolic aaRSs tested and the AME components. A potential implication of vaceMRS in TORC1 inhibition was also observed.

Keywords: aminoacyl-tRNA synthetase, *S. cerevisiae*, echoforms, mitochondria, vacuole, TORC1